

SWBSS 2014

**Third International Conference on
Salt Weathering of Buildings and Stone Sculptures**

Brussels, 14-16 October 2014

SWBSS 2014

3rd International Conference on
Salt Weathering of Buildings and Stone Sculptures

14-16 October 2014

Edited by
Hilde De Clercq

Proceedings of SWBSS 2014

Third International Conference on
Salt Weathering of Buildings and Stone Sculptures

Royal Institute for Cultural Heritage, Brussels, Belgium
14-16 October 2014

Published by the Royal Institute for Cultural Heritage | Koninklijk Instituut
voor het Kunstpatrimonium (KIK) | Institut royal du Patrimoine artistique
(IRPA)

Jubelpark 1 | Parc du Cinquenaire 1 B-1000 Brussels
www.kikirpa.be

All rights reserved. No part of this publication may be reproduced, stored
in a retrieval system, or transmitted, in any form or by any means, without
the prior permission in writing of the publisher, or as expressly permitted
by law, or under terms agreed with the appropriate reprographics rights
organization.

Editor: Hilde De Clercq

Every effort has been made to comply with legal copyright requirements.
The publisher will be pleased to rectify any omission brought to their
notice at the earliest opportunity.

Front illustration: microscopic image of thenardite (actual picture size
approximate 5x4 mm) by Sebastiaan Godts

Printed in September 2014 by Peeters Printers (Herent, Belgium).
Printed on acid free paper norm ISO 9706.
D/2014/0613/4



ISBN 978-2-930054-24-7

Published online
www.saltwiki.net

Previous SWBSS Conferences

SWBSS 2008, organized by L.M. Ottosen, The National Museum
Copenhagen, Denmark, 22-24 October 2008

SWBSS 2011, organized by I. Ioannou & M. Theodoridou, University of
Cyprus, Limassol, Cyprus, 19-22 October 2011

SWBSS 2014

Scientific Committee

De Clercq Hilde, Royal Institute for Cultural Heritage, Brussels, Belgium

Flatt Robert, ETH Zürich, Switzerland

Hamilton Andrea, University of Strathclyde Engineering, Glasgow, UK

Ioannou Ioannis, University of Cyprus, Nicosia, Cyprus

Laue Steffen, University of Applied Science Potsdam, Germany

Lubelli Barbara, Delft University of Technology, The Netherlands

Ottosen Lisbeth, Technical University of Denmark, Lyngby, Denmark

Scherer George, Princeton University, US

Siedel Heiner, Dresden University of Technology, Germany

Steiger Michael, University of Hamburg, Germany

Török Akos, Budapest University of Technology and Economics, Hungary

Vergès-Belmin Véronique, Laboratoires de Recherche des Monuments
Historiques, Champs-sur-Marne, France

Organizing committee

De Clercq Hilde, Royal Institute for Cultural Heritage, Brussels, Belgium

Godts Sebastiaan, Royal Institute for Cultural Heritage, Brussels, Belgium

Berto Tanaquil, Royal Institute for Cultural Heritage, Brussels, Belgium

Laue Steffen, University of Applied Science Potsdam, Germany

Sponsored by

DGO4-Département du Patrimoine, Belgium

Service Publique de Wallonie, Belgium

Preface

Welcome to Brussels to the Royal Institute for Cultural Heritage!

The first SWBSS-event was held in Copenhagen, Denmark in 2008, with Lisbeth Ottosen as driving force; the second was organized by Ioannis Ioannou and Magdalini Theodoridou, in Limassol, Cyprus, in 2011.

This is the third conference in the series. It is a great pleasure to see that SWBSS2014 managed to attract the interest from so many different countries within Europe and abroad. We received almost 50 contributions, consisting of papers and extended abstracts, bringing together conservators, engineers, academics, young students and experienced researchers.

The success confirms the significance of the SWBSS topic to the scientific community. Being aware that salt crystallization is of a major importance on the weathering of porous building materials, I do hope that these kind of events contribute to an exchange of knowledge, the creation of new research ideas and future collaborations within this interesting field.

I would like to thank the Salze im Kulturgut e.V. - Fachhochschule Potsdam, Germany, Mr. Steffen Laue, for co-organizing this third version. The honor and opportunity is yours to host the fourth event, as offered in Limassol, to which I will collaborate with pleasure.

A thanks goes to all my colleagues for their assistance in organizing this international event, especially Sebastiaan Godts, Tanaquil Berto and our precious ICT unit.

Last but not least, I would like to express my deepest gratitude to our sponsors DGO4 and SPW for offering us support for the conference.

I sincerely hope that you will enjoy SWBSS2014 and wish you a pleasant stay in Brussels!

Hilde De Clercq

Conference Chair
Royal Institute for Cultural Heritage, Brussels

Table of Contents

Salt phase and transport phenomena

Drying of porous building materials possibly contaminated with soluble salts: summary and findings of the DRYMASS research project <i>T. Diaz Gonçalves, V. Brito, J. Musacchi, L. Pel, T. Saidov, J. Delgado Rodrigues, D. Costa and J.M. Mimoso</i>	1
Nucleation and growth of sodium chloride in confined geometries <i>J. Desarnaud, H. Derluyn, J. Carmeliet, D. Bonn and N. Shahidzadeh</i>	17
Influence of the salt concentration on the damage potential of mirabilite and thenardite <i>A. Stahlbuhk, J. Nissen, K. Linnow and M. Steiger</i>	35
Salt damage risk prediction for porous limestones <i>H. Derluyn, P. Moonen, T. Diaz-Gonçalves, V. Cnudde and J. Carmeliet</i>	49
Peering into the rock: a 4D synchrotron study of salt solution movement within masonry sandstone <i>C. Graham, M. Lee, V. Phoenix and M. Young</i>	61
Paradoxical drying due to salt crystallization; the effect of ferrocyanide <i>L. Pel and S. Gupta</i>	77
The effect of ferrocyanide ions on sodium chloride crystallization in salt mixtures as studied by NMR <i>L. Pel, S. Gupta, and M. Steiger</i>	89
Investigating a method to limit damage in Globigerina Limestone, a soft porous stone widely used in historic buildings <i>S. Sammut, J. Cassar, A. Marrocchi, C. Russo, L. Sommei and M.L. Santarelli</i>	101

Gypsum efflorescence under laboratory conditions: preliminary study <i>J. Chwast, H. Janssen and J. Elsen</i>	117
Numerical simulation of gypsum transport and crystallization <i>J. Todorović and H. Janssen</i>	133
Crystallization behavior of a Na ₂ SO ₄ –MgSO ₄ salt mixture and comparison to single salt behavior <i>N. Lindström, T. Talreja, K. Linnow and M. Steiger</i>	151
The crystallization behavior of sodium magnesium sulfate in limestone <i>S. Godts, R. Hendrickx and H. De Clercq</i>	167
Common salt mixtures database: a tool to identify research needs <i>S. Godts, R. Hayen and H. De Clercq</i>	185
 Measurement techniques	
Further steps towards the solution of Correns' dilemma <i>F. Caruso and R. J. Flatt</i>	199
Experimental study on salt deterioration of salt contaminated earthen materials under dry-wet cycles <i>Y.X. Shen, W.W. Chen, J. Kuang and W.F. Du</i>	211
Determination of the deliquescence point in salt mixtures and in in-situ multicomponent salts with DVS equipment <i>I. Rörig-Dalgaard</i>	223
Measurement of sorption isotherm of porous materials influenced by salt <i>M. Abuku, D. Ogura, S. Hokoi, C. Iba, S. Wakiya and T. Uno</i>	237
Porosity changes after different temperature regimes for a salt weathering simulation test on Mekkattam limestone <i>N. Aly, M. Gomez-Heras, A. Hamed, M. Alvarez de Buergo and F. Soliman</i>	247

Salt crystallization damage: how realistic are existing ageing tests? <i>B. Lubelli, R.P.J. van Hees and T.G. Nijland</i>	259
Monitoring of the salt mist aging test with DRMS <i>D. Costa and J. Delgado Rodrigues</i>	275
Study of NaCl crystallization using Infrared Thermography <i>P. Vázquez, C. Thomachot-Schneider, K. Mouhoubi, M. Gommeaux, G. Fronteau, V. Barbin and J.L. Bodnar</i>	289
 Conservation issues	
Salt sources revisited <i>C. Bläuer and B. Rousset</i>	305
Salt crystallization resistance of nano-modified repair lime mortars <i>M. Theodoridou, L. Kyriakou and I. Ioannou</i>	319
Limestone resistance to sodium sulfate degradation after consolidation by hydroxyapatite and TEOS <i>E. Sassoni, E. Franzoni, G. Graziani and F. Sagripanti</i>	335
Consolidation of fired-clay bricks by ethyl silicate: durability to salt crystallization <i>E. Franzoni, E. Sassoni, G. Graziani and A. Fregni</i>	347
 Conservation issues – desalination	
Testing the durability of hemp-based mortars under Mediterranean climatic conditions in coastal and inland areas: does the presence of salt alter hemp bio receptivity? <i>A. Arizzi, H. Viles, I. Martin-Sanchez and G. Cultrone</i>	357
Effect of ethyl silicate on salt crystallization resistance of Maastricht limestone <i>B. Lubelli, R.P.J. van Hees, T.G. Nijland and J. Bolhuis</i>	371

Sodium sulphate test on lime-based mortars: attaining degraded material to test conservation products and assessing salt resistance <i>C. Nunes, Z. Slížková and J. Delgado Rodrigues</i>	389
Electrodesalination of sandstones with irregular shapes and uneven distribution of salts <i>L.M. Ottosen, G. Skibsted and T. Præstholm</i>	405
Salt extraction of limestone by means of electrophoresis: some results on type of contact material and electrode position <i>H. De Clercq, Y. Vanhellemont and V. De Swaef</i>	421
Poulticing sandstone: implications for subsequent weathering response <i>C.M. Gerrow, C. Gerdwilker, P.A. Warke, S. McCabe and J.M. McKinley</i>	435
 Case studies	
Salt extractions of brickwork: a standard procedure? <i>H. De Clercq and S. Godts</i>	457
Desalination of the painted vault ribs of the Franciscan monastery church of Zeitz <i>W. Wedekind and Y. Rieffel</i>	469
In-situ 'vacuum' desalination - case study of a baroque tombstone <i>H. Siedel, C. Franzen and E. Pummer</i>	481
Salt conversion, backfilling, and back anchoring: the securing of the painted ceiling of the Red Hall in the Neues Museum, Berlin <i>W. Wedekind and J. Rüdrieh</i>	497

Posters

- Wall paintings salt induced decay in residential buildings in Hierapolis of Phrygia (Turkey) 517
E. Cantisani, B. Sacchi, S. Bracci, C. Riminesi and S. Vettori
- Salt weathering processes of reconstituted stone used in the Orval Abbey (Belgium) 521
M. Gommeaux C. Thomachot-Schneider, G. Fronteau, S. Eyssautier, K. Mouhoubi, T. Fujimaki, and C. T. Oguchi
- Limiting salt crystallization damage in lime mortar by using crystallization modifiers 525
S.J.C. Granneman, N. Shahidzadeh, B. Lubelli and R.P.J. van Hees
- A salt-storing modular mortar system developed for the salt loaded brick masonry of the Kampischen Hof, Stralsund (Germany) 527
G. Hilbert, J. Weber and P. Butz
- Measurement of salt solution uptake by ceramic brick using γ -ray projection 529
D. Ogura, M. Abuku, S. Hokoi, C. Iba, S. Wakiya, and T. Uno
- The effect of salt crystallization on the drying kinetics of building materials 533
M. D. Seck, P. Faure, M. Van Landegheb, and P. Coussot
- Nanocomposite coatings for the protection of marble against salt weathering 535
P. Spathis, I. Karapanagiotis, P. Manoudis, A. Zacharopoulou, V. Melfos and G. Vourlias
- Thermal behaviour of building stones contaminated with Na_2SO_4 543
C. Thomachot-Schneider, P. Vázquez, N. Lelarge, A. Conreux, C. Bouvy, M. Gommeaux, K. Mouhoubi and J.L. Bodnar

Drying of porous building materials possibly contaminated with soluble salts: summary and findings of the DRYMASS research project

**T. Diaz Gonçalves^{1*}, V. Brito¹, J. Musacchi¹, L. Pel², T. Saidov²
J. Delgado Rodrigues¹, D. Costa¹ and J.M. Mimoso¹**

¹ National Laboratory for Civil Engineering (LNEC), Lisbon, Portugal

² Eindhoven University of Technology (TU/e), The Netherlands

* teresag@lnec.pt

Abstract

Moisture causes severe and recurring anomalies in the built heritage, but removing it from the solid and thick masonry walls of old constructions is not easy, especially when soluble salts are present. These salts crystallize during drying, may harm the materials and their aesthetics. Moreover, the salts themselves and the alterations they cause affect the underlying drying process through mechanisms that require clarification.

The DRYMASS project aimed at improving the current understanding of drying and of how soluble salts can influence it. It also had the objective of verifying if drying can be accelerated by means of surface layers such as coatings, which would be of high technical interest for conservation.

The work of the project involved evaporative drying tests on porous building materials contaminated with different salts. It included also a novel use of optical profilometry for monitoring salt decay processes, and NMR measurements to determine the crystallizing Na₂SO₄ phases.

Main conclusions were that salts hinder drying because they reduce sorptivity and also, when compact efflorescence or a salt crust occurs, because these types of deposit obstruct vapour transport. It was also concluded that lime coatings can accelerate drying of several types of porous building material initially saturated with pure water. However, this effect may not manifest when salts are present because efflorescence morphology incorporates a component of chaotic uncertainty.

Keywords: soluble salts, drying, porous material, optical profilometry, lime coating

1 Introduction

Moisture causes severe and recurring anomalies to the architectural heritage. This involves the loss of historic materials, aesthetical problems, poor comfort and health conditions, as well as expensive repairs. Eliminating moisture, which is present in the pores of materials such as stone, brick and mortars, may be difficult because old masonry walls are typically solid and thick.

Moreover, historical materials often contain soluble salts. During drying, these salts crystallize as efflorescence or subflorescence, which is one of the most destructive alteration mechanisms of porous building materials.

The salts themselves and the alterations they cause to the materials influence the drying process. Understanding the mechanisms through which this influence is exerted is of paramount importance for the conservation of the architectural heritage because it is essential to enable prediction of decay.

The research project *DRYMASS – Drying of porous materials possibly contaminated with soluble salts* (<http://www-ext.lnec.pt/drymass/>) was launched in this context and took place from February 2010 to January 2014. Its main scientific objective was to provide a better understanding of drying and of how soluble salts can affect it. This included clarifying, for example, the effects that soluble salts, in solution or as solid crystals, have on liquid and vapour transport across the pores.

Another important objective of the project was finding out whether it is possible to accelerate the drying rate of a porous material by means of a surface layer (for example, a coating). Such possibility was suggested by the fact that the drying rate of a porous material can be higher than the evaporation rate of free water surface, depending on the pore structure of the material [1–4]. Therefore, manipulating the physical properties of the material, for instance by using a surface layer, could allow accelerating its drying rate. This technology would have high technical interest for the architectural heritage, in which moisture and dampness are recurrent. However, in this heritage, salts are also frequent. Therefore, the response of the surface layer needs to be evaluated not only with pure water but with salt solutions too.

The present article summarizes most of the experimental work undertaken to respond to the above mentioned questions, and the main conclusions that it eventually led to. More detailed information, for example on the methods and results, can be found in the articles published in the course of the research [4–11].

2 Methods and results

2.1 How do soluble salts influence liquid and vapour transport during drying?

We started by examining experimentally the drying kinetics of three natural stones impregnated with solutions of NaCl or NaNO₃. The natural stones were the Bentheimer sandstone (B), the Ançã limestone (CA) and a current Portuguese limestone of lower porosity which we have called “grey limestone” (CC). These materials are thoroughly characterized in [5].

The tests were carried out with four NaCl solutions and three NaNO₃ solutions with a different concentration. The experiments consisted in assessing sequentially, on the same specimens, the following properties and aspects: a) capillary absorption with water and with the salt solutions; b) vapour pressure above the solution-filled materials; c) drying kinetics, as expressed by the evaporation curve; d) morphology of the efflorescence formed during drying; and, e) water vapour conductivity of the efflorescence-covered specimens.

In tests a, c and e, RILEM procedures [12] were followed. In test b, vapour pressure was measured using a capacitive water activity analyser (Hygrolab 3, by Rotönic). In test d the study of efflorescence morphology was carried out visually or, in some cases, by optical microscopy.

The test specimens were small stone cubes with 24-mm edge, except for the Bentheimer of which taller specimens (120 mm height) had to be used to measure capillary absorption because this was very fast. A minimum of three test specimens of each type of stone was always used at each experimental condition.

The vapour conductivity was measured through the dry cup method in a climatic chamber at 23°C and 50% RH. RH of around 0% was achieved inside the cups by the use of anhydrous calcium chloride. Measuring the vapour conductivity of porous materials with efflorescence (e) was a particularly innovative aspect of this work. To the best of our knowledge, such direct method of quantifying the obstruction posed by the efflorescence had never been tried before.

The results of drying test c revealed two main facts: (i) the higher the salt concentration the slower the drying, which agrees with what is usually observed in practice and in lab; (ii) some isolated specimens arbitrarily deviated from the general behaviour, depicting even slower drying kinetics (Figure 1). The arbitrary deviations in drying kinetics correspond to (also apparently random) variations in the morphology of the efflorescence formed during drying (test d), as also seen in Figure 1.

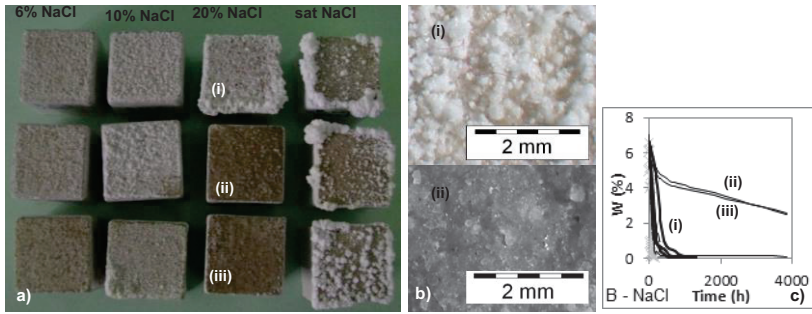


Figure 1: Decay patterns and drying kinetics of Bentheimer sandstone with NaCl solutions of different concentration: (a) vitreous salt crusts were observed on two out of three specimens tested with 20% NaCl solution; (b) details of the two types of efflorescence obtained with the 20% NaCl solution; (c) drying curves showing that the vitreous NaCl crusts on specimens (ii) and (iii) correspond to a much slower drying kinetics.

As to the capillary absorption (test a), it was observed that sorptivity decreased with the concentration of the absorbed salt solution and also varied with the type of salt [5]. Sorptivity ($m s^{-1/2}$) is an experimental quantity that expresses the tendency of a material to absorb and transmit liquids by capillarity [13]. It is the slope of the first linear segment of the absorption curve obtained when the cumulative volume of liquid absorbed per unit area, i.e., inflow velocity i (m), is plotted against the square root of time t (s). This is expressed by Equation (1), in which ΔM is the cumulative mass of absorbed liquid (kg), A the area of the absorption surface (m^2) and ρ the density of the liquid ($kg m^{-3}$).

$$S = i t^{-1/2}, \text{ with } i = \Delta M A^{-1} \rho^{-1} \quad (1)$$

The observed changes in sorptivity were proportional to $(\sigma/\eta)^{1/2}$, which means that they were due to the effect of the salts on surface tension (σ) and viscosity (η) of the salt solution. Indeed, when the sorptivity of a given material is measured using different liquids, it should scale as $(\sigma/\eta)^{1/2}$. This is shown in Equation 2, in which σ (mN/m) and η (cP) are the surface tension and viscosity of the liquid, respectively, and S is the intrinsic sorptivity of the material [13].

$$S = (\sigma/\eta)^{1/2} S \quad (2)$$

This indicates that salts can hinder liquid capillary transport, which could explain, at least partially, the observed differences in drying kinetics. However, this influence agrees with what is predicted theoretically from thermodynamic principles [13] and, therefore, cannot account for the seemingly arbitrary variations observed in some cases.

The vapour pressure measurements (test b) were carried out above the surface of CA and CC specimens saturated with NaCl solutions of different concentrations. They took place 24h after drying had begun, i.e., at the start of the process as this lasted in total close to one month or more. The results showed that, regardless of the initial concentration of the solution, the RH above the specimens was similar to the RH_{eq} of the saturated salt solution [5]. This means that the solutions saturated very early at the evaporation front and, so, that the initial differences in vapour pressure are not relevant to explain the differences in drying behaviour.

The results of the vapour conductivity test (test e) are given in Figure 2 in terms of equivalent air layer thickness S_d . As seen, the S_d of the efflorescence-covered specimens is, in most cases, similar to that of the blank specimens. This means that no significant blocking of vapour transport by the efflorescence took place in these cases.

By crossing these results with those of test d, it was verified that the deviant drying kinetics correspond to dense salt deposits, namely the mentioned vitreous NaCl crusts formed on Bentheimer specimens ii and iii (Figure 1) and compact NaCl efflorescence formed on the Ançã specimens [5]. The rest corresponds to porous efflorescence. Therefore, it was concluded that only dense salt layers effectively hinder the transport of vapour.

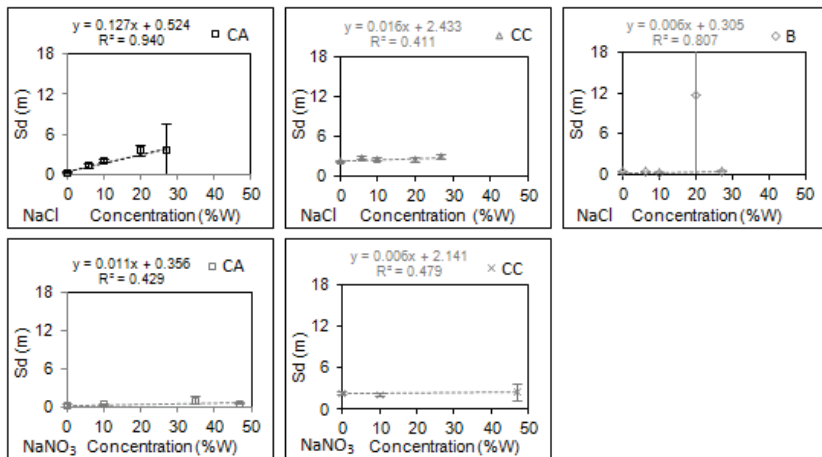


Figure 2: Equivalent air layer thickness (S_d) of the efflorescence-covered specimens as a function of the initial concentration of the salt solution [5]

In fact, when the efflorescence present on the surface was porous and, therefore, had no relevant blocking effect in relation to vapour transport, the drying kinetics is similar for solutions with similar σ/η ratio (Figure 3, on

the left). This indicates that, in these cases, the differences in drying kinetics are due to the changes salts induce on sorptivity.

Differently, when compact salt crusts which hinder vapour transport are present, there is an additional decrease in drying kinetics, as seen for the CA limestone with NaCl (Figure 3, on the right). This indicates that compact salt crusts can further slowdown the drying kinetics.

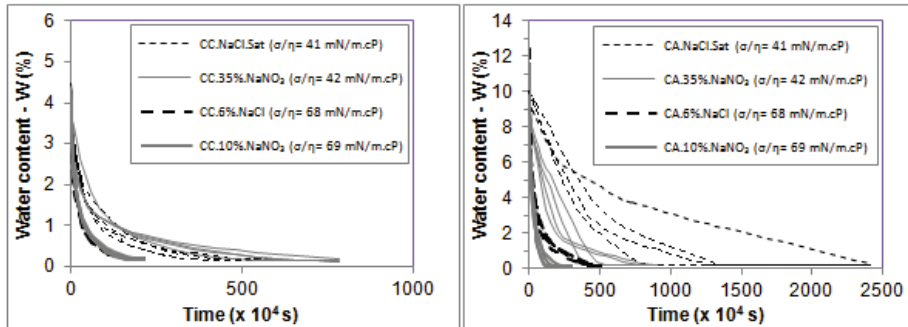


Figure 3: Drying kinetics, for solutions with similar σ/η ratio, of specimens depicting either: (i) only porous efflorescence (on the left, CC stone); (ii) porous efflorescence and compact salt crusts, respectively (on the right, CA stone) [5]

2.2 Unpredictability in salt decay

The results presented in the previous section show that thermodynamic considerations are not enough to explain the drying kinetics of porous materials in the presence of soluble salts. As seen, the drying kinetics of several specimens suffered occasional deviations which derive from apparently random variations in efflorescence morphology. This shows that there is also a component of unpredictability in the process [5].

This kind of uncertainty was observed also in a second experimental study of the project carried out with NaCl and Na₂SO₄ [7]. Figure 4 shows some of the results. As seen, the drying kinetics are not only slower, but also more irregular showing higher dispersion for the salt solutions than for pure water. Also, it sometimes diverges among specimens of the same material subjected to similar experimental conditions. These chaotic features [14] are in agreement with the decay patterns and suggest that soluble salts amplify the effects of the natural heterogeneity of porous materials.

A third study of the DRYMASS project [10, 11] showed that this type of phenomenon occurs not only in relation to efflorescence, but also in relation to decay patterns that involve material degradation. Fissures and

disaggregation, for example, can create preferential pathways for vapour transport.

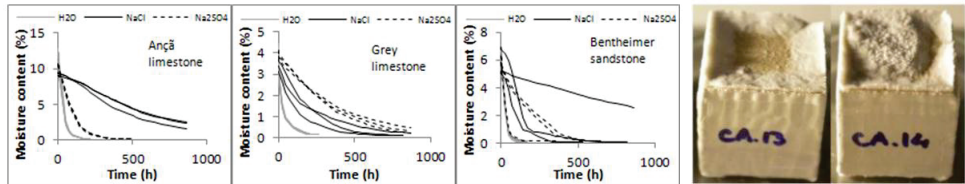


Figure 4: On the left: drying kinetics of the three tested stones. On the right: variation in the decay patterns of two specimens of Ançã limestone tested simultaneously and under similar conditions with saturated NaCl solution [7]

This study was carried out with six individual salts, NaCl, NaNO₃, Na₂SO₄, Na₂CO₃, KCl and KNO₃, on two current materials, lime mortar (A) and red ceramic brick (T). It involved measuring the sorptivity and the drying kinetics of the salt laden materials, the last over a span of more than 7 months. The testing protocols are those described in the previous section.

Figure 5 shows variations in the decay patterns and drying kinetics of brick and mortar with NaNO₃ and Na₂CO₃.

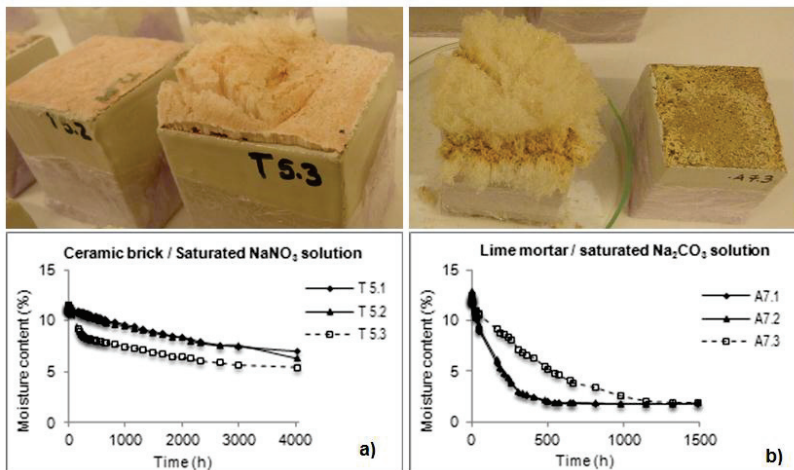


Figure 5: Variations in the decay patterns and drying kinetics of brick and mortar laden with NaNO₃ and Na₂CO₃: (a) one brick specimen depicted fluffy efflorescence while the other two developed compact salt crusts and had slower drying kinetics; (b) two lime mortar specimens showed abundant efflorescence that caused material disintegration and was accompanied by faster drying kinetics, while the other did not [8].

This figure illustrates that also in this study the degradation patterns varied occasionally for similar materials subjected to the same experimental conditions. And, again, the drying kinetics varied accordingly: in this case, the more altered the material the faster the drying.

2.3 Measuring the alterations

But it is not only arbitrariness that makes it hard to predict and deal with decay salt processes. Another important problem is that salt crystallization tests, which are used to assess treatments and materials, are often unrepresentative of reality. This happens because, to obtain measurable changes within a reasonable period of time, the specimens are typically subjected to extreme conditions, such as high temperatures or successive wet/dry cycles. The consequent distortion of results can be particularly significant for salts such as Na_2SO_4 , which in these extreme conditions can give rise to massive contact-induced [15] or temperature-induced [16] crystallization processes that hardly occur in the architectural heritage.

To overcome this major difficulty, a novel method based on optical profilometry was developed within the DRYMASS project [6]. Topographic profiles are measured during drying, from which an alteration kinetics curve is afterwards calculated (Figure 6). Each point in the alteration curve corresponds to a different profile, so, this curve expresses the (average) lifting of the surface during the process. As we are able to measure the small changes undergone by the material at the micrometre scale, it becomes unnecessary to subject it to extreme experimental conditions.

This new method was used in a set of crystallization tests with saturated Na_2SO_4 solution. The specimens, laterally sealed with epoxy, were first lead to capillary saturation by partial immersion in the salt solution. Then, their bottom face was sealed with polyethylene sheet, which was followed by a single drying event at 20°C and 50% RH.

The results showed that, under these less radical conditions, Na_2SO_4 can develop decay patterns similar to those observed in buildings. Ançã limestone, for example, developed a typical delamination pattern (Figure 6). As shown, the alteration process was successfully monitored by optical profilometry and, afterwards, characterized by the alteration curve [6].

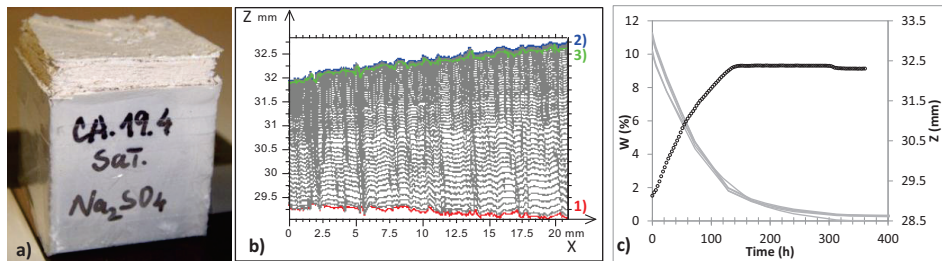


Figure 6: Delamination of Ançã limestone: (a) image of a test specimen at the end of drying; (b) topographic profiles obtained every 3 h during drying: 1) first profile; 2) uppermost profile after 305 h of drying; 3) last profile after 320 h of drying; (c) alteration kinetics curves in black, and drying kinetics curves in grey [6]

2.4 NMR identification of sodium sulfate phases crystallizing on Ançã limestone

NMR experiments showed that the Na_2SO_4 phase causing the damage seen in Figures 6 and 7 was mirabilite [9]. Indeed, the two Na_2SO_4 hydrated phases, mirabilite and the metastable heptahydrate, can form under a wide range of conditions, including the present (20°C / 50% RH).

The NMR tests were repeated under different experimental conditions of temperature and RH (20°C-50%RH, 20°C-0%RH and 7.5°C-0%RH). The two last conditions included also pre-heating the specimens at 40°C to ensure that no mirabilite crystals were present in the pores when drying started. That would exclude heptahydrate crystallization because heptahydrate is metastable and, therefore, the two phases cannot coexist.

The conclusions were that both mirabilite and heptahydrate can be responsible for this type of decay, as seen in Figure 7. The heptahydrate tends to crystallize first when there is no previous presence of mirabilite crystals in the porous material [9].

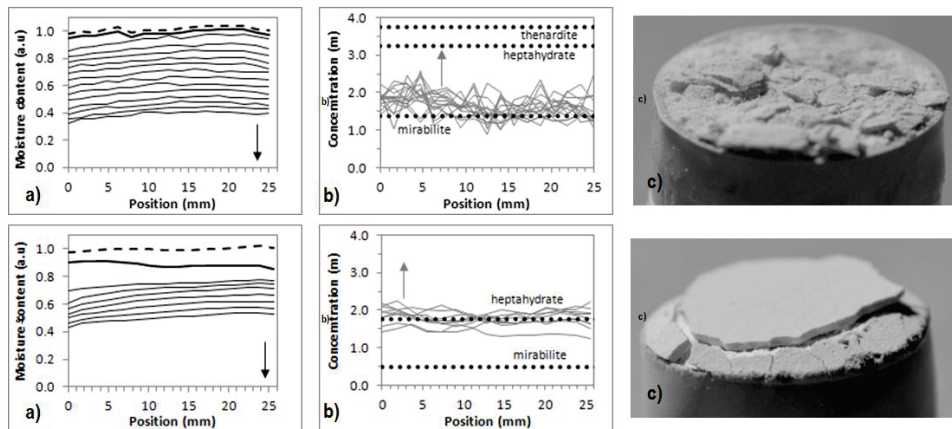


Figure 7: NMR-monitored drying experiments on Ançã limestone specimens at 20°C / 50% RH (left) and 7.5°C/0% RH with pre-heating (right): (a) moisture profiles, (b) ion concentration profiles, (c) test specimens after the experiment [9]

2.5 Influence of a traditional lime coating on drying

To find out whether it is possible to accelerate the drying rate of porous building materials by means of surface layers, we started by evaluating experimentally the influence of a traditional lime coating on the drying of five materials [7]. The materials were the previously mentioned Ançã limestone (CA), grey limestone (CC) and Bentheimer sandstone (B), as well as the well-known Maastricht limestone (M).

Lime coatings were considered a good first choice for this work because they are hydrophilic and vapour permeable, and also because of the relevance they have in conservation. The traditional lime coating used in our study had a 1.4 water/lime ratio and was applied manually, by brush or with a spatula, depending on the substrate material [7].

The drying tests were carried out, as previously, according to the RILEM procedure [12]. The outputs of the test were quantified: (i) through the drying index (DI), an empirical quantity which translates the drying curve into a single quantitative parameter and is based on the measurement of the area below that curve [17]; (ii) through the Stage I drying rate which is the drying rate of the material while its moisture content is high enough to sustain a saturated condition at the surface and is given by the slope of the initial straight branch of the evaporation curve.

The results obtained with pure water were extremely interesting. They showed that the lime coating not only does not hinder drying, but it is also able to accelerate it (Figure 8).

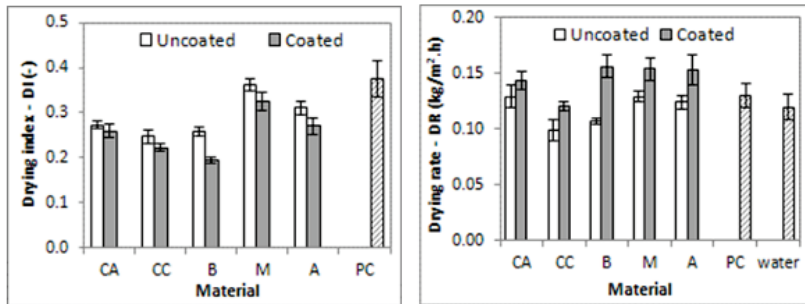


Figure 8: Results of the drying test with pure water on lime coated materials given in terms of: drying index (on the left) and Stage I drying rate (on the right) [7]

The increase in drying rate was very significant under Stage I conditions (Figure 8, on the right), i.e., when the moisture content of the substrate is high, as it often happens at the base of walls suffering from rising damp. It has, therefore, nothing to do with the vapour permeability of the coating, because during Stage I the drying front is at the surface of the material.

The main explanation for the observed increase in the Stage I drying rate is that, due to the complexity of its pore structure, the coating is able to generate a larger effective surface of evaporation.

2.6 Behaviour of the traditional lime coating with soluble salts

To verify the behaviour of the traditional lime coating when salts are present, we carried out a set of crystallization tests on coated and uncoated specimens with solutions of NaCl or Na₂SO₄ [8].

As seen in Figure 9, the coating can still, in few cases, enhance drying when soluble salts are present. However, in comparison to pure water, the drying kinetics are slower. The drying behaviour is also more irregular and has higher dispersion, which suggests that salt decay processes have a high sensitivity to the initial conditions. This means that small changes in the microstructure of the materials may result in large differences in terms of decay patterns and, consequently, of drying kinetics. That explains why, as previously, the drying kinetics occasionally diverged between specimens of the same material subjected to similar experimental conditions.

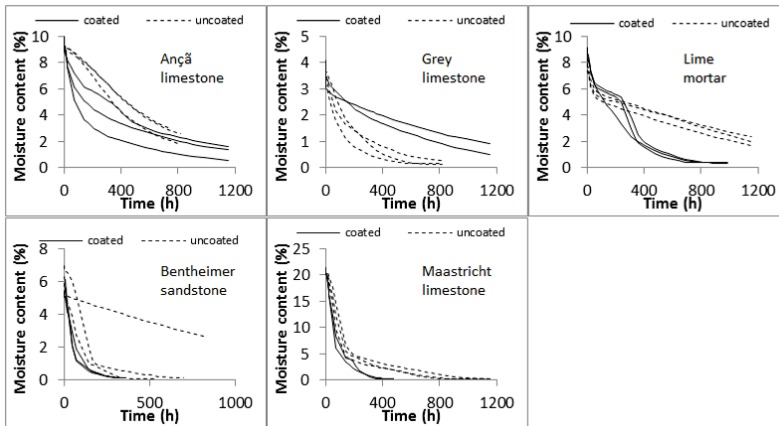


Figure 9: Drying kinetics of coated and uncoated materials contaminated with NaCl [8]

3 Conclusions and perspectives

In relation to the first objective of the DRYMASS project, of advancing the understanding of how soluble salts affect the drying of porous materials, two main conclusions were reached:

- Factors that influence drying

The drying kinetics of the tested materials were generally slower with salt solutions than pure water. This was expected because it is what is normally observed in practice and in the lab.

Our work indicates that this slower drying has two main causes that may overlap. The first is a reduction in sorptivity due to the effect that salts have on surface tension and viscosity. The second is the obstruction to vapour transport by the crystallized salt.

Only compact salt crusts can obstruct the pores, and these occurred only occasionally in our experiments. In most cases, porous efflorescence occurred, which poses no obstruction to water vapour transport.

In addition to these two main factors of influence, others may occur, which often have the opposite effect. For example, fissures and disaggregation can create preferential pathways for vapour transport and, therefore, accelerate drying.

- Unpredictability in salt decay

When soluble salts are present, the drying kinetics are more irregular and show higher dispersion than for pure water.

Furthermore, it may diverge significantly among specimens of the same material subjected to similar conditions.

We believe this happens because salt decay processes have a chaotic component and, therefore, salts amplify the dispersion effects that material heterogeneity has on the drying kinetics. Due to this chaotic character of salt decay, the morphology of efflorescence, and of other decay patterns with an influence on drying, incorporates a component of unpredictability [14]. This explains the apparently random variations in drying kinetics that were observed.

In relation to the second objective of the project, i.e. of finding out whether it is possible to enhance the drying rate of porous building materials using a surface layer, there were two main conclusions:

- Lime coatings such as traditional lime washes not only do not hinder drying, but can even accelerate it. This happens when the moisture content in the substrate is high enough so that the drying front is at the surface, and is likely to occur because the coating generates a larger effective surface of evaporation.
- In the presence of soluble salts, lime coatings can, sometimes, still enhance drying, but not systematically, and this due to the chaotic nature of the salt crystallization process.

In addition, the DRYMASS project allowed developing a novel method to monitor and quantify salt decay patterns by optical profilometry:

- This new method allows defining more realistic salt crystallization tests because we are able to measure the small changes undergone at the micrometre scale. Therefore, it becomes unnecessary to subject the material to (unrealistically) extreme experimental conditions.
- It was confirmed that sodium sulfate can be very destructive in field-representative conditions, i.e., in the absence of high temperature or fast successive wet/dry cycles. A delamination pattern similar to that found in real constructions was observed on the well-known Ançã limestone, which was thoroughly characterized with the help of the new optical method.

Finally, the work allowed concluding that NMR is appropriate to determine which crystal phases are crystallizing during drying. It showed that both mirabilite and heptahydrate can cause delamination of Ançã limestone under different environmental conditions. The heptahydrate tends to crystallize first when there is no previous presence of mirabilite crystals in the porous material.

Among future research perspectives suggested by the project, we highlight those related to the uncertainty in salt decay processes. In parallel to establishing an effective theoretical framework, there is a pressing need for data about what happens in reality. This will allow defining ranges of situations (types of salt, salt contents, etc.) to be considered in experiments and modelling.

Acknowledgments

This study was funded by the Portuguese Foundation for Science and Technology (FCT) under the research project DRYMASS (ref. PTDC/ECM/100553/2008). We thank Veerle Cnudde and Timo G. Nijland for providing the Bentheimer sandstone, as well as Cerâmica Vale de Gândara and Lusical for offering the ceramic brick and the dry hydrate, respectively. We also gratefully acknowledge the support provided by José Costa, Luis Nunes, Paula Menezes and Etelvina Leitão.

References

- [1] Hammecker C. Importance des transferts d'eau dans la dégradation des pierres en œuvre. Thèse de doctorat, Université Louis Pasteur, Strasbourg, France, 1993.
- [2] Tournier B, Jeannette D, Destrigneville C. Stone drying: an approach of the effective evaporating surface area. In Proceedings of 9th International Congress on Deterioration and Conservation of Stone, Venice, 19-24 June 2000, 629-635.
- [3] Tang R, Etzion Y. Comparative studies on the water evaporation rate from a wetted surface and that from a free water surface. *Building and Environment* 39 (2004), 77–86.
- [4] Diaz Gonçalves T, Brito V, Pel L Water vapour emission from rigid mesoporous materials during the constant drying rate period. *Drying Technology* 30 (2012), 462–474.
- [5] Brito V, Diaz Gonçalves T. Drying kinetics of porous stones in the presence of NaCl and NaNO₃: experimental assessment of the factors affecting liquid and vapour transport. *Transport in Porous Media* 100 (2013), 193-210.
- [6] Diaz Gonçalves T, Brito V. Alteration kinetics of natural stones due to sodium sulphate crystallization: can reality match experimental simulations? *Environmental Earth Sciences* (in press). DOI:10.1007/s12665-014-3085-0.

- [7] Brito V, Diaz Gonçalves T. Artisanal lime paints and their influence on moisture transport during drying. HMC13 - 3rd Historic Mortars Conference, Glasgow, 11-14 September 2013. Available at http://www-ext.lnec.pt/drymass/pdfs/Brito_DiazGoncalves_HMC13.pdf.
- [8] Diaz Gonçalves T, Brito V, Musacchi J. The whole and the parts: can lime coatings enhance the drying of salt laden materials? *Construction and Building Materials* 57 (2014), 179–189.
- [9] Brito V, Saidov T, Diaz Gonçalves T, Pel L. NMR identification of sodium sulfate phases crystallizing on Ançã limestone under different environmental conditions. *Journal of Building Physics* (accepted June 2014)
- [10] Azevedo J. Absorção por capilaridade de soluções salinas em materiais porosos (Capillary absorption of salt solutions in porous building materials, in Portuguese). MSc Thesis, Faculty of Engineering of the University of Porto, 2013. Available at http://www-ext.lnec.pt/drymass/pdfs/Tese_JoanaVFinal.pdf.
- [11] Azevedo J, Guimarães AS, Diaz Gonçalves T. Uncertainty in the processes of absorption and drying of a mortar and a brick contaminated with six different binary salts. Crispom IV-4th international workshop on crystallization in porous media, Amsterdam, 11-13 June 2014 (abstract).
- [12] RILEM TC 25-PEM. Recommended tests to measure the deterioration of stone and to assess the effectiveness of treatment methods, *Materials and Structures* 13 (1980), 175-253.
- [13] Hall C, Hoff WD. *Water Transport in Brick, Stone and Concrete*. Second edition. CRC Press, Taylor & Francis, 2012.
- [14] Werndl C. What are the new implications of chaos for unpredictability?, *British Journal for the Philosophy of Science* 60 (2009), 195-220.
- [15] Chatterji S, Jensen AD. Efflorescence and breakdown of building materials, *Nordic Concrete Research* 8 (1989), 56-61.
- [16] Doehne E, Selwitz C, Carson DM. The damage mechanism of sodium sulfate in porous stone In *Proc. SALTeXPERT Meeting, Prague*. Stefan Simon and Miloš Drdácý (ed.) *European Research on Cultural Heritage. State-of-the-Art Studies, Vol.5* (2006), 127-160.
- [17] Commissione NORMAL. *Misura dell'indice di asciugamento (drying index)*. Roma, CNR/ICR. Normal 29/88, 1991.

Nucleation and growth of sodium chloride in confined geometries

J. Desarnaud^{1*}, H. Derluyn², J. Carmeliet², D. Bonn¹ and N. Shahidzadeh¹

¹Van der Waals-Zeeman Institute, Institute of Physics, University of Amsterdam, The Netherlands

²ETH, Institut für Technologie in der Architektur, Zürich Hönggerberg, Switzerland

* j.e.desarnaud@uva.nl

Abstract

Experiments on evaporation of aqueous sodium chloride solutions from micro capillaries demonstrate for the first time that there is a metastability limit to the solubility of NaCl. The supersaturation of the solution reached at the onset of crystallization is found to be very high, almost twice the saturation concentration. At this concentration, we observe a peculiar form of crystal growth: the very rapid growth of a single Hopper crystal in which many crystallites grow outwards from a single central nucleus. The high supersaturations achieved at the onset of crystal growth are found to be independent of the size, shape and surface properties of the micro capillary.

Keywords: metastability limit, NaCl, supersaturation, salt damage

1 Introduction

Nucleation and crystallization in porous media are very important subjects in different fields such as the semiconductor industry, oil recovery, soils mechanics, purification of pharmaceuticals and proteins [1-4]. There are also many direct applications, biomineralization [5], CO₂ sequestration where NaCl crystals that precipitate can completely block the porous medium in which the CO₂ should be injected [6,7]. For civil engineering, geology and conservation of cultural heritage, frost [8-9] and salt crystallization is one of the major cause of mechanical and physical weathering leading to the disintegration of rocks and building materials [10-14], and its influence is expected to increase due to global climate change [15].

In practice, the precise conditions under which the salt crystals nucleate and grow are very important but still unknown. The existence of a supersaturation in the salt solutions can account for an excess pressure exerted by the salt crystals against the pore walls (crystallization pressure) [16, 17] and hence damage the stone. In fact, any crystallization in solution process consists of two major steps: crystal nucleation and growth. The rate of nucleation and the growth speed are driven by the supersaturation ($\Delta\mu$) of the solution, since the latter is the driving force of both processes

$$\Delta\mu = \mu_s - \mu_c \approx \nu RT \ln S \quad (1)$$

where μ_s and μ_c are the chemical potentials of a molecule in solution and in the bulk of the crystal phase, respectively; k is the Boltzmann constant, T is the absolute temperature and S is the relative supersaturation defined as ($S=C/C_{\text{sat}}$ with C concentration of the solution and C_{sat} concentration of the solution at saturation).

For a given supersaturation, by taking into account the non-ideal behaviour of the liquid phase, the total number of ions present and the interactions, the crystallization pressure due to the crystal growth may be expressed as [16]:

$$\Delta P = \frac{\nu RT}{V_m} \left(\ln \frac{C}{C_0} + \ln \frac{\gamma_{\pm}}{\gamma_{\pm,0}} + \frac{\nu_0}{\nu} \ln \frac{a_w}{a_{w0}} \right) \quad (2)$$

where ν is the total number of ions per dissolved molecule (2 for NaCl) and V_m the molar volume of the crystalline phase. The first term in the parenthesis describes the supersaturation in terms of concentration, the second and third terms describe the no ideal behaviour of the concentrated salt solutions.

But this mechanism cannot explain all the degradations observed. It does not consider the influence of surface properties of the materials itself on the salt nucleation and crystallization even if it is well known that the intensity of damage depends on the quantity of salt as well as the characteristics of the porous network and the pore geometry. Indeed, a stone is a porous material composed of a network of angular pores of different sizes and shapes. Taber [18], Everett and [9] Scherer [12] claim that damaging stresses are expected only if the crystallization takes place in small pores because the salt solution constrained in fine pores could maintain a higher supersaturation [19-21]. It is also well established that the surface chemistry, the morphology and the shape of the surface play a crucial role in the nucleation [22-26].

New studies have shown that the kinetics of salts crystallization play an important role in the degradation [27,28]. It is clear that when the salts crystallize within the stone (a phenomenon called subflorescence) the decay is strong, harmful for the stone and a loss of material can be observed (i.e flaking and scaling).

Consequently a detailed understanding of how crystals nucleate and grow within porous media and lead to damage is needed.

In this study we have investigated at the microscale the role played by the nature, shape and size of the porous media on the kinetics of nucleation and growth of sodium chloride. Then, at the macroscale the damage process on Prague sandstone when the NaCl-solution is entrapped inside the stone and the salt crystallizes as subflorescence is studied.

2 Experimental section

At a microscale, using a phase contrast microscopy and direct imaging we have investigated the drying of a NaCl-solution in glass capillaries which are considered as simple model for a single pore in a porous medium. Different sizes of microcapillaries have been used (50 to 2000 μm) and chemically different surfaces: hydrophobic (silanised: treated with OCTEO (Octyltriethoxysilane)) and hydrophilic (cleaned) [29]. The geometry of the microcapillaries is also changed; besides cylindrical we also use rectangular shapes since in real porous media liquid can be trapped within corners of the porous network [24, 30-32]. We study situations with slow evaporation (and consequently no large salt concentration gradients) by choosing the initial concentration in such a way that the surface tension and the contact angle of the salt solution were high enough to avoid the formation of wetting films. This corresponds to the most harmful situation where the solution cannot reach the surface of a porous medium like stone (because of the presence of a treatment product: water repellent, consolidant, anti-graffiti, wax, etc) [33] or very high concentration of salt solution or finally because of extreme conditions of drying [24] and the salts will crystallize as subflorescence.

Because the NaCl-solution evaporates and concentrates during the experiment, we measured the variations of the surface tension and the contact angles of the NaCl-solution on glass with regards to the salt concentration with an Easy-Drop device. The initial salt solutions (molar concentrations from 0,616 to 6,160 M) were prepared by dissolving NaCl (Sigma-Aldrich purity 99.9%) in Millipore water.

All experiments have been done in well controlled relative humidity (RH in a range from 2% to 68% \pm 0.5%) and temperature ($T = 22 \pm 2^\circ\text{C}$)

A known volume (V_0) of the solution is introduced into the capillary and placed into a miniature climatic chamber with dimensions 1.5x2x6 cm³ [27] under a microscope. By fixing the relative humidity of the ambient air in the climatic chamber [27], the evaporation rate of the solution is controlled. The volume change during the evaporation of the solutions inside the microcapillaries is subsequently followed by recording the displacement of the two menisci while simultaneously visualizing the onset of crystal growth in the solution directly with the optical microscope (Leica IDRM) coupled to a CCD camera.

At macroscale we investigated the crystallization of sodium chloride as subflorescence inside Prague Sandstone (porosity $\Phi \approx 29\%$, pore diameter $d_p \approx 25 \mu\text{m}$ [34]) using scanning electron microscope (SEM, HITACHI TM 3000). To avoid the formation of efflorescence, the upper face of the sandstone samples (5x5x10mm) were treated with a consolidant (@)funcosil) and the 4 lateral faces were covered with parafilm. Then, the samples were impregnated with NaCl-solution by capillarity with an initial concentration of 4.9 M and left to dry in a homemade climatic chamber in which both temperature and humidity are imposed at $T \approx 22 \pm 2^\circ\text{C}$ and $\text{RH} \sim 50 \pm 2\%$.

3 Results and Discussion

3.1 Microscale experiments

The liquid/vapor surface tension (γ_{lv}) of the NaCl solution and its contact angle on glass slide (θ) increase linearly with the NaCl concentration (Figure 1). Using this relation, we define a critical salt concentration ($S = 4.47 \text{ M}$, i.e $S = C/C_{\text{sat}} = 0.72$) above which the formation of wetting films in the edges of the square geometry is avoided [30] (the critical angle defined as $\theta_c = \pi/N$ with N the number of sides, $\theta_c = 45^\circ$). The solution will be trapped inside the capillary without any connection with the entrance, and the crystallization will happen within it.

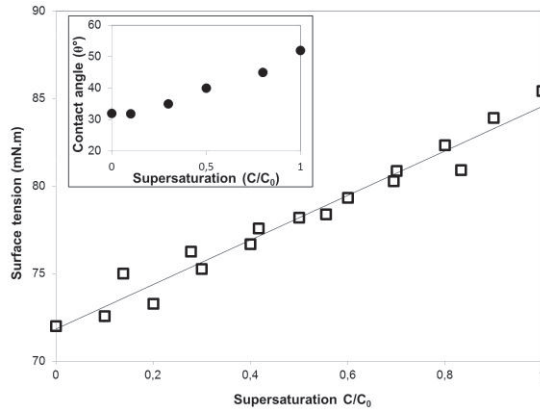


Figure 1: Linear increase of the surface tension of a NaCl-solution with regards to the supersaturation (C/C_{sat} with C concentration of the solution and C_{sat} concentration at saturation). In the frame, the contact angle θ of the NaCl-solution as a function of the supersaturation of the solution is plotted. ($T \approx 22.0 \pm 0.5^\circ\text{C}$ and $\text{RH} \sim 50 \pm 2\%$)

With regards to these results, we investigated the drying kinetics of $0.1 \mu\text{l}$ of NaCl-solution with an initial concentration of 4.9M (above the critical salt concentration) in the different capillaries.

As we expected no wetting films are observed in these experiments. The concentration for which nucleation is observed is constant and independent of the size, the shape of the microcapillary and the evaporation rate of the solution, the latter being controlled by the relative humidity (Figure 2). From more than 100 experiments, a supersaturation S of 1.6 ± 0.2 is calculated at the onset of crystallization ($S=C/C_{\text{sat}}$, with C the solution concentration at the moment when the crystallization occurs) (Figure 2).

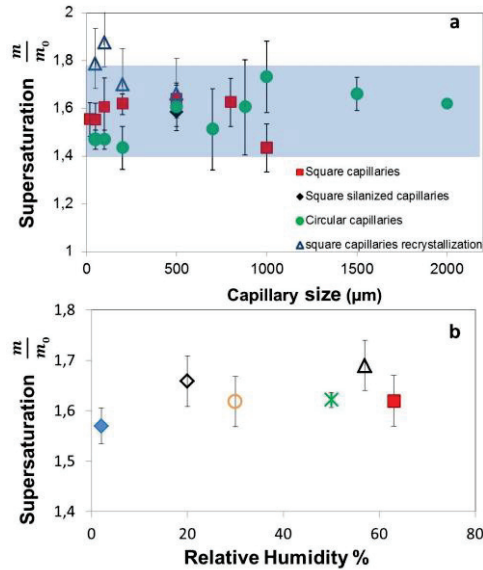


Figure 2: Supersaturation ($S = m/m_0$) of NaCl solutions reached by evaporation under isothermal conditions ($22.0 \pm 0.5^\circ\text{C}$) in various confined geometries and situations. (a) Data for microcapillaries of different sizes (from 20 to 2000 μm , i.e. below and above the capillary length), with two geometries (square and circular) and with different wetting properties (hydrophilic and hydrophobic). Recrystallization was studied after complete deliquescence of salt crystals. All measurements were done at a relative humidity (RH) of $52 \pm 2\%$. (b) Data for 200 μm square capillaries at different evaporation rates (RH ranging from 2 to 68%) at the onset of spontaneous crystallization.

To assess the effect of impurities on the concentration for which nucleation is first observed, recrystallization experiments were conducted by performing repeated cycles of complete deliquescence (dissolution by water vapour) of the salt crystals followed by drying, a procedure that is known to efficiently expel impurities [25,27]. Our results show again that the value of 1.6 of supersaturation at the onset of crystallization is not affected within the experimental uncertainty (Figure 2a). One consequence of the evaporation is that, when the ion transport in the liquid phase is slower than the evaporation rate, there may be concentration gradients in the salt solution. This leads to a higher concentration of ions close to the meniscus, where the evaporation takes place. To see whether our limit of metastability is well defined in terms of NaCl concentration we calculated the Peclet number (Pe), which is a measure of the heterogeneity of the ion distribution. Pe is defined as the ratio between the convective and the diffusive transport of ions in the solution and can be calculated from various parameters such as the time-dependent NaCl

diffusion coefficient and the characteristic time of the displacement of the meniscus: $Pe \approx t_{diff}/t_s$ [30]. These can be calculated from $t_{diff} \approx z_0^2/D_{NaCl}(t)$ and $t_s \approx z_0/(dz/dt)$, with z_0 the initial meniscus position, z the position at the time t , and $D_{NaCl}(t)$ the diffusion coefficient at time t , which depends on the concentration and viscosity of the solution [30].

We find that at the start of the evaporation, Pe is of order unity at low relative humidity and in small microcapillaries, reflecting a rather heterogeneous distribution of ions in the solution (figure 3). However, the increase of the solute concentration in time leads to both a lower evaporation rate and a higher viscosity [35], reflected in a decrease of Pe . At the onset of crystallization, Pe reaches values on the order of 10^{-2} to 10^{-3} revealing that the ions are very homogeneously distributed in the solution and the limit of metastability is well defined.

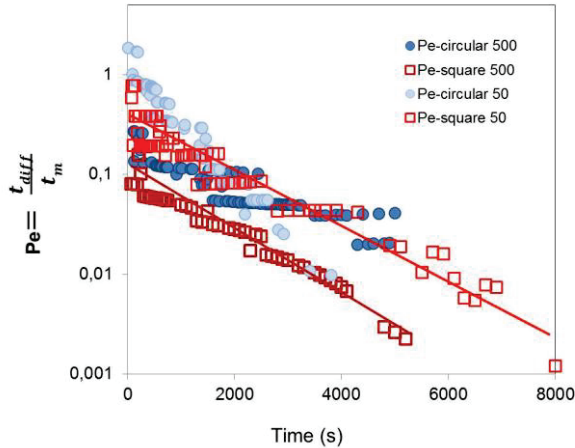


Figure 3: Peclet number Pe calculated at the meniscus as a function of evaporation time in square and circular capillaries with a size of 50 and 500 μm at $RH = 52 \pm 2\%$ and $T = 22.0 \pm 0.5^\circ\text{C}$. The straight lines are guides to the eye.

From classical nucleation theories, one would also expect the probability of nucleation increase with time for which the solution has been supersaturated [36]. However the results as a function of the relative humidity show that the nucleation is only observed when a concentration of 1.6 ± 0.2 is achieved, independently of the time necessary to reach it. In our experiment, the necessary time to reach the limit of metastability strongly depends on the relative humidity and varies over more than an order of magnitude (figure 4).

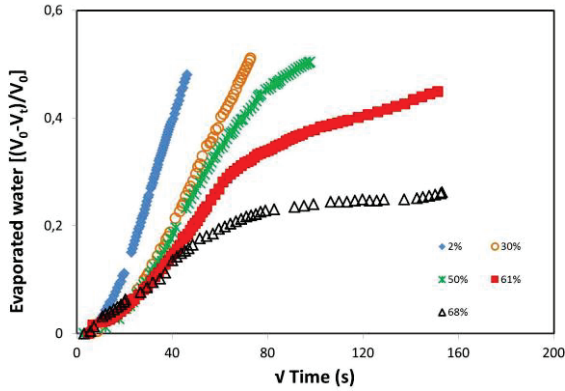


Figure 4: Normalized evaporated water volume from a 4.9M NaCl solution in 200 μm square capillaries as a function of time at different relative humidities (ranging from 2 to 68%) until spontaneous growth is observed. At an RH of 68% no crystals were formed. All measurements were done at $T = 22.0 \pm 0.5^\circ\text{C}$

As can be observed in figure 4, the evaporation rate decreases in time but does not follow a \sqrt{t} scaling as it would be for a simple diffusive process [37]. In fact, when the evaporation rate e is limited by diffusive vapor

transport through the gas phase, it follows $e \approx \rho_g D \frac{(c_i - c_\infty)}{\delta}$ with ρ_g the vapor density, D the diffusion coefficient of water vapor through the gas, c_∞ the controlled water vapour concentration of the climatic chamber and c_i the water vapor concentration just above the menisci; δ is the characteristic distance over which diffusion takes place [30,36]. The drying rate is consequently controlled by δ and $c_i - c_\infty$; during the evaporation, $c_i - c_\infty$ decreases because the saturated vapor concentration decreases when the salt solution becomes more concentrated ($c_i / c_{\text{pure water}} = 1 - 0.24 S$) [38]; on the other hand δ is roughly the distance between the meniscus and the outlet of the capillary, which increases: both effects then lead to a decrease in evaporation rate, consequently a simple diffusive \sqrt{t} scaling is not expected [36].

As a consequence, for humidities higher than 61%, corresponding to the equilibrium water vapour concentration above a solution close to $S \sim 1.6$, the evaporation rate goes to zero as soon as $c_i = c_\infty$ (see e.g. the black symbols in Figure 4). Here, although the solution is supersaturated, no nucleation is observed because the value of 1.6 is not reached. In the experiments performed at humidities higher than 68 %, crystals no longer precipitate, since the evaporation stops until a perturbation is imposed to the system (i.e. rapid decrease of the temperature or relative humidity). This independently provides another value for the onset of nucleation: $S = 1.60 \pm 0.07$ (Figure 2b), in agreement with the findings above.

It is worthwhile noting here that the time delay between the actual nucleation and our first observation of the crystal is given by its growth rate, which is typically in the order of a few (~ 5) $\mu\text{m/s}$ for the cubic NaCl crystal [27]. This means that within a few seconds of its formation, the crystal is consequently observable. This results in an error on the supersaturation that is negligible, since the evaporation takes place over several hours. Moreover, any crystallization in the solution would change the equilibrium water vapor pressure above the solution and consequently the evaporation rate; we only notice such a change once the crystal is observed.

Since the nucleation appears to be homogeneous, Classical Nucleation Theory (CNT) can be used to predict the rate of crystal nucleation for sodium chloride as a function of the supersaturation. According to CNT, the rate of nucleation per unit volume can be calculated as the product of an exponential factor and a kinetic pre-factor [39,40]:

$$J = \kappa \exp\left(-\frac{\Delta G^*}{kT}\right) \quad (3)$$

In the exponential factor, ΔG^* is the free energy cost of creating a critical nucleus and kT the thermal energy. The total Gibbs free-energy cost to form a spherical crystallite has a bulk and a surface term and can be expressed as:

$$\Delta G = \frac{4}{3}\pi R^3 \rho_s \Delta\mu + 4\pi R^2 \gamma \quad (4)$$

With ρ_s is the number density of the solid, $\Delta\mu$ the difference in chemical potential of the solid and the liquid and γ is the interfacial tension of the NaCl crystal with the solution ($\gamma_{lc} \sim 0.08 \text{ N}\cdot\text{m}^{-1}$ [39,40]). Here, the difference in chemical potential of the solid and the liquid, can be written in terms of the mean ionic activity of the solute a_{\pm} [16,36], as:

$$\frac{\mu_l - \mu_c}{RT} = \nu \ln\left(\frac{a_{\pm}}{a_{0\pm}}\right) = \nu \ln\left(\frac{\gamma_{\pm} m}{\gamma_{\pm 0} m_0}\right) \quad (5)$$

where m and m_0 are the molalities at crystallization and equilibrium ($\text{mol}\cdot\text{kg}^{-1}$) and γ_{\pm} is the corresponding mean ionic activity coefficient and ν the sum of ions (2 for NaCl).

The energy of the critical nucleus ΔG^* is then:

$$\Delta G^* = \frac{4\pi}{3} \gamma R_c^{*2} \quad \text{with} \quad R_c^* = \frac{2\gamma}{\nu kT \ln\left(\frac{\gamma_{\pm} cm}{\gamma_{\pm 0} m_0}\right)} \quad (6)$$

The kinetic pre-factor κ , which relates to the efficiency with which collisions between supernatant ions and the crystal interface produce crystal growth and is determined from $\kappa = \rho j Z$, where ρ is the number density of molecules in the liquid phase, Z the Zeldovich factor : $Z \approx 1/(n^*)^{2/3}$ with n^* the excess number of molecules in the critical nucleus and j the rate at which molecules attach to the nucleus causing its growth. j is approximated as $j \sim \rho D R_c^*$ with D the diffusion constant of the molecules and R_c^* the radius of the critical nucleus [40].

The rate of nucleation J ($m^{-3}s^{-1}$) is plotted as a function of the supersaturation in Figure 5. It can be noticed that for supersaturation values lower than ~ 1.6 the nucleation rate is extremely small while very large in case of higher values. At $S \sim 1.6$ the rate of the nucleation of sodium chloride is found to be $0.004 m^{-3}s^{-1}$, which roughly corresponds to one nucleus in a typical volume considered here within our experimental time window (typically 5000 s). Moreover, the variation of the experimental parameters here (volume V , relative humidity etc.) does not significantly change the value of $S \sim 1.6$ for which the nucleation becomes observable. Simply said, the nucleation rate depends so steeply on the supersaturation that all other parameters are irrelevant, in excellent agreement with all our observations.

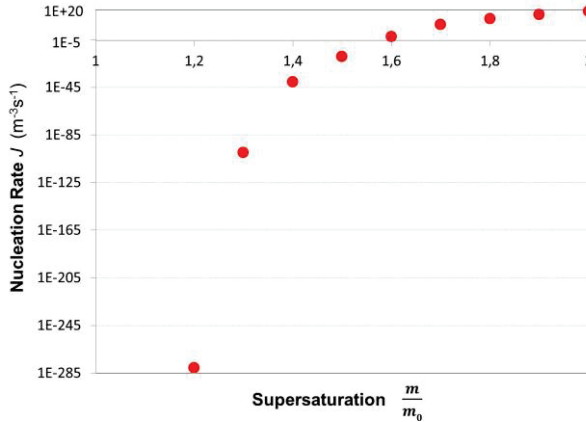


Figure 5: Nucleation rate J ($m^{-3}s^{-1}$) as a function of supersaturation $S = m/m_0$ of the solution calculated using equation (3)

Very recent simulations on NaCl solutions show surprisingly that already at a relatively low supersaturation, nucleation can be observed in smaller

system than ours on the time scale of a simulation [41,42] which is shorter than our experimental time. This discrepancy could be related to restrictions of the model used for the simulations or due to a difference in theoretical parameters (attempt frequency, dielectric constant, chemical potential difference and surface tension) compared to the experimental ones. For example, the solubility of NaCl is under estimated in the simulations compared to the real value; this seems an interesting item for further investigations.

Another very interesting observation is that at the onset of crystallization a single nucleus is observed to be growing very rapidly with a peculiar shape: a Hopper (skeletal) crystal (figure 6a,b). Such a hopper shaped crystal appears at high supersaturation because of the so-called “Berg-Effect” (on a flat surface, there is an excess of supersaturation near the edges) [43]. A new growth layer will be generated by the 2D nucleation near the edges and then the growth layer will spread inward from the edges forming the macrosteps [43,44].

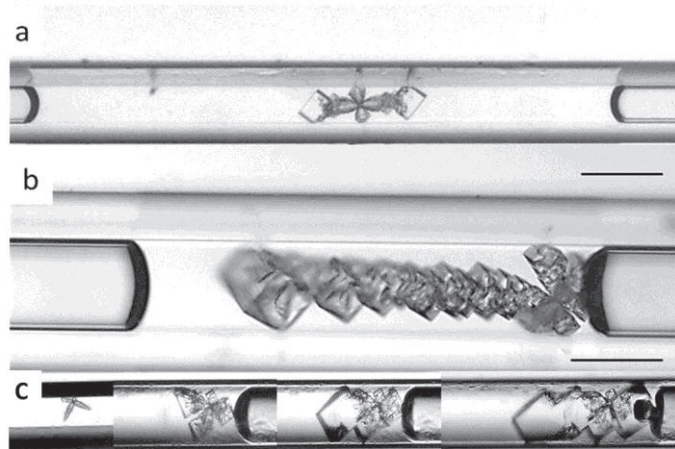


Figure 6: Spontaneous formation of Hopper crystals at $S = 1.6 \pm 0.2$ in (a) 50 μm capillary: and, (b) 100 μm capillary. (c) Evolution of the growth of a Hopper crystal in the first 10 minutes (Scale=100 μm)

However, since the nucleation rate depends very strongly on the concentration, such a rapid growth of the critical nucleus will lead to a very rapid decrease of the local supersaturation and consequently favors the formation of only a single skeletal crystal with a peculiar shape. It is noticed that the morphology of the Hopper crystals changes during the growth process, due to the gradual decrease of the ion concentration in the solution accompanying the formation of the crystals (figure 6c). At the late stages of growth regular cubic crystals start to form from the extremities of the Hopper crystal.

The Hopper crystals are growing in these experiments at a speed up to ten times that of the growth of a regular cubic crystal under the same conditions [27-45]; it is likely that such fast growth dynamics are accomplished with high supersaturations of the solution [45], hence provoking damage in porous materials. Indeed, the crystallization pressure that is responsible for the damage is known to depend strongly on the supersaturations reached [46,47].

3.2 Macroscale experiments

To see whether our conclusions from the capillaries also apply to real porous media, we compare the crystal morphologies at the late stages in microcapillaries with the NaCl crystals formed in experiments on porous sandstone. The surface of the latter was also treated as described in the experimental section to slow down the evaporation, prevent salt crystallization at the exterior of the stone and facilitate the formation of liquid pockets.

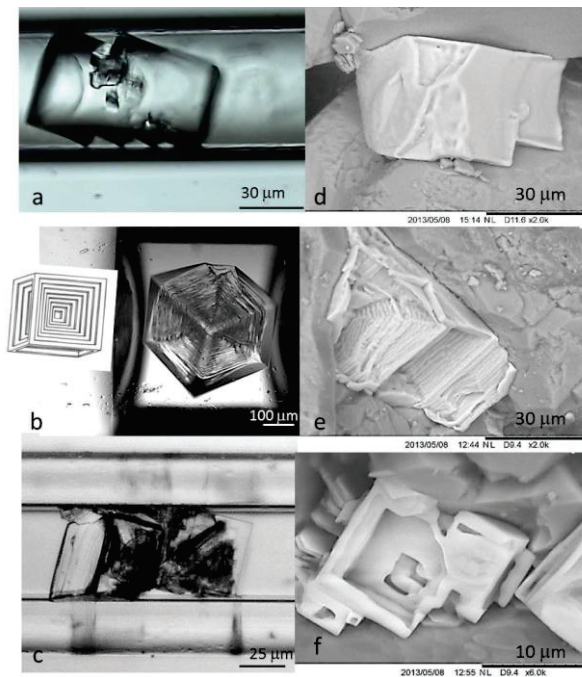


Figure 7: Comparison between NaCl crystals formed in capillaries after reaching our limit of supersolubility $S \sim 1.6$ (a-c) and those obtained in the sandstone (d-f). All the experiments are performed at ($T=22^{\circ}\text{C}$, $\text{RH} \sim 50\%$).

For that, the Mesne stone saturated with a NaCl solution ($C_0=4.9M$) is dried under the same conditions as the capillaries. Subsequently, the sample is fractured and the salt crystal morphology inside the stone is investigated by Scanning Electron Microscopy (SEM).

Figure 7 shows the remarkable similarities between the crystal structures formed in the stone and in the capillaries: in the stone also Hopper crystals have been formed. Observations on several samples show that these crystals are plentiful in some parts of the stone, while almost absent in others, suggesting that very concentrated residual fluid pockets had formed. Both these observations indicate that the liquid pockets in the stone behave similarly to the microcapillaries where high supersaturations were reached before crystallization starts.

This supersaturation seems to be sufficient to provoke damage. In fact, at $S = 1.6$ the crystallization pressure is about $\Delta P \sim 160$ MPa [16]. If we assume that only 15% of local volume fraction is filled with the salt, the related effective stress [48] in the sandstone will be $\sigma \sim 1,65$ MPa which is higher than the tensile strength of the Mesne sandstone (0.9 MPa). This is in a good agreement with the recent study on the damaging capacity of sodium chloride in stones, in which the formation of a crack in the drying front due to the development of enough effective stress was clearly shown [49].

4 Conclusion

In summary, we have demonstrated by controlled evaporation experiments of sodium chloride solutions, that the supersaturation achieved at the onset of spontaneous primary nucleation and growth is around 1.6 and remains independent of the size, shape and surface properties of the microcapillary. These results are consistent with expectations from classical nucleation theory. The metastability limit obtained here clearly shows that, contrary to what is commonly assumed for this salt [19,50], high concentrations can be reached before spontaneous crystal growth. This in turn leads to the formation of a Hopper crystal, which we also detected in analogous experiments conducted on real sandstone. Our findings therefore have far-reaching implications for the widespread consequences of salt crystallization [1-14] since the salt weathering of rocks, stones and monuments is related to the crystallization pressure which is directly dictated by the supersaturation.

References

- [1] Pfann W.G. US Patent 3423189, (1969)
- [2] Dutton R.L., Sharer J.M. Advanced technologies in biopharmaceuticals processing, (Blackwell publishing) (2007).
- [3] Hunte C., von Jagow G., Schagger H., Membrane protein purification and crystallization; a practical guide (Academic press) (2003).
- [4] Rengasamy P., Olsson K. A., Sodcity and soil structure. Aust. J. Soil. Res. (29) (1991), 935 - 952.
- [5] Oelkers E.H., Gislason S.R., Matter J., Mineral carbonation of CO₂, Elements (4) (2008), 333-337.
- [6] Muller N., Qi R., Mackie E., Pruess, K., Blunt, M. J., CO₂ injection impairment due to halite precipitation. Energy Proc. (1) (2009), 3507-3514.
- [7] Peysson Y., Permeability alteration induced by drying of brines in porous media. Eur. Phys. J. Appl. Phys. (60) (2012), 24206.
- [8] Fitzner B., Sneathlage R., Einfluß der Porenradienverteilung auf das Verwitterungsverhalten asugewälter Sandsteine. Bautenschutz und Bausanierung. (3) (1982), 97–103
- [9] Everett D.H., The thermodynamics of frost damage to porous solids, Trans. Faraday. Soc. (57) (1961), 1541-1551.
- [10] Goudies A. S., Viles H. A., Salt Weathering Hazard (Wiley, London, (1997).
- [11] Novak G.A., Colville A.A., Efflorescence mineral assemblages associated with crack and degraded residential concrete foundation in south California. Cem. Concr. Res. (1) (1989), 1-6.
- [12] Scherer G.W., Stress from crystallization of salt, Cem. Concr. Res. (34) (2004), 1613-1624.
- [13] Lubelli B., van Hees R. P. J., Huinink H. P., Groot C. J. W. P., Irreversible dilation of NaCl contaminated lime-cement mortar due to crystallization cycles, Cement and concrete research. (36) (2006), 678-687.
- [14] Shahidzadeh-Bonn N., Desarnaud J., Bertrand F., Chateau X., Bonn D., Phys. Rev. E, (81) (2010), 066110.

- [15] Viles H. A., Implication of future climate change for stone deterioration, *Geo. Soc. Spec. Publ.* (205) (1997), 407-418.
- [16] Steiger M., Crystal growth in porous materials-1: The crystallization pressure of large crystals. *J. Cryst. Growth.* (282) (2005), 455.
- [17] Flatt R. J., Salt damage in porous materials: how high supersaturations are generated? *J. Cryst. Growth.* (242) (2002), 435-454.
- [18] Taber S., The growth of crystals under external pressure, *American Journal of Science* (41A) (1916), 532-557.
- [19] Emmanuel S., Berkowitz B., Effect of pores size controlled solubility on reactive transport in heterogeneous rock, *Geophys. Res. Lett.* (34) (2010), L06404.
- [20] Putnis A., Mauthe G., The effect of pore size on cementation in porous rocks, *Geofluids* (1) (2001), 37-41.
- [21] Putnis A., Prieto M., Fernandez-Diaz L., Fluid supersaturation and crystallization in porous media, *Geol. Mag.* (132) (1995), 1-13.
- [22] Aizenberg J., Black A.J., Whitesides G. M., Control of crystal nucleation by patterned self-assembled monolayers, *Nature* (398) (1999), 495-498.
- [23] Diao Y., Harada T., Myerson A.S., Hatton T.A., Trout B.L.. The role of nanopore shape in surface induced crystallization. *Nature Materials* (10) (2011), 867-871.
- [24] Shahidzadeh-Bonn N., Rafai S., Bonn D., Wegdam G., Salt crystallization during evaporation: Impact of interfacial properties, *Langmuir* (24) (2008), 8599-8605.
- [25] Desarnaud J., Shahidzadeh-Bonn N., Salt crystal purification by deliquescence/crystallization cycling, *Euro. Phys. Lett.* (95) (2011), 48002.
- [26] Page A.J., Sear R.P., Crystallization controlled by geometry of surface, *J. Am. Chem. Soc.* (131) (2009), 17550-17551.
- [27] Shahidzadeh N., Desarnaud J., Damage in porous media: role of the kinetics of salt (re)crystallization, *Eur. Phys. J. Appl. Phys.* (60) (2012), 24205.

- [28] Desarnaud J., Bertrand F., Shahidzadeh N., Impact of the kinetics of salt crystallization on stone damage during Rewetting/Drying and Humidity cycling, *J. Appl. Mech.* (80) (2013), 020039.
- [29] Shahidzadeh-Bonn N., Azouni A., Coussot P., Effect of wetting properties on the kinetics of drying of porous media, *J. Phys. Condens. Matter.* (19) (2007), 112101.
- [30] Camassel B., Sghaier N., Prat M., Nasrallah S.B., Evaporation in a capillary tube of square cross-section: application to ion transport, *Chem. Eng. Sci.* (60) (2005), 815-826.
- [31] Chauvet F., Duru P., Geoffroy S., Prat M., The three periods of drying of a single square capillary tube, *Phys. Rev. Lett.* (18) (2009), 124502.
- [32] Wong H., Morris S., Radke C. J., Three dimensional menisci in polygonal capillaries, *J. Colloid. Interf. Sci.* (48) (1991), 317.
- [33] Lubelli B., van Hees R.P.J., Groot C., Gunneweg J., Risks of the use of water repellent and consolidating treatments on salt contaminated masonry: the case of a wind mill in the Netherlands, *Restoration of building and monument* (13), 319-330.
- [34] Pavlík Z., Michálek P., Pavlíková M., Kopecká I., Maxová I., Černý R., Water and salt transport and storage properties of Mšené sandstone, *Construction and Building Materials* (22) (2008), 1736-1748.
- [35] Kestin J., Khalifa E., Correia R. J., Tables of the dynamics and kinematic viscosity of aqueous NaCl solutions in the temperature range 20-150°C and the pressure range 0.1-35 MPa. *J. Phys. Chem. Ref. Data.* (10) (1981), 71-87.
- [36] Mullin J. W., *Crystallization*, (Butterworths-Heinemann, 4th edition), (2001).
- [37] Bird R. B., Stewart W. E., Lightfoot E. N., *Transport phenomena* (Wiley, New York), (1960)
- [38] Robinson R. A., The Vapour Pressures of Solutions of Potassium Chloride and Sodium Chloride, *Trans. Roy. Soc. New Zealand.* (122) (1945), 203-217.
- [39] Valeriani C., Sanz E., Frenkel D., Rate of Homogeneous Nucleation in Molten NaCl, *J.Chem.Phys.* (122) (2005), 194501 1-6.

- [40] Sear R., Nucleation: Theory and Applications to Protein Solutions and Colloidal Suspensions, *J. Phys. Condens. Matter.* (19) (2007), 033101 1-28.
- [41] Mucha M., Jungwirth P., Salt Crystallization from an Evaporating Aqueous Solution by Molecular Dynamics Simulations, *J. Phys. Chem. B* (107) (2003), 8271-8274.
- [42] Chakraborty D., Patey G.N., How Crystals Nucleate and Grow in Aqueous NaCl Solution. *J. Phys. Chem.Lett.* (4) (2013), 573-578.
- [43] Sunagawa I., Growth and morphology of crystals. *Forma* (14) (1999), 147-166.
- [44] Kuroda T., Irisawa T., Ookawa A. Growth of a polyhedral crystal from solution and its morphological stability, *J. Cryst. Growth* (42) (1972), 41-46.
- [45] Al-Jibbouri S., Ulrich J., The growth and dissolution of sodium chloride in a fluidized bed crystallizer, *J. Cryst. Growth* (2002) (234), 237.
- [46] Correns C. W., Growth and dissolution of crystals under linear pressure, *Discussions of the Faraday Soc.* (5) (1949), 267–271.
- [47] Steiger M., Crystal Growth in Porous Materials II: Influence of Crystal Size on the Crystallization Pressure, *J. Cryst. Growth* (282) (2005), 470-481.
- [48] Espinosa-Marzal R., Hamilton A., McNall M., Whitaker K., Scherer G.W., The Chemomechanics of Crystallization During Rewetting of Limestone Impregnated with Sodium Sulfate, *J. Mater. Res.* (26) (2011), 1472-1481.
- [49] Derluyn H., Mooneen P., Carmeliet J., Deformation and Damage due to Drying Induced Salt Crystallization in Porous Limestone. *J. Mech. Phys. Solids* (63) (2014), 242-255.
- [50] Bouzid M., Mercury L., Lassin A., Matray J. M., Salt Precipitation and Trapped Liquid Cavitation in Micrometric Capillary Tubes. *J. Colloid and Interf. Sci.* (360) (2011), 768-776.

Influence of the salt concentration on the damage potential of mirabilite and thenardite

A. Stahlbuhk*, J. Nissen, K. Linnow and M. Steiger

Department of Chemistry, University of Hamburg,
Inorganic and Applied Chemistry, Hamburg Germany

* Amelie.stahlbuhk@studium.uni-hamburg.de

Abstract

The present study reports on the damage potential of the crystallization of either thenardite or mirabilite in porous sandstone. Specimens of Sand sandstone with different loads of sodium sulfate were exposed to wetting-drying cycles at different conditions to rank the damage potential of different crystallization pathways and to investigate the influence of the salt concentration on the damage process. The damage intensity was assessed by visual inspection and mass loss curves. In general, the well-known extreme damage potential of thenardite dissolution and subsequent mirabilite crystallization is confirmed. Under such conditions, the damage potential increases with increasing salt load which is confirmed by the calculation of the effective stresses and comparison with the tensile strength of Sand sandstone. Considering the pore filling ratio with respect to the crystallizing phase, it turns out that thenardite crystallization during evaporation can cause as much damage as the crystallization of mirabilite during wetting of thenardite. Finally, it is demonstrated that wetting by slow deliquescence of thenardite can also be very destructive, though it is yet unclear which phases actually crystallize out under such conditions.

Keywords: damage potential, thenardite, mirabilite, salt concentration, pore filling ratio

1 Introduction

Precipitation of salts in contact with their supersaturated solution is the key mechanism for damage to porous materials. Sodium sulfate has been repeatedly reported as one of the most aggressive salts. Although sodium sulfate is commonly used in laboratory weathering tests, little is known about the influence of different crystallization pathways and the influence of the salt concentration on the damage potential. In general the interaction between a salt, the material and the climatic conditions related to the manifestation of damage is complicated. The interactions of the different influences are given schematically in Figure 1. The damage is influenced by the crystallization pressure and the mechanical properties of the stone, i.e. the tensile strength. The theoretical crystallization pressure can be calculated if the supersaturation of the crystallizing phase is known [1]. To relate the crystallization pressure to the macroscopic stress, the pore filling ratio must be taken into account because the theoretical pressure is not effectively transmitted through a porous material when the pores are not sufficiently filled with crystals [2,3]. The supersaturation during growth depends on the crystallization pathway and might change according to the climatic conditions, e.g. evaporation or cooling rates, and the presence of nucleation sites within the material.

Typically, in laboratory tests a porous material is repeatedly impregnated with a sodium sulfate solution at room temperature (r.t.) and dried at a higher temperature. For a long time damage was attributed to the volume increase associated with the hydration reaction. Today, it is well known that the damage is due to the growth of mirabilite ($\text{Na}_2\text{SO}_4 \cdot 10\text{H}_2\text{O}$) crystals from the supersaturated solution formed by the dissolution of thenardite (Na_2SO_4). Such a dissolution-crystallization mechanism not only occurs during wetting by impregnation but also during wetting at relative humidities above the deliquescence humidity of thenardite. Direct hydration without formation of a solution is also possible [4]. However, up to now the damage potential of this reaction is not well investigated,

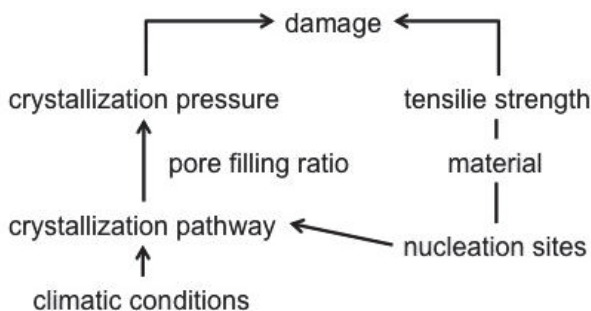


Figure 1: Overview of the aspects influencing the magnitude of damage.

whereas several investigations showed that dissolution of thenardite and recrystallization of mirabilite is extremely destructive [e.g. 5,6].

In a recent study [7] it was shown that the crystallization of sodium sulfate phases from a saturated solution can in fact lead to severe degradation patterns, even in the absence of temperature or wet/dry cycles. In contrast, another study shows that thenardite crystallization during evaporation produces less damage than the thenardite dissolution - mirabilite crystallization mechanism occurring during wetting [8]. However, comparing the two salts it is often ignored that, for a given sodium sulfate content in a porous material, the pore filling ratio of thenardite is much lower than that of mirabilite. For example, repeated impregnations with a solution saturated with respect to mirabilite at room temperature are often used to enhance the damage. The pore filling ratio increases with the cycle number. Assuming complete saturation of the pore space, repeated impregnations at 20 °C with a saturated solution ($1.35 \text{ mol}\cdot\text{kg}^{-1}$) lead to pore filling ratios of 29 %, 49 %, 64 %, 74 % and 82 % with respect to mirabilite in the first, second, third, fourth and fifth cycle, respectively.

The same concentration is often used to investigate the damage potential of thenardite alone. In the first cycle the pore filling ratio of 29 % is then reduced to 7 %, i.e. by a factor of 4.1, with respect to thenardite. In the following cycles during the impregnation above 32.4 °C thenardite dissolves in the brine due to the undersaturation with respect to thenardite (saturation concentration of $3.51 \text{ mol}\cdot\text{kg}^{-1}$ at 32.4 °C) of the used brine. It follows that the increase of the pore filling ratio is less steep than for mirabilite at 20 °C. Therefore the damage produced by mirabilite crystallization has to be more pronounced in these investigations simply because there is a much higher pore filling.

For this reason, the present study has two objectives, a ranking of different crystallization pathways involving both thenardite and mirabilite, and, the investigation of the influence of the salt concentration on the damage potential. For this purpose, Sand sandstone samples with different sodium sulfate concentrations were exposed to four different wetting-drying cycles. The first set of samples was both wetted with liquid water and dried at 40 °C to avoid the formation of mirabilite during wetting as well as during drying. The second set of samples was wetted with liquid water at temperature of the lab (22–26 °C) to induce the crystallization of mirabilite during wetting. The third set was exposed at 90 % RH at temperature of the lab, above the deliquescence humidity of thenardite to induce mirabilite crystallization from its supersaturated solution. Finally, the fourth set was exposed at 84 % RH at temperature of the lab below the deliquescence humidity of thenardite but above the equilibrium humidity of the thenardite-mirabilite transition. In this case, the hydration should occur as a true solid state reaction without dissolution.

2 Materials and methods

2.1 Sample preparation

Sand sandstone (Middle Keuper) was cut into blocks with the dimension of 30 x 30 x 15 mm³. The major constituents of this sandstone are quartz, rock fragments, plagioclase and alkali feldspars. The porosity is 20 %v/v and the bulk density is 2.13 g·cm⁻³ [9]. Exchangeable cations in Sand sandstone [10] were replaced with sodium immersing the specimens in a sodium sulfate solution (1.35 mol·kg⁻¹). This solution was replaced three times. To remove excess sodium sulfate, the samples were subsequently washed three times by immersion in doubly distilled water. Different salt loads were achieved by impregnation with salt solutions of different concentrations. For low salt content, solutions of 0.32, 0.68 and 1.35 mol·kg⁻¹ were used, whilst higher loads were obtained by one or up to three impregnations with a 3.2 mol·kg⁻¹ solution. These impregnations were carried out at 40 °C to avoid the formation of mirabilite during the impregnation. All specimens were dried at 130 °C after each impregnation.

2.2 Climatic conditions of the cycling

The cycles were carried out at four different conditions. Each cycle started with the wetting of the specimen and ended with complete drying. Depending on the temperature and the method used for wetting, different mechanisms of damage should affect the stones. Regarding the thermodynamic stabilities in the Na₂SO₄—H₂O system, mirabilite cannot be formed above 32.4 °C. Thus, in order to study the influence of thenardite crystallization, repeated cycles of wetting and drying, both at 40 °C, were carried out (A_{then}). At room temperature, thenardite forms a saturated solution and subsequently mirabilite precipitates from its supersaturated solution (method B_{mir}). Wetting with water vapor may induce two different hydration mechanisms [4]. Above the deliquescence humidity of thenardite a dissolution re-crystallization mechanism takes place in addition to the solid gas reaction (method C_{mir}), where the specimens were stored during the wetting process in a desiccator above a saturated MgSO₄ solution (90% RH). Below the deliquescence humidity of thenardite (86–87 % RH at 20–25 °C) the hydration takes place as a true solid state reaction, which was found to be incomplete for the pure salt [4]. In order to study this process the specimens were stored in a desiccator above a saturated KCl solution at about 84% RH (method D_{mir}). The reaction equations of the different methods are summarized in Figure 2.

The amount of liquid water for the wetting in methods A_{then} and B_{mir} was adapted to the salt load of each specimen to allow the full hydration of thenardite to mirabilite. The calculated volume varies from 10 µL to 589 µL. It turns out that the penetration of the pipetted water takes some time during which evaporation takes place. To compensate for this evaporative loss, an additional 100 µL was added to the samples.

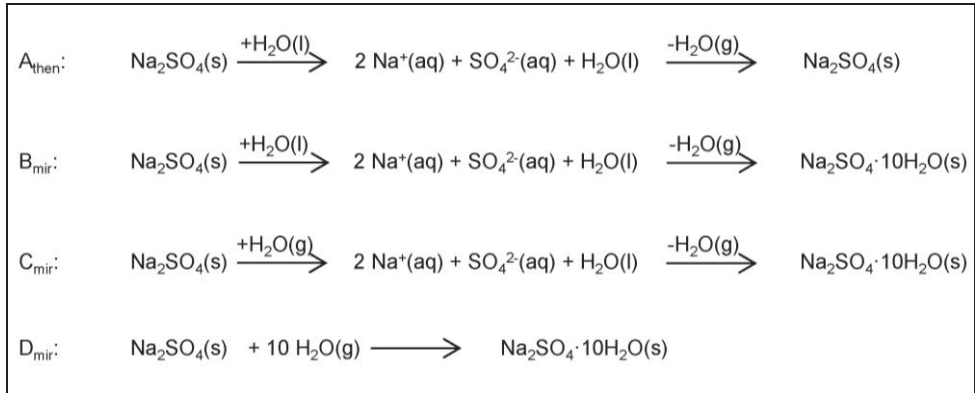


Figure 2: Overview of the cycling methods and the relevant reaction mechanism.

After wetting, samples of method A_{then} were dried in a desiccator above silica at 40 °C till constant weight, while those of methods B_{mir} , C_{mir} and D_{mir} in a desiccator above silica at temperature of the lab. In addition a flow of dry air was used to reduce the drying times (methods B_{mir} , C_{mir} , and D_{mir}). The mass of the dried specimens was measured after each cycle. The damage in the specimens having different salt loads is assessed by the mass decrease with ongoing cycling and visual observations. One sample was tested for each method and salt load. The total cycle number is up to 17.

3 Results and discussion

3.1 Load and visual appearance after impregnation

Obvious damage of the specimens and efflorescences were not visible after the initial impregnation and drying procedure. The average salt loads of equally impregnated stones and the pore filling of each individual specimen are given in Table 1. These pore fillings are only average values that do not reflect the fact that gradients of salt concentration, hence, the pore filling evolve during drying.

3.2 Damage

Visual rating (Table 2)

In general the damage appeared in different forms, which can be described as sanding, crumbling, formation of big cracks and total breakdown of the specimens. The localization of salt deposit played a major role on the visible damage. Specimens of method A_{then} did not show

any efflorescences (see for example Figure 3a) and mostly do not show visually detectable damage such as rounding of the corners and edges by sanding, or crumbling. Damage was only observed for the specimen A8, where a big crack was observed after cycle 4. With ongoing cycling the crack enlarged accompanied by sanding and ended in the total breakdown of the sample after cycle 6, obviously caused by subflorescences.

Table 1: Average salt load of the specimens, given in mg Na₂SO₄ per g stone, with the standard deviation of the mean value, and average pore filling ratio Φ with respect to the crystal volume of the damaging phase.

Specimen	salt load (mg·g ⁻¹)	A _{then} Φ_{then} (%)	B _{mir} Φ_{mir} (%)	C _{mir} Φ_{mir} (%)	D _{mir} Φ_{mir} (%)
1	0.55 ± 0.05	0.20	1.00	— ⁽¹⁾	— ⁽¹⁾
2	2.2 ± 0.2	0.86	4.03	3.47	3.62
3	4.3 ± 0.8	1.74	7.25	8.50	6.04
4	10.5 ± 1.3	4.10	16.9	19.6	16.01
5	13.9 ± 0.5	5.65	22.6	23.7	22.23
6	24.5 ± 2.5	9.24	39.3	— ⁽¹⁾	— ⁽¹⁾
7	31.1 ± 1.8	12.2	54.8	50.4	50.9
8	44.8	17.8	— ⁽¹⁾	— ⁽¹⁾	— ⁽¹⁾

(1): not tested

Table 2: Cycle number at which visible damage is observed.

Specimen	A _{then}	B _{mir}	C _{mir}	D _{mir}
1	> 6 ⁽¹⁾	> 6 ⁽¹⁾	— ⁽²⁾	— ⁽²⁾
2	> 5 ⁽¹⁾	> 5 ⁽¹⁾	> 5 ⁽¹⁾	> 5 ⁽¹⁾
3	> 17 ⁽¹⁾	> 7 ⁽¹⁾	> 9 ⁽¹⁾	> 9 ⁽¹⁾
4	> 17 ⁽¹⁾	9 (sanding)	> 9 ⁽¹⁾	> 9 ⁽¹⁾
5	> 17 ⁽¹⁾	4 (sanding)	> 9 ⁽¹⁾	> 9 ⁽¹⁾
6	> 6 ⁽¹⁾	3 (small cracks)	— ⁽²⁾	— ⁽²⁾
7	> 3 ⁽¹⁾	1 (small cracks) 3 (breakdown)	> 5 ⁽¹⁾	2 (big crack) 4 (breakdown)
8	4 (big crack) 6 (breakdown)	— ⁽²⁾	— ⁽²⁾	— ⁽²⁾

(1): > n: no damage observed after n cycles

(2): not tested

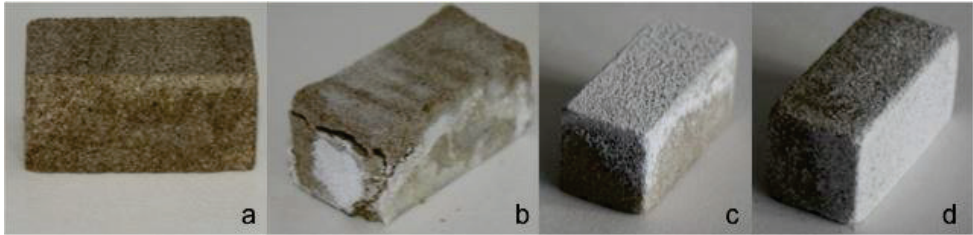


Figure 3: Damage of different specimens; a) A6 after the fourth cycle, b) B6 after the fourth cycle, c) C5 after the eighth cycle and d) D4 after the eighth cycle.

All specimens of method B_{mir} showed some efflorescences and damage in the form of sanding and loss of debris. Rounded edges and corners and loss of small particles were clearly visible on specimens B4–B7, whilst B1–B3 showed no damage. In addition, small cracks formed in samples B6 and B7 after the third and the first cycle, respectively. With ongoing cycling the cracks enlarged. As an example, specimen B6 is shown in Figure 3b after the fourth cycle, illustrating the enhanced cracks. The total breakdown of B7 occurred in the third cycle during wetting. A huge amount of sodium sulfate was present as efflorescences on the specimens subjected to conditions of method C_{mir} (see example in Figure 3c) and those with a high salt load are nearly fully covered by fine salt grains. As no efflorescence was noticed after impregnation, its appearance evidenced the formation and transport of a salt solution as expected in a deliquescence-recrystallization mechanism. However, no damage was observed on the specimens subjected to conditions of method C_{mir}.

Surprisingly, the specimens of method D_{mir} also showed efflorescences after some cycles (see Figure 3d as an example), despite an expected solid state hydration mechanism as the RH is below the deliquescence humidity of thenardite. As mentioned before the formation of efflorescences gives evidence of the presence of a solution which may be formed due to the water vapor sorption behavior of the stone itself, the secondary porosity of the thenardite grains or the presence of Na₂SO₄(III) (phase III) which deliquesces at about 83 % RH (20–25 °C). Damage was only observed in the specimen with the highest salt load (D7). The formation of a big crack after cycle 2 ended in the total breakdown of the sample after cycle 4.

Mass loss

The specimens were dried until constant weight at the end of each cycle. The normalized weight w_n was calculated by Equation (1):

$$w_n = \frac{m_i}{m_0} \quad (1)$$

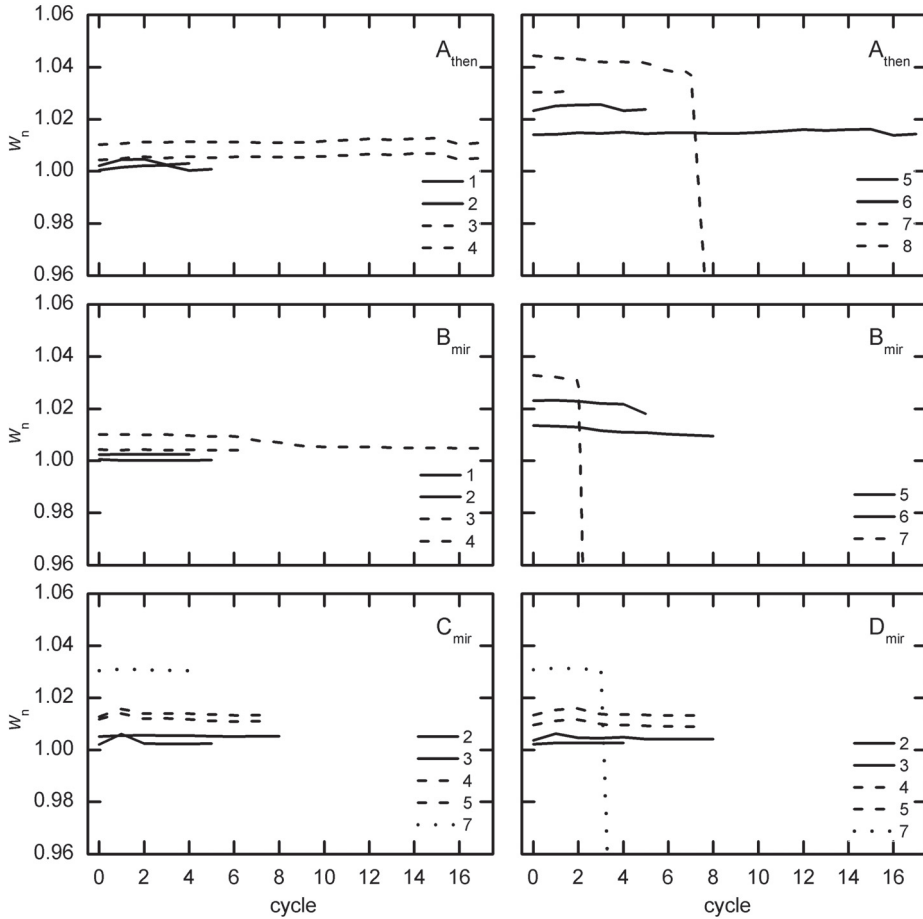


Figure 4: Normalized weight w_n with ongoing cycling.

where m_i is the dry weight after each cycle and m_0 the dry mass of the untreated sample. The evolution of the normalized weight is depicted in Figure 4. The number of cycles is not the same for all methods as some experiments were started later (A1,2,6,7; B1–3,5,6; C2,7; D2,7).

Moreover, the water uptake of the specimens subjected to conditions of methods C_{mir} and D_{mir} was very slow, thus, substantially increasing the total time required for a complete cycle. Figure 5 depicts the time consuming water sorption of sample D7 that finally lasted 20 days.

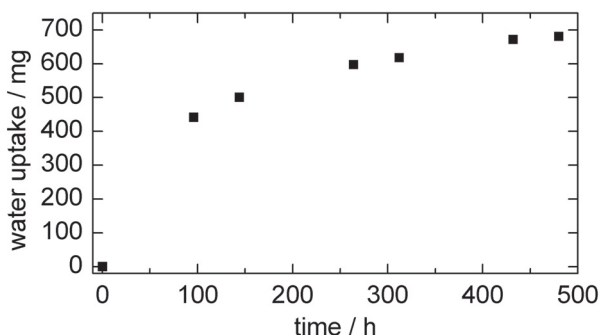


Figure 5: Water uptake versus time during the wetting of specimen D7 at 84 % RH.

Minor fluctuations of mass losses, noticed for nearly all samples, are explained by hygroscopic water uptake during weighing of samples previously dried at a very low humidity. However, the observed mass increase of the specimens A1, A6, C2, C4, C5 and D3–5 after the first cycle seems to be the result of pore clogging [11] and incomplete drying.

In general, a mass loss for successive cycling was not found, except for the specimens A8 and B4–B7. The slight mass loss in samples B4–B6 is in accordance with the observation that only slight sanding occurred on the surfaces of these specimens. Significant damage of the specimens of method A_{then} was only observed for the highest salt load (A8), it is important to note that the absence of damage for the next lower load (A7) might also be due to the low number of cycles. If and at which cycle damage occurs will be seen by further ongoing cycling. The mass loss of the specimens B_{mir} increases with increasing salt load. In contrast, a significant mass loss could not be detected for any of the specimens related to methods C_{mir} and D_{mir} , whatever the salt load, not even for sample D7 that broke down completely after the fourth cycle.

For the method D_{mir} it turns out that the expected condition of a solid state reaction was not fulfilled although the humidity was kept constantly below the deliquescence humidity of thenardite. The water uptake curve of specimen D7 is given as an example for all specimens of method D_{mir} in Figure 5. For sample D7 laden with 440 mg (3.09 mmol) of sodium sulfate, after drying a water uptake of 556 mg would be sufficient for the hydration of thenardite to mirabilite. The higher water uptake of about 695 mg provides evidence for the formation of a solution, explaining the aforementioned formation of efflorescences during cycling. However, this higher water uptake is not yet understood.

Both methods, C_{mir} and D_{mir} , involve a deliquescence–crystallization process. Considering the salt load, the observed damage confirms that method B_{mir} , the thenardite dissolution with liquid water and mirabilite crystallization, is the most harmful process. But regarding the pore filling ratio with respect to the crystalline phase the results could be interpreted differently. To discuss that more clearly the average mass losses,

calculated from the slope of the mass loss curves before the total breakdown, were plotted against the pore filling ratio for both crystalline phases in Figure 6. The average mass losses reflect sanding and crumbling of the specimens or in other words the superficial damage due to crystallization close to the surface.

Some scattering of the average mass loss is observed, which might be due to either the aforementioned error during weighing or due to pore clogging. However, significant values above 0.5 mg per g stone and cycle were only reached by the specimens A8, B4–B6. In case of the specimens A8, B6 and B7 the formation of cracks (Table 2) indicated that damage originated from the formation of subflorescences and their enlargement was accompanied by a mass loss. The specimens B4 and B5 were the only samples where the mass loss was produced solely by sanding of the surface, whilst the sticky behavior of the efflorescences noticed on the specimens related to methods C_{mir} and D_{mir} seems to prevent sanding.

Regarding the pore filling ratio it turns out that the damage caused by thenardite at 17.8 % pore filling (A8) is less than the damage observed for mirabilite crystallization at a pore filling of 51.6 % (B7) but more pronounced than at pore fillings of 23.1 % (B5) and 17.4 % (B4). In order to understand this result, a comparison of the effective stresses σ^* , calculated by Equation (2) [2], is useful.

$$\sigma^* = b \cdot \Phi \cdot \Delta p \quad (2)$$

where b is the Biot coefficient, Φ the degree of pore filling with salt crystals, and Δp the theoretical crystallization pressure. The crystallization pressure for method A_{then} was calculated assuming that the growth of thenardite proceeds in contact with a solution saturated with respect to the better soluble Na_2SO_4 phase III [12]. This assumption seems quite reasonable because it is frequently observed that both solids, thenardite and phase III, can coexist during evaporation at low relative humidities [13,14,15]. It is important to note, that this is a minimum value for the supersaturation with respect to thenardite due to the unknown supersaturation of phase III necessary for its crystallization. In method B_{mir} the supersaturation with respect to mirabilite at a given temperature is given by the solubility of thenardite at the same temperature. A Biot coefficient of $b = 1$ was used in the calculations in lack of experimental values for Sand sandstone. It is important to note that average values of the pore filling ratio were used for the calculations yielding only a rough estimation of the effective stress. Due to salt transport during cycling, which was clearly more pronounced in method B_{mir} as in A_{then} (see Figures 3a and 3b), accumulation of salts can reveal higher pore filling ratios in some pores and in turn to higher effective stresses according to Equation (2). Average effective stresses σ^* are given in Table 3. Cracks were observed in those specimens (A8, B6, B7) where the average effective stress was higher than 4.27 MPa. Sanding occurred on the surfaces of

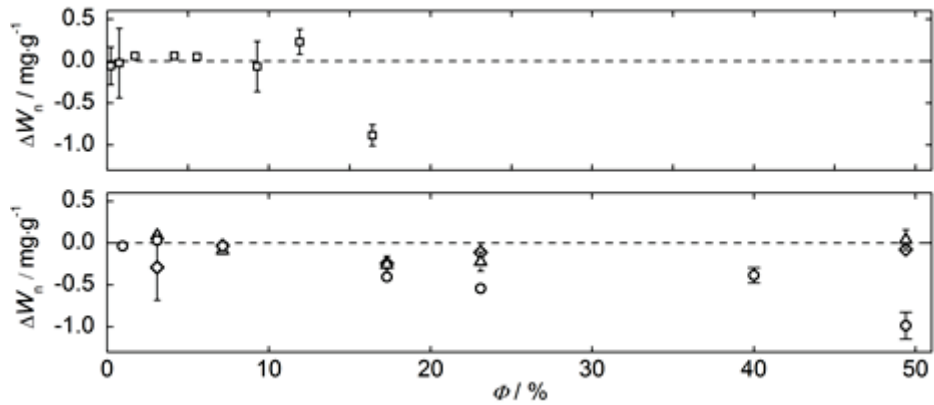


Figure 6: Average mass loss Δw_n per cycle versus pore filling ratio after impregnation with respect to thenardite in the upper diagram and mirabilite in the lower diagram. Squares represent method A_{then} , circles method B_{mir} , diamonds method C_{mir} and triangles method D_{mir} . Error bars reflects the standard deviation of the slope yielded by the linear regression. The dashed line is used as guide for the eye representing a mass loss of zero.

Table 3: Average effective stresses σ^* calculated for methods A_{then} and B_{mir} with the average pore filling ratios and the crystallization pressure (see text).

Specimen	σ^* (MPa)	σ^* (MPa)
	A_{then}	B_{mir}
1	0.058	0.096
2	0.234	0.383
3	0.457	0.749
4	1.12	1.83
5	1.48	2.42
6	2.60	4.27
7	3.30	5.42
8	4.76	— ⁽¹⁾

(1) not tested

specimens B4 and B5 at average effective stresses of 1.83 MPa and 2.42 MPa. Due to the efflorescences observed on the surfaces of these specimens, the assumption of a salt enrichment closely beneath the surface is reasonable resulting in a higher effective stress near the surface than the calculated average value. The effective stresses may be

compared with the tensile strength of Sand sandstone. Values reported by different authors are quite scattered but most values reported are close to about 2 MPa [16,17,18]. This value is in reasonable agreement with our experimental observation and the calculated effective stresses.

In general it turns out that wetting with humid air is less harmful than wetting with liquid water, although the pore filling ratio with respect to mirabilite is the same as in the specimens of method B_{mir}. Hence, the average effective stress could be the same for the crystallization of mirabilite. As observed by Shahidzadeh and Desarnaud [13] in a capillary experiment, the precipitation of phase III and thenardite is more likely after dissolution via deliquescence than the crystallization of mirabilite. Hence, it is also possible that damage of the specimens treated with humid air (C_{mir} and D_{mir}) is caused by the crystallization of thenardite. In this case, the average effective stress would be the same as calculated for the specimens of method A_{then}. Up to now however, it is unclear which phases do actually crystallize within the porous network of Sand sandstone which will be the focus of future research. Therefore, an estimate of an average effective stress is more complicated. In addition, the appearance of a large amount of efflorescences yields a decrease of the average pore filling ratio resulting in a lower average effective stress. Contrarily, the salt accumulation due to salt transport during wetting leads to higher effective stresses in the pores with a higher salt load. Anyhow, the formation of cracks and the total breakdown observed for the specimen D7, give evidence that wetting with humid air at high salt loads can also be extremely destructive within few cycles.

4 Conclusion

In general the extreme destructiveness of the thenardite dissolution and mirabilite crystallization process (B_{mir}) is confirmed. The magnitude of damage increases with increasing salt load. Taking the degree of pore space filling with respect to the crystalline phase into account, it turns out that liquid wetting at 40 °C and subsequent drying, i.e. conditions where thenardite crystallization takes place, can cause more damage to Sand sandstone than mirabilite crystallization during wetting at 23 °C. The experiments carried out so far do not yet allow for an assessment of the influence of the pore filling ratio on the damage potential of thenardite. More insight is expected from our ongoing cycling experiments with the specimen A7. A study with even higher salt loads for cycling with liquid water (A_{then}) at 40 °C and for cycling including the deliquescence (C_{mir} and D_{mir}) has to be the subject of future research. Nonetheless, the study clearly reveals that the deliquescence of thenardite at high salt loads might also be very destructive at about 23 °C. Up to now it is unclear whether mirabilite or thenardite crystallization is responsible for the damage under such conditions.

Acknowledgement

This research was funded by Deutsche Forschungsgemeinschaft (DFG).

References

- [1] Steiger M., Crystal Growth in porous materials. I: The crystallization pressure of large crystals. *J. Cryst. Growth* 282 (2005) 455-469.
- [2] Espinosa-Marzal R. M. and Scherer G. W., Crystallization of sodium sulfate salts in limestone. *Environ. Geol.* 56 (2008) 605-621.
- [3] Espinosa-Marzal R. M., Hamilton A., McNall M., Whitaker K. and Scherer G. W., The chemomechanics of crystallization during rewetting of limestone impregnated with sodium sulfate, *J. Mater. Res.* 26 (2011) 1472-1482.
- [4] Linnow K., Niermann M., Bonatz D., Posern K. and Steiger M., Experimental studies of the mechanism and the kinetics of hydration reactions. *Energ. Proc.* 48 (2014) 394-404.
- [5] Angeli M., Hébert R., Menéndez B., David C. and Bigas J.-P., Influence of temperature and salt concentration on the salt weathering of a sedimentary stone with sodium sulfate. *Eng. Geol.* 115 (2010) 193-199.
- [6] Tsui N., Flatt R. J. and Scherer G. W., Crystallization damage by sodium sulphate. *J. Cult. Herit.* 4 (2003) 109-115.
- [7] Diaz Gonçalves T., Brito V., Alteration kinetics of natural stones due to sodium sulfate crystallization: can reality match experimental simulations? *Environ. Earth Sci.* (2014) doi: 10.1007/s12665-014-3085-0.
- [8] Yu S., Oguchi C. T., Is sheer thenardite attack impotent compared with cyclic conversion of thenardite-mirabilite mechanism in laboratory simulation tests? *Eng. Geol.* 152 (2013) 148-154.
- [9] Grimm W.-D., *Bildatlas wichtiger Denkmalgesteine*, Lipp-Verlag, München, 1990.
- [10] Schäfer M., Steiger M., A rapid method for the determination of cation exchange capacities of sandstones: preliminary data. *Geological Society Special Publication* 52 (2002) 431-439.
- [11] Espinosa-Marzal R. M., Scherer G. W., Impact of in-pore salt crystallization on transport properties. *Environ. Earth. Sci.* 69 (2013) 2657-2669.
- [12] Steiger M., Asmussen S., Crystallization of sodium sulfate phases in porous materials: The phase diagram $\text{Na}_2\text{SO}_4\text{-H}_2\text{O}$ and the

- generation of stress. *Geochim. Cosmochim. Acta* 72 (2008) 4291–4306.
- [13] Shahidzadeh N., Desarnaud J., Damage in porous media: role of the kinetics of salt (re)crystallization. *Eur. Phys. J. Appl. Phys.* 60 (2012) 24205p1-p7.
- [14] Linnow K., Steiger M., Lemster C., De Clerq H., Jovanovic M., In situ Raman observation of the crystallization in $\text{NaNO}_3\text{-Na}_2\text{SO}_4\text{-H}_2\text{O}$ solution droplets. *Environ. Earth Sci.* 5 (2013) 1609-1620.
- [15] Rodriguez-Navarro C., Doehne E., Sebastian E., How does sodium sulfate crystallize? Implications for the decay and testing of building materials, *Cem. Concr. Res.* 30 (2000) 1527-1534.
- [16] Möller U., Thermo-hygrische Formänderungen und Eigenspannungen von natürlichen und künstlichen Mauersteinen. Dissertation University Stuttgart (2004).
- [17] Alfes C., Bruchmechanisches Werkstoffverhalten von Sandstein unter Zugbeanspruchung. Dissertation RWTH Aachen, 1993.
- [18] Siegesmund S., Dürrast H., Physical and mechanical properties of Rocks. In: Siegesmund S., Snethlage R. (eds.), *Stone in Architecture*. Springer, Berlin, 2011.

Salt damage risk prediction for porous limestone

H. Derluyn^{1,*}, P. Moonen², T. Diaz Gonçalves³, V. Cnudde¹ and J. Carmeliet^{4,5}

¹Ghent University, Department of Geology and Soil Science – UGCT, Ghent, Belgium

²Université de Pau et des Pays de l'Adour (UPPA), Pau Cedex, France

³Laboratorio Nacional de Engenharia Civil (LNEC), Lisbon, Portugal

⁴ETH Zürich, Chair of Building Physics, Zürich Hönggerberg, Switzerland

⁵EMPA, Laboratory for Building Science and Technology, Dübendorf, Switzerland

* hannelore.derluyn@ugent.be

Abstract

We present a model coupling heat, moisture and salt transport, salt crystallization, deformation and damage in porous building materials with the aim of predicting crystallization-induced damage. The model performance is illustrated by simulating the damage caused by sodium chloride crystallization in a porous limestone. The results are compared with experimental observations based on neutron and X-ray imaging, showing a good agreement. The effective stresses that can cause damage are the result of the crystallization pressure combined with a sufficient amount of precipitating salt crystals in a localized zone.

Keywords: salt crystallization, salt damage, porous media, FEM modeling

1 Introduction

Many damage cases in civil constructions and in cultural heritage are related to the presence of salts. Water and dissolved salt ions penetrate into porous materials due to diffusive and convective transport. Upon changes in the environmental conditions (temperature and vapor pressure), salts can crystallize. When salt crystals form inside the material (subflorescence), crystallization pressures develop. This may lead to spalling and cracking of the building material, reducing its service life time.

The availability of a model providing a full coupling between heat, moisture and salt transport, salt crystallization, deformations and damage would be an important asset for engineers and conservators. It would allow them to assess and compare different maintenance, repair or conservation techniques or to assess the durability of a new building material under different climatic conditions, without having to perform long-term experiments. Several models for salt transport and crystallization or for damage in porous media are described in the literature. There remains however a need for bringing together the available approaches within a single unifying framework. Such a framework was only recently established, by developing a fully coupled finite element model to improve the prediction of salt damage risks in porous materials [1,2].

This paper summarizes the salt damage prediction model, and presents a case study of a hydrophobized Savonnières limestone, initially saturated with NaCl-solution, that cracks due to halite precipitation.

2 Salt damage prediction model

The model is developed in-house using the FORTRAN programming language and includes conservation of mass, energy and momentum, combined with the description of salt crystallization and crystallization damage. As this paper focuses on the salt damage prediction potential of the model, we limit this section to the description of salt crystallization and damage. For the description of the conservation laws, we refer to [2].

2.1. Salt crystallization

The salt crystal mass balance reads:

$$\Phi \frac{\partial (S_{cr} \rho_{cr})}{\partial t} = e_{crf} \quad (1)$$

with Φ the total open porosity, S_{cr} the crystal saturation degree and ρ_{cr} the crystal density. The mass exchange e_{crf} between the liquid and the crystal phase is described by the kinetics of salt crystallization or dissolution. It is

assumed that the supersaturation U is the driving force for crystallization, and that the mass exchange during crystallization is given by [3]:

$$e_{crl} = \zeta K_{m,cr} (U - 1)^{g_{cr}} \text{ for } U > U_{thr} \quad (2)$$

where $K_{m,cr}$ and g_{cr} are kinetic parameters and ζ is the fraction of the capillary active pore space filled with salt solution. In order for new crystals to nucleate and grow, the supersaturation has to exceed a threshold value U_{thr} . Dissolution is described by a similar type of equation, only the kinetic parameters differ and the threshold is $U < 1$.

For the modelling of the crystallization, besides the kinetics, also the availability of pore volume space needs to be considered. If no space is available for crystals to grow, crystallization will stop and consequently the concentration in the solution will remain higher than when the crystals could grow freely. Moreover, dissolution can only take place as long as there are crystals present. Finally, the presence of crystals at a certain location influences nucleation and growth of crystals at neighbouring locations. In order to get a stable numerical method incorporating all these constraints, the mass exchange term e_{crl} is implemented as:

$$e_{crl} = f(S_{cr}, 1) \zeta K_{m,cr} (\max(U, U_{thr}) - U_{thr})^{g_{cr}} + f(S_{cr}, 0) \zeta K_{m,diss} (1 - \min(U, 1))^{g_{diss}} \quad (3)$$

where the first term represents crystal growth and the second term represents crystal dissolution. The function f accounts for the constraints related to the pore and crystal volume and is described as:

$$f(x_1, x_2) = \text{sgn}(x_2 - x_1) \left(1 - \exp\left(-\left|\frac{x_1 - x_2}{HBW}\right|\right) \right) \quad (4)$$

where $\text{sgn}()$ represents the signum function, x_1 and x_2 are values, and HBW is a (numerical) parameter controlling the gradual transition between situations in which a constraint is active or not. A very low value ($HBW=0.01$) is selected in order to assure that the exponential function rapidly approaches zero as the difference $|x_1 - x_2|$ increases and that the function f approximates as closely as possible a step function. The function f is introduced to ensure that: (1) crystallization stops when the available pore volume is occupied by salt crystals and (2) dissolution can occur as long as there are still crystals present. As long as $S_{cr} < 1$, $f(S_{cr}, 1)$ equals 1 and the crystallization kinetics are active. When the pore volume is filled with crystals, $S_{cr} = 1$, no crystallization occurs anymore and consequently $f(S_{cr}, 1)$ equals 0. As long as $S_{cr} > 0$, $f(S_{cr}, 0)$ equals -1 (where the sign indicates that the crystal mass decreases). When all crystals are dissolved and $S_{cr} = 0$, the dissolution kinetics stop and $f(S_{cr}, 0)$ equals 0.

The function U_{thr} is defined as:

$$U_{thr} = 1 + (U_{start} - 1) \cdot \exp(-\nu \bar{S}_{cr}) \quad (5)$$

and represents the drop of the crystallization threshold from U_{start} to 1. For primary crystallization (i.e. if no crystals are present) the supersaturation has to exceed the supersaturation value U_{start} before crystallization starts. The drop from U_{start} to 1 is related to the nucleation and growth kinetics.

These kinetics determine how long a certain supersaturation U is maintained until a sufficient amount of crystals have nucleated and/or sufficiently large crystals have grown so that new crystals start to grow at lower supersaturation levels. These phenomena are incorporated in the parameter ν and the function \bar{S}_{cr} . S_{cr} is a measure for the amount of crystals in the immediate neighborhood, influencing the crystallization kinetics at the location being evaluated. ν quantifies how important the presence of already formed crystals is for the crystallization threshold U_{thr} . A non-local formulation is developed for the function \bar{S}_{cr} :

$$\bar{S}_{cr} = \frac{\int_{\Omega} w_f S_{cr} d\Omega}{\int_{\Omega} w_f d\Omega} \quad (6)$$

with w_f a weighting function, defined as a multivariate normal distribution:

$$w_f = \frac{1}{(2\pi)^{\frac{k}{2}} l^k} \exp\left(-\frac{r^2}{2l^2}\right) \quad (7)$$

with r the distance away from the evaluated point and l the influence length. k represents the number of dimensions (1, 2 or 3). The influence length l controls the extent of the crystallization zone. The smaller its value, the more localized crystallization will be.

2.2 Crystallization damage

The solid momentum balance, in the absence of body forces, reads:

$$\nabla \cdot \boldsymbol{\sigma}_s = 0 \quad (8)$$

with $\boldsymbol{\sigma}_s$ the partial stress tensor, expressed as:

$$\boldsymbol{\sigma}_s = \boldsymbol{\sigma} - b p_s \mathbf{I} \quad (9)$$

with $\boldsymbol{\sigma}$ the effective stress tensor, b the Biot coefficient, p_s the solid pressure and \mathbf{I} the second order unit tensor. p_s accounts for the mechanical effects of the constituents in the pore space on the macroscopic behavior of the porous material and is defined as [2]:

$$p_s = \int_{p_{c,ref}}^{p_c} (S_l + S_{cr}) dp_c + S_{cr} (p_x - p_{x,ref}) \quad (10)$$

with S_l and S_{cr} the liquid and crystal saturation degree, respectively, p_c the capillary pressure and p_x the crystallization pressure. The effective stress tensor is given by:

$$\boldsymbol{\sigma} = \mathbf{D}(\boldsymbol{\varepsilon} - \alpha \mathbf{I}(T - T_{ref})) \quad (11)$$

where \mathbf{D} is the 4th order elasticity tensor, $\boldsymbol{\varepsilon}$ is the second-order strain tensor, α is the thermal expansion coefficient and T the temperature.

We assume that damage occurs, i.e. that a crack develops, when the j^{th} principal component σ_j of the effective stress tensor exceeds the material strength f_t^0 .

3 Case study

3.1 Stone properties

The total open porosity Φ of the Savonnières limestone used for the experimental study was determined by vacuum saturation and amounts 26.9%. The density of the limestone equals 1975 kg/m³. During capillary saturation, only 56% of the pore space gets filled. The capillary active porosity of untreated Savonnières limestone amounts $\Phi_{unt} = 14.9\%$. The other pores are only active in the over-capillary regime. When a hydrophobic treatment is applied, the treatment deactivates a fraction of the capillary active pore space, defined by the porosity Φ_h . The capillary active pore space reduces to $\Phi_{unt} \cdot \Phi_h$. The porosity occupied by the hydrophobic treatment Φ_h at a certain position x is found by:

$$\Phi_h(x) = \Phi_{unt} - \frac{w_{l, cap}(x)}{\rho_l} \quad (12)$$

with $w_{l, cap}(x)$ the capillary moisture content at the position x , determined from the moisture profile in the capillary saturated sample, as quantified by neutron radiography. When salt crystals are precipitating, they as well reduce the capillary active pore space. The crystals occupy a fraction of the pore space $\Phi_{cr} = \Phi \cdot S_{cr}$, with S_{cr} the crystal saturation degree. The capillary active pore space reduces to $\Phi_{unt} \cdot \Phi_h \cdot \Phi_{cr}$.

The moisture retention curve, describing the liquid saturation degree S_l in function of capillary pressure p_c , is approximated by a sum of power functions [4]:

$$S_l(p_c) = \sum_{j=1}^s l_j (1 + (c_j p_c)^{n_j})^{-\frac{1-n_j}{n_j}} \quad (13)$$

with s the number of pore systems, l_j weight factors, and c_j and n_j model parameters. The parameters as determined by [5] are adopted. When the capillary active porosity is reduced by a hydrophobic treatment and/or the presence of salt crystals, the liquid saturation degree is reduced in a simplified way by multiplying with the factor $1 - \Phi_h / \Phi_{unt} - \Phi_{cr} / \Phi_{unt}$.

The liquid permeability for pure water, $K_{w, unt}$, in function of capillary pressure was determined from the moisture profiles obtained by neutron imaging during a capillary uptake test [6]. The liquid permeability for a salt solution $K_{l, unt}$ is calculated from the liquid permeability of pure water as:

$$K_{l, unt} = K_{w, unt} \frac{\eta_w \rho_l}{\rho_w \eta_l} \quad (14)$$

where η is the viscosity. This relation is experimentally confirmed in [6]. When the capillary active pore space is reduced by a hydrophobic treatment and/or the presence of salt crystals, the liquid permeability is reduced, similar to the liquid saturation degree, by multiplying with the factor $1 - \Phi_h / \Phi_{unt} - \Phi_{cr} / \Phi_{unt}$.

The vapor permeability δ_v was measured following EN ISO 12572:2001 and can be described in function of the vapor pressure p_v as:

$$\delta_v = \delta_{v,air} \left(a + b \exp \left(c \cdot \frac{p_v}{p_{v,sat}} \right) \right) \quad (15)$$

with a , b and c parameters and $p_{v,sat}$ the saturated vapor pressure. The vapor permeability in air $\delta_{v,air}$ is given by Schirmer's equation [7]. For flow perpendicular to the bedding direction of the limestone, the parameters a , b and c amount 0.0109, $8.86 \cdot 10^{-6}$ and 8.55, respectively.

The thermal conductivity λ was measured following EN 1946-3:1999. An average thermal conductivity of 0.99 W/mK was found for dry Savonnières limestone. To incorporate the influence of moisture, the thermal conductivity of water λ_w , multiplied with the volume fraction of water, is added to the dry thermal conductivity:

$$\lambda(S_l) = \lambda_{dry} + \lambda_w \Phi S_l \quad (16)$$

The thermal capacity $c_{p,s}$ of Savonnières limestone is estimated to be 900 J/kgK. The thermal expansion coefficient α_s was determined by measuring the thermal dilation in a dynamic mechanical analyzer during a heating-cooling cycle, an average value of 5.5 $\mu\text{m}/\text{mK}$ was obtained.

The E-modulus was measured during a compression test, an average E-modulus of 13.9 GPa was found perpendicular to the bedding direction. When the stone is capillary saturated, the E-modulus perpendicular to the bedding direction reduces to 11.2 GPa. The tensile strength of dry Savonnières limestone $f_{t,dry}^0$ was determined from a tensile test and equals 1.8 MPa perpendicular to the bedding. In the capillary saturated state, the tensile strength reduces to 1.46 MPa. The Biot coefficient of Savonnières limestone was not measured experimentally, but estimated from literature data of a similar limestone [8]. The Biot coefficient is 0.77.

3.2 Salt properties

The supersaturation U is calculated using the Pitzer ion interaction approach as described by [9], thus accounting for the non-ideal behavior of pore solutions. The crystallization pressure p_x is expressed as [10]:

$$p_x = \frac{RT}{\bar{V}_{cr}} \ln U \quad (17)$$

with R the universal gas constant, T the absolute temperature and \bar{V}_{cr} the molar volume of the crystal, being 27 cm^3/mole for sodium chloride. The kinetic growth parameters $K_{m,cr}$ and g_{cr} for sodium chloride equal 0.41 $\text{kg}/\text{m}^3\text{s}$ and 1. Values of 100, 10^{-4} and 1.5 are taken for the kinetic parameters ν , l and U_{start} in the U_{thr} -function.

3.3 Drying experiment

Drying of a Savonnières limestone sample ($10 \times 10 \times 8.5 \text{ mm}^3$) at 45°C and 5% RH, initially saturated with a 5.8 molal sodium chloride solution, has been visualized and quantified using neutron imaging analysis [1]. The sample was prepared by applying a water and vapor tight membrane on the lateral sides (aluminum tape) in order to create a one-dimensional drying process. Drying occurred in the direction perpendicular to the bedding. A hydrophobic treatment (SILRES BS 280, Wacker) was applied on the upper 3 mm of the sample. Drying could only occur through the water repellent upper part as the bottom face was sealed. The hydrophobic treatment was intended to prevent salt efflorescence and induce in-pore crystallization. During the drying, the high spatial resolution neutron radiographs (nominal pixel size of $13.5 \mu\text{m}$) indicated considerable deformations after about 100 minutes (Fig. 1a). These deformations represent the displacements induced by crack formation due to the crystallization of sodium chloride. The cracks resulting from the salt crystallization were characterized using X-ray micro-computed tomography. The experiment revealed that the salt crystals precipitate in the upper region of the sample, mainly in the hydrophobic zone, but below the top surface. Consequently, cracks form in this zone (Fig. 1b).

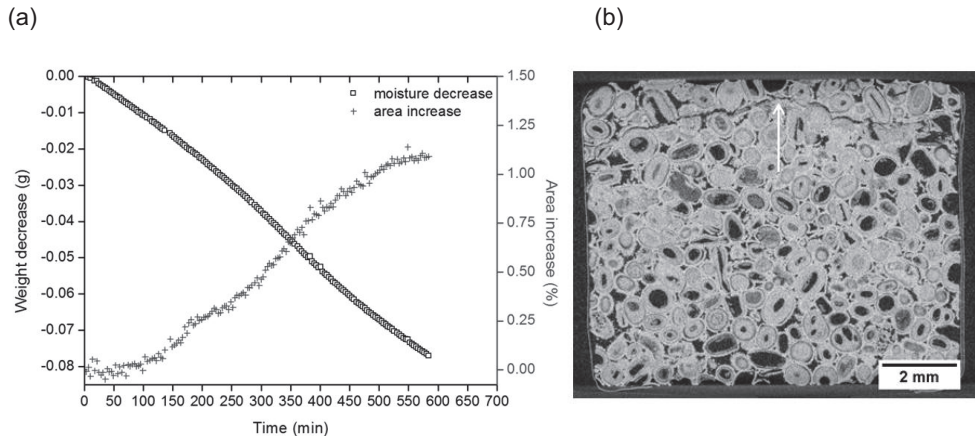


Figure 1: (a) Weight decrease due to drying and area increase due to crystallization-induced deformations in the Savonnières sample as quantified from time-lapse neutron radiographs. After approximately 100 min. the sample starts to deform. (b) A crack, visualized by X-ray micro-tomography, is observed in the upper region of the sample after the drying process.

4 Results

We simulate the coupled heat-moisture-salt transport and salt crystallization and predict the risk for salt damage for the experiment described in section 3. The simulation is performed on a 1-dimensional mesh of length L , where L equals the height of the sample used in the drying experiment, being 8.19 mm. The mesh consists of 100 equidistant elements. The mass flux and heat flux at the sample's boundary are described by boundary conditions of the Neumann type:

$$\begin{aligned}\bar{q}_m &= CMTC(p_{v,env} - p_{v,surf}) \text{ with } p_{v,env} = p_{v,sat}(T_{env}) \cdot RH_{env} \\ \bar{q}_e &= HTC(T_{env} - T_{surf}) + (c_{p,v}(T_{surf} - T_0) + L_v) \cdot \bar{q}_m\end{aligned}\quad (18)$$

$p_{v,surf}$ and T_{surf} are the vapor pressure and the temperature at the boundary surface and $p_{v,env}$, T_{env} and RH_{env} the vapor pressure, temperature and relative humidity of the environment. The convective mass transfer coefficient $CMTC$ amounts $3.95 \cdot 10^{-9}$ s/m [1] and the heat transfer coefficient HTC 5.67 W/m²K.

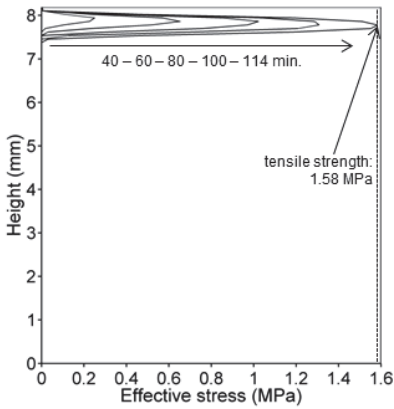


Figure 2: Effective stress evolution.

The U_{start} -value of 1.5 is reached after 23 minutes. The effective stress evolution with time is given by the profiles in Fig. 2. We observe that the highest stresses develop at about 0.4 mm from the top of the sample. This is in agreement with the observed crack pattern in the sample (Fig. 1b). A crack developed at the same position as where the effective stress reaches the tensile strength of 1.58 MPa, (corresponding to a saturation degree of 2%). This tensile strength is reached after 114 min., similar to the time at which the deformations due to crack formation were observed in the experiment. The effective stresses are directly related to the crystal saturation degree S_{cr} and the crystallization pressure p_x (Fig. 3). It is the product of

these two quantities that determines the effective stress, as expressed by equation (10). As our sample can deform freely, the solid stress σ_s equals zero (i.e. is equal to the external mechanical stress). This means that the effective stress σ is only determined by the solid pressure p_s . Using equation (10) and considering that our simulation is 1-dimensional, so that we can denote the stresses by a scalar (i.e. we describe the stress along the height of the sample), lead to:

$$\sigma = b \left(\int_0^{p_c} \left(S_{l,unt} \left(1 - \frac{\Phi_h}{\Phi_{unt}} \right) \right) dp_c + S_{cr} p_x \right)$$

The effect of the hygric stresses, expressed by the first term, is found to be negligible in this simulation, as they only range in the order of magnitude of 1000 Pa. Thus the effective stress is approximated by $\sigma \approx b S_{cr} p_x$.

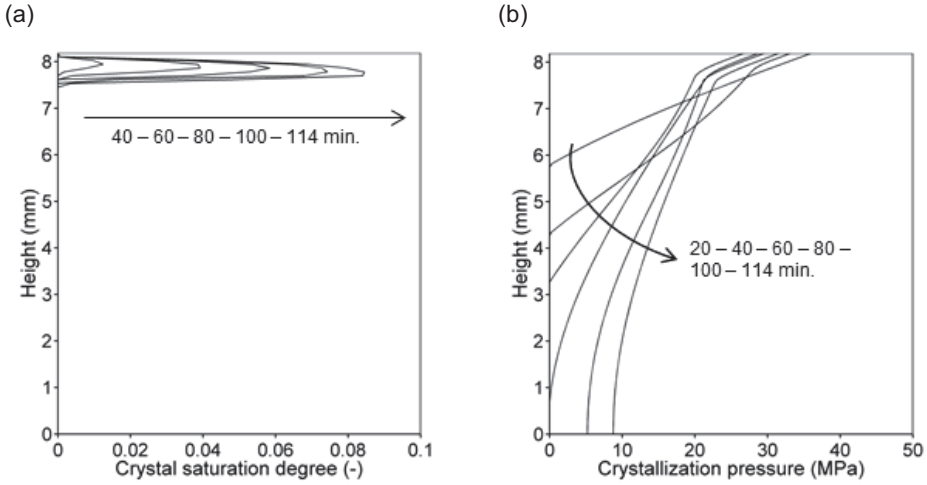


Figure 3: Evolution of (a) the crystal saturation degree S_{cr} and (b) the crystallization pressure p_x .

5 Conclusions

We have developed a fully coupled computational model that describes heat, water and salt transport, salt crystallization and deformations and damage induced by hygro-thermal and crystallization stresses. The model predicts the macroscopic behavior and physical degradation of porous materials. The model has been discussed with the focus on the prediction of salt damage caused by the formation of sodium chloride crystals in a porous limestone during drying. The simulation results show a good agreement with experimental data, obtained from neutron and X-ray imaging techniques, when choosing adequate parameters for the crystallization kinetics. The simulations show that the effective stresses resulting from salt crystallization do not only depend on the crystallization pressure, which is related to the supersaturation, but also on the amount of salt crystals forming and the localization of these crystals.

Acknowledgements

Hannelore Derluyn is a postdoctoral fellow of the Research Foundation - Flanders (FWO) and acknowledges its support.

References

- [1] Derluyn, H. Salt transport and crystallization in porous limestone: neutron – X-ray imaging and poromechanical modeling, PhD Thesis, ETH Zurich, Switzerland, 2012.
- [2] Derluyn, H., Moonen, P., Carmeliet, J. Deformation and damage due to drying-induced salt crystallization in porous limestone, *Journal of the Mechanics and Physics of Solids* (63) (2014) 242-255.
- [3] Espinosa, R.M., Franke, L., Deckelmann, G. Phase changes of salts in porous materials: crystallization, hydration and deliquescence, *Construction and Building Materials* (22) (2008) 1758-1773.
- [4] van Genuchten, M.T. A closed-form equation for predicting the hydraulic conductivity of unsaturated soils, *Soil Science Society of America Journal* (44) (1980) 892-898.
- [5] Roels, S., Elsen, J., Carmeliet, J., Hens, H. Characterisation of pore structure by combining mercury porosimetry and micrography, *Materials and Structures* (34) (2001) 76-82.
- [6] Derluyn, H., Griffa, M., Mannes, D., Jerjen, I., Dewanckele, J. et al. Characterizing saline uptake and salt distributions in porous limestone with neutron radiography and X-ray micro-tomography, *Journal of Building Physics* (36) (2013) 353-374.
- [7] Ochs, F., Heidemann, W., Mullersteinhagen, H. Effective thermal conductivity of moistened insulation materials as a function of temperature, *International Journal of Heat and Mass Transfer* (51) (2008) 539-552.
- [8] Lion, M., Skoczylas, F., Ledésert, B. Determination of the main hydraulic and poro-elastic properties of limestone from Bourgogne, France, *International Journal of Rock Mechanics and Mining Sciences* (41) (2004) 915-925.
- [9] Steiger, M., Kiekbusch, J., Nicolai, A. An improved model incorporating Pitzer's equations for calculation of thermodynamic

properties of pore solutions implemented into an efficient program code, *Construction and Building Materials* (22) (2008) 1841-1850.

- [10] Steiger, M. Crystal growth in porous materials – I: the crystallization pressure of large crystals, *Journal of Crystal Growth* (282) (2005) 455-469.

Peering into the rock: a 4D synchrotron study of salt solution movement within masonry sandstone

C. Graham¹, M. Lee¹, V. Phoenix¹ and M. Young²

¹School of Geographical and Earth Sciences, University of Glasgow, U.K

²Historic Scotland, Conservation Directorate, Edinburgh, U.K

* c.graham.1@research.gla.ac.uk

Abstract

Here we report results from an initial study on salt solution movement within masonry sandstone. The capillary uptake of 6M calcium iodide solution into Blaxter and Locharbriggs sandstone was imaged by micro computed tomography scanning at three minute intervals. Over a scanning period of seven seconds/360° scan, the solution movement was successfully visualised and quantified. Results show distinct differences in the uptake characteristics of Blaxter and Locharbriggs sandstone. Flow is dominant within permeable layers in the Locharbriggs samples forming thin layers, coating grains that permit the movement of solution without filling pores. It is thought that preferential flow through these confined permeable layers may be an important determinant of salt crystallisation processes.

Keywords: Sandstone, Synchrotron CT Scanning

1 Introduction

The crystallisation of soluble salts is one of the major decay mechanisms affecting sandstone masonry. Salts are introduced into masonry through a number of pathways including (i) capillary rise from de-icing salts, fertilizers and soils saturated into groundwater [1], (ii) inappropriate chemical cleaning methods, (iii) sea spray and air pollution [2,3] and (iv) the alteration and mobilisation of inherent materials such as mortars [4,5]. Salt solution ingress and the subsequent drying pathways are extremely important factors that influence both the location and severity of salt crystallisation. Unsaturated flow dominates the movement of liquid within porous building materials and is controlled by capillary forces. The extent of capillary flow depends on (i) the petrographic properties of the stone, (ii) solution properties, such as surface tension and viscosity and (iii) environmental parameters including temperature and relative humidity (RH). Several salt types have been identified as being major destructive agents within building stone. These include sodium sulphate [6-8], magnesium sulphate [9, 10], gypsum [3] and sodium chloride [9, 11]. Mixtures of salt ions are generally found within buildings, leading to the dynamic crystallisation of many salt types throughout a relatively short space of time [12]. The most damaging mechanisms responsible for damage within natural stone include (i) the thermal expansion of salts [13], (ii) hydration pressures [14] and (iii) crystallisation pressures [15, 16]. Alongside environmental conditions and solution properties, the pore characteristics of the stone influence the uptake and distribution of moisture as well as the rate and magnitude of decay. Both the total connected porosity and distribution of pore sizes, particularly of micropores (<0.1 μm) have been shown to be important factors in the generation of high crystallisation pressures [17, 18].

The uptake and crystallisation of salts within building stone is an extremely complex system that contains many variable parameters. The mechanisms by which salts damage building materials cannot be fully understood by invasive sampling and analysis after crystallisation because the key to the process lies in the feedbacks between salt solution movement, salt crystal growth and rock microstructure at the pore scale. A suitable technique in the visualisation of material pore space and recently fluid movement is x-ray micro-computed tomography scanning (μCT). μCT has been used extensively in the fields of geology [19, 20], archaeology [21], palaeontology [22, 23] and cultural heritage [24] to quantify pore space [25-27] and weathering processes [28]. Recent research has made use of synchrotron facilities [29] that allow greater versatility and precision of measurements. Synchrotron μCT and neutron imaging have been used successfully to image and quantify solution movement through sand [30] and limestone [31].

In order to visualise the uptake and movement of salt solution within building stone a non-destructive 4-dimensional μCT study was undertaken using the I12 beamline at the Diamond Light Source synchrotron, UK.

2 Materials and methods

Two sandstones are used within this study, representative of replacement and historic sandstones used through the UK. Petrographic analyses of each rock type took place using transmitted light microscopy and scanning electron microscopy (SEM). The hydric behaviour and subsequent pore system was measured on six repeat samples (6cm³ cubes) using a range of British Standard tests including: (i) water absorption coefficient (BS EN 13755:2008), (ii) capillary absorption coefficient (BS EN 1925:1999), (iii) saturation coefficient, (iv) effective open porosity by buoyancy weighing (BS EN 1936:2006) and porosity and pore size distribution analysis by helium porosimetry and mercury intrusion porosimetry (MIP).

2.1 Sandstone

Locharbriggs is a red aeolian sandstone of lower Permian age quarried in Dumfries and Galloway, southern Scotland from the oldest and largest red sandstone quarry in Scotland, first quarried in 1759. Locharbriggs is a mineralogically mature, medium grained and poorly sorted sandstone containing abundant clean, sub-rounded –angular quartz grains and a lower percentage of feldspar grains. Grain sizes are variable but contain well established hematite rims throughout. The stone matrix is composed of poorly sorted and broken lithic fragments, quartz grains, smectite clay and weak silica cement. There is a strong and distinguishable fabric throughout the stone that is visible in hand specimen. Layers measure between 1-3mm in thickness and are characterised by small, poorly sorted quartz grains, small Fe-oxides and small, poorly connected pores, separated by thicker layers of larger pores and grains. It has an average porosity of 19.5%, a water absorption coefficient of 9.82% and a capillary coefficient of 309 g/m²/sec^{1/2}. Locharbriggs contains a bimodal distribution of pore sizes, with an average of 50% of pores within the 5µm - 25µm radius range and 9% within the 0.05µm – 0.5µm radius range. Locharbriggs is an extremely important and popular building stone across the UK, with historically important buildings constructed of Locharbriggs dating back to the 1700s. Locharbriggs sandstone has been used extensively in other research looking at (i) building stone cleaning [32], (ii) sandstone weathering [33] and (iii) the mechanical and hydraulic properties of deformation bands [34].

Blaxter is a blonde-buff, medium grained carboniferous sandstone of fluvial origin, quarried in Northumberland, northern England. It is a mineralogically immature sandstone containing a high abundance of feldspar and muscovite grains that are clearly visible in hand specimen. Most grains are sub-angular but of a consistently similar size (180-200µm). Many of the feldspar and muscovite grains show high weathering characteristics and many have decomposed into kaolinite and illite clay. Fe-coatings of quartz and feldspar grains are common, with detrital clays providing secondary cement to silica between the grains. Blaxter has an average porosity of 15.5%, a water absorption coefficient of 6.15% and a

capillary coefficient of $52\text{g/m}^2/\text{s}^{1/2}$. Blaxter contains 53.5% of pores within the $1\mu\text{m} - 25\mu\text{m}$ radius range and 17.6% within the $0.05\mu\text{m} - 0.5\mu\text{m}$ radius range. Blaxter is widely used throughout the UK for both new builds and as replacement stone in restoration projects.

2.2 Methods

The sandstone samples were cubes with an 8-10mm edge length, and cylinders $>10\text{mm}$ height by 8mm diameter. From the data presented in this paper, the Blaxter and one Locharbriggs sample were cut into cubes and the remaining two Locharbriggs samples were cylinders. The experiment set-up consisted of a bespoke cylindrical chamber 110mm in height by 50mm in diameter and constructed from 2mm thick Perspex. It consisted of two sections: a top part containing a small platform that was used to hold sandstone specimens, and a bottom section that was used to house a small reservoir of salt solution. Both parts of the chamber were connected and sealed together using a large, tight rubber band, with small holes drilled into the platform in the upper section to allow the circulation of air and connection with the reservoir in the lower section. The chamber was sealed using a large rubber bung. In all experiments, samples were held in place using moulded foam to ensure their stability during stage rotation.

The initial proposal of work called for a process whereby solution that was contained in a small reservoir in the bottom section of the chamber was transferred by a filter-paper wick to a piece of 1mm thick filter paper situated on the platform in the top section. Salt solutions would then enter the sample via non-forced capillary uptake from the saturated filter-paper. This would provide solution at a rate that allowed for a five minute time interval before solution entered the stone, during which time safety checks and sample stage positioning could take place. Due to poor contrast between the solution and stone at low solution concentrations, a 6M concentrated calcium iodide (CaI_2) solution, as has been used previously in other similar studies [31], was chosen to ensure sufficient contrast. At this high concentration however, wicking between the lower reservoir and the filter paper prior to safety checks did not take place. In order to solve this problem, pre-saturated filter-paper was used. This provided a second problem as by the time scanning was initiated capillary intrusion into the sample had already started. This meant that the field of view had to be moved to a higher position on the sample to enable fluid movement through the stone to be imaged.

Dynamic, high speed tomography scanning was performed on the I12 beamline at the Diamond Light Source synchrotron, Oxfordshire, UK. Images were captured using module 2 of the Phantom v7.3 camera. This had a field of view of 9.8mm by 7.3mm and a resolution of $\sim 12\mu\text{m}/\text{pixel}$. With this arrangement the sample stage rotation was set as to ensure that one 360° scan took only seven seconds to complete and therefore the dynamic movement of solution into and throughout the sample could be

imaged. Five hundred and eighty projections were captured in each 360° scan; however specific images from either the start or end of each scan were omitted due to poor definition of phase boundaries. Unlike conventional laboratory CT scanners, synchrotron radiation is generated by the movement of electrons as they pass through magnetic fields at close to the speed of light. As these electrons are steered through the magnetic fields they lose energy in the form of synchrotron light. This light is harnessed and subsequently filtered and focused, with the subsequent x-rays used for a number of scientific applications. This results in faster scanning of a better signal-noise ratio than lab based CT systems.

Reconstructed scans were visualised in Avizo 7 software. Each scan was placed through two filters to enhance contrast between greyscale phases and to enhance the edge detection of each separate phase. By using the greyscale distribution of each scan, grain, pore and solution phases were separated and quantified to provide the porosity and solution values through each slice. Each separate scan was then registered to a reference scan to ensure each scan was aligned in each scan set. In order to visualise the change in solution movement from two neighbouring scans, the arithmetic tool was used to calculate the difference between each scan. The resulting difference field was used to visualise and quantify the movement of solution between scans. Some samples were also cropped prior to any analysis to eliminate background “porosity” from out-with the sample.

3 Results

Four individual scan-sets will be discussed in this section. One set from a Blaxter sample (B) and the following three sets from three individual Locharbriggs samples (L1, L2 and L3). Samples B and L1 are scans from cropped cubic samples and samples L2 and L3 from small cores.

3.1 Blaxter (B)

A 3-dimensional visualisation of the open pores, solution and stone grains and a cropped horizontal cross section through the middle of this block are shown in Fig 1. It shows a high percentage of filled pores with sporadic empty porosity of different pore sizes located between larger clusters of solution. Solution within this sample fills a range of pore sizes, likely the most open and accessible pores as highlighted in Fig 1B. Solution does not follow any petrographic structures within the sample and highlights a well distributed range of pore connectivity within the stone. Due to problems associated with the rapid rate of solution uptake, this was the only scan suitable for analysis and therefore does not provide an initial “dry” scan for comparison.

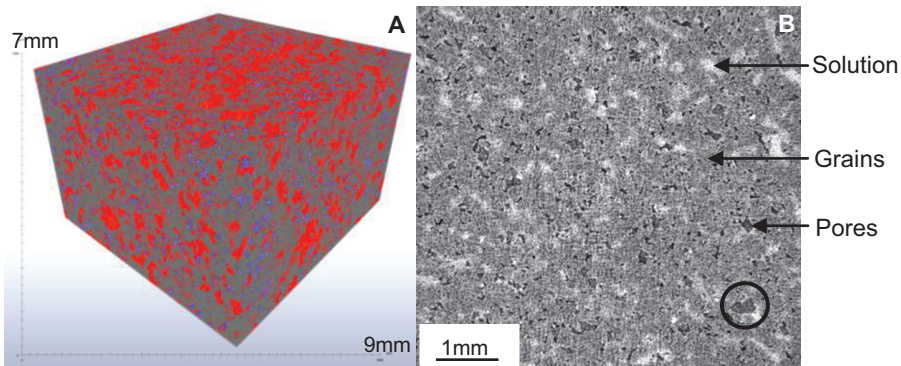
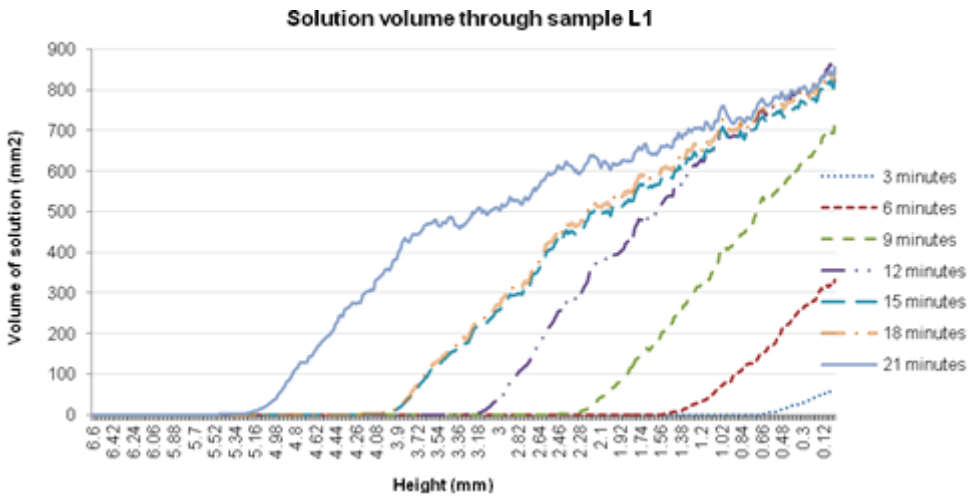


Figure 1: A: 3D visualisation of pores (blue), solution (red) and stone grains (grey). B: 2D cropped horizontal cross section showing each distinct phase. Black circle shows partial ingress of solution into an empty pore, with a white halo at the edge of the pore.

3.2 Locharbriggs 1 (L1)

Seven scans were acquired at three minute intervals. The volumes of solution, porosity, quartz/feldspar grains and Fe-oxides are segmented and calculated at each time interval. The initial porosity values throughout the sample show an average of ~ 17%, which shows little variation throughout the height of the sample. The sample was subject to capillary uptake experiments parallel to bedding. The data show that solution ingress and subsequent transport through the stone is significantly influenced by the internal pore structure, specifically in relation to pore size distributions and the internal fabric (ie bedding) of the stone. The solution transport is restricted to one half of the sample, separated from the rest of the sample by the bedding horizon and a change in mineralogical texture. Porosity in this other, separated layer is significantly lower and less well connected than the coarser layer, thus inhibiting solution penetration. It is likely that this solution has hydraulic connectivity throughout the height of the sample. Initial solution ingress is restricted to a small section in the centre of the coarse layer.

Graph 1 shows the solution volume distribution throughout the sample at each three minute interval. It reveals a steady increase of solution volume height reached by capillary rise in the sample and total solution volume. A noticeable peak is evident around 1.032mm in height from twelve minutes onwards. Solution volumes below this height appear very similar, with little fluctuation as to suggest that most of the accessible pores below this point have been filled by twelve minutes. Open pores below this height in the 9, 12, 15, 18 and 21 minute scans shows that saturation has not been met however. Rather than solution moving through the sample by consecutively filling pores, the solution instead moves through the sample by coating and "wetting" grains. In this process, solution uptake is highly influenced by the viscosity and surface tension of the solution. From twelve minutes onwards, vertical solution movement above 1.032mm is supplied by solution already within the sample at a rate equal to solution ingress into the base of the stone. This would ensure that pores below 1.032mm would not become filled and solution volume below this height would remain stable. From both the visualisation of solution at each time step within the stone and from graph 1, it can be seen that lateral dispersion of solution is more prominent within the first nine minutes of solution uptake. From twelve minutes onwards capillary rise of solution becomes prominent.



Graph 1: Solution volume per slice through sample L1 at different time periods

From solution visualisation at each time step it is shown that the wetting front is not laterally consistent, with a leading ridge of solution at the centre of the volume (Fig 2). This is in contrast to analysis of B1, whereby solution moves through the sample in individual channels as opposed to homogeneous flow with a defined wetting front.

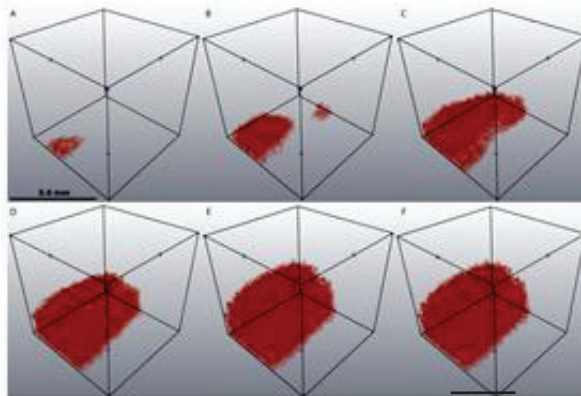


Figure 2: Solution movement through sample L1. A= 3minutes, B= 6minutes, C= 9minutes, D= 12minutes, E= 15minutes, F= 21minutes.

3.3 Locharbriggs 2 (L2)

Sample L2 is a scan of the upper 7mm (Fig 3A) of the sample due to problems associated with the rapid uptake of solution and so does not represent the initial ingress of solution into the stone. Unlike sample L1, Fig 3 shows evidence of complete pore filling in sample L2. The black boxes highlight the infilling of a pore with solution over the full period of scanning. The solution does not neatly “outline” the shape of the pore but instead is imaged within the pore and pore-throats that are undetected at this resolution. The red circles highlight the partial infilling of a smaller pore whereby the solution adheres to the surrounding grain surfaces due to capillary forces. These capillary forces will allow the flow of solution throughout the pore network, in which pores are hydraulically connected through this thin solution layer. Fig 4 shows a 3D visualisation of a cropped section within sample L2 of the same time frames as highlighted in Fig 3.

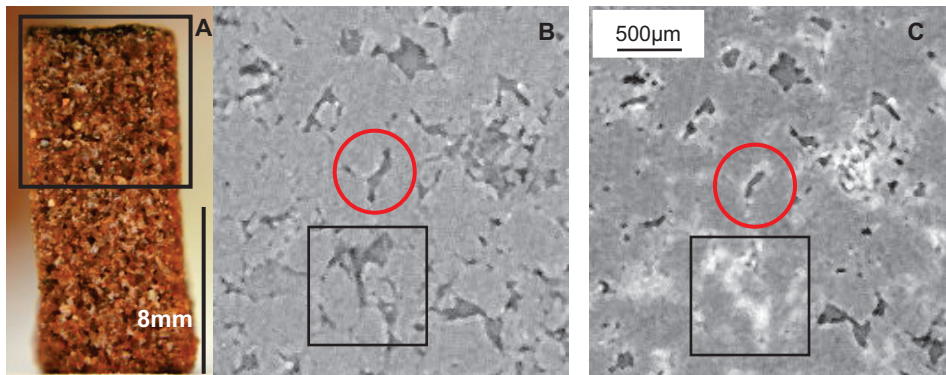
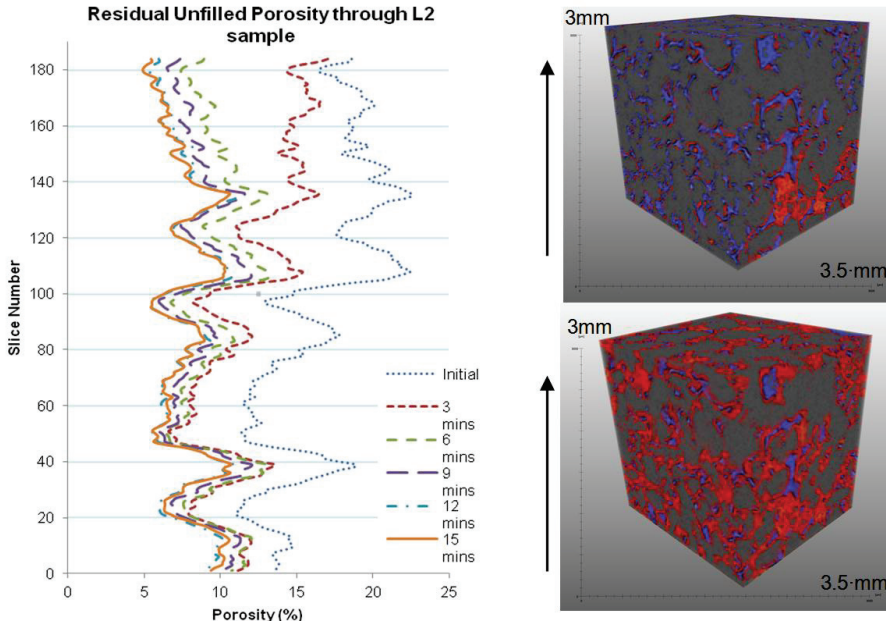


Figure 3: A: Black box highlights the scanned area of L2. B+C: 2D images of L2. Black boxes highlight the infilling of a pore. Red circles highlight the partial infilling of a pore. B: Initial scan. C: Final scan (approximately 15minutes later).

It is clearer to see the infilling of the pore network in Fig 4, whereby the segmentation of solution in Fig 4B helps to define smaller pore-throats that are not detected otherwise. Fig 4A shows that solution moves through the rock by capillary action, adhering to the grain surfaces while staying in hydraulic connectivity with the larger solution volume present at lower levels within the sample. Larger pores at this height are not completely filled with solution over this short scanning period. Graph 2 shows the change in porosity values through the cropped section visualised in Fig 4. It shows the natural variation of porosity within the Locharbriggs sandstone as highlighted by the high porosity peaks at slice numbers 39, 108 and 138. It shows that at the start of scanning some of the porosity of the lower slices were already partially filled. The infilling of porosity is

clearly shown, especially over the first six minutes of scanning. From six to nine minutes the change in unfilled porosity over each slice is compressed and shows greater evidence of the infilling of pore throats (that aren't counted in porosity values) and the capillary rise of solution, whereby only the partial filling of pores takes place due to greater capillary forces causing the vertical transportation of solution.



Graph 2: Porosity measurements through the cropped section Fig 4.

Figure 4: Visualisation of porosity (blue), solution (red) and grains (grey). Black arrow shows direction of fluid movement. A: Initial scan showing partial infilling of large pore network and grains coating within other pores allowing solution movement through the pore network. B: The final scan (15minutes from the initial scan) showing pore infilling and highlighting narrow pore throats that weren't initially detected.

3.4 Locharbriggs 3 (L3)

Sample L3 represents the scan of the upper 7mm of the sample, similar to L2. It shows a similar process of fluid movement, whereby the flow is concentrated within more permeable bedding planes of the stone. Preferential solution movement takes place near the edges of stone and within bedding planes of the stone. The visualisation of differences between neighbouring scans highlights the lack of horizontal flow. From

the visualisation of pores that have lost fluid it indicates that the rate of vertical, capillary flow is not constant throughout the full section. If this was true then there would be no loss of solution in the feeder pores as they would be continually filled as solution moved through them, penetrating the open pores above.

4 Discussion

Analysis of four samples from two sandstone types has shown that the uptake characteristics and flow through each of these sandstone types differs significantly. Specifically, the mechanisms by which solution is absorbed and transferred through the stone are comparable, however the distribution of solution within the stone is different and is influenced by pore structure. An interesting and important result from analysis of Locharbriggs sandstone regards the preferential solution uptake and movement through confined permeable layers that was evident in all Locharbriggs samples. This may be an important determinant of salt crystallisation processes. The drying of sandstone is a complex and extremely important factor that significantly influences the distribution and damage potential of salt crystallisation. Damaging crystallisation pressures can develop during this drying process. Drying is influenced by solution properties, the pore network and surface modifications such as biological growth and hard surface crusts. The margin between permeable and impermeable layers in the Locharbriggs samples (specifically L1) presents a boundary in pore size distributions and a potential barrier for hydraulically controlled drying. This would lead to a vapour dominated drying regime, whereby the drying front would be located at the boundary, leading to salt crystallisation. This process could result in the preferential crystallisation of salts within a small layer within the stone. The distribution of high crystallisation pressures extending over such an area could lead to the development of fracture chains and scaling decay processes.

5 Conclusions and future work

The movement of 6M concentrated CaI_2 solution was successfully imaged in one sample of Blaxter sandstone and three samples of Locharbriggs sandstone over a period of ~21minutes. Over a scanning period of seven seconds, it was possible to image the grains, pore structure and salt solution within the samples. From repeated scans over three minute intervals the change in solution volume and porosity was visualised and calculated. Differences between neighbouring scans also allowed the visualisation and quantification of solution change within the stone. Images from the Blaxter sample show that the solution is well distributed within the stone, filling pores, while other, possibly disconnected pores remain unfilled. Solution distribution isn't influenced by any obvious structural features of the stone. Rather, it is likely influenced by the random distribution of pore sizes. All three Locharbriggs samples showed

similar fluid flow characteristics whereby more permeable layers permitted preferential flow through the stone. Vertical capillary uptake was the dominant flow mechanism, with thin solution films that coated grains evident in the L2 sample. This preferential flow within certain layers may influence the location and subsequent intensity of salt crystallisation during the drying stage of the stone.

An important issue that must be acknowledged is the effect of such a highly concentrated CaI_2 solution on fluid dynamics within the sandstones. In order to enable sufficient contrast between solution and the rock, and after several attempts at lower concentrations, a 6M concentration was accepted. This significantly increased the viscosity and the surface tension of the solution. This would impact on the fluid dynamics and influence the flow rate and accessibility into certain pore sizes. It was with this issue and problems associated with the experimental design that no attempt to calculate fluid flow rate were made. This increase in contrast did however allow the visualisation of pore-throats to be made that were otherwise undetected. It highlighted that pore throats were preferentially filled while larger pores remained partially filled.

Results from this study demonstrate that synchrotron X-ray μCT is a useful and valuable tool in the non-destructive analysis of building materials, specifically in the continued research of fluid flow dynamics in porous materials. It shows that with an extremely simple set-up, high quality data can be produced. It is believed that this study serves as a starting point for further research of salt crystallisation processes in building materials using dynamic synchrotron techniques. Advances would include the increased speed of imaging, an increased data set of stones containing contrasting pore structures and research of the drying regimes experienced by these sandstone types. Further study must strive to use more realistic solution concentrations as to replicate, as close as possible, natural conditions.

Acknowledgements

Thanks are extended to Robert Atwood and Nghia Vo of the I12 beamline at Diamond Light Source and to Kate Dobson of the Manchester X-ray Imaging Facility for their assistance and advice both during and after the experimental work. Thanks are also extended to Alison Wright and Emma Fairley of The University of Glasgow for their help and assistance during the allocated beamtime at Diamond, as part of a four person team and for supplying samples L2 and L3.

References

- [1] Charola, E. A. "Salts in the deterioration of porous materials: An overview." *Journal of the American Institute for Conservation* (39) Number 3, Article 2. (2000) 327 – 343.
- [2] Cardell, C. Delalieux, F. Roumpopoulos, K. Moropoulou, A. Auger, F. and Van Grieken, R. "Salt-induced decay in calcareous stone monuments and buildings in a marine environment in SW France" *Construction and Building Materials* (17) (2003) 165 – 179.
- [3] Lubelli, B. van Hees, R. P.J. and Groot, C. J. W. P. "The role of sea salts in the occurrence of different damage mechanisms and decay patterns on brick masonry" *Construction and Building Materials* (18) (2004) 119 – 124.
- [4] Perry, S.H. and Duffy, A.P. "The Short-term effects of mortar joints on salt movement in stone" *Atmospheric Environment* (31) (1996) 1297 – 1307.
- [5] Ruedrich, J. and Siegesmund, S. "Salt and ice crystallisation in porous sandstones" *Environmental Geology* (52) (2007) 225 – 249.
- [6] Rodriguez-Navarro, C. Doehne, E. and Sebastian, E. "How does sodium sulphate crystallize? Implications for the decay and testing of building materials" *Cement and Concrete Research* (30) (2000) 1527-1534.
- [7] Espinosa, R.M. Franke, L. and Deckelmann, G. "Model for the mechanical stress due to the salt crystallization in porous materials" *Construction and Building Materials* (22) (2008) 1350 – 1367.
- [8] Espinosa-Marzal, R.M. and Sherer, G.W. "Mechanisms of damage by salt" *Geological Society, London, Special Publications* (331) (2010) 61-77.
- [9] Lopez-Arce, P. Doehne, E. Greenshields, J. Benavente, D. and Young, D. "Treatment of rising damp and salt decay: the historic masonry buildings of Adelaide, South Australia." *Materials and Structures* (41) (2009) 827 – 848.
- [10] Balboni, E. Espinosa-Marzal, R. M. Doehne, E. and Scherer, G. W. "Can drying and re-wetting of magnesium sulphate salts lead to damage of stone?" *Environmental Earth Science* (63) (2011) 1463 – 1473.

- [11] Ruedrich, J. Seidel, M. Rothert, E. and Siegesmund, S. "Length changes of sandstones caused by salt crystallization." Geological Society, London, Special Publications (271) (2007) 199 – 209.
- [12] Zehnder, K. and Schoch, O. "Efflorescence of mirabilite, epsomite and gypsum traced by automated monitoring on-site." Journal of Cultural Heritage (10) (2009) 319-330.
- [13] Al-Naddaf, M. "The effect of salts on thermal and hydric dilation of porous building stone" Archaeometry (51) (2009) 495-505.
- [14] Flatt, Robert. J. "Salt damage in porous materials: how high supersaturations are generated" Journal of Crystal Growth (242) (2002) 435 – 454.
- [15] Theoulakis, P. and Moropoulou, A. "Salt Crystal Growth as Weathering Mechanism of Porous Stone on Historic Masonry" Journal of Porous materials (6) (1999) 345 – 358.
- [16] Scherer, G. W. "Stress from crystallization of salt" Cement and concrete research (34) (2004) 1613 – 1624.
- [17] Buj, O. and Gisbert, J. "Influence of pore morphology on the durability of sedimentary building stones from Aragon (Spain) subjected to standard salt decay tests" Environmental Earth Science (61) (2010) 1327 – 1336.
- [18] Yu, S. and Oguchi, C.T. "Role of pore size distribution in salt uptake, damage, and predicting salt susceptibility of eight types of Japanese building stones" Engineering Geology (115) (2010) 226 – 236.
- [19] Snelling, A.M. Zalasiewicz, Jan. A. and Reeds, I. "Using X-ray images to analyse graptolite distribution and alignment in Welsh mudrocks." Proceedings of the Yorkshire Geological Society (58) (2010) 129 – 140.
- [20] Needham, A. W. Abel, R. L. Tomkinson, T. and Grady, M. M. "Martian subsurface fluid pathways and 3D mineralogy of the Nakhla meteorite." Geochimica et Cosmochimica Acta (116) (2013) 96 – 110.
- [21] Hiller, J. C. and Wess, T. J. "The use of small-angle X-ray scattering to study archaeological and experimentally altered bone." J. Archaeol. Sci 33 (4) (2006) 560 – 572.
- [22] Clark, N. D. L. Adams, C. Lawton, T. Cruickshank, A. R. I. and Woods, K. "The Elgin marvel: using magnetic resonance imaging to

- look at a mouldic fossil from the Permian of Elgin, Scotland, UK." *Magnetic Resonance Imaging* (22) (2004) 269 – 273.
- [23] Douarin, M. Sinclair, D. J. Elliot, Mary. Henry, L. Long, D. Mitchison, F. and Roberts, J.M. "Changes in fossil assemblage in sediment cores from Mingulay Reef Complex (NE Atlantic): Implications for coral reef build-up." *Deep-Sea Research II* (99) (2014) 286 – 296.
- [24] Rozenbaum, O. "3-D characterization of weathered building limestones by high resolution synchrotron X-ray microtomography." *Science of the Total Environment* (409) (2011) 1959 – 1966.
- [25] Cnudde, V. Cwirzen, A. Masschaele, B. And Jacobs, P. J. S. "Porosity and microstructure characterization of building stones and concrete" *Engineering Geology* (103) (2009) 76 – 83.
- [26] Long, H. Swennen, R. Foubert, Anneleen. Dierick, M. and Jacobs, P. "3D quantification of mineral components and porosity distribution in Westphalian C sandstone by microfocus X-ray computed tomography." *Sedimentary Geology* (220) (2009) 116 – 125.
- [27] Cnudde, V. Dewanckele, J. Boone, M. De Kock, T. Boone, M. Brabant, L. Dusar, M. De Ceukelaire, M. De Clercq, H. Hayen, R. and Jacobs, P. "High-Resolution X-Ray CT for 3D Petrography of Ferruginous Sandstone for an Investigation for Building Stone Decay." *Microscopy Research and Technique* (74) (2011) 1006 – 1017.
- [28] Dewanckele, J. De Kock, T. Boone, M. A. Cnudde, V. Brabant, L. Boone, M. N. Fronteau, G. Van Hoorebeke, L. and Jacobs, P. "4D imaging and quantification of pore structure modifications inside natural building stones by means of high resolution X-ray CT." *Science of the Total Environment* (416) (2012) 436 – 448.
- [29] Derluyn, H. Dewanckele, J. Boone, M.N. Cnudde, V. Derome, D. and Carmeliet, J. "Crystallization of hydrated and anhydrous salts in porous limestone resolved by synchrotron X-ray microtomography." *Nuclear Instruments and Methods in Physics Research B* (324) (2014) 102 – 112.
- [30] Shokri, N. Lehmann, P. and Or, D. "Liquid-phase continuity and solute concentration dynamics during evaporation from porous media: Pore-scale processes near vapourization surface." *Physical Review* (81) (2010) 1 – 7.

- [31] Dewanckele, J. De Kock, T. Fronteau, G. Derluyn, H. Vontobel, P. Dierick, M. Van Hoorebek, L. Jacobs, P. and Cnudde, V. "Neutron radiography and X-ray computed tomography for quantifying weathering and water uptake processes inside porous limestone used as building material." *Materials Characterization* (88) (2014) 86 – 99.
- [32] Young, M. E. Urquhart, D. C. M. and Laing, R. A. "Maintenance and repair issues for stone cleaned sandstone and granite building façades." *Building and Environment* (38) (2003) 1125 – 1131.
- [33] McCabe, S. Smith, B. J. McAllister, J. J. Gomez-Heras, M. McAllister, D. Warke, P. A. Curran, J. M. and Basheer, A. M. "Changing climate, changing process: Implications for salt transportation and weathering within building sandstones in the UK." *Environmental Earth Sciences* (69) (2013) 1225 – 1235.
- [34] Main, I, Mair, K. Kwon, Ohmyoung. Elphick, S. and Ngwenya, B. "Experimental constraints on the mechanical and hydraulic properties of deformation bands in porous sandstones: a review" *Geological Society, London, Special Publications* (186) (2001) 43 – 63.

Paradoxical drying due to salt crystallization; the effect of ferrocyanide

L. Pel * and S. Gupta

Eindhoven University of Technology, Eindhoven, The Netherlands

* l.pel@tue.nl

Abstract

Salt damage of historical porous materials is mainly due to the crystallization of soluble salts due to drying. It is known that efflorescence changes the drying kinetics of porous media by changing the boundary conditions near material/air interface. In this study we focused on the influence of NaCl on the drying behavior. The results show that salt changes the drying process. At low relative humidities (RH ~ 0%), the drying rate of a brick saturated with NaCl solution is much lower than the drying rate of water saturated brick. Moreover, the presence of salt suppresses the development of a receding front. In this case homogenous drying of the material continues to very low saturation values. This is due to salt crystallization near the surface of the brick that causes blockage of the pores. This blockage reduces the evaporation rate at the surface. Increasing the relative humidity to 55% and 70% RH with the brick saturated with the salt solution leads to a paradoxical situation with evaporation rates greater than for 0% RH. The paradox is explained by the impact of the efflorescence microstructure on the evaporation rate, leading to the formation of a blocking crust for sufficiently high evaporation rates and non-blocking efflorescence for sufficiently low evaporation rates.

With the addition of ferrocyanide crystallization inhibitor at low relative humidity, due to its effect on crystal morphology, salt crystallizes as efflorescence and the saturation concentration was attained very slowly inside the brick; the fired-clay brick dries much faster than without inhibitor.

Keywords: NaCl, crystallization, drying, inhibitor, NMR

1 Introduction

Salt damage of historical porous materials is mainly due to the crystallization of soluble salts due to drying. Salt can enter a material along with moisture in various ways, such as capillary rise of groundwater, absorption of sea water and atmospheric pollution. Almost all water that enters porous materials will leave by evaporation or drying. Lewin [1] proposed that the location of salt crystallization is determined by a dynamic balance between the rate of escape of water at the surface (evaporation or drying) and the rate of supply of water to the surface. If salt crystallizes inside the material, i.e., the so-called sub-efflorescence, it can cause damage, whereas, if salts crystallize outside the material, also called efflorescence, it may appear non aesthetic but it is often not harmful for a material. The location of salt crystallization is in general determined by the competition of diffusive and advective fluxes. This can be characterized in terms of a Peclet number [2].

The drying behaviour of porous materials in the presence of salt is still a topic of discussion, especially with regard to the impact of salt crystallization on drying. By varying the mean pore size of the porous material, it has been shown that the crystallization of the salt at the porous material surface could either severely reduce the evaporation rate compared to pure water or have no impact at all [3]. Hence two main types of efflorescence can be identified, referred to as patchy (or non-blocking) and crusty (or blocking).

The aim of this work is to study the drying behaviour of porous materials saturated with a salt solution. In this study we will focus on NaCl as this is a common salt found in many salt related problems in situ. We will investigate to what extent this drying behavior resembles the standard drying behaviour of water saturated materials. To study this, we have used a specially designed Nuclear Magnetic Resonance (NMR) set-up with a static magnetic field of 0.78 T [4]. With this set-up we can measure non-destructively, quantitatively and simultaneously both the hydrogen and sodium profiles in fired-clay brick samples.

2 Materials and methods

2.1 Materials

The material used in this study was a fired-clay brick of a type typically found in the Netherlands. It has an average porosity (as measured by water immersion method) of $0.32 \text{ m}^3\text{m}^{-3}$, and a pore size distribution ranging from a few tens of nanometers to $100 \text{ }\mu\text{m}$ (with 80% of the total pore space corresponding to pores in the range $1\text{--}10 \text{ }\mu\text{m}$), as determined by MIP [5].

2.2 Methods

An extensive description of the NMR set-up can be found elsewhere [4, 5]. A schematic representation is given in Fig. 1. The tuned circuit can be toggled between 33 MHz for ^1H and 8.9 MHz for ^{23}Na , giving the possibility to quasi-simultaneously measure the H and Na content and thereby the concentration. For the echo time used in the experiment (viz., $TE=250 \text{ }\mu\text{s}$ for ^1H and $450 \text{ }\mu\text{s}$ for ^{23}Na), only the dissolved Na and H nuclei are measured and no signal is obtained from the nuclei incorporated in the crystals. The magnetic field gradient was chosen so that a slice of less than 2 mm is measured. The cylindrical samples of 20 mm in diameter and 40 mm in length were vacuum saturated with water and 3 m NaCl solution. These samples were sealed using Teflon tape on all sides except the top surface and placed in the NMR sample chamber. In this way a one-dimensional drying experiment can be performed. The samples were then exposed to dry air at a flow rate of 1 L/min. The relative humidity was varied from 0% to 70% at room temperature. The sample was moved in the vertical direction using a stepper motor to allow the measurement of moisture and sodium content throughout the sample length. Measuring one profile takes about 2.5 h. As the complete drying experiment takes in the order of a few days, small variations in the moisture and ion profiles during a single scan can be neglected. After each drying experiment was completed, the efflorescence formed on the top of the sample was collected and weighed.

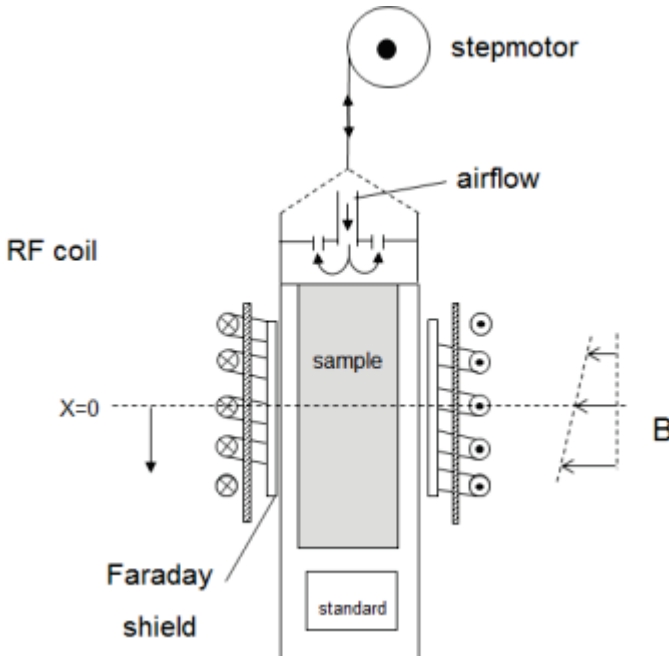


Figure 1: NMR set-up for measuring the moisture and Na-ion profiles during drying. The Teflon holder with the saturated sample is moved in the vertical direction by means of a stepmotor.

3 Results and discussion

3.1 Drying behaviour as studied by NMR

Initially, the drying behavior of fired-clay brick samples vacuum-saturated with water and salt solution (3 m NaCl) was studied. The samples were dried at 0% RH and 1 L/min air flow rate. Figure 2 shows the measured moisture profiles during drying of water- and solution-saturated samples, respectively [5, 6]. The recurrent irregularities in the profiles result from inhomogeneities of the sample, e.g., at 15 mm in case of the water-saturated sample.

In the case of a water-saturated sample, the first few profiles are almost horizontal, representing the first (externally limited) drying stage where liquid transport is dominant and the transport is limited by the evaporation at the surface. Afterwards, a drying front develops which recedes below the sample surface. This represents the second (internally limited) drying stage. As can be seen, the addition of salt changes the drying behavior of

the fired-clay brick significantly (Fig. 2). Two effects can be seen. First, the presence of NaCl reduces the drying rate compared to that of the water-saturated fired-clay brick. Complete drying of water-saturated fired-clay brick took about one day. In comparison, it took more than one week for a NaCl solution-saturated fired-clay brick of the same dimensions and at the same drying conditions. Secondly, the receding drying front vanishes and homogenous drying of the material continues till low saturation values. Hence, drying is prolonged and homogenous drying is maintained till low saturation values.

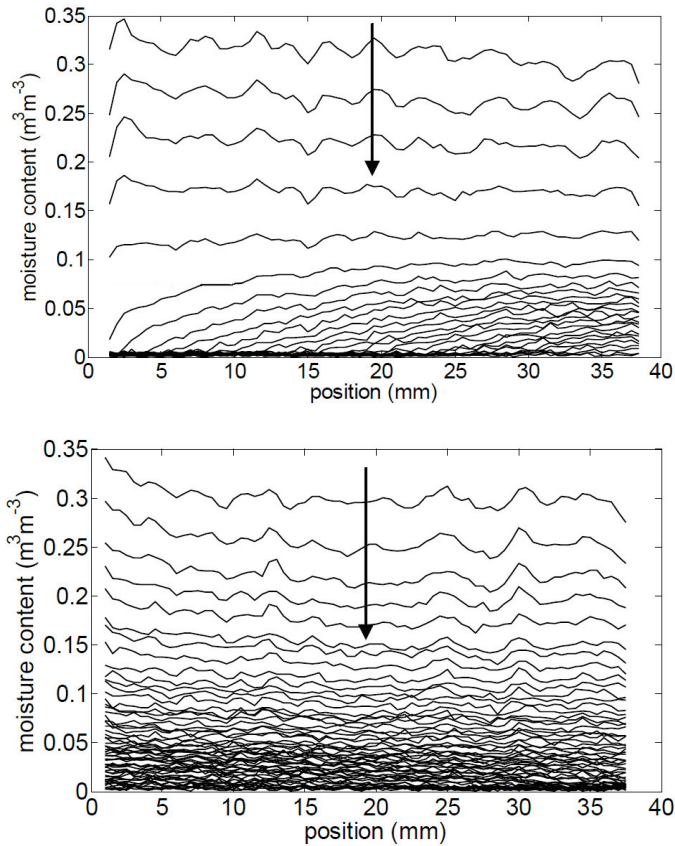


Figure 2: The measured moisture profiles for (top) water saturated and (bottom) 3M NaCl saturated fired-clay brick plotted as a function of position. The profiles are given for every 0.45 h for water and 2.26 h for salt saturated fired-clay brick. The samples were dried using dry air with a flow of 1 l/min and 0% RH. The drying surface is at 0 mm.

3.2 Drying curves

Since the evaporation rates are markedly different between the pure water experiment and the salt experiment, it is interesting to get more insight into the effect of evaporation rate on the drying process. To this end, experiments were also performed on both water- and solution-saturated fired-clay brick at high humidity conditions (viz., 55% and 70% RH) [5, 6]. In Fig. 3 we have plotted the normalized integrated hydrogen signal (S_H) as a function of time (t), i.e., the so-called drying curve. The integrated hydrogen signal at a given time represents the total amount of water in the fired-clay brick. As can be seen in Fig. 3, the drying rate of water-saturated bricks was slower at high relative humidity, which can be understood by considering that the moisture flux is proportional to the relative humidity difference. With increasing environmental humidity, the water vapor pressure in the surrounding air also increases. This decreases the humidity gradient between the air/material interface and the surrounding air and slows down the drying as is also observed.

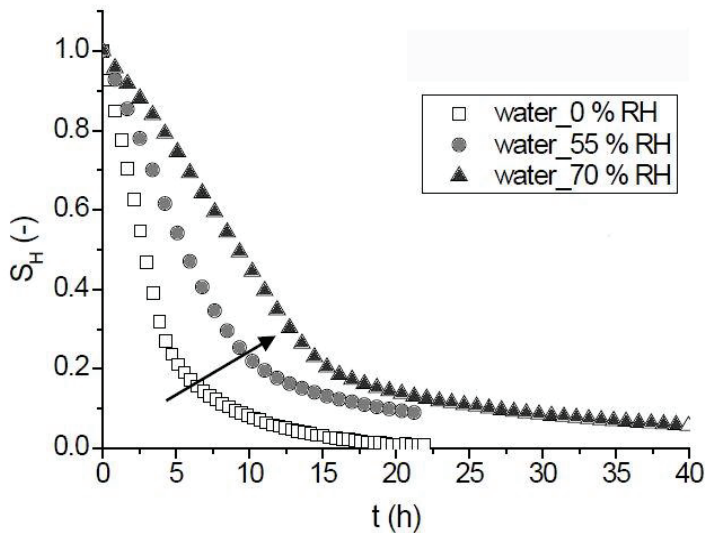


Figure 3: Normalized integrated hydrogen signal (S_H) as a function of time (t) for water saturated fired-clay bricks dried at different relative humidity conditions.

Fig. 4 shows the results for similar experiments using fired-clay bricks saturated with 3 m NaCl solution. The drying rate of solution-saturated bricks is lower than that of water-saturated bricks. After approximately 15 hours, the drying rate of the fired-clay brick dried at low humidity became even lower than that of the bricks dried at higher humidity. However, the

drying rate of bricks dried at 70% RH was lower than that of bricks dried at 55% RH. This leads to a paradoxical drying situation since the evaporation rate is greater for 55% RH and 70% RH than for 0% RH. At the end of the experiment, the efflorescence formed on the surface of the fired-clay brick was collected and weighed.

Pictures of the efflorescence formed on the surface of the materials are shown in Fig. 5. In the case of 0% RH, the efflorescence had the form of a very thin crust on the outer surface of the fired-clay brick and was strongly adhered to the substrate. It was not easy to remove the efflorescence from the substrate. At 0% RH, 6% - 7% of the NaCl crystallized as efflorescence. At 55% and 70% RH, a significant amount of NaCl crystallized as efflorescence, about 48% and 40%, respectively. The type of efflorescence formed at high humidities was rather fragile and was easy to remove from the substrate by rubbing. The efflorescence is clearly quite different at 0% RH compared to the efflorescence at 55% and 70% RH. Similarly as in Eloukabi et al. [3], this suggests distinguishing two types of efflorescence, referred to as “patchy” and “crusty” and that can be referred to as well as “non-blocking” and “blocking”. The efflorescence obtained at 0% RH is blocking and thereby slowing the moisture transport, whereas the efflorescence at 55% and 70% RH is non-blocking. This blocking of the pores will be a function of the pore-size distribution of the material [7].

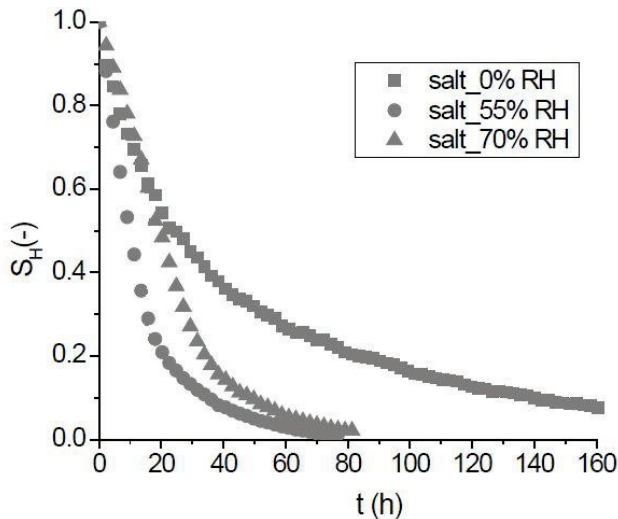


Figure 4: Normalized integrated hydrogen signal (S_H) as a function of time (t) for water saturated fired-clay bricks dried at different relative humidity conditions.

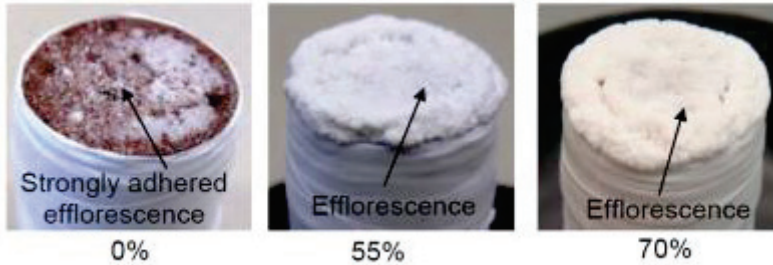


Figure 5: Pictures of the efflorescence formed at the end of drying experiment in the case of 3m NaCl saturated brick dried at 0%, 55% and 70% relative humidity. The amount of efflorescence increases at higher humidity.

This blocking efflorescence does not form suddenly, but progressively covers the porous medium surface. This is explained by the non-uniformity of the evaporation flux at the porous medium surface. As explained for instance in Eloukab et al. [3] and Veran-Tissoires et al. [8], efflorescence starts forming in the region of higher evaporation fluxes at the surface and then progressively colonizes the rest of the surface. Other factors, such as possible local spatial variations of porosity and/or permeability, especially in the top region of the sample, may also play a role in the localization and development of efflorescence [3]. Thus, the pore blockage essentially starts where the evaporation flux is the highest and next progressively develops over the rest of the surface of the material. The net effect is a progressive reduction of the surface left free for evaporation and consequently a continuous decrease of the flux with decreasing moisture content. At high humidities NaCl crystallizes as efflorescence, which is open and not transport limiting.

3.3 Influence of salt inhibitor

The use of crystallization inhibitors has been proposed as a potential preventive treatment method. In this study potassium hexa-cyanoferrate (II) tri-hydrate $K_4[Fe(CN)_6] \cdot 3H_2O$ was tested as a crystallization inhibitor. Here we will focus on the drying at 0% RH as this will result in subflorescence which can give much damage.

The drying curves for the samples saturated with 3M NaCl+ inhibitor solution dried at 0% RH are given in Fig. 6, where the normalized integrated hydrogen signal is plotted as a function of time. Based on our previous results [5], two concentrations of inhibitor were tested, i.e., 0.001 m and 0.01 m. For comparison, results for water and solution-saturated bricks dried at 0% RH are included in Fig. 6. Three main observations can be made. Firstly, in the presence of inhibitor the initial drying rates of

solution- and solution + inhibitor-saturated materials were similar. Secondly, after approx. 15 hours a dramatic decrease in the drying rate of the solution-saturated material without inhibitor was observed. However, in the presence of inhibitor at this time no drop in the drying rate was seen. Thirdly, in the presence of 0.01 m inhibitor after approx. 25 hours a dramatic decrease in drying rate occurred. No such drop in flux was seen in case of 0.001 m inhibitor.

The initial drying behavior of the systems with and without inhibitor was the same. This is caused by the fact that with the addition of inhibitor the equilibrium relative humidity of salt solution does not change. Therefore, the humidity gradient and hence the evaporative fluxes remain the same.

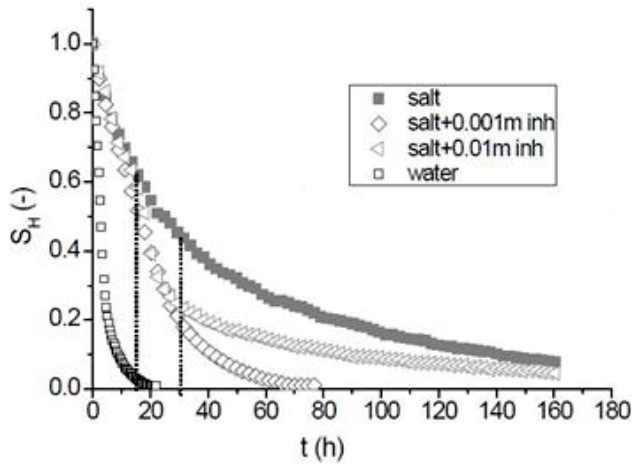


Figure 6: Normalized integrated hydrogen signal (S_H) as a function of time (t) for salt loaded bricks with and without inhibitor dried at 0% relative humidity



Figure 7: Pictures of the efflorescence formed at the end of drying experiment in case of solution-saturated brick dried at 0% RH in the absence (left) and the presence of 0.001 m (middle) and 0.01 m (right) inhibitor.

No drop in the drying rate was seen in the presence of inhibitor in contrast to what was observed in the absence of inhibitor. In the absence of inhibitor after approx. 15 hours, the saturation concentration was achieved in the top few mm of the sample. This causes a dramatic drop in the drying rate for salt saturated brick. Since most of the salt crystallized as sub-florescence, it causes a more severe blockage of the pores near the drying surface. However, in the presence of inhibitor, the crystal morphology changes from cubic to dendritic. The salt solution creeps along the branches of the dendrites and transports more and more dissolved salt ions towards the drying surface causing the efflorescence observed at the end of drying experiment. Pictures of the materials with efflorescence are shown in Fig. 7. Approximately 26% and 69% of the salt crystallized as efflorescence in the presence of 0.001 m and 0.01 m inhibitor respectively. Because of the formation of efflorescence in the presence of inhibitor, the average salt ion concentration inside the brick remained below saturation. Therefore, the system remained open and less blockage occurred compared to the solution-saturated system without inhibitor. Consequently, no dramatic drop in drying rate was seen. An extremely low drying rate was seen at later stages of drying ($t > 30\text{h}$) in the case of 0.01m inhibitor (see Fig. 6). This is attributed to drying out of the efflorescence at the end of the drying process.

4 Conclusions

Drying of a NaCl loaded fired-clay brick is faster at high humidity than at low humidity. This seeming paradoxical behavior is caused by the fact that at low humidity, moisture transport is dominant in the initial stage of drying process, so that ions quickly crystallize and form a crusty efflorescence that blocks the surface. At high humidity, salt crystallizes outside the material as patchy efflorescence. This prevents blockage of the pores, thereby keeping the system open to transport more and more salt outside the material. The addition of inhibitor was found to be useful at low humidity conditions. At low humidity, due to the crystal morphology in the presence of inhibitor, salt crystallizes as non-destructive efflorescence. This prevents a severe blockage, as was seen for solution-loaded material at low humidity.

This study helps to understand that the success of adding an inhibitor strongly depends on the local climate. The effect of inhibitor on the sheltered areas of a monument would be different from that on the areas exposed to sun and wind. Before using inhibitor in practice these aspects should be considered carefully.

References

- [1] S. Z. Lewin, The mechanism of masonry decay through crystallization. In Conservation of historic stone buildings and monuments. Washington, D.C., National Academy Press. (1982) 120–44.
- [2] H.P. Huinink, L. Pel and M.A.J. Michels, How ions distribute in a drying porous medium - A simple model, *Phys. Fluids* (14) (2002) 1389-1395.
- [3] H. Eloukabi, N. Sghaier, S. Nasrallah Ben and M. Prat, Experimental study of the effect of sodium chloride on drying of porous media: the crusty-patchy efflorescence transition, *Int. J. Heat Mass Transf.* (56) (2013) 80–93.
- [4] K. Kopinga and L. Pel, One dimensional scanning of moisture in porous materials with NMR, *Rev. Sci. Instrum.* (65) (1994) 3673-3681.
- [5] S. Gupta, Sodium chloride crystallization in drying porous media: influence of inhibitor, Ph.D. thesis, Eindhoven University of Technology, the Netherlands 2013
- [6] S. Gupta, H.P. Huinink, L. Pel, and K. Kopinga, How ferrocyanide influences NaCl crystallization under different humidity conditions, *Cryst. Growth Des.* (14) (2014) 1591–1599.
- [7] R.M. Espinosa-Marzal and G.W. Scherer, Impact of in-pore salt crystallization on transport properties, *Env. Earth Sci.* (69) (2013) 2657–2669.
- [8] S. Veran-Tissoires, M. Marcoux, M. Pratt, Salt crystallization at the surface of a heterogeneous porous medium, *Europhys. Lett.* (98) (2012) 1–6.

The effect of ferrocyanide ions on sodium chloride crystallization in salt mixtures as studied by NMR

L. Pel *¹, **S. Gupta**¹ and **M. Steiger**²

¹Eindhoven University of Technology, Eindhoven, The Netherlands

²Hamburg University, Hamburg, Germany

* l.pel@tue.nl

Abstract

The use of crystallization inhibitors such as ferrocyanide has been proposed as a potential preventive treatment against salt damage of historical monuments. It has been extensively tested for crystallization of single salts, where it has shown to be effective. However, in practice there are always mixtures of salts present. Therefore, before using inhibitors in practice, there is a strong need to explore their effect on salt mixtures. A main obstacle is the measurement of the individual salt concentration in a mix, which is necessary to determine the ternary phase diagram. We have developed a NMR setup in which we are able to measure quasi-simultaneously Na, Li and H, giving the possibility to measure both the Na and Li concentration. We have also incorporated a digital microscope, giving the possibility to perform time-lapse microscopy of the crystallization. This gives the possibility to connect the measured concentrations in a mixture with the visual point of crystallization. In this research, we studied the effect of ferrocyanide ions on NaCl crystallization as single salt and in a mixture with LiCl. A series of micro droplet drying experiments was undertaken. For a NaCl solution droplet, in the presence of the inhibitor, a significantly higher supersaturation, in the order of 10 M, prior to the onset of crystallization and a change in crystal morphology were observed. For the mixtures of NaCl - LiCl, the NaCl supersaturation was much lower in the presence of the inhibitor than for the single salt. However, a significant change in the crystal morphology was seen in the presence of inhibitor for these salt mixtures.

Keywords: salt mixture, crystallization, drying, inhibitor, NMR

1 Introduction

The use of crystallization inhibitors has been proposed as a potential preventive treatment against damage and is extensively tested for crystallization of single salts. However, in practice salt mixtures are present. To stop or reduce salt damage, preventive methods are required. In the past, intensive research has been carried out to test various protective treatments; however, all these tests have been performed on single salts, which are rarely found in practice, where always salt mixtures are present. The crystallization behavior of mixed salt systems is much more complicated than that of pure single salts. For instance, the crystallization of one salt from a mixture does not occur at a specific value of the relative humidity, but rather across a range of values [1]. The crystallization of salt mixtures occurs at lower humidities than expected for single salts [1]. Few studies have been carried out to understand the crystallization behavior of salt mixtures [1-3]. Linnow et al. have reported a study in which the complexity of the kinetic and thermodynamic properties of the salt mixtures is considered [1]. The authors investigated the crystallization sequence of complex salt mixtures using Raman microscopy and polarization microscopy. This work has been extended by De Clercq et al., who studied the crystallization behavior of this mixture in porous limestones [2].

Recently, the use of crystallization inhibitors has been proposed as a potential preventive treatment. These inhibitors are known to act either by preventing or by delaying the onset of nucleation and hence crystallization or by changing the crystal growth mechanism by adsorbing onto specific crystal faces. Ferrocyanide, $[\text{Fe}(\text{CN})_6]^{4-}$, is one of the most researched crystallization inhibitors against NaCl damage. For bulk solutions, an increase in NaCl supersaturation has been reported in the presence of ferrocyanide ions [4, 5]. If such a supersaturation can be sustained inside a porous material it can be dangerous for the material. However, recently it has been shown that no high supersaturation is generated inside building materials in the presence of ferrocyanide ions [4, 6]. Additionally, ferrocyanide ions promote the formation of non-destructive efflorescence on building materials [6]. However, to the best of our knowledge, no studies have been reported where the influence of ferrocyanide ions on salt mixture has been studied. The reason is the difficulty to measure simultaneously different types of ions during in-situ measurements. However, with the help of a specially designed NMR set-up, we are able to

measure H, Na and Li ions simultaneously during dynamic drying experiments. The concentration of dissolved salt ions can be calculated from the ratio of the Na / H content and the Li / H content. In this work, we focused on the effect of ferrocyanide ions on the drying and crystallization behavior of NaCl in mixtures with LiCl. All drying tests have been performed in salt solution droplets.

2 Experimental setup

In this study, a specially designed Nuclear Magnetic Resonance (NMR) set-up was used. NMR is used for carrying out non-destructive, quantitative and simultaneous measurements of hydrogen (H), sodium (Na) and lithium (Li) ions in the droplet. NMR is based on the principle that in a magnetic field, nuclei have a specific resonance frequency and can be excited by a radio frequency field. The resonance frequency f (Hz) depends linearly on the magnitude of the magnetic field:

$$f = \gamma/2\pi B_0 \quad (1)$$

where, $\gamma/2\pi$ (Hz T⁻¹) is the gyromagnetic ratio and B_0 (T) is the main magnetic field. The signal intensity (S) of a spin echo as used in the experiment is given by:

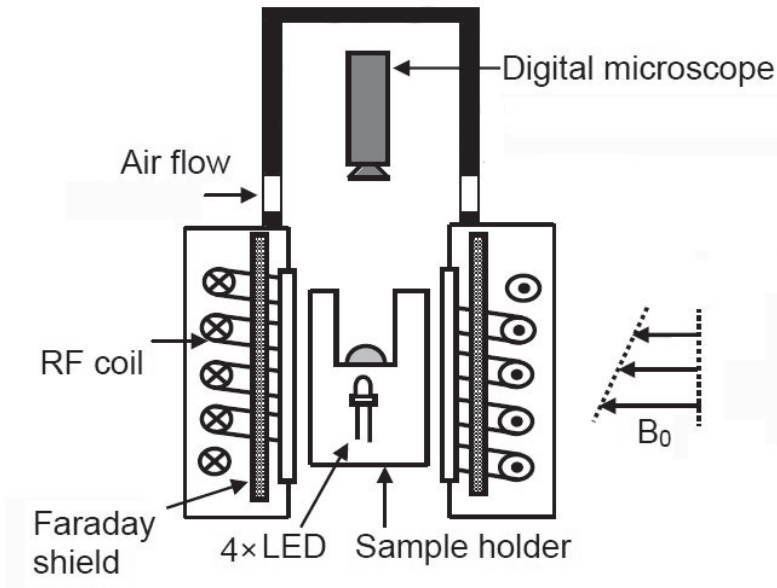
$$S = k \rho \exp(T_e/T_2)(1 - \exp(-T_r/T_1)) \quad (2)$$

where S is the signal intensity, k is the sensitivity of the nuclei relative to hydrogen, ρ is the density of the nuclei, T_r and T_1 are the repetition time of the pulse sequence and spin-lattice relaxation time, T_e and T_2 are the spin-echo time and spin-spin relaxation time. The gyromagnetic ratio ($\gamma/2\pi$), the magnitude of the nuclear spin (I), the relative NMR sensitivity, and the values of T_1 (spin-lattice relaxation time) and T_2 (spin-spin relaxation time) of the H, Na and Li nuclei are given in table 1.

Table 1: The gyromagnetic ratio, magnitude of the nuclear spin, relative NMR sensitivity, and T_1 and T_2 values for H, Na and Li nuclei.

Nucleus	^1H	^{23}Na	^7Li
Spin (I)	1/2	3/2	3/2
$\gamma/2\pi$ (MHz/T)	42.58	11.26	16.55
Relative sensitivity	1	0.093	0.29
T_1 (ms)	2670	75	2502
T_2 (ms)	2000	30	1793

Using NMR we can selectively measure just H, Li or Na. For the experiments presented in this chapter, a home-built NMR scanner with a static magnetic field of 0.78 T was used, which can quasi simultaneously measure both H, Na and H. A schematic diagram of the setup is given in Figure 1.

**Figure 1:** A schematic diagram of the NMR set-up for the droplet drying experiments. A 300 μL droplet of NaCl and NaCl-LiCl mixture was placed on the glass holder after which the drying was started.

An extensive description of this set-up can be found elsewhere [6, 7]. The signal is obtained only from the dissolved Na, Li and H nuclei, because the signal from the nuclei incorporated in the crystals decays too fast to be detected. To obtain a sufficient signal-to-noise ratio, 256 and 64 averages of the spin echo measurements are taken for sodium and lithium ions, respectively. The magnetic field gradient was chosen such that the whole droplet is covered in a measurement. To obtain visual information time-lapse microscopy of the crystallization was performed using a Dino-lite® digital microscope along with the NMR measurements. Using NMR, the average concentration (C_{avg}) is determined over the whole volume of the droplet. The drying was carried out at room temperature. A 300 μL salt solution droplet was placed on a cylindrical quartz sample holder and airflow of about 1 L min^{-1} was used to control the humidity in the Perspex chamber.

3 Results and discussion

3.1 Single salt solution of NaCl

In this study potassium hexa-cyanoferrate (II) tri-hydrate $\text{K}_4[\text{Fe}(\text{CN})_6] \cdot 3\text{H}_2\text{O}$ was tested as a crystallization inhibitor. First, the influence of ferrocyanide inhibitor on NaCl crystallization was studied. For this purpose, droplets of NaCl solution with and without inhibitor were dried inside the NMR set-up. Using NMR, the hydrogen and dissolved sodium content was measured and using the digital microscope, the onset of crystallization and crystal morphology were recorded. From the ratio of the Na and H content (Na / H), the NaCl concentration is calculated. We have studied the effect of various inhibitor concentrations on NaCl nucleation (supersaturation), crystal size and crystal morphology. For this purpose 0.0001 m, 0.001 m and 0.01 m inhibitor concentrations were tested. For the single salt, NaCl supersaturation can be calculated as $C_{\text{NaCl}} / C_{\text{NaCl},o}$, where C_{NaCl} is the measured NaCl concentration and $C_{\text{NaCl},o}$ is the saturation concentration of NaCl (6.14 m).

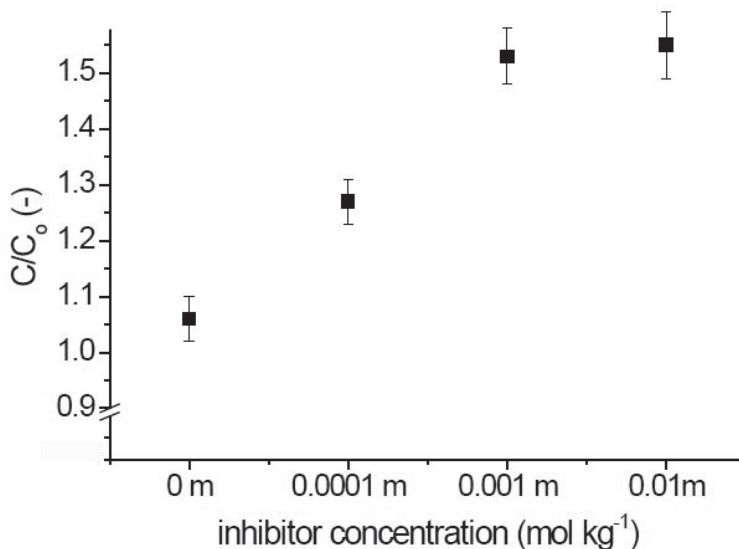


Figure 2: The supersaturation as measured using NMR plotted as a function of the concentration of the inhibitor used.

The results are shown in Figure 2, where supersaturation is plotted as a function of inhibitor concentration. For the droplet without inhibitor, the onset of crystallization was observed at a concentration of 6.3 ± 0.5 m, giving a supersaturation of 1.03 ± 0.08 . In the presence of inhibitor, the crystallization was observed at a concentration higher than the saturation concentration of NaCl; that is, the droplet supersaturates. The supersaturation increases with increasing inhibitor concentration. A maximum supersaturation of 1.55 is observed for 0.01 m inhibitor. These results clearly indicate that ferrocyanide ions act as a strong nucleation inhibitor for NaCl crystallization. The results are in line with other studies, where higher supersaturation in the presence of ferrocyanide ions was reported. The inhibiting action of ferrocyanide ions on NaCl crystallization can be caused by the fact that they can reduce the concentration of the available solvent, i.e., water, in the system, thereby increasing the relative supersaturation, and by adsorbing Na^+ ions they can interfere with ion transport towards more or less developed NaCl clusters with dimensions below the critical radius.

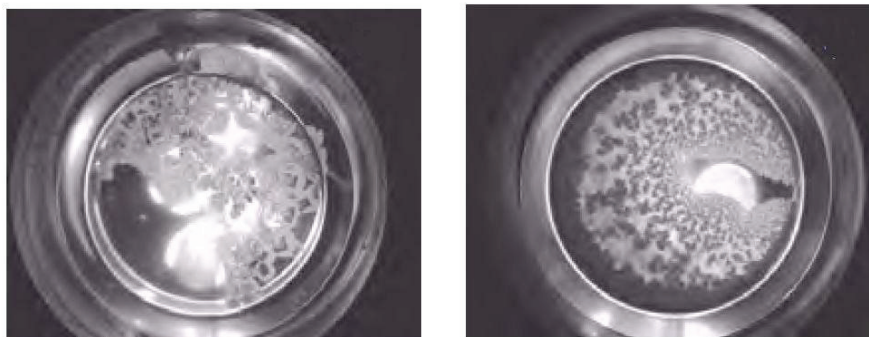


Figure 3: Images showing the crystal morphology at the end of a drying experiment: (left) with no inhibitor (right) with 0.01 M inhibitor

The digital microscope images in Figure 3 show that ferrocyanide also acts as a habit modifier for NaCl. In case of drying of a NaCl solution droplet without inhibitor, cubic crystals were seen growing at the liquid/air interface, whereas, in the presence of inhibitor dendritic crystals first form at the liquid/air interface. These crystals then spread very rapidly all over the substrate. Spreading of the crystals was more extensive at higher inhibitor concentration. The branches of dendritic crystals provide a pathway for spreading of solution over a much larger surface area. This phenomenon is commonly known as ‘salt creep’.

3.2 Salt mix of NaCl-LiCl-H₂O

In the case of salt mixtures having one ion in common (e.g. NaCl - KCl and NaCl – LiCl), due to an additional chlorine (Cl) from the second salt, supersaturation $S \neq C_{NaCl} / C_{NaCl,o}$. For a mixture of monovalent salts, e.g., NaCl - KCl, supersaturation is defined as, $S = [a / a_o]^{1/2}$, where, $a = C_{NaCl} (C_{NaCl} + C_{KCl})$ and $a_o = C_{NaCl,o} (C_{NaCl,o} + C_{KCl,o})$, where C_{NaCl} is the actual concentration of sodium chloride and C_{KCl} is that of potassium chloride. The index ‘o’ refers to the saturation concentration. The concentration (C) in this work is defined as the number of moles of salt dissolved in one kilogram of solvent (molality). In this study we have looked at a mixture of NaCl and LiCl, as we can measure simultaneously the H, Na and Li ions. From the concentrations of both the Na and Li ions, we can determine the exact location of the mixture in the phase diagram. This way, it was possible to check whether the equilibrium solubility line is followed after

the onset of crystallization. The ternary phase diagram of a NaCl-LiCl-H₂O mixture at 25 °C is given in Figure 4, where LiCl concentration is plotted as a function of NaCl concentration. The solubilities were calculated using the Pitzer electrolyte solution model [8]. The ion interaction model parameters for LiCl (aq) and NaCl - LiCl mixed solutions were obtained from experimental water activity data (LiCl) and solubilities in the ternary system at 25 °C [9]. The calculated solubilities in Figure 4, agree with available experimental data within the expected experimental uncertainty of $\pm 0.05 \text{ mol kg}^{-1}$. The solubility equilibrium line is shown by a solid black line. Everywhere on this line NaCl will crystallize and LiCl will precipitate only at very high concentrations (viz., 19.84 m LiCl and 0.03 m NaCl). As an example, the expected paths during evaporation of a solution are shown by the solid lines A, B and C for three different initial ion concentrations.

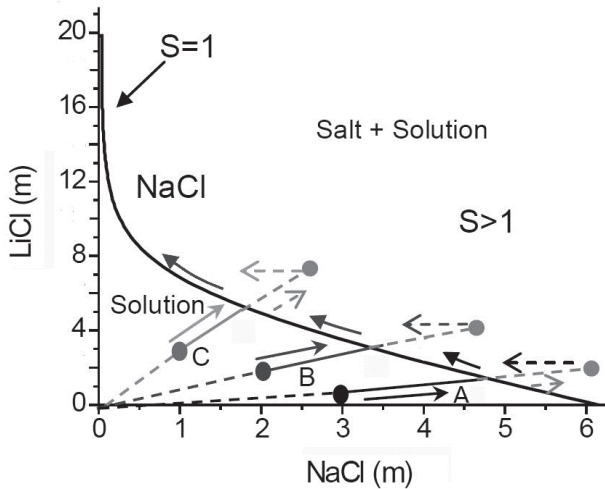


Figure 4: The ternary phase diagram of NaCl-LiCl-H₂O at 25°C. During evaporation the paths A, B and C will be followed for salt mixture of compositions 1 m NaCl - 3 m LiCl, 2 m NaCl - 2 m LiCl, and 3 m NaCl - 1 m LiCl, respectively. If no crystal appears at the intersection of path A, B, C and the equilibrium line ($S = 1$), the concentration will keep on increasing (supersaturation), as indicated by dashed lines. After crystallization the system will return to the equilibrium solubility line.

Initially, the influence of inhibitor was tested on LiCl only. These results indicated that ferrocyanide ions have no influence on LiCl nucleation and crystal morphology. Next, the influence of inhibitor was tested on a mixture of NaCl - LiCl. Three different salt concentrations were tested: 3 m NaCl -

1 m LiCl, 2 m NaCl - 2 m LiCl, and 1 m NaCl - 3 m LiCl. For all these experiments, 0.01 m inhibitor concentration was used. The results are shown in Figure 5. The solid lines are the expected paths to be followed upon drying of the droplet. As can be seen from the figure, the experimental data points coincide very well with the expected paths. The salt concentration first increases to the equilibrium line. At this point a salt crystal appears, as was confirmed from the pictures taken by the digital microscope. After the onset of crystallization the concentration of NaCl decreases and the equilibrium solubility line is followed, as shown by dotted arrows. These results show that multi-nuclear NMR is a powerful experimental tool to validate the phase diagrams.

For the mixture of NaCl - LiCl, no significant NaCl supersaturation was observed in the presence of inhibitor. These results indicate that in the presence of another salt, ferrocyanide ions are not able to supersaturate NaCl as highly as was seen in case of single salt. A higher supersaturation means a higher crystallization pressure; however, it must be kept in mind that calculating the crystallization pressure assuming ideal behavior can lead to significant errors. This is because the intermolecular interactions between liquids cannot be simply neglected. For example, in case of NaCl, for a given value of supersaturation e.g., 1.2, assuming ideal behavior the calculated value of $P_c = 33.45$ MPa (calculated using eq. $P_c = \nu RT/V_m \ln S$, $C_{NaCl,o}$ is 6.14 mol kg^{-1} at 298.15 K, $\nu = 2$ for NaCl, $V_m = 27.02 \text{ cm}^3 \text{ mol}^{-1}$). However, including non-ideal behavior, the calculated value of crystallization pressure (P_c) = 59.14 MPa, which is approx. 1.76 times higher than the one calculated assuming ideal behavior. A clear habit modification was also seen in the presence of inhibitor. The photos in Figure 6 show that more spreading occurred and dendritic crystals were formed in the presence of inhibitor.

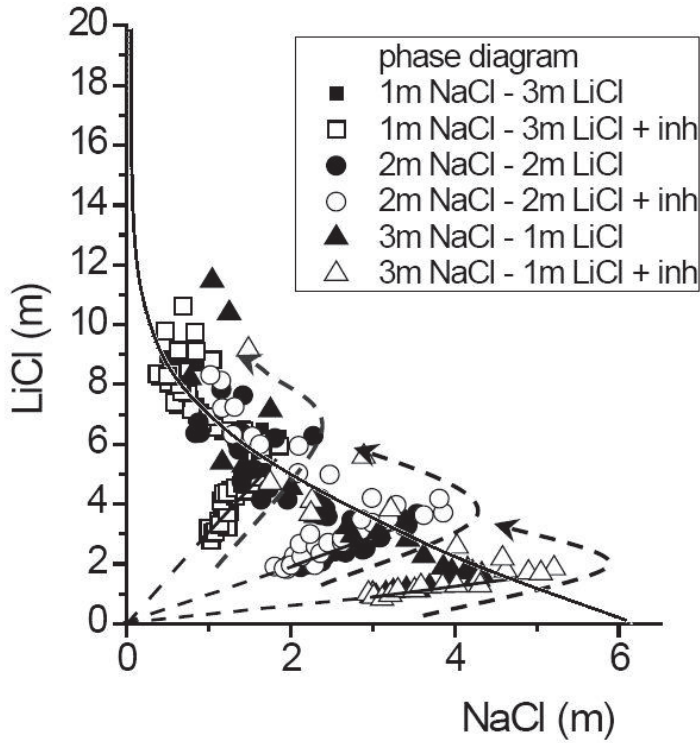


Figure 5: The three tested concentrations of NaCl - LiCl mixtures shown in the ternary phase diagram of the NaCl - LiCl - H₂O system. The open symbols denote salt mixtures with inhibitor and the closed symbols denote salt mixtures without inhibitor. The solid lines show the expected pathways to be followed before the equilibrium line is reached.

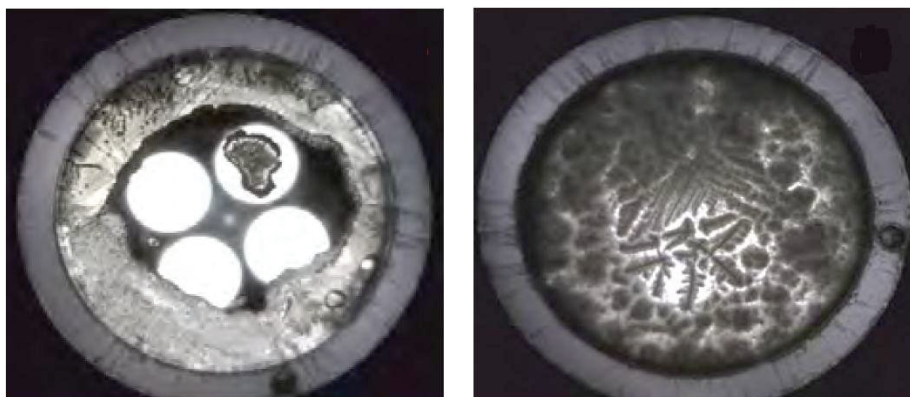


Figure 6: Images showing the crystal morphology at the end of a NaCl-LiCl drying experiment: (left) with no inhibitor (right) with 0.01 M inhibitor.

4 Conclusions

The results show that ferrocyanide ions act as a strong nucleation inhibitor for NaCl when it is the only salt present. A significant higher NaCl supersaturation was observed in the presence of inhibitor and the supersaturation increases with increasing inhibitor concentration. For salt mixtures, it is found that the inhibitor will result in a lower supersaturation than that of the single salt. For both single salt and salt mixtures, the crystal morphology changes completely from bigger cubic crystals to dendritic crystals in the presence of inhibitor. The crystal size decreases significantly at high inhibitor concentrations.

This dendritic crystal morphology with immense spreading is seen for all the cases. In a porous material, this morphology can promote the formation of efflorescence that causes only little structural damage. The crystals formed in the presence of inhibitor were more powdery and fluffy and were easy to remove from the substrate. Consequently, the ferrocyanide ions may be beneficial for building materials that are contaminated with a salt mixture. Moreover, as the solution does not highly supersaturate in the presence of inhibitor, the risk of damage will be reduced.

References

- [1] K. Linnow, M. Steiger, C. Lemster, H. De Clercq and M. Jovanović, In-situ Raman observation of the crystallization in $\text{NaNO}_3\text{-Na}_2\text{SO}_4\text{-H}_2\text{O}$ solution droplets, *Environ. Earth Sci.* (69) (2012), 1609–1620.
- [2] H. De Clercq, M. Jovanović., K. Linnow and M. Steiger. (2012): Performance of limestones laden with $\text{Na}_2\text{SO}_4\text{-NaNO}_3$ and $\text{Na}_2\text{SO}_4\text{-K}_2\text{SO}_4$ mixtures, *Environ. Earth Sci.* (69) (2012), 1751–1761.
- [3] C. Cardell, D. Benavente and J. Rodríguez-Gordillo, Weathering of limestone building material by mixed sulfate solutions. Characterization of stone microstructure, reaction products and decay forms, *J. Mater Charact* (59) (2008), 1371–1385.
- [4] S. Gupta, K. Terheiden, L. Pel, and A. Sawdy, Influence of ferrocyanide inhibitors on the transport and crystallization processes of sodium chloride in porous building materials, *Crystal Growth and Design* (12) (2012), 3888-3898.
- [5] C. Rodriguez-Navarro, L. Linares-Fernandez, E. Doehne and E. Sebastian, Effects of ferrocyanide ions on NaCl crystallization in porous stone, *J Cryst Growth* (243) (2002), 503–516.
- [6] S. Gupta, Sodium chloride crystallization in drying porous media: influence of inhibitor, Ph.D. thesis, Eindhoven University of Technology, the Netherlands 2013.
- [7] K. Kopinga and L. Pel, One dimensional scanning of moisture in porous materials with NMR, *Rev. Sci. Instrum.* (65) (1994), 3673-3681.
- [8] M. Steiger, J. Kiekbusch, A. Nicolai, An improved model incorporating Pitzer's equations for calculation of thermodynamic properties of pore solutions implemented into an efficient program code, *Construction and Building Materials* (22) (2008) 1841-1850
- [9] M. Steiger, private communication (2013)

Investigating a method to limit damage in Globigerina Limestone, a soft porous stone widely used in historic buildings

S. Sammut^{1*}, J. Cassar¹, A. Marrocchi², C. Russo², L. Sommei² and M.L. Santarelli³

¹Department of the Built Heritage, Faculty for the Built Environment, University of Malta, Malta

²Department of Chemistry, Biology and Biotechnology, Università degli Studi di Perugia, Perugia, Italy

³Centro di Ricerca in Scienza e Tecnica per la Conservazione del Patrimonio Storico-Architettonico, Università di Roma La Sapienza, Rome, Italy

*svetlana.sammut.00@um.edu.mt

Abstract

A programme of studies is ongoing to investigate the action of environmentally-friendly functionalized polycarboxylates as organic crystallization modifiers on salts on two types of Globigerina Limestone of Malta, to compare their action and behaviour. This was mainly done to verify the potential of such compounds to control, and therefore, limit damage on this locally unexplored territory. The main thrust of the research, at this stage, was to observe modifications to solution transport and salt crystal growth induced in two varieties of the stone by treating under controlled laboratory conditions; work under uncontrolled conditions has also commenced, but will not be discussed here. In this paper, indications of the modifications obtained are discussed, in the context of former trials, the fact that they are still under investigation and with a view on way forward. A discussion establishing a classification for damage limitation is postulated.

Keywords: Globigerina Limestone conservation, salt damage, crystallization modifiers

1 Research aims

Research relating to the conservation of the built heritage, and in particular, behaviour of materials, stone conservation practices and possible environmental effects, has acquired great importance, also in Malta. The unsuitability of currently available treatments for conservation was often only understood following their application, in turn encouraging a generation of new research for the development of new materials and procedures, also with respect to salt weathering [1, 2].

As one of the most common causes of deterioration, salt damage in porous materials remains not yet fully understood, and hence has been the subject of study by many authors (examples are [3-8]). The crystal pressure against pore walls and volumetric changes during the growth of crystals during de/hydration and crystallization cycles under variable environmental conditions, are amongst the most investigated modes of damage for porous materials [1, 4, 9].

It is in this context of an incomplete understanding of damage, as well as the ever-present water (containing soluble salts) in porous building materials in the built heritage, that studies which directly target salt damage within porous building materials, are being undertaken.

The main aim of the research has been to observe, and compare, modifications to salt crystal growth induced in two varieties of Globigerina Limestone by the application of crystallization modifiers. This was done with a focus on the potential of such compounds to control, and therefore, limit damage. This study on this locally unexplored territory, has primarily focused on the damaging action of sodium sulphate, as one of the most damaging salt types [9-12], but also on sodium chloride, sodium nitrate and binary mixtures of the first two.

In this paper, the results obtained using this still experimental method of limiting salt damage on local stone are outlined. Indications on any effect on deterioration and changes to the crystallization habit of contaminant salts, following the application of salt crystallization modifying products on the stone systems, have also been visually and microscopically observed. The way forward is also anticipated.

2 The materials

The Globigerina Limestone under study originates from the geological sequence of the Maltese Islands consisting of four major and one minor sedimentary formations [13]. This archipelago, lies in the middle of the Mediterranean Sea, between Sicily and North Africa and is limited to circa 316 square kilometres. The Globigerina formation has been the primary building stone used for construction, for well over 5000 years [14]. It primarily consists of high purity calcite (>92%) with a fine grain and contains trace amounts of other minerals [15-17]. The porosity is very high

and can be up to 40% [12]. Its colour is mainly cream, with occasional inclusions of hard shell fragments, bioturbation and other variations in an otherwise generally homogenous matrix.

There are two basic classifications (by quarry owners) of this stone, namely the *franka* (freestone) 'good quality' and 'bad quality' *soll*, which generally lie at the extreme ends of the different 'grades' of this natural material. The latter type is generally less resistant when exposed to weathering, generally varying in geochemical and mineralogical composition and having a lower overall porosity with a higher degree of small pores [12, 15, 18-20]. The pores of *franka* are both inter- and intra-granular, with fossil chambers generally empty, while those of *soll* pores are mainly inter-granular, with parts of the fossil chambers often lacking voids [15]. The different stone types can hardly be distinguished visually on fresh material; however, the difference becomes evident on exposed surfaces showing different weathering patterns.

The *franka* can be further sub-classified, namely, the *bajda* (whitish) and *safra* (pale yellow variety). This paper only presents data relating to *bajda*. Studies on *safra*¹ are ongoing and are not reported in this paper. All types of stones have been identified by the respective quarry owners at this stage of the study, based on their experience in their own quarry.

2.1 General material physical properties

The porosity of Globigerina Limestone can reach values up to 40%, depending on location/depth, however, it generally varies between 24 and 37% [21]. The total porosity of the *Bajda* variety used in this research is 37% [22]. Pore radii lie in the range 0.001-6 μm , with smaller pore sizes not being detectable.

With respect to pore size distribution, the major part of pores (about 70%) has a size $>1\mu\text{m}$. The remaining pore volume corresponds mainly to smaller pores. On the other hand, the proportion of small pore sizes for *soll* generally lies in a 40% range, with a much higher proportion of smaller (less than $1\mu\text{m}$) pores, of the order of 60% [20, 22].

2.2 The crystallization modifiers

The types of modifiers selected for this study are functionalized polycarboxylates, as part of a broader research project on a range of materials, on different porous materials [12, 23-27]. To date, the use of these compounds has resulted in positive effects in inhibiting salt

¹ Results on *safra* are consistently similar to those of *bajda*, both in terms of physical properties, as well as those obtained to date with crystallization inhibitors (Cassar et al. 2008)

crystallization. Citrate ($C_6H_8O_7^{3-}$) and phosphocitrate ($C_6H_8PO_7^{5-}$), hereinafter referred to as CA and PCA respectively, are the principal systems used in conjunction with porous materials contaminated with sodium sulphate (Na_2SO_4), sodium chloride (NaCl), sodium nitrate ($NaNO_3$), and binary mixtures of the first two, in these tests.

Both modifying compounds were applied at very low concentrations, between 1 and 100 ppm, for reasons of their application on calcite, but possible because of the positive chemical affinity between the molecule structures in the system, enabling an interaction with the mineral surface even when present in trace amounts. Previous studies have shown that a concentration between 1 and 10 seems the most effective to induce crystallization inhibition [12, 22-27].

The pH of the solution ranges between 6 and 7.

Salt concentrations were kept to realistic levels of 0.35M, which, in comparison to most reported experiments in literature, are quite low; consequently, dramatic results as reported elsewhere [3, 28-30] were not obtained. Here, an incremental approach has been designed.

3 Experimental section

Sodium sulphate, with the addition of sodium chloride and sodium nitrate, was applied in simple and binary mixtures (binary mixtures were only used with the former two salts), in conjunction with treatments with salt crystallization modifying compounds, in three concentrations.

The development of the initial tests with sodium sulphate, particularly in binary mixtures, aimed at giving indications on the possible action of these modifiers in more complex, closer to in-situ situations, where the presence of different types of salts is ubiquitous.

Solution transport behaviour, general macro scale crystallization patterns/efflorescences and modifications to surface morphology of the stone, indicating salt crystallization damage, have been studied, in conjunction with microscopy. Other observations such as quantity of material disaggregation and efflorescence formation have also been noted.

3.1 Methodology

The work carried out to date was performed under controlled laboratory conditions. A methodology explored here is related to the treatment on sound stone, followed by a salt contamination, and related to the one on salt contaminated stone, so as to analyse any differences consequent to the alteration of the sequence in the modes of application/contamination. Such a sequence also enabled observation of any possible effects on sound stone.

The test combinations undertaken are outlined in Table 1 which indicates treatment/contaminant types, as well as environmental conditions.

Tests A02 and A05 relate to samples first contaminated with salts followed by a treatment. The application method of the modifiers in A03 was then changed to the brush type, but also introduced that of the poultice application of the crystallization inhibitor treatment.² The aim of these modifications in the test routines was the creation of a 'model' which is more realistic, in terms of any eventual in-situ application. Repeat sets of tests were also performed to confirm previous obtained results.

3.1.1 Crystallization tests

Two basic methods were adopted for the crystallization/drying tests. Sound cubes, initially 5x5x12.5cm, then reduced to 2.5x2.5x12.5cm (to manage more samples), were used. These stones were cleaned and dried to constant weight and then either:

1. treated with the modifiers in question, using either capillarity, brush or paper pulp application, followed by drying to constant weight and then contamination with the respective salt solution via capillarity in both controlled and uncontrolled laboratory conditions (the latter conditions in a closed room with a ceiling mounted extraction facility provided variations in relative humidity by circa $\pm 15\%RH$ and at times also up to $20\%RH$), or
2. contaminated with the saline solution, dried to constant weight and cleaned to remove efflorescence deposit, followed by treatment with modifying compounds in solution in both controlled and uncontrolled laboratory conditions.

Following the above procedures, a set up similar to that described elsewhere in literature [12] with sealed containers to promote capillary rise through the specimens, was adopted. The evaporative weight loss was measured and plotted in relation to the exposed surface area of sample to extrapolate a direct relationship. In all tests, a minimum of three samples was used per treatment type, with the equivalent control/blank samples.

The initial drying/crystallization tests were carried out with sodium sulphate, considering that this particular salt has proved to be the most damaging under laboratory controlled conditions [9-12]. Further tests and observations were then carried out with sodium chloride and sodium nitrate. Controlled conditions for the tests, including the single salts and binary mixtures, were those carried out at 20 and 23°C and an established

² This type of application was preferred over the partial immersion method, since it is more applicable to the in-situ situations.

50% relative humidity in a climatic chamber³ (Weiss Technik Sr. no.:201982-8-0001).

The formation of efflorescences and eventual limestone damage, were photographically recorded for all samples and the debris weighed to obtain the amount of material loss and efflorescence formation on the samples. The crystal formation and damage were viewed by optical (Nikon Microscope Optiphot – 100 in conjunction with Leica Digital camera DFC290) and digital microscopy (Dino-Lite Pro series AD413T). Elemental analyses of the samples were also performed using a Scanning Electron Microscope (SEM) Merlin FE-SEM by Carl Zeiss with enhanced Gemini II column in conjunction with EDS Edax having an SDD Apollo X detector, for blanks and samples showing the most positive results in terms of increase in evaporative water loss.

³ It must be noted that the controlled conditions in the climatic chamber are maintained by the operation of a rotating blade at the back of the chamber, thus increasing air flow around the samples and influencing evaporation rate. This has been noted to lead to the formation of efflorescences at a faster rate than in ambient, lower air velocity conditions, irrespective of the humidity levels.

Table 1: Actual comprehensive list of drying tests. A01-A04 and (part of) A05, B01, B03, C01 & C03 were carried out in controlled conditions, whereas (part of) A05, B02, B04, C02 & C04 in uncontrolled laboratory conditions

Test ref.	Stone type	Treatment type		Contaminant salt			Conditions		Application method		
		CA (ppm)	PCA (ppm)	Na ₂ SO ₄	NaCl	NaNO ₃	Ambient Av. Temp(°C)/RH(%)	Controlled	Capillary	Brush	Paper pulp
A01	bajda, soll	1	10	0.17M				23/50	✓		
A02*	bajda	1	10	0.35M				20/50	✓	✓	
A03	bajda, soll	1	10	0.35M				20/50		✓	✓
A04	bajda, soll	10	100	0.35M				20/50		✓	✓
A05*	bajda	10	100	0.35M			20/70			✓	✓
B01	soll	1	10		0.35M	0.35M		20/50		✓	✓
B02	soll	1	10		0.35M	0.35M	24/50			✓	✓
B03	bajda	1	10		0.35M	0.35M		20/50		✓	✓
B04	bajda	1	10		0.35M	0.35M	20/60			✓	✓
C01	soll	10	100	0.35M (1:1 & 1:2)				20/50		✓	✓
C02	soll	10	100	0.35M (1:1 & 1:2)			17/70			✓	✓
C03	bajda	10	100	0.35M (1:1 & 1:2)				20/50		✓	✓
C04	bajda	10	100	0.35M (1:1 & 1:2)			20/70			✓	✓

*Contamination followed by treatment was applied in these tests, otherwise, treatment, followed by contamination with saline solution of the types was adopted.

Specific areas studied were those in the upper 8mm, produced by chipping pieces (with a chisel and hammer) from the 'crust'. This zone appeared most affected by salt accumulation towards mid-height of the exposed part of the cubes (circa 3cm from the upper surface). No grinding was carried out so as to limit modifications incurred to the stone sample following such an operation.

4 Results

4.1 Crystallization tests

The initial results obtained for the two varieties of stone, utilizing various application methods indicated, included those for treatment by partial immersion, by brush and via paper pulp. These methods generally indicated a positive tendency of increase in evaporative water loss in the presence of the crystallization modifiers under study (Fig. 1). In general, the use of higher concentrations of CA, as well as the highest concentration of PCA (10 ppm) gave the most positive results, especially on the 'weaker' *soil* stone variety. This means that the crystallization modifiers used tend to influence the rate of transport of saline solutions within Globigerina Limestone, which is being taken as a sign of the effectiveness of the treatment. These compounds generally act as crystallization inhibitors, particularly in the first days following the application of treatment.

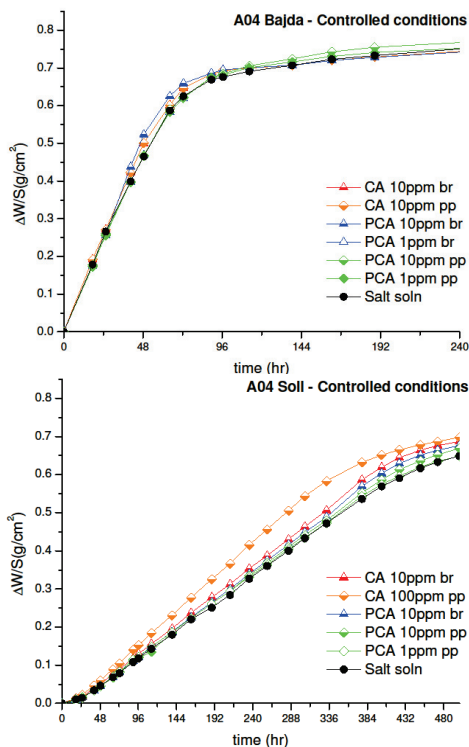


Figure 1: Evaporative weight loss results - Test run A04 using 0.35M Na₂SO₄, on both *bajda* and *soll*

4.1.1 Observations on the effect of the treatment compounds

The effects of the treatment, which varied widely, appear to primarily depend on the material type, but also on the treatment/contamination sequence, the salt type and environmental conditions, confirming observations by other studies [28, 31], whereas they appear to be less dependent on the mode of application of modifying products, as well as the presence or otherwise of a phosphate group in the inhibitor skeleton (over 450 samples have been tested under controlled conditions).

In the *bajda* type, an improved inhibiting effect of CA over PCA is observed in most conditions. Nevertheless, no particular pronounced efficacy was observed with varying mode of application. In the *soll* type, the presence of both CA and PCA indicates inhibiting properties, but, again, without a significant influence with respect to the application method.

It was also noticed that the most pronounced differences observed in evaporation graphs relate to those treated prior to contamination. In this case the drying is delayed; besides a generally reduced distinction between treated and reference samples is observed. This effect is probably due to precipitated salt crystals occluding pores.

The quantity of material disaggregation and efflorescence formation have also been measured, however, the differences obtained in various conditions were too small to draw conclusions, mainly as a consequence of the limited size of sample being used, unlike results reported in [12]. Table 2 (below) summarizes the results obtained so far.

Table 2: Summary of results relating to tests carried out with pure sodium sulphate under controlled conditions

Observations	<i>Bajda</i>	<i>Soll</i>	Remarks
General variance of enhancement in evaporative water loss within executed tests	Distinction between modes of application ranges from: insignificant to 0.2g/sqcm	Distinction between modes of application ranges from: 0.1 to 0.3g/sqcm	<i>Soll</i> exhibits a wider variability, possibly due to composition/pore size distribution
Influence of salt type – macroscopic and evaporative weight loss observations	Primarily filamental strands over exposed part of samples, 'extending' pore structure. This layer eventually crumbles to a powder	Primarily filamental strands, 'extending' pore structure, eventually crumbles to powder in the lowest exposed part of the sample	- Enhancement in evaporation rate is more pronounced with single salt types. - A variance in formation of efflorescence type could be observed macroscopically, with <i>bajda</i> , more readily allowing solution flow, reflecting prevalent larger pore size
Damage to stone	Surface damage generally limited to light superficial disaggregation, sometimes, more pronounced in the corners of the cuboid samples.	Concentrated in lower (exposed) parts of samples. Most pronounced with pure Na ₂ SO ₄ & results in 'peeling/lifting' effect of outer layer exposing a weaker disaggregated surface. Horizontal splits of base of stone observed.	- Damage mainly limited to specific exposed parts. - Appears to be heavily dependant on salt type, other than treatment. - Varies widely between the two stones tested - Least damage observed with salt mixtures.

4.1.2 Crystal morphological changes

Observations to date on representative stone samples⁴, were carried out by optical and digital microscopy⁵ but more importantly SEM, particularly on those samples showing a highly enhanced evaporation rate. Modifications in crystallization patterns and habits, in comparison with unconfined crystal formation have been noted. Crystal morphology generally appears to be far from the regular habit, especially in the presence of inhibitors. Indications are that crystals are more skeletal (especially for NaCl), with prevalent preferential development of specific faces.

A comprehensive SEM investigation of the tested samples to confirm these positive indications are planned, particularly for comparison with untreated, but salt-laden samples. This information shall be studied in the context of interpreting any changes vis-à-vis the modification solution transport and eventually contributing to data for building a mathematical model to understand the trends of action of crystallisation modifiers in question. The latter is deemed to be essential considering the heterogeneity of these natural materials, which broadens the scope in establishing a model of action.

5 Discussion and conclusions

The actual results obtained using the local stone, Globigerina Limestone, both 'good' and 'bad' qualities, confirm the need for the further deepening of the study of the action of the crystallization modifiers as inhibitors, particularly with respect to modification of evaporation rate as well as crystal habit modification.

The following observations and conclusions can be made at this point:

- The most significant modification of evaporation rate is observed in the initial period of the test, particularly when the solution within the pores is uninterrupted;
- The action of the inhibitors is very much dependent on the substrate type, but also on the solution composition and environmental factors, especially relative humidity levels which

⁴ Chippings from the outer 8mm of the stone cuboids were analysed.

⁵ Difficulties obtaining a clear image at various depths of the stone have been experienced, due to the limited aperture variation of available equipment (Nikon Microscope Optiphot – 100 in conjunction with Leica Digital camera DFC290). Such observations merit further investigations to obtain a better picture of changes; these will be reported in future.

appear to influence evaporation rate, but more importantly efflorescence patterns;

- Given the range of tests carried out, it can be concluded that a precise mode of action cannot be pre-determined, mainly due to the nature of the substrate, which in this case, is a heterogeneous natural material. Other variables come into play when dealing with such situations, particularly the more complex salt/environmental conditions in-situ type. A larger sample set is therefore recommended at this stage in conjunction with further analysis, also using statistical tools such as Cluster Analysis and Principal Component Analysis to identify trends.
- The application methods tested are also considered to limit the damage incurred to replacement fresh stone in the context of the presence of salts in existing structures.

References

- [1] Rodriguez-Navarro, C., Doehne, E. & Sebastian, E. Influencing crystallization damage in porous materials through the use of surfactants: experimental results using sodium dodecyl sulfate and cetyldimethylbenzylammonium chloride. *Langmuir*, (16), (2000) 947–954.
- [2] Price, C. A., Doehne, E. *Stone Conservation – An Overview of Current Research*. The Getty Conservation Institute, Los Angeles, California (2010).
- [3] Rodriguez-Navarro, C. & Doehne, E. Salt weathering: influence of evaporation rate, supersaturation and crystallization pattern. *Earth Surf Processes Landforms* (24), (1999) 191–209.
- [4] Scherer, G. W., Flatt R. & Wheeler, G.. *Materials Science Research for Conservation of Sculpture and Monuments*. *MRS Bulletin*, (2001), 44–50.
- [5] Flatt, R.J., Salt damage in porous materials: How high supersaturations are generated. *Journal of Crystal Growth*, (242), (2002) 435–454.
- [6] Sawdy, A., Heritage, A., Pel, L., A review of salt transport in porous media, assessment methods and salt reduction treatments. In: Ottosen, L. M.; Rørig-Dalgaard, I.; Larsen, P. K.; Brajer, I.; Bøllingtoft, P.; Marciniak, M.; Svane, M. (eds.): *Salt Weathering on Buildings and Stone Sculptures*, Proceedings from the Int. Conf. 22–

- 24 (October 2008), National Museum Copenhagen, Denmark, Technical University of Denmark, Lyngby (2008) 1-28.
- [7] Espinosa-Marzal, R.M. & Scherer, G.W., Advances in understanding Damage by Salt Crystallization. *Accounts of Chemical Research*, 2010, 43 (6), (2010 a) 897–905.
- [8] Espinosa-Marzal, R.M. & Scherer, G.W. Mechanisms of Damage by Salt. In: *Limestone in the Built Environment: Present-Day Challenges for the Preservation of the Past - Geological Society Special Publications* (2010 b).
- [9] Shahidzadeh-Bonn, N., Desarnaud, J., Bertrand, F., Chateau X, & Bonn D. Damage in porous media due to salt crystallization, *Physical Review E*, (81), (2010) 066110.
- [10] Charola, A. E. Salts in the deterioration of porous materials: an overview. *Journal of the American Institute for Conservation*, (39-3), (2000) 327–343.
- [11] Doehne, E., Salt weathering: a selective review In: *Natural Stone, Weathering Phenomena, Conservation Strategies and Case Studies*: Edited by S. Siegesmund, T. Weiss and A. Vollbrecht - Geological Society of London (2002).
- [12] Cassar, J., Marrocchi, A., Santarelli, M. L. & Muscat, M. Controlling crystallization damage by the use of salt inhibitors on Malta's limestone. *Materiales de Construcción*. (58) 289–290, (2008) 281–293.
- [13] Pedley, M., Clarke, M. H., Galea, P., *Limestone Isles in a Crystal Sea: The Geology of the Maltese Islands*. PEG, Malta (2002).
- [14] Trump, D.H. *Malta. Prehistory and Temples*. Midsea Books, Malta (2002).
- [15] Cassar, J., Deterioration of the Globigerina Limestone of the Maltese Islands. In: *Natural Stone, Weathering Phenomena, Conservation Strategies and Case Studies*. Geological Society of London, (2002) 33-49.
- [16] Gatt, P.A., Model of limestone weathering and damage in masonry: Sedimentological and geotechnical controls in the Globigerina Limestone Formation (Miocene) of Malta. In: *Xjenza*. (11), (2006) 30-39.

- [17] Cassar, J., The use of limestone in a historic context – the experience of Malta. In: *Limestone in the Built Environment: Present-Day Challenges for the Preservation of the Past - Geological Society Special Publications* (2010).
- [18] Farrugia, P., Porosity and related properties of local building stone. Unpublished B.E. & A. dissertation. Faculty of Architecture and Civil Engineering, University of Malta, Malta (1993).
- [19] Fitzner, B., Heinrichs, K., Volker, M. Model for salt weathering at Maltese Globigerina Limestones. In: Zezza, F. (ed.) *Origin, Mechanisms and Effects of Salt on Degradation of Monuments in Marine and Continental Environments. Proceedings, European Commission Research Workshop on Protection & Conservation of the European Cultural Heritage, Italy. Research Report, (4), (1996) 333–344.*
- [20] Rothert, E., Eggers, T., Cassar, J., Ruedrich, J. & Fitzner, B. “Stone properties and weathering induced by salt crystallization of Maltese Globigerina Limestone.” In: *Geological Society, London. Special Publication, (271), (2007) 189-198.*
- [21] Cassar, J., Composition and Property Data of Malta's Building Stone for the Construction of a Database. In R. & S.P. Prikryl, ed. *Architectural and Sculptural Stone in Cultural Landscape. Prague: Karolinum Press. (2004) 11-28.*
- [22] Muscat Azzopardi, E. Investigation of Hydraulic Lime Mixes Used in Building Conservation & their Effects on Globigerina Limestone. Unpublished thesis (M.Sc.), University of Malta (2011).
- [23] Marrocchi, A., Santarelli, M. L., Taticchi, A., Minuti, L., Broggi, A., New products for the inhibition of salt efflorescences in masonries, in *Atti del Seminário COMPASS “Sais solúveis em argamassas de edifícios antigos”, Lisboa (Portogallo), 14-15 Febbraio (2005).*
- [24] Marrocchi, A., Santarelli, M. L., Taticchi, A., Minuti, L., Broggi, A., Inibitori della crescita di cristalli di solfato di sodio in materiali lapidei, *Sci. Technol. Cultural Heritage, 15 (1-2), (2006) 101-108.*
- [25] Marrocchi, A., Taticchi, A., Santarelli, M.L., Orrù, M., Minuti, L., and Librando, V. Inibitori organici della cristallizzazione di sali nei materiali lapidei porosi. *4. Sci. Technol. Cultural Heritage, 1/2 (2007) 143-151.*

- [26] Cardinali, F., Una strategia innovativa ed eco-compatibile per il controllo del degrado dei materiali lapidei dovuti all'umidità di risalita capillare; gli inibitori di cristallizzazione salina. Il caso del Tempio di Veiove a Roma, Tesi Specialistica in Scienze e Tecnologie per la Conservazione e il Restauro del Patrimonio Storico-Artistico, Università degli Studi di Perugia (2010).
- [27] Franceschini, M.; Broggi, A.; Bracciale, M.P.; Sommei, L.; Santarelli, M. L.; Marrocchi, A., "On the effectiveness of phosphocitrate as salt crystallization inhibitor in porous materials: the case-study of the Roman mosaic of "Orpheus and the Beasts" (Perugia, Italy)" *Int. J. of Architectural Heritage*, (2013), doi: 10.1080/15583058.2012.760121.
- [28] Lubelli, B., van Hees, R., Effectiveness of crystallization inhibitors in preventing salt damage in building materials. *Journal of Cultural Heritage*, (8) (2007) 223–234.
- [29] Rodriguez-Navarro, C., Linares- Fernandez, L., Doehne, E. & Sebastian, E. Effects of ferrocyanide ions on NaCl crystallization in porous stone. *Journal of Crystal Growth*, 243 (2002) 503–513.
- [30] Selwitz, C., Doehne, E. The evaluation of crystallization modifiers for controlling salt damage to limestone *Journal of Cultural Heritage* 3: 3. (2002) 205-216.
- [31] Ruiz-Agudo, E., Rodriguez-Navarro, C. & Sebastian-Pardo, E. Sodium Sulfate Crystallization in the Presence of Phosphonates: Implications in ornamental stone conservation. *Crystal Growth and Design*, 6, (2006) 1575–1583.

Gypsum efflorescence under laboratory conditions: preliminary study

J. Chwast^{1*}, H. Janssen² and J. Elsen¹

¹KU Leuven Department of Earth and Environmental Sciences, Leuven, Belgium

²KU Leuven Building Physics Section, Department of Civil Engineering, Leuven, Belgium

*jacek.chwast@ees.kuleuven.be

Abstract

Gypsum efflorescence (GE) is a recent problem affecting modern clay brick masonry and permanently alters an aesthetic aspect of a building. This type of efflorescence affects exclusively masonry built in the last 30 years and usually appears a couple of years after construction. The GE characteristics indicate that the components are derived from the masonry itself and not from the atmosphere. The GE genesis and mechanism, and specifically the gypsum crystallisation behaviour in porous materials, are poorly understood.

We have designed and executed a series of crystallisation experiments, to compare gypsum behaviour with common efflorescing salts: NaCl and Na₂SO₄. Our experimental wick test setup consists of a brick sample mounted in a cell. The salt solution is supplied to the bottom sample side while the drying process exclusively occurs at the top. The experiments are carried out under three drying regimes: 'accelerated' (35 °C, 19% RH), 'laboratory' (24 °C, 58% RH) and 'cold' (12 °C, 80% RH). The first simulates accelerated efflorescence formation, the second is comparable to common wick tests while the third and last imitates early spring conditions. The experiments demonstrated that gypsum accumulates below the surface, unlike natural GE occurrences. Since the basic wick test does not simulate frequent masonry wetting, we have implemented wetting cycles which resulted in a considerable GE formation. We conclude that gypsum intrinsically has a subflorescing tendency, but frequent surface wetting progressively leads to GE formation.

Keywords: gypsum, efflorescence, masonry

1 Introduction

Gypsum efflorescence (GE) is a recent problem affecting clay brick masonry. It is reported to occur in the UK [1] and the Netherlands [2], and there is a growing number of cases in Belgium. It concerns the formation of a thin white film at the brick surface, what considerably alters the aesthetic aspect of a construction. This problem affects exclusively recently erected constructions, while older buildings remain unblemished. White discoloration develops only on wind and rain exposed facades, leaving the sheltered ones intact. This indicates that the GE components are solely derived from the masonry, transported with moisture and accumulated at the surface. GE is apparent only after a few years, hence either its formation is delayed or very slow.

Apart from the recent gypsum efflorescence on brick masonry and the established black crust formation on calcareous stones, gypsum is rarely reported to create surface deposits. For non-calcareous stones gypsum is reported to be found just below the surface [3]. The same is observed for wick tests, where feeding a historic brick [4] or limestone sample [5] with gypsum solution resulted in solely subsurface enrichment with gypsum. It remains to be seen whether this behaviour is also valid for the alternating wetting and drying of facade masonry, since the typical salt crystallisation tests simulate only the drying process. Aside from these few studies, little work is devoted to gypsum crystallisation in porous materials: such studies are mostly focused on crystallisation of more soluble salts like alkali sulphates and chlorides. It is thus of interest to investigate further this controversial gypsum behaviour.

Consequently, in this investigation we apply a wick test setup to study efflorescing potential of salts. The choice of the wick test setup is motivated by maintaining the drying front at the surface, and then promoting efflorescence formation. We present preliminary results on gypsum crystallisation behaviour in porous clay brick, and compare it with this of common efflorescing salts: NaCl and Na₂SO₄, under various drying regimes. This comparison aims at evaluating whether severe drying conditions are suitable for reproduction and acceleration of efflorescence formation, and assessing whether efflorescing tendency is salt-dependent. Nevertheless, wick test simulates solution uptake via the bottom sample side only, unlike in field conditions, where the fluid is supplied at the drying side. Additional tests are therefore carried out to investigate the effect of frequent surface wetting on the efflorescing potential of gypsum.

2 Materials and methods

Cylindrical samples with a diameter of 3 cm are drilled out of a common Belgian clay brick (density 1826 kg/m³, capillary absorption coefficient 0.68 kg/(m²·s^{0.5}), and capillary and saturated moisture content 210 and

325 kg/m³ respectively). Experiments on raw samples in demineralised water resulted in quick formation of sample-derived salt deposits. To limit this undesirable effect samples are initially subjected to a leaching procedure by placing them in a tank with demineralised water maintained at a temperature of 40 °C. Each 24 hours the leachate's conductivity is measured. The samples are then dried with a towel to aid in extracting the leachate from their pores, and are again submerged in fresh demineralised water. This procedure is repeated until the measured leachate conductivity reaches a constant background value. Once this requirement is achieved, samples are dried at 105 °C.

An optimal drying setup for promoting efflorescence formation should maintain the drying front at the sample surface. We have accordingly selected a wick test setup, which is depicted in Figure 1. The experimental setup consists of a cylindrical brick sample mounted in a cell. The top sample surface, being the original brick stretcher side, is exposed to the external conditions. The bottom side is in continuous contact with a chosen solution. The lid closing the experimental cell contains an inlet allowing for pressure levelling between the setup and the drying environment. The inlet is covered with a perforated tape, to limit solution evaporation from the cell. The complete setups are frequently weighed and pictures of the drying surfaces are taken to monitor the drying rate (DR) and the surface appearance, respectively.

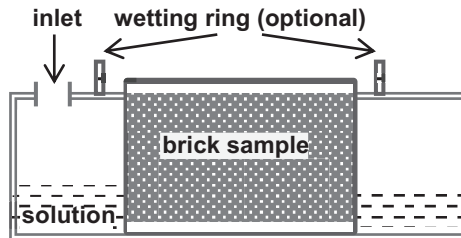


Figure 1: Scheme of the experimental wick test setup.

Natural GE is often observed to occur only after a couple of years, what might be related to 'slow drying' field conditions. We have thus investigated the effect of more severe drying conditions on reproduction and acceleration of the efflorescence formation. The experiments are carried out in parallel under different drying conditions and by use of various salt solutions. An overview of the setups is presented in Table 1.

Three drying regimes are applied where both temperature and relative humidity (RH) are fixed during the experiment. The 'accelerated' (35 °C, 19% RH) conditions are implemented by a climatic chamber. This severe drying regime is chosen to accelerate the efflorescence formation. Both the 'laboratory' (24 °C, 58% RH) and 'cold' conditions (12 °C and 80% RH) are realised in an air-conditioned laboratory room. The former is similar to conditions commonly implemented in salt crystallisation tests,

while the latter imitates early spring conditions, as this season is often believed to favour efflorescence formation [1].

Despite widespread GE occurrence, gypsum is reported to crystallise below the surface of porous materials, while under the same experimental conditions other salts form efflorescence [4, 5]. The efflorescing tendency of gypsum is compared with those of sodium chloride and sodium sulphate, while setups impregnated with demineralised water are used as a reference. Both additional salts are often reported as efflorescing, and are as such suitable for assessing gypsum crystallisation behaviour. This is realised by impregnating the samples with appropriate salt solutions, prepared from pro-analysis quality salts: calcium sulphate dihydrate ($\text{CaSO}_4 \cdot 2\text{H}_2\text{O}$), sodium chloride (NaCl) and anhydrous sodium sulphate (Na_2SO_4). All salt solutions are prepared at the same concentration of 2.2 g/L, equivalent 85% gypsum saturation at 20 °C. This way we aim to limit the effect of solubility on the rate of salt accumulation at the surface, what in turn allows for a better comparison of the efflorescence formation tendency. For convenience, we refer to the experimental wick setups containing brick samples impregnated with different salts or pure water, by simply gypsum, Na_2SO_4 , NaCl or water setups. Each measurement, for each drying conditions and salt solution, is carried out in triplicate (see Table 1).

Table 1: Summary of the investigated wick test setups.

Conditions \ Setup	Accelerated (35 °C, 19% RH)	Laboratory (24 °C, 58% RH)	Cold (12 °C, 80% RH)	Accelerated + Wetting
Gypsum	3 setups	3 setups	3 setups	3 setups
NaCl , Na_2SO_4 , water	9 setups	9 setups	X	X

Under the wick test conditions solution is supplied to a brick sample through the bottom side only. On the other hand, under field conditions it is the drying surface which receives wind-driven rain, being absorbed and then evaporated via the same masonry side. In order to simulate surface wetting we have modified the wick test by mounting a plastic ring around the exposed sample surface (see Figure 1), allowing for applying water on top of the sample, while the sample is maintained in gypsum solution. The wetting procedure is carried out under the accelerated conditions and involves 44 wetting episodes over 30 days, realised by applying 2 g of demineralised water on top of the sample.

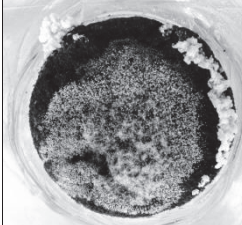
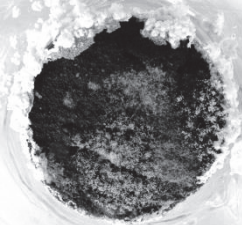
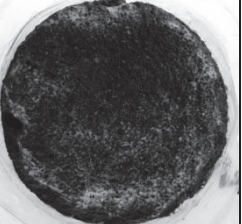
3 Results

3.1 Visual observations

The photographs in Table 2 show sample surface appearance at the end of the experiment. Under laboratory conditions, surface appearance of the NaCl and Na_2SO_4 setups is greatly affected by mould growth.

Nevertheless, it is still possible to distinguish between salt accumulation limited to peripheries and organic deposits.

Table 2: Comparison of sample surface appearance after the wick test.

NaCl setups		Na ₂ SO ₄ setups	
Laboratory (59d)	Accelerated (14d)	Laboratory (59d)	Accelerated (14d)
			
Gypsum setups			
Cold (50d)	Laboratory (59d)	Accelerated (66d)	Accelerated + wetting (30d)
			

The water setup samples do not show any deposit formation under both the accelerated and laboratory conditions (results not shown in Table 2). Deposit formation is absent or limited for all the gypsum setups under all the drying conditions, with few exceptions. Some fine dendrite growth on the sample edges is observed during the first days of the experiment under the accelerated conditions, but mostly it does not progress after two days into the experiment. Surprisingly, only one out of three samples under the cold conditions shows deposit growth at multiple locations over the surface which progresses, but only after 30 experimental days. In contrast, all three samples subjected to wetting cycles developed significant GE. For all the NaCl setups, both under the accelerated and laboratory conditions, a significant amount of salt deposit is formed. Even though the deposit formed under the accelerated conditions is covering almost the entire sample surface, it is almost uniquely anchored to the sample edges, where its growth was initiated and is then progressively wrapping over the sample surface. Under the laboratory conditions the deposit is localised uniquely at the edges, whereas substantial growth is observed only after 30 days. The Na₂SO₄ setups behave similarly to NaCl under the laboratory conditions, but the accelerated setups produced only a slight deposit, most of it formed during the first two days after which it does not progress any further.

3.2 Drying rate

Figure 2 shows the DR of different setups under the accelerated conditions. The water and NaCl setups show the highest DR, which is progressively decreasing. For both gypsum and Na₂SO₄ setups a rapid DR decrease takes place within the first days, after which it stays at a low and stable level. However, one of the gypsum setups exhibits elevated DR compared to the rest.

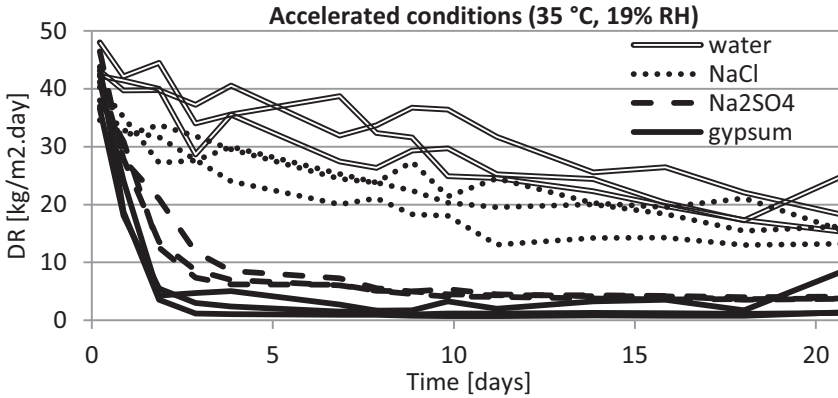


Figure 2: DR evolution of brick samples laden with water and various salt solutions and exposed to accelerated conditions.

Under the laboratory conditions (Figure 3) a stable DR is observed for all setups besides the gypsum ones, which exhibit a slow but steady drop in the DR, levelling after 40 days at a low DR.

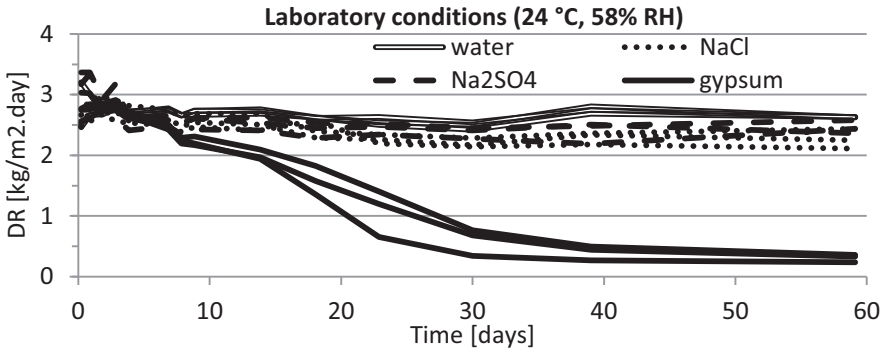


Figure 3: DR evolution of brick samples laden with water and various salt solutions and exposed to the laboratory conditions.

A DR drop is also observed for the gypsum setups under the cold conditions (Figure 4), which stabilises after around 60 days. However, for one sample an increase in the DR is observed after 30 days.

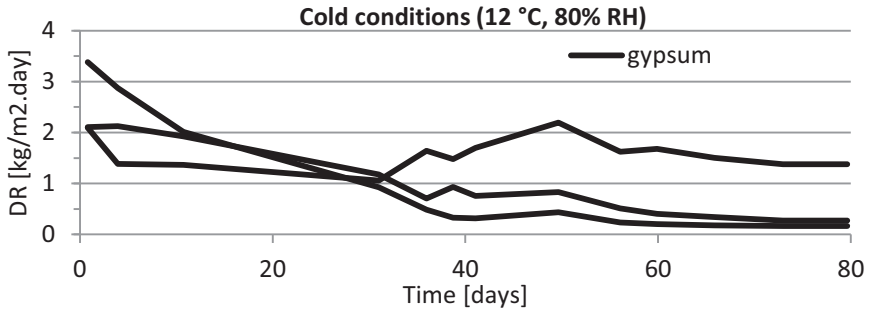


Figure 4: DR evolution of brick samples laden with gypsum solution and exposed to the cold conditions.

Table 3 compares the initial and final DR between different setups.

Table 3: Comparison of the initial and final DR for all investigated wick test setups.

Drying regime	Initial DR [kg·m ² /day]			
	gypsum	NaCl	Na ₂ SO ₄	water
Accelerated	40.5 ± 3.7	37.3 ± 2.8	42.3 ± 4.2	43.4 ± 2.3
Laboratory	2.7 ± 0.1	2.5 ± 0.1	3.2 ± 0.2	2.7 ± 0.4
Cold	2.5 ± 0.7	X	X	X
Drying regime (number of days)	Final DR [kg·m ² /day]			
	gypsum	NaCl	Na ₂ SO ₄	water
Accelerated (21d)	1.3 ± 0.1*	14.9 ± 1.5	3.8 ± 0.2	19.5 ± 5.1
Laboratory (59d)	0.3 ± 0.1	2.3 ± 0.2	2.5 ± 0.1	2.6 ± 0.0
Cold (80d)	0.2 ± 0.1*	X	X	X

* A single particularly elevated DR curve is excluded for this estimation

4 Discussion

4.1 Crystallisation at the peripheries

In cases where a substantial salt deposit develops at the sample surface, it is mostly limited to the sample's edges. Such localised crystallisation behaviour is also reported by Veran-Tissoires et al. [6] and explained by a variable evaporation flux over the exposed sample surface, which is highest at the sample's peripheries. Nevertheless, their study demonstrates that this effect can be eliminated by means of rings shielding the sample surface, which results in a similar efflorescence extent but distributed evenly. For this reason, the edge-localised salt accumulation reported here is a valid measure for evaluating salts' efflorescing behaviour.

4.2 Water samples' performance

The water laden samples under the accelerated conditions exhibit a considerable DR drop (see Figure 2), which is not accompanied by any major surface discoloration. To indicate the origin of this phenomenon, the samples were halved and subjected again to the wick test (see Figure 5). The bottom face exhibits a much higher DR than the top, demonstrating that some brick-derived components are accumulated under or within the brick surface and hindering the evaporation process.

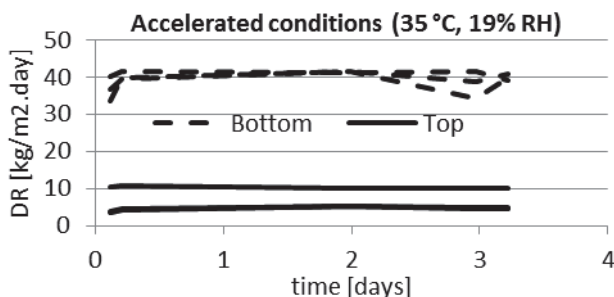


Figure 5: DR of water setups through bottom and top face. The samples were first subjected to a wick test under the accelerated conditions.

Sample surface analysis with a stereomicroscope revealed some local inter-grain deposit formation (see Figure 6A). A cross-section scanning electron microscope (SEM) image (see Figure 6B) from the same sample shows that it forms a thin sheet of a few micrometres thickness. SEM-EDAX analysis shows presence of 50% CaO, 30% of SiO₂ and a few other oxides. This is consistent with the formation of a portlandite layer, which is further carbonated to calcite, on a brick matrix rich in SiO₂.

The water setups prepared with raw (not leached) brick samples resulted in the formation of abundant, water soluble deposits. This undesirable effect was successfully eliminated by applying the leaching procedure. Accordingly, the majority of well soluble brick components, for instance the alkali sulphates, are likely extracted from the samples. Nevertheless, raw bricks may contain CaO which hydrates to Ca(OH)₂ upon contact with water. The latter exhibits low solubility at 0.14 g / 100 mL (40 °C), thus it may persist in brick samples after the leaching procedure. The applied leaching procedure is in consequence effective against well soluble salts, but the low soluble compounds like calcium hydroxide are likely to be preserved. This undesirable effect appears also to affect the drying behaviour of the NaCl setups, as their drying behaviour follows the same trend (see Figure 2).

However, no such effect is observed for the water samples at the laboratory conditions after 60 days (see Figure 3). An equivalent amount of water evaporated after only 4 days under the accelerated conditions, and was accompanied by a considerable DR decrease of 15%. It appears therefore that this effect takes place exclusively under the accelerated

conditions, or is significantly delayed under the laboratory conditions. The solubility of calcium hydroxide at 25 °C is only 8% lower than at 35 °C, so does not seem to account for this effect. On the other hand the difference in the drying conditions is translated into a 16 times higher initial DR for the water samples under the accelerated conditions (see Table 3). Slower drying conditions favour the diffusion process over the advective transport, which may help to delay portlandite precipitation under the laboratory conditions. Under the accelerated conditions local calcium hydroxide saturation at the surface can be reached much faster leading to its precipitation, which inhibits the drying process.

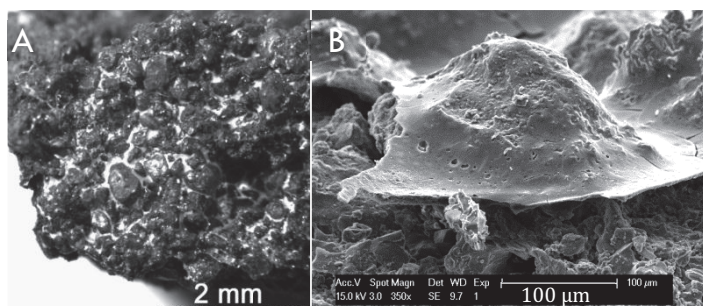


Figure 6: Surface (A) and cross-section (B) images of a water sample tested under the accelerated conditions, pictures taken with stereomicroscope (A) and SEM (B).

4.3 Mineral-specific efflorescing potential

The three tested salt setups demonstrate distinctly different crystallisation behaviour, even though tested under the same experimental conditions.

4.3.1 Sodium chloride

Sodium chloride crystallises exclusively as halite under both drying regimes. Irrespective of the drying regime, halite forms extensive deposits accompanied by drying rates similar to these of water samples.

4.3.2 Sodium sulphate

The Na_2SO_4 setups display heterogeneous responses: under the accelerated conditions they exhibit a DR decrease and scarce efflorescence, while under laboratory conditions they behave like NaCl ones, with extensive efflorescence and a DR at the level of a water sample (see Figures 2 and 3).

Steiger and Asmussen (2008) discuss in their paper the Na_2SO_4 crystallisation pathways [7], what aids in explaining the different crystallisation behaviour of the Na_2SO_4 setups. Even though thenardite ($\text{Na}_2\text{SO}_4(\text{V})$) is the stable phase under both drying regimes according to the $\text{Na}_2\text{SO}_4\text{-H}_2\text{O}$ phase diagram, the crystallisation pathway for its formation may include intermediate crystallisation of mirabilite

($\text{Na}_2\text{SO}_4 \cdot 10\text{H}_2\text{O}$). The origin of the observed discrepancies for the Na_2SO_4 setups may stem from the fact that the experiments at 24 °C and 35 °C are carried out below and above the thenardite-mirabilite transition temperature of 32.4 °C, respectively. Assuming that the process is completely controlled by the thermodynamics, mirabilite crystallisation takes place first under the laboratory conditions, followed by dehydration to the thenardite phase during drying while thenardite precipitates directly under the accelerated conditions. Our results then show that mirabilite shows a tendency to form extensive efflorescence, while direct crystallisation of thenardite results in pore clogging and only scarce surface deposits. Nevertheless, thenardite formation upon mirabilite dehydration does not alter the overall efflorescence formation tendency.

It appears that the propensity towards efflorescence formation may be mineral-specific, even in case where both forms are different hydrates of the same base anhydrous compound, as demonstrated for Na_2SO_4 .

4.3.3 Calcium sulphate

Calcium sulphate occurs in the mineral forms of anhydrite (CaSO_4), hemihydrate ($\text{CaSO}_4 \cdot 0.5\text{H}_2\text{O}$) and gypsum ($\text{CaSO}_4 \cdot 2\text{H}_2\text{O}$), but only the last one crystallises under ordinary conditions [3], including the three drying regimes. Sodium chloride also crystallises as a single phase, halite, and thus is a good proxy for evaluating gypsum crystallisation behaviour. The surface appearance and DR trend illustrate that the two minerals show contrasting crystallisation behaviour. Halite forms extensive deposits and the NaCl setups exhibit DR similar to that of water setups, while gypsum setups display a DR drop without or with scarce efflorescence formation. This DR drop is followed by a low and stable drying phase irrespective of the drying conditions, as shown in Figures 2-4. Two particular samples show a fast drying behaviour, each under either the accelerated or cold conditions which, unlike others, show some gypsum crystallisation at the surface. Table 4 shows characteristic data derived from gypsum DR plots, comparing the DR before (Initial DR) and after the transition to the low DR phase (Transition DR), and the time and amount of gypsum solution needed to accomplish this transition.

Table 4: Comparison of characteristic data derived from DR plots for gypsum setups under various drying conditions.

Drying regime	Initial DR [$\text{kg} \cdot \text{m}^2/\text{day}$]	Time [days]	Transition DR [$\text{kg} \cdot \text{m}^2/\text{day}$]	Gypsum solution [kg/m^2]
Accelerated	40.5 ± 3.7	$6 \pm 4^*$	$2.0 \pm 1.3^*$	$32 \pm 8^*$
Laboratory	2.7 ± 0.1	52 ± 12	0.3 ± 0.0	57 ± 10
Cold	2.5 ± 0.7	$60 \pm 0^*$	$0.3 \pm 0.1^*$	$61 \pm 8^*$

* A single particularly elevated DR curve is excluded for this estimation

The initial DR is considerably higher under the accelerated conditions, compared to the laboratory and cold ones. Nevertheless, the beneficial effect of the fast drying is abruptly suppressed, as the DR drops by a factor of 20 after about six days. The same effect is observed under

laboratory and cold conditions, though it is taking place less rapidly and less extensively. Under both drying regimes the transition is accomplished after about 60 days, yielding a DR decrease by a factor of nine. This is also associated with a two times higher amount of gypsum solution evaporated during the slow transition, than under the accelerated conditions. A higher amount of gypsum can be hence accumulated during a slow process, before the DR drop is accomplished. This indicates that the amount of accumulated gypsum is not directly related to the DR drop. Instead, its distribution in the pore structure likely has a more profound effect on the permeability decrease.

The DR drop occurs for all gypsum setups, thus is not related to a specific drying regime. It is then rather the consequence of an intrinsic gypsum property, an apparent tendency for crystallisation under the surface, even under efflorescence-favourable conditions. This observation seems at odds with the commonly observed GE phenomenon, but is in line with some literature reports [4, 5]. Calcium sulphate is a ubiquitous component of various building materials, but gypsum deposits are rarely reported to accumulate on their surface, apart from the recent occurrence of GE on masonry and crusts formed via the interaction with atmosphere. This rare occurrence might therefore be a consequence of both its tendency to crystallise below the surface and its limited solubility.

4.3.4 The factors determining crystallisation location

The location of the crystallisation depends on the complex interplay between many factors like properties of supersaturated solution, drying conditions, matrix porosity, and crystal growth pattern. The first parameter is of importance for highly soluble salts of which supersaturated solutions may show significantly altered viscosity and surface tension. Nevertheless, it does not seem significant for scarcely soluble gypsum. We have demonstrated that, on one hand, gypsum tendency for subflorescence formation is not directly related to the drying rate. On the other hand, formation of halite and intermediate mirabilite efflorescence shows that the brick porous matrix is not a barrier itself for crystallisation at the surface. It appears hence that the propensity for efflorescence formation may be mineral-specific, as shown on the example of efflorescing halite and mirabilite and subflorescing thenardite and gypsum. It is not clear though, whether the origin of this behaviour is specific crystal growth or other mineral related parameter.

4.4 Accelerated efflorescence formation

The difference in the drying conditions between the laboratory and accelerated setups translates into a 16 times higher initial DR for the water samples (see Table 3). The vapour pressure difference between surface and environment, under the 'accelerated' and 'laboratory' conditions is 4500 Pa and 1200 Pa, respectively, thus they do only partly contribute to such a high difference in the DR. It is hence the higher air flow in the climate chamber which enhances this effect. The effect of fast drying

conditions on the efflorescence formation is evident for the NaCl setups, resulting in a rapid formation of an extensive deposit under the accelerated conditions and reflected by a high DR similar to this of the water sample (Figure 2). Under accelerated conditions efflorescence is initiated very early, after only two days, while it takes more than 30 days under laboratory conditions. In both cases, deposition continues over time.

The long delay under the laboratory conditions may be explained by a high supersaturation necessary for triggering NaCl crystallisation, which is achieved much slower under these conditions. The slower evaporation rate may also facilitate the diffusion process to counteract advection, further delaying supersaturation and NaCl precipitation. A similar argument can be made for the Na₂SO₄ setups under the laboratory conditions.

Gypsum setups under all the 3 drying regimes and Na₂SO₄ setups at the accelerated conditions behave differently than NaCl ones, the effect of the fast drying conditions is quenched by the pore clogging effect of gypsum and thenardite respectively, markedly reducing the DR (see Figures 2-4).

The acceleration of efflorescence formation by applying more severe drying regime is consequently mineral dependent. It can be easily realised for halite, whereas the pore-clogging effect for gypsum and direct thenardite crystallisation inhibits efflorescence. Consequently, it is likely that sodium sulphate efflorescence formation may be accelerated by carrying the experiment just below the thenardite-mirabilite transition temperature of 32.4 °C.

4.5 The effect of wetting-wicking cycles

The application of wetting cycles resulted in a significant gypsum efflorescence formation. This was not achieved for the basic wick test, irrespectively of the drying conditions (see Table 2). We have then followed more closely the drying behaviour during the wetting phase of an 11 days old sample, subjected already to 18 wetting episodes.

Figure 7 shows the evolution of the setup mass in function of time, from the moment when 2 g of water is placed over the sample surface (point A). The water gets absorbed slowly: it was observed that the sample surface turned dry only at the point B, corresponding to 1 g of absorbed water. Therefore during the phase A-B 1 g of added water has evaporated, and 1 g was absorbed. The phase B-C corresponds to the evaporation of 1 g water, absorbed and supplied to the surface by wick action. From the C point onwards all wetting water has evaporated and gypsum solution is brought to the surface followed by evaporation of water from the solution. From the graph it is evident that the DR during A-B is similar to B-C, while the C-D is characterised by a very low DR. The C-D low DR is related to the pore clogging caused by crystallisation upon evaporation of water from the gypsum solution. This effect can be eliminated by wetting the sample surface, which dissolves the pore plugs. The similar magnitude of the

water-wick DR (B-C) and the free water surface drying rate (A-B) indicates that the drying process is no longer constrained by pore blockage.

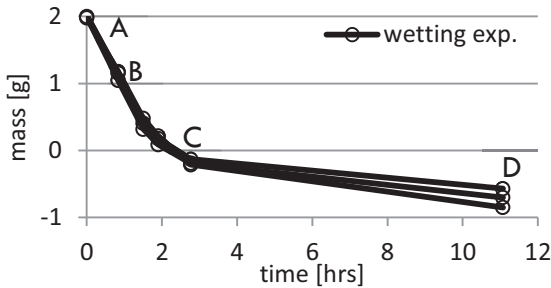


Figure 7: Evolution of mass of the gypsum setups after wetting with 2g of water.

During the 11 days preceding the experiment, water from about 30 g of gypsum solution has evaporated via the top sample surface leaving gypsum behind. For the wetting experiment only 2 g of water is used, which is then able to dissolve only a small fraction of the accumulated gypsum. Nonetheless, it effectively restores the high DR, even though much gypsum is still present in the sample pores. It is plausible then that most of the accumulated gypsum narrows the pores, without completely closing them, allowing for a persistent high DR (phase B-C). The DR decrease is then caused by an increasing number of pores becoming completely blocked by gypsum-plugs. Once a pore is clogged, no further gypsum accumulation can take place in an isolated pore, what makes the pore plugs relatively fine and susceptible to dissolution even with a low amount of wetting water.

The basic gypsum wick test demonstrates that, although a low amount of gypsum may initially crystallise at the surface, its further growth is quickly inhibited by pore clogging. However, these short episodes of surface accumulation may be repeated by wetting cycles, reopening the pores and progressively leading to efflorescence formation.

Even though wetting appears to contribute remarkably to GE formation, it does not explain its only recent occurrence. Nevertheless, implementation of the wetting cycles allows for further investigation of the problem. The factor which has actually led to GE triggering may be either source or process related. Considering the former, it appears that there were no recent changes leading to an increased availability of sulphates in either brick or cement. However, the recent GE occurrence might be associated with significant changes in mortar quality, particularly in recent application of various surfactant-based admixtures. There are premises showing an important role of such compounds in enhancing gypsum crystallisation on masonry [1]. However, the admixtures potential for exerting a long time effect in real masonry systems remains questionable.

5 Conclusions

However exploratory, this study offers some insights into elucidating the salt's efflorescing tendency. The results obtained from a series of wick experiments allow formulating the following conclusions:

- 1) Salt's efflorescing tendency appears to be mineral specific: halite (NaCl) and mirabilite ($\text{Na}_2\text{SO}_4 \cdot 10\text{H}_2\text{O}$) tend to form extensive efflorescence while gypsum ($\text{CaSO}_4 \cdot 2\text{H}_2\text{O}$) and thenardite (Na_2SO_4 (V)) accumulate under the surface. The former is accompanied by a high drying rate, sustaining salts' growth at the surface. The latter results in pore clogging and consequently a major drying rate drop, reducing efflorescence development.
- 2) Under wick test conditions only halite efflorescence formation can be accelerated by applying more severe drying regime. It is likely that the same holds for direct crystallisation of mirabilite, hence for temperatures below the thenardite-mirabilite transition. For gypsum and thenardite the effect of severe drying conditions is quenched by the salt's pore clogging tendency.
- 3) A standard wick test is not effective in simulating efflorescence formation when minerals show a pore clogging tendency. However, it was possible to simulate gypsum efflorescence formation by implementing frequent surface wetting into the standard procedure. This allows the re-opening of plugged pores and progressive events of gypsum crystallisation at the surface, resulting in significant efflorescence development. The improved procedure is consistent with frequent masonry wetting under field conditions.

Acknowledgements

This work is supported by the funding of IWT Baekeland (No. 120193). We would like to thank Paul Verbeek for brick samples preparation.

References

- [1] G. K. Bowler and N. B. Winter, "Investigation into causes of persistent efflorescence on masonry," *Mason. Int.*, vol. 11, no. 1, pp. 15–18, 1997.
- [2] H. Brocken and T. G. Nijland, "White efflorescence on brick masonry and concrete masonry blocks, with special emphasis on sulfate efflorescence on concrete blocks," *Constr. Build. Mater.*, vol. 18, no. 5, pp. 315–323, 2004.

- [3] A. E. Charola, J. Pühringer, and M. Steiger, "Gypsum: a review of its role in the deterioration of building materials," *Environ. Geol.*, vol. 52, no. 2, pp. 339–352, Dec. 2006.
- [4] L. Franke and J. Grabau, "Influence of salt content on the drying behavior of brick," in *Conservation of historic brick structures*, Baer N. S., Fitz S, Livingston R.A., Donhead, 1998, pp. 59–68.
- [5] C. Cardell, D. Benavente, and J. Rodríguez-Gordillo, "Weathering of limestone building material by mixed sulfate solutions. Characterization of stone microstructure, reaction products and decay forms," *Mater. Charact.*, vol. 59, no. 10, pp. 1371–1385, Oct. 2008.
- [6] S. Veran-Tissoires, M. Marcoux, and M. Prat, "Discrete Salt Crystallization at the Surface of a Porous Medium," *Phys. Rev. Lett.*, vol. 108, no. 5, Feb. 2012.
- [7] M. Steiger and S. Asmussen, "Crystallization of sodium sulfate phases in porous materials: The phase diagram $\text{Na}_2\text{SO}_4\text{-H}_2\text{O}$ and the generation of stress," *Geochim. Cosmochim. Acta*, vol. 72, no. 17, pp. 4291–4306, Sep. 2008.

Numerical simulation of gypsum transport and crystallization

J. Todorović and H. Janssen

KU Leuven, Department of Civil Engineering, Leuven, Belgium

* jelena.todorovic@bwk.kuleuven.be

Abstract

Over the last few decades, brick masonry buildings in the UK, The Netherlands and Belgium have started suffering from a new type of salt efflorescence. This new efflorescence consists of sparingly soluble gypsum, and is therefore strongly persistent. Although gypsum efflorescence has already been known for several decades, there are still many open questions regarding the mechanisms behind this phenomenon. Numerical simulation of the transport and crystallization of gypsum in porous materials can contribute to a better understanding of the underlying processes, hence being helpful in the search for causes and solutions. However, due to the low solubility of gypsum and insensitivity to changes in temperature and relative humidity, calcium sulphate is generally not included in simulation software for salt transport and crystallization in porous materials. Therefore, this paper focuses on the numerical implementation of gypsum transport and crystallization in the Delphin simulation environment. As initial application, the simulation of wicking test is performed. The uptake test comprises an initially dry material sample in contact with gypsum solution at the bottom surface, while evaporation is allowed only at the top surface. The main objective is the study of the processes of transport and crystallization of gypsum in porous media, with relation to gypsum efflorescence on brick masonry.

Keywords: gypsum efflorescence, numerical simulation, transport and crystallization, gypsum solution uptake test.

1 Introduction

Gypsum efflorescence is an aesthetical problem of masonry facades which has started appearing in the UK, The Netherlands and also in Belgium over the last few decades. It is a form of persistent white-grey discoloration, mainly developing on walls which are highly exposed to wind-driven rain [1–3]. This new type of efflorescence brought a growing number of complaints to the Belgium brick industry, which motivated a field survey and case study in Belgium [3]. After investigating 28 cases it was concluded that the efflorescence is composed of relatively insoluble gypsum and that it solely affects buildings which were erected over the last twenty years. The facades oriented towards South and West showed to be most affected. According to the building owners, the efflorescence started to develop several years after the construction, making it unclear whether it is a slow or delayed process. The relevant brick types were identified, but no connection between gypsum efflorescence and brick properties - moisture transfer properties and calcium sulphate content specifically - was found.

Despite the fact that this phenomenon has been known for several years already, the exact mechanisms and reasons for its appearance remain unknown. Therefore a numerical simulation of the transport and crystallization of gypsum in porous materials can contribute to a better understanding of the underlying processes, and hence help in the search for causes and solutions. Although there are several works that deal with the numerical modelling of salt transport and crystallization in porous materials [4, 5], neither of them includes gypsum or any other form of calcium sulphate. Its low solubility, insensitivity to changes in relative humidity and temperature, and the different mechanisms of causing damage, are all the reasons why it is excluded from numerical models [6]. However, to simulate gypsum transport and crystallization in the building materials, the same parameters and properties as for any other salt and salt solution are required. This includes the basic physical and chemical properties of gypsum and its solution, such as the density, solubility, heat capacity, viscosity, surface tension and heat of dissolution. The diffusion coefficient and activation energy are required for the simulation of transport, while the kinetic parameters for crystallization and dissolution are necessary for description of phase transitions [4, 5]. All these properties are equivalent to those of free salt solutions. Their connection and relation with the salts in porous building materials are not going to be the focus of this work, as they are detailed explained elsewhere [4, 5].

Therefore, the objective of this paper is to gather and implement all the parameters of calcium sulphate dihydrate and its solution, necessary for simulation of gypsum transport and crystallization in the Delphin simulation environment. Furthermore, the model application is illustrated via the simulation of gypsum solution wicking experiment. The test comprises an initially dry sample in contact with gypsum solution at the bottom face, while evaporation is allowed only at the top face. These

simulations make up the first step towards a better insight into how gypsum is transported, where it crystallizes and which parameters and properties are of a great importance for numerical modelling of calcium sulphate transport. Additionally the limitations of the model and needs for further research are discussed.

2 Parameterization of calcium sulphate

2.1 Molality based numerical model

Even though tabulated values of many electrolyte solution properties are available in the literature, most of them are only valid within limited ranges of temperature and concentration. Therefore, the molality based Pitzer ion interaction approach is used to predict many of the desired binary and salt mixture solution properties in the Delphin program. This well-known model is used in the area of electrolyte chemistry as well as geology. Developed by Kenneth S. Pitzer, it represents a system of equations which describe the thermodynamic properties of mixed and pure electrolyte solutions, within an experimental accuracy. The main objective of such a model is to reproduce the properties of solutions by using simple mathematical equations for pure electrolyte solutions as well as for mixed solutions. These equations require only a few parameters, which are obtained from experimental data and mainly tabulated in the work of Pitzer [7].

2.2 Basic properties of gypsum and gypsum solution

This part of the paper deals with the description and calculation of the basic physical and chemical properties of gypsum and gypsum solution. Firstly, ion and water activities, depending on temperature and concentration, are determined in order to calculate the density and solubility. Secondly, the viscosity, surface tension, heat capacity and heat of dissolution are discussed.

2.2.1 Ion activity

One of the most important parameters in the thermodynamic calculations is the ion activity. It describes the effective concentration of chemical substances in the solution. For ideal solutions, the activity of an ion equals its concentration. However, an increase of concentration results in a deviation from ideal solutions, which is described by the activity coefficient γ . General equations for the calculation of the ion activity and the activity coefficients are available in the paper of Pitzer [7], while the calculation for pure calcium sulphate solution is given by the following equations:

$$\ln a_i = \ln \gamma_i + \ln m_i \quad (1)$$

$$\ln \gamma_M = z_M^2 F + \sum_a m_a (2B_{Ma} + zC_{Ma}) + z_M \sum_c \sum_a m_c m_a C_{ca} \quad (2)$$

$$\ln \gamma_X = z_X^2 F + \sum_a m_c (2B_{cX} + ZC_{cX}) + |z_X| \sum_c \sum_a m_c m_a C_{ca} \quad (3)$$

$$B_{MX} = \beta_{MX}^{(0)} + \beta_{MX}^{(1)} g(\alpha_1 I^{\frac{1}{2}}) + \beta_{MX}^{(2)} g(\alpha_2 I^{\frac{1}{2}}) \quad (4)$$

$$g(x) = 2[1 - (1+x)e^{-x}] / x^2 \quad (5)$$

$$F = -A_\Phi \left[\frac{1}{(1+bl^2)} + \frac{2}{b} \ln(1+bl^2) \right] + m_c m_a B'_{ca} \quad (6)$$

$$B'_{MX} = \frac{1}{I} \left[\beta_{MX}^{(1)} g'(\alpha_1 I^{\frac{1}{2}}) + \beta_{MX}^{(2)} g'(\alpha_2 I^{\frac{1}{2}}) \right] \quad (7)$$

$$g'(x) = \frac{-2}{x^2} [1 - (1+x + \frac{x^2}{2})e^{-x}] \quad (8)$$

where a_i is the ion activity [-], m_i is the molality of ion species [mol/kg], γ_M and γ_X are the activity coefficients [-] of the cation C_a^{2+} and the anion SO_4^{2-} respectively. The subscripts c and a refer to anions and cations present in a solution. B_{MX} and C_{MX} are the second and the third virial coefficients [-]; I is the ionic strength [mol/kg] and Z is the charge density [mol/kg]; b is the constant $1.2 \text{ kg}^{0.5}/\text{mol}^{0.5}$. A_Φ is the Debye-Hückel parameter for the osmotic coefficient [$\text{kg}^{0.5}/\text{mol}^{0.5}$], whose temperature dependence is described by equation (9) [8]:

$$A_\Phi(T) = -0.817653 - \frac{0.8685276}{T - 222K} + \frac{19251}{T^2} + 5.251484 \cdot 10^{-3}T + 9.338559 \cdot 10^{-12}T^4 \quad (9)$$

In the expression for the second virial coefficient, $\beta^{(i)}$ are adjustable binary interaction parameters. Parameters α_i are constants which have values of $\alpha_1 = 2.0$ and $\alpha_2 = 0$ for all electrolytes, except for 2-2 type salts, like calcium sulphate [7]. According to Pitzer and Mayorga [9], 2-2 electrolytes tend to form ion pairs, due to electrostatic forces. Nevertheless, considering ion pairs as separate species would make the calculations much more complex. The solution was found by adding the $\beta^{(2)}$ term in the expression for the second virial coefficient and setting the values of α to $\alpha_1 = 1.4 \text{ kg}^{0.5}/\text{mol}^{0.5}$ and $\alpha_2 = 12 \text{ kg}^{0.5}/\text{mol}^{0.5}$. Although Pitzer [7] provides binary interaction parameters for calcium sulphate, with values of 0.2, 3.1973 and -54.24 for $\beta^{(0)}$, $\beta^{(1)}$ and $\beta^{(2)}$ respectively, they are constant and thus independent of temperature. In the work of Steiger et al. [8] the

temperature dependence of all interaction parameters of different salts is described with the following function:

$$P(T) = q_1 + q_2 \left(\frac{1}{T} - \frac{1}{T_R} \right) + q_3 \ln \left(\frac{T}{T_R} \right) + q_4 (T - T_R) + q_5 (T^2 - T_R^2) + q_6 \ln(T - 225) \quad (10)$$

where $T_R = 298.15\text{K}$ is a reference temperature and q_i are tabulated values for many salts. This improved model and parameterization of Steiger et al. [8] was implemented and used in Delphin. However, the parameterization of the temperature dependence of calcium sulphate is not provided. Møller [10] studied the prediction of mineral solubilities in natural waters, for the system of Na-Ca-Cl-SO₄-H₂O. In her work, the temperature dependence of binary interaction parameters, $\beta^{(i)}$ and C^Φ , is described with equation (11):

$$f(T) = a_1 + a_2 T + \frac{a_3}{T} + a_4 \ln T + \frac{a_5}{T-263} + a_6 T^2 + \frac{a_7}{680-T} + \frac{a_8}{T-227} \quad (11)$$

For calcium sulphate, $\beta^{(0)}$, $\beta^{(1)}$ and C^Φ are set as constants with values of 0.15, 3.0 and 0 respectively, with following fitting parameters: $a_1 = -129.399287$ and $a_2 = 0.400431027$, while the rest is equal to 0. Since the temperature dependence of interaction parameters in Delphin is described by equation (10) [4], the constants for calcium sulphate from equation (11) are fitted to function (10). The constant values for $\beta^{(0)}_{\text{CaSO}_4}$, $\beta^{(1)}_{\text{CaSO}_4}$ and $C^\Phi_{\text{CaSO}_4}$ are kept the same, while for the $\beta^{(2)}_{\text{CaSO}_4}$ values of $q_1 = -10.01077629995$ and $q_4 = 0.400431027$ are obtained and the rest is equal to zero. The obtained parameters for calcium sulphate are valid for temperatures from 0 to 50°C [10], which is acceptable for the scope of this work. Although the difference between $\beta^{(2)}$ suggested by Pitzer and the one from Møller seems large, based on the calculated ion activity at a reference temperature of 25°C, this difference seems to be negligible (see Figure 1a). Even though it would be possible to use Pitzer's constant values of $\beta^{(i)}$ for the present work, we proceed with the suggestion of Møller; this leaves us the possibility to include interactions with other ions, where the influence of temperature can be significant. In addition, the model of Møller is generally valid for higher levels of concentration [10].

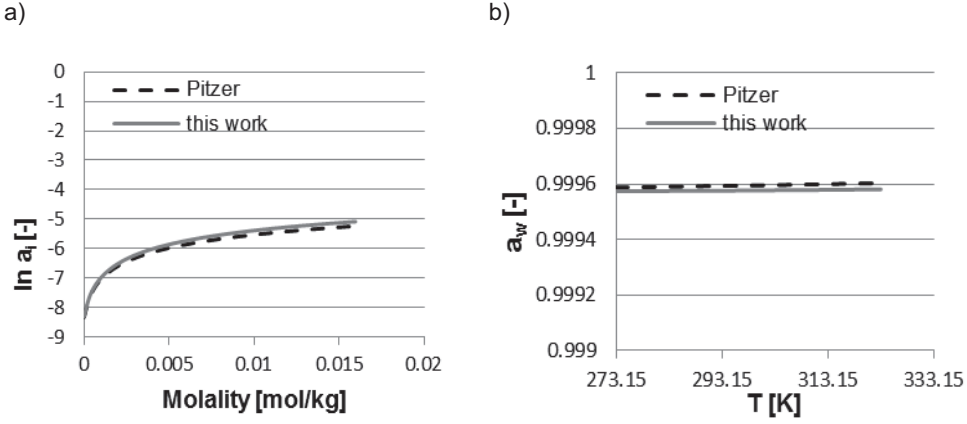


Figure 1: a) Activity of ions in function of molality at 298.15K; b) water activity in function of temperature, at saturation level

2.2.2 Water activity

As the vapour diffusion inside the porous materials is influenced by the moisture saturation level as well as the salt content, the water activity is a quantity which describes the reduction of vapour pressure over the salt solution inside unsaturated porous media [4]. It is also necessary for the calculation of the equilibrium constant and thus the saturation ratio, which is essential for determining whether crystallization or dissolution will occur. Therefore, the calculation of this property is one of the advantages of the Pitzer ion interaction approach. The water activity is described by the following equation:

$$\ln a_w = -\phi M_w \sum_i m_i \quad (12)$$

where ϕ is the osmotic coefficient [-], M_w is the molar mass of water [kg/mol] and m_i is the molality of dissolved ions. The general equation for the osmotic coefficient is presented in the work of Pitzer [7], while the reduced one, for the pure solution of calcium sulphate is given by the equation (13):

$$(\phi - 1) = \frac{2}{\sum_i m_i} \left[\frac{-A_\phi I^{\frac{3}{2}}}{(1 + bI^{\frac{1}{2}})} + \sum_c \sum_a m_c m_a (B_{ca}^\phi + ZC_{ca}) \right] \quad (13)$$

$$B_{MX}^\phi = \beta_{MX}^{(0)} + \beta_{MX}^{(1)} e^{-\alpha_1 I^{1/2}} + \beta_{MX}^{(2)} e^{-\alpha_2 I^{1/2}} \quad (14)$$

Fitting parameters for the virial coefficients, B_{MX}^ϕ and C_{MX} , are the same as for the ion activities. As the solubility of gypsum is only 0.015 mol/kg of water at room temperature [11], the influence of dissolved calcium and sulphate ions on the water activity is almost negligible. For the temperature range from 0 to 50°C, the water activity does not differ much from unity (see Figure 1b), which also confirms that gypsum is insensitive to the changes in the temperature.

2.2.3 Density of solution

Although, the tabulated values of densities for different electrolyte solutions are available in the literature, they are often valid for limited ranges of temperature and concentration. Therefore the Pitzer ion interaction model can be used for the calculation of densities for salt mixtures as well as for binary solutions [4]. The density of a solution, containing 1kg of water, can be calculated by equation (15):

$$\rho_{sol} = \frac{1\text{kg} + \sum_i m_i M_i}{\frac{1\text{kg}}{\rho_w} + \sum_i m_i V_i^0 + V_{mix}^{ex}} \quad (15)$$

where m_i and M_i are the molality and molar mass of ions, respectively. V_w^0 and V_i^0 are the molar volume of water and the partial molar volumes of the ions, while ρ_w is water density. V_{mix}^{ex} is the excess molar volume, which is the result of the interaction between ions and water. The temperature dependence of the partial molar volumes V_i^0 is described by equation (16):

$$f(T) = a_0 + a_1 \left(\frac{1}{T-225} \right) + a_2 \frac{1}{T} + a_3 T + a_4 T^2 + a_5 \ln T \quad (16)$$

The fitting parameters a_i for calcium and sulphate ions are listed in Table 1 [8].

Table 1: Fitting parameters for the partial molar volumes of calcium and sulphate ions

	a_0	a_1	a_2	a_3	a_4	a_5
Ca	4.79700693	-429.486853	0	-0.0568315647	0	0
SO ₄	409.4060315	-618.1208309	-56791.12672	-0.65897533	0	0

The calculated values of the partial molar volumes for calcium and sulphate ions at the reference temperature of 298.15K are -18.0186 and 14.0 cm³/mol respectively, which is in a good agreement with the values $V_{Ca} = -18.4\text{cm}^3/\text{mol}$ and $V_{SO_4} = 13.98\text{cm}^3/\text{mol}$ reported in the work of Konstantinos and Georg [12]. The Pitzer ion interaction approach plays the role in the calculation of the excess molar volume (equation (17)).

$$V_{\text{mix}}^{\text{ex}} = A_v \frac{1}{b} \ln(1+b\sqrt{I}) + RT \left[\sum_c \sum_a m_c m_a (2B_{\text{ca}}^V + ZC_{\text{ca}}^V) \right] \quad (17)$$

$$B_{\text{MX}}^V = \beta_{\text{MX}}^{(0)V} + \beta_{\text{MX}}^{(1)V} g \left(\alpha_1 |z| \right) + \beta_{\text{MX}}^{(2)V} g \left(\alpha_2 |z| \right) \quad (18)$$

Although, $\beta^{(i)V}$ and C_{ca}^V are also expressed with the function (16), due to the low solubility of calcium sulphate, these parameters can be neglected in the calculation of $V_{\text{mix}}^{\text{ex}}$ [13]. Nicolai [4] obtained a similar observation: for low concentration solutions, the influence of excess volume is negligible, while in the case of high ionic strengths, ion interaction can significantly influence the solution volume. Since the values for $\beta^{(i)V}$ and C_{ca}^V are not established for the present work, the calculation of the solution density was executed in two ways. The first one excluded the excess molar volume completely, while the other included $V_{\text{mix}}^{\text{ex}}$, which is calculated taking into account only the first term of equation (17). Due to the very low solubility of gypsum, the solution density is only slightly different from that of pure water, both when taking into account $V_{\text{mix}}^{\text{ex}}$ and not (Figure 2). From Figure 2 it can be assumed that the density of gypsum solution is the same as that of pure water. However, in order to maintain as accurate as possible it is decided to calculate gypsum solution density by taking into account $V_{\text{mix}}^{\text{ex}}$.

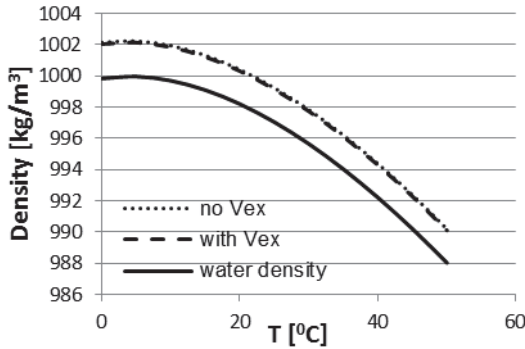
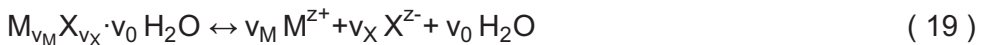


Figure 2: Density of water and saturated gypsum solution

2.2.4 Equilibrium constant

Once the ions and the water activities are calculated it is possible to determine the equilibrium constant for the dissolution and the crystallization reaction for a given salt, equation (19).



of which the equilibrium constant K_{MX} can be determined by the following equation:

$$\ln K_{MX} = v_M \ln a_M + v_X \ln a_X + v_0 \ln a_w \quad (20)$$

where v_M , v_X and v_0 are the stoichiometric numbers of cations, anions and water molecules respectively. The ratio of the equilibrium constant calculated for real activities and molalities, and temperature dependent equilibrium constant K_o at zero ionic strength, determines the level of saturation U , and thus crystallization or dissolution [4].

$$U = K_{MX}/K_o \quad (21)$$

One can assume that for low soluble salts, solubility can be calculated from the solubility product (product of concentrations of ions). However, this cannot be considered very accurate when it comes to 2-2 electrolytes. Due to the ion pairing effects, which has been discussed before, it cannot be safely assumed that concentrations of ions are equal to the solubility of the solid phase, as a significant number of ion pairs can be present. Therefore, very accurate calculations of solubility can be obtained using the ion activities as these are corrected for the effect of ion pairing.

Since the temperature dependence of all ion interaction parameters was described with equation (10), it was suggested to use the same equation for the temperature dependence of the equilibrium constant $\ln K_o$ [8].

For gypsum, the equilibrium constant was determined from solubility data taken from the paper of [11] and Azimi et al. [14], based on equation (22) [12]:

$$m_{CaSO_4 \cdot 2H_2O} = \sqrt{K_o}/\gamma a_w \quad (22)$$

Using least square analysis, equation (10) was fitted according to obtained data and corresponding parameters, listed in the Table 2.

Table 2: Fitting parameters for temperature dependent solubility constant $\ln K_o$

q_1	q_2	q_3	q_4	q_5	q_6
-10.23145825	-25770	-137.6	0.1747	0	0

Figure 3 shows that the calculated gypsum solubility, obtained from the temperature dependent solubility constant K_o is in a good agreement with the experimental data, up to a temperature of 50°C.

2.2.5 Heat capacity of gypsum and gypsum solution

In the case of the solid phase of calcium sulphate dihydrate and its anhydrite, the heat capacities are 1455 J/kgK and 732 J/kgK respectively. In general, the heat capacity of a salt solution represents the sum of the heat capacities of the solvent, dissolved ions and the capacity which results from the interaction between ions and with the solvent. In case water is the solvent, the heat capacity of a solution can be assumed to be

equal to the heat capacity of pure water, as the presence of ions has an insignificant influence [4]. Since gypsum solution is already characterised by its low concentration, it is feasible to assume that its heat capacity is equal to that of pure water, with a value of 4180 J/kgK.

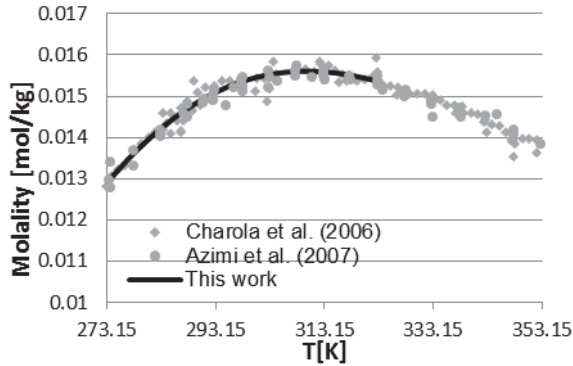


Figure 3: Solubility of gypsum calculated with equation (22), taking into account K_0 determined from function (10)

2.2.6 Viscosity, surface tension and heat of dissolution

Viscosity and the surface tension are the solution properties that could have an impact on the moisture storage and transport in porous materials. However, in the case of the low soluble gypsum, it is again acceptable to assume that the change in viscosity and surface tension is negligible, and thus that both are the same as for pure water. The same assumption is made regarding the heat of dissolution. Since there is a lack of information about this quantity, it is completely neglected from the model. The justification of this decision is again based on the low solubility of calcium sulphate dihydrate.

2.3 Transport parameters

2.3.1 Diffusion coefficient

Modelling of salt transport in building materials includes modelling the movement of ions within water, driven by the concentration gradient. This is known as diffusion. In order to describe diffusion of a salt, the diffusion coefficient needs to be determined. As for the other salt properties, the diffusion coefficient can be determined for free salt solutions. It is dependent on the concentration and the temperature, although the last has no significant impact [4]. Taking into account the low solubility of gypsum, a concentration-independent value of the diffusion coefficient can be accepted, assuming that the influence of the concentration is insignificant relative to other effects related to the transport inside a porous media. The value of $1 \times 10^{-9} \text{ m}^2/\text{s}$ was proposed by Colombani and Bert [15] and accepted in this work.

2.3.2 Activation energy

Information for the values of the activation energy is not obtained. Nevertheless, taking into account the low concentration of a saturated gypsum solution, it can be expected that this lack will not affect the results.

2.4 Kinetics of dissolution and crystallization

The damages of building materials are quiet often caused by the salts present in the pores of materials. The numerical models of heat, moisture and salt transport in porous materials are developed aiming to study and hence mitigate these damages [16]. In the work of Nicolai [4], and thus in Delphin, salt phase transition rates are based on the model of Espinosa et al. [16] and given by the following equations:

$$\sigma^{m_{p,j}} = -k_{sol}(1-U_j)^{g_{sol}} \qquad \sigma^{m_{p,j}} = k_p(U_j-1)^{g_p} \qquad (23)$$

where k_{sol} , g_{sol} , k_p , g_p are the kinetic parameters for dissolution and crystallization respectively. U_j is the saturation ratio, discussed in section 2.2.4. In the case of $U_j < 1$, dissolution will take place, while for $U_j > 1$ crystallization will occur. In order to develop an accurate and reliable numerical model it is necessary to obtain and evaluate the kinetic parameters from the experimental data. As calcium sulphate dihydrate is known for its low solubility, there are limited data regarding the kinetic parameters for dissolution and crystallization in porous materials.

However, Serafeimidis and Anagnostou [17] studied the gypsum precipitation and obtained $5 \times 10^{-7} \text{ kg/m}^2\text{s}$ and 2 as k_p and g_p whereas Jeschke et al.[18] performed rotating disk and batch experiments aiming to determine accurate dissolution kinetic parameters for gypsum. As a result they found almost a linear dissolution rate law, with dissolution constant $k_{sol} = 1.1 \times 10^{-4} \text{ mmol/cm}^2\text{s}$ and $g_{sol} = 1.2 \pm 0.2$ from the rotating disc measurement, and $1.3 \times 10^{-4} \text{ mmol/cm}^2\text{s}$ and $g_{sol} = 1.2 \pm 0.2$, from the batch experiments. Nevertheless, they discussed about dissolution kinetic parameters found in the literature, and although they stated that different experimental measurements and set ups can give different results, the order of magnitude for k_{sol} is $10^{-4} \text{ mmol/cm}^2\text{s}$. Since both kinetic parameters are determined without the presence of a porous material, they are expressed per surface area; for precipitation this represents the surface available for crystal growth, while for dissolution it implies the surface area in contact with water and from which dissolution occurs.

However, considering salt phase transitions inside porous materials, the kinetics of dissolution and crystallization are not only dependent on the salt type, but also on the material and its porosity [16]. In order to translate the values of gypsum kinetics to porous materials, some assumptions have to be made. The first one is that the total surface area of pores is available for gypsum dissolution and precipitation. Knowing the pore volume and the pore size, with the assumption of a cylindrical shape of

pores, it is possible to determine the total surface area of pores per cubic meter of material. As an example, the brick type often affected by efflorescence in Belgium has a porosity of 34% and a characteristic pore radius of about $1\mu\text{m}$ yielding a total pore surface area of $680000\text{ m}^2/\text{m}^3$, which lead to material-specific parameters for crystallization and dissolution of $0.34\text{ kg}/\text{m}^3\text{s}$ and $140\text{ kg}/\text{m}^3\text{s}$ respectively. The impact of different assumptions regarding the availability of pore surface area is discussed in the next section.

3 Application of the model

Now that all the required parameters are determined, their implementation into the code of Delphin can be made. As the objective is to get an insight into how gypsum is transported and where it crystallizes, a simulation of gypsum wicking experiment is performed. The model is based on the accelerated experiment which is developed at the Department of Geology at KU Leuven [19]. The experiment comprises an initially dry brick sample in contact with a gypsum solution at the bottom face with evaporation allowed only from the top side. The concentration of the gypsum solution is $0.013\text{ mol}/\text{kg}$, which is about 80% of a saturated solution. The wicking experiment runs for 5 days at a constant temperature and RH of 35°C and 20%, respectively. The results reveal that the advective transport of gypsum is very fast; after 4 hours it already reaches the top face (see Figure 4). Since the phase transition is determined by the saturation ratio, the time and the location of gypsum crystallization is determined by when and where the super-saturation of a solution is reached. Knowing that the solubility of gypsum is $0.015\text{ mol}/\text{kg}$, saturation of gypsum solution is reached near the surface after 4h. Based on these observations it can be expected that gypsum starts crystallizing near the brick surface, 4 to 5 hours after the start of the experiment, which is confirmed in Figure 5. Additionally, it can be seen that whether 100% or 0.1% of pore surface area is available for crystallization, in both cases crystallization starts after 4h and the location of the precipitation is situated in the top 5mm. However, for the lower versus the higher kinetic constant, the width of crystallized zone is larger while the amount of solid phase is smaller (Figure 5).

Similar observations follow the laboratory study of gypsum transport in porous material reported by Franke and Grabau [20]. Although it was expected that during the laboratory measurements, gypsum would appear at the surface and form efflorescence, the opposite occurred. Contrary to very soluble salts that form efflorescence, gypsum crystallized below the surface in the form of subflorescence, inducing pore clogging and a drop in the drying rate [20]. After analysing the samples they reported that gypsum completely crystallized just below the brick surface at a depth of a few millimetres. The same observations were made from the experiments of Jacek et al.[19].

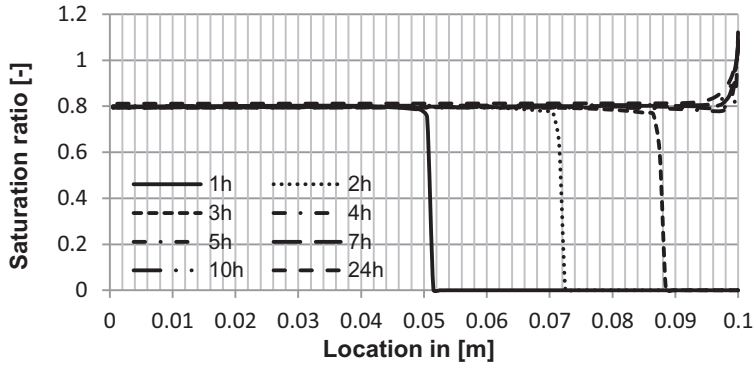


Figure 4: Saturation ratio as a function of time and location

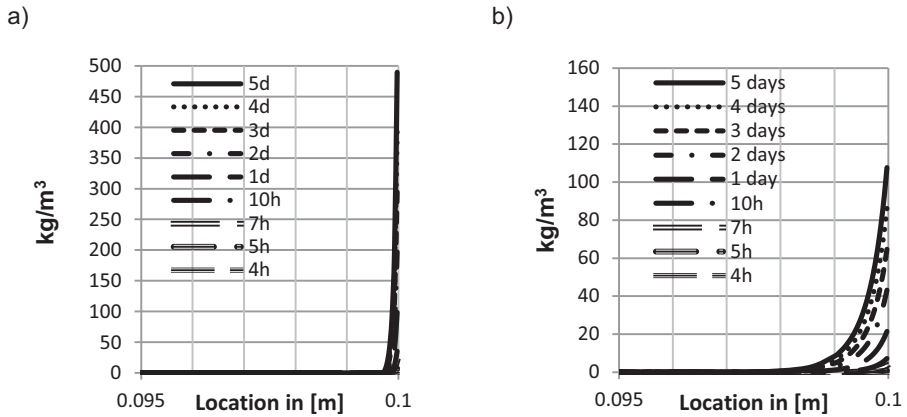


Figure 5: Precipitated gypsum within 5mm below the top surface; a) 100% of pore surface area available for precipitation; b) 0.1% of pore surface area available for precipitation

4 Limitations of the model

While the results from laboratory measurements indicated the drop in the drying rate after 2 to 3 days [19], this observation was not obtained from the simulation. The reason is that the phenomenon of pore clogging is inadequately addressed in the Delphin program

Additionally, even if during the laboratory measurements, gypsum formed efflorescence instead of subflorescence, this would not be the case when it comes to this numerical model. Since the formation of efflorescence is not included in the code of Delphin, regardless of the type of salt that is used in the model, and regardless of the environmental conditions, crystallization will always be located below the surface.

5 Conclusions

The motivation for the numerical implementation and simulation of gypsum transport and crystallization in a porous material is the development of a new type of efflorescence, the so called gypsum efflorescence. Although it has been known for several years already, there are still many uncertainties and questions in relation to the source of gypsum, the recent occurrence and the crystallization behaviour [3]. Therefore, numerical modelling of transport and crystallization of gypsum could provide a better understanding and more insight into the physico-chemical mechanisms behind this phenomenon. Even though Delphin is a software developed for simulation of heat, air, moisture and salt transport and crystallization in porous materials, it does not include gypsum. Mainly due to its low solubility and insensitivity to changes in temperature and relative humidity it is typically not considered as important. On one hand, the low solubility is the limiting factor for the determination of different properties of gypsum solution, but on the other hand many of these properties could be considered as equal to those for pure water. Although these specific characteristics are aggravating factors even for many experimental measurements, it was still possible to accomplish the parameterization of the solid phase as well as of a solution. The Pitzer ion interaction approach was proven to be applicable for the description of the basic physical properties in this case as well as for highly soluble salts.

The initial application of the model is a simulation of a gypsum solution wicking experiment. Based on this simulation, several observations were made. First of all, it was seen that despite the low solubility, gypsum is transported via advection and diffusion, like any other salt. Although transport is also dependent on the material properties, gypsum solution reaches the top surface of a sample after only a few hours, where in the same time frame, it becomes fully saturated. When oversaturation of the solution was obtained near the surface, gypsum started precipitating. Moreover, it was noticed that even after 5 days of the experiment, the total amount of crystallized gypsum was located just below the surface. However, the width of crystallized zone and the amount of precipitated gypsum depend on the magnitude of the kinetic constant. Although similar observations were found from the gypsum solution wicking experiments conducted in the laboratory, this numerical model has several limitations. First of all, pore clogging is not included in the code of Delphin in a sufficient way. While under the laboratory conditions, a drop in the drying rate was noticed after several days, this cannot be achieved with the present model. Secondly, the motivation for this work was the development of gypsum efflorescence. However, the impossibility of the simulation of efflorescence in general is another limitation of the model.

Despite of these limitations and deficiencies, this model is still a great starting point for further research and additional improvements. Since the validation of the numerical model of gypsum transport and crystallization is the subject of ongoing research, first the present limitations will have to be

addressed. Additionally, the interaction with other ions and salts will be studied and included in the model, in order to analyse whether there is a significant change in the gypsum solution characteristics which could be the reason for the development of the new efflorescence type.

References

- [1] G. Bowler and N. B. Winter, "New form of salt staining on external masonry.pdf," *Br. Ceram. Trans.*, (95) (1996) 82–86.
- [2] H. Brocken and T. G. Nijland, "White efflorescence on brick masonry and concrete masonry blocks, with special emphasis on sulfate efflorescence on concrete blocks," *Constr. Build. Mater.*, (18) (2004) 315–323.
- [3] J. Chwast, J. Todorović, H. Janssen, and J. Elsen, "Gypsum efflorescence on clay brick masonry: field survey and literature study," in *13th International conference on durability of building materials and components*, Sao Paulo, Brasil, 2014
- [4] A. Nicolai, "Modeling and numerical simulation of salt transport and phase transitions in unsaturated porous building materials," PhD thesis, Syracuse University, USA, 2007.
- [5] H. Derluyn, "Salt transport and crystallization in porous limestone: neutron - X-ray imaging and poromechanical modeling," PhD thesis, ETH, Zurich, 2012.
- [6] M. Steiger and A. Heritage, "Modelling the crystallisation behaviour of mixed salt systems: input data requirements," in *12th International Congress on the Deterioration and Conservation of Stone*, 2012.
- [7] K. S. Pitzer, "Ion interaction approach: Theory and data correlation," in *Activity coefficients in electrolyte solutions*, edited by K. Pitzer, chap.3, CRC Press., (1991), 75–152.
- [8] M. Steiger, J. Kiekbusch, and A. Nicolai, "An improved model incorporating Pitzer's equations for calculation of thermodynamic properties of pore solutions implemented into an efficient program code," *Constr. Build. Mater.*, (22) (2008) 1841–1850.
- [9] K. S. Pitzer and G. Mayorga, "Thermodynamics of electrolytes. III. Activity and osmotic coefficients for 2-2 electrolytes," *J. Solution Chem.*, (3) (1974) 539–546.

- [10] N. Møller, "The prediction of mineral solubilities in natural waters : A chemical equilibrium model for the Na-Ca-Cl-SO₄-H₂O system, to high temperature and concentration," *Geochim. Cosmochim. Acta*, (52) (1988) 821–837.
- [11] E. Charola, J. Pühringer, and M. Steiger, "Gypsum: a review of its role in the deterioration of building materials," *Environ. Geol.*, (52) (2006) 339–352.
- [12] S. Konstantinos and A. Georg, "On the Solubilities of Anhydrite and Gypsum," in *Constitutive Modeling of Geomaterials*, edited by Q. Yang, J. Zhang, H. Zheng and Y. Yao, 2013, 333–339.
- [13] M. Steiger, "Total volumes of crystalline solids and salt solutions," in *An expert chemical model for determining the environmental conditions needed to prevent salt damage in porous materials*, edited by C. Price, chap.6, vol.0135, 2000, 53-63.
- [14] G. Azimi, V. G. Papangelakis, and J. E. Dutrizac, "Modelling of calcium sulphate solubility in concentrated multi-component sulphate solutions," *Fluid Phase Equilib.*, (260) (2007) 300–315.
- [15] J. Colombani and J. Bert, "Holographic interferometry study of the dissolution and diffusion of gypsum in water," *Geochim. Cosmochim. Acta*, (71) (2007) 1913-1920.
- [16] R. M. Espinosa, L. Franke, and G. Deckelmann, "Phase changes of salts in porous materials: Crystallization, hydration and deliquescence," *Constr. Build. Mater.*, (22) (2008) 1758–1773.
- [17] K. Serafeimidis and G. Anagnostou, "Simultaneous anhydrite dissolution and gypsum precipitation in a closed swelling rock system," in *46th US Rock Mechanics / Geomechanics Symposium*, Chicago, IL, USA, 2012.
- [18] A. A. Jeschke, K. Vosbeck, and W. Dreybrodt, "Surface controlled dissolution rates of gypsum in aqueous solutions exhibit nonlinear dissolution kinetics," *Geochim. Cosmochim. Acta*, (65) (2001) 27–34.
- [19] J. Chwast, H. Janssen, and J. Elsen, "Gypsum efflorescence under laboratory conditions : preliminary study," in *3rd International conference of salt weathering of buildings and stone sculptures*, Brussels, Belgium, 2014, 117-131.

- [20] L. Franke and J. Grabau, "Influence of salt content on the drying behavior of brick," in Conservation of historic brick structures, Baer N.S., Fitz S., Livingston R.A., Donhead, (1998) 59–68.

Crystallization behavior of a Na₂SO₄–MgSO₄ salt mixture and comparison to single salt behavior

N. Lindström*, T. Talreja, K. Linnow and M. Steiger

Department of Chemistry, University of Hamburg,
Inorganic and Applied Chemistry, Hamburg, Germany

* Nadine.Lindstroem@chemie.uni-hamburg.de

Abstract

Crystals growing in confined spaces can generate stress and are a major cause of damage in porous materials. While the behavior of several single salts is well characterized, only few studies have been carried out on the behavior of salt mixtures and, especially, mixtures involving the formation of double salts have not been systematically investigated. Double salts show a complex crystallization behavior and an incongruently soluble salt may have a great damage potential, because a solution supersaturated with one of its single salt compounds is formed during its dissolution. In this study we report on wetting–drying experiments with an equimolar Na₂SO₄–MgSO₄ salt mixture. In situ Raman microscopy was used to study the phase transformations during the wetting of the double salts Na₂Mg(SO₄)₂·4H₂O (bloedite) and Na₂Mg(SO₄)₂·5H₂O (konyaite). Though both salts are incongruently soluble and should form mirabilite upon dissolution, it was found that they behave similar to congruently soluble salts. Most likely, the resulting supersaturation is not sufficient for mirabilite nucleation to occur. Due to the low supersaturation the damage potential of the dissolution of the incongruently soluble double salts bloedite and konyaite is not only much lower than that of sodium sulfate and magnesium sulfate but also in comparison to the incongruently soluble double salt darapskite.

Keywords: sodium sulfate, magnesium sulfate, salt mixtures, bloedite, konyaite

1 Introduction

Crystals growing in confined spaces can generate stress if in contact with their own supersaturated solution and are a major cause of damage in porous materials. The behavior of several single salts that are commonly found in building materials is well characterized. Many studies focused on the behavior of sodium sulfate and magnesium sulfate as these salts were found to be particularly damaging [e.g. 1–8 among others]. However, contamination of building materials with a single salt is uncommon. Usually, the salt systems found are comprised of many different ions. Compared to single salts, the crystallization behavior of salt mixtures is much more complicated. It is not a trivial task to predict, for a given mixture composition, the crystallization sequence, i.e. the nature of the solid phases that crystallize out. Only few experimental studies have been carried out on the crystallization behavior and the damage potential of salt mixtures [e.g. 9,10]. One complicating factor in studies with salt mixtures is that a number of double salts may form in mixed solutions [11], a problem that was tackled in several recent studies [12–14]. These authors studied behavior of Na_2SO_4 – NaNO_3 and Na_2SO_4 – K_2SO_4 salt mixtures including the formation of the incongruently soluble double salts $\text{Na}_3\text{NO}_3\text{SO}_4\cdot\text{H}_2\text{O}$ (darapskite) and $\text{K}_3\text{Na}(\text{SO}_4)_2$ (glaserite). The present study reports on experiments on the crystallization behavior of Na_2SO_4 – MgSO_4 mixtures including the formation of the incongruently soluble double salts $\text{Na}_2\text{Mg}(\text{SO}_4)_2\cdot 4\text{H}_2\text{O}$ (bloeditite, also known as astrakanite) and $\text{Na}_2\text{Mg}(\text{SO}_4)_2\cdot 5\text{H}_2\text{O}$ (konyaite).

Most double salts found in building materials are incongruently soluble which means that they precipitate from solution compositions different from their own stoichiometric composition. Incongruent dissolution of a double salt is accompanied by the formation of a secondary solid phase, i.e. one of the pure single salts that form the double compound crystallizes out. In this respect, the behavior of double salts during wetting is similar to that of other salts, e.g. anhydrous Na_2SO_4 (thenardite), that form metastable solutions, i.e. solutions supersaturated with respect to other solids (e.g. $\text{Na}_2\text{SO}_4\cdot 10\text{H}_2\text{O}$, mirabilite). Consequently, double salts may have a great damage potential because a solution supersaturated with respect to one of the single salt compounds is formed during their dissolution. Therefore, crystallization and damage may occur at high relative humidity (deliquescence of the double salt) or during wetting. Recently, this behavior was confirmed in wetting experiments with thenardite and darapskite by in situ Raman spectroscopy [14]. During wetting of both thenardite and darapskite we observed the formation of mirabilite. In the present study, similar wetting–drying experiments were carried out with an equimolar salt mixture Na_2SO_4 – MgSO_4 . In situ Raman microscopy was used to study the phase transformations during wetting.

2 Materials and methods

2.1 Syntheses of double salts

As discussed in more detail in Section 3.1, the only stable phases in the ternary system Na_2SO_4 – MgSO_4 at 23 °C are epsomite ($\text{MgSO}_4 \cdot 7\text{H}_2\text{O}$), mirabilite and bloedite. However, initial experiments on evaporation of equimolar solutions revealed that a second double salt, konyaite, formed next to bloedite depending on the climatic conditions during evaporation. Pure bloedite was prepared by addition of NaCl to a MgSO_4 solution at 40 °C and cooling to room temperature as described in reference [15]. The identity of the product was confirmed by XRD (PDF 19-1215) and a sample was used to record the Raman spectrum. Evaporation of an equimolar mixed solution at room temperature yielded two different types of crystals that could be separated using tweezers. The two solids were identified by XRD as thenardite (PDF 37-1465) and konyaite (PDF 35-0649). Thenardite was also identified via Raman spectroscopy using the reference spectrum reported earlier [13]. The konyaite crystals were used to determine the Raman spectrum of the double salt.

For the preparation of the bloedite crystals used in the wetting experiments, an equimolar mixed solution was prepared by dissolving 23.76 g (0.167 mol) Na_2SO_4 and 38.5 g (0.168 mol) $\text{MgSO}_4 \cdot 6\text{H}_2\text{O}$ in 142.1 g doubly distilled water. Few milliliters were filled in Petri dishes and evaporated in a desiccator over a saturated solution of $\text{Ca}(\text{NO}_3)_2 \cdot 4\text{H}_2\text{O}$ (50% RH) at room temperature. After 51 days, pure bloedite crystals were obtained and identified via Raman spectroscopy.

The synthesis of konyaite crystals followed the same way as for bloedite. The amount of salts used were 123.3 g (0.868 mol) Na_2SO_4 and 198.3 g (0.867 mol) $\text{MgSO}_4 \cdot 6\text{H}_2\text{O}$ dissolved in 1406 g double distilled water. As desiccant, a saturated solution of $\text{K}_2\text{CO}_3 \cdot 1.5\text{H}_2\text{O}$ generating a relative humidity of about 43%, was used. After a few days, pure konyaite crystals were obtained and identified via Raman spectroscopy.

2.2 Wetting experiments and in situ Raman observations

The in situ Raman observations during wetting of salt crystals were performed on glass slides which were cleaned with hydrogen peroxide to remove all organic substances. Experiments were done with pure crystals of bloedite and konyaite. In situ observations started with the recording of the Raman spectrum of the pure educt phases. Subsequently, the sample was carefully wetted with 2–4 μL of doubly distilled water using a microliter pipet. The amount of water used was chosen in order to avoid complete dissolution and the formation of a dilute undersaturated solution. In this

case, no information on the precipitation of a new phase is obtained and the subsequent drying will be similar to a droplet evaporation experiment. Right after the addition of water Raman spectra were continuously recorded at the same spot of the sample surface. Occasionally, the crystal under investigation changed its position slightly due to the presence of the solution. In these cases, the laser was adjusted accordingly.

2.3 Instrumentation

Raman spectra were recorded on a Senterra Raman dispersive microscope (Bruker Optics GmbH, Germany) with an automated Raman frequency calibration system (SurCal technology) using MPlan M 10x and LMPlanFL N 20x objectives (Olympus Deutschland GmbH, Germany). The diode-laser excitation source was operated at 532 nm and 20 mW.

The Raman spectrum of a mixture of different solid phases can be expressed as the linear combination of the spectra of the pure compounds:

$$I(\lambda) = \sum_i (b_i I_{r,i}(\lambda)) \quad (1)$$

where $I(\lambda)$ is the intensity at wavelength λ (the observed Raman spectrum) and $I_{r,i}(\lambda)$ are the spectra of the reference compounds r . The coefficients b_i can be determined by multiple linear regression and ordinary least squares analysis using reference spectra of all compounds that might be present in the mixture under investigation. Details on the measurements of the reference spectra are provided in reference [13]. The least squares analysis was carried out using a selected number of wavenumbers at which the measured intensities in both the sample and the reference spectra were sufficiently high. The coefficients b_i represent the contributions of the reference spectra to the sample spectrum. No attempts were made to calibrate the method, i.e. the values of b_i do not represent but are related to the mole fractions of a compound.

3 Results and discussion

3.1 Solubilities in the ternary system $\text{Na}_2\text{SO}_4\text{-MgSO}_4\text{-H}_2\text{O}$

There is a number of solid phases that may be formed in the ternary system $\text{Na}_2\text{SO}_4\text{-MgSO}_4\text{-H}_2\text{O}$ [16]. These are listed in Table 1. Nine of these phases do have ranges of stable existence, only six phases (thenardite, mirabilite, kieserite, hexahydrate, epsomite and bloedite) can be stable at near ambient temperatures, meaning that these solids have lower solubili-

Table 1: Possible phases in the ternary system of Na₂SO₄–MgSO₄–H₂O

Compound	Formula	Thermodynamics
thenardite (phase V)	Na ₂ SO ₄ (V)	stable ^(a)
phase III	Na ₂ SO ₄ (III)	metastable
sodium sulfate heptahydrate	Na ₂ SO ₄ ·7H ₂ O	metastable
mirabilite	Na ₂ SO ₄ ·10H ₂ O	stable ^(a)
kieserite	MgSO ₄ ·H ₂ O	stable ^(a)
magnesium sulfate 5/4 hydrate	MgSO ₄ ·1.25H ₂ O	metastable
sanderite	MgSO ₄ ·2H ₂ O	metastable
magnesium sulfate trihydrate	MgSO ₄ ·3H ₂ O	metastable
starkeyite	MgSO ₄ ·4H ₂ O	metastable
pentahydrate	MgSO ₄ ·5H ₂ O	metastable
hexahydrate	MgSO ₄ ·6H ₂ O	stable ^(a)
epsomite	MgSO ₄ ·7H ₂ O	stable ^(a)
meridianiite	MgSO ₄ ·11H ₂ O	stable ^(b)
loedite	Na ₂ Mg(SO ₄) ₂ ·4H ₂ O	stable ^(a)
konyaite	Na ₂ Mg(SO ₄) ₂ ·5H ₂ O	metastable
loewite	Na ₁₂ Mg ₇ (SO ₄) ₁₃ ·15H ₂ O	stable ^(c)
vanthoffite	Na ₆ Mg(SO ₄) ₄	stable ^(c)
disodium magnesium sulfate decahydrate	Na ₂ Mg(SO ₄) ₂ ·10H ₂ O	metastable

^(a) stable at near ambient temperatures
^(b) stable at low temperatures (<0.7 °C)
^(c) stable at enhanced temperature (loewite: >57 °C, vanthoffite: >60 °C)

ties (for a given mixture composition) than the metastable phases which have higher saturation concentrations. However, due to the tendency of several stable solids to supersaturate, the saturation concentrations of various metastable solids can be reached and exceeded during evaporation. Mirabilite and kieserite exhibit a particularly strong tendency to supersaturate. Therefore, the formation of metastable sodium [4,17] and magnesium sulfate phases [16] is quite commonly observed.

The solubility diagram of the Na₂SO₄–MgSO₄-system at 23 °C is shown in Figure 1. The solubilities were calculated using our thermodynamic model [16,18] and validated with available experimental data [16]. There are three thermodynamically stable phases: mirabilite,loedite and epsomite. Their solubilities are represented by the solid black lines. The dashed lines represent the solubilities of the metastable phases thenardite, phase III, heptahydrate, hexahydrate, starkeyite, kieserite and the metastable branch of theloedite solubility curve. The solid grey line indicates an equimolar mixed solution of both salts. During evaporation the solution will first reach

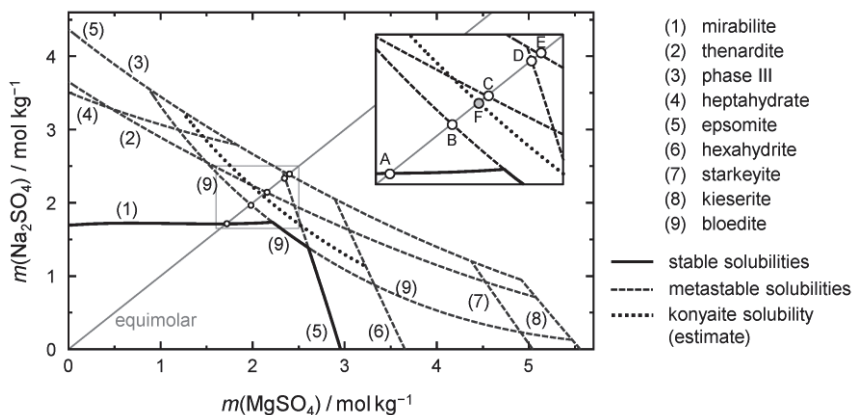


Figure 1: Solubility diagram of the system $\text{Na}_2\text{SO}_4\text{--MgSO}_4\text{--H}_2\text{O}$ at 23 °C calculated using an equilibrium model [16,18]. Solid and dashed curves denote stable and metastable solubilities, respectively. The gray solid line represents an equimolar mixed solution. Points A, B, C, D, E and F represent saturation concentrations in the equimolar solution with mirabilite, bloedite, thenardite, epsomite, phase III and konyaite, respectively. The dotted curve represents estimated solubilities of konyaite.

saturation with the stable solid mirabilite (at point A) confirming that bloedite is incongruently soluble.

In our evaporation experiments with an equimolar mixed solution the formation of mirabilite was not observed due to its strong tendency to supersaturate. Upon further evaporation into the supersaturated region the concentration increases and reaches successively saturation with bloedite, thenardite, epsomite and phase III (points B–E). An enlarged view is provided in the inset of Figure 1. It can be understood that bloedite is formed in our evaporation experiments with an equimolar mixed solution. If the evaporation rates are not too large (at about 50% RH), the critical concentrations for thenardite and phase III nucleation are obviously not reached. However, increasing the evaporation rate by slightly decreasing the RH in the desiccator results in higher supersaturation and crystallization of konyaite. In some experiments the simultaneous crystallization of konyaite and thenardite was also observed.

Unfortunately, the available thermodynamic data for konyaite do not permit the calculation of its solubility. However, it is certain that konyaite is metastable with respect to bloedite and, most likely, will have a solubility close to that of thenardite at 23 °C. Based on these assumptions we have

drawn an estimated solubility curve for konyaite in Figure 1 (dotted line). Saturation with konyaite is indicated by point F.

3.2 Raman reference spectra

The use of Raman microscopy for the in situ analysis of phase transformations in the wetting experiments requires Raman reference spectra of all possible phases. Phase identification is possible by comparison of the position of the total symmetric stretching vibration (ν_1) of the sulfate ion. The reference spectra with the spectral range dominated by the ν_1 Raman peak positions of the compounds relevant to this work are depicted in Figure 2. There is a systematic shift of the ν_1 peak position that can be used for phase identification. In cases when the difference in the ν_1 peak position is only small, additional information may be gained from less intense Raman bands (not shown in Figure 2).

Usually, it is possible to identify unambiguously the different phases present in a mixture. In case of a very complex mixture composition, additional information, e.g. from phase diagrams, can be used to assess the

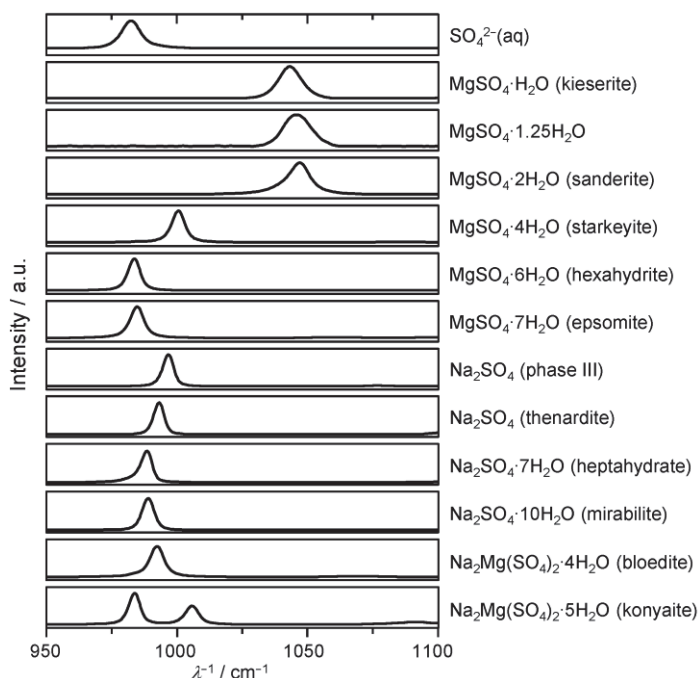


Figure 2: Raman reference spectra in the spectral range dominated by the symmetric stretching vibration of the SO_4 tetrahedra (950 cm^{-1} and 1100 cm^{-1}).

most likely phase assemblages. However, it is always very difficult to distinguish epsomite and hexahydrate unambiguously.

3.3 In situ Raman observations during wetting

3.3.1 Wetting of pure konyaite crystals

The results of the in situ Raman measurements during the wetting of pure konyaite are shown in Figure 3. The spectrum on top of the left diagram was recorded right before the addition of water and confirms the presence of pure konyaite with two characteristic peaks assigned to the symmetric stretch of sulfate. The two peaks correspond to two distinct sulfate tetrahedra in the structure of konyaite [19]. Only one of them is coordinated directly to the Mg^{2+} ion. The second spectrum (0 min) was recorded right after the addition of water. The konyaite peaks no longer occur in the spectrum and the peak assigned to the aqueous sulfate ion appears instead. At that moment in time, the sample was not yet completely dissolved. However, the laser was focused on a spot in the center of the droplet where the dissolution was already complete. At the edge of the droplet (not shown in the respective micrograph) there was still a solid residue of konyaite.

After about 11 min the re-appearance of the peak at 1005 cm^{-1} indicates the precipitation of konyaite during evaporation of the droplet. In the following spectra the peak caused by $\text{SO}_4^{2-}(\text{aq})$ continuously diminishes while the konyaite peaks increase indicating ongoing evaporation and precipitation of konyaite. Assuming that konyaite is the only solid phase present we calculated by least squares analysis the contributions of dissolved sulfate and crystalline konyaite to the various spectra. The result of these calculations is depicted in Figure 3 (right diagram) and yields an approximate composition after wetting and during evaporation. Although konyaite is an incongruently soluble salt its behavior in the wetting and drying experiment is that of a congruently soluble salt, i.e. it dissolves without precipitation of a second salt (which would be mirabilite in this case) and is re-precipitated during evaporation.

From the Raman spectra it may be speculated that hexahydrate or epsomite might have been formed as well. However, this is very unlikely as these salts exhibit much higher solubilities than bloedite, konyaite and thenardite (cf. Figure 1). Also, if a magnesium sulfate hydrate would have been formed, for stoichiometric reasons, a sodium sulfate phase would have to be formed as well which is clearly not the case. Finally, it is surprising that the calculations predict the presence of a solution still after 28 min (cf. Figure 3). It is not clear whether this is an indication that there is

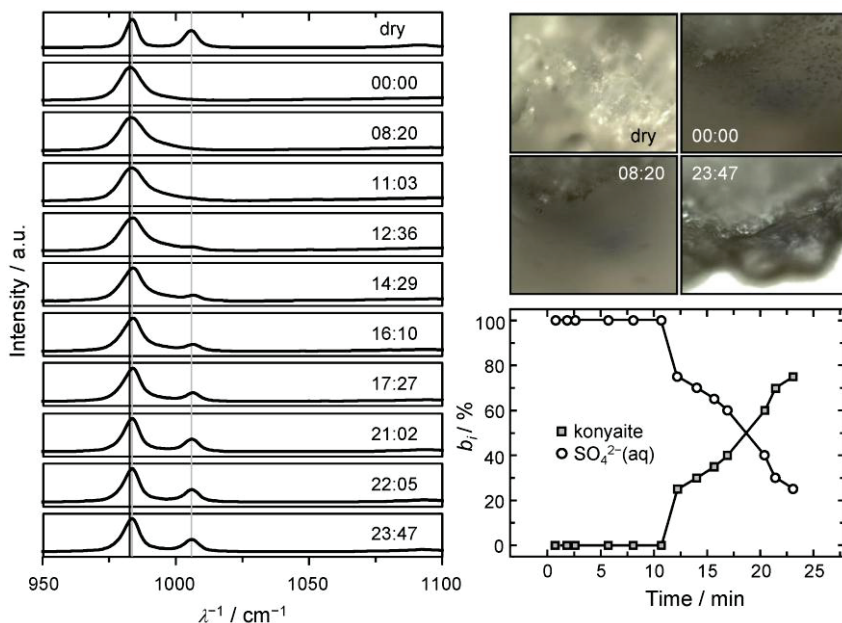


Figure 3: In situ Raman microscopy after wetting of konyaite. Left diagram: initial Raman spectrum of dry konyaite sample and successively recorded spectra after wetting; the vertical lines represent the peak positions in the reference spectra of konyaite (grey) and of an aqueous sulfate solution (black). The micrographs show the sample before and at different times after wetting. Lower right diagram: approximate composition of the sample during wetting (represented by the coefficients b_i of Eq. 1).

really solution left at the end of the measurements and the resolution of micrographs is not sufficient to identify the presence of a solution with certainty. However, additional Raman spectra were recorded after several days. Only konyaite could be identified in the spectra of this completely dried sample.

3.3.2 Wetting of pure bloedite crystals

The interpretation of the wetting experiment with bloedite crystals turned out to be more complicated. The results are shown in Figure 4. The first spectrum confirms bloedite as the starting material which is dissolved completely after the addition of water (second spectrum in Figure 4). During the following 40 min a precipitate forming a thin layer on top of the solution droplet started to grow (see micrographs after 18 and 41 min). Upon closer inspection of the Raman spectra a slight shift of the peak maximum can be seen and also a decrease in the peak width. This is a

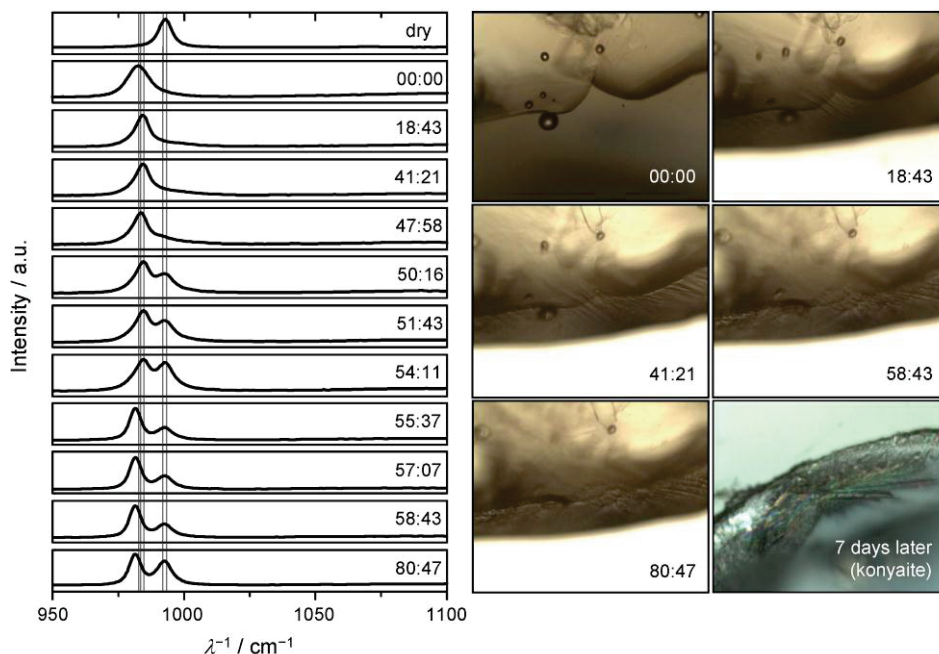


Figure 4: In situ Raman microscopy after wetting of bloedite. Left diagram: initial Raman spectrum of dry bloedite sample and successively recorded spectra after wetting; the vertical lines represent the peak positions in the reference spectra of aqueous sulfate, hexahydrate, epsomite, bloedite and thenardite (from left to right). The micrographs show the sample before and at different times after wetting.

clear indication for the presence of either hexahydrate or epsomite as the main constituent of the crystalline layer. This is in agreement with the observation of such layers in droplet evaporation experiments with pure MgSO_4 solutions. In these experiments the crystalline layers hindered further evaporation of the droplet and made it extremely difficult to detect other crystalline phases or aqueous solutions that are present underneath.

There is no significant change in the Raman spectra during the first 50 min after the addition of water although the micrographs clearly show the continuous growth of the layer. Only then, a second peak at about 993 cm^{-1} occurred in the spectrum (50 min). This peak may be assigned to thenardite, however, the peak position is also close to the peak in the reference spectrum of bloedite (992.3 cm^{-1}) and it is impossible to ascribe this peak to either one of these two solids with certainty. Due to the uncertainties regarding the identity of the solid phases no calculations of the sample compositions were carried out.

In the following 30 min the spectra do not alter very much apart from changes in the intensity ratios of the two peaks that may be caused by minor movements of solution and crystalline deposits during evaporation resulting in a small displacement of the laser spot. According to the micrographs, solution is still present after 80 min, therefore, the last spectrum probably represents a mixture of dissolved sulfate, epsomite (or hexahydrate) and either thenardite or bloedite.

After 7 days of drying several Raman spectra of the completely dry sample were recorded. Surprisingly, konyaite was found as the main constituent with minor contributions of a second phase (thenardite or bloedite). Since it is unlikely that konyaite is formed by conversion from bloedite (usually the opposite is observed [19]), we conclude that a likely crystallization pathway after wetting includes the initial formation of epsomite (or hexahydrate) followed by thenardite precipitation and, subsequently, with ongoing evaporation the formation of konyaite. Considering the solubility diagram (Figure 1), the crystallization of epsomite (or hexahydrate) is surprising as this requires very high supersaturation with respect to bloedite, konyaite and thenardite. However, if it is accepted that a magnesium sulfate hydrate crystallizes first (epsomite being more likely), the remaining solution becomes enriched in sodium sulfate. It can then be understood that thenardite is the second solid phase that is precipitated as the solution is no longer equimolar (cf. Figure 1). In contrast to the wetting experiment with konyaite, this compound did not crystallize as the first solid in the wetting experiment with bloedite. One reason may simply be that nuclei acting as seed crystals were still present after the initial dissolution of konyaite.

In conclusion, also bloedite does not follow the expected behavior of an incongruently soluble salt upon wetting. For incongruent dissolution the precipitation of mirabilite is expected (cf. Figure 1). Obviously, the supersaturation with respect to mirabilite in a solution saturated with bloedite is not sufficient for the nucleation of mirabilite. Crystallization only occurs after further increase of the solution concentration during evaporation. Under these conditions other phases than mirabilite are formed.

3.3.3 Comparison to single salt behavior and damage potential

Sodium sulfate is considered as one of the most damaging salts in building materials and is frequently used in laboratory crystallization tests. It is well known that the destructive process is the growth of mirabilite crystals from the highly supersaturated solutions originating from the dissolution of anhydrous Na_2SO_4 [4,20]. Recently, we have confirmed this reaction pathway by in situ Raman microscopy [14]. In that study we carried out wetting experiments with thenardite similar to the experiments with bloedite and

konyaite in the present work. Wetting of thenardite with a limited amount of water leads to the formation of a solution saturated with thenardite. At 23 °C, the temperature of the wetting experiments, the solubility of thenardite is more than twice that of mirabilite. Hence, mirabilite crystallization occurs under conditions of very high supersaturation resulting in substantial crystallization pressure [4].

Similar behavior is expected in the case of magnesium sulfate. However, the resulting supersaturation depends on the nature of the lower hydrated phase, i.e. on the degree of dehydration after drying. Very high supersaturation resulting in significant stress is generated during the wetting of the lowest hydrate of magnesium sulfate, i.e. $\text{MgSO}_4 \cdot \text{H}_2\text{O}$ (kieserite) [7,8].

Similar behavior was also demonstrated in wetting experiments with the incongruently soluble double salt $\text{Na}_3\text{NO}_3\text{SO}_4 \cdot \text{H}_2\text{O}$ (darapskite). After wetting of darapskite rapid crystallization of mirabilite from a substantially supersaturated solution was observed by Raman microscopy [14]. In the wetting experiments carried out in the present work, the supersaturation with respect to mirabilite of a solution just saturated with bloedite is only about 15%. This is obviously not enough for nucleation to occur in our experiment. However, even if nucleation occurred, the resulting crystallization pressure is expected to be low at such moderate supersaturation. Assuming that the supersaturation of 15% can be maintained during crystal growth, a maximum crystallization pressure of only 2.2 MPa is calculated at 23 °C. This value is significantly lower than the values of 12.3 MPa and 10.6 MPa that are obtained for the wetting of thenardite and phase III, respectively, at the same temperature, thus indicating that the damage potential of the dissolution of the incongruently soluble double salt bloedite is much lower. Also in comparison to the wetting of darapskite, which yields a crystallization pressure of 4.4 MPa at the same temperature, the damage potential of bloedite appears to be lower. This is also confirmed by our ongoing wetting-drying experiments with sandstone specimens contaminated with an equimolar Na_2SO_4 – MgSO_4 mixture. The results of these experiments will be reported elsewhere.

4 Conclusions and outlook

The dissolution of thenardite and lower hydrated phases of magnesium sulfate leads to highly supersaturated solutions. In effect, the respective higher hydrated phases, i.e. mirabilite and epsomite or hexahydrate, crystallize out. If crystal growth occurs in confinement, a high crystallization pressure can be generated. In theory, the same mechanism also applies to incongruently soluble double salts. Their dissolution leads to a solution that is supersaturated with respect to one of the single salt compounds.

Depending on the degree of supersaturation, wetting of an incongruently soluble double salt in a porous material may also cause high crystallization pressures. This mechanism was confirmed in a recent study with darapskite; its dissolution was followed by crystallization of mirabilite. In contrast, the wetting experiments carried out in the present work show that the dissolution of these salts does not lead to the expected crystallization of mirabilite. Obviously, the degree of supersaturation is not sufficient for mirabilite nucleation in our experiment. The calculation of crystallization pressures confirms that bloedite and, most likely, also konyaite are less damaging than both their single compounds, i.e. sodium sulfate and magnesium sulfate, and in comparison to darapskite, another incongruently soluble double salt.

Acknowledgement

This research was funded by Deutsche Forschungsgemeinschaft (DFG).

References

- [1] Tsui N., Flatt R.J., Scherer G.W. Crystallization damage by sodium sulfate. *J. Cult. Heritage* 4 (2003) 109–115.
- [2] Espinosa Marzal R.M., Scherer G.W. Crystallization of sodium sulfate salts in limestone. *Environ. Geol.* 56 (2008) 605–621.
- [3] Angeli M., Bigas J.-P., Benavente D., Menéndez B., Ronan H., David C. Salt crystallization in pores: quantification and estimation of damage. *Environ. Geol.* 52 (2007) 205–213.
- [4] Steiger M., Asmussen S. Crystallization of sodium sulfate phases in porous materials: The phase diagram Na_2SO_4 - H_2O and the generation of stress. *Geochim. Cosmochim. Acta* 72 (2008) 4291–4306.
- [5] Schiro M., Ruiz-Agudo E., Rodriguez-Navarro C. Damage mechanisms of porous materials due to in-pore salt crystallization. *Phys. Rev. Lett.* 109 (2012) 265503.
- [6] Desarnaud J., Bertrand F., Shahidzadeh N. Impact of the kinetics of salt crystallization on stone damage during rewetting/drying and humidity cycling. *J. Appl. Mech.* 80 (2013) 020911.
- [7] Steiger M., Linnow K., Juling H., Gülker G., El Jarad A., Brüggerhoff S., Kirchner D. Hydration of $\text{MgSO}_4 \cdot \text{H}_2\text{O}$ and generation of stress in porous materials. *Cryst. Growth Des.* 8 (2008) 336–343.

- [8] Balboni E., Espinosa-Marzal R.M., Doehne E., Scherer G.W. Can drying and re-wetting of magnesium sulfate salts lead to damage of stone? *Environ Earth Sci*, 63 (2011) 1463–1473.
- [9] Cardell C., Benavente D., Rodríguez Gordillo J. Weathering of limestone building material by mixed sulfate solutions. Characterization of stone microstructure, reaction products and decay forms. *Mater. Charact.* 59 (2008) 1371–1385.
- [10] De Clercq H. Behaviour of limestone contaminated with binary mixtures of sodium sulphate and treated with a water repellent. *Int. J. Restor. Build. Monum.* 14 (2008) 357–364.
- [11] Steiger M., Charola A.E., Sterflinger K. Weathering and deterioration. In: Siegesmund S., Snethlage R. (eds.) *Stone in architecture*, Springer, Berlin (2011) pp. 227–316.
- [12] De Clercq H., Jovanović M., Linnow K., Steiger M. Performance of limestone laden with Na_2SO_4 – NaNO_3 and Na_2SO_4 – K_2SO_4 mixtures. *Environ. Earth Sci.* 69 (2013) 1751–1761.
- [13] Linnow K., Steiger M., Lemster C., De Clercq H., Jovanović M. In-situ Raman observation of the crystallization in NaNO_3 – Na_2SO_4 – H_2O solution droplets. *Environ. Earth Sci.* 69 (2013) 1609–1620.
- [14] Lindström N., Heitmann N., Linnow K., Steiger M. Crystallization behavior of NaNO_3 – Na_2SO_4 salt mixtures in sandstone and comparison to single salt behavior. 12th International Conference on the Deterioration and Conservation of Stone. New York, 2012.
- [15] Autenrieth H., Braune G. Die Lösungsgleichgewichte des reziproken Salzpaars Na_2Cl_2 + MgSO_4 + H_2O bei Sättigung an NaCl unter besonderer Berücksichtigung des metastabilen Bereichs. *Kali Stein-salz* 3 (1960) 15–30.
- [16] Steiger M., Linnow K., Ehrhardt D., Rohde M. Decomposition reactions of magnesium sulfate hydrates and phase equilibria in the MgSO_4 – H_2O and Na^+ – Mg^{2+} – Cl^- – SO_4^{2-} – H_2O systems with implications for Mars. *Geochim. Cosmochim. Acta* 75 (2011) 3600–3626.
- [17] Hamilton A., Hall C, Pel L. Sodium sulfate heptahydrate: direct observation of crystallization in a porous material. *J. Phys. D* 41 (2008) 212002-1/5.

- [18] Steiger M., Kiekbusch J., Nicolai A. An improved model incorporating Pitzer's equations for calculation of thermodynamic properties of pore solutions implemented into an efficient program code. *Construct. Build. Mater.* 22 (2008) 1841–1850.
- [19] Leduc E.M.S., Peterson R.C., Wang R. The crystal structure and hydrogen bonding of synthetic konyaite, $\text{Na}_2\text{Mg}(\text{SO}_4)_2 \cdot 5\text{H}_2\text{O}$. *Am. Mineral.* 94 (2009) 1005–1011.
- [20] Flatt R.J. Salt damage in porous materials: how high supersaturations are generated. *J. Cryst. Growth* 242 (2002) 435–454.

The crystallization behavior of sodium magnesium sulfate in limestone

S. Godts*, R. Hendrickx and H. De Clercq

Royal Institute for Cultural Heritage (KIK-IRPA), Brussels, Belgium

* sebastiaan.godts@kikirpa.be

Abstract

The deterioration of porous building materials caused by single salts has been investigated extensively. Recently, more emphasis is given to the assessment of salt mixtures. Since a few years the ECOS/RUNSALT model is being used for the interpretation of the crystallization behavior of detected ion mixtures. The double salt bloedite or $\text{Na}_2\text{Mg}(\text{SO}_4)_2 \cdot 4\text{H}_2\text{O}$ is frequently found in the output of the predictive model. However, the crystallization behavior and the destructive effects of double salts such as bloedite are generally not documented. This paper presents the results of a research project carried out to assess the behavior of sodium magnesium sulfate in limestone related to that of the respective single salts. Limestone samples were contaminated with aqueous solutions of equimolar mixtures of sodium and magnesium sulfate at different concentrations and conditioned at different environmental conditions. The drying behavior as well as the crystallization behavior upon repeated drying-rewetting cycles was investigated. Identification of efflorescence was carried out by micro-Raman spectroscopy and XRD. The results indicate in general that the (initial) drying rate is an important factor for efflorescence development, which is influenced by ambient RH as well as the concentration of the salt solution used for the contamination of the samples. For samples contaminated with equimolar mixtures of Na_2SO_4 — MgSO_4 , konyaite $\text{Na}_2\text{Mg}(\text{SO}_4)_2 \cdot 5\text{H}_2\text{O}$ precipitates during the first cycles, while only after several cycles bloedite $\text{Na}_2\text{Mg}(\text{SO}_4)_2 \cdot 4\text{H}_2\text{O}$ is identified.

Keywords: bloedite, konyaite, limestone, deterioration, conservation

1 Introduction

Damage to porous building materials and stone sculptures caused by the expansion pressures of salts is a well-known phenomenon, as described in a selective review by Doehne [1]. Over the past decade the thermodynamic ECOS/RUNSALT model [2], a mole-fraction-based model, is being used for the interpretation of the crystallization behavior of detected ion mixtures. The double salt bloedite or $\text{Na}_2\text{Mg}(\text{SO}_4)_2 \cdot 4\text{H}_2\text{O}$ is frequently found in the output of the predictive model. However, the real behavior of the salt in practice or in lab is not documented.

This paper describes the results of the investigation on the crystallization behavior and damage potential of sodium magnesium sulfate on Maastricht limestone related to that of the respective single salts. The solution transport and drying behavior are investigated and compared to numerical calculations. The salt crystallization behavior in climatic conditions of 35 and 70% RH (25°C) is discussed.

2 Experimental procedure

Maastricht limestone samples are cut into 35 mm sided cubes. To avoid evaporation from the sides during absorption and drying, they are covered with sheets of dental modeling wax (Cavex[®]) applied with a heated spatula (Figure 1). The wax cover extends the height of the sample to avoid loss of efflorescence and to allow the addition of water during rewetting cycles.

Three sulfate concentrations are selected: 0.578, 1.100 and 1.700 mol/kg for a contamination with MgSO_4 and the equimolar mixture of Na_2SO_4 and MgSO_4 . In case of Na_2SO_4 , only the highest concentration (1.700 mol/kg) was tested as the lower ones have previously been investigated [3]. Per type of salt solution (7 in total), plus one reference test with pure water, four samples are used, which brings the total number of samples to 32.

Contamination was carried out by putting the bottom in contact with the salt solution or pure water. The capillary absorption rate was measured during the solution uptake, one sample per solution. Then, the bottom was closed off with transparent tape. Half of the samples (two of each group) were conditioned in a ventilated climate chamber at 35% RH and 25°C while the other half at 70% RH and 25°C to evaluate the drying behavior

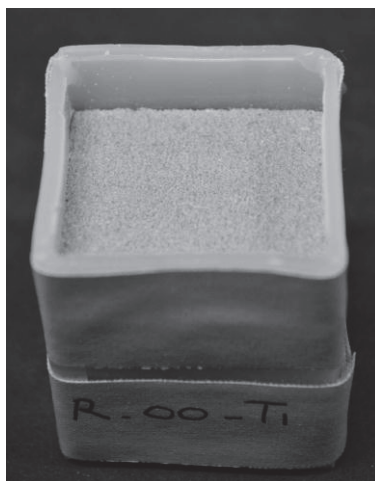


Figure 1: Sample with wax cover

and eventually the occurrence of damage over time upon repeated drying-rewetting cycles. The samples were weighed and photographed daily. After 14 days, an amount of water equal to the amount of evaporated water is poured on the top surface, dissolving all or most of the efflorescence. Consecutive rewetting and drying cycles are carried out (drying time of 14 days) until damage was visible. Due to practical circumstances the drying time of the sixth cycle was extended to 50 days. In total, 11 cycles were carried out. At the end of the program each sample was left to dry until constant weight was reached.

Efflorescence was identified with micro-Raman spectroscopy (Renishaw InVia). The measurements were carried out with a 780nm near infrared diode laser through a long-distance objective with a magnification of x5 or x50 reaching approximately 17,7 mW or 14,3 mW at the sample. An exposure time of 10 sec and a measurement range between 100.00 and 2000.00 cm^{-1} was sufficient to obtain identifiable spectra. At the end of the cycles the efflorescence is subjected to X-Ray Diffraction analysis (BRUKER D8 theta/2theta configuration).

3 Maastricht stone

Maastricht stone [4-6] is a pale yellow limestone, consisting mainly of microfossils and sand-sized fragments of microcrystalline carbonate. It is extremely light (density between 1300-1450 kg/m^3) and porous, has a low mechanical resistance (a compressive strength of 13.4-50 kg/cm^2), is easily scratched, and has a fine-grained, sandy structure. The microscopic structure resembles weakly cemented loose-packed sand. Because it is so easily workable and relatively frost resistant, it has been used frequently as a building stone in the Limburg region (Belgium and The Netherlands), especially during the Middle Ages and the Renaissance period.

The average porosity of the stone used for this investigation is 51%. The dominant pore size between 10 and 100 micron corresponds to the space between the grains. About 80% of the pore space corresponds to pores falling in this range, which means that the pore structure is highly monomodal. Some 20% of the pores (in volume) are smaller than 10 micron; this can be related to the intragranular porosity, like the hollows of fossils.

Because of its specific microstructure and properties, it is easily damaged by salts (fast and abundant uptake of solution and rapid drying). This has motivated researchers in Belgium and Europe to use it as a model material in lab experiments and it was also the reason why it was selected for the current test program.

The dry density of the Maastricht stone used in the tests is $1278 \pm 20 \text{ kg/m}^3$ (based on volume and measured dry mass). The average capillary water absorption coefficient derived from 5 measurements is 3.88 ± 0.74

$\text{kg/m}^2\text{s}^{0.5}$ with an average capillary saturated water content (w_{cap}) of $418 \pm 18 \text{ kg/m}^3$. This corresponds to a capillary saturation coefficient of $(41.8/51.0) * 100 = 82\%$. Due to the extremely fast absorption, it is not easy to measure the absorption rate because the process has to be interrupted at each measuring point. Apart from the intrinsic variations in the stone, this leads to a relatively important scatter in the results.

4 Results

4.1 Absorption and drying of limestone with salt solutions

The absorption rate of each of the salt solutions is expected to be equal to the one of water, scaled to the ratios of density and dynamic viscosity of the liquids. This was validated for very homogeneous materials [7-10], but not quantitatively for the Maastricht stone (Figure 2), although a trend of decreasing absorption rate (in volume units) and increasing saturation (in mass units; it remains approximately constant in volume units), was clearly observed for each case. One plausible explanation for this deviation is that the sharp front equation is an approximation and also that the increased surface tension, which leads to a higher capillary suction, was not accounted for. The theoretical approach is not further described in this paper.

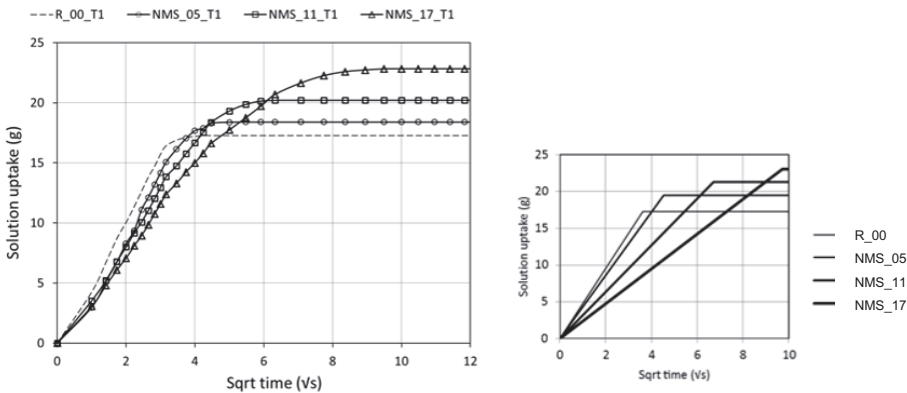


Figure 2: Absorption curves of one sample contaminated with sodium and magnesium sulphate in 3 concentrations and pure water, on the right the predicted curves. R: reference samples, NMS: sodium and magnesium sulfate, MS: magnesium sulfate in different concentrations 05: 0.578 mol/kg; 11: 1.100 mol/kg; 17: 1.700 mol/kg.

Drying of Maastricht stone with salts is expected to be slower than with water. The evaporation flux at the surface q_{evap} ($\text{kg/m}^2\text{s}$) is driven by the difference in vapor pressure at the surface ($p_{v,\text{surf}}$, Pa) and in the surrounding atmosphere ($p_{v,\text{atm}}$, Pa) and can be expressed by a simplified formula:

$$q_{\text{evap}} = \beta(p_{v,\text{surf}} - p_{v,\text{atm}})$$

with β a transfer coefficient which depends on the air flow pattern and the topography of the surface. In the case of pure water in the pores, the surface vapor pressure will remain equal to the saturation vapor pressure at the current temperature (RH 100%) as long as liquid water is transported to the surface from inside the stone.

Knowing that drying at 20°C and 50%RH leads to an initial rate of 0.42 $\text{kg/m}^2\text{h}$ for a vapor pressure difference of 2339-1169=1170 Pa in these test conditions, the expected initial drying rates for the salt solutions can be calculated (knowing the transfer coefficient $\beta = 3.59\text{e-}4 \text{ h/m} = 9.97\text{e-}8 \text{ s/m}$). It is assumed that liquid and gas phases are in equilibrium; i.e. the water activity (a_w) of the liquid phase equals the RH in the gaseous phase. The measured initial drying rates are an average over a period of the first 24 h. Although a substantial decrease of drying rate can already occur within 24h, for the sake of clarity and to keep the focus on the long-term effect, we kept the nomenclature of the "initial drying rate".

The experimentally measured initial drying rates are quite different from the calculated ones, and it appears that the difference can be related to the RH of the environment, the salt concentration and the type of salts introduced (Figure 3). A lower RH of 35% should theoretically lead to much faster drying. A trend in this sense could be observed, but not to the extent as could be expected theoretically. The lower-than-expected drying rates can be attributed to the blocking or clogging effect of crystallized salts near the surface, as was demonstrated for sodium chloride in brick by Gupta [11]. It was found that rapid drying (at little more than 0% RH) leads to the formation of "patchy" efflorescence, which tends to block the pores and prevents the formation of a receding drying front, while a slower drying leads to the formation of more protruding, cauliflower-shaped, "crusty" efflorescence that do conduct liquid. Eloukabi [12] also relates these two distinct drying regimes to the different types of efflorescence.

Similar remarks can be made on the effect of concentration: higher concentrations have systematically lower initial drying rates, but the effect is much stronger than expected and this deviation can again be attributed to clogging. Systematic trends according to the type of salt could not be observed from this analysis.

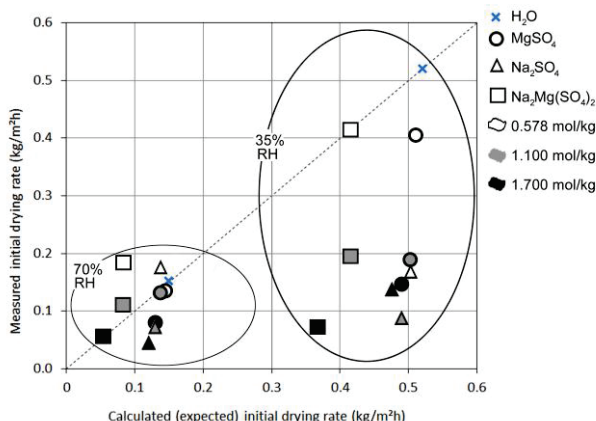


Figure 3: Experimentally measured (average of two samples) and calculated drying rates during the first 24 h after the uptake of salt solutions or pure water (1st cycle); the data are presented according to: the environmental RH (35 or 70 %) at 25°C, the molal concentration of the solutions, and the type of salt.

The experimentally measured initial drying rates (measured 24 hours after the start of each cycle) with pure water show a drying rate of about 0.52 kg/m²h for the samples conditioned at 35% RH and a lower rate of approximately 0.15 kg/m²h for the samples conditioned at a RH of 70%. The initial drying rate for the salt contaminated samples is generally lower compared to that of pure water (Figure 4). A significant drop of the drying rate occurs after the first cycle for the Maastricht stone contaminated with the lowest concentration of the equimolar mixture of sodium and magnesium sulfate (0.578 mol/kg) at 35% RH. There is a general trend of slower initial drying rates for all the samples during the first cycles, which stabilizes and then speeds up again after several cycles. This can be related to pore clogging and redistribution of salts after the addition of water at the start of each cycle.

Notable changes are observed over time when comparing the average evaporation rates over the last 24 h of each cycle (Figure 5). The water evaporation rate of the samples contaminated with magnesium sulfate in all three concentrations and those with 0.578 mol/kg sodium magnesium sulfate have is logically lower at higher RH. It becomes more complicated for the samples contaminated with a solution of 1.100 mol/kg as the evaporation rate dramatically increases after each cycle when conditioned at 70% RH, surpassing the evaporation rate of the samples conditioned at 35% (Figure 6). For the samples contaminated with a 1.700 mol/kg sodium magnesium sulfate solution this starts from the first cycle onwards. The increase of evaporated water at higher RH can be associated with a

decreased pore clogging, an increase in efflorescence and perhaps an increase in deterioration.

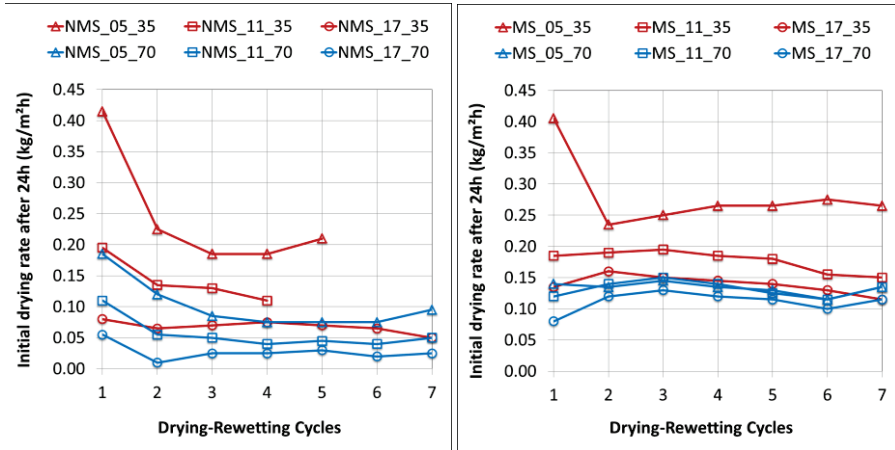


Figure 4: Average initial drying rate of samples contaminated with an equimolar mixture of sodium and magnesium sulfate (NMS, left) and magnesium sulfate (MS, right) in concentrations 0.578, 1.100 and 1.700 mol/kg conditioned at 35 (red) and 70% RH (25°C) for each rewetting cycle.

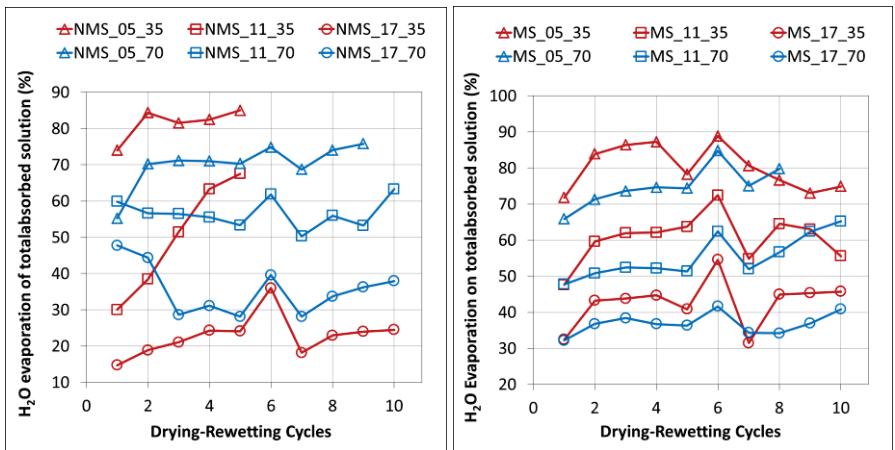


Figure 5: Evolution of the average evaporation of water (%) at the end of each cycle (after 14 days drying) except the 6th that ran over 50 days) of samples contaminated with sodium magnesium sulfate (NMS, left) and magnesium sulfate (MS, right) in different concentrations (05: 0.578 mol/kg ; 11: 1.100 mol/kg ; 17: 1.700 mol/kg) conditioned at 35 (red) and 70% RH (25°C).

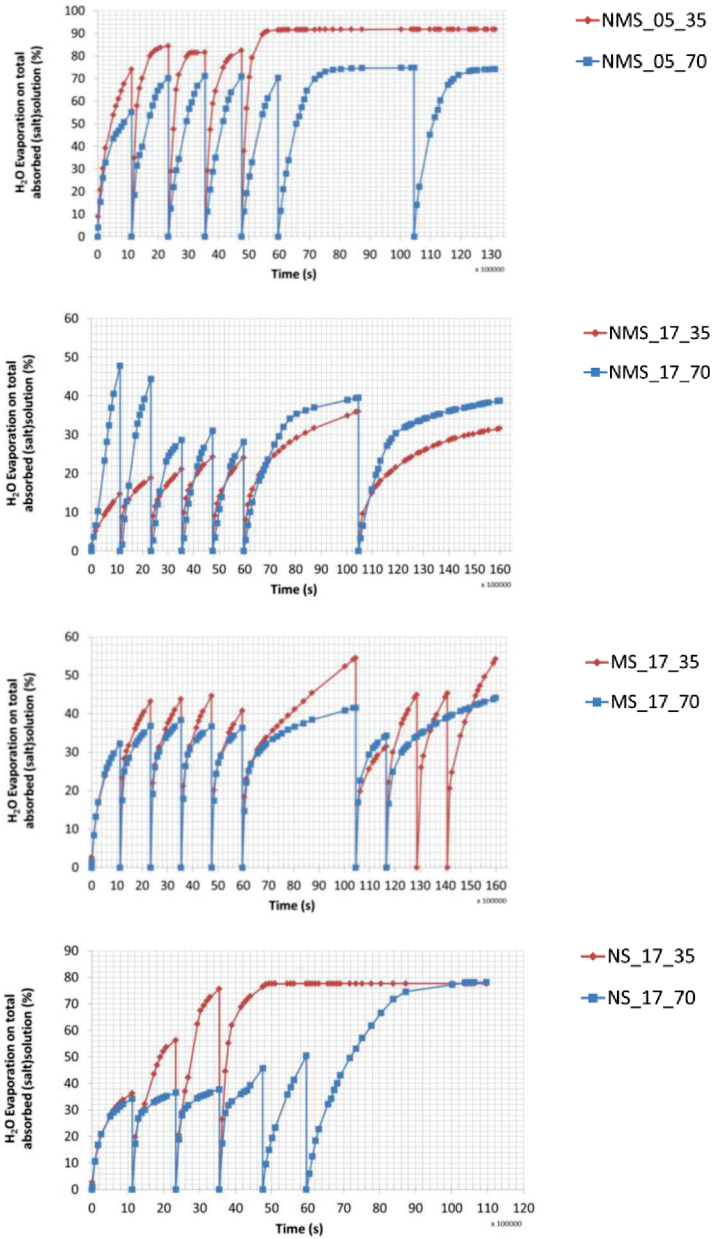


Figure 6: Average % evaporation of H₂O over time (sec) of two samples contaminated with sodium magnesium sulfate (NMS), magnesium sulfate (MS) or sodium sulfate (NS) at different concentrations (05: 0.578 mol/kg or 17: 1.700 mol/kg) at 35 (red) and 70% RH (25°C)

4.2 Salt crystallization processes

4.2.1 Evaporation properties and crystal growth

By observing the efflorescence deposit on the stone surface, significant differences are noticed (Figure 7). Where 35% RH generally leads to a rapid initial drying, patchy efflorescence develops (subsequently slowing down the process), a higher RH of 70% allows for slower but more sustained drying, leading to cauliflower-shaped efflorescence which doesn't block the moisture transport towards the evaporation face. Figure 7 illustrates this trend. Only the 2nd series from the top is an exception to this behavior as efflorescence develops on the surface of the samples at the lowest concentration of sodium magnesium sulfate. Apparently in this case at this stage the amount of salt is not sufficient to block the pores.

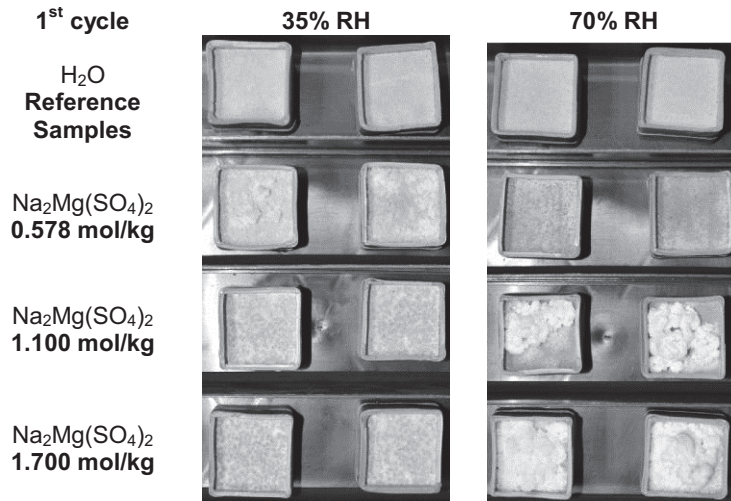


Figure 7: Images of the top faces of the specimens after 1 week of the 1st drying cycle at 35% RH (left) or 70% RH (right) at 25°C. Two specimens per case, contaminated with sodium magnesium sulfate in increasing concentrations from top (pure water) to bottom (1.700 mol/kg). Drying at high RH leads to cauliflower-shaped efflorescence, while low RH leads to efflorescence in patches.

After 1 week of the 2nd drying cycle at 35% RH, a decreasing amount of efflorescence for increasing salt concentration is observed (visually), while the opposite in case of a high RH (Figure 8). The explanation is the same: upon fast drying, a higher salt concentration leads to faster pore clogging

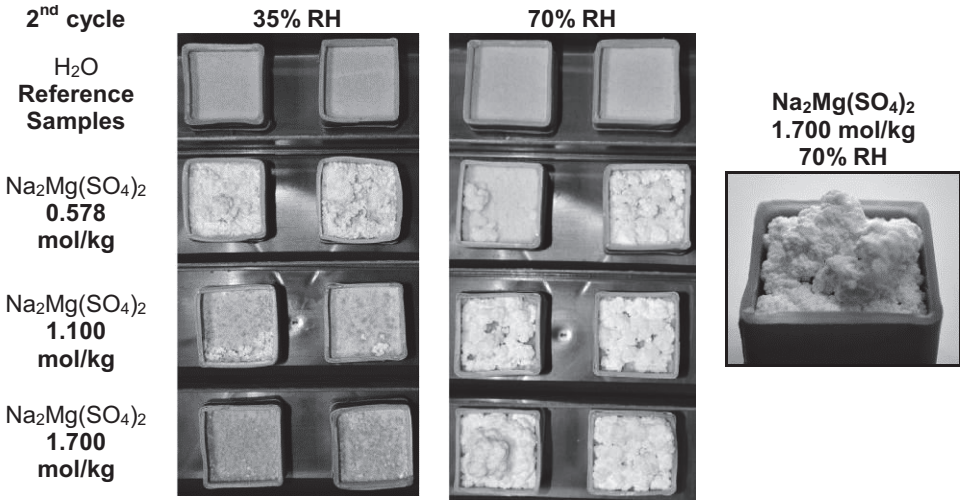


Figure 8: Image of the top faces of the specimens after 1 week of the 2nd drying cycle at 35% RH (left) or 70% RH (middle) at 25°C. Two specimens per case, contaminated with sodium magnesium sulfate in increasing concentrations from top (pure water) to bottom (1.700 mol/kg). Side view of a sample contaminated with sodium magnesium sulfate (1.100 mol/kg) conditioned at 70% RH (right).

This interpretation cannot be generalized to other types of salt. Figure 9 shows the top surfaces of the specimens contaminated with the single salts magnesium sulfate and sodium sulfate after one week of the 3rd cycle. Whereas the Maastricht stone is known for its rapid drying at the surface, magnesium sulfate is known for causing preferential subflorescence within limestone instead of efflorescence, when compared to sodium sulfate [13]. The higher viscosity of the magnesium sulfate solutions at equal molality, also decreasing the absorption rate, slows down their transportation (Table 1).

Sodium sulfate seems to be much less influenced by this pore clogging phenomenon: a drier environment leads to faster drying and more damage. The initial drying rate recorded in the first cycle is rather low (Figure 6) but increases a lot due to cracks formed, probably upon re-wetting in between the cycles.

Table 1: Solution Properties. Measurements obtained from: ■ Raf De Dier, Dept. of Applied Rheology, KULeuven, (viscometer Ubbelohde); ■ Michael Steiger, Dept. of Chemistry, UHamburg; ■ CRC Handbook interpolated; ■ Estimated based on ratio η_{25}/η_{20} of $MgSO_4$; ■ Wikipedia

mol/kg	Na ₂ SO ₄			MgSO ₄			Na ₂ Mg(SO ₄) ₂			H ₂ O
	0.578	1.100	1.700	0.578	1.100	1.700	0.578	1.100	1.700	
density at 25°C (kg/l)	1.066	1.123	1.183	1.064	1.120	1.182	1.127	1.229	1.331	0.997
kinematic viscosity at 25°C (mm ² /s)				1.226	1.634	2.367	1.246	2.497	4.832	0.901
dynamic viscosity at 25°C (mPas)	1.104	1.418	1.904	1.304	1.831	2.797	1.405	3.069	6.431	0.898
density at 20°C (kg/l)	1.067	1.152	1.185	1.066	1.122	1.183				0.998
kinematic viscosity at 20°C (mm ² /s)				1.382	1.860	2.689	1.667	2.860		1.026
dynamic viscosity at 20°C (mPas)	1.255	1.611	2.164	1.473	2.087	3.182				1.002

During the 9th cycle at 35% RH efflorescence is still not visible on the top face of the samples contaminated with magnesium sulfate at all concentrations (Figure 10). The surface of the samples contaminated with the lowest concentration starts to bulge. By the end of the test when the wax around the samples is removed, as shown in figure 10, it becomes clear that sub-efflorescence has deteriorated a superficial layer of approximately 3mm thickness.

At 70% RH a decreasing amount of efflorescence for increasing salt concentration is noticed, in contrary with the results obtained for sodium magnesium sulfate. The explanation is the same in both dry and moist conditions: upon drying, a higher salt concentration leads to faster pore clogging. The discrepancy compared to the sulfate mixtures can be caused by the higher viscosity of the magnesium sulfate solutions (Table 1).

Further evidence is found in the earlier plotted drying rates (Figure 3). It shows that the highest concentration reduces significantly the drying rate compared to the lower concentrations, and that magnesium sulfate tends to cause a further reduced decrease of the expected initial drying rate when compared to sodium sulfate and the sulfate mixture (Figure 6).

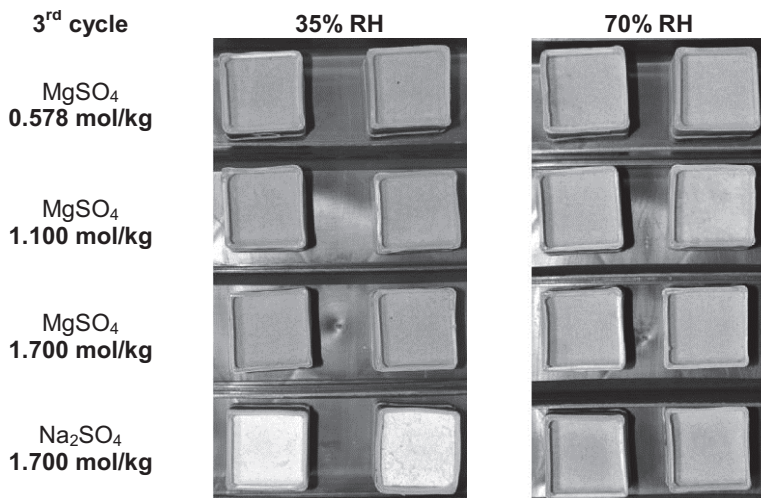


Figure 9: Photograph of the top faces of the specimens after 1 week of the 3rd drying cycle at 35% RH (left) or 70% RH (right) (25°C). Two specimens per case, contaminated with, from top to bottom, magnesium sulfate in increasing concentrations starting from 0.578 to 1.700 mol/kg or sodium sulfate (1.700 mol/kg).

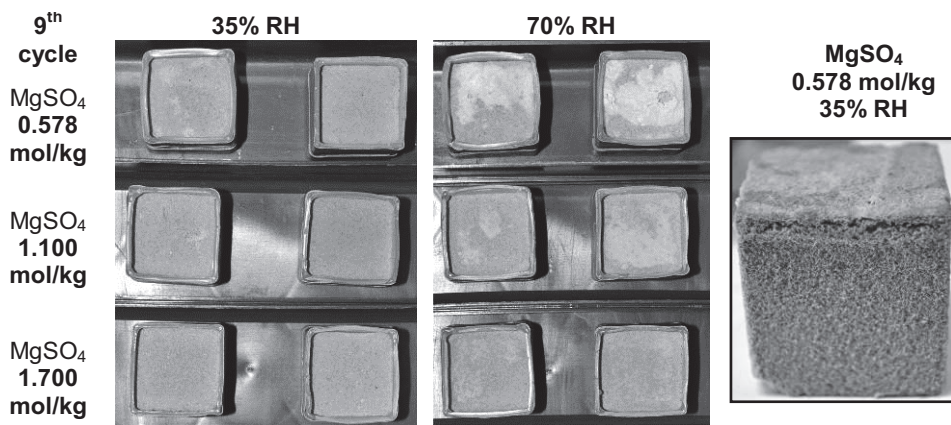


Figure 10: Photograph of the top faces of the specimens after 1 week of the 9th drying cycle at 35% RH (left) or 70% RH (middle) at 25°C. Two specimens per case, contaminated with magnesium sulfate in increasing concentrations starting from top (0.578 mol/kg) to bottom (1.700 mol/kg). Side view of a sample contaminated with magnesium sulfate (0.578 mol/kg) conditioned at 35% RH (right).

4.2.2 Identification of efflorescence

Efflorescence on the samples is investigated with Raman spectroscopy during the second week of each cycle. An average of five measurements is systematically carried out each time efflorescence is visible on the top face. When efflorescence with a different morphology is observed under the microscope, it is also investigated. The obtained spectra are identified with reference spectra obtained from [14] (Table 2). Five main spectra were identified during the entire program (Figure 11). The Raman spectrum of konyaite shows in the range of 900–1100 cm^{-1} a double band at 983.2 and 1005.3 cm^{-1} , while that for bloedite shows only one band at 992.1 cm^{-1} . The efflorescence of samples contaminated with 0.578 mol/kg of $\text{Na}_2\text{SO}_4\text{—MgSO}_4$ conditioned at 70% RH show one strong band at 980.4 cm^{-1} that could not be attributed to a particular phase (Figure 11).

The results show that for all the samples containing equimolar mixtures of $\text{Na}_2\text{SO}_4\text{—MgSO}_4$ at all tested concentrations, only konyaite or $\text{Na}_2\text{Mg}(\text{SO}_4)_2 \cdot 5\text{H}_2\text{O}$ effloresces during the first cycles (Table 3) while bloedite or $\text{Na}_2\text{Mg}(\text{SO}_4)_2 \cdot 4\text{H}_2\text{O}$ later on. Both double salts bloedite and konyaite are analyzed by XRD at the end of the cycles.

For the samples contaminated with MgSO_4 only sub-efflorescence is visibly clogging the pores at the surface of all the samples conditioned at 35% RH with a rare exception for the highest concentration. In case of increased RH, almost no efflorescence is visible on the top face until the 5th cycle with an exception of the samples contaminated with a solution of 1.100 and 1.700 mol/kg of MgSO_4 . Only after the longer 6th cycle efflorescence becomes visible on all the samples conditioned at 70% RH.

The Raman spectra revealed the crystallization of hexahydrite (983.2 cm^{-1}). Although the main band of it is quite close to that of $\text{MgSO}_4 \cdot 7\text{H}_2\text{O}$ (984.5 cm^{-1}), and hence not easy to distinguish, XRD confirmed the presence of hexahydrite. As expected the efflorescence on the samples containing Na_2SO_4 consists of thenardite (Raman band at 993.0 cm^{-1}), further confirmed by XRD at the end of the program.

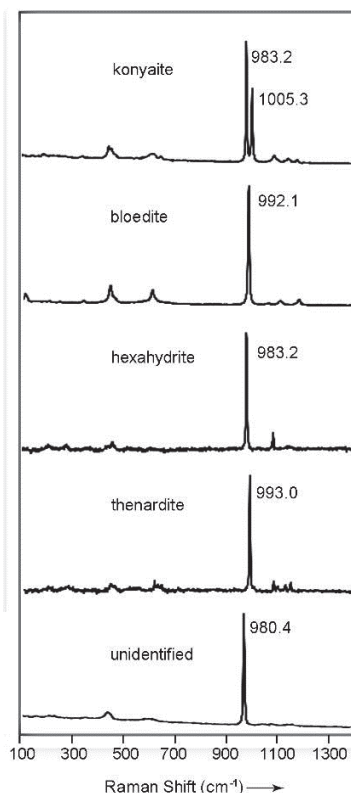


Figure 11: Raman spectra of the efflorescence

Table 2: Main Raman bands (cm^{-1}) of the identified efflorescence compared to the reference spectra and literature

	Measured	Reference spectra [14]	[15]	[16]
Konyaite	983.2	983.5	981	—
	1005.3	1005.5	1003	—
Bloedite	992.1	992.0	995	—
Hexahydrate	983.2	983.0	—	983.6
Epsomite	—	984.5	—	984.1
Thenardite	993.0	993.0	—	—

Table 3: Identification of salt efflorescence with micro-Raman spectroscopy during the second week of each cycle and identification with XRD at the end of the program. The samples for which bloedite was detected are marked in gray.

sample / cycle	C1	C2	C3	C4	C5	C6	C7	C8	C9	C10	C11
NMS_05_35	K	K	K	K	K	K/B	K/B	K/B	K/B	K/B	K/B (X)
NMS_05_70	U	K/U	K	K	K/B	K	K/U	K/B	K/B	K/B	K/B (X)
NMS_11_35	K	K	K	K	K	K/B	K/B	K/B	K/B	K/B	K/B (X)
NMS_11_70	K	K	K	K	K	K	K/B	K/B	K/B	K/B	K/B (X)
NMS_17_35	K	K	K	K	K	K/B	K/B	K/B	K/B	K/B	
NMS_17_70	K	K	K/B								
MS_05_35						S	S	S	S		
MS_05_70						H	H	H	H	H	H (X)
MS_11_35						S	S	S	S		
MS_11_70		H	H	H	H	H	H	H	H		
MS_17_35					H	H	S	S	S	S	
MS_17_70	H					H	H	H	H		
NS_17_35		T	T	T	T	T	T	T	T	T	T (X)
NS_17_70	T			T	T	T	T	T	T	T	T (X)

Legend:

NMS: $\text{Na}_2\text{Mg}(\text{SO}_4)_2$ **MS:** MgSO_4 **NS:** Na_2SO_4 **05:** 0.578 mol/kg**11:** 1.100 mol/kg**17:** 1.700 mol/kg**35:** 35% RH, 25°C**70:** 70% RH, 25°C**C:** cycle number**K:** konyaite**B:** bloedite**U:** unidentified**S:** sub-florescence**H:** hexahydrate**E:** epsomite**T:** thenardite**(X):** XRD

5 Conclusions

The absorption rate of each of the sulfate solutions in the experiments with the Maastricht stone did not correspond to the expected rates. However, the decreased absorption and increased saturation compared to pure water remain rather constant for each case. The results show significant differences in drying behavior between the individual salts and the salt mixture, between different concentrations and RH conditions. Important deviations were found for drying at the lower RH: a fast initial drying leads to pore clogging in almost all cases, subsequently slowing

down the process. This confirms previous studies which stated that, for salts which are prone to pore clogging, high RH drying appears more effective because it reduces the clogging effect. The preliminary observations on the damage potential of the single salts Na_2SO_4 and MgSO_4 are generally in agreement with recent literature [13, 17].

In general it can be concluded that a lower concentration and a lower RH leads to higher amounts of efflorescence deposited at the surface of samples contaminated with Na_2SO_4 — MgSO_4 while higher concentrations tend to lead to a stronger pore clogging reducing efflorescence, and vice versa at a higher RH. This phenomenon can also be concluded for samples contaminated with the single salt MgSO_4 with an important discrepancy in case of more humid conditions where higher concentrations also tend to lead to a stronger pore clogging and a reduced efflorescence.

The Na_2SO_4 contaminated samples dry fast and large amounts of thenardite sub- and efflorescence are produced causing rapid deterioration and layer detachment, which is first observed for the samples conditioned at 35% RH. MgSO_4 contaminated samples dry slower; damage is mainly caused by hexahydrate subflorescence causing bulging, followed by the collapse of the surface layer, probably occurring during rewetting. The subflorescence causes internal crack formation after a significant amount of cycles, which is first detected for the samples conditioned at 70% RH while only later at 35%. For samples contaminated with an equimolar mixture of sodium and magnesium sulfate, konyaite or $\text{Na}_2\text{Mg}(\text{SO}_4)_2 \cdot 5\text{H}_2\text{O}$ precipitates during the first cycles, while only after several cycles bloedite $\text{Na}_2\text{Mg}(\text{SO}_4)_2 \cdot 4\text{H}_2\text{O}$ crystallized, although frequently appearing in the output of ECOS/RUNSALT.

From this investigation it can be concluded that the salt crystallization behavior depends on the cycle numbers. In order to understand the behavior of double salts the execution of a sufficient amount of crystallization cycles is crucial. In general we can state that the (initial) drying rate is an important factor for the damage potential, which is influenced by the ambient RH as well as the salt type and concentration of the solution. A lower concentration leads to a higher damage potential in samples contaminated with $\text{Na}_2\text{Mg}(\text{SO}_4)_2$. Again, this can be explained by the stronger pore clogging effect when using higher concentrations. Furthermore, the preliminary results indicate that the formation of bloedite possibly causes a further decrease in the drying rate perhaps due to its less soluble nature compared to konyaite.

References

- [1] E. Doehne. Salt weathering: a selective review. In: *Natural Stone, Weathering Phenomena, Conservation Strategies and Case Studies*: Edited by S. Siegesmund, T. Weiss and A. Vollbrecht - Geological Society of London, (2002)
- [2] C. Price (Ed.). An expert chemical model for determining the environmental conditions needed to prevent salt damage in porous materials. European Commission Research Report No 11, (Protection and Conservation of European Cultural Heritage). London: Archetype Publications, (2000)
- [3] H. De Clercq, M. Jovanović, K. Linnow, M. Steiger. Performance of limestones laden with mixed salt solutions of $\text{Na}_2\text{SO}_4\text{-NaNO}_3$ and $\text{Na}_2\text{SO}_4\text{-K}_2\text{SO}_4$, *Environmental earth sciences*, 69 (5), (2013), pp 1751-1761
- [4] CW. Dubelaar, M. Duser, R. Dreesen, WM. Felder, TG. Nijland. Maastricht limestone: a regionally significant building stone in Belgium and the Netherlands. Extremely weak, yet time-resistant. In Fort R, de Buergo MA, Gomez-Heras M and Vazquez-Calvo C (eds): *Proceedings of the International Heritage, Weathering and Conservation Conference*, Taylor&Francis Group, London, (2006), pp 9-14
- [5] E. Roekens, E. Leysen, E. Stulens, J. Philippaerts, R. Van Grieken. Weathering of Maastricht Limestone Used in the Construction of Historical Buildings in Limburg, Belgium. In Ciabach J (ed): *Proceedings of the 6th International Congress on Deterioration and Conservation of Stone*, Nicholas Copernicus University Press Department, Torun, (1988), pp 45-56
- [6] M. Duser, R. Dreesen, A. De Naeyer. *Renovatie & Restauratie, Natuursteen in Vlaanderen, versteend verleden*. Wolters Kluwer België NV, (2009), pp 427-437
- [7] R. Hendrickx, S. Roels, H. De Clercq, Y. Vanhellemont. Experimental Determination of Liquid Transport Properties on Salt-Contaminated Porous Stone. In V. De Freitas, H. Crovacho, & M. Lacasse (Eds.), *12th International Conference on Durability of Building Materials and Components*, Porto, 12-15 April 2011, Rotterdam (2011), pp 125-132

- [8] H. Derluyn, M. Griffa, D. Mannes, I. Jerjen, J. Dewanckele, P. Vontobel, A. Sheppard, D. Derome, V. Cnudde, E. Lehmann, J. Carmeliet. Characterizing saline uptake and salt distributions in porous limestone with neutron radiography and X-ray microtomography, *Journal of Building Physics*, 36 (4), (2013), pp 353–374, doi:10.1177/1744259112473947
- [9] C. Hall, WD. Hoff. Water transport in brick, stone and concrete. London: Taylor & Francis, (2002)
- [10] AS. Poupeleer. Transport and crystallization of dissolved salts in cracked porous building materials. PhD thesis KU Leuven, (2007)
- [11] S. Gupta. Sodium chloride crystallization in drying porous media: influence of inhibitor. PhD thesis Eindhoven University of Technology, (2013)
- [12] H. Eloukabi, N. Sghaier, S. Ben Nasrallah, M. Prat. Experimental study of the effect of sodium chloride on drying of porous media: The crusty–patchy efflorescence transition, *International Journal of Heat and Mass Transfer*, 56 (1-2), (2013), pp 80–93
- [13] A. Ruiz-Agudo, F. Mees., P. Jacobs, C. Rodriguez-Navarro. The role of saline solution properties on porous limestone salt weathering by magnesium and sodium sulfates. *Environ Geol* (52), (2007), pp 269-281
- [14] Reference spectra obtained from Kirsten Linnow and Nadine Lindstroem, University of Hamburg, Department of Chemistry, Inorganic and Applied Chemistry, Michael Steiger Research Group.
- [15] P. Vargas Jentzsch, B. Kampe, P. Rösch, J. Popp. Raman Spectroscopic Study of Crystallization from Solutions Containing $MgSO_4$ and Na_2SO_4 : Raman Spectra of Double Salts, *The Journal of Physical Chemistry* 115 (22), (2011), pp 5540-5546
- [16] A. Wang, JJ. Freeman, BL. Jolliff, IM. Chou. Sulfates on Mars: A systematic Raman spectroscopic study of hydration states of magnesium sulfates. *Geochimica et Cosmochimica Acta* 70, (2006), pp 6118-6135
- [17] M. Steiger, K. Linnow, H. Juling, G. Gülker, A. El Jarad, S. Brüggerhoff, D. Kirchner. Hydration of $MgSO_4 \cdot H_2O$ and generation of stress in porous materials. *Crystal Growth & Design* 8 (1), (2008), pp 336–343

Common salt mixtures database: a tool to identify research needs

S. Godts*, R. Hayen, and H. De Clercq

Royal Institute for Cultural Heritage (KIK-IRPA), Brussels, Belgium

* sebastiaan.godts@kikirpa.be

Abstract

Salt mixtures found in building materials and stone sculptures have been analyzed in the Monuments Laboratory at KIK-IRPA since the early 1960's. The common salt mixtures database is a spreadsheet based on the results of quantitative ion analyses carried out with Ion Chromatography at KIK-IRPA since 2004, currently counting almost 6000 records of samples from Belgian monuments and sculptures, e.g., about 1600 brick and mortar samples, 300 wall plaster and 581 natural stone samples. Today, approximately 500 samples are yearly analyzed and added to the database. The samples are classified by location, type of material, depth and height. The main objective of this database is to generate average compositions of salt mixtures according to different criteria such as the geographic region, the type of building material, the depth and the height and hence to narrow down specific research needs and move from single salts to relevant salt mixtures. The average ion content representative for a selected group of samples is entered into the program ECOS/RUNSALT to predict the crystallization behavior. The outputs reveal a complex mixture consisting of kieserite, starkeyite, thenardite, nitratine, niter, darapskite, halite, bloedite and aphanthalite. Ultimately the location data will be linked to a geographic information system (GIS) and the database will be made available online so that researchers active in the field of salt analyses can add data.

Keywords: salt, database, conservation, monuments, ecos

1 Introduction

A database was established containing quantitative ion data of the aqueous extract of powder samples lifted from Belgian monuments since 2004. The database currently contains the results of almost 6000 samples classified among others by date, location, material type, depth and height. From the database common occurring salt mixtures can be derived according to selected criteria. For example, from a total of 244 brick samples lifted from the first centimeter at a height up to 30 cm from the floor level, an average ion composition can be calculated. This data can then be entered into the RUNSALT software [1] based on the thermodynamic model ECOS (Environmental Control of Salts) [2]. The output represents in this specific case the salt crystallization behavior of the average ion mixture typical for the first cm of brick at a height up to 30 cm, consisting of halite, bloedite, niter, nitratine, starkeyite, kieserite and thenardite (Figure 1) with a total average content of 0.64 wt%. This result is obtained after a correction for an excess of calcium ions, which corresponds to approximately 0.08 wt% and also excluding gypsum to an average extent of approximately 1.26 wt%. The main objective of the database is to generate the average composition of salt mixtures according to different criteria such as the geographic region, the type of building material, the depth and the height and thus to narrow down specific research needs and move from single salts to relevant salt mixtures.

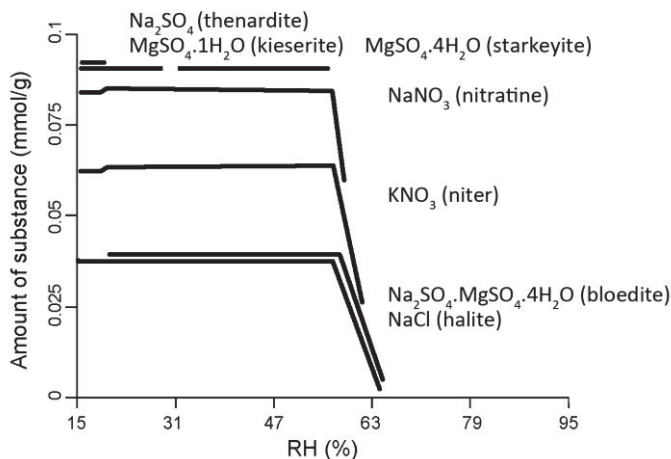


Figure 1: ECOS/RUNSALT output (25°C) derived from the average ion composition of 244 brick samples lifted in the 1st cm at a height up to 30 cm in Belgian monuments. A correction for an excess of calcium ions is applied and gypsum was removed

2 Sampling procedure

Most of the samples have been lifted from building materials by powder drilling (diameter: 5 mm) into the substrate at different depths and heights. The powdered samples are individually and hermetically sealed in pre-weighed containers and transported to the laboratory. The ambient moisture content is determined gravimetrically by weighing the samples at 60°C until a constant weight is reached. Then the samples are conditioned at 20°C and 95% RH to determine the hygroscopic moisture content. The weight increase is related to that of the dry sample and presented as weight percentage (wt%).

The salt content is determined by adding approximately 1 g of the dried sample to 100 ml pure water, which is mixed to extract soluble ions. The quantity of anions (Cl^- , NO_3^- and SO_4^{2-}) and cations (Na^+ , K^+ , Ca^{2+} and Mg^{2+}) of the filtered extract is analyzed with Ion Chromatography (IC, Metrohm). The results in parts per million (ppm) are converted into milli-equivalents/g and presented as wt%. The data expressed as millimole per gram (mmol/g) are entered into the ECOS/RUNSALT thermodynamic model. Currently this is done for the average ion content of a selected group of samples.

3 Database setup

The spreadsheet database is arranged into two pages. The first page contains the entire dataset while the second page the legend with abbreviations used.

The sample data include a Sample Code, the analytical methods used, such as, Ion Chromatography (IC), X-Ray Diffraction (XRD), Raman Spectroscopy and/or the ambient- and hygroscopic moisture content, the month and year when the sample was lifted, the location by “city”, the “object” describing the type of artefact (monument, archaeological site, sculpture, ...), and, if applicable, information related to the documentation method of the institution having performed the investigation.

The following columns contain the material type, sampling height and depth. These data are completed with a code as described in Table 1. The numerical data related to the weight of the sample container, the initial sample weight, its weight after drying as well as after conditioning at 20°C and 95% RH, the weight of the dried sample used for analysis with IC, the amount of pure water added to bring the ions into solution and the data derived from the analysis with IC in ppm are included as well.

The ion concentrations are converted into milli-equivalents per gram (mEq/g), useful to interpret possible connections between anions and cations and to evaluate the balance between the two. An excess of Ca^{2+} ions is generally identified due to a small amount of CaCO_3 dissolved from the substrate or to the presence of non-carbonated lime. A further

imbalance can be associated with the presence of sodium carbonate, which is further confirmed by a slight increased pH around 8, if so; the amount of NaCO_3 in wt% is calculated. Further, the amount of gypsum is calculated. The database includes the input data (mmol/g) for the ECOS/RUNSALT model followed by the results of XRD and Raman Spectroscopy analyses of efflorescence lifted in-situ, if available.

The legend is found on the second page of the database. It contains for example the parameters related to the sampling: materials, depth, height and their codes (Table 1).

Table 1: sampling parameters and their codes used in the database

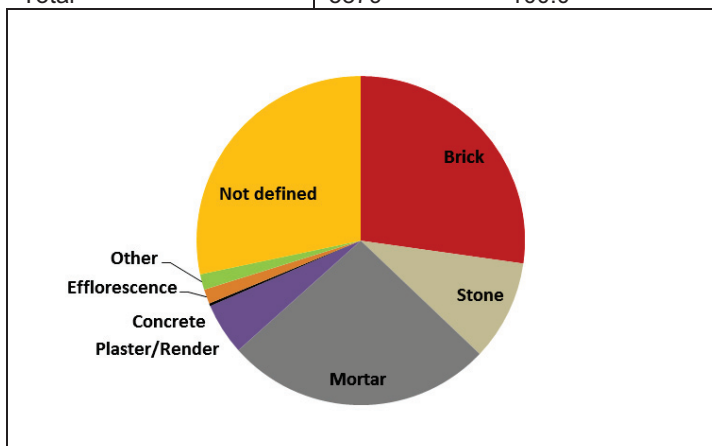
Materials	Code	Depth (cm)	Code	Height (cm)	Code
Efflorescence	E	Efflorescence	0	Low 0 to 30	L
Plaster (indoors)	P	0 to 1	1	Middle low 30 to 60	Mi
Render (outdoors)	R	0 to 2	2	Middle high 60 to 100	MiHi
Wall painting	W	0 to 3	3	High >100 <600	Hi
Brick	B	1 to 3	4	Vault or wall >600	T
Mortar/Joint	M	2 to 5	5		
Stone	S	3 to 5	6		
Earth/Soil/Dirt	D	5 to 7	7		
Concrete	C	7 to 10	8		

4 Database content and calculations

The database currently contains the results of 5879 samples that can be split up among different types of materials (Table 2). The largest group, entitled “not defined”, relates to samples for which their identification is missing. The brick samples constitute the second largest group, followed by mortar, stone and plaster/render. Less than 5% can be associated with other materials, efflorescence and concrete.

Table 2: Distribution of the samples

Substrate	Amount	Percentage
Brick	1600	27.2
Stone	581	9.9
Mortar	1546	26.3
Plaster/Render	300	5.1
Concrete	15	0.3
Efflorescence	84	1.4
Other	90	1.5
Not defined	1663	28.3
Total	5879	100.0



To establish a statistical evaluation of the data, both the numerical and alphanumeric data were transferred and classified from the database to Matlab. In Matlab a graphical user interface was developed to represent a user-defined selection of the data, i) the frequency distribution of the samples for a selected parameter (amount of salt, anions, cations or individual ions) and ii) the correlation between two ions of choice, presented in a 2D-graph. The criteria for data grouping are the type of substrate and the sampling height and depth.

5 Statistical analysis of the salt data

5.1 Average salt concentrations

The average ion concentration of anions and cations, expressed in milli-equivalents per gram (mEq/g), for each type of material is given in Table 3. For all material types, the average total amount of cations is in excess of the anion amount.

The average total ion content is noticeably higher for the group of plasters and renders, and decreases significantly for the mortars followed by both bricks and stones. This difference can be associated with a higher gypsum content, which is regularly detected in plasters and renders (Figure 2). Only 33% of these samples contain less than 1,5 wt% of gypsum, against 64,2% for the mortar samples. Nevertheless, the amount of samples containing at least 1,5 wt% of gypsum in stone and brick is considerably high, respectively 27,7% and 28,3%.

Table 3: Average concentration of anions and cations (mEq/g)

	Brick	Stone	Mortar	Plaster/Render	All
Anions	0.273	0.248	0.386	1.344	0.522
Cations	0.312	0.300	0.441	1.517	0.607
Total	0.584	0.548	0.827	2.861	1.129

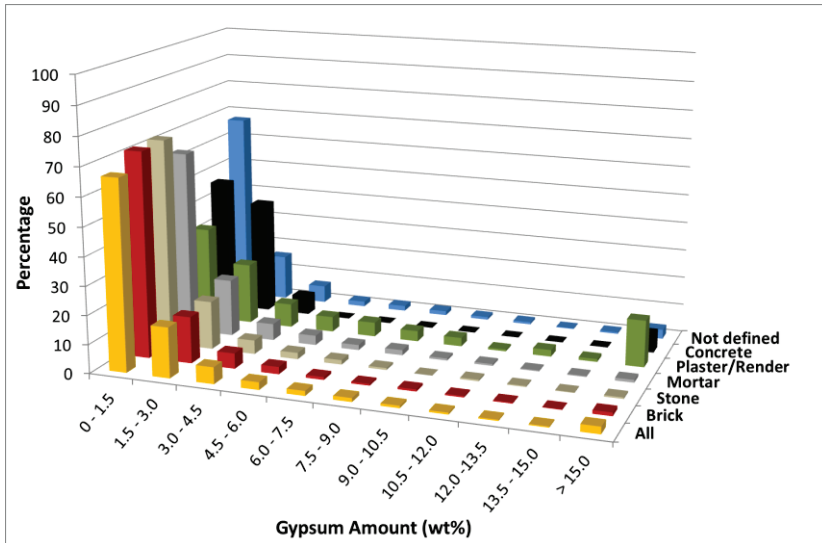


Figure 2: The frequency distribution of the gypsum content within different material types

The brick and stone samples contain similar average total salt concentrations, approximately 3.91 wt%, while the average increases for mortar samples to 2,86 wt% and up to 9,68 wt% for the plaster and render sample group (Table 4). When comparing the total amounts of salts, excluding gypsum (Figure 3), the same trend can be noticed. However, for the renders and plasters the amount of salts now only doubles instead of quadruples, explained by their high gypsum load.

Table 4: Average salt concentrations in wt%

	Brick	Stone	Mortar	Plaster/Render	All
Total	2.00	1.88	2.86	9.68	3.91
Total (excl. gypsum) (approximation)	0.83	0.87	1.38	1.82	1.77

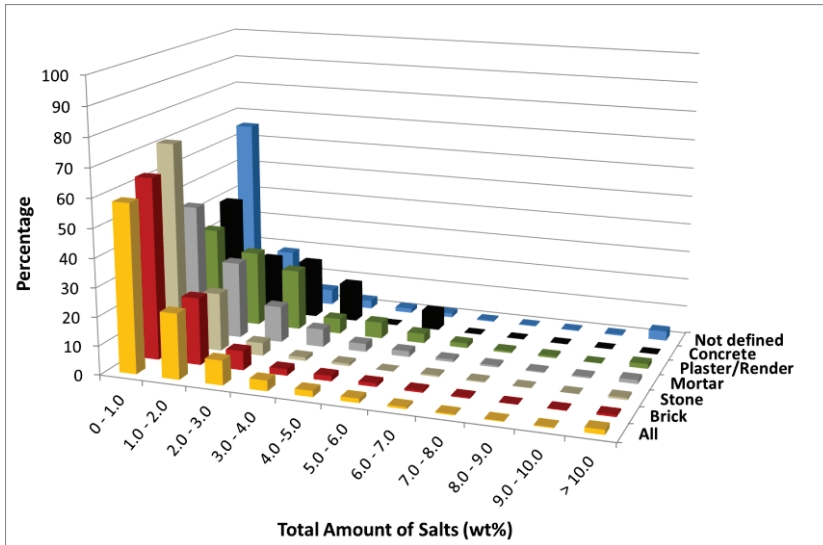


Figure 3: The frequency distribution of the total amount of salts, excluding gypsum, for the different material types

5.2 Treatment of the average ion concentrations

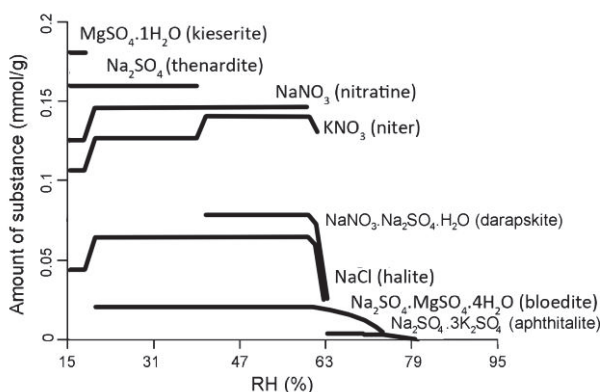
It becomes even more interesting when looking at the crystallization behavior of the average ion mixtures, shown in Table 5, as examined with ECOS/RUNSALT. Three approaches can be distinguished. The first approach (Figure 4) is derived from the average ion mixture of all the samples. All salts presented in Table 6 show up in the output, with the exception of starkeyite.

Table 5: Average ion concentrations (mmol/g)

Ion	Overall	Brick	Stone	Mortar	Plaster/Render
Chlorides	0.0441	0.0391	0.0146	0.0634	0.0481
Nitrate	0.0822	0.0430	0.0253	0.0750	0.0880
Sulphate	0.1978	0.0952	0.1042	0.1236	0.6038
Sodium	0.1329	0.0642	0.0790	0.1030	0.1866
Potassium	0.0626	0.0233	0.0266	0.0429	0.0468
Calcium	0.1424	0.0867	0.0656	0.1103	0.5400
Magnesium	0.0209	0.0058	0.0058	0.0095	0.0152

Table 6: Salts present in the ECOS/RUNSALT outputs based on the average ion contents (table 5). (✓: present in the output; —: not present in the output)

Salts	All	Brick	Stone	Mortar	Plaster/ Render
MgSO ₄ .1H ₂ O (kieserite)	✓	✓	✓	✓	✓
MgSO ₄ .4H ₂ O (starkeyite)	—	✓	—	✓	—
Na ₂ SO ₄ (thenardite)	✓	✓	✓	✓	✓
NaNO ₃ (nitratine)	✓	✓	—	✓	✓
KNO ₃ (niter)	✓	✓	✓	✓	✓
NaNO ₃ .Na ₂ SO ₄ .H ₂ O (darapskite)	✓	—	✓	—	✓
NaCl (halite)	✓	✓	✓	✓	✓
Na ₂ SO ₄ .MgSO ₄ .4H ₂ O (bloedite)	✓	✓	✓	✓	✓
Na ₂ SO ₄ .3K ₂ SO ₄ (aphthitalite)	✓	✓	✓	✓	✓


Figure 4: ECOS/RUNSALT output (25°C) of the average ion composition of all 5879 samples (table 5). Gypsum was removed from the ion mixture.

A second approach is based on the average ion concentration representative for the group of the brick samples (Figure 5). The output contains all the salts presented in Table 6, with the exception of darapskite in this case. A similar output is derived for the average ion mixture typical for the mortar samples.

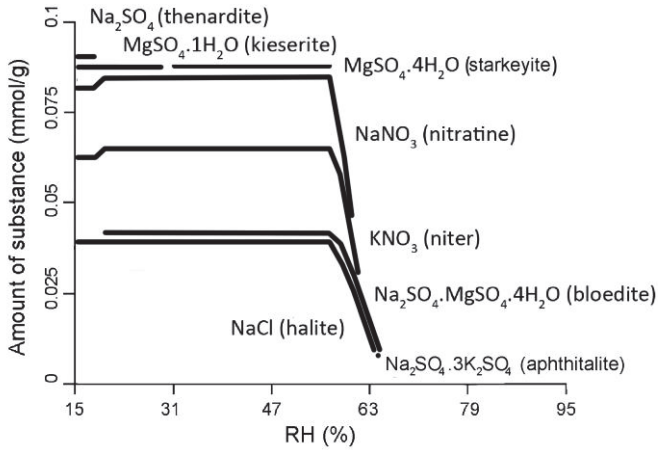


Figure 5: ECOS/RUNSALT output (25°C) of the average ion composition of the brick samples (table 5), after correction for gypsum.

The third approach deals with the average ion concentration found in the plaster and render samples (Figure 6). All of the salts presented in Table 6 with the exception of starkeyite are present in the output. A similar output is derived from the stone samples, however excluding nitratine.

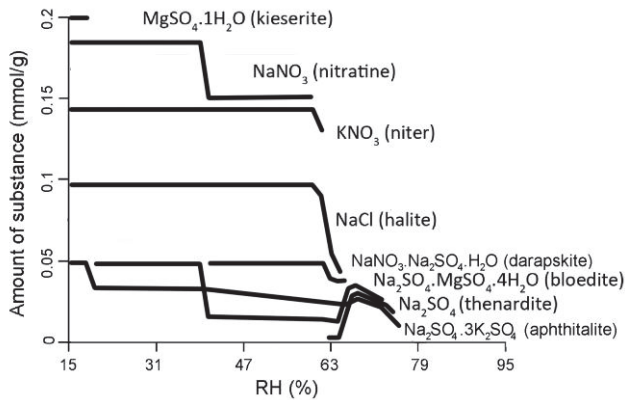


Figure 6: ECOS/RUNSALT output (25°C) of the average ion composition of plaster and render samples (table 5), after correction for gypsum.

The data structure further enables the study of the correlation amongst the ions as well, possibly identifying recurrent ion ratios. For example, the

quantities of calcium versus nitrate ions and the calcium versus sulfate ions of all samples are plotted in Figures 7 and 8. Between the calcium and nitrate ions, a spurious correlation can be noticed for a small number of samples and this up to a calcium-concentration of 0.2 mmol/g at a ratio of approximately 1:2 (calcium versus nitrate). A noticeably higher correlation between the sulfate and calcium ions is obtained (Figure 8) from which the omnipresence of gypsum is evidenced.

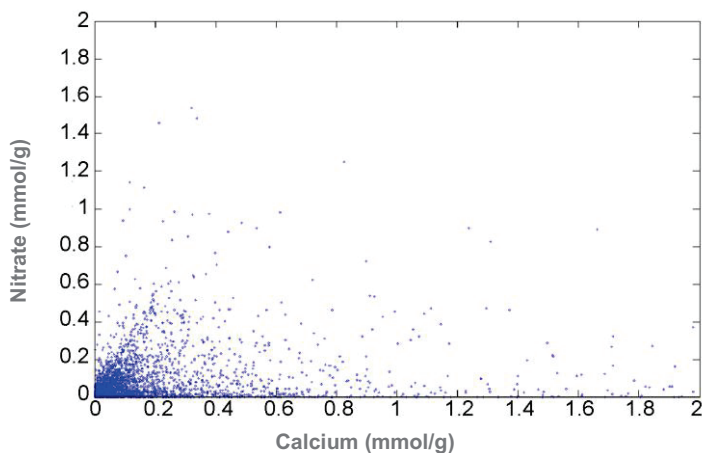


Figure 7: Correlation of the amount of calcium versus that of nitrate ions (mmo/gl).

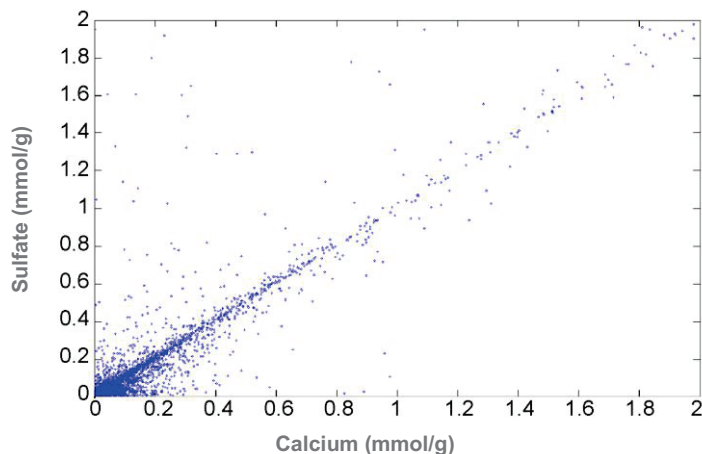


Figure 8: Correlation of the amount of calcium and that of sulfate ions (mmol/g).

5.3 Spatial distribution of salts

The total amount of salts according to the sampling height is plotted in Figure 9. The majority of samples contain, regardless the height, a maximum of 2 wt% of salts. Samples lifted above 1 m contain a higher salt content resulting from rising damp transporting ions to the drying front where salts are deposited. The content in the vaults is generally less when compared to the walls, however a significant amount of samples contain a higher salt content above 10 wt% when compared to samples lifted above 60 cm in the walls.

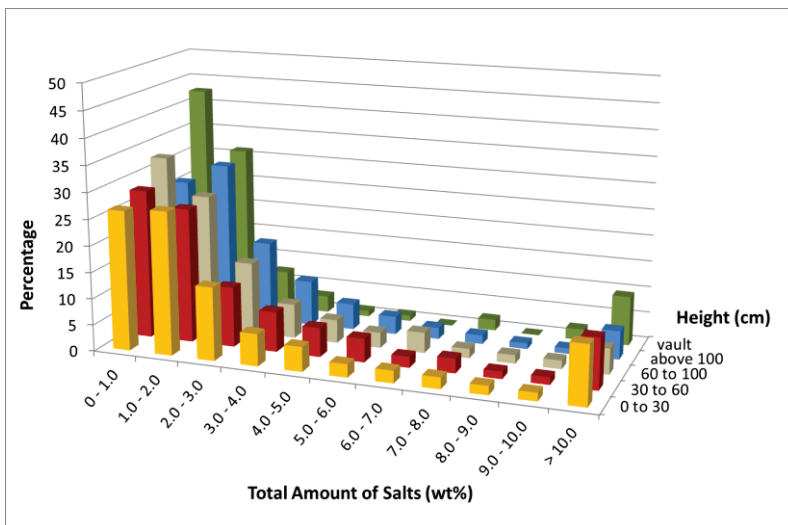


Figure 9: Variation of the total amount of salts, including gypsum, according to the height at which the samples were lifted.

The total amount of salts according to the sampling depth is plotted in Figure 10. Closer to the surface of the material the average amount of salts tends to increase. An exception can be seen at a depth between 5 and 7 cm, where a larger percentage of samples contain a salt concentration above 10 wt%. Naturally, such an evaluation is bias as in normal conditions samples are only lifted up to a depth of 5 cm while drilling samples at a greater depth are only lifted when severe damage or large amounts of efflorescence are visible.

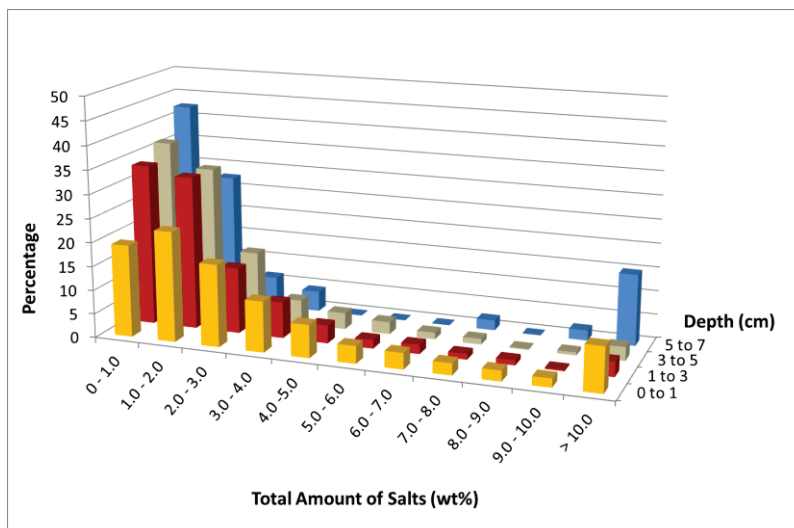


Figure 10: Variation of the total amount of salts, including gypsum, according to the sampling depth.

6 Conclusions

The presented database has become KIK's main location to collect quantitative ion data of the aqueous extract of powder samples lifted in Belgian monuments. The samples are classified by date, location, material, depth and height. Within the database calculations are automated to aid the interpretation of the salt distribution within the monument, sculpture or archaeological site that is under investigation. Furthermore, it can be used as an educational tool to further the understanding of the complexity of ions and salt mixtures for many conservation practitioners.

Statistical analysis of the data evidences average ion mixtures per material, which can then be interpreted with the ECOS/RUNSALT program to analyze the thermodynamic behavior of the ion mixture. The results show complex mixtures with the presence of kieserite, starkeyite, thenardite, nitratine, niter, darapskite, halite, bloedite and aphanthalite. However the program has its limitations as it excludes gypsum and carbonate salts. It also has a known error relating to the magnesium sulfates, as hexahydrite is not shown in the output. Hexahydrite is however the most likely reaction product with increasing RH [3, 4]. Additionally, the formation and deterioration potential of the double salts darapskite, aphanthalite and bloedite can be questioned when in the presence of other salts or within different porous materials [3, 5].

The main goal of the database is to generate average salt mixtures found in the different materials according to various criteria such as the geographic region, the type of building material, the depth and the height to narrow down specific research needs and to move from single salts to relevant complex mixtures. Ultimately the location data will be linked to a geographic information system (GIS) and the database will be made available online such that other research institutions can add data to further increase the relevancy of the database.

References

- [1] D. Bionda. 'Modelling indoor climate and salt behaviour in historical buildings: A case study', PhD thesis, Diss. Nr. 16567 ETH Zürich. (2006)
- [2] C. Price, (Ed.). An expert chemical model for determining the environmental conditions needed to prevent salt damage in porous materials. European Commission Research Report No 11, (Protection and Conservation of European Cultural Heritage). London: Archetype Publications (2000)
- [3] S. Godts, R. Hendrickx, H. De Clercq. The crystallization behavior of sodium magnesium sulfate in limestone. Proceedings SWBSS2014, 3rd International Conference on Salt Weathering of Buildings and Stone Sculptures, H. De Clercq (Ed.), (2014), pp 167-183.
- [4] M. Steiger, K. Linnow, H. Juling, G. Gülker, A. El Jarad, S. Brüggerhoff, D. Kirchner. Hydration of $\text{MgSO}_4 \cdot \text{H}_2\text{O}$ and generation of stress in porous materials. *Crystal Growth & Design* 8(1), (2008), pp 336–343.
- [5] H. De Clercq, M. Jovanović, K. Linnow, M. Steiger. Performance of limestones laden with mixed salt solutions of Na_2SO_4 – NaNO_3 and Na_2SO_4 – K_2SO_4 , *Environmental Earth Sciences*, 69(5), (2013), pp 1751-1761, DOI 10.1007/s12665-012-2017-0

Further steps towards the solution of Correns' dilemma

F. Caruso* and R.J. Flatt*

Physical Chemistry of Building Materials, Institut für Baustoffe, ETH Zürich, Switzerland.

* fcaruso@ethz.ch and flattr@ethz.ch

Abstract

Correns' and Steinborn's pioneering experiment is probably the most intriguing one in the field of salt crystallization. It consisted of the measurement of the force needed to prevent a monocrystal of potassium alum (potassium and aluminium sulfate dodecahydrate, $\text{KAl}(\text{SO}_4)_2 \cdot 12 \text{H}_2\text{O}$) from growing in various supersaturated solutions. What is puzzling is that they obtained very good agreement between their experimental data and an ideal equation of crystallization pressure.

We report here the experimental advances in our modern reproduction of this milestone experiment. We developed a setup that includes a universal testing machine, custom-made glassware, and an external stirring system. Here, we present and comment on the data derived from the first 11 experiments. We found that many aspects of the work by Correns and his collaborators should be put into question, along with a thorough analysis of the non-ideal thermodynamics of potassium alum. Slowly, we are getting closer to answering the mystery that continues to surround this experiment.

Keywords: crystallization pressure, potassium alum, supersaturation, thermodynamics

1 Introduction

Crystallization of salts from aqueous solutions is an important weathering phenomenon of porous building materials and concerns different fields of studies. The underlying thermodynamics, kinetics, and mechanics have been extensively studied, and it is now well established how the resulting crystallization pressure can cause significant stresses and, therefore, damage [1–9]. However, quantitative data are still relatively rare to find in literature [10–15].

Correns and Steinborn derived the first equation for crystallization pressure in their paper in 1939 [11,16] (a subsequent and much more succinct paper in English with Correns as the only author was published in 1949 [12,16]):

$$P = RT/v \ln(c/c_s) \quad (1)$$

In (1), P is the crystallization pressure, R is the gas constant, T is the temperature, v is the molar volume of the solute, c is the actual concentration, and c_s is the saturation concentration at T . The system studied by Correns was potassium alum (potassium and aluminium sulfate dodecahydrate, $KAl(SO_4)_2 \cdot 12 H_2O$), probably because of its low cost, easy availability, relative stability of the supersaturated solutions, and ease of obtaining good single crystals [17]. With his ingenious pressure balance (*Druckwaage* in German), Correns observed growth or no growth of a potassium alum single crystal in its supersaturated solution, when loaded below or above the value of pressure resulting from (1), respectively [11,12,16].

The results in Correns' papers show an excellent agreement between the experimental data and (1). However, the latter equation is – at best – incomplete because it neglects the non-ideal behaviour of concentrated solutions of electrolytes [16]. In fact, the correct version of (1) for large crystals is:

$$P = RT/v \ln(Q/K) \quad (2)$$

where Q is the ion activity product and K is the solubility product, the other symbols are the same as in (1).

Furthermore, in both Correns' papers [11,12,16] relatively few experimental details are given; some more are present in the work by Brehler (one of Correns' doctoral students [18]) but several doubts about the validity of his findings persist.

Correns' work remains however pioneering for what concerns his identification of the role of surface energies. In fact, he showed that growth is observed at different extents if the surfaces between which the crystal is loaded are made of materials other than glass, or if the crystal is differently oriented.

This paper extensively illustrates the method for obtaining and characterising potassium alum crystals, and the setup used to measure the thickness of potassium alum crystals after their (111)-faces loading in supersaturated solutions between glass surfaces. We present and comment also some first measurements at low supersaturations (1.10 and 1.15), so to neglect the role of the different surface energies of the faces of the crystals.

The contents of this paper questions aspects of the work by Correns and his collaborators, others than the ones already discussed by Flatt *et al.* in their commented translation of the 1939 paper [16]. This work follows a preliminary one in which potassium alum supersaturated solutions were characterized [17].

2 Experimental

2.1 Instrument

The application of a constant load and the measurement of the displacement were performed on a 10 kN universal testing machine 1454 by Zwick GmbH (Ulm, Germany). The employed load cell was a high precision 1 kN one. The load is applied through a custom-made aluminum pushrod, previously described in [17]. The load application rate is 5 N/min. The machine keeps a constant load by continuously adjusting the position of its traverse. Therefore, it does not allow a direct and continuous recording of a possible displacement of the crystal.

The nominal resolution of the machine is 0.2 μm . The program used for the acquisition of data was TestXpert II by Zwick.

2.2 Glassware

For the purpose of the experiment, we designed crystallizing dishes and glass sockets with flat faces and thus parallel to the potassium alum single crystals. A specialized glassblower (Comandè Saskia, Monreale, Italy) produced the pieces of glassware. The crystallizing dish has a diameter of 10 cm and a height of 5 cm for containing a volume of around 400 mL of solution. The socket has a diameter of around 2.3 cm and a height of 5.5 cm. The socket is designed to completely cover the face of the crystal under load [16].

Before the use in the experiments, all the glassware has been carefully washed and dried in a laboratory dishwasher, using only demineralised water.

Both the crystallizing dish and the socket are shown in Figure 1, left.

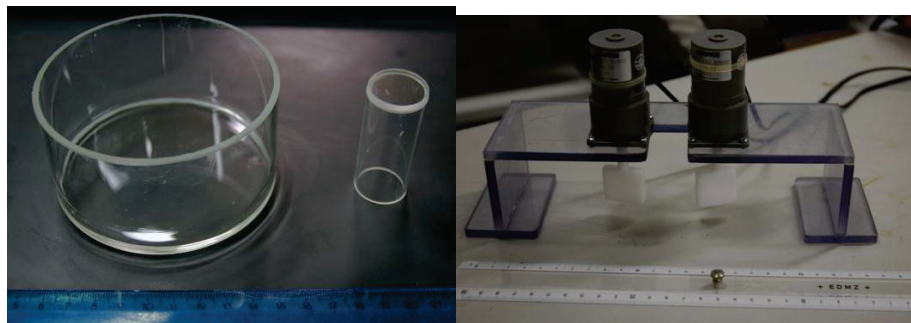


Figure 1: The custom-designed borosilicate glass crystallizing dish and socket (left) and the custom-made powered stirring system with poly(methylene oxide) pads (right) used for the experiments.

2.3 Potassium alum supersaturated solutions and crystals

Supersaturated solutions were prepared (and stored) in borosilicate glass bottles with screw caps by stirring and heating ultrapure water (UPW) and analytical grade potassium alum from either Merck KGaA (Damstadt, Germany) or Sigma-Aldrich Chemie GmbH (Buchs, Switzerland).

The refractive index of such solutions was measured with a pocket refractometer PAL-RI by Atago (Tokyo, Japan), after performing the zero setting with UPW.

The solubility value of potassium alum (5.9 g/100 g water at 20 °C for the anhydrous salt, corresponding to a solubility of 11.4 g/100 g water for the dodecahydrate at the same temperature) is taken from the literature [19].

Single crystals were obtained by cooling down supersaturated potassium alum solutions (with a concentration of around 13.1 g/100 g water) from 20 °C to 5 °C in a Vötsch VC 4060 climatic chamber (Vötsch Industrietechnik GmbH, Balingen-Frommern, Germany) in the above-described crystallizing dishes covered with a Petri dish. The cooling rate was 1 °C/h. Under these conditions, around 1 day is necessary for the potassium alum to nucleate and crystallize. Only crystals with a good overall aspect (absence of cracking and asperities on the surface) and not twinned to others were chosen. A micrograph of a typical crystal is shown in Figure 2.

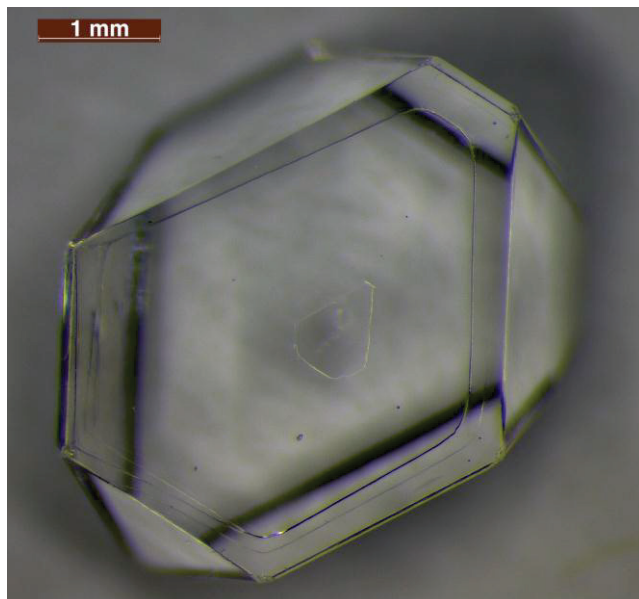


Figure 2: Micrograph of a potassium alum single crystal oriented on the (111) face.

The masses of the crystals were recorded with a Mettler-Toledo NewClassic MS-204S analytical balance (Mettler-Toledo GmbH, Greifensee, Switzerland).

All the crystals were then observed under an M60 stereomicroscope by Leica Microsystem AG (Heerbrugg, Switzerland). Micrographs at different magnification were taken using the LAS program by Leica.

The values of the (111) surface areas were obtained by analysing the above-mentioned micrographs with the image-processing program ImageJ 1.47v, created by Wayne Rasband (National Institutes of Health, USA).

The measurement of the thickness of the crystal – before and after the experiment – was carried out as follows: i) the crystal is put at the centre of the crystallizing dish; ii) the machine applies a 5 N load on the crystal through the pushrod (without the glass socket) at a rate of 5 N/min; iii) the height of the pushrod on the crystal is recorded when the machine reaches such load. This procedure allows a precise (the standard deviation on 5 replicates is, generally, around 1-2 μm , and ranged from < 1 μm to around 20 μm in the experiments reported in this work) and reproducible value of the thickness of the crystals.

2.4 Stirring system and other experimental parameters

A powered stirring system (Figure 1, right) with poly(methylene oxide) pads was designed and built in house. When the stirring system was not employed, a glass rod was then used.

A sponge pad – kept wet with ultrapure water – was used on the edges of the crystallizing dish to ensure minimum evaporation of the solutions.

All the experiments were carried out in a climatic room at constant temperature ($20\text{ }^{\circ}\text{C} \pm 2\text{ }^{\circ}\text{C}$) and relative humidity ($50\% \pm 8\%$).

11 experiments (Figure 3) were carried out with solutions at supersaturation either 1.10 or 1.15. The applied load ranged from the crystallization pressure predicted by (1) to 1.9 times it.

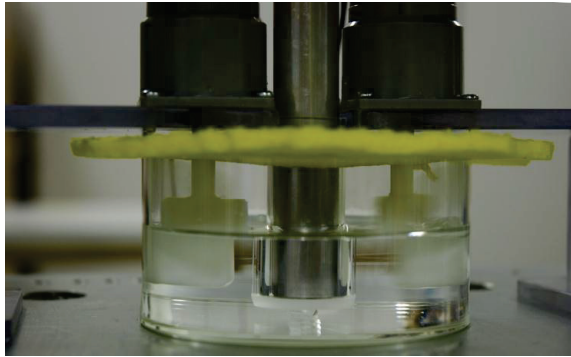


Figure 3: A close-up of a running experiment. The crystallizing dish, the glass socket, the aluminium pushrod, the powered stirrer, and the potassium alum crystal are visible.

3 Results and discussion

A table showing the relevant data and the outcome of the experiment is here reported (Table 1).

Table 1: Outcome of the 11 experiments discussed in this paper. " c/c_s " stands for supersaturation and it refers at that value at 20 °C. The applied load is expressed as a multiple of the crystallization pressure resulting from (1). The thickness of the crystal after the loading in the supersaturated solution is reported in the "Outcome" column. The "Surface" refers to the mean value of surface area of the two (111) faces of the potassium alum crystal. The standard deviation of the thickness of the crystal is given in parenthesis.

ID	Surface (mm ²)	Mass (mg)	c/c_s	Load (P_{Correns} -fold)	Thickness (mm)	Duration	Outcome
1	21.2	148.2	1.15	1.45	3.921(0)	12 h 25'	Not grown (3.89(2) mm) and broken
2	55	317.2	1.10	1.45	4.031(0)	14 h 30'	Not grown (4.028(3) mm)
3	58	211.7	1.15	1	3.068(1)	---	Broken during exp.
4	9.8	13.2	1.15	1	1.183(5)	20 h 30'	Not grown (1.18(1) mm)
5	10	21.2	1.10	1	1.533(0)	1 h	Not grown (1.513(1) mm)
6	13	22.1	1.10	1	1.342(1)	1 h 40'	Grown (1.394(1) mm)
7	12	25.4	1.10	1.9	1.444(0)	40'	Not grown (1.431(1) mm)
8	5.3	8.6	---	---	---	---	Broken during thickness meas.
9	9	16.1	1.10	1	1.343(0)	2 h 5'	Not grown (1.337(1) mm) and broken
10	16	31.8	1.10	1	1.505(0)	45'	Not grown (1.476(1) mm) and broken
11	10	19.8	1.10	1.52	1.452(0)	1 h 50'	Not grown (1.449(1) mm) and broken

For experiments 1-3, we employed bigger crystals than the ones used after. Correns did not report any information about the dimension of the employed crystals [11,12,16] but Brehler did [18] and referred to quite small crystals (similar in dimensions to the ones reported in this study). The use of large crystals means higher probability of defects and a corresponding higher probability of breakage of the crystal during the loading phase. However, Brehler fails to indicate how he obtained the values of the surface areas of the crystal faces, despite being precise to the mm^2 [18]. An accurate value is critical for the calculation of the load to be applied.

In 6 experiments out of 11, the crystal broke either after the loading or during the measurement of the thickness. Such a frequent occurrence of breakage may be attributed to three factors: i) an intrinsic fragility of the crystals when under load; ii) the presence of defects in the crystals; iii) the dynamic application of the load by the machine. Excluding the last factor, this evidence questions the possibility of carrying out experiments at supersaturations (and, therefore, loads) higher than the ones reported in this work.

From Table 1, it can be noted that experiments 1, 2, and 4 had higher duration than the others. In fact, from experiment 5 on, when the first crystal appeared (nucleated) on the bottom of the crystallizing dish, the experiment was interrupted. It is worth remembering that when two crystals are immersed in a supersaturated solution and one of them is loaded, the unloaded crystal will grow at the expense of the loaded one.

The external powered stirrer was a cause of disturbance to the system and enhanced nucleation. Correns – probably aware of the concentration gradient that would result if the solution during the experiment were unstirred – reported that the solutions were stirred [11,12,16]. Considering that he did not describe any automatic stirring system and that the experiments were rather long (up to a couple of days), it is hard to imagine that: i) continuous stirring of the solutions (probably, by hand with a glass rod) during the experiments was performed; ii) nucleation (especially at high supersaturations) did not occur.

Only experiment no. 6 showed a growth of the crystal. This experiment indicates that the calculated value of the potassium alum crystallization pressure by Flatt *et al.* [16] is probably overestimated. It also suggests that other treatment of the activity coefficients may be needed for this system. Buil [10] reports that taking this into account resolves the discrepancy, but his work was never published. A more detailed consideration of the non-ideal solution thermodynamics of supersaturated potassium alum solutions however appears necessary in addition to the continuation of our experiments.

4 Conclusions and outlook

We presented a setup designed to carry out experiments of constant loading of potassium alum single crystals immersed in supersaturated solutions. We also presented a robust (albeit not continuous) method to measure the thickness of the single crystal before and after the loading in its supersaturated solution.

From the first results we obtained, we put into question further aspects of the work by Correns and his collaborators: the dimension of the potassium alum crystals, the stirring, and the resulting stability of the solutions (especially at high values of supersaturations). Furthermore, considering the shape of the chosen crystals, it is not clear how Correns and collaborators could have carried out loading experiments on faces others than the (111).

We will continue performing experiments at different loads to verify if further improvements to our setup are necessary or if the load range we are working on is correct.

For the future, a continuous recording of the movements of the crystal when loaded would be desirable. A custom-made accessory for the pushrod for mounting three independent displacement transducers on it has already been designed and produced. The implementation for the transducer is under development.

Finally, our still preliminary results suggest that the non-ideal solution thermodynamics of potassium alum supersaturated solutions may have to be re-examined.

Acknowledgments

The authors would like to thank Mr. Heinz Richner (IfB – ETH Zürich) for support in the use of the universal testing machine and advice on the experiments. The authors are also grateful to Mr. Jakob Scherrer (IfB – ETH Zürich) for producing the custom-designed parts and the fittings necessary for the experiment with the universal testing machine.

References

- [1] G.W. Scherer, Crystallization in pores, *Cem. Concr. Res.* 29 (1999) 1347–1358. doi:10.1016/S0008-8846(99)00002-2.
- [2] G.W. Scherer, Stress from crystallization of salt, *Cem. Concr. Res.* 34 (2004) 1613–1624. doi:10.1016/j.cemconres.2003.12.034.

- [3] R.J. Flatt, Salt damage in porous materials: how high supersaturations are generated, *J. Cryst. Growth.* 242 (2002) 435–454. doi:10.1016/S0022-0248(02)01429-X.
- [4] A.E. Charola, Salts in the Deterioration of Porous Materials: An Overview, *J. Am. Inst. Conserv.* 39 (2000) 327–343. doi:10.2307/3179977.
- [5] R.M. Espinosa-Marzal, G.W. Scherer, Advances in Understanding Damage by Salt Crystallization, *Acc. Chem. Res.* 43 (2010) 897–905. doi:10.1021/ar9002224.
- [6] N. Shahidzadeh-Bonn, J. Desarnaud, F. Bertrand, X. Chateau, D. Bonn, Damage in porous media due to salt crystallization, *Phys. Rev. E.* 81 (2010) 066110. doi:10.1103/PhysRevE.81.066110.
- [7] M. Schiro, E. Ruiz-Agudo, C. Rodriguez-Navarro, Damage Mechanisms of Porous Materials due to In-Pore Salt Crystallization, *Phys. Rev. Lett.* 109 (2012) 265503. doi:10.1103/PhysRevLett.109.265503.
- [8] M. Steiger, A.E. Charola, K. Sterflinger, Weathering and Deterioration, in: S. Siegesmund, R. Snethlage (Eds.), *Stone in Architecture*, Springer Berlin Heidelberg, 2014: pp. 225–316.
- [9] R.J. Flatt, F. Caruso, A.M. Aguilar Sanchez, G.W. Scherer, Chemo-mechanics of salt damage, accepted on *Nat. Commun.*
- [10] M. Buil, Thermodynamic and experimental study of the crystallization pressure of water-soluble salts, in: F.H. Wittmann (Ed.), *Materials science and restoration. Proceedings of the international conference. Esslingen, 6-8 Sept. 1983*, Lack und chemie, Esslingen, 1983: pp. 373–377.
- [11] C.W. Correns, W. Steinborn, Experimente zur Messung und Erklärung der sogenannten Kristallisationskraft, *Z. Kristallogr.* 101 (1939) 117–133.
- [12] C.W. Correns, Growth and dissolution of crystals under linear pressure, *Discuss. Faraday Soc.* 5 (1949) 267–271. doi:10.1039/DF9490500267.

- [13] V.Y. Khaimov-Mal'kov, Experimental Measurement of Crystallization Pressure, in: A.A.V. Shubnikov, D.G.-M.S.N.N. Sheftal' (Eds.), *Growth of Crystals*, Springer US, (1995) pp. 14–19.
- [14] J. Desarnaud, Mécanisme de croissance et dissolution de cristaux de KCl sous charge : Apport dans la connaissance des mécanismes d'altération des pierres par les sels, Ph.D. thesis, Université Paul Cézanne - Aix-Marseille III, 2009.
- [15] J. Désarnaud, O. Grauby, P. Bromblet, J.-M. Vallet, A. Baronnet, Growth and Dissolution of Crystal under Load: New Experimental Results on KCl, *Cryst. Growth Des.* 13 (2013) 1067–1074. doi:10.1021/cg3013359.
- [16] R.J. Flatt, M. Steiger, G.W. Scherer, A commented translation of the paper by C.W. Correns and W. Steinborn on crystallization pressure, *Environ. Geol.* 52 (2007) 187–203. doi:10.1007/s00254-006-0509-5.
- [17] F. Caruso, R.J. Flatt, Measuring crystallization pressure: can Correns' experiment be repeated?, in: *Proceedings of the 12th International Congress on the Deterioration and Conservation of Stone*, New York, 2012.
- [18] B. Brehler, Über das Verhalten gepreßter Kristalle in ihrer Lösung, *Neues Jahrb. Mineral. Monatsh.* (1951) 110–131.
- [19] W.M. Haynes, ed., *Physical Constants of Inorganic Compounds*, in: *CRC Handbook of Chemistry and Physics*, 94th Edition, CRC Press/Taylor and Francis, Boca Raton, 2013: pp. 4–43 – 4–101.

Experimental study on salt deterioration of salt contaminated earthen materials under dry-wet cycles

Y.X. Shen^{1*}, W.W. Chen¹, J. Kuang¹, and W.F. Du²

¹School of Civil Engineering and Mechanics, Lanzhou University, 222 Southern Tianshui Rd, Lanzhou City, Gansu Province, 73000, China

²China JK Institute of Engineering Investigation and Design, Xi'an, 710043, China

* shenyx08@lzu.edu.cn

Abstract

On the Silk Road in the northwest of China, there is a large number of precious ancient relics, such as the Great Wall with beacon towers and castles, the Jiaohe Ruins etc. Most of these ancient relics are earthen architecture sites, which is different from many monuments that are usually made of rocks or metal materials. Specifically, these ancient relics have suffered different levels of deterioration due to long term dry-wet cycles in this typical arid and semi-arid region. The damage patterns have been studied by field investigations, and the dynamics of salt precipitation have been confirmed to be crucial for understanding the deterioration mechanism in these earthen relics. However, the influence of the nature of the salt and its content on the mechanical properties and erosion responses of relic soils under dry-wet cycles are not well understood. In the present research, the deterioration of the saline ancient relics soil under dry-wet cycles was investigated in comparison to the mechanical properties (i.e., direct shear test, unconfined compression test and tensile test) and the effect of erosion response to artificial sandstorms. The specimens studied were remoulded samples from the Jiaohe Ruins loaded with different concentrations of NaCl, Na₂SO₄ and a mixture of these two salts. Meanwhile, the deterioration process was monitored by an ultrasonic test. It is found that the P-wave velocity decreases with increasing number of dry-wet cycles and the salts added to the samples accelerate the deterioration process. The degree of deterioration is reflected by the decrease of shear strength, compression strength and tensile strength of the relic soils. We also conducted wind erosion tests to investigate the erosion characteristics of remoulded samples by

considering different salt distributions. The results indicate that most serious deterioration is on the surface of the samples due to salt crystallisation. Na_2SO_4 contributed most of the surface weathering of the soils while NaCl played little role in the weathering.

Keywords: Jiaohe Ruins, dry-wet cycles, mechanical properties, wind erosion, salt crystallisation

1 Introduction

The Silk Road has been the main passage for commerce and cultural exchange between Central Asia and Europe for thousands of years. Hence, a large number of precious ancient relics, such as the Jiaohe Ruins, the Great Wall with beacon towers and castles etc. remain along this road. In contrast to many foreign monuments that are usually made of rocks or metal materials, most of these ancient sites are composed of soil. Due to continuous deterioration under adverse environmental conditions, only a small proportion of the ancient relics survived to the present day. Therefore, to provide effective treatments to preserve them, learning the fundamental deterioration mechanisms of this material is necessary.

Recently, based on the field investigations of many earthen relics, the damage patterns and the cause of damage have been described in detail [1]. The dynamics of salt precipitation under long term dry-wet cycles have been confirmed to be crucial for understanding the deterioration mechanism in these earthen relics. Salt crystallisation is widely recognized as a cause of damage in porous materials. A century and a half ago, Lavalley [2] provided the evidence that growing crystals can exert pressure and the research in salt deterioration has begun. The mechanism of salt damage including thermodynamic aspects was studied in detail [3-7]. Although these mechanisms are applied universally in porous materials, the applicability for earthen relics is unknown due to the lack of relevant research.

In this study, the influence of salt content and type of salts on the deterioration of contaminated earthen material under dry-wet cycles was examined experimentally by using a non-destructive ultrasonic wave velocity instrument. In addition, according to the results of the mechanical performance tests, the degree of deterioration was estimated. Finally, a wind tunnel erosion test was carried out with the salt contaminated specimens after dry-wet cycles.

2 Study area (Jiaohe Ruins)

The Jiaohe Ruins are located in the Xinjiang Uygur Autonomous Region, an arid and semi-arid area in the northwest of China. The main climate

characteristic of this area is low rainfall in combination with high evaporation. Details are summarized in Table 1.

Table 1: The climate characteristics of Jiaohe Ruins

Climate factor	Characteristics	Data
Evaporation	High evaporation	Annual average 2787.1 mm
Precipitation	Arid and semi-arid	Annual 2.9-48.4 mm; Annual average 16.2 mm
Temperature	High temperature difference	High 47.4 °C Low -28 °C; Difference 21.9 °C (daily)
Wind	Wind with sand	Max speed >40 m/s; Strong wind 36.2 days/year; Sandstorm 11.2 days/year

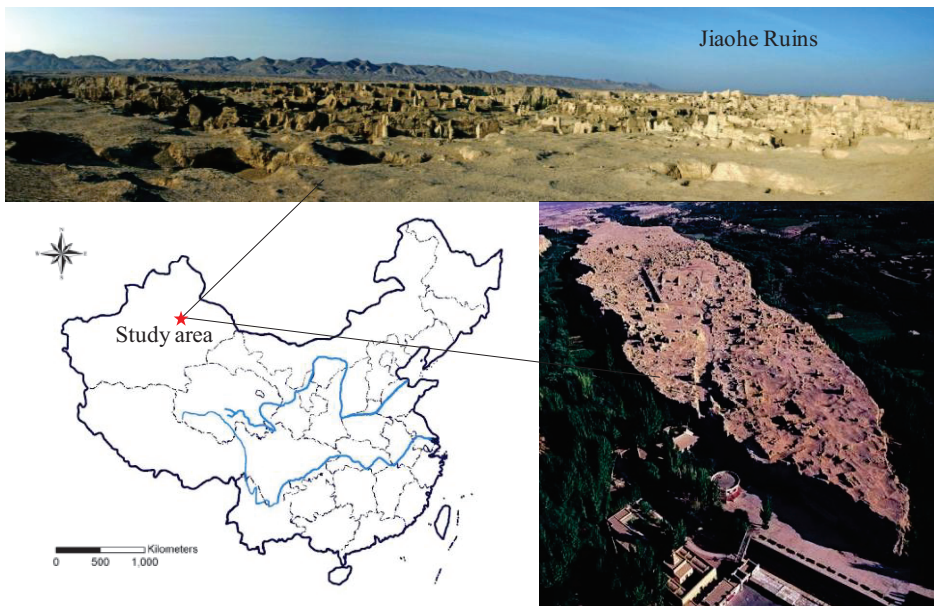


Figure 1: Jiaohe Ruins

The Jiaohe Ruins are the largest, oldest and best-preserved earthen relics over the world (Figure 1). The total area of the Jiaohe site is more than 350,000 m², including a 220,000 m² construction area. This large city was built during the Han dynasty (206 BC-AD 220), on a willow leaf-shaped loess plateau atop a cliff of over 30 meters. After the conversion and

expansion of several dynasties, it achieved most prosperity in the Tang Dynasty and was abandoned during Yuan dynasty (AD 1271-1368). Most of the ancient earthen structures that have been preserved to the present were built in the 3rd to 6th century AD.

Most buildings of the city were dug from earth and the soils have been used for the manufacture of mud bricks, rammed earth and cob. Hence, the material of Jiaohe Ruins is soil, a soft material much more easily damaged than stone and brick. After thousands of years of exposure to the environment, these structures show significant damage such as erosion, cracks and even collapse. Specifically, the ancient relics that contain soluble salts have suffered severe deterioration due to long term dry-wet cycles.

3 Materials and methods

3.1 Sample preparation

Soil for the experiments was collected from blocks of a collapsed part of the cliff of the Jiaohe Ruins. This consists of undisturbed loess material, named raw soil. All the soil samples were desalinated using distilled water until the electrical conductivity of the filtered water was less than 300 $\mu\text{s}/\text{cm}$ followed by drying at 105 °C [8]. Physical properties of the desalinated soil (Table 2) were determined according to the Chinese National Standards (CNS) GB/t50123-1999.

The salt content and the type of salt were determined on the basis of an analysis of the ion concentration of aqueous extracts from more than 100 samples collected from many different earthen ruins. The results indicate that Na_2SO_4 and NaCl are the most common salts in this material with contents up to 2% and 1%, respectively. Therefore, the two particular single salts and mixtures of them were used for the laboratory deterioration experiments. Details are listed in Table 3.

Table 2: Basic physical properties of the sample

Initial water content (%)	Specific gravity (g/cm^3)	Atterberg limits (%)		Particle size distribution (mm,%)		
		Liquid limit (%)	Plastic limit (%)	Clay (<0.002)	Silt (0.002-0.075)	Sand (0.075-2)
0.77	2.76	29.9	19.6	11.54	88.25	0.21

Cubic specimens, $7.07 \times 7.07 \times 7.07 \text{ cm}^3$ [9], were remoulded with the optimum moisture content (21.0%) and maximum dry density ($1.71 \text{ g}/\text{cm}^3$), which was determined by the compaction test. Before being remoulded, the dried soil was thoroughly mixed with the brine, then placed in plastic

bags and kept in a humidity-controlled room (100% relative humidity) for at least 48 hours to ensure water in the specimens in the state of equilibrium. All specimens were subjected to three cycles of wetting and drying (temperature: 25 °C; relative humidity: 95%-15%). The samples were kept at constant humidity for one month.

Table 3: The salts and salt contents used in the laboratory deterioration experiments

Remoulding water content	21.0%	Remoulding dry density	1.71 g/cm ³
Type of salts	Salt content *(wt %)	Type of salts	Salt content (wt %)
NaCl	0.2	Na ₂ SO ₄	0.2
NaCl	0.4	Na ₂ SO ₄	0.4
NaCl	0.6	Na ₂ SO ₄	0.6
NaCl	0.8	Na ₂ SO ₄	0.8
NaCl	1.0	Na ₂ SO ₄	1.0
NaCl+Na ₂ SO ₄	0.2+0.4	Na ₂ SO ₄	1.2
NaCl+Na ₂ SO ₄	0.4+0.8	Na ₂ SO ₄	1.4
NaCl+Na ₂ SO ₄	0.6+1.2	Na ₂ SO ₄	1.6
NaCl+Na ₂ SO ₄	0.8+1.6	Na ₂ SO ₄	1.8
NaCl+Na ₂ SO ₄	1.0+2.0	Na ₂ SO ₄	2.0

*the salt content is related to the dry material.

3.2 Methods

3.2.1 Ultrasonic test

The basic principle of the ultrasonic test (US) is to analyse the change of the US wave velocity through the sample to estimate its internal structure. The primary wave (P-wave) is normally used in such tests due to its fast velocity and low interference. In order to monitor the influence of the salt content and the number of wet-dry cycles on the soil deterioration induced by salt, the P-wave velocities of all the specimens were determined after every cycle using the RSM-SY5 ultrasonic instrument manufactured by the Institute of Rock and Soil Mechanics, Chinese Academy of Sciences. Transmitter and receiver were coupled to the surface of the specimens using vaseline. The instrument was calibrated with a standard material before every test. All the P-wave velocities of specimens were measured after complete drying at 15% RH, due to the high sensitivity of the US velocity to the moisture content.

3.2.2 Mechanical performance tests

Soil is a particularly loose material composed of particles. The stability and deterioration behaviour of this material can be estimated from its mechanical properties, including the resistance to external forces such as the shear resistance, the compression resistance and the tensile resistance. The mechanical performance tests were conducted after three dry-wet cycles, including direct shear test, unconfined compression test and tensile test. The specimens for the shear test were cut from the cubic samples due to the limited acceptable sample height of 20mm of the instrument used. Therefore, only the shear strength close to the surface of the specimens was measured while the mechanical properties of the whole cubic specimens are better represented by the compressive strength and the tensile strength.

3.2.3 Wind tunnel test

Erosion can be a common problem for monuments in deserts. Thus, the different effect of erosion response to artificial sandstorms is an effective and direct way to evaluate the salt deterioration under wet-dry cycles. The wind tunnel test was carried out in the multifunctional wind tunnel laboratory in Lanzhou University in China, with four different wind speeds, 18m/s, 21m/s, 24m/s and 28m/s, for 100s, 200s, 300s, 400s and 600s duration wind erosion. The sands used in the experiment are taken from the Tengger Desert in Minqin County of Gansu Province, China. The average particle diameter of these sands is approximate 0.288mm. In addition, the samples were weighed each time to calculate the mass loss under the different erosion conditions.

4 Results and discussion

4.1 Ultrasonic test

Soil deterioration was recorded as the P-wave velocity evolution, illustrated in Figure 2. It is seen that after the third cycle the wave velocity declines compared to after the first one, and this the more for increasing salt content. The decrease of the P-wave velocity is attributed to salt crystallisation exerting pressure on the soil material, hence causing damage. Moreover, this decrease caused by salt crystallisation accumulates with increasing cycle number as the wave velocities of the samples decreased significantly after each cycle. However, a decreasing US wave velocity for increasing cycle number was also observed for the salt free samples, indicating that swelling of clay minerals cannot be ignored. The result is consistent with the viewpoint proposed in the previous studies [10-11].

The degree of damage should be different for samples treated with different salts. According to the results of the experiments, for the single

salts, the wave velocity of the sample contaminated with Na_2SO_4 is always lower than that of the one containing a similar amount of NaCl , indicating that crystallisation of the last creates less damage to the soil. The salt mixture reflects the largest damage potential to the soil material. Although the deterioration mechanism is still unknown, it ensured that the internal structure of the salt contaminated sample has changed, such as pore distribution, amount of voids and the inter-particle bonds in soil, under dry-wet cycles.

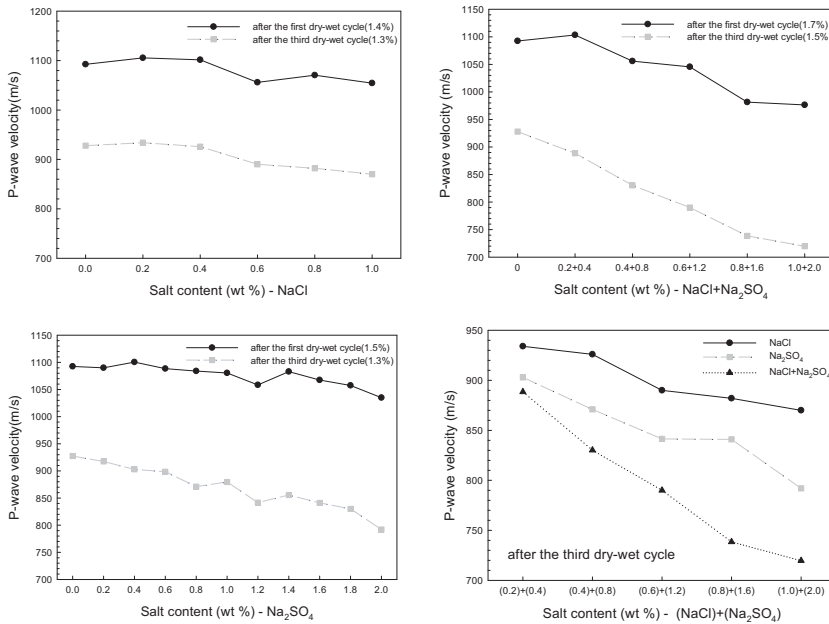


Figure 2: Relationship between P-wave velocity and salt content of the samples after different dry-wet cycles

4.2 Mechanical performance test

Different from the ultrasonic test, the degree of deterioration of the soil can be shown clearly from the results of the mechanical performance test. Figure 3 shows the relationship between mechanical strength parameters and salt content of the sample. For all samples in this experiment, the strength decreases with increasing salt content, thus, confirming the strong influence of the salt content on the magnitude of damage that was also demonstrated in the ultrasonic test.

Comparing the tensile strength and the compressive strength of samples contaminated with NaCl , Na_2SO_4 and their mixtures, respectively, similar results are obtained as with the ultrasonic test. Samples prepared with the salt mixtures have the lowest strength, followed by those mixed with Na_2SO_4 while NaCl shows the lowest destruction potential.

However, there is a slight difference in the shear strength. The cohesion of samples prepared with the salt mixture is higher than that of the samples containing pure Na_2SO_4 when the content is less than 1.2%. This is an apparent contradiction to the results of the compression and tensile tests. However, the reasonable interpretation of this difference is simply that the shear parameter was determined on smaller specimens (2 cm height) that were cut from the cubic ones. Therefore, the shear measurements only represent the deterioration closed to the surface of the cubic samples. In other words, the degree of deterioration in the samples is inhomogeneous from the interior to the surface. Low RH (relative humidity) promotes rapid evaporation, driving the flow through the pores to the surface. Thus, the salt normally crystallises on the exterior surface or near the surface of the sample. Due to the presence of NaCl, the solubility of Na_2SO_4 in the mixture is lower than that of the single salt, so it can be that the precipitation of Na_2SO_4 occurs at greater depths, resulting in less damage close to the surface of the specimens where the shear measurements were carried out.

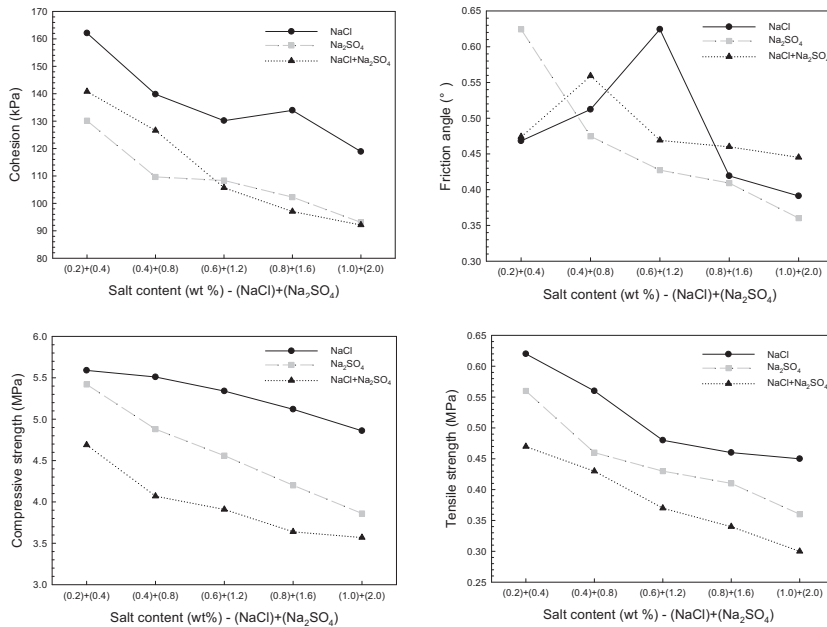


Figure 3: Relationship between mechanical strength parameters and salt content of the samples

In addition, the angle of internal friction of the soil, another important shear performance parameter usually used to describe the friction shear resistance of soil, exhibits an increasing trend at first and then decreases with increasing salt content. The value of the friction angle depends on the roughness of the contact surface between particles and the compactness of the soil. Salts precipitated in the pores can increase the roughness of the contact surface between adjacent particles, while crystallisation

pressure decreases the compactness of the soil as well. Therefore, when the salt content is smaller, the friction angle increases due to the filling of the pores with growing salt crystals, whereas in case of larger salt contents, the reduction of the compactness is primarily controlling the angle of internal friction.

4.3 Wind tunnel test

The following observations should be considered in order to evaluate the influence of the salt content on the erosion response of relic soils under dry-wet cycles. Erosion is usually considered as a minor problem for stone monuments or sculptures. However, the mass loss of soil due to the erosion is an obvious result of its loose structure. Moreover, typical soil, they crumble very easily under an external force such as salt crystallisation pressure. Therefore, the mass loss during wind tunnel tests reveals the deterioration combining salt crystallisation and erosion.

Apparently, the mass loss is largely dependent on the speed of wind-sand flow and time of duration (Figure 4). This means that the greater the wind speed and the longer the duration, the more serious the mass loss. On the contrary, the mass loss is low when the wind speed is low with short time of duration. Thus, the deterioration caused by the erosion can not be ignored for the earthen relics.

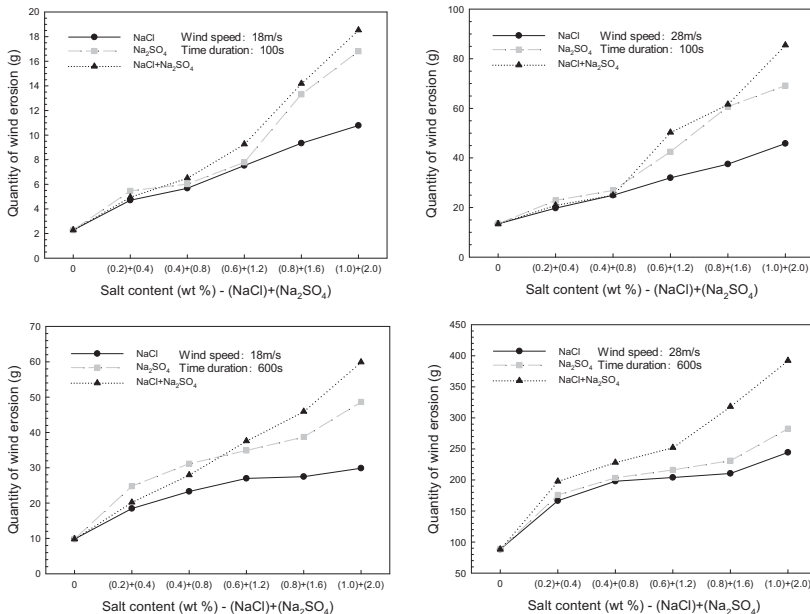


Figure 4: Relationship between quantity of wind erosion and salt content of the samples. However, for the same conditions (wind speed and duration), the effect of increasing wind erosion on samples with increasing salt content is striking.

The maximum mass loss due to the salt weathering is several times that of the salt free sample. It is also observed that the mass loss rate of the same sample decreases with increasing time duration under constant wind speed (Figure 5). In other words, the outmost zone of the sample is more deteriorated and less resistant to erosion. Therefore, salt crystallisation not only deteriorates the soil but also makes the samples inhomogeneous.

Moreover, according to the experimental results of the mechanical performance, the degree of deterioration is determined by the crystallisation behaviour of different salts as well, which is consistent with the results obtained in the wind tunnel experiment. In the beginning, the erosion process is largely controlled by the Na_2SO_4 content (Figure 4). With increasing mass loss, the influence of the salt mixture is obvious.

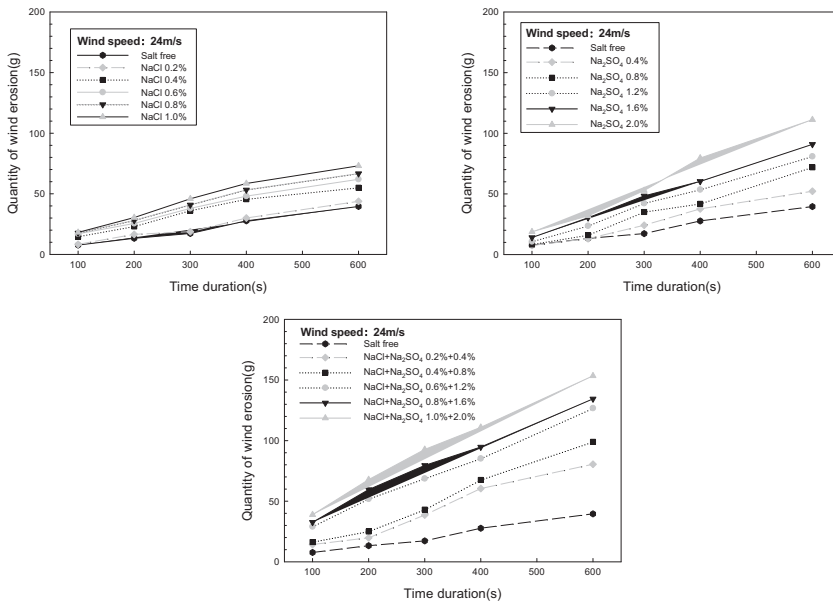


Figure 5: Relationship between quantity of wind erosion and time duration

5 Conclusions

To investigate the salt deterioration of salt contaminated soil under dry-wet cycles, an experimental program was conducted to test the mechanical performance and erosion characteristics of salt contaminated specimens. In addition, the deterioration process was monitored by means of ultrasonic tests. The factors of salt content and type of salts were considered. From the results presented and discussed above, the following conclusions can be drawn.

- 1) The dependence of the degree of deterioration on the salt content is obvious. Moreover, a mixture of Na_2SO_4 and NaCl added to the sample has the largest damage potential while the crystallisation of NaCl caused the lowest damage to the soil.
- 2) The deterioration caused by salt crystallisation accumulated with increasing cycle number. However, the presence of swelling clay minerals also causes damage during dry-wet cycles that cannot be ignored.
- 3) It is found that the degree of deterioration in the samples is inhomogeneous from the interior to the surface. Most serious deterioration is at the surface of the samples due to salt crystallisation. Na_2SO_4 contributed most to the surface weathering of the soils while NaCl played a minor role in the weathering.

References

- [1] M.S. Shao, L. Li, S.J. Wang, E.Z. wang, Z.X. Li, Deterioration mechanisms of building materials of Jiaohe ruins in China, *J. Cult. Heritage* 14 (2013) 38-44.
- [2] J. Lavalle, Recherches sur la formation lente des cristaux à la température ordinaire, *Compt. Rend. Acad. Sci. (Paris)* 36 (1853) 493-495.
- [3] K. Zehnder and A. Arnold, Crystal growth in salt efflorescence, *J. Cryst. Growth* 97. (1989) 513-521.
- [4] G.W. Scherer, Crystallisation in pores, *Cement Concr. Res.* 29 [8] (1999) 1347-1358.
- [5] R.J. Flatt, Salt damage in porous materials: how high supersaturations are generated, *J. Cryst. Growth* 242 (2002) 435-454.
- [6] Steiger M, Crystal growth in porous materials—I: the crystallisation pressure of large crystals. *J. Cryst. Growth* 282 (2005) 455–469.
- [7] Steiger M, Crystal growth in porous materials—II: Influence of crystal size on the crystallisation pressure. *J. Cryst. Growth* 282 (2005) 470–481.
- [8] Standardization Administration of China (SAC), Ministry of Water Resources, 1999. China National Standards GB/T50123-1999: Standard for Soil Test Method, China Planning Press, Beijing (in

Chinese).

- [9] Standardization Administration of China (SAC), Shaanxi Building Research Institute, 1999. China Standards JGJ/T70-1999: Standard for test method of performance on building mortar, China Construction Industry Press, Beijing (in Chinese).
- [10] F.Z. Zhang and X.P. Chen, Influence of repeated drying and wetting cycles on mechanical behaviors of unsaturated soil, *Chinese J. Geotech. Eng.* 32 (1) (2010) 41-46.
- [11] H.Y. Zhang, G.S. Yan, T.Y. Zhao, X.D. Wang, Y.X. Zhang, Durability of earthen architecture ruins under cyclic wetting and drying, *Rock Soil Mech.* 32 (2) (2011) 347-355 (in Chinese).

Determination of the deliquescence point in salt mixtures and in in-situ multicomponent salts with DVS equipment

I. Rørig-Dalgaard*

Technical University of Denmark, Department of Civil Engineering

* ird@byg.dtu.dk

Abstract

Accelerated salt induced deterioration occurs by frequently changes across the deliquescence point. Therefore does the actual deliquescence point of the present salts have a major impact on preventive conservation being able to ensure a relative humidity not causing salt phase transition and to in-situ desalination as dissolution of the salts is the essential criterion to enable transport of salt (ions) in the construction.

In the present work deliquescence points were measured with dynamic vapor sorption (DVS) equipment in salt mixtures and the results are shown to be in agreement with values from the literature. Also in-situ-multi salt samples were measured including the difference between the second critical relative humidity and the efflorescence relative humidity being a measure for the critical supersaturation required for crystallization at the specific experimental conditions. The DVS equipment seems to be able to make accurate determinations of the deliquescence points in complex salt systems and could be an expressive determination in in-situ investigations.

Keywords: deliquescence point, salt mixtures, second critical relative humidity, efflorescence relative humidity, DVS, critical supersaturation

1 Introduction

The precise deliquescence point in constructions is of major importance in relation to preventive conservation being able to ensure a relative humidity not causing salt phase transition and to in-situ desalination as dissolution of the salts is the essential criterion to enable transport of salt (ions) in the construction.

For single salts deliquescence points are and has for decades been well defined [1]. Regarding salt mixtures some deliquescence points are available in the literature as e.g. given in [2] though due to the comprehensive possibilities by far all combinations are available. Two and three component salt mixtures can be thermodynamically calculated [2-5]; however in-situ-multi salt mixtures are difficult to calculate. In the conservation science community is the model ECOS-Runsalt becoming increasingly popular to predict the deliquescence humidities of very complex salt mixtures. However, experimental investigations are desired for validation of the model and for illustration of kinetic effects.

In [2] the deliquescence points of salt mixtures were measured in a cell that can be evacuated and backfilled with water vapor and the phase transformation of the aerosol particle was monitored by laser light scattering. The RH at the transition point was determined by directly measuring the water vapor pressure in the cell. They also developed a theoretical model for the composition and temperature dependence of the deliquescence properties for single- and two-salt aerosol systems.

In preliminary work [6] it was made probable to determine the deliquescence point of single salts with dynamic vapor sorption (DVS) equipment by measuring mass changes during constantly changing partial pressure. In the present work the accuracy of the equipment was determined by salt calibration validation test with single salts. Deliquescence points were measured in salt mixtures at conditions identical to data from the literature and in in-situ-multi salt samples with DVS equipment.

2 Deliquescence point in salt mixtures and multicomponent mixtures

The presence of other ions also impacts the solubility. This effect is opposite to the common ion effect and was called the “secondary salt effect”. If other ions are dissolved, the total ionic concentration of the solution increases and interionic attractions become important. Activities become smaller than the stoichiometric or measured concentrations. Higher concentrations are necessary before equilibrium is established [7].

In case of at least three salts a multiphase region can exist during absorption. At the deliquescence point (Mutual Deliquescence Relative Humidity, MDRH, being the RH at which the mixture starts to pick up moisture) only one component of the solid mixture dissolves completely and subsequently the composition consists of an aqueous solution and undissolved solids following growing into a common saturated solution droplet at the second critical RH (SCRH) at which the dissolution is completed.

Increasing mass after the deliquescence point has been reached is a consequence of continuous water droplet growth by water vapour condensation. At the deliquescence point an equilibrium exists between the solid phase and the aqueous solution. Evaporation will occur until the RH becomes sufficient low and the droplet suddenly crystallizes in a point, expelling the remaining water content. A significant difference between the deliquescence point during absorption and desorption was shown in [8] in case of the salts: KCl-NaCl. According to [2] a significant difference in the deliquescence point during absorption and desorption can exist in salt mixtures consisting of at least 3 salts.

In [3] non-ideal mixture of two salts is described. Regarding two salts in a solution as the ambient relative humidity is lowered, one of the salts eventually becomes saturated, and its crystalline phase forms. As the relative humidity is further lowered, more of the solid phase of this salt forms, and the residual solution becomes more concentrated in the other salt. At a certain relative humidity, referred to as the mutual deliquescence relative humidity (MDRH), the two salts crystallize together and form a mixed solid phase at the eutonic composition. The MDRH is always lower than the DRH of the individual solutes.

The resulting dried particles are composed of a pure salt core surrounded by a mixed salt coating, where the core composition is solely determined by the original aerosol composition, but the coating is identical with the eutonic composition and is independent of the original aerosol composition. If the ambient relative humidity is increased, the size of the dried particle remains unchanged until the relative humidity in the atmosphere becomes identical with the water activity of eutonic. The solid coating having eutonic composition at the particle surface is then dissolved in the absorbed water. Due to surface tension, the remaining pure salt solid core stays at the center of the particle and is surrounded by saturated solution of eutonic composition. Further increasing the relative humidity results in more water absorption into the particle, and part of the pure salt solid core is dissolved to maintain water equilibrium between the solution and the atmosphere. At a certain relative humidity, which is a function of the overall composition of the original particle, the pure salt solid core is completely dissolved into the solution, and the particle becomes a pure aqueous droplet [3].

3 Principle description of the DVS

The dynamic vapour sorption (DVS) equipment can generate a desired pressure; the pressure is changeable according to a programmable sequence and simultaneously the mass can be recorded. This gives the possibility continuously to increase or decrease the relative humidity.

The pressure within the DVS is generated by control of the supply of dry and moist air respectively. The accuracy of the mixed air supply is checked through calibration tests and preformed with single salts covering RH from 11 to 93 % (LiCl; MgCl₂; MgNO₃; NaCl; KNO₃). The salt calibration principle is based upon the principle that the vapour pressure above a saturated salt solution in equilibrium with its surroundings is a constant at a particular temperature. In case of equilibrium conditions in the vicinity of the deliquescence point, mass change (dm) per change in pressure related to the saturation pressure (d(%P/P₀)) is equal to the pressure (P) multiplied with a constant (c):

$$\frac{dm}{d(\% \frac{P}{P_0})} = c \cdot P \quad (1)$$

At the point where the DVS-generated %P/P₀ is equal to the %P/P₀ above the saturated salt solution, the rate of change of mass is zero defining the deliquescence point, resulting in eq. 1 can be simplified to:

$$\frac{dm}{d(\% \frac{P}{P_0})} = 0 \quad (2)$$

In praxis this means that the change in partial pressure must be appropriate slow throughout the measurements to ensure equilibrium conditions to come into existence. In order to determine the most accurate deliquescence points it is of importance to ensure that the DVS is accurate calibrated which is done with single salt calibration tests. To obtain reliable salt calibration tests it is essential to ensure the salts have been prepared into the right condition prior to the salt calibration test (this is not described in this paper).

4 Materials

4.1 Preparation of salt mixtures

Based on the solubilities of single salts in 100 mL distilled water the soluble mass of two salts was mixed together in 100 mL distilled water in a 1L beaker. The beaker was placed in a pot with boiling water and covered with a slightly curved transparent glass on the top. The solution was heated until the solution was around 100°C or till nucleation occurs at the surface whereupon the beaker is taken up of the pot and placed for cooling in a fume cupboard. Crystals will be formed at the surface and gradually fall down to the bottom. A small amount of the solution was poured into a petri dish to accelerate evaporation. The used masses for preparation of each of the salt mixtures are listed in Table 1.

Table 1: Masses of each single salt added into 100 mL distilled water for preparation of the salt mixture.

	NaCl [g]	NaNO ₃ [g]	Na ₂ SO ₄ [g]	(NH ₄) ₂ SO ₄ [g]
NaCl-NaNO ₃	39.1	180		
NaCl-Na ₂ SO ₄	39.1		42.7	
(NH ₄) ₂ SO ₄ -Na ₂ SO ₄			42.7	103.8
NaCl-Na ₂ SO ₄ -NaNO ₃	39.1	180	42.7	

4.2 In-situ multi salt sample

The in-situ-multi-salt sample was taken from the upper side of the vault in Rørby church, Denmark, Zealand, in February 2011 and is one of the analysed samples in [9]. The samples consisted mainly of sodium and chloride but did also include potassium, magnesium, nitrate and sulphate. The measured ion contents in the in-situ multi salt samples are shown in Table 2 as an average of a trippel determination.

Table 2: The measured ion contents in the in-situ-multi-salt sample as an average of a trippel determination.

	Na ⁺ [wt%]	Ca ²⁺ [wt%]	K ⁺ [wt%]	Mg ²⁺ [wt%]	Cl ⁻ [wt%]	NO ₃ ⁻ [wt%]	SO ₄ ²⁻ [wt%]
Rørby church Feb. 2011	0.36	0.08	0.03	0.02	0.74	0.05	0.09

5 Results and discussion

5.1 Check of the generated RH in the DVS by calibration tests with single salts

In order to determine the accuracy of the results for salt mixtures initial salt calibration tests were to be made on well-defined single salts with a deliquescence point close to the expected values for the salt mixtures. Salt calibration tests were carried out at 25°C with a salt with a deliquescence relative humidity (DRH) around 70 % RH and with a salt having a lower DRH being NaCl and $\text{Mg}(\text{NO}_3)_2$ with a deliquescence point of 75.29 +/- 0.12 % RH and 52.91 +/- 0.22 % RH respectively [1].

The deliquescence point is found by a combination of the result for the point at which no mass change occur (equation 2) and made more robust by following the development in the desorption and absorption around the deliquescence point (equation 1). The point at which no mass change occurs is represented by the intersection with the X-axis in Figure 1, see the grey lines. By creating a fitted line (see the dotted black line in Figure 1) on basis of the measured values for desorption across the deliquescence point showing mass change per change in RH, the black dotted line is generated. On the basis of this a calculated intersection with the x-axis can be found and thereby a RH found at which no mass change occurs defining the deliquescence point. By creating the same data for the absorption phase the deliquescence point found with the DVS equipment is an average of two determinations with a deviation in the deliquescence point found between the desorption and absorption phase.

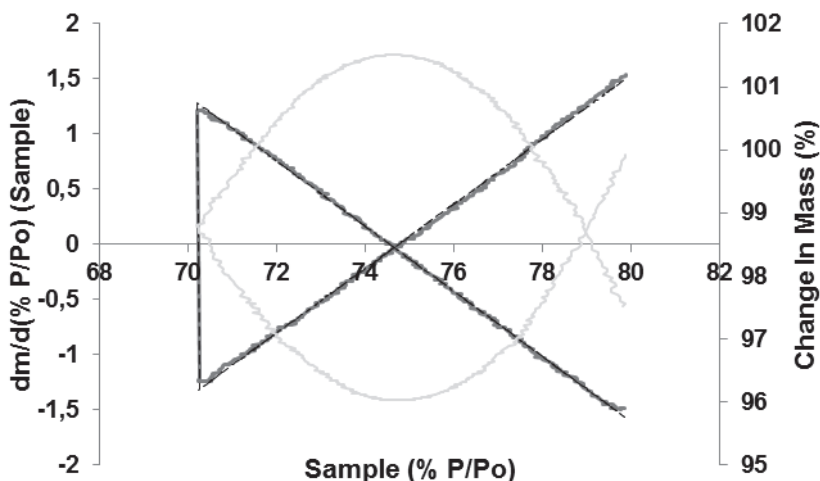


Figure 1: A plot of the salt validation calibration for NaCl. — Measured $\text{dm}/\text{d}(\%P/P_0)$ (Sample), — fitted $\text{dm}/\text{d}(\%P/P_0)$, — change in mass (%) at 25.0°C.

The results of the salt calibration validations test for NaCl is shown in Figure 1. The bright grey color in figure 1 illustrates a continuously changing mass as a function of changing RH. An absence of mass change was measured and imaged in the middle of the graph showing the presence of a deliquescence point. The measured mass change as a function of change in RH occurred continuously as shown as the dark grey line and was very close to the fitted line (black dotted). The fitted line which minimizes experimentally induced circumstances is representative for the actual measured values. A relative little deviation between the desorption deliquescence point and the absorption deliquescence point further make probable that the salt calibration validation tests were performed accurately ensuring the most reliable result.

Figure 1 was made on the basis of the available standard add-ins in excel to the DVS enabling an easy check of the reliability of the obtained data.

The results from the salt calibration validation tests are besides a test of the generated RH used to increase the accuracy of the measured results as deviations from the reference values for single salts must be attributed to experimental induced causes. Several salt calibration tests were carried out with NaCl and $Mg(NO_3)_2$, see Table 3 and Table 4.

Table 3: Salt validation calibration tests with NaCl.

	Reference value from the literature	1 th run	2 th run	3 th run	4 th run	5 th run	Average
NaCl	75.29 +/- 0.12	74.65 +/- 0.09	74.58 +/- 0.09	74.51 +/- 0.17	74.40 +/- 0.07	74.69 +/-0.10	74.57 +/- 0.04
Deviation from reference	-	0.64	0.71	0.78	0.89	0.60	0.72

Table 4: Salt validation calibration tests with $Mg(NO_3)_2$.

	Reference value from the literature	1 th run	2 th run	3 th run	Average
$Mg(NO_3)_2$	52.91 +/- 0.22	52.21 +/- 0.03	52.20. +/- 0.02	52.25 +/- 0.11	52.22 +/- 0.05
Deviation from reference	-	0.70	0.71	0.66	0.69

The average of the salt calibration validation test for $\text{Mg}(\text{NO}_3)_2$ was found to 52.22 % RH which is a difference of 0.69 % RH from the reference values of 52.91 % RH \pm 0.22. The average of the measured deliquescence point for NaCl was found to 74.57 % RH meaning a difference of 0.72 % RH from the reference value of 75.29 \pm 0.12 % RH.

The repeated salt calibration validation tests showed an accuracy of the measurements of 0.05 % RH and 0.10 % RH for $\text{Mg}(\text{NO}_3)_2$ and NaCl respectively and make probable the results are reproducible and representative for the preformed measurements.

5.2 Determination of the deliquescence point in salt mix

Since the general definition of the deliquescence point is an absence of mass change at a specific relative humidity this criterion can also be used in case of salt mixtures. The measured deliquescence points for NaCl- NaNO_3 ; NaCl- Na_2SO_4 ; $(\text{NH}_4)_2\text{SO}_4$ - Na_2SO_4 and NaCl- Na_2SO_4 - NaNO_3 are shown in Table 5. The deliquescence point for these salt mixtures were previously measured by [2] and [3] at 25°C and used as reference values.

Table 5: Deliquescence point at 25°C for salt mixtures. The recalculated values are the measured values \pm the documented deviation from the reference values (see Table 3 and 4).

	Literature % RH	1 th run	2 nd run	3 rd run	Average/ deviation	Re- calculated
NaCl- NaNO_3	68.0 \pm 0.4	66.52 \pm 0.01	66.19 \pm 0.11	66.35 \pm 0.14	66.35 \pm 0.07	67.07
NaCl- Na_2SO_4	74.2 \pm 0.3	73.78 \pm 0.10	73.73 \pm 0.08	73.50 \pm 0.05	73.67 \pm 0.03	74.39
$(\text{NH}_4)_2\text{SO}_4$ - Na_2SO_4	71.3 \pm 0.4	74.61 \pm 1.33	75.75 \pm 0.35	-	75.18	75.90
NaCl- Na_2SO_4 - NaNO_3	71.8 \pm 0.5	65.96 \pm 0.16	-	-	-	66.68

Taking the determined difference between the RH measured in the DVS and reference values into account being 0.72 % RH at a RH around 75 % RH, the recalculated deliquescence point for NaCl- Na_2SO_4 was found to 74.39 % RH. The present found deliquescence point is in consistence and does not differ significantly from the deliquescence point found by [2] of 74.2 \pm 0.3 % RH. In addition this clarifies that it is possible to measure a significant difference in the deliquescence point between NaCl (75.29 \pm 0.12 % RH) and NaCl- Na_2SO_4 (74.2 \pm 0.3 % RH) meaning two salts have a deliquescence point relative close to each other.

The recalculated value for the deliquescence point for NaCl- Na_2SO_4 was determined to 67.07 % RH. In [3] the deliquescence point for this salt

mixture was thermodynamically calculated to 67 % RH whereas in [2] it was measured to 68.0 +/- 0.4 % RH. The setup was described in [8] where the reproducibility of the measurement was described to be better than +/- 2%. They also developed a theoretical model resulting in the same deliquescence point as they had measured. The present measured deliquescence point is in consistence with the thermodynamically calculated result by [3] which is close to but differs significantly from the calculated and measured values by [2].

In two salt calibration validation tests where the deviation was improved by narrowing the interval of the applied RH, the recalculated deliquescence point of $(\text{NH}_4)_2\text{SO}_4\text{-Na}_2\text{SO}_4$ was determined to 76.47 % whereas it was found to 71.3 +/- 0.4 % RH [2]. Likewise was the recalculated deliquescence point for $\text{NaCl-Na}_2\text{SO}_4\text{-NaNO}_3$ determined to 66.56 % RH whereas it was measured to 71.8 +/- 0.5 % RH in [2].

In case of sodium sulfate there is no unique DRH and the value depends on the nature of the solid phase. At 25°C is the DRH 93.6 % RH for mirabilite, 86.9 % RH for thenardite (Na_2SO_4) and 83.5 % RH for phase III. Regarding the salt mixture $\text{NaCl-NaNO}_3\text{-Na}_2\text{SO}_4$ two different possible compositions of the solid mixture exist at room temperature being a) $\text{NaCl} + \text{Na}_2\text{SO}_4 + \text{Na}_3\text{NO}_3\text{SO}_4\cdot\text{H}_2\text{O}$ (darapskite) (MDRH = 69.7 % RH) or b) $\text{NaCl} + \text{NaNO}_3 + \text{Na}_3\text{NO}_3\text{SO}_4\cdot\text{H}_2\text{O}$ (MDRH = 66.2 % RH) and a third possibility exists due to the preparation of the salt through evaporation from a boiling solution being c) $\text{NaCl} + \text{Na}_2\text{SO}_4 + \text{NaNO}_3$. In [3] they characterizes salt mixtures as simple and less simple systems the former one being independent of the present mole fractions of the salt in contrast to the latter. The differences between the present determined MDRH and the values from the literature [2] is most likely a result of different composition of the solid salt mixture caused by differences in salt preparation and different fractions of each salt. For future work it must be ensured that identical fractions are used for preparation of the salt mixtures and identical salt preparation procedures must be followed to obtain comparable results. Comparison with results from ECOS-runsalt should also be carried out in future work for common validation of results.

The measured deliquescence points for the salts and salt mixtures are in good agreement with reference values both regarding single salt, salt mixtures and found differences can be theoretically explained, making probable the determination of the deliquescence point in in-situ multi salt samples with the dynamic vapor sorption equipment.

5.3 Determination of the deliquescence point in in-situ multi salt samples

In case of an in-situ multi salt sample the deliquescence point and the second critical relative humidity (SCRH) at which the dissolution is complete are unknown. Therefore the below procedure was followed:

- 1) Initially it was necessary to make a relative fast screening of the sample between 0 and 95 % RH to determine the interval where phase changes occur both regarding complete dissolution of the salt at SCRH during absorption and efflorescence relative humidity (ERH) where crystallization is initiated during desorption. It is to be noticed that a fast screening is not carried out at equilibrium conditions which can result in slightly misleading results.
- 2) Based on the results from the initial screening a new test was started within a limited interval with a decreased change in partial pressure as a function of time. The decreased change in partial pressure as a function of time was made to ensure equilibrium conditions throughout the experimental duration.
- 3) Further narrowing of the test interval though still ensuring both the SCRH and ERH were included in the interval and simultaneously decreasing the change in partial pressure as a function of time.

Article 3 was repeated until equilibrium conditions were ensured through an absence of change in SCRH and ERH at further reduced interval or further decreased change in partial pressure as a function of time; an example of this is given in Figure 2.

The sorption isotherms in Figure 2 represent both brick powder and a salt mixture. Regarding a sorption isotherm for brick powder a weight gain up to 1.5 wt% has been measured dependent on the brick type [10]. The water absorption to the brick powder could partly explain the mass increase at low RH e.g. was a weight gain of 0.3 wt% measured at 40 % RH [10] where the present weight gain at 40 % RH was measured to 0.6 wt%. This implies that at a RH of 40 % there is a significant water uptake and an initial dissolution of the salt mixtures defining the deliquescence point. A more precise deliquescence point could e.g. be calculated by the use of ECOS-Runsalt and verified by measurements with the DVS.

In [11] the water uptake during absorption occurred in a step meaning a sudden increase in absorbed water whereas in contrast the evaporation path yields metastable phases resulting in partly continuous water decrease. Regarding the curved evolution in Figure 2 it is seen that the second critical relative humidity (SCRH) during absorption differs significant from the efflorescence relative humidity (ERH) during desorption. At equilibrium there is no difference between the RH at which crystallization starts and the RH at which dissolutions is completed.

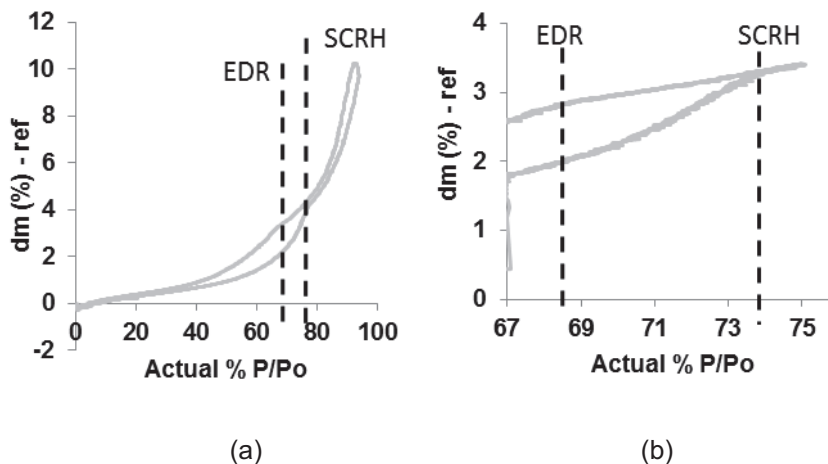


Figure 2: The measured mass change as a function of relative humidity at 25.0°C. The results shown in (a) were obtained from measurements performed in conjunction with a change of 1% RH per hour and in b) with a change of 0.08 % RH per hour.

Table 6: Second critical relative humidity (SCRH) and efflorescence relative humidity (ERH) in three different in-situ samples extracted above the vault in Rørby Church. The results from the three samples were found as a function of different changes in RH/h, intervals and measuring modes.

	Sample 1 Closed loop	Sample 2 Closed loop	Sample 2 Open loop	Sample 3 Closed loop
Initial screening $\Delta 1$ % RH per hour	SCRH: 77 ERH: 67	SCRH: 83 ERH: 72	SCRH: 87 ERH: 73.6	SCRH: 84 ERH: 74
Limited interval $\Delta 0.35$ % RH per hour	SCRH: 74 ERH: 67.5	-	-	-
Second limited interval $\Delta 0.18$ % RH per hour	SCRH: 74 ERH: 68	-	-	-
Third limited interval $\Delta 0.08$ % RH per hour	SCRH: 73.8 ERH: 68.6	SCRH: 80 ERH: 74	SCRH: 78.6 ERH: 74.6	-

The measured hysteresis between absorption and desorption for RH between 40 and 80 % is a clear indication that supersaturation occurred during evaporation and differences between the two curves in Figure 2 must be attributed to differences between kinetic influences and the state of equilibrium. The supersaturation is dependent on the experimental conditions and is related to the porous structure, material, temperature, RH during evaporation, salt mixture composition and solid phase. The

difference between SCRH and ERH is therefore a measure for the critical supersaturation required for crystallization which clarifies salt induced deterioration RH at the present experimental conditions.

This pattern for the absorption and desorption isotherm including phase change in the sample from Rørby church is in consistence with the theoretical considerations made by [2] which make probable the presence of at least three different salts. The actual presence of at least three different salts is documented by measurements of the ionic contents shown in Table 2.

The SCRH will vary in case of varying fractions of the different salts in the mixtures for less simple salt systems. Extracting three different samples from a several hundreds of years old in-situ location it is most probably that these salt systems are less simple and that they do vary in the fraction of the different salts [3].

The measured SCRH was found to be between 73.8 and 80 % RH and the ERH between 68.6 and 74.6 % RH. Such significant differences between SCRH and ERH point have a practical influence on preventive conservation and for dissolution of salts prior to desalination campaigns. According to the present results dissolution of all parts of the salt mixture occurs at RH above 80 % RH and in case of subsequent lowering of the RH to ERH crystallization is initiated which potentially can cause damages. Therefore to avoid salt induced damages the RH should be kept above the SCRH of the salt mixture. Also to carry out desalination the salts must be completely dissolved which only is possible in case of total dissolution of the present salts. Therefore is the SCRH the determining parameter in case of preventive conservation and for desalination.

5.4 Considerations in relation to the practical case (here church vaults)

The present SCRH and ERH were determined at a temperature of 25°C even though this is a high temperature in connection with constructions. This temperature was chosen since most research is carried out at 25°C enabling comparison with the largest amount of data. In future research deliquescence points are also to be made at other temperatures to make the determination of the deliquescence points with DVS valid in a more general context and to make the method more useful for practical purposes.

In case of establishing a climate chamber with steady temperature and RH to prevent further salt induced deterioration determination of the SCRH and ERH gives valuable information on the most appropriate RH. As seen in Table 6 the SCRH and ERH can vary considerably as a consequence of varying salt fractions in the salt mixture out of which a sufficient accuracy of the present determined DRH and ERH are concluded.

Prior to desalination treatments climate data including temperature and RH are most often recorded through a year to clarify seasonal variations

[12] which makes it possible to determine SCRH and ERH at relevant temperatures. In previous work with electrochemical desalination of an artificial salt contaminated wall section with the single salt NaCl it was shown possible to obtain a high desalination effect when a microclimate was established ensuring a RH above the well-known deliquescence point of this single salt [13]. Therefore knowledge of the deliquescence points and ensuring these can have major impact on the desalination effect and success.

6 Conclusion

It was shown possible to determine ERH and DRH for single salts. The determined ERH and DRH for single salts did not differ significantly. The difference between the determined deliquescence point and reference values from the literature for single salts was used to increase the accuracy of the DVS determined values. A consistence was found between the measured deliquescence point for salt mixtures and values from the literature enabling to determine the deliquescence point in in-situ multi salt samples as shown for a sample lifted from above a church vault in Denmark. For the in-situ multi salt sample a significant difference was found between the SCRH and the ERH being a measure for the critical supersaturation required for crystallization. Due to the extensive possible combinations of salt mixtures, the determination of phase transition with the dynamic vapor sorption equipment seems like an expressive tool useful for in-situ multi salt samples.

Acknowledgements

The A.P. Møller and Chastine Mc-Kinney Møller Foundation is gratefully acknowledged for financial support to this project. Staffan Svensson and Kurt Kielsgaard Hansen are acknowledged for many fruitful discussions regarding general DVS issues, practical help with and for an introduction to the DVS. This is highly appreciated.

References

- [1] Greenspan L., Humidity Fixed Points of Binary Saturated Aqueous Solutions, Journal of research of the National Bureau of Standards – Physics and Chemistry, (81A), (1977), 89-96.
- [2] Tang I. N. & Munkelwitz H.R., Aerosol Phase Transformation and Growth in the Atmosphere, J. Appl. Meteorol. (33), (1994), 791-796.
- [3] Ge Z., Wexler A.S. & Johnston M.V., Deliquescence Behavior of Multicomponent Aerosols, J. Phys. Chem, (102), (1998), 173-180.

- [4] Steiger M., Salts in Porous Materials, Thermodynamics of Phase Transitions, Modeling and Preventive Conservation, Bauinstandsetzen und Baudenkmalpflege 11 (6), (2005) 419-432.
- [5] Steiger M., Asmussen S, Crystallization of sodium sulfate phases in porous materials: The phase diagram $\text{Na}_2\text{SO}_4\text{-H}_2\text{O}$ and the geration of stress. *Journal of Geochimica et Cosmochimica Acta* 72, (2008) 4291-4306.
- [6] Rörig-Dalgaard, I. (2012), Determination of the deliquescence point in salt mixtures by utilizing the dynamic vapour sorption method. *The 3th International Workshop on Crystallization in Porous Media*. (ed.) Teresa Diaz, Troja, Portugal, 2012. 37-38.
- [7] Rijck G.D. & Schrevens E., Elemental bioavailability in nutrient solutions in relation to precipitation reactions, *Journal of Plant Nutrition*, (21:10), (1998), 2103-2113.
- [8] Tang I. N. & Munkelwitz H.R., Composition and temperature dependence of the deliquescence properties of hygroscopic aerosols, *J. Atmospheric Environment*, (27A) No. 4 (1993), 467-473.
- [9] Rörig-Dalgaard, I. & Bøllingtoft P. (2011), Electrochemical desalination of the ionic mixture measured in the vault of Rørby Church – Laboratory scale. *Salt Weathering on Buildings and Stone Sculptures*, (ed.) Ioannou I. & Theodoridou M., Limassol, Cyprus, 2011. 365-372.
- [10] Koronthalyova O., Moisture storage capacity and microstructure of ceramic brick and autoclaved aerated concrete, *J. Construction and Building Materials*, (25), (2011), 879-885.
- [11] Tang I.N., Fung K.H., Imre D.G. & Munkelwitz H.R., Phase Transformation and Metastability of Hygroscopic Microparticles, *J. Aerosol Science and Technology* (23), (1995), 443-453.
- [12] Larsen P.K., The salt decay of medieval bricks at a vault in Brarup Church, Denmark, *Environ Geol*, (52), (2007), 375-383.
- [13] Rörig-Dalgaard, I. (2009), Desalination for preservation of murals by electromigration and regulated climate. *Structural Studies, Repairs and Maintenance of Heritage Architecture XI*, (ed.) Brebbia C.A., Tallinn, Estonia, 2009. 71-82.

Measurement of sorption isotherm of porous materials influenced by salt

M. Abuku^{1,*}, D. Ogura², S. Hoko², C. Iba², S. Wakiya³, and T. Uno⁴

¹Faculty of Architecture, Kinki University, Higashi-Osaka, Japan

²Graduate School of Engineering, Kyoto University, Kyoto, Japan

³Nara National Research Institute for Cultural Properties, Nara, Japan

⁴Department of Architecture, Mukogawa Women's University, Nishinomiya, Japan

* abuku@arch.kindai.ac.jp

Abstract

This paper compiles the past data of the sorption isotherm of Autoclaved Aerated Concrete (AAC) laden with salts ($MgCl_2$ and $NaCl$) and some new experimental data for AAC that contains Na_2SO_4 . The results are related to the type of salt, the salt concentration and the mass of salt that is considered to be crystallised. Finally the existing mathematical model that uses the sorption isotherm for pure water and the salt content in the material is applied to predict the sorption isotherm of AAC laden with Na_2SO_4 . It is shown that even salts like Na_2SO_4 , whose equilibrium relative humidity is 94%, significantly alter the sorption isotherm when a large amount of salt is crystallised in the material and this to an extent depends on the amount as well as the type of salt.

Keywords: moisture, water retention curve, absorption, desorption, salt crystal

1 Introduction

The relation between the water content of a porous material and the relative humidity of the surrounding air in a condition that no exchange of moisture between the material and the air occurs, i.e. sorption isotherm, can be different when the material contains salts. This is because the vapour pressure of a salt solution is lower than that of pure water and because crystallising salts can alter the pore structure of the material.

Water sorption isotherm of porous materials in presence of salts has been measured by Bresler [1], Tanimoto et al. [2], Harimoto et al. [3], Hashikata et al. [4], Abuku et al. [5], etc. and modelled by Bresler [1], Brocken et al. [6], Rucker et al.[7], Abuku et al. [5, 8], etc. Most work was focused on porous materials containing salt solution at low concentration or saturated without salt crystals in the material. Recently, Abuku et al. [5] extended the existing models to a model for a material that contains undissolved salts (salt crystals).

This paper compiles the past data of the sorption isotherm of Autoclaved Aerated Concrete (AAC), commonly called ALC (Autoclaved Light-weight Concrete) in Japan, laden with two different types of salt ($MgCl_2$ and $NaCl$) and some new experimental data for AAC that contains sodium sulphate (Na_2SO_4). Here, AAC was not selected for its susceptibility to salt damage but for academic reasons chosen as model material to study the sorption isotherm of a salt-laden porous material. However, the methodology proposed here is considered to be similarly applicable to other porous materials. In the new measurement, we observe both absorption and successive desorption processes. The results are discussed with respect to the type of the salt and the salt content that is considered to be crystallised. Finally the existing model that uses the sorption isotherm for pure water and the salt content in the material is applied to predict the sorption isotherm of a salt-laden material.

2 Parameters and sorption isotherm model

This section briefly describes some important parameters required to understand the measurement data in the following section and the existing model developed in Abuku et al. [5], which predicts the sorption isotherm of a salt-laden porous material on the basis of the sorption isotherm of the same salt free material, the salt concentration and the amount of undissolved (crystallised) salts.

2.1 Definition of parameters

The moisture content w_w is given by:

$$w_w = \frac{m - m_0 - m_s}{m_0} \quad (1)$$

with m the mass of the material (kg), m_0 the dry mass of the material (kg), m_s the mass of salt in the material (kg).

The salt solution content w_{sw} is given by:

$$w_{sw} = \frac{m - m_0}{m_0} \quad (2)$$

The salt concentration C based on the solvent (water) is given by:

$$C = \frac{m_s}{m - m_0 - m_s} \leq C_{sat} \quad (3)$$

with C_{sat} the saturated salt concentration (kg/kg).

The content of salt crystals w_c is given by:

$$w_c = \frac{m_c}{m_0} \quad (4)$$

Here m_c can be calculated by:

$$m_c = m_s - w_w m_0 C_{sat} \quad (5)$$

2.2 Sorption Isotherm Model

The relative humidity φ' of a material that contains a salt solution with a concentration C is given by:

$$\varphi' = \varphi(1 - x_s) \quad (6)$$

where x_s is the molar fraction (-) and φ is the relative humidity (-) that the material would have when containing pure water of the same volume as the salt solution φ is related to the chemical potential μ_0 of water in the material that depends on the volume of the solution:

$$\varphi = e^{\frac{\mu_0}{TR_v}} \quad (7)$$

with T the temperature (K) and R_v the gas constant (J/kgK) of water vapour (4.616×10^2). Based on data for pure water, the relation between μ_0 and the water content w_w can generally be obtained as:

$$\mu_0 = \sum_{i=1}^n c_{i,1} \exp(c_{i,2} w_w) \quad (8)$$

with $c_{i,1}$ and $c_{i,2}$ constants. For a material that contains a salt solution, Eq.(8) is replaced by:

$$\mu_0 = \sum_{i=1}^n c_{i,1} \exp\left(c_{i,2} \frac{\rho_w}{\rho_{sw}} w_{sw}\right) \quad (9)$$

with ρ_w the density of water (kg/m^3), ρ_{sw} the density of a salt solution (kg/m^3), and w_{sw} the salt solution content (kg/kg).

When the salt concentration C reaches the saturated salt concentration C_{sat} and salt crystals are deposited, the relative humidity ϕ' predicted with the existing model (Eq. (6)) can thus be modified to the relative humidity ϕ'_{mod} by:

$$\phi'_{mod} = \left(1 - k_c \frac{w_c}{w_{sw}}\right) \phi' \quad (10)$$

where $k_c w_c / w_{sw}$ represents the degree of the influence of salt crystallisation.

3 Experiment

3.1 General

Some new measurements were conducted at a constant temperature of 23 °C. Equilibrium moisture content of AAC in absorption and successive desorption processes is measured in a manner similar to [5]. The porosity Φ_0 and density ρ_0 of the material are respectively $0.786 \text{ m}^3/\text{m}^3$ and 494 kg/m^3 [9].

In the measurement, the following six steps are taken:

- (1) 21 specimens of approximately $10 \times 10 \times 10 \text{ mm}^3$ are dried at 95 °C in an oven. The mass of each dry specimen m_0 is measured at a temperature of 23 °C and a relative humidity of 30 %.
- (2) Three desiccators that contain respectively pure water and Na_2SO_4 solution at a concentration $C_i = 0.0038 \text{ kg/kg}$ or $C_i = 0.0501 \text{ kg/kg}$, are prepared. Seven, eight and six specimens are dipped into respectively pure water, salt solution of $C_i = 0.0038 \text{ kg/kg}$ and a salt solution of $C_i = 0.0501 \text{ kg/kg}$. The air in the specimens is then evacuated by means of a vacuum pump.

- (3) All specimens are kept in the desiccators for more than one week, during which the air in the specimens is continuously evacuated. So all the specimens are considered to have been completely dried.
- (4) The specimens are stored in a large desiccator with a constant relative humidity of 11% that is controlled with saturated LiCl solution. The weight m of the specimens is measured every a few days.
- (5) When a constant weight is reached, the saturated salt water in the desiccator is changed successively from LiCl (11% RH), $MgCl_2$ (33% RH), NaCl (75% RH), to KCl (84% RH). At each relative humidity level, step (4) is repeated.
- (6) The salt-laden specimen are finally dried at 95 °C. The mass of each dry specimen is then measured to determine the sum of m_0 and m_s , which allows to determine the value of m_s by calculating $m_0 + m_s$ minus m_0 .

Given m , m_0 , and m_s , the moisture content w_w is obtained according to Eq. (1), the salt concentration C by Eq. (3), and the value of w_c by Eqs. (4) and (5).

It should be noted that it is assumed that all parameters are uniform in the specimen. To check whether the surface of the specimen is not blocked by salt crystals, AAC specimens are examined with an optical microscope at a dry condition (RH ~ 30%). However salt crystals were not found at the surface of the specimens. Only when a specimen that was initially saturated with a saturated salt solution and dried, salt crystals were observed at the surface of the specimen. In case parameters are not uniform in the specimen or pores at the surface zone are blocked by salt crystals, the measurement procedure presented in this section and the model may no longer be valid.

3.2 Results

The equilibrium moisture content at different conditions of relative humidity for specimens laden with Na_2SO_4 , related to salt free ones, in absorption and desorption mode is presented in Figure 1. The plotted values are obtained by averaging the data for the 7, 8 and 6 specimens. In the case of salt-laden specimens, the salt concentration during absorption and desorption processes is considered to be equal to the saturated salt concentration C_{sat} , so only the content of undissolved (crystallised) salt w_c calculated using Eqs. (4) and (5) is displayed in Figure 2(a) for the salt solution with the lower C_i and in Figure 2(b) for that with the higher C_i .

Although the equilibrium relative humidity of a Na_2SO_4 solution is 94 % at 23 °C, and hence no significant vapour pressure depression can be expected, the results show that the relative humidity values which are considered to give the same equilibrium moisture content can be very

different when the material contains salt crystals. This can be attributed to the influence of undissolved (crystallised) salts that are considered to change the pore structure.

The moisture content differences between the absorption and desorption processes for pure water and salt solution of the lower C_i are larger than in case of the higher C_i .

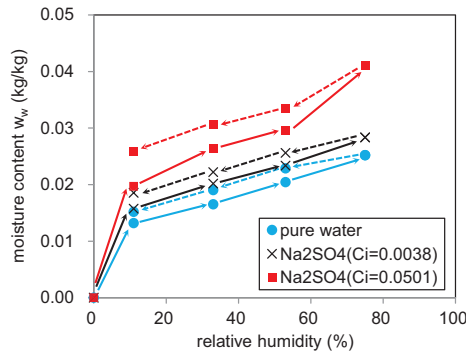


Figure 1: The measured sorption isotherm in absorption (solid line) and desorption (dashed line) processes of an autoclaved aerated concrete specimen laden with Na_2SO_4 solutions at two different concentrations

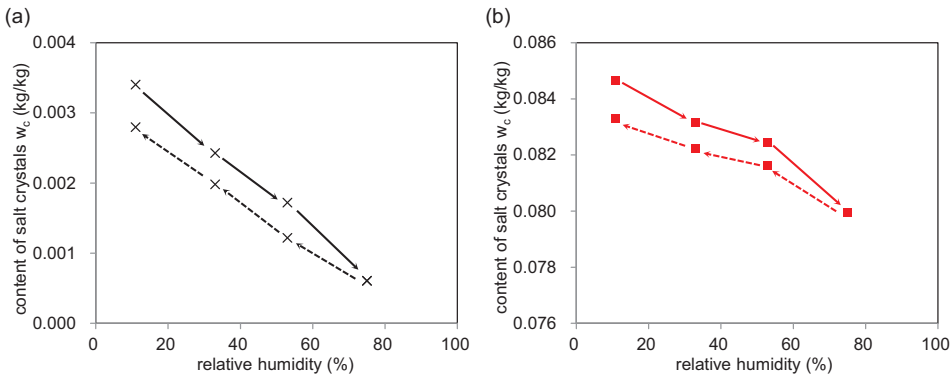


Figure 2: The measured content of salt crystals in absorption (solid line) and desorption (dashed line) processes

4 Discussion

The measurement data for absorption process were modelled using the equations described in section 2.2.

First, the data for pure water are fitted using Eqs. (7) and (8) with $n = 3$, $c_{1,1} = 1 \times 10^7$, $c_{1,2} = -210$, $c_{2,1} = 4 \times 10^4$, $c_{2,2} = -20$, $c_{3,1} = -3.75 \times 10^{-12}$, and $c_{3,2} = 0$. A good agreement is obtained between the measured data and the calculated ones as given in Figure 3. The values of n , $c_{i,1}$ and $c_{i,2}$ obtained here are used below as well.

Abuku et al. [5] found that k_c in Eq. (10) for AAC that contains NaCl and $MgCl_2$ under the conditions of the study can be obtained by:

$$k_c = c_{k,1} \exp\left(c_{k,2} \frac{m_s}{m_0}\right) \quad (11)$$

with $c_{k,1} = 0.0853$ and $c_{k,2} = 0.0495$. Using this same equation, we also determined $c_{k,1}$ and $c_{k,2}$ to be respectively 0.1229 and 0.0209 for AAC that contains Na_2SO_4 . The values of $\ln(k_c)$ given by $c_{k,1} = 0.0853$ and $c_{k,2} = 0.0495$ are compared to those experimentally obtained in Figure 4, showing the dependency of k_c on the type of salt. This dependency becomes larger with increasing ratio m_s/m_0 .

Figure 5 compares the measured and predicted relations between the water content and relative humidity, which confirms that using the model presented in section 2.2 and the model for k_c in this section allows to predict the sorption isotherm of salt-laden AAC given the type and amount of salt in the material. Note that the relative humidity predicted by only Eqs. (7) and (9) and the one by Eq. (6) as well as Eqs. (7) and (9) are also included in Figure 5. By comparing the predicted results, it can be noticed that the influence of salt crystals on the sorption isotherm can become much larger than that of the vapour pressure depression.

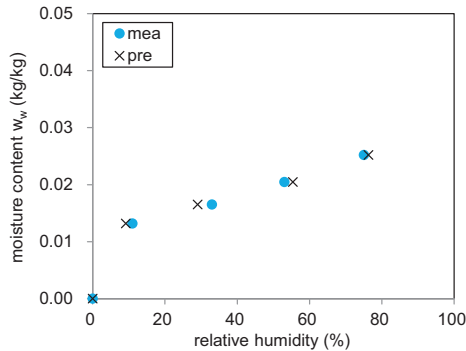


Figure 3: The measured and predicted relation between the water content and relative humidity for pure water

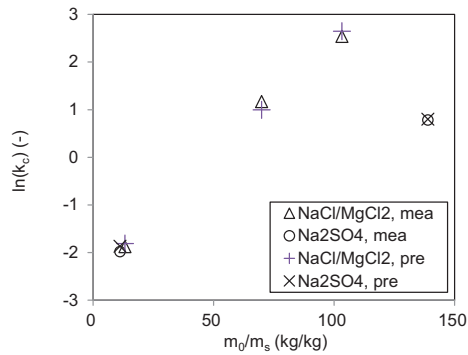


Figure 4: The measured and predicted $\ln(k_s)$ for NaCl/MgCl₂ and Na₂SO₄

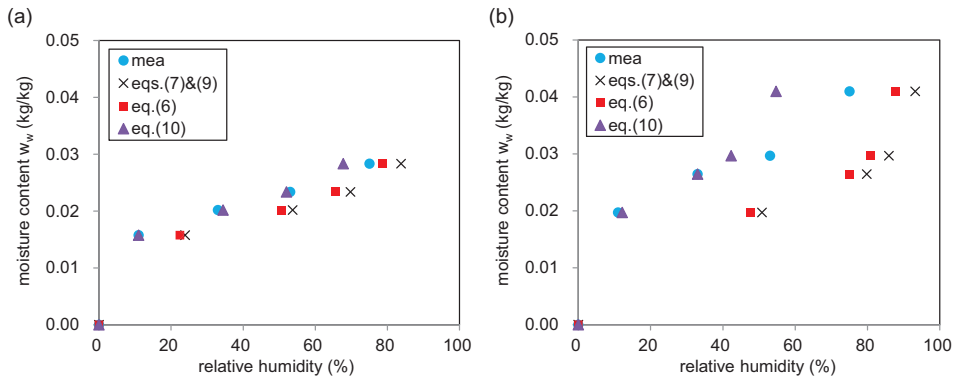


Figure 5: The measured and predicted relation between the water content and relative humidity for salt solution at (a) $C_i = 0.0038$ kg/kg and (b) $C_i = 0.0501$ kg/kg.

5 Conclusions

In this paper, we conducted some new experiments to measure the sorption isotherm of Autoclaved Aerated Concrete (AAC), commonly called ALC (Autoclaved Light-weight Concrete) in Japan, that contains sodium sulphate (Na₂SO₄). The measured data were compared to those obtained for different types of salt (MgCl₂ and NaCl). The compiled data were discussed in relation to the type of material and salt and the salt content that is considered to be crystallised. The mathematical model that uses the sorption isotherm for pure water and the salt content in the material to predict the sorption isotherm of a salt-laden material is validated. A good agreement was obtained also for AAC laden with Na₂SO₄. Moreover, by compiling and comparing the past and present data, it is shown that the degree of the influence of salt crystals is

dependent on the type of salt and the ratio of the salt mass to the mass of the dry material at least for AAC that contains MgCl_2 , NaCl and Na_2SO_4 .

Acknowledgement

This work was supported by JSPS KAKENHI Grant Numbers 23560694 (Grant-in-Aid for Scientific Research (C)) and 26709043 (Grant-in-Aid for Young Scientists (A)). We also thank Mr. Y. Ishii and Mr. K. Shikata for their assistance in the experiments.

References

- [1] Bresler, E. 1981. Transport of salts in soils and subsoils. *Agricultural Water Management* 4: 35-62.
- [2] Tanimoto, J., Harimoto, K., Kimura K. 1995. Development of High Performance Type of Moisture Regulatory Materials Impregnated with Chlorides Part 1 : Measurement of Moisture Characteristics, in: *Summaries of technical papers of annual meeting, Architectural Institute of Japan (AIJ) D-2: 305-306.*
- [3] Harimoto, K., Tanimoto, J., Kimura K. 1995. Development of High Performance Type of Moisture Regulatory Materials Impregnated with Chlorides Part 2 : Measurement of Equilibrium Water Content and Evaluation of the Effects of Different Building Materials Impregnated with Chlorides, in: *Summaries of technical papers of annual meeting, Architectural Institute of Japan (AIJ), D-2: 307-308.*
- [4] Hashikata, M., Hokoi, S., Takada, S. 2000. Transient Response of Human Body to Thermal Environment, Considering Moisture Movement and Accumulation in Clothing, Part 10 : Measurement of Sorption Isotherm of Saline Clothing and Analysis of Sweat Evaporation Process, in: *Proceedings of annual research meeting Kinki chapter, Architectural Institute of Japan (AIJ), Environment 40: 53-56.*
- [5] Abuku, M., Ogura, D., Hokoi, S. 2013. Modelling salt effects on sorption isotherm of porous materials, in: *Proceedings of the 2nd Central European Symposium on Building Physics (CESBP 2013), Vienna, Austria, September 9 -11, 2013, pp. 605-612.*

- [6] Brocken, H.J.P., Rook, T.N.O., Adan, O.C.G. 1999. Salinization Effects on the Water Sorption of Porous Building Material, in: Proceedings of CIB W40 Meeting: 191-196.
- [7] Rucker, P., Holm, A. Krus, M. 2000. Determination of moisture and salt content distributions by combining NMR and gamma ray measurements, Materialsweek, Sep.
- [8] Abuku, M., Hokoi, S., Takada, S., Hashikata, M. 2007. Heat and moisture transfer in cloth considering salt influences, Part 1 - Experiment of salt water uptake and absorption isotherm of cloth considering salt influences, Transactions of the society of heating, air conditioning and sanitary engineers of Japan 119: 17-22.
- [9] Ogura, D., Hokoi, S., Shimizu, T., Noguchi, H. 2009. Influence of hysteresis in sorption isotherm and moisture conductivity on condensation and evaporation processes, Journal of environmental engineering (Transactions of AIJ) 643: 1065-1074.

Porosity changes after different temperature regimes for a salt weathering simulation test on Mokattam limestone (Egypt)

N. Aly^{*1,2}, M. Gomez–Heras^{2,3,4}, A. Hamed¹, M. Alvarez de Buergo² and F. Soliman⁵

¹Faculty of Petroleum and Mining Engineering, Suez University, Egypt

²Geosciences Institute IGEO (CSIC, UCM) Madrid, Spain

³CEI Campus Moncloa (UPM, UCM, CSIC) Madrid, Spain

⁴ETS Arquitectura (UPM) Madrid, Spain

⁵Faculty of Science – Suez Canal University, Ismalia, Egypt

* nev_ali2007@yahoo.com

Abstract

This study deals with the characterization of the pore structure of fresh quarry limestone samples belonging to the Mid-Eocene Mokattam Group, and porosity changes in samples subjected to salt crystallization tests at different temperatures (20, 30 and 40 °C) in a purpose-made simulation chamber based on feeding samples by capillary imbibitions. NaCl with fixed concentration (10%) was used in the different experimental tests. One more experiment was performed using only distilled water to discriminate changes due to salt crystallisation from those resulting just from wetting. In order to characterize the changes of the pore structure, fresh and weathered samples subjected to different temperature regimes tests were investigated by means of Mercury Intrusion Porosimetry (MIP), and Scanning Electron Microscopy (SEM). These results show the critical role of temperature in controlling the porosity changes after salt crystallisation.

Key words: stone decay, limestone, salt weathering, pore structure.

1 Introduction

Many researchers have studied the relation between durability of building stones and their petrophysical properties, including pore structure and strength [1]. Salts are known to be one of the most effective agents in stone decay. Therefore it is very important to study the factors controlling their crystallisation to be able to establish measures to minimize their effects [2]. Also, porosity and pore-size distribution of the stone play an important role in determining the movement of water and its dynamic properties and therefore the extent of the decay process [3].

When a saline solution accesses the pore structure of a stone, different mechanisms can subsequently lead to crystal growth [4]. Most commonly, evaporation usually prompts salt crystallization [5]. The loss of cohesion between the stone grains/crystals, splitting and surface deterioration and the change of the pore size distribution can result from the repeated cycles of crystallization/dissolution of salt solution within the porous network of the stone, which may lead to the modification of the porous media and the petrophysical properties of the stone [5-6] and also crystallisation pressure is an important factor controlling the decay pattern during salt crystallisation test [7].

Recently, some models describing how the balance between capillary transport and evaporation processes determine the zone of salt accumulation and crystallisation are available [8-9]. In this study, a set of experimental tests based on the partial immersion of stone samples in a saline solution, which accesses into the specimens by capillary rise, have been carried out. This method is based on what Goudie [10] referred to as "the wick effect" in which the solution rises to a certain height characterised by the evaporation and salt crystallisation processes. In this area, efflorescences and/or subflorescences may appear, accompanied by material loss; this effect being mainly controlled by the mean pore size of the stone material [6, 11]. Temperature is also a factor controlling when and how salts crystallise on or within stone [3, 12]. The paper aims mainly to study the effect of temperature during this process and how it controls the occurrence of salt crystallisation, affecting the pore structure, and determining the decay forms.

2 Materials and methods

Limestone samples were extracted from Helwan quarries; an area South of Cairo, Egypt (Fig.1), which belongs to the Mid Eocene Mokattam Group, a biomicrite limestone, out of which cores of 2 cm diameter and 4 cm height were drilled.



Figure 1: General view of limestone quarry at Helwan, Egypt.

Limestone cores were subjected to different temperature regimes (20, 30 and 40°C) in a simulation chamber (Fig. 2a) based on continuous capillary imbibitions of samples designed by Hamed et al. [13]. Samples are placed in a set of drawers made of polyvinyl chloride (Fig. 2b). Each drawer can fit up to 32 samples, which are placed in connected containers, so all samples are fed continuously by a running solution. The chamber is equipped with temperature/humidity measuring sensors and connected to an air conditioning unit (Fig. 2c). A set of samples was tested for each temperature regime for 144 hours.

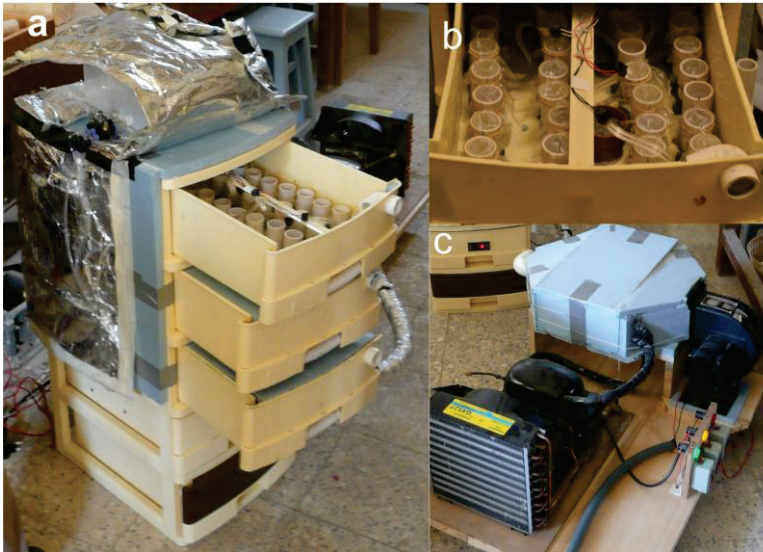


Figure 2: General view of the simulation chamber used for the experiments (a). Close up of one of the drawers showing sample holders. Air conditioning unit (c)

A 10 % sodium chloride solution in distilled water was used in this experiment as it is a common salt in building stones in Egypt and elsewhere [14-18]. In addition to this, another experiment was performed at 20 °C using distilled water to study the effects of a non-saline solution in the stone porosity.

The effect of the different simulation regimes on the porous media of the stone samples was evaluated by means of Mercury Intrusion Porosimetry (MIP). A Micromeritics Autopore IV 9500 with a maximum injection pressure of 230 MPa and a pore size range detection of 0.001- 400 micrometers was used. Pores below 5 micrometers were considered microporosity, as capillary height increases dramatically for pores below this threshold. Four cores were analysed after 144 h for each different simulation regime beside one fresh reference core.

Scanning Electron Microscopy in Secondary Electrons mode (SEM-SE) with a JEOL JSM 6400 microscope equipped with an Energy Dispersive X-ray (EDX) detector facility (Oxford INCA) was used for the examination of one fresh core and another one after 40 °C regime test to see how salts may have crystallised within the pores. Samples were around 5 mm oriented fragments and were either gold metallised or graphite sputtered depending if they were used just for taking pictures or for analyses.

3 Results

Figure 3 shows the visual appearance of the tested samples after the different experimental regimes. The samples show a variation after different temperature regimes: while samples submitted to a 20 °C regime appear undamaged, those tested at 30 °C displayed efflorescences at the top of the cores and the ones at 40 °C showed deep scaling, cracking and loose of material.

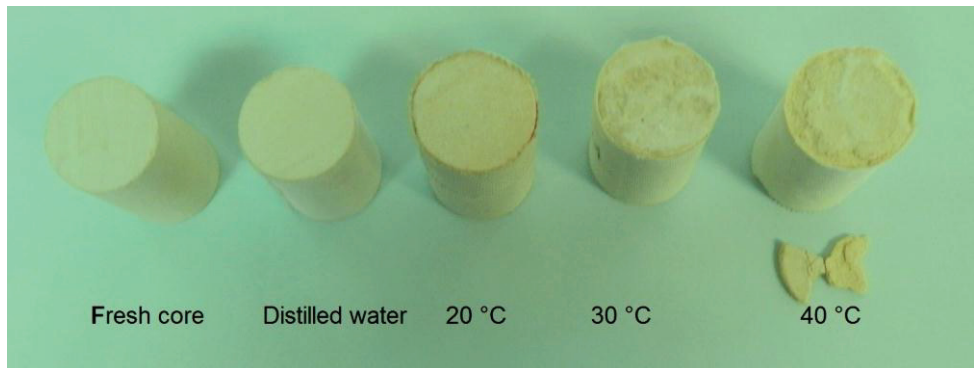


Figure 3: Visual appearance of limestone cores before and after the experiments.

3.1 Mercury Intrusion Porosimetry (MIP)

Table 1 and Figure 4 show the results of different porosity parameters and pore size distribution of fresh core and samples subjected to the different experimental regimes. Pore size distribution and porosity parameters changed after the tests for all different temperature regimes in comparison to the reference fresh core except for the porosity of cores tested with distilled water that did not change significantly.

Table 1: Mercury Intrusion Porosimetry parameters of fresh core, one contaminated with distilled water and salt laden cores submitted to different temperature conditions.

	Fresh core	Dist. water	20°C	30°C	40°C
Porosity (%)	33.4	33.6	22.5	29.9	20.6
Average pore diameter(4V/A) (µm)	0.14	0.17	0.16	0.13	0.16
Apparent Density (g/ml)	1.76	1.75	1.72	1.85	2.10
Total microporosity (%)	33.23	33.23	22.32	29.51	20.18

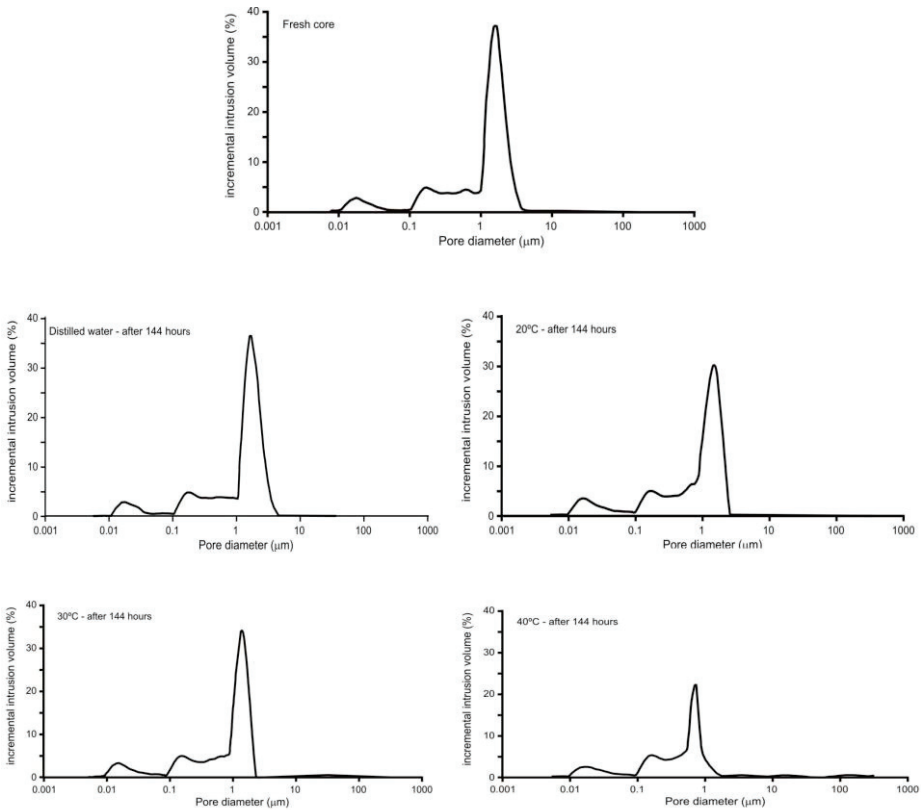


Figure 4: Pore size distribution of a fresh core (top), one contaminated with distilled water (middle left) and salt laden cores submitted to different temperature conditions (20°C, middle right; 30°C, bottom left; 40°C, bottom right)

After the 20 °C test the total Hg-porosity decreased to 22.5 %.The average pore diameter (4V/A) increased slightly from 0.14 μm to 0.16 μm and the relative intensity of a secondary peak at 0.65 μm increased.

After the 30 °C test the total Hg-porosity decreased slightly to 29.9%. The average pore diameter shows a very slight decrease to 0.13 μm .

After the 40 °C test the total Hg-porosity decreased significantly to 20.6%. The average pore diameter increases slightly to 0.16 μm and the main peak shifted from 1.50 μm to 0.75 μm and decreased its relative intensity.

3.2 Scanning Electron Microscopy (SEM)

SEM-EDX analysis show minor amounts of dolomite ($\text{CaMg}(\text{CO}_3)_2$) and quartz (SiO_2) and also P-rich skeletal remains (Fig. 5).

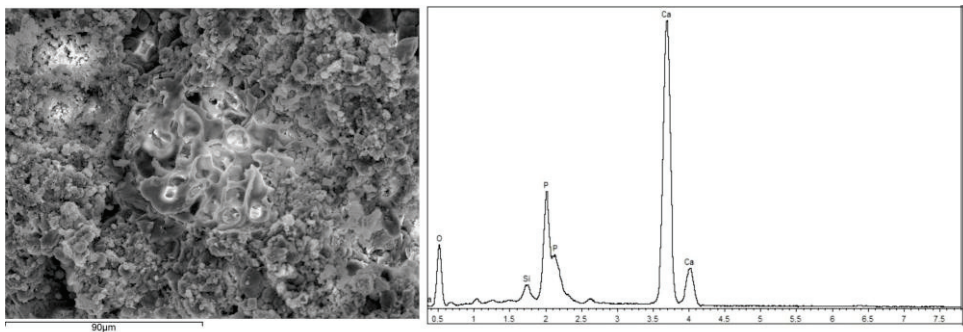


Figure 5: SEM – SE image (left) with EDX analysis (right) for the fresh limestone used in all the experimental tests.

Samples after 40 °C tests showed the largest decrease of porosity and this was verified through SEM observations in which halite crystals have been observed filling stone cracks (Fig. 6) and pores (Fig. 7).

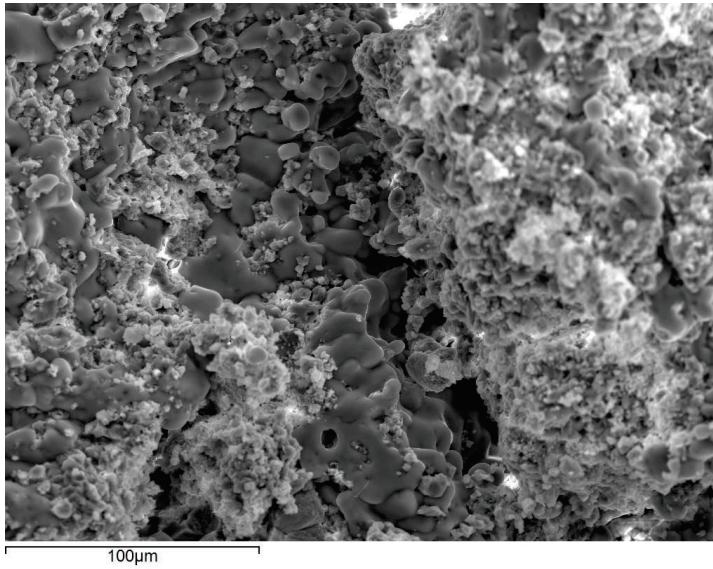


Figure 6: SEM – SE image after 40 °C test, halite crystals filling a crack.

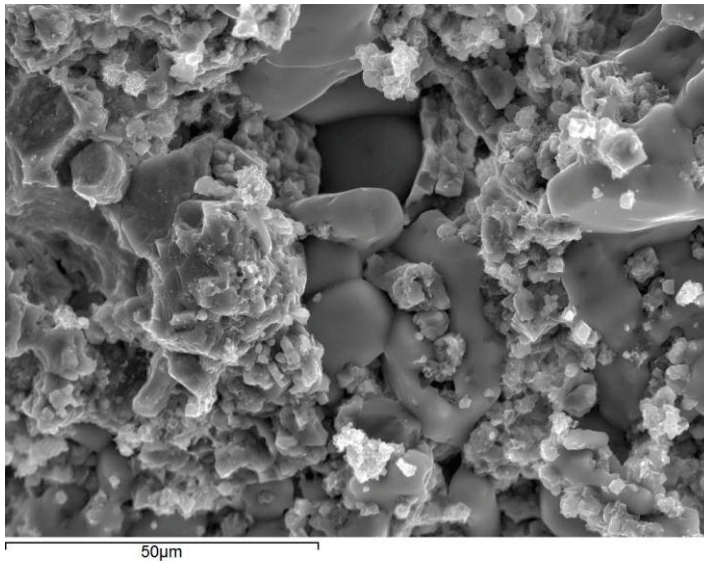


Figure 7: SEM – SE image after 40 °C test, halite crystals filling the stone pores.

4 Discussion and conclusions

Significant differences have been noticed, as a result of different temperature regimes, in the salt crystallisation occurrence under the same conditions of salt concentration and %RH during the partial immersion capillary method. MIP results confirm NaCl crystals tend to grow on the top surface (efflorescences) of most of the tested stone cores after the 30 °C regime cycles, as a result of increasing of the evaporation rate which promotes the growth of NaCl on the top surface. As a consequence, total Hg-porosity and average pore size show only a slight decrease. Pore size distribution and porosity parameters show a more intense change after 20 and 40 °C in experimental tests than at 30 °C, showing salt crystallisation tends to occur preferably within the pores. The extent of this process is limited during the 20 °C regimes and does not generate any real damage on the core surfaces nor lead to the development of cracks.

However, crystallisation of salts within pores during 40 °C regime is largely more predominant. Total Hg-porosity decreases significantly and obvious cracking was observed with SEM. NaCl crystals fill these cracks and the pore system as subflorescences. The crystallisation pressure leads to visible damage, with scaling and loss of material in most of the tested core surfaces.

These results show that when saline solutions enter into the rock by capillary imbibitions, environmental temperature regimes may be crucial to promote changes in the crystallisation occurrence for the same salt (i.e. efflorescence or subflorescence) and, therefore changes on the decay patterns exhibited, as a result of differences on the balance between water ingress and evaporation.

Acknowledgements

We would like to thank to the Mission Sector of the High Education Ministry, Egypt and to Geomateriales programme (S2009/MAT-1629) for financial support. We also thank Rock Mechanics Laboratory, Faculty of Petroleum and Mining Engineering – Suez University, Egypt and the Petrophysics Laboratory at the Instituto de Geociencias IGEO (CSIC-UCM), where laboratory tests have been performed. Research by MG was supported by a PICATA postdoctoral fellowship of the Moncloa Campus of International Excellence (UCM-UPM, CSIC).

References

- [1] Benavente D, García del Cura MA, Bernabeu A, Fort R, Ordoñez (2004) Durability estimation of porous building stones from pore structure and strength. *Engineering Geology* (74) 113 – 127.
- [2] Angeli M, Bigas J-P, Benavente D, Menendez B, Hebert R (2007) Salt crystallization in pores: quantification and estimation of damage. *Engineering Geology* (52) 168 – 178.
- [3] Gomez-Heras M, Fort R (2007) Patterns of halite (NaCl) crystallisation in building stone conditioned by laboratory heating regimes. *Environmental Geology* (52) 239–247.
- [4] Thaulow N, Sahu S (2004) Mechanism of concrete deterioration due to salt crystallization. *Materials Characterization* (53) 123 – 127.
- [5] Coussy O (2006) Deformation and stress from in-pore drying-induced crystallization of salt. *Journal of the Mechanics and Physics of Solids* (52) 1517-1547.
- [6] Benavente D, García del Cura, MA, Bernabeu A, Ordoñez S (2001) Quantification of salt weathering in porous stones using an experimental continuous partial immersion method. *Engineering Geology* (59) 313–325.
- [7] Benavente D, García del Cura, MA, Fort R, Ordoñez S (1999) Thermodynamic modelling of changes induced by salt pressure crystallisation in porous media of stone. *Journal of Crystal Growth* (204) 168–178.
- [8] Lewin SZ (1982) The mechanism of masonry decay through crystallization – *Conservation of Historic Stone Buildings and Monuments*. 120 – 144.
- [9] Hall C, Hoff WD (2007) Rising damp: Capillary rising dynamics in walls. *Proceedings of the Royal Society A*. (463) 1871- 1884.
- [10] Goudie AS (1986) Laboratory simulation of “the wick effect” in salt weathering of rock. *Earth Surface Processes and Landforms* (11) 275–285.
- [11] Uchida E, Ogawa E, Maeda N, Nakagawa T (1999) Deterioration of stone materials in the Angkor monuments, Cambodia. *Engineering Geology* (55) 101-112.

- [12] Aly N, Hamed A, Gomez-Heras M , Alvarez de Buergo M (in press) The influence of temperature in a capillary imbibition salt weathering simulation test on Mokkattam limestone. *Mater. Construc.*
- [13] Hamed A, Aly N, Gomez-Heras M, Alvarez de Buergo M (submitted) New experimental method to study the combined effect of temperature and salt weathering. In Prikryl R et al. (Eds.). Geological Society Special Publication, Sustainability of traditional construction materials in modern Geol. Soc. Publishing House, Bath, series Special Publication.
- [14] Goudie A S (1974) Further experimental investigation of rock weathering by salt and other mechanical processes. *Zeitschrift fur Geomorphologie supplement band (21)* 1-12.
- [15] Sperling CHB, Cooke RU (1985) Laboratory simulation of rock weathering by salt crystallization and hydration processes in hot, arid environments. *Earth Surf. Process Land.* 10(6) 541–555.
- [16] Grossi CM, Esbert RM (1994) Las sales solubles en el deterioro de rocas monumentales; revisión bibliográfica. *Mater. Construc.* (44)15–30.
- [17] Benavente D, García del Cura MA, Ordoñez S (2003) Salt influence on evaporation from porous building rocks. *Construction and building materials (17)* 113- 122.
- [18] Lubelli B, van Hees RPJ (2008) Sodium chloride to porous building materials: effect of RH changes. SWBSS proceedings, 1-27. Ottosen LM et al. (Eds). *Salt Weathering on Buildings and Stone Sculptures*. Technical university of Denmark – Department of civil Engineering, Lyngby, Denmark.

Salt crystallization damage: how realistic are existing ageing tests?

B. Lubelli*^{1,2}, R.P.J. van Hees^{1,2} and T.G. Nijland¹

¹TNO Technical Sciences, Delft, The Netherlands

²Delft University of Technology, Delft, The Netherlands

* barbara.lubelli@tno.nl

Abstract

Salt crystallization is a major cause of damage in porous building materials. Notwithstanding the extensive research in this field, the complexity of the problem has hindered the use of mathematical models for forecasting ageing and damage due to salt crystallization. Nowadays, the durability of materials with respect to salt crystallization is mostly determined by accelerated ageing tests, carried out in laboratory following different test procedures. An effective ageing test should simulate in laboratory, in a reliable way and within a relatively short period of time, the behaviour in practice. The question is whether existing test procedures are able to do so. This paper reports a critical overview of existing procedures and suggests directions for further research.

Keywords: salt crystallization, ageing test, porous building materials, damage.

1 Introduction

Salt crystallization is a major cause of damage in porous building materials. When selecting a stone or stone-like material for building and/or restoration purposes, its resistance to salt crystallization is an important factor influencing the final choice. At present, the ability of a building material to withstand salt crystallization is generally evaluated by subjecting the materials to accelerated salt crystallization tests in laboratory. In fact, the complexity of the salt crystallization process in porous building materials has limited up to now the development and the use of durability estimators and mathematical models for forecasting ageing due to salt crystallization, as done e.g. for other weathering processes (e.g. chloride ingress in concrete).

According to most current models, damage due to salt crystallization occurs when the crystallization pressure developed by salts precipitating in pores overcomes the strength of the material. Crystallization pressure depends on supersaturation of the solution and on pore size and these two factors are interrelated [a.o. 1]. When trying to assess a relation between properties and durability of a material with respect to salt crystallization, parameters as pore size and related properties (e.g. specific surface area, capillary absorption, etc.), being easy to measure, have been used more often than supersaturation in pores. In some cases simple correlations have been proposed between some material properties (e.g. porosity, pore size distribution, water absorption, mechanical strength, swelling clay content) and the damage due to salt crystallization [e.g. 2]. Mostly different parameters have been combined in durability estimators [e.g. 3-5]. Notwithstanding the fact that usually correlations can be identified between these parameters or indicators and the durability of the stone, they are not straightforward nor unique.

Existing mathematical models applied to durability of materials with respect to salt crystallization all starts from the assumptions of the already mentioned salt crystallization theory, without taking into account other possible mechanisms [e.g. 6-8]. Besides, most models focus mainly on the calculation of the development of pressures in singles pores [a.o. 1, 9]. The process of salt solution transport during drying (governing the location of crystallization) and the translation of the crystallization pressure developed in a pore to the damage at the macro scale of the building material are generally not included in the model. Some attempts have been undertaken to come to more complex models considering the different factors governing salt crystallization damage in porous building materials [10-12]. However, the complexity of the process has hindered until now the use of these mathematical models for forecasting the effect of salts crystallization on ageing of materials.

Another approach to the problem has been attempted by developing stochastic models on ageing on the basis of experimental results from laboratory or in situ measurements [13-14]. However, as these models are generally based on a limited set of data (e.g. data from a limited number of

building materials, contaminated with a certain type of salt and under specific environmental exposure conditions), their validity is limited to similar cases only.

The considerations described above, make clear why, still nowadays, the durability of materials with respect to salt crystallization is mostly determined by accelerated ageing tests, carried out in laboratory following different test procedures.

The following sections of this paper report a critical overview of existing procedures and suggest directions for further research.

2 Comparing existing salt crystallization laboratory tests

The first known example of a test procedure for the determination of stone durability with respect to salt crystallization dates back to 1828; the so-called Brard test, published by Héricart de Thury [15] was actually meant for the determination of the frost resistance, but it used a sodium sulfate solution to simulate frost decay. This test was further modified during the 19th century [16]. In the first decades of the 20th century, the idea of classifying stone durability on the basis of salt crystallization tests was proposed [a.o. 17]. A detailed report of the early history of salt crystallization tests can be found in [18-19]. During the 20th and 21st centuries a large number of different salt crystallization procedures has been developed: an extensive overview can be found in [20]. Some of these test procedures have resulted in codes and recommendations, which are generally used for the evaluation of the durability of building materials to salt crystallization.

Most common test procedures for the evaluation the durability of material to salt weathering, reproduce the process of salt solution penetration on one side of the material, transport of the salt solution through the pore network and drying (with consequent salt crystallization) on the opposite side; a process as occurring in practice e.g. in the case of rising damp transporting salts in a wall. Next to these procedures, sea-salt spray test exists too, reproducing the effect of sea-salt spray in buildings in marine environment. This last type of test procedure will not be further discussed in this paper.

A test procedure includes the type of specimens (a.o. single material or combination), the salt type and load, the contamination procedure, the temperature and relative humidity conditions and the assessment method: each of these parameters can differ from one test procedure to another, in one or more details. Hereafter, some commonly used international recommendations for salt crystallization tests (RILEM MS-A.1 [21] and MS-A.2 [22], WTA [23], EN 12370 [24]) are compared with respect to the above mentioned parameters (table 1).

An effective ageing test should simulate in laboratory, in a reliable way and within a short period of time, the behaviour of the investigated material in the field. In order to accelerate the ageing, laboratory tests generally use conditions harsher than in practice. Questions arise as to what extent laboratory conditions need to be similar to those in the field and if the chosen harshest conditions would still give reliable results. In the following sections the effect of the choices for each of the parameters is discussed.

Table 1: Most common salt crystallization standard procedures

Standard/recommendations	Specimen	Salt type	Salt load Wet-dry cycles	Wet-dry cycles	T & RH during drying	Assessment method
RILEM MS-A.1	Combined (masonry)	Na ₂ SO ₄ or NaCl	Different Wet-dry cycles	yes	Constant 20 °C 50%RH	Visual/mass debris
RILEM MS-A.2	Single (Brick/stone)	Na ₂ SO ₄	Saturated solution Wet-dry cycles	yes	Constant 20 °C 50%RH	Visual
EN 12370	Single (stone with porosity >5%)	Na ₂ SO ₄	14% Wet-dry cycles	yes	105 °C high RH	Mass change specimen
WTA	Single (plaster)	NaCl+ Na ₂ SO ₄ + NaNO ₃	Continuous absorption from salt solution (55g salt/l water)	no	Constant 20°C 65%	Visual

2.1 Specimens

The first step in an accelerated test is the choice of the type of specimen, which should be as much as possible representative for the practice situation. From table 1 it is clear that most procedures are carried out on single materials, while it is well known that salt accumulation (and thus damage) depends on the moisture transport properties of the combination of materials [25]; testing single materials can thus lead to misleading results. On the other hand, the use of large masonry specimens [26] or even full scale models [27] while being more realistic, may require too long test periods. A compromise between fully representative test specimens and duration of the test is therefore necessary.

An interesting example with respect to this issue, is given by the definition of an adequate laboratory specimen for the assessment of the salt resistance of mortars (bedding, pointing, plaster or render). Experience

shows that the behaviour of a mortar is strongly affected by the material with which it is combined [28-29]. Moreover, the pore structure of the mortar itself is different and depends on whether this is prepared on a non-absorbing substrate (e.g. Teflon or metal mould) or on a porous substrate, (e.g. brick or stone unit) [30-31]. Therefore testing 40 x 40 x 160 mm³ mortar specimens prepared in a metal mould for evaluating salt resistance of a 15 mm thick plaster layer on a brick/stone substrate might lead to distorted results. For testing of mortar, a 20 mm thick layer prepared on (plaster/render) or in between a brick or stone substrate (bedding mortar), might give a more realistic specimen for salt crystallization tests (figure 1) [32].



Figure 1: Specimens for testing the durability to salt crystallization of plaster (left) and bedding mortar (right)

When discussing the reliability of predictions made on the basis of an accelerated laboratory test, it should also be stated that the durability of a fresh stone from the quarry differs, and is not always higher, from that of a stone in a historic building. The results of ageing of the stone, as for example gypsum crust formation on limestones, can affect the response of the stone to salt degradation processes [33-34]. Also the water absorption / hygric behaviour and strength of a material itself may be time dependent, as is the case for many volcanic tuffs. Such aspects are generally not taken into account in any durability tests.

Another situation in which the choice and preparation of specimens is of outermost importance, is that in which durability of conservation treatments, in particular consolidant products, to salt crystallization needs to be assessed. Consolidants are meant to restore the cohesion of decayed surfaces and they are therefore applied in practice on already decayed substrates. This implies that, in order to achieve reliable data on the behaviour, also the substrate used in laboratory tests should be artificially aged prior to the application of the treatment and the execution of the salt crystallization test. However, mainly due to the difficulty to prepare decayed substrates in a reproducible way, this is usually not the case and surface treatments are commonly tested on sound (fresh)

substrates. Recently, different methods to prepare reproducible, decayed specimens for testing consolidation treatments have been proposed (figure 2) [35-36].



Figure 2: Specimen with a surface layer presenting insufficient cohesion, obtained by re-aggregating stone grains used for testing consolidant products

2.2 Salt type and amount

The salt type chosen in the test is extremely relevant for the obtained results. Sodium sulfate is the most damaging salt type in crystallization tests, for this reason it is often prescribed in test procedures. However, the harmfulness of sodium sulfate strongly depends on the test conditions used (wet-dry cycles, temperature and RH). The harmfulness of sodium sulfate in salt crystallization tests lays mainly in its tendency to supersaturate (and thus to develop high crystallization pressures) and in the different solubility of its different (hydrated) forms [a.o. 37]. Research has demonstrated that high crystallization pressures are developed by rewetting by liquid water and partial dissolution of anhydrous sodium sulfate (thenardite) followed by immediate re-crystallization into agglomeration of fine crystals of mirabilite ($\text{Na}_2\text{SO}_4 \cdot 10\text{H}_2\text{O}$) at a very high supersaturation [38]: re-wetting with water is in fact a crucial part of most crystallization tests. From this it is clear that the salt type should be chosen keeping in mind that using one salt or another is not simply a way to speed up the damage, but might simulate damage mechanisms different from those occurring in practice. Studying the aging of a wall exposed to marine environment by immersing a brick repetitively in a saturated sodium sulfate solution might lead to unreliable results.

Next to the salt type, the salt amount should be realistic: saturating a specimen with a salt solution at high concentration several subsequent times [EN 12370] or by continuous supply [e.g. 39] might be unrealistic with respect to the practice situation, not only because such saturated solutions do not exist in practice, but also because the type of damage

obtained might be unrealistic. Salt damage manifests in the field usually in the form of powdering and scaling of the material surface, sometimes accompanied by fluffy or whisker-like efflorescences; features as cracks perpendicular to the evaporation surface or dense salt crusts as observed in accelerated tests with highly concentrated solutions [5, 39-40] are quite unusual in practice.

A high salt content might in some cases, for example in sodium chloride crystallization tests, even be contra-productive for the effectiveness of the test. Slightly higher salt amounts than generally observed in practice can obviously be used in accelerated tests, but our experience shows that in case of NaCl, increasing the salt amount too much might sometimes even delay damage development. It is mainly the number of dissolution/re-crystallization cycles of the salt that may speed up the damage; increasing the amount of salt delays the drying speed of the salt contaminated specimen and thus decreases the number of wet-dry cycles possible in a certain time period. 1-2% Na₂SO₄ and 2-4% NaCl (weight salt/weight dry specimen) are realistic salt contents, which are sufficient to make a test effective [e.g. 41].

2.3 Test conditions: wet-dry cycles, temperature and RH

A very important parameter in crystallization tests is constituted by the presence of wet-dry cycles and by the environmental conditions (temperature, RH and air speed) during these [42]. First of all, not all test procedures foresee cycles of wetting and drying. In some cases continuous wetting from one side of the specimen and continuous drying on the other side (tested side) are used (e.g. 23, 43). Most tests include wet-dry cycles, by re-wetting of the specimens with water or with salt solution, either by full immersion or capillary absorption from the side opposite to that to be tested. As wet/dry cycles are the trigger for the occurrence of damage, it is advantageous when a sufficient number of wet-dry cycles occurs in a limited period of time. A wetting cycle (dissolution of the salt) is useful if the specimen is sufficiently dry, i.e. if a large part of the salt present has crystallized. For this reason, it might be advantageous to speed up the drying phase and to re-wet the specimen only when most of the water (> 80%) has evaporated. When using 20 °C/50% RH drying conditions and relatively large specimens, as prescribed e.g. by RILEM MS-1, it might take longer than a year to get some conclusions from the test. Apart from reducing the specimen size [a.o. 29], enhancing the drying within reasonable limits can be an option to speed up the test. A temperature of 105 °C, as prescribed in EN 12370, is clearly unrealistic. A too fast drying leads to salt accumulation in-depth with consequent cracking in the specimen [e.g. 5, 44]. As mentioned, this is not the typical type of damage for salt crystallization. Moreover, such high drying temperatures may provoke breakdown of some phases (such as primary ettringite) in for example a cement-based mortar or (reversible)

dehydration of phases (zeolites) in for example zeolitized volcanic tuffs (common natural stones in many European countries).

Another approach to speed up the test, consists of introducing, next to rewetting, RH changes across the RH of equilibrium of the salt used during the drying phase. In this way, not the complete specimen is re-wetted but, by hygroscopic adsorption, only the outer layer in which the salts have accumulated. Even if the presence of a high RH period slightly increases the drying time, the alternation of RH across the RH of equilibrium of the salt causes several dissolution/crystallization cycles in a limited period of time. This procedure has been proven particularly effective for testing the resistance of material to sodium chloride [29, 45]. This type of salt, well-known for its aggressiveness in the field, is generally just slightly damaging in accelerated laboratory tests based on continuous supply of solution or on re-wetting and drying. The additional use of RH cycles improves the effectiveness of the test, ensuring at the same time a realistic simulation of the field situation.

2.4 Assessment method

In order to assess the effects of salt crystallization in laboratory tests, different methods can be used. In most procedures visual and photographic observations are used. Salt damage is mainly affecting the surface, therefore those techniques measuring changes of the surface are appropriate. The limit of visual observations is their subjectivity and the absence of numerical values, which might be used for an easy comparison between results or for the development or the validation of a model. In order to overcome this limit, other techniques (e.g. laser scanning of the surface [a.o. 27, 46]) are sometimes applied.

The weight of the specimen during the execution of the test, as recommended by the EN 12370 standard, is often used as criterion too [a.o. 40, 44, 47]. The main limit of this last method is that the weight of the specimen depends both from salts absorbed and material loss, and these two factors cannot be distinguished, unless washing of the specimen is performed to remove the salts, an action only possible at the end of the test. A better way in the authors' opinion, consists in measuring the weight of the debris (salt + material) which can be brushed from the surface of the specimen after each wetting cycle; the salt and material can then be further separated by dissolving the salts in water followed by a filtration of the aqueous solution [45].

The reduction in strength of the specimens is considered in some cases as criterion for evaluation, measured by mechanical tests or by ultrasonic measurements [a.o. 5, 48-49]. This last technique has the advantage of being non-destructive and might, in theory, be used for monitoring the development of damage during time. However, also in this case the presence of the salts can alter the results; washing of the specimens

before the measurements solves the problem, but, again, this procedure can only be done at the end of the test.

3 How far can accelerated tests predict the in-situ durability of materials with respect to salt crystallization?

The aim of a salt crystallization test is the evaluation and, whenever possible, the prediction of the durability of materials subjected in-situ to the action of salt crystallization. At present, results from crystallization tests cannot easily be translated to in-situ situations. A step forward in this direction might be achieved by the definition of classes of material durability to salt crystallization, following the approach used in the Dutch NEN 2872 standard [50] for the determination of the frost resistance of materials.

A first factor limiting the definition of a classification of material according to their durability, is the use of many different procedures in crystallization tests. The reluctance of researchers to the use of a common standard procedure hinders comparison between results of different studies. As previously discussed, this may be caused by the unrealistic character of some existing standards as well as by the necessity of simulating situations which are not well represented by the existing standard tests. A reliable and commonly accepted standard procedure should be the first step towards a classification of materials according to their durability with respect to salt crystallization.

To reproduce in laboratory the different aggressiveness of different in-situ situations an approach, which recalls the one used by Van der Klugt [51-52] in the definition of the Dutch NEN 2872 standard [50] for frost testing, might be used. Van der Klugt defines 3 classes of aggressiveness of the test (by varying some variables as the water saturation degree of the specimens), each of which can be used to simulate different in-situ situations. Even if frost damage is perhaps a better understood process which can be described by relatively few variables (mainly saturation degree and temperature, next to material properties), whereas the mechanism of salt crystallization damage is still under discussion and much more complex, this kind of approach might be valid. By considering parameters such as salt type, salt content, wet-dry cycles, temperature and RH cycles and defining their importance for the development of the damage, aggressiveness classes of salt crystallization tests can be defined.

For the choice of a suitable aggressiveness of laboratory test, the aggressiveness of environmental in-situ conditions should be considered. Most relevant parameters in this case would have to include moisture supply, salt type, salt load and environmental conditions, as frequency and amplitude of temperature and RH changes.

Next to different aggressiveness classes of the test, the standard procedure should include objective measuring methods and criteria for the evaluation of the decay. Nowadays, the durability of a material, as resulting from the salt crystallization test, is only rarely measured in absolute values (e.g. material loss after n cycles, % of decayed surface); often durability is expressed in a relative sense, i.e. with respect to that of other substrates included in the study. This complicates the comparison between results from different experiments (even if performed according to the same standard) and hinders a classification of materials on the basis of their salt resistance. Defining objective methods for the measurement of the damage and criteria (see examples reported in section 2.4) is a first step in this direction. Durability classes can be then defined and the materials could be classified according to these at the end of the test, on the basis of the test conditions used and the damage observed.

A further step in the classification of materials according to their durability with respect to salt crystallization, is represented by models able to predict service life of material in different in-situ situations.

For the development and validation of models for service life prediction on the basis of laboratory test results, which include a time ratio between lab and in-situ durability, first of all field studies are necessary. Unfortunately, these are limited because of the difficulty of retrieving historical information about the studied buildings (age, eventual historic events as fire, flooding etc. , past conservation interventions, etc.), the co-presence of different weathering agents and the large number of samples which need to be collected in order to get statistical significance (see e.g. [53]). Moreover, direct comparison between practice and laboratory is complicated due to the following factors [19, 33]:

- The use of a single damage process (in this case salt crystallization) and often of a single salt in laboratory, while in the field a combination of different salt types and different weathering mechanisms, enhancing or delaying the decay, is generally present.
- The use of a fixed number of cycles (e.g. wet-dry cycle, temperature and RH) with a unified frequency and magnitude in laboratory, whereas in the field cycles are more heterogeneous.
- The uncertainties, deriving from 1 and 2, in estimating the effect of differences, with respect to environmental conditions, salt and moisture load etc., between the real situations and the laboratory.
- The lack of quantitative data on the evolution of the damage in-situ; this is due not only to the long-time monitoring necessary on site, but also to the difficulty of defining a method for a quantitative and objective assessment of the damage. Damage assessment in laboratory is generally done by measuring changes in weight and strength of the specimens, methods, which are not easily applicable on site.

Defining a relation in time between the laboratory and the field is therefore very complex, since it would require a long term monitoring of the behaviour of the material in the field (according to the same method used in the laboratory) as well as of the environmental conditions relevant to salt crystallization, as salt types and content, moisture supply, drying conditions (temperature and RH) amplitude and length of RH cycles. Moreover, the relative importance of each of these parameters as well as their interaction should be evaluated. This knowledge is at the moment not fully available and hindered also by the lack of a definitive and complete understanding of the damage mechanism of salt crystallization.

4 Conclusions

For the time being laboratory crystallization tests are the main source of information for forecasting material durability with respect to salt crystallization. They still constitute, with all the above discussed limits, a useful method for the a evaluation of the resistance of porous building materials to salt weathering.

A step forward in forecasting material durability in situ by accelerated test can be done by defining a classification of materials according to their durability to salt crystallization. This objective can be pursued by:

- Defining an effective standard salt crystallization test, i.e. a test reproducing in a realistic way and within a relatively short time the damage mechanism and decay patterns occurring in situ.
- Including different aggressiveness classes in the test procedure (by varying some of the parameters as salt content and moisture supply), corresponding to different aggressiveness of conditions in-situ. Depending on the foreseen application of the material, the most suitable class within the laboratory test can be chosen.
- Defining an objective, quantitative, method for measuring the decay (e.g. material loss, % decayed area).
- Determining different classes of durability of materials with respect to salt crystallization on the basis of their response to the test.

References

- [1] Steiger M. Crystal growth in porous materials—I: The crystallization pressure of large crystals, *J Crys Grow* 282 (2005) 455–469.
- [2] Rossi Menaresi R and Tucci A, Pore structure and disruptive or cementing effect in salt crystallization in various types of stone, *Stud Cons* 36 (1) (1991) 53-58.

- [3] Benavente D, Garcia del Cura MA, Fort R, Ordonez S, Durability estimation of porous building stones from pore structure and strength, *Eng Geol* 74 (2004) 113-127.
- [4] Yu S, Oguchi CT, Role of pore size distribution in salt uptake, damage, and predicting salt susceptibility of eight types of Japanese building stones, *Eng Geol* 115 (2010) 226–236.
- [5] Molina E, Cultrone G, Sebastian E, Alonso FJ Evaluation of stone durability using a combination of ultrasound, mechanical and accelerated aging tests, *J. Geophys. Eng.* 10 035003 (2013) 18 pp.
- [6] Pühringer J, Salzwanderung und Verwitterung durch Salze. In: Wittmann, FH (Ed.) *Materials Science and Restoration*. Edition Lack + Chemie, (1983) 361-366.
- [7] Pühringer J, Möglichkeit zur Verhinderung von Schäden durch Salze. In: Wittmann, FH (Ed.) *Materials Science and Restoration*. Technische Akademie Esslingen, Ostfildern, (1986) 359-364.
- [8] Pühringer H, Berntsson L, Hedberg B, Hydrate salts and degradation of materials. In: Félix, G (Ed.) *Proc. 5th Int. Congr. Det. Cons. Stone*. Presses Polytechniques Romandes, Lausanne, (1985) 231–240.
- [9] Scherer GW, Stress from crystallization of salt, *Cem Concr Res* 34 (2004) 1613–1624.
- [10] Coussy O, Deformation and stress from in-pore drying-induced crystallization of salt, *Journal of the Mechanics and Physics of Solids* 54 (2006) 1517–1547.
- [11] Espinosa RM, Franke L, Deckelmann G, Model for the mechanical stress due to the salt crystallization in porous materials, *Cons Buil Mater:22* (7) (2008) 1350-1367.
- [12] Derluyn H, Moonen P, Carmeliet J, Deformation and damage due to drying-induced salt crystallization in porous limestone, *Journal of the Mechanics and Physics of Solids* 63 (2014) 242–255.
- [13] Garavaglia E, Lubelli B, Binda L, Two different stochastic approaches modelling the decay process of masonry surfaces over time, *Mater Struc* 34 (248) (2002) 246-256.
- [14] Koster T, Nijland TG, van Hees RPJ, Faalkansen van zoutbelast natuursteen- een probabilistische benadering, *Praktijksreeks Cultureel Erfgoed* 8 (21) (2009) 33 pp.
- [15] Thury H De, Sur le Procédé proposé par M. Brard pour reconnoitre immédiatement les pierres qui ne peuvent pas résister à la gelée, et que l'on désigne ordinairement par les noms de pierres gelivs ou pierres gelisses, *Annales de Chimie et de Physique* 38 (1828) 160-192.

- [16] Luquer L, The relative effects of frost and the sulphate of soda efflorescence tests on building stones, Transactions of the American Society of Civil Engineers 33 (1985) 235-256.
- [17] Visser CK, Korte mededeeling in verband met het onderzoek van cement, Luiksche kalk en schelpkalk, ten behoeve van de restauratie der Groote Kerk te Dordrecht'. In: Mededelingen van de Afdeling B van de Rijkscommissie voor de Monumentenzorg B2736 (mededeling I, 2 februari 1925) (1925).
- [18] Nijland TG, van Hees RPJ, Lubelli B, Touret JLR, Zoutschade aan natuursteen en metselwerk, Praktijkreeks Cultureel Erfgoed 20 (27) (2010) 49 pp.
- [19] Prikryl R, Durability assessment of natural stone, Q J Eng Geol Hydr 46 (2013) 377-390.
- [20] Goudie AS, Viles H, Salt Weathering Hazards, John Wiley, Chichester, UK, 1997.
- [21] RILEM Recommendation MS-A1 Determination of the resistance of wallettes against sulphates and chlorides, Mat Struc 31 (1998) 2-19.
- [22] RILEM Recommendation MS-A2, Unidirectional salt crystallization test for masonry units, Mat Struc 31 (1998) 10-11.
- [23] WTA Merkblatt 2-9-04/D – Sanierputzsysteme, 2004, 24 pp.
- [24] EN 12370 - Natural stone test methods- Determination of resistance to salt crystallization, 1999.
- [25] Petković J, Huinink HP, Pel L, Kopinga K, van Hees RPJ, Moisture and salt transport in three-layer plaster/substrate systems, Cons Buil Mater 24 (1) (2010) 118-127.
- [26] Laycock EA, Spence K, Jefferson DP, Hetherington S, Martin B, Wood C Testing the durability of limestone for Cathedral facade restoration, Environ Geol 56 (2008) 521–528.
- [27] Baronio G, Binda L, Cantoni F, Rocca P, Outdoor models to assess the durability of masonry, Masonry International, 6 (2) (1992) 50-53.
- [28] Lubelli B, van Hees RPJ, Pel L, The role of the pointing mortar in the damage due to salt crystallisation in Proceeding of the STREMAH VII, Bologna, Italy, 28-30 May 2001, (2001) 537-547.
- [29] Wijffels T, Lubelli B, Development of a new accelerated salt crystallization test, Heron 51 (1) (2006) 63-75.
- [30] Groot CJWP, Effect of water on mortar-brick bond, PhD thesis, Delft University of Technology, The Netherlands (1993)
- [31] Wijffels TJ, van Hees RPJ, The influence of the loss of water of the fresh mortar to the substrate on the hygric characteristics of so-called restoration plaster. In: Proceedings International Workshop on Urban Heritage and Building Maintenance VII (2000) 49-54

- [32] Lubelli B, van Hees RPJ, Huinink HP, Groot CJWP, Irreversible dilation of NaCl contaminated lime–cement mortar due to crystallization cycles, *Cem Concr Res* 36 (2006) 678 – 687.
- [33] Viles HA, Durability and conservation of stone: coping with complexity, *Q J Eng Geol Hydr* 46 (2013) 367–375.
- [34] Smith BJ, McCabe S, McAllister D, Adamson C, Viles HA, Curran JM A commentary on climate change, stone decay dynamics and the ‘greening’ of natural stone buildings: new perspectives on ‘deep wetting’, *Environ Earth Sci* 63 (2011) 1691–1700.
- [35] Franzoni E, Sassoni E, Scherer GW, Naidu S, Artificial weathering of stone by heating, *J Cult Heri* 14S (2013) 85–93.
- [36] Lubelli B, van Hees RPJ, Nijland TG, Re-aggregated stone specimens as replicas of decayed stone for testing the effectiveness of consolidation treatments, submitted to *Journal of Cultural Heritage*
- [37] Steiger M, Asmussen S, Crystallization of sodium sulfate phases in porous materials: The phase diagram $\text{Na}_2\text{SO}_4\text{--H}_2\text{O}$ and the generation of stress, *Geoc Cosm Act* 72 (2008) 4291–4306.
- [38] Shahidzadeh-Bonn N, Desarnaud J, Bertrand F, Chateau X, Bonn D, Damage in porous media due to salt crystallization, *Phys Rev E* 81 066110 (2010).
- [39] Cardell C, Benavente D, Rodriguez-Gordillo J, Weathering of limestone building material by mixed sulfate solutions. Characterization of stone microstructure, reaction products and decay forms, *Mater Char* 59 (2008) 1371–1385.
- [40] Angeli M, Hébert R, Menéndez B, David C., Bigas JP, Influence of temperature and salt concentration on the salt weathering of a sedimentary stone with sodium sulphate, *Eng Geol* 115 (2010) 193–199.
- [41] De Witte E (ed.) *Salt Compatibility of Surface Treatments (SCOST)*, Final report of the EU project ENV4-CT98-0710, (2002), unpublished
- [42] Lubelli B, van Hees RPJ, Groot CJWP, The effect of environmental conditions on sodium chloride damage – a step in the development of an effective weathering test, *Stud Cons* 51 (1) (2006) 41–56.
- [43] Ruiz-Agudo E, Mees F, Jacobs P, Rodriguez-Navarro C, The role of saline solution properties on porous limestone salt weathering by magnesium and sodium sulfates, *Environ Geol* 52 (2007) 269–281.
- [44] Akin M, Ozsan A, Evaluation of the long-term durability of yellow travertine using accelerated weathering tests, *Bull Eng Geol Environ* 70 (2011) 101–114.

- [45] Lubelli B, Sodium chloride damage in porous building materials, PhD thesis, Delft University of Technology (2006).
- [46] Gomez-Heras M, Smith BJ, Viles HA, Meneely J, McCabe S, High definition laser scanning for the evaluation of salt decay in laboratory simulation of building limestone, in Ottosen LM; Rørig-Dalgaard I, Larsen PK, Brajer I. Bøllingtoft P, Marciniak M, Svane M (Eds), "Salt weathering on Buildings and Stone Sculptures – Proceedings from the International conference, Copenhagen 22-24 October 2008, Nyt teknisk Forl, Copenhagen, (2008) 149-158.
- [47] Kamh GME, Oguchi CT, Watanabe K, Factors Controlling Salt Susceptibility and Alteration Indices on Salt Weathering of Oolitic Limestone Using Single Salt at Five Weathering Regimes, a Case Study, Restoration of Buildings and Monuments 19 (6) (2013) 393-416.
- [48] Alm D, Brix S, Howe Kjoergaard, Kielsgaard Hansen K., Grell B (2008) Determination of resistance to salt crystallization on natural stone measured with ultrasonic wave, in Ottosen LM; Rørig-Dalgaard I, Larsen PK, Brajer I. Bøllingtoft P, Marciniak M, Svane M (Eds), "Salt weathering on Buildings and Stone Sculptures – Proceedings from the International conference, Copenhagen 22-24 October 2008, Nyt teknisk Forl, Copenhagen, (2013) 159-167.
- [49] Cardenes V, Mateos FJ, Fernandez-Lorenzo S, Analysis of the correlations between freeze-thaw and salt crystallization tests, Environ Earth Sci 71 (2014) 1123–1134.
- [50] NEN 2872 Beproeving van steenachtige materialen - Bepaling van de vorstbestandheid - Eenzijdige bevroering in zoetwatermilieu, (1989) 12 pp.
- [51] van der Klugt LJAR Durabilité par gel - Belgisch-Nederlands onderzoek naar de betrouwbaarheid van een aantal vorstbestandheid-onderkeningsproeven voor vormvaste steenachtige bouwmaterialen; intern TNO-rapport BI-86-25, (1986) 68 pp.
- [52] van der Klugt LJAR, A European perspective of freeze-thaw issues, paper presented at Building Research Establishments seminar on 'Frost susceptibility issues', Edinburgh, 16 April 1997 (1997).
- [53] Mottershead DN, Weathering of coastal defensive structures in south West England: a 500 year stone durability trial, Earth Surf. Process. Landforms 25, (2000) 1143-1159.

Monitoring of the salt mist aging test with DRMS

D. Costa* and J. Delgado Rodrigues

National Laboratory for Civil Engineering, Lisbon, Portugal

* drcosta@lnec.pt

Abstract

Salt mist test can be used to evaluate the durability of porous materials. Besides mass loss, the paper discusses the use of DRMS (drilling resistance measurement system) to monitor changes in strength due to salt crystallisation. Drilling resistance was used to characterize changes promoted in very different lithotypes, namely carbonate rocks and one variety of sandstone. The results show that this technique is able to identify fingerprints of the presence of salts on the profiles seen as increments in resistance. Damage zones can also be detected on the profiles of the aged samples, after desalination. The results clearly indicate the influence of moisture content on the drilling data. Although considered as a minimally invasive action, the method produces a small hole that has some influence on the ongoing decay process. In this paper illustrative examples are presented, some advantages and drawbacks are indicated in order to correctly evaluate the results when it is possible to use it to evaluate the action of salts.

Keywords: salt mist test, drilling resistance, natural stone, drill bit wear effect.

1 Introduction

Salts are considered as the most effective factor of decay, operating in very different climatic conditions, and are particularly relevant when repeated moisture and temperature cycles enhance the dynamism of their action. The evaluation of the durability of stone materials in face of this mechanism is a relevant research topic with implications in several domains, including stone conservation.

In laboratory, the behaviour of porous materials in salt crystallization tests has been extensively studied and results obtained in different stone types from all over the world are available in scientific journals and conference proceedings. *Salt crystallization test* has a long tradition of use to assess the stone durability to salts. The original version was introduced by Brard in 1828 [1] to evaluate the susceptibility of stone to frost damage. According to it, stone samples are subjected to cycles of immersion in a salt solution followed by drying in an oven, using a concentrated solution of sodium sulphate. Now as then, the protocol of testing prepared by CEN uses a similar procedure [2] to determine the relative resistance to salt crystallisation of natural stones. The test results are expressed as “mass loss”. This test method is considered suitable for the evaluation of very porous stones (higher than 5% porosity) but it is also commonly used for low porosity materials evaluation. It is a very aggressive test, able to produce damage on porous materials very rapidly. To get information in a short period of time justifies the extreme conditions very often used in aging tests. However, this test is criticized due to the fact that the preconized conditions are extreme and far from reality.

Moreover, in particular when exposed to marine conditions, the materials are submitted to very different conditions from those considered above. Natural weathering due to salt crystallisation is quite often related with marine spray action. In the lab, the simulation of this action can be achieved by using a climatic chamber where the marine spray is simulated by the production of spray with the testing solution. As in the previous protocol, wet and dry cycles promote damage but softer action is expected for the salt spray. In this protocol, sodium chloride solutions are often used instead of sodium sulphate.

The equipment is able to create a salted and humid environment during the wet phase, followed by a period of drying created through the increase of temperature in the cabinet. The duration of each phase can be programmed and changed according to the objectives and always taking into account the characteristics of the materials to be tested. Besides a better similitude to reality, this test promotes smaller increments in decay between cycles and therefore it allows following the decay process in a better controlled way.

In both test procedures, the absorption of salt solutions into the void system of the materials is a determinant factor of decay. Successive cycles of wet and dry phases are responsible for decay, which is mainly attributed to the processes of physical disintegration of the materials as the result of salt crystallization pressure created inside the material.

2 Objectives

Both types of tests are currently considered in the European normative of stone testing, as previously mentioned. The two procedures use the quantification of damage expressed as a “mass loss” value determined after a certain number of cycles. Values are usually expressed as a single number per test.

In research studies, the results are usually expressed in a different way; the “mass loss value” is determined in each step to allow defining a trend line representing the overall behaviour of the stone during the test.

Besides “mass loss”, which is considered a very relevant parameter, other physical properties can also be used to quantify physical changes. Porosity, water absorption and ultrasound velocity are examples of properties that can be successfully used to evaluate global mass modifications on stone materials, in particular when used in a comparative basis, before and after salt aging test.

Salt crystallization changes the original porous space configuration and new fissures, cracks or voids can be created whose presence is reflected in a lower mechanical strength. Visual damage can be identified as flaking, disaggregation, disintegration and rupture of the stone specimens. Quite surprisingly, the effect of the presence of salts inside the materials is not usually considered when analysing the test results. Though in some cases desalination is recommended, the operating conditions defined to achieve it hardly correspond to an effective desalination process. The presence of salts may induce damage but, depending on the materials, they can also artificially increase mechanical strength, or modify the ultrasound velocity usually used to assess degradation in a non-destructive way. Salt accumulation during aging test is already known in other stone types, namely on granites, where a very small amount of salts was detected using ultrasonic pulse velocity [3].

Natural weathering profiles can also be developed due to salt damage. The methods mentioned can hardly detect or identify the characteristics of the material in depth, although the final values can be skewed by their presence. Taking all these facts into consideration the *drilling resistance method* showed up as potentially interesting to investigate physical changes due to the presence of salts, especially when small changes of the resistance in depth are expected to occur.

This paper aims to support the use of drilling resistance measurements to control the changes induced during salt crystallisation tests, by presenting data taken from a salt mist test carried out in very different stone materials commonly used in Europe.

3 Materials and test conditions

Five lithotypes are considered in this work, including carbonate stones and sandstones. One marble (with heteroblastic fabric), three limestones (fine and coarse grained, more or less homogeneous) and one variety of sandstone with transverse anisotropy, tested in specimens (cut parallel to the bedding plane).

The marble samples (MC) are from Camaioire, in Italy. The fine grained limestone comes from Portland, UK (PW), and the coarse grained limestone from Vicenza (Va), Italy. Sander is an anisotropic sandstone, from Hassberge in Germany, (S). Some tests were also performed on a Portuguese limestone from Coimbra (Ti), a very soft and homogeneous stone, taken as a reference in the interpretation of drilling test data. Besides the wide range of chemical and mineral composition, these materials also present very different physical properties, including very low porosity materials, like marbles, as well as very high porosity ones, such as Vicenza (Va) and Portland stone (PW).

Porosity, water absorption and mechanical resistance properties of raw material used are presented in Table 1 for comparison.

Table 1: Physical properties of the raw materials

Lithotypes	Porosity accessible to water (%)	Maximum water content (%)	Water absorption by capillarity [Kg/(m ² *h ^{0.5})]	Compressive strength (MPa)	Drilling resistance force (N)
MC	0.4	0.1	3.9 - 4.2 x 10 ⁻²	131.7	66 - 61
PW	21.1	9.9	8.5 - 9.4	53.2	18 - 25
Va	28.5	14.8	8.0 - 8.3	20.8	6 - 11
PW	21.1	9.9	8.5 - 9.4	53.2	18 - 25
S	17.8	8.2	1.5 - 1.9	51.8	11 - 14
Ti	19.0	8.7	nd	nd	6-8

Note: MC - marble; PW - limestone; Va - limestone; S - sandstone; Ti- limestone. For complementary information see text above

3.1 Salt mist test

The stone specimens were submitted to cycles of alternate conditions of salt mist and drying, in a climatic chamber capable of maintaining the temperature from lab conditions to about 40°C. The salt mist consists of a solution of sodium chloride in deionized water at 1:20 in weight. Ten hours in a salt mist atmosphere (flowing rate of 2.5ml/h) under ambient temperature were followed by 38 hours of drying at 35°C.

Prismatic specimens were used in this study. Lateral faces were coated with an epoxy resin in order to leave exposed only the two faces orientated in one direction. During the test the debris detached from the surface were carefully collected to help control the induced damage.

The samples were characterized to determine the original characteristics (T0) and photographed for visual inspection.

At the end of the test (or in specified intermediate control steps), the specimens were immersed in de-ionised water to remove salts before proceeding to characterisation. This is a very slow process and the water had to be changed periodically until total desalination. Then, specimens were dried, weighed and visually inspected. Mechanical characterisation was performed using non-destructive techniques selected from those currently in use in laboratories. *Drilling Resistance Measurement System, from SINT (Italy)* was used to evaluate resistance in depth.

In a preliminary test aiming at defining the protocol adequate to test the selected rock categories, two specimens of each rock type were used. The duration of drying and wetting phases, the possibility to test sequentially the same specimen in each step of the test are examples of questions then considered as relevant. The purpose of the present paper is to use the information obtained in that study to discuss the use of drilling data to monitor changes due to salt mist action. The wide range of materials object of analysis will also help to frame the range of validity of the suggested procedures.

The ultrasound methods allow a non-destructive monitoring of each individual sample throughout the test, consequently reducing the number of specimens required to test and avoiding the uncertainty induced by the comparison of results taken from different specimens at each step of the test. The use of drilling resistance to complement “ultrasound pulse velocity” data was also under analysis.

A total number of 50 cycles were performed; one phase of control was done between the 23 and the 25 cycles, in dry and wet phase. At the 25th cycle, in the beginning of the drying phase, the specimens were cleaned for removal of detached particles and dried in a ventilated oven at 100°C, for about 72hours. After 50 cycles the specimens were tested in wet and dry phases, cleaned and desalinated for 30 days to remove the salt from the

interior. Dry mass loss was measured and final characterization of the material after 50 cycles was performed.

Considering the protocol used and summarized above, it is worth mention that EN 14147 protocol [4] follows a similar general philosophy. However, the concentration of the sodium chloride solution and the cycle conditions are different from those used in this test. A longer cycle and a more concentrated solution were considered to be more effective to test simultaneously so different stone materials.

3.2 Drilling resistance measurements

The drilling resistance measuring system (DRMS) is a power drill with constant feed and a force transducer that measures the thrust as a function of the drilling depth. It is considered a quasi-non-destructive technique due to the fact that a hole is produced during the test, typically a 5mm diameter hole. The equipment used was a prototype originally developed through the European HARDROCK project [5].

The drilling test has been used to characterize stone resistance in depth. To interpret the results several variables must be taken into consideration, namely grain size and homogeneity of the material or the water content, a variable that has not been very studied up to now. The presence of quartz grains is a serious drawback, in particular in very compact mineral textures, since it is responsible for the drill bit wear effect and a strong base noise in the drilling graphs. When drill bit wear exists, the correction of the original test data is absolutely mandatory [6].

4 Results and discussion

4.1 Salt damage patterns and their quantification with “mass loss”

Macroscopic observation can spot slight changes during the test, when they modify the original roughness of stone surfaces. Damage is more evident when the material is wet due to the fact that drying allows a formation of efflorescences, which are particularly evident in very porous materials able to absorb higher amounts of solution. Detachment of single grains or aggregates of grains (*disintegration*, *powdering*) or as thin scales (*flaking*) on Sander specimens (S) were evident deterioration signs.

Due to evaporation, salts formed a thin but hard crust on the surface of Vicenza stone specimens and fluffy efflorescences “randomly” dispersed on Sander specimens. Very often, deterioration patterns were not uniformly distributed. Original heterogeneities of the materials can justify differences on the level of damage observed in adjacent areas. Some examples are indicated in Figure 1.

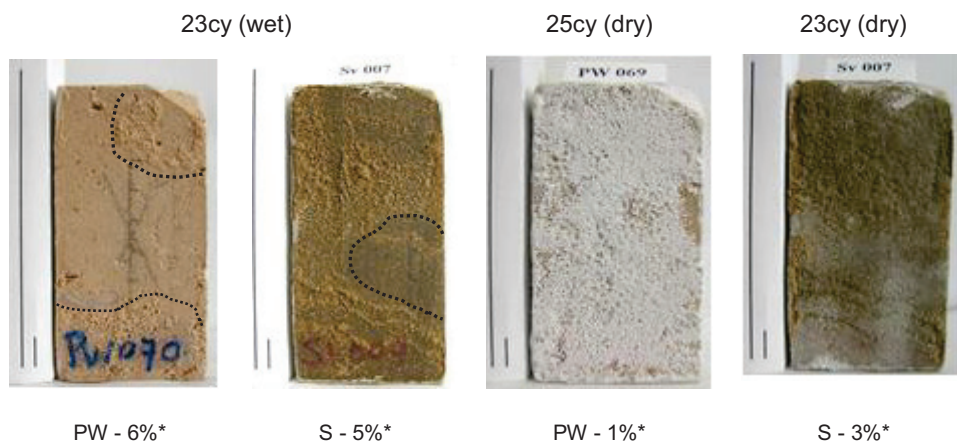


Figure 1: Heterogeneous distribution of damage during salt mist test. Macroscopic aspect of the surfaces during wet and dry phase at 23th cycle; * the numbers (in %) represent the residual "salt solution content" in each phase, before drilling test

Table 2 presents mass loss values after 50 cycles of salt mist and the quantity of solution absorbed in the wet phase. Figure 2 allows the comparison of different types of stone using *mass loss* values.

Table 2: Salt solution content estimation on wet phase and mass loss after 50 cycles

Stone types	MC	PW	Va	S	Ti
Mass loss (%)	0.07 - 0.11	0.75 - 0.97	0.37 - 0.82	1.69 - 2.22	0.33 - 0.46
Salt solution content (wet phase)	0.12 - 0.13	5.7 - 6.7	11.3 - 11.5	4.6 - 6.1	6.6 - 6.8

Note: MC - marble; PW - limestone; Va - limestone; S - sandstone; Ti- limestone.

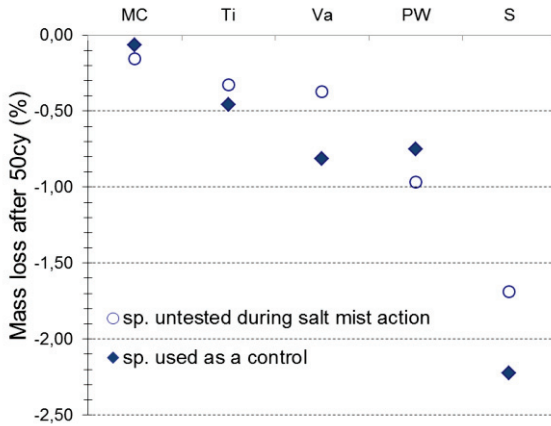


Figure 2: Mass loss after 50 cycles of salt mist test

Marble (MC) is the stone variety that was less affected by salt mist action. This is justified by its very low porosity and consequently by the reduced absorption of the salt solution.

Other lithotypes show different behaviours, which remain unexplained through these properties. Vicenza stone (Va), in spite of its high porosity, revealed a modest value of mass loss during this test. On the contrary, similar salt solution absorptions allowed different levels of damage in PW, S and Ti, as their mass loss values indicate, claiming for other suitable explanations.

4.2 Using drilling resistance to identify the damage due to salt mist action

Drilling resistance test is a very sensitive test to evaluate resistance in depth. Concerning this application, the main raised question is related with the possible interference of the presence of salts on the results. The presence of water (as salt solution) inside the materials also influences the strength values, a fact that has to be taken into account, in particular if a well-defined reference for moisture condition cannot be guaranteed. Besides these specific questions, others aspects must be taken into account for a correct use of this technique, namely the influence of grain size and heterogeneity of the material, as well as the drill bit wear due to the presence of abrasive quartz grains, in particular in compact materials.

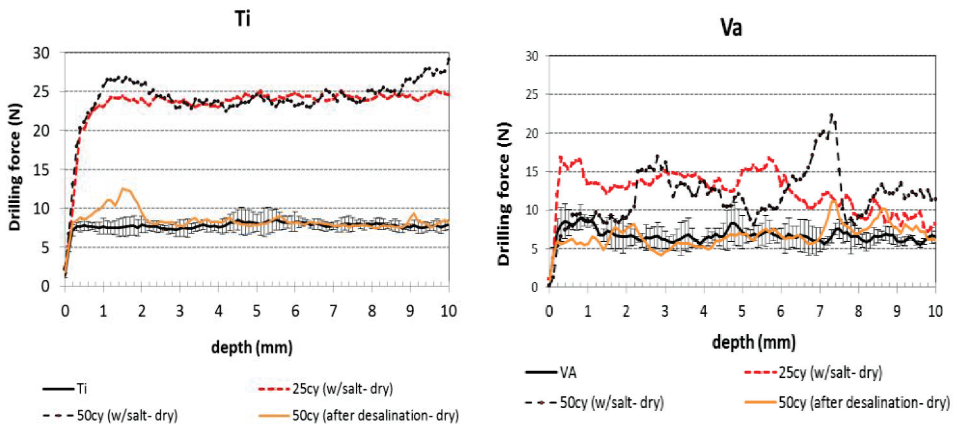
In the following graphs some examples of drilling test profiles are presented in order to illustrate what kind of information can be expected. For comparative purposes, in all the graphs T0 values are projected as the average values of at least five drillings (and their respective standard

deviation), in black. All tests were performed using 600 rpm of rotation speed and the penetration of 10mm/min.

4.2.1 Soft and non-abrasive stones

Good results are usually obtained on very homogeneous materials, in particular if they are non-abrasive like the Portuguese limestone (Ti). Concerning salt mist test, the presence of the salt increases the resistance of the material, as shown in Figure 3a, graphs “25cy-dry” and “50cy-dry”. In this case, the tested length is fully “impregnated” with salt and the force resistance more than doubles the original value. Desalination removes the salt and consequently lowers the drilling resistance. However, desalination was not complete since a peak is still detected near the surface (1-2mm) thus illustrating how sensitive the method is to minimum amounts of salt. Damage was limited to scarce powder detachments and has no fingerprints in the drilling profile.

In this type of stone it is very common to have drilling graphs showing some artificial increase of force in depth due to the accumulation of fine dust during the drilling process, as seen in Ti specimen at the 50th cycle with salt (Figure 3a). To limit the occurrence of this packing effect, the hole-in-hole procedure can be adopted when small size specimens (till 4cm thickness) are used [7].



a) Portuguese homogeneous limestone (Ti)

b) Vicenza heterogeneous limestone (Va)

Figure 3: Drilling tests on limestones.

A very different situation is obtained on Vicenza stone (Figure 3b) due to its marked heterogeneity. Graphs are much rougher, but the presence of

salt is still detected by the increase of force values in the salinated condition.

Portland stone (PW) is a harder and very heterogeneous material (Figure 4). In spite of this fact, the hardness profiles clearly demonstrate the presence of salt, more pronounced on the two first millimetres while less in depth, from 4-9 mm (Figure 4a).

The effect of moisture to promote packing in depth is also clear in this stone when it is wet (Figure 4b). Packing, produced by dust accumulation and favoured by the presence of moisture, can be overcome by using the pilot-hole technique, as indicated before.

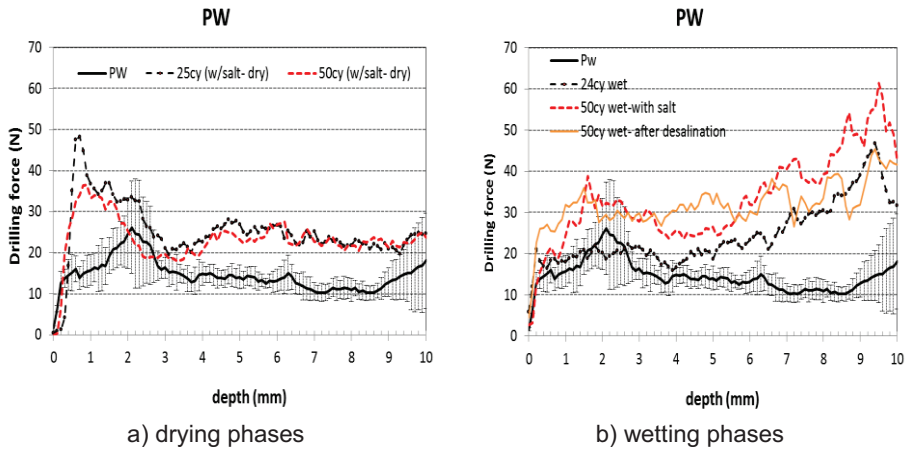


Figure 4: Drilling tests on heterogeneous Portland limestone (PW); dry and wet phases

Vicenza stone (Va) shows a surface damage in the first 2mm, where previously a peak of salt accumulation was detected (Figure 5a).

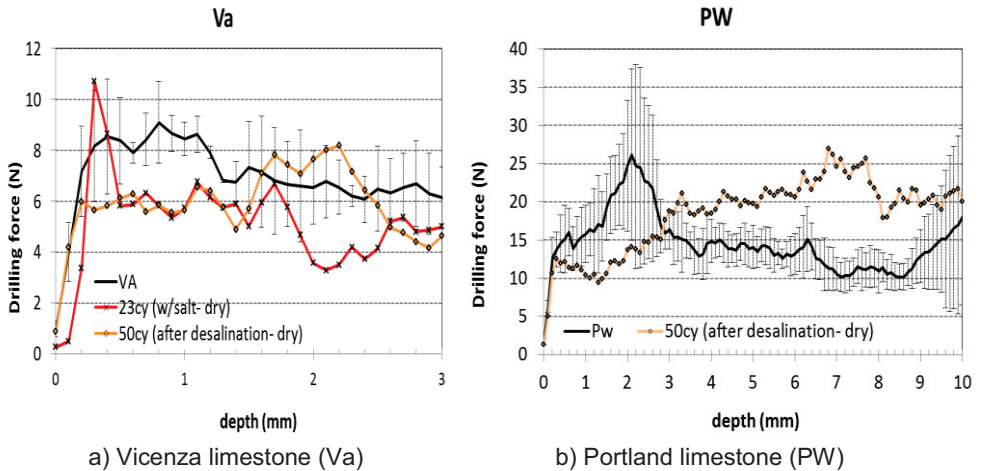


Figure 5: Drilling tests on heterogeneous limestones varieties after salt mist, in desalinated specimens

In other cases, some salt can still remain in depth (Figure 5b), although in the first three millimetres near the surface a decrease of resistance is registered and considered to be the result of salt damage. In fact, on Portland limestone, the desalination was not fully achieved when it was tested but the profile shows some surface damage in the first millimetres.

4.2.2 Hard and abrasive materials

When the stone is abrasive, like Sander sandstone (S), drilling tests must be carried out using a specific protocol to determine the abrasive law and to ultimately correct the drilling resistance data against the drill bit wear [6]. In this study, drilling data were obtained before the correction methodology was entirely developed and therefore corrections had to be made in a slightly different way, with the corrections being supported in drilling tests carried out in the To reference samples above defined.

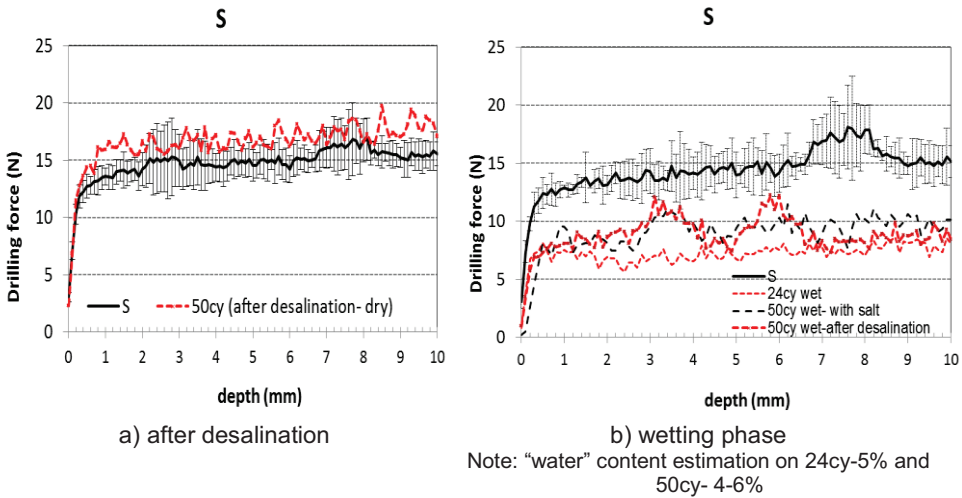


Figure 6: Drilling tests on abrasive Sander sandstone (S)

In this type of stone the presence of moisture is particularly relevant and it is responsible for a decrease of the resistance values (Figure 6). After salt mist action, no evident signs of damage or accumulation of salt were detected. The slight increase of force compared to non-decayed values (represented by "S" in Figure 6b) must be considered in the range of error introduced by the correction process in this particular case.

Marbles can be also slightly abrasive. However, in the present case, the values of forces were corrected due to the fact that only one drill bit was used to test all the materials. The wear effect promoted by Sander sandstone was responsible for the artificial increase of the values obtained on marble and justifies the need for the correction.

The drilling tests on marbles did not detect significant changes after salt mist action (Figure 7a) but the influence of moisture must also be considered in this stone variety. Even in small amounts, the force values decreased dramatically, as it is evident in the holes drilled during wetting and drying phases of the cycle (Figure 7b).

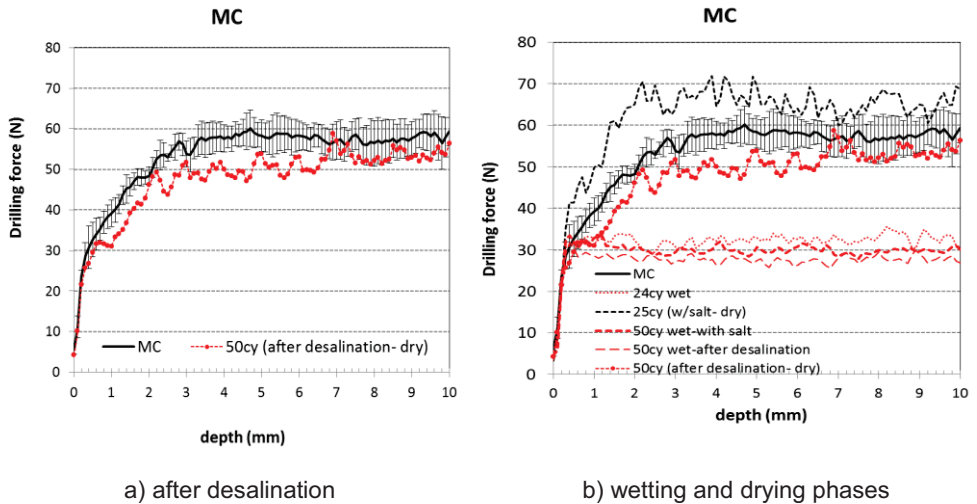


Figure 7: Drilling tests performed on marble (MC)

5 Conclusions

The use of drilling resistance on salt mist samples allow to confirm the sensitivity of the method for stone rock profiles characterization.

In fact, salt mist action promotes slight changes, hardly detectable after test. Great part of the damage is removed due to the fact that sand disintegration or small flakes produced are removed in each cycle.

However, the experience allows considering that it can be successfully used to detect the presence of salt accumulations or the damage promoted by salt damage. The slight decrease of mechanical resistance near the evaporitic zone on the profile is, in this case, considered the result of the action of salts.

From the results obtained an influence of the moisture on the drilling profiles is noticed. In most of the cases it reduces the force, and this means that stone hardness decreases due to this fact. Actually, this finding confirms the influence of the presence of water in the lowering of mechanical resistance of materials.

Acknowledgement

This work was carried out in the framework of the project “Effects of the weathering on stone materials: assessment of their mechanical durability” (McDUR), contract G6RD-2000-00266.

References

- [1] Schaffer, R. J. "The weathering of natural building stones". Department of Scientific and industrial research. Building Research. Special report N°18. London, (1932), pp.149.
- [2] European Committee for Standardization "Natural stone test methods. Determination of resistance to salt crystallisation", Brussels, CEN, EN 12370 European standard, 2001.
- [3] Costa, D. Delgado Rodrigues, J. "Consolidation treatment of salt laden materials. Methodology for their laboratory study". Proceedings of the 11th Int. Congress on "Degradation and Conservation of Stone", Ed. Lukaszewicz, J. & Niemcewicz, P., Torun, (2008), 827-836.
- [4] European Committee for Standardization "Natural stone test methods. Determination of resistance to aging by salt mist", Brussels, CEN, EN 14147 European standard, 2003.
- [5] Tiano, P., Filareto, C., Ponticelli, S., Ferrari, M., and Valentini, E. "Drilling force measurement system, a new standardisable methodology to determine the "superficial hardness" of monument stones: prototype design and validation". *Int. Journal for the Restoration of Buildings and Monuments*, vol. 6, No.2, (2000), 115 - 132.
- [6] Delgado Rodrigues, J. & Costa, D. "A new method for data correction in drill resistance tests for the effect of drill bit wear". *International Journal for Restoration*, Vol.10, (2004) No 3, 219-236.
- [7] Mimoso, J.M. & Costa, D. "The DRMS drilling technique with pilot holes". *HWC 2006 – Heritage, Weathering and Conservation*, Madrid, 19-26 June, vol. 2, (2006), 651-655.

Study of NaCl crystallization using Infrared Thermography

P. Vázquez^{1*}, C. Thomachot-Schneider¹, K. Mouhoubi²,
M. Gommeaux¹, G. Fronteau¹, V. Barbin¹ and J. L. Bodnar²

¹GEGENAA EA 3795, University of Reims Champagne-Ardenne, Reims (France)

²CATHERM, GRESPI EA 4694, University of Reims Champagne-Ardenne, Reims (France)

*patricia.vazquez@univ-reims.fr

Abstract

The Infrared Thermography (IRT) technique has been widely developed during the last years. IRT is useful to observe changes in the fields of physics and chemistry, and has turned out to be an important and indispensable non-destructive technique used for investigation of civil engineering works, with special attention to cultural heritage.

In this research IRT has been used to study the crystallization of NaCl solution droplets with different initial concentrations (3.5, 14 and 26% weight). The crystallization was induced by evaporation of the solvent (water). Tests were carried out at two temperatures (25 and 50°C). We explained how the crystallization process is observed with IRT. The variations in emissivity recorded by the IRT described distinctly the different stages of salt crystallization. IRT allowed observing three phases. In phase I the mass diffusion within the droplet and differences in concentration and volume of the solution around the crystal germs nuclei were observed. Phase II is related to the final crystallization step, with the crystal growth and the complete evaporation of the solution. Phase III describes creeping associated with efflorescence formation. This phenomenon takes place as an intermittent decrease in the IR thermosignal which can be repeated up to 100 times in a 10 minutes interval.

Different morphologies corresponded to different IRT phases. Thus, if only phases I-II are present, crystals have cubic shape or efflorescence-like

with fan-shape. If phase III occurs, efflorescence-like crystals with spherulite shape develop. These spherulites can crystallize on the substrate or on previous crystals, growing by top-supplied creeping and showing an intermittent decrease of thermosignal.

The study and comprehension of salt droplets crystallization by IRT is the first step in our research. Currently, we are testing different salt types and the response of salt crystallization in porous stones.

Keywords: Infrared Thermography, emissivity, creeping, NaCl, temperature

1 Introduction

Salt crystallization in stones is widely recognised as an important mechanism of deterioration. The knowledge of the crystallization mechanism itself is crucial to understand stone decay [1-4]. This process can exert a destructive pressure if it occurs within the porous system [5-7] or less damage, but leading to a change in the stone appearance, if crystallization takes place on the outer surface as efflorescence [1, 8, 9]. Several authors studied these processes with new and ultraprecise tools such as Environmental Scanning Electron Microscopy [3], Atomic Force Microscopy [10], X-ray Computed Tomography [11] or Nuclear Magnetic Resonance [4].

The use of Infrared thermography (IRT) has been widely developed during the last years [12] in several areas due to its non-destructive character, including civil engineering works [13, 14] with special attention to cultural heritage [15-20]. This technique allows, on the basis of a photothermal signal, studying the moisture transfer [21] and detecting defects in a material [13, 20]. There are two main methodologies in the use of IRT, the stimulated and the passive method. In the stimulated IRT, the studied object is initially in a steady state and it is artificially put in a transient state by exciting the material with an external energy source. Stimulated IRT has been widely used for detecting defects in works of art [17, 18] and recently for salt detection in stone [22]. Passive infrared thermography is used when the study case is a process which shows temperature and emissivity variations. This is the case of moisture movement [21] or salt crystallization processes [23].

Before studying crystallization within a complex system such as a porous media, it is essential to understand the IRT response of single saline solution during crystallization. In this study, we observed and analyzed the crystallization of NaCl from solution droplets with passive IR thermography. Different solution concentrations were tested at two temperature ranges. We discuss the thermosignal variations related to the crystallization processes.

2 Methodology

2.1 Principle of Infrared Thermography

Infrared thermography is a method based on the measurement of the intensity of infrared radiation emitted by materials, commonly interpreted as changes in surface temperature. For a given material Stefan-Boltzmann's law states, in a simple form, that the quantity of radiation emitted is a function of its temperature:

$$TS = \varepsilon \cdot \sigma \cdot T^4 \quad (1)$$

where TS is the thermosignal measured by the sensor (expressed in isotherm units, I.U.), ε is the emissivity of the material (dimension-less), σ is the Stefan-Boltzmann constant ($\approx 5.67 \cdot 10^{-8} \text{ J} \cdot \text{s}^{-1} \cdot \text{m}^{-2} \cdot \text{K}^{-4}$) and T is the temperature of the material (in K).

In the present study, crystallization was produced by evaporation at two different temperatures, 25 and 50°C. The former was the laboratory condition, the latter was reached and maintained constant during the tests with a hotplate (see setup description in next section).

The acquisition system was a FLIR infrared thermography camera SC655. It works in the longwave infrared spectrum range [7.5 – 14 μm], which enables to investigate a temperature range from -20 to 150 °C for most common materials. The detector is an uncooled array of microbolometers that provides images of 640 x 480 pixels. The noise signal is about 40 mK. The camera was equipped with an additional macro-objective with a magnification x1.6 which gives a spatial resolution of 50 μm / pixel.

In order not to interfere with the evaporation, all measurements were conducted in passive IRT mode. In addition, the recording of the thermosignal along the crystallization tests was done in absolute darkness to avoid the heat release from the laboratory illumination. Prior tests concluded that the optimal recording speed in this test for the IRT was 5 images per second throughout the test. The images were treated and analyzed with the ThermaCAM Researcher 2.10 software (FLIR).

2.2 Experimental procedure

To be ready for crystallization, a saline solution must be supersaturated. In this study, the supersaturation was produced by evaporation of the solvent. We prepared three solutions of different concentration with distilled water and NaCl (purity of > 99%, Sigma Aldrich). The concentrations of NaCl were 35, 140 and 260 $\text{g} \cdot \text{L}^{-1}$ (thereafter referred to as 3.5%, 14% and 26% weight), the latter corresponding to near-saturation. The solutions were filtered to remove any impurities. The crystallization was studied in 10 μL droplets of each concentration. Two drops of each concentration were placed on black adhesive tape (3M), serving as a reference material, which was stuck to a glass slide. The

experimental set-up was placed inside a Plexiglas open-top box of 50 x 40 x 30 cm (Fig. 1). Inside the box, there was enough silica gel to keep a constant humidity at $25 \pm 5\%$. This low RH was chosen to enhance the precipitation/crystallization. In order to avoid the air flow, the open side was covered with a transparent and mate plastic film that did not interfere with the IR detection (transparent in the wavelength analyzed by the camera [24]). Hygrometers and thermocouples were set in contact with the black tape, in order to monitor the temperature and humidity every second.

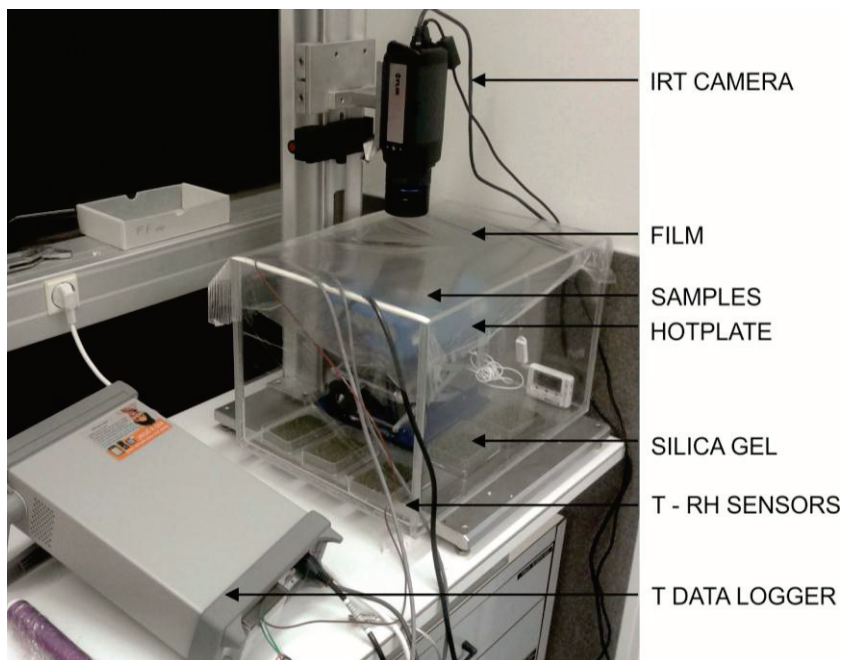


Figure 1: Experimental set-up.

The glass slides with the solution droplets were placed on a hot-plate. This hot-plate was switched off in the test carried out at 25°C , acting as support, and set at a constant temperature of $50 \pm 1^\circ\text{C}$ in the second series of experiments, in order to accelerate the evaporation. The tests lasted until the thermosignal remained stable, once the salts were crystallized. All the equipment was plugged to a computer in order to obtain the image “in vivo” as well as the data from the thermocouples and hygrometers. In addition to whole-image observation, variations of the thermosignal during the experiments were recorded and compared between several points of the droplets and the black tape reference.

Once the droplets had crystallized, they were compared to the observed thermosignals, in order to establish the relation between some processes and crystal morphology. Photographs were taken with a stereomicroscope Olympus SZH-ILLB, with digital Tri-CCD camera (Sony, DXP 930).

Measurements of the sizes and numbers of crystals were done with the image analysis software from MicroVision Instruments.

3 Results and discussion

3.1 Factors affecting the thermosignal in this study

Initially, this study was conceived in order to detect the exothermic process of NaCl crystallization. The observed images, processes and measurements indicated, however, a decrease in thermosignal, contrary to what was expected. Since the black adhesive tape and the droplets are at the same temperature $\pm 0.5^{\circ}\text{C}$ (measured with thermocouples) these variations (1 - 10 I.U.) have to be due to emissivity. Distilled water and the 3M black tape have the same emissivity (0.96, [24]). Comparison between pure water droplets and the different saline solution droplets at the same temperature did not exhibit any difference in thermosignal. In spite of that, the thermosignal of the droplets was always lower than that of the black tape. In addition, differences in the thermosignal were observed within one droplet (e.g. higher thermosignal in the centre). All these emissivity differences between salt solution and tape and between different points of the same droplet are thus mainly due to shape factor and were taken into account for the interpretation of thermosignal variations in terms of crystallization processes. NaCl crystals have a reference emissivity close to 0.82 [25], that is also variable depending on several factors, such as the crystal size, if it was a single crystal or an aggregate or if the measure was made on one face or on a crystal edge.

3.2 Crystallization phases

NaCl crystallization process differed in relation to temperature and concentration of the solution. The study with the IRT revealed three main phases: (I) homogeneous evaporation and crystal nucleation, (II) crystal growth driven by evaporation, and (III) crystal growth fed by solution creeping. The presence and duration of these phases depended mainly on the solution concentration and evaporation rate. Furthermore, at certain times these phases coexisted in different zones within a drop. In general, with low and medium concentration (3.5 - 14 %), crystallization followed sequences of phases I-II. In occasions an additional and weak phase III (creeping) could be found within phase II. In drops with a higher concentration (26%) phase III occurred after or instead of phase II, leading to sequences I-II-III or I-III.

Phase I: Progressive homogenous evaporation and crystal nucleation. At the beginning of the test, there was a marked difference in thermosignal between the droplets and the reference tape (ΔTS). In Figure 2a and 2e, for $t=0$ the droplet thermosignal was clearly lower than in the black support. In Figures 3 and 4 the thermosignal differed at the

beginning of the test from 1 I.U. at 25°C to 3-10 I.U. at 50°C. Considering that temperature of droplets and support was the same (measured with thermocouples), emissivity had an important weight in the received signal,

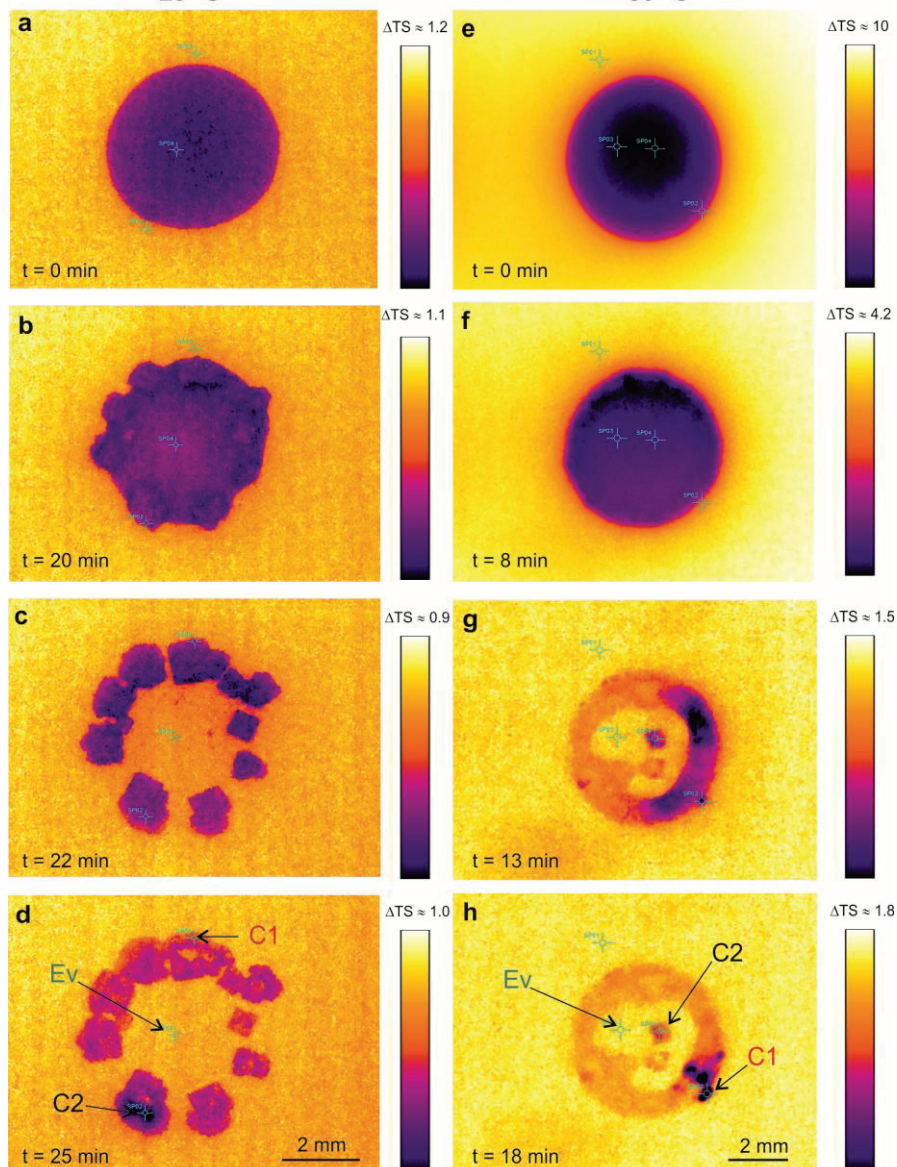


Figure 2: Crystallization sequence observed with IRT for two droplets at 25 °C (left) and 50 °C (right). Both droplets have 14% NaCl concentration. Marks in 2.d and 2.h correspond to profiles in figures 3 and 4. Ev: evaporation zone; C1: creeping zone 1; C2: creeping zone 2.

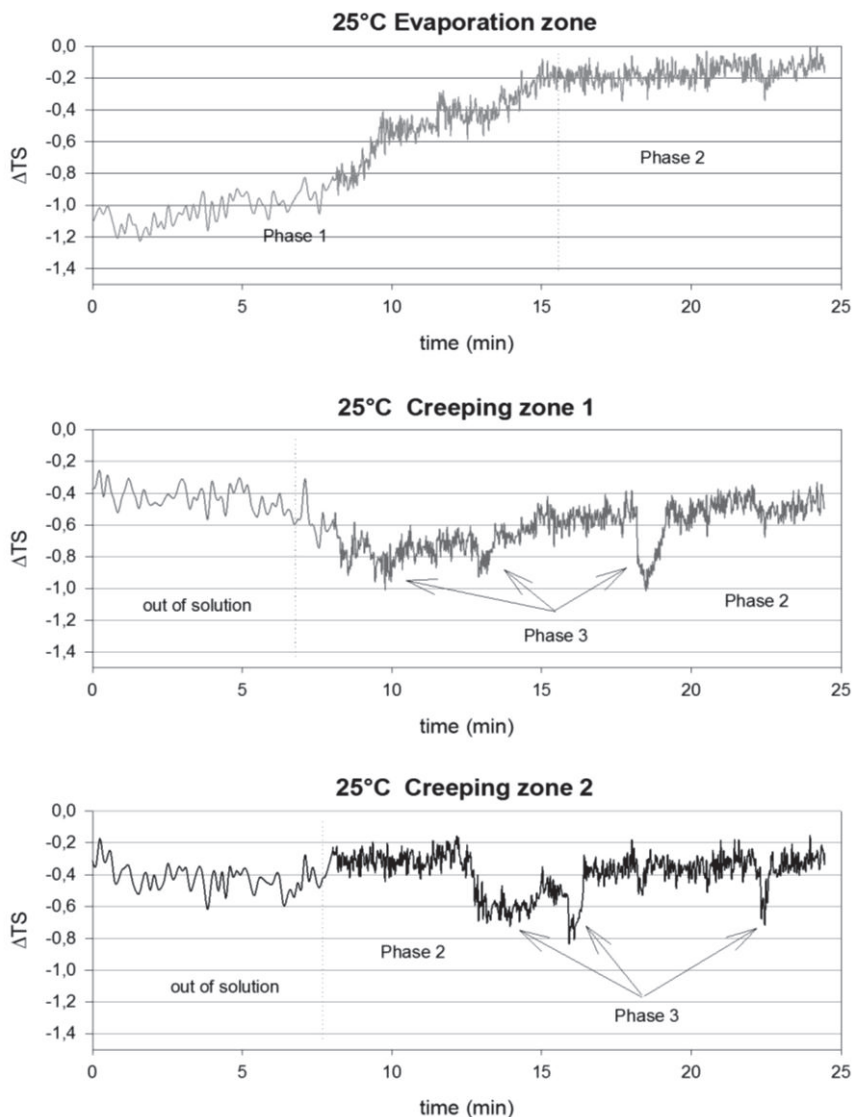


Figure 3: Thermosignal profiles of the crystallization sequence at 25°C. Profiles corresponded to measurements of the TS in spot mode (points indicated in Figure 2d as EV, C1 and C2). Phase I, II and III are shown. “Out of solution” corresponds to a point that is initially out of the droplet edge (reference material) but that is later reached by developing crystals. Phase III last several seconds and was more an isolated phenomena.

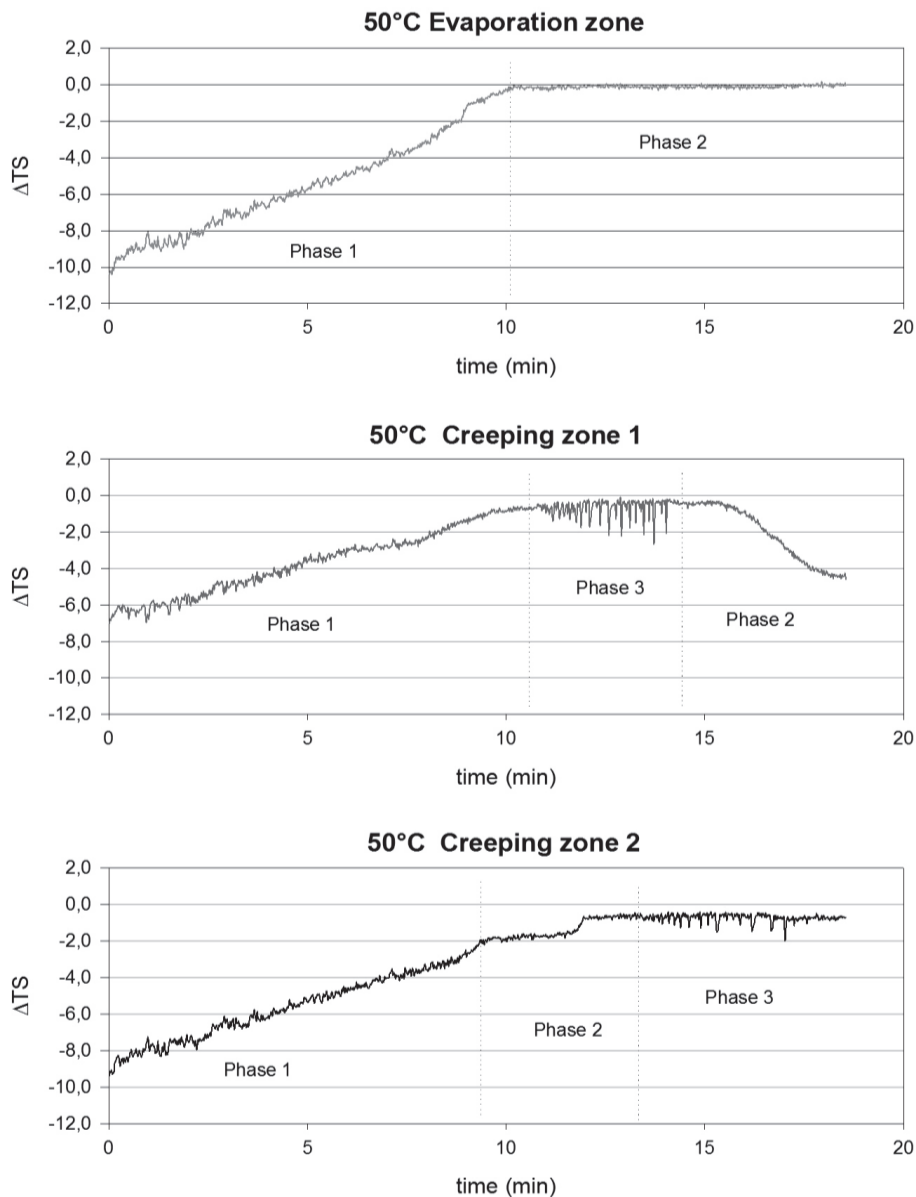


Figure 4: Thermosignal profiles of the crystallization sequence at 50°C. Profiles corresponded to measuring points signals in Figure 2h as EV, C1 and C2. Phase I, II and III are present. Creeping is shown as an intermittent decrease in thermosignal.

mainly due to the shape factor. During this phase I, ΔTS decreased steadily over time (Figures 3, 4). The increase of emissivity with time was due to evaporation, which induced a decrease of the thickness of the droplets.

This homogeneous increase in thermosignal may be due to mass diffusion as a result of the first crystals formation, since sometimes, crystal germs could be distinguished in the solution edge due to their lower emissivity (Figure 2 b, f).

Phase II: Crystal growth driven by evaporation. This phase is featured by a higher thermosignal zone that expanded from the centre to the edges and to the growing crystals. This corresponded to water evaporation and a final visible mass diffusion from lowest concentrated areas towards the highest concentrated ones, that is the crystal surface [4]. The thermosignal profile differed depending on the measured spot.

The transition between phase I and phase II differs depending on the formation or not of visible crystals in the measured point. In areas where crystals formed, the transition from phase I to phase II is observed as a sharp increase of the thermosignal (Fig. 4) at the moment of evaporation. These abrupt increases of thermosignal had maximal values around 0.2 I.U. in the test at 25°C and 2 I.U. in the tests at 50°C. The ΔTS after stabilization was always below zero. The thermosignal was lower, since NaCl emissivity is lower than that of the black tape [24, 25]. At 25°C, this stabilization occurred with a negative ΔTS around 0.2-0.4 (Figure 2d, h, Figure 3) up to 1 I.U. in a few cases, depending mainly on the crystal shape. In those places where all the solution had totally dried out and were apparently devoid of crystals, the thermosignal stabilized at values similar to the black reference (around 0 I.U.) (Fig 4 top). The transition from phase I to phase II was observed to be progressive. In low concentrated droplets, the phase II marked the complete evaporation and the end of the thermal effect.

Phase III: “Pop-cold events”. After phase II, no more solution remained visible with the IRT. However, in medium and high concentrated droplets (14 and 26%), intermittent decreases of the thermosignal around and on the previously formed crystals were observed (Figure 3-4). These indicated that evaporation was not yet completed and stepped crystal growth processes were still occurring.

At that step, crystals were formed by creeping mechanism. Creeping is explained as the evaporation-driven extension of crystals. Hazlehurst [27] described the creeping as an intermittent process, where crystal growth is halted temporarily and more crystals grow outside the first crystal layer. The creeping crystals, formed after the first regular layer of crystals, are disposed in irregular layers in localized regions. These episodic pulses are the consequence of the release of water of crystallization at the edge of the droplet [27, 28].

Creeping leads to an intermittent process of dissolution-crystallization. A hypothesis would be that each new dissolution on the surface resulted in a decrease in thermosignal and each crystallization in an increase. Since in this study temperature remained constant during each test and NaCl crystallization is an exothermic reaction, this decrease in thermosignal depended mostly on emissivity changes. When this intermittent variation of emissivity stopped, and signal became stable again, we considered that evaporation was completed. This phenomenon may take place in several points of the droplet but not at the same time (Figure 34). The measured number of “pop-cold events” in each measuring point ranged from 1 to more than 100. The decrease in thermosignal varied between 0.5 and 5 I.U according to the concentration of the droplets and the temperature of the test. The presence of phase III, the number of events and the intensity in the variation of thermosignal are related mainly to concentration of the NaCl solution and to a lesser extent to temperature.

3.5% concentration droplets.

This low concentration permitted that crystals were formed and the evaporation/crystallization was in equilibrium. Exceptionally, in one droplet at 25 °C, an intermittent and very weak decrease in thermosignal was observed in germ crystals. However, most of the solution remained at that stage, so we cannot consider it as creeping at the scale of the study.

14% concentration droplets.

At 25°C four areas were observed and measured in one droplet and seven areas in the other one. The number of events were from 1 isolated “pop-cold event” in one of the droplets to 13 in the other one. The maximal decrease in thermosignal was of 0.5 I.U (Figure 3). At 50 °C at least twelve different points were recorded during this phase in each droplet. The areas which experimented the largest creeping showed about 20-22 “pop-cold events” with a maximum decrease of 2.50 I.U. of the thermosignal (Figure 4) and 30 events with only a decrease of 0.5 I.U. Some areas showed a low number of measured events of 6-8 and a thermosignal decrease of 0.5-1 I.U.

26% concentration droplets.

At 25°C only a few areas showed phase III, with a variable number of events, from 3 to 20. The decrease of emissivity was still less intense than at higher temperatures. At 50°C, phase III started directly without any previous phase or sometimes just after a short phase I. At the beginning of phase III, more than 30 small active areas were identified and selected to be measured. However, some of these areas joined together. The number of pop events were from 40 to 70, although there were also exceptional cases with more than 100 events. The average decrease of the thermosignal was about 4 and 5 I.U. compared to the black tape.

3.3 Relation between IRT signal and crystal morphology

Crystal morphologies and numbers depended on several variables such as operating conditions [29] and contact angle of the droplet with the support [30]. Clear differences in crystal size and distribution were observed in relation to salt concentration and temperature. In the study with IRT each morphology gave a different signal. Some authors [2, 29, 30] described the different morphologies observed during the crystallization of a NaCl droplet. In agreement with their observations, we found cubic crystals at the centre and the edge of the droplet. This morphology corresponded to a sequence of phases I-II, with an abrupt transition between phases, related to the crystal size. In some of the tests, efflorescences-like crystals with various morphologies grew (Figure 5). They can be formed by two mechanisms: Top-Supplied Creeping (TSC) and Bottom-Supplied Creeping (BSC). In TSC, the fresh solution necessary to the creeping process is supplied by the liquid flow aside and on top of growing crystallites, whereas in BSC, the liquid flow occurs in narrow spaces between the crystallites and the substrate [27, 28, 31]. Three different morphologies of creeping aggregates were observed by optical microscopy.

- 1) Fan-shaped crystals in contact with the substrate: in 3.5 and 14% concentrated droplets, dendritic crystals with flat fan shape that corresponded to BSC were observed. They grew from the droplet edge towards the interior and exterior of the droplet (Fig. 5 a, c). The crystallization sequence corresponded to phase I-II. This type of creeping is not observed in phase III.
- 2) Spherulite-like crystals in contact with the substrate: the crystal growth corresponded both to the BSC and TSC mechanisms because the crystal was in contact with the substrate (BSC) but also grew in height (TSC) (Fig. 5 a, d). This kind of efflorescence growth was linked to the “pop-cold events”.
- 3) Spherulite-like crystals on the surface of previous crystals: formed by hairy crystals aggregates and found mainly in medium and high concentration droplets (14 and 26%, Fig. 5 a, b, d), always corresponding to phase III “pop-cold” observations. The number and size of visible aggregates varied depending on the temperature and concentration. Figure 5 (a, d) shows that for the same concentration, spherulites are bigger at 50°C, due to the union of several spherulites to form a unique aggregate.

4 Conclusions

Infrared thermography (IRT) has turned out to be an appropriate technique to observe, analyze and even quantify salt crystallization. IRT allows observing “in vivo” evaporation phases and types of crystallization.

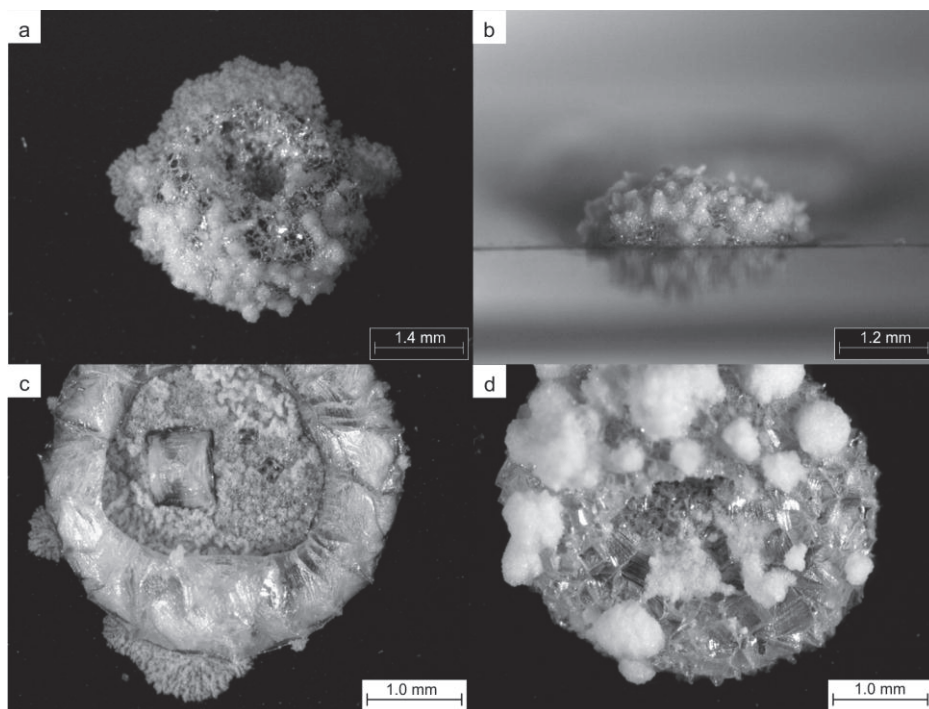


Figure 5: Efflorescence-like crystals. (a) and (b) 14% solution droplet crystallized at 25 °C. Small spherulite-like crystals grew on cubic crystals by TSC; (c) 14% solution droplet crystallized at 50 °C. Fan-shaped crystals grew by BSC; (d) 14% solution droplet crystallized at 50 °C. Aggregates of spherulite-like crystals grew by TSC.

In this study, different droplets of NaCl solution at different initial concentrations were dried at constant temperature (25 and 50 °C) under an IRT camera. Since temperature remained constant, in this study the thermosignal recorded depended mainly on the emissivity and was expressed as a difference compared to a reference material. Three phases were detected: (I) homogeneous evaporation and crystal nucleation, (II) crystal growth and (III) creeping. Creeping was related to the formation of efflorescence-like crystals. They may result from bottom-supplied creeping (BSC) with mainly fan shapes and found around the droplet in contact with the support or they may result from top-supplied creeping (TSC) with spherulite shape and growing on and around the precipitated crystals. TSC showed a spectacular phenomenon when recorded with IRT. It exhibited an intermittent decrease of IR thermosignal of a few seconds (called by the authors “pop-cold events”). Even if no liquid solution is visible, creeping demonstrated that evaporation was not completed and crystallization process was still occurring. At lower temperatures, creeping occurred over a longer period and decreases in thermosignal may last from several seconds up to one minute. At 50 °C

“pop-cold events” occur consecutively and are more numerous, more intense and shorter than at 25°C.

IRT is a non-destructive technique that gives information about the thermal properties of materials and their weathering degree. However, this technique is highly influenced by environmental parameters when used outdoors, and sometimes its accuracy is not enough in research field.

This study is the beginning of a wide research about saline solution behaviour studied by IRT and serves as basis for further investigations dealing with salt crystallization in porous stones and salt damage in built heritage.

References

- [1] K. Zehnder, A. Arnold, Crystal growth in salt efflorescence, *J. Cryst. Growth* 97(2) (1989) 513-521.
- [2] C. Rodriguez-Navarro, E. Doehne, Salt weathering: influence of evaporation rate, supersaturation and crystallization pattern. *Earth Surf Proc Land*, 24(3) (1999) 191–209.
- [3] C. Rodriguez-Navarro, E. Doehne, E. Sebastian, How does sodium sulfate crystallize? Implications for the decay and testing of building materials, *Cement Concrete Res.* 30 (10) (2000) 1527–1534.
- [4] L. Pel, H. Huinink, K. Kopinga, Salt transport and crystallization in porous building materials. *Magn. Reson. Imaging*, 21(3-4) (2003) 317–320.
- [5] M. Steiger, Crystal growth in porous materials - I: The crystallization pressure of large crystals. *J. Cryst. Growth*, 282(3-4) (2005) 455–469.
- [6] E.M. Winkler, P.C. Singer, Crystallization pressure of salts in stone and concrete, *Geol Soc Am Bull*, 83 (1972) 3509-3514.
- [7] A.S. Goudie, Experimental salt weathering of limestones in relation to rock properties, *Earth Surf. Proc. Land*. 24 (1999) 715-724.
- [8] F.J. Alonso, P. Vázquez, R.M. Esbert, J. Ordaz, Ornamental granite durability: evaluation of damage caused by salt crystallization test, *Materiales de Construcción* 58 (289-290) (2008) 191-201.
- [9] P. Vázquez, A. Luque, F.J. Alonso, C.M. Grossi, Surface changes on crystalline stones due to salt crystallization. *Envir. Earth Sci.*, (2012) 1-12.

- [10] N.N. Piskunova, V.I. Rakin, Statistical analysis of dynamics of elementary processes on the surface of the growing crystal (by the AFM data), *J. Cryst. Growth*, 275(1-2), (2005) 1661–1664.
- [11] J. Dewanckele, T. De Kock, M.A. Boone, V. Cnudde, L. Brabant, M. N. Boone, G. Fronteau, L. Van Hoorebeke, P. Jacobs, 4D imaging and quantification of pore structure modifications inside natural building stones by means of high resolution X-ray CT, *Sci. Total Environ.*, 416 (2012) 436-48.
- [12] S. Bagavathiappan, B.B. Lahiri, T. Saravanan, J. Philip, J., T. Jayakumar, Infrared thermography for condition monitoring – A review, *Infrared Phys. Techn.*, 60 (2013) 35–55.
- [13] E. Grinzato, V. Vavilov, T. Kauppinen, Quantitative infrared thermography in buildings. *Energ. Buildings*, 29(1), (1998) 1–9.
- [14] H. Wiggenhauser, Active IR-applications in civil engineering. *Infrared. Phys. Techn.*, 43(3-5) (2002) 233–238.
- [15] N.P. Avdelidis, A. Moropoulou, Applications of infrared thermography for the investigation of historic structures. *J Cult Herit*, 5(1) (2004) 119–127.
- [16] A. Moropoulou, M. Kouli, N.P. Avdelidis, Infrared thermography as an NDT tool in the evaluation of materials and techniques for the protection of historic monuments. *Insight: Non-Destructive Testing and Condition Monitoring*, 42(6) (2000) 379-383.
- [17] F. Mercuri, N. Orazi, U. Zammit, S. Paoloni, M. Marinelli, P.P. Valentini, Thermographic analysis of Cultural Heritage: recent applications and perspectives, *E-preservation Sciences* 9, (2012) 84–89.
- [18] J.L. Bodnar, J.L. Nicolas, K. Mouhoubi, V. Detalle, Stimulated infrared thermography applied to thermophysical characterization of cultural heritage mural paintings. *Eur. Phys. J-Appl. Phys.* 60 (02) (2012) 21003.
- [19] M. Danese, U. Demsar, N. Masini, M. Charlton, Investigating material decay of historic buildings sing visual analytics with multi-temporal infrared thermographic data. *Archeometry*, 52, 3 (2010) 482-501.
- [20] J.L. Bodnar, J.L. Nicolas, K. Mouhoubi, J.C. Candore, V. Detalle, Characterization of an inclusion of plastazote located in an academic

- fresco by photothermal thermography, *Int. J. Thermophys.* 34 (2013) 1633-1637.
- [21] N.P. Avdelidis, A. Moropoulou, P. Theoulakis, Detection of water deposits and movement in porous materials by infrared imaging. *Infrared Phys. Techn.*, 44(3) (2003) 183–190.
- [22] C. Thomachot-Schneider, P. Vázquez, N. Lelarge, A. Conreux, C. Bouvy, M. Gommeaux, K. Mouhoubi and J.L. Bodnar. Thermal behaviour of building stones contaminated with Na₂SO₄. *Proceedings SWBSS2014, 3rd International Conference on Salt Weathering of Buildings and Stone Sculptures*, H. De Clercq (Ed.), (2014), 543-547
- [23] P. Vázquez, C. Thomachot-Schneider, K. Mouhoubi, G. Fronteau, M. Gommeaux, V. Barbin, J.L. Bodnar. Infrared thermography monitoring of the NaCl crystallization process. (submitted)
- [24] FLIR user manual. Series SC 655.
- [25] M. Marchetti, V. Muzet, R. Pitre, S. Datcu, L. Ibos, J. Livet, Emissivity Measurements of Road Materials, *Quantitative InfraRed Thermography Journal*, Vol 1 (1) (2004) I.2.1-I.2.7.
- [26] S. Al-Jibbouri, J. Ulrich, The growth and dissolution of sodium chloride in a fluidized bed crystallizer. *J. Cryst. Growth*, 234 (1) (2002) 237–246.
- [27] T.H. Hazlehurst Jr, H. C. Martin, L. Brewer, The Creeping of Saturated Salt Solutions, *J. Phys. Chem.* 40.4 (1936) 439-452.
- [28] E.R. Washburn, The creeping of solutions, *J. Phys. Chem.* 31.8 (1927) 1246-1248.
- [29] H. Takiyama, T. Otsuhata, M. Matsuoka, Morphology of NaCl crystals in drowning-out precipitation operation, *Chemical Engineering Research and Design* 76.7 (1998), 809-814.
- [30] N. Shahidzadeh-Bonn, S. Rafai, Salima, D. Bonn, G. Wegdam, Salt Crystallization during Evaporation: Impact of Interfacial Properties, *Langmuir* (2008), 24, 8599-8605.
- [31] W.J.P. Van Enckevort, J.H. Los, On the Creeping of Saturated Salt Solutions. *Cryst. Growth Des.* 13(5) (2013) 1838–1848.

Salt sources revisited

C. Bläuer* and B. Rousset

Conservation Science Consulting Sàrl, Fribourg, Switzerland

* csc@conservation-science.ch

Abstract

The hierarchy of possible approaches to conservation if maximal effectiveness and sustainability are aimed for, are preventive conservation i.e. addressing the causes, passive intervention i.e. addressing the activation mechanisms, remedial intervention i.e. strengthening the object and the least efficient restoration, which camouflages the damage.

To apply this principal of minimal intervention on buildings suffering from salt damage and especially when aiming to conserve preventively it is necessary to know the sources of the salts.

The possible sources of salts are:

Autochthonous salts – salts coming from the materials they damage.

Salts from neighbouring building materials.

Salts from human activity in the vicinity of the building.

Salts in connection with the use of the monument throughout history.

Salts having to do with the general geographic situation of the building.

In the paper general indications are given which salts can be released from which sources and some examples for common as well as uncommon salt sources are reported on, some of which for the first time.

Keywords: salt source

1 Introduction

Salt weathering is mainly a physical process. Even though the exact mechanisms provoking this kind of weathering are still not completely understood [1], the weathering itself has been observed on countless monuments and shown by laboratory experiments. It is generally agreed that this weathering process is mainly triggered by the salt system reacting with a changing environment, by letting different salt phases crystallise, re-crystallise, hydrate, de-hydrate, deliquesce according to the environmental conditions. On non-porous materials salt growth or transformation processes will not lead to damage, as can easily be demonstrated with laboratory experiments with salts e.g. in glass containers. When the salts are however sitting within an inorganic porous material such as most natural stones or mortars, the recurring change of their physical form will, in many cases, lead to the degradation of the material [2]. It can be observed that the porous system of a material determines the type and intensity of salt deterioration caused by a specific salt system in a specific environment to a large extent [3].

If maximal effectiveness and sustainability are aimed for, the most effective approaches to conservation are preventive conservation i.e. addressing the causes or passive intervention i.e. addressing the activation mechanisms [4]. On buildings, suffering from salt damage passive intervention consists of sheltering from unsuitable environmental conditions. Preventive conservation consists in stopping the salt supply, which requires to know the salt source.

Practitioners confronted with the task of finding the sources of the salts occurring in a specific case might find this text and its bibliography useful and it might enlarge the appreciation of the question to newcomers in the field.

2 Salts

Salts are chemical compositions consisting of cations (metal ions) and anions (acid residue anions) connected by ionic bonds. Therefore most of them are at least slightly soluble in water. The ions found most commonly on monuments are sodium (Na^+), potassium (K^+), ammonium (NH_4^+), calcium (Ca^{2+}), magnesium (Mg^{2+}), chloride (Cl^-), sulphate (SO_4^{2-}), carbonate (CO_3^{2-}), hydrogen carbonate (HCO_3^-), nitrate (NO_3^-) and oxalate ($\text{C}_2\text{O}_4^{2-}$) [2]. But salts with less common ions like nickel (Ni^{2+}) [5], copper (Cu^{2+}) [6] or aluminium (Al^{3+}) [7], to name only a few, can be found as well.

Some salts can crystallise either in a hydrated or non-hydrated form according to the environmental conditions surrounding them. In humid air salts can take up water from their environment, start to creep, deliquesce and finally form a salt solution. If ionic solutions from different sources are mixed, their cations and anions can regroup on drying and form “new” salt

species. The specific salt minerals found in an efflorescence will strongly reflect the environmental conditions at or shortly before the time of sampling and they can be formed by only some of the ions actually present within the pores of the material while the other ions remain in solution (see e.g. [8]).

Looking for the sources of salts means therefore looking for the sources of the different ions rather than the sources of individual salt minerals. More so because in most cases the ions found in a porous material on a monument are coming from diverse sources to form the salt system on hand at the time and place of observation.

3 Sources for salt ions

3.1 Salt ions from building materials

3.1.1 Salts in stone materials and natural waters

Most minerals and hence stones are at least partly soluble in water. Therefore, the mineralization of spring water depends on the geological environment the water passed through on its way to the surface [9].

Basically all natural stones contain at least small amounts of water-soluble ions. For instance the average values measured in seven different types of molasse-sandstones from Bern, Switzerland (CH), per gram of material were: Na^+ (32 μg), K^+ (96 μg), NH_4^+ (7 μg), Ca^{2+} (510 μg), Mg^{2+} (111 μg), Cl^- (12 μg), NO_3^- (1 μg), HCO_3^- (2249 μg), SO_4^{2-} (29 μg) [10]. In spite of the fact that such values would be necessary to estimate the salt input from the stone material itself, autochthonous salt contents astonishingly seldom are published.

Common natural rocks do not contain nitrates, if these ions are present in spring water or a rock they indicate a contamination from the infiltration of surface waters.

Like water in the soil, rainwater will contain ions. The main source of dissolved material over the ocean and near coasts, is sea salt [9]. Other sources of dissolved matter in rain are diverse atmospheric pollutants including sulphates, nitrates and ammonia as well as organic acids. Generally “the composition of rain in any one location may vary greatly with time. The first drops of rain at the beginning of a storm may contain most of the soluble material available in the atmosphere; rain toward the end of a storm is relatively dilute” [9].

3.1.2 Salts in mortars

Most mineral mortars contain water-soluble parts. This is not astonishing as mortars are mainly made by mixing natural rock particles (gravel, sand, clay) with a binder, produced by calcinating natural rock materials, and

adding water. As explained before all these constituents can contain water-soluble parts.

Historical mortars usually have been made using local materials. If the locally found sand contains water soluble parts, these will contribute to the salt content of the mortar. Such was the case for a lime mortar from the Luegisland tower in Luzern (CH) where the sand contained a noticeable amount of gypsum ($\text{CaSO}_4 \cdot 2\text{H}_2\text{O}$). During a few hundred years this did not cause any degradation problems, but it “falsified” our salt analysis, in fact the measured high calcium and sulphate content only could be explained after the thin section analysis of the mortar had revealed the gypsum grains.

Some building materials such as gypsum stucco or plaster of Paris consist predominantly of soluble salts. On the Swiss Plateau pure gypsum mortars were e.g. used frequently as jointing mortars for facades out of sandstones. In a recent study, sulphates participating in stone deterioration could be attributed not only to air pollution but also to nearby gypsum mortars [11].

Another group of mortar binders consisting mainly of water-soluble minerals are dolomitic limes. In the central Alpine regions, until quite recently, these materials were not well known and the common assumption was that the binders of historical mortars consisted generally of lime. Recent analysis however has shown that especially in remote areas with no suitable limestone but abundant dolomite, the latter was the (logical) material to use for the production of mortar binders. One such an example is Müstair monastery, a world cultural heritage site situated in the Val Müstair (CH) where dolomites are the predominant sedimentary rocks [12]. Analysis of plasters, wall painting supports and white washes dating from the 9th until the 19th century have shown that dolomitic lime had been used quite exclusively. These mortars and washes contain amongst other minerals the following slightly water soluble minerals hydromagnesite ($3\text{MgCO}_3 \cdot \text{Mg}(\text{OH})_2 \cdot 3\text{H}_2\text{O}$), brucite ($\text{Mg}(\text{OH})_2$) and periclase (MgO) [13].

The mortars at the ruined church San Gaudenzio in Casaccia consisted of dolomitic lime too. When the restoration works began the architect was puzzled by the occurrence of strange salt efflorescence, which could be identified as being hydromagnesite, washed out of the mortars and deposited on stone and plaster surfaces as efflorescence and crusts.

Modern hydraulic lime or cement mortars contain water soluble sodium and potassium reacting with CO_2 of the surrounding air to form alkali carbonate or hydrogen carbonate salts [14]. Our analysis of mortars that contain such binders have shown that another major water soluble constituent of such materials seems to be sulphate. After setting these materials contain abundant amounts of calcium hydroxide, which, if washed out and getting in contact with CO_2 from the air, will cause white calcite crusts on monument surfaces.

Tetmajer reports in 1894 of the addition of sodium chloride to the fresh mortar mixture when building at low temperatures in winter, giving examples from Switzerland, Germany and France [15]. He suggests to use combinations of alum, sodium chloride, sodium carbonate and burnt lime when building at temperatures below -10°C .

3.2 Pollution situations

3.2.1 Air pollution

A few decades after the end of the Second World War the damaging effects of air pollution, primarily SO_2 and NO_x , on stones became a major subject of concern amongst conservators and conservation scientists especially from the highly developed and industrialized countries [16]. The phenomenon at that time was however not new as already in 1864 the effects of air pollutions on stone are studied [17]. Today air pollution seems not anymore to be considered to be a major problem for stone conservation in Europe. In fact the SO_2 emissions measured in today's Switzerland even in the most polluted areas do not even reach a tenth of the values measured in the nineteen eighties [18] and the pollution levels evolved probably similarly all over Europe. However, in other parts of the world the situation seems to be very different [19] and even in Europe the sulphate (and other) ions deposited on stone and mortar surfaces during the high times of air pollution are of course still present within the material surfaces and continue to exert their deleterious effects [11].

3.2.2 Waste water and faeces

Faeces are generally rich in nitrogen from which ammonium and nitrate ions can derive. Soils near human settlements contain salts from the decomposition of organic materials and especially from faecal matter. The hygienic conditions in cities and other settlements in ancient times, were quite different from today's [20]. Evacuation systems for faeces and other waste waters were rather open systems and cattle, draught and other animals lived all around the houses and in the streets. Important amounts especially of nitrates have infiltrated into the soils and from there into the walls during these times [20].

Apart from the nitrogen containing ions, the manure of cattle and other herbivore animals is dominated by potassium [21]. In the urine of ruminant animals, potassium is generally largely dominant over sodium (oral communication 2005, Ms. Dr. Kaufmann, Tierspital, Bern). In human urine, however sodium and chloride are quite abundant and the content in inorganic ions of a so called 24 hours human urine are [22]: Na^+ (5.9 g), K^+ (2.7 g), NH_4^+ (0.8 g), Ca^{2+} (0.5 g), Mg^{2+} (0.4 g), Cl^- (8.9 g), PO_4^{3-} (4.1 g), SO_4^{2-} (2.4 g). From the same source, it can be calculated that a 24h human urine contains about 10 g of nitrogen, which would result in over 40 g of nitrate per human being per day.

In Durham Cathedral, nitromagnesite ($\text{Mg}(\text{NO}_3)_2 \cdot 6\text{H}_2\text{O}$) together with a little gypsum and quartz (SiO_2) was at the basis of slippery, oily looking patches occurring locally on the floors [23]. When looking for the sources of the magnesium nitrate the authors could exclude the local sandstones “employed in the cathedral flooring” which “are normally exceedingly poor in magnesium, and contain virtually no nitrogenous material” [23]. The most likely source of magnesium is the seating crushed Magnesian Limestone from the region upon which these flagstones were formerly laid. As for the nitrate source decomposition of cadavers, extensive use of incandescent gas mantles or the storage of gun powder in the cathedral, were considered but could be excluded [23]. It could finally be shown that the most likely source for the nitrate are a few 1000 prisoners that were kept in winter 1650-1651 in the cathedral and who most likely stayed at the warmer end of the cathedral and used the colder end for their toilet.

On the ruined castle of Belfort in Brienz/Brinzauls (CH) where severe degradations had been found below two medieval toilets (garderobes) one of which had been only in use a rather short time and the other had been used for over a hundred years. The salt composition beneath the latter was clearly dominated by sodium and chloride in very similar proportions to human urine [24]. The salt system underneath the precociously abandoned garderobe, was however, clearly dominated by potassium and nitrate. This could be attributed to a herd of Alpine Ibex (a sort of wild goats) regularly gazing and resting on top of the walls, right above the former toilet. To verify this attribution we analysed the water extraction of faeces from these animals and found the following inorganic ion content per gram sample: Na^+ (49 μg), K^+ (5166 μg), NH_4^+ (157 μg), Ca^{2+} (741 μg), Mg^{2+} (629 μg), Cl^- (674 μg), NO_3^{2-} (2538 μg), PO_4^{3-} (651 μg), SO_4^{2-} (247 μg).

3.3 Common salt, table salt

Many human activities involve the use of sodium chloride, which explains the huge importance this material always has and had [25]. In former times, salt was transported in wooden barrels or linen sacks [25] and it often was stored as piles of salt without any container. Whoever has handled salts in laboratory knows that salts have an annoying tendency to creep up the walls of their containers and even out of them [26, 27], it is therefore easily imaginable that such creeping can explain how salts moved away from their stocking places into the surrounding materials. Fact is, that big amounts of this salt are found in walls at or near places where the salt market took place, e.g. at the Salzlaube in Bern [28] or where salt was stocked e.g. in the crypt of St. Maria im Kapitol in Köln [3].

3.4 Professions dealing with salt and general salt uses

Many food-producing professions use apart from sodium chloride diverse other salts for different purposes. For example: Salt-cured meat is

produced using sodium chloride but also sodium and potassium nitrate. Cheese making facilities use the same salts. Bakeries use potassium nitrate and sodium carbonate or hydrogen carbonate.

The process of tanning of leather consists of many steps where acids, lyes and salts are used. Amongst others, sodium, chloride, sulphate and aluminium ions can have their source in this activity [29].

Since the end of the 16th century it was known that mixtures of ice, water and salts can be used to reach temperatures well below freezing [30]. Before the invention of the refrigerator, this was used to cool for medical or laboratory purposes or to cool drinks or food. An often used and easily available salt for this purpose was potassium nitrate [31].

On the other hand, salts are used for de-icing. Apart from NaCl de-icing salts can contain: potassium chloride, calcium chloride, magnesium chloride, potassium and sodium acetate; potassium and sodium formate or even urea [32].

Very hygroscopic salts like calcium chloride are used to keep natural tracks humid to bind the dust.

We have observed that sodium chloride is sometimes used as an herbicide on paved surfaces adjacent church walls to prevent herbs growing between the stones.

Synthetic fertilizers contain nitrates, phosphates, potassium, calcium and magnesium; they often are applied as a powder or in granulated form. These materials are distributed over the fields like seeds would be and can be thrown this way far away from the fields. We have observed such materials landing on nearby surfaces of monuments [33].

Potassium nitrate is an important constituent of gun powder. In historic time, it was mainly produced by leaching out the floors of stables and settlements [34]. In Switzerland this was mainly done while the cattle were on the mountain pastures during summertime by the so-called "Salpetersieder", a highly regulated profession [35].

3.5 Salts resulting from conservation or restoration measures

Waterglass is a solution of sodium, potassium or sodium and potassium silicate in water. In a building context, it is used e.g. as the binding media for silicate mineral paint, for fireproofing or in injection materials against rising moisture in walls. Waterglass is applied as a liquid and sets to an insoluble aqueous SiO_2 and water soluble sodium or potassium carbonates [2]. During the 1950ies and 1960ies waterglass was extensively used in the German Rheinland to consolidate wall paintings in most cases with quite disastrous side effects due to the high sodium and/or potassium input [36].

Interesting enough since a few years lithium waterglass is sold for the consolidation of mortars and renders [37]. We are actually expecting lithium salts to occur in the future at buildings treated with these materials.

Desalination poultices can not only extract salt ions from the treated support but also release ions into the support; this should be controlled before the use of such material. In a commercial poultice material containing cellulose fibres and montmorillonite, 1051 ppm of sodium as well as traces of ammonium, potassium and chloride were analysed in the water extraction [38].

In the vaults of the St. Johannes chapel in the monastery Allerheiligen in Schaffhausen (CH) we did find large amounts of calcium nitrates, whose occurrence can only be explained as the residue of the uncovering of the wall paintings by using nitric acid [39].

Acid cleaning can easily lead to salt damages and the salts involved will strongly reflect the acid used. Accordingly, [40] report on formate salts effloresce after the use of formic acid.

After acidic cleaning lyes might be used to neutralize and by this of course producing salts. Lyes such as sodium hydroxide and ammoniac can be constituents of paint removers or cleaning poultices. P. and L. Mora have suggested a poultice containing ammonium and sodium bicarbonate and sodium EDTA for the cleaning of crusts on limestone surfaces [41].

Since a long time people have observed the deleterious effects of salts concentrated at the bases of walls and many attempts have been made to remedy by transforming the harmful salts present to less harmful ones. An early such proposal was published in 1845 [42], who believed that the salts consisted mainly in the very deliquescent calcium nitrate sometimes together with some calcium chloride. Therefore he suggested that the salts should be transformed to much less deliquescent salts by applying solutions of sodium sulphate, phosphate or carbonate of which he clearly preferred the sodium carbonates. He believed that the newly formed calcium salt would remain insoluble and trapped within the sandstone whereas the also resulting sodium nitrate would form efflorescence on the surface from where it could easily be washed off.

Even today new restoration techniques are liable to add salts into the treated stones. For example, to increase the stability of a newly proposed consolidation treatment based on the formation of hydroxyapatite ($\text{Ca}_{10}(\text{PO}_4)_6(\text{OH})_2$), it is proposed to add calcium salts such as calcium chloride to the other reagents [43, 44].

Up until today attempts are made to chemically transform harmful salts present within porous building materials into less or not harmful salts. There are situations where such methods correctly applied can be very successful to fulfil the task wanted [45]. However the products sold nowadays as remedy for salt problems on a grand scale do seem to be rather potential producers of salts than real solutions to the problem. In the

course of a very recent expertise, we did come across products containing amongst other things the following constituents alone or in various mixtures: barium phosphate, phosphoric acid, magnesium, zinc or lead fluorosilicates. All sellers of these products indicated that none of the products can be used when nitrates are present, because the nitrates formed as a result of such a treatment are all very water soluble and/or hygroscopic and additionally the nitrates of barium, zinc and lead are highly toxic. This means that these products cannot be applied in the zone of rising humidity at the basis of walls, which for many buildings are the parts that are the most contaminated by salts.

It has been suggested already more than 100 years ago to use fluorosilicates as stone and mortar consolidants [46] and these products are in use until today. Other treatment products were en vogue at former times but are now forgotten. One such treatment was called Testalin; it consisted in a consecutive impregnation of the stone surface with aluminium acetate and potassium soaps [47]. The mentioned historical treatments are suspected to be at the basis of aluminium and ammonium salts found on diverse buildings in northern and north-eastern Germany [7, 48-50] and recently in Switzerland too [51].

4 Conclusions

To find the sources of the salts of an individual building, it is necessary to know the autochthonous soluble salt content of the original and repair building materials, the potential salt input from the environment, how the building and its surroundings have been used throughout its history and what restorations have taken place.

If uncommon ions are found when analysing the salts from a monument, uncommon sources have to be looked for. Very often these sources have to do with the use of the building or with former conservation/restoration treatments. Conservation projects often take place on objects that have been treated at least once in the course of the past fifty or sixty years and in many cases (modern) materials have then been used. Such materials might be at the basis of the problems encountered nowadays. Our latest encounters in this direction are acrylates and probable lactates as efflorescence on historical monuments.

References

- [1] <http://www.saltwiki.net/>
- [2] Arnold, A., Zehnder, K., Monitoring wall paintings affected by soluble salts, The Conservation of Wall Paintings, Proc. Symp. Courtauld

Institute of Art and Getty Conservation Institute, London, July 13-16, 1987, The Getty Conservation Institute, 1991, 103-135.

- [3] Laue, S., Bläuer Böhm, C., Jeannette, D., Salt weathering and porosity - Examples from the crypt of St. Maria im Kapitol, Cologne, 8th International Congress on Deterioration and Conservation of Stone, Berlin, 1996, 513-522.
- [4] Cather, S., Assessing the causes and mechanisms of detrimental change to wall paintings. Conserving the painted past: developing approaches to wall painting conservation, Post-prints of a conference organised by English Heritage, London 2-4 December, 1999, Gowing R., Heritage A. (Eds), London, 2003, 64-74.
- [5] Blanco Varela, M. T., Menendez, E., Hoyos, M., Study of surface decay of the marbles and serpentine from the Descalzas Reales convent at Madrid, La conservation des monuments dans le bassin méditerranéen, Actes du 2ème symposium international, 19-21 novembre, Genève, 1991, 167-175.
- [6] Steiger, M., Behlen, A., Neumann, H.H., Willers, U., Wittenburg, C., Sea salt in historic buildings: Deposition, Transport and accumulation, Proc. 4th Int. Symp. Conservation of Monuments in the Mediterranean, Rhodes, 6.-11. May, Vol. 1, 1997, 325-335.
- [7] Neumann, H.-H., Aufbau, Ausbildung und Verbreitung schwarzer Gipskrusten, dünner schwarzer Schichten und Schalen sowie damit zusammenhängender Gefügeschäden an Bauwerken aus Naturstein. Dissertation, Universität Hamburg, 1994.
- [8] Steiger, M., Neumann, H.-H., Grodten, T., Wittenburg, C., Richter, U., Dannecker, W., Salze in Natursteinmauerwerk - Probenahme, Messung und Interpretation, Denkmalpflege und Naturwissenschaft - Natursteinkonservierung II, Sneathlage, R. (Ed.), Fraunhofer IRB Verlag, Stuttgart, 1998, 61-91.
- [9] Drever, J. I., The geochemistry of natural waters, Prentice Hall, N. J. 1988.
- [10] Bläuer, C., Verwitterung der Berner Sandsteine. Dissertation, Universität Bern, 1987.
- [11] Kloppmann, W., Bromblet, P., Vallet, J.M., Vergès-Belmin, V., Rolland, O., Guerrot, C., Gosselin, C., Building materials as intrinsic sources of sulphate: A hidden face of salt weathering of historical

- monuments investigated through multi-isotope tracing (B, O, S), *Science of the Total Environment* 409 (2011) 1658–1669.
- [12] Trümpy, R., *Zur Geologie des Münstertals (Val Müstair), Müstair, Kloster St. Johann, Sennhauser, H.R. (Ed), Naturwissenschaftliche Beiträge, vdf Hochschulverlag, Zürich, 4, 2007, 11-22.*
- [13] Bläuer, C., GR, Müstair, Heiligkreuzkapelle. Analysen von Mörtel und Malschichtproben, unpubl. report CSC Sàrl, Fribourg, 2013.
- [14] Arnold, A., *Moderne alkalische Baustoffe und die Probleme bei der Konservierung von Denkmälern, Arbeitshefte des Bayerischen Landesamtes für Denkmalpflege, (31), (1985), 152-162.*
- [15] Tetmajer, L., *Ueber Mauer- und Cementarbeiten bei niedrigen Temperaturen, Schweizerische Bauzeitung, (23/24), (1894), 136+137 / 142-144 / 151-154.*
- [16] Rosvall, J. [Ed.], *Air Pollution and Conservation. Safeguarding Our Architectural Heritage, Swedish Institute of Classical Studies in Rome, Department of Conservation, University of Göteborg, 1986.*
- [17] Voelcker, A., *On the injurious effects of smoke on certain building stones and on vegetation, J. Royal Soc. Arts, (12), (1864), 146-151.*
- [18] Swiss Federal office for the Environment, *Graphics of annual values NABEL: Sulfur dioxide.*
http://www.bafu.admin.ch/luft/luftbelastung/blick_zurueck/01693/09016/index.html?lang=en ; 10.5.2014
- [19] <http://aqicn.org/map/world/> ; 14.5.2014
- [20] Künzel, H., *Bauphysik und Denkmalpflege. Fraunhofer IRB Verlag, Stuttgart, 2007.*
- [21] Saskatchewan Soil Conservation Association, *Soil Facts. Solid Cattle Manure.*
http://www.soilcc.ca/ggmp_fact_sheets/pdf/Cattle%20manure.pdf ; 2.3.2014
- [22] Römpp, electronic edition, Harn.
<https://roempp.thieme.de/roempp4.0/do/data/RD-08-00423>
11.5.2014
- [23] Whitworth, T. A., George, M. C., *A note on a curious effect observed in Durham Cathedral, Durham University Journal, LXII, (1970), 172-176.*

- [24] Bläuer Böhm, C., Technologische Fragestellungen bei der Ruinenerhaltung. Das Beispiel der Burgruine Belfort, Brienz/Brinzauls GR. Gesicherte Ruine oder ruinierte Burg? Erhalten-Instandstellen-Nutzen. Schweizer Beiträge zur Kulturgeschichte und Archäologie des Mittelalters, (31), (2005), 129-144.
- [25] Treml, M. H., Salz Macht Geschichte, Bayerische Staatskanzlei, Veröffentl. zur Bayer. Geschichte und Kultur, 30, Augsburg, 1995.
- [26] Washburn, E. R., The Creeping of Solutions, J. Phys. Chem., 31 (8), (1927), 1246–1248.
- [27] Enckevort, W. J. P. van, Los, J. H., On the Creeping of Saturated Salt Solutions. Crystal Growth & Design 13 (5), (2013), 1838–1848.
- [28] Bläuer, C., BE, Bern, Burgerbibliothek, Gewölbekeller, Salzanalysen und Massnahmenempfehlungen, unpubl. report CSC Sàrl, Fribourg, 2014.
- [29] http://en.wikipedia.org/wiki/Tanning#Vegetable_tanning ; 20.4.2014.
- [30] Fischer, F. Ueber die Herstellung von Eis. Dingler's Polytechnisches Journal, Band 224, (1877), 165–174.
<http://dingler.culture.hu-berlin.de/article/pj224/ar224040> ; 5.5.2014
- [31] Blume, R., Wiechoczek, D., Mit Kältemischungen gibt es auch im Sommer Eis, 2010.
http://www.chemieunterricht.de/dc2/tip/08_98.htm ; 14.4.2014
- [32] Gartiser, S., Reuther, R., Gensch, C.-O., Machbarkeitsstudie zur Formulierung von Anforderungen für ein neues Umweltzeichen für Enteisungsmittel für Strassen und Wege, in Anlehnung an DIN EN ISO 14024; Ed. Umweltbundesamt, Berlin, 2003.
<http://www.umweltbundesamt.de/sites/default/files/medien/publikation/long/2230.pdf> 14.11.2013
- [33] Bläuer, C., Rousset, B., BE, Münsingen, Mosaïques romaines, Analyses de sels, unpubl. report CSC Sàrl, Fribourg, 2007.
- [34] LeConte, J., Instructions for the Manufacture of Saltpetre, Columbia, S.C., Charles P. Pelham, State Printer, 1862.
<http://docsouth.unc.edu/imls/lecontesalt/leconte.html> ; 5.5.2014
- [35] Anonymous, Gesetze, Dekrete und Verordnungen des Kantons Bern. Bey Wittwe Stämpfli in der obrigkeitlichen Buchdruckerey,

- Vol.4, 1813. <http://retro.seals.ch/digbib/view?lp=120&rid=gdv-001%3A1813%3A4%3A%3A397&Submit=ok> ; 4.4.2014
- [36] Christ, A., Der Einsatz von Wasserglas in der Konservierung von Wandmalereien. Untersuchungen an ausgesuchten Beispielen des Rheinlandes, Zeitschrift für Kunsttechnologie und Konservierung, 1994, 1, 25-77.
- [37] Lithiumwasserglas, Verfestigungsmittel für mineralische Schichten. http://www.kremer-pigmente.com/media/files_public/31402.pdf; 10.5.2014
- [38] Bläuer, C., GR, Chur, St. Stephan, Sarkophag, Salzanalysen, unpubl. report CSC Sàrl, Fribourg, 2009.
- [39] Bläuer, C., SH, Schaffhausen, Allerheiligen, Johanneskapelle, Materialanalysen, unpubl. report CSC Sàrl, Fribourg, 2014.
- [40] Arnold, A., Zehnder, K., Verwitterungsschäden durch Ameisensäure. Eine Fallstudie am Erlacherhof in Bern. Schweizer Ingenieur und Architekt, (36), (1983), 841-845.
- [41] Amoroso, G. G., Fassina, V., Stone decay and conservation. Atmospheric pollution, cleaning, consolidation and protection, Elsevier, Amsterdam - Lausanne - Oxford - New York, 1983.
- [42] Pagenstecher, Über die Erzeugung des Salpeters im Sandsteine und ein geeignetes Mittel, denselben daraus zu entfernen, Mitt. natf. Ges. Bern, (1845), 101-105.
- [43] Naidu, S., Sassoni, E., Scherer, G. W., New treatment for corrosion-resistant coatings for marble and consolidation of limestone, in Jardin de Pierres, SFIC, Champs-sur-Marne, 2011, 289-294.
- [44] Sassoni, E., Naidu, S., Scherer, G. W., The use of hydroxyapatite as a new inorganic consolidant for damaged carbonate stones, Journal of Cultural Heritage, (12), (2011), 346–355.
- [45] Matteini, M., In review: an assessment of Florentine methods of wall painting conservation based on the use of mineral treatments, Proc. Symp. Courtauld Inst. of Art and Getty Conservation Inst., London, July 13-16, 1987, The Getty Conservation Institute, 1991, 137-148.
- [46] Tetmajer, L., Ueber Conservirung und Erhärtung des Ostermündiger Sandsteins, Schweizerische Bauzeitung, (19/20), (1892), 51-52.

- [47] Farrak, H., Steinkonservierung vor 100 Jahren. Untersuchungen zu Steinbehandlungen in Sachsen um 1900, *Restauro*, (5), (2001), 352-358.
- [48] Schad, J., Brüggerhoff, S., Kettelhack, C., Die Renaissance-Fassade des Lübecker Rathauses - Untersuchungen und Testmassnahmen zur Erhaltung des Naturstein-Inventars, *Denkmalpflege und Naturwissenschaft - Natursteinkonservierung II*, Snethlage, R. (Ed.), Fraunhofer IRB Verlag, Stuttgart, 1998, 229-269.
- [49] Steiger, M., Neumann, H. H., Wittenburg, C., Behlen, A., Schmolke, S., Stoffregen, J., et al., Sandsteinverwitterung in schadstoffbelasteter Atmosphäre am Beispiel des Erfurter Doms, *Jahresber. a. d. Forschungsprogr. Steinerfall-Steinkonservierung*, (4), (1994), 215-243.
- [50] Visser, H., Steinerfall am Leineschloss in Hannover. Teil 1: Untersuchung der Schäden und Schadensursachen im Forschungsverbund des BMFT-Projektes, *Jahresberichte aus dem Forschungsprogramm Steinerfall – Steinkonservierung*, (2), (1992), 381-399.
- [51] Bläuer, C., BE, Bern, Muenster, Historische Konservierungen und Salze, unpubl. report CSC Sàrl, Fribourg, 2013.

SWBSS2014

3rd International Conference on Salt Weathering of Buildings and Stone Sculptures
14-16 October 2014

Salt crystallization resistance of nano-modified repair lime mortars

M. Theodoridou*, L. Kyriakou and I. Ioannou

Department of Civil and Environmental Engineering, University of Cyprus, Nicosia, Cyprus

*mtheodo@ucy.ac.cy

Abstract

This paper describes the results of the application of nano-binders (SiO₂ and TiO₂) in repair lime mortars, focusing on the durability of the composites against salt crystallization. A total of 12 new mixtures have been designed, produced and investigated in the laboratory, in an effort to produce durable, environmentally friendly, energy-efficient, sustainable composites, primarily for conservation purposes but also for contemporary applications. The effect of different aggregates and binders on the end-product was also investigated using a combination of physico-mechanical tests and analytical experimental techniques (e.g. MIP, capillary absorption, flexural and compressive strength tests). The results show that the use of nano-binders generally enhances the mechanical properties of lime mortars, without significantly affecting their pore structure. They also suggest that nanosilica enhances the durability of aerial lime mortars, while nanotitania significantly improves the resistance of hydraulic lime mortars subjected to salt weathering by full immersion. Nevertheless, attention should be drawn to the development of a standardized salt crystallization test methodology, which would be more appropriate for relatively weak masonry materials, such as lime mortars.

Keywords: lime, mortars, nanosilica, nanotitania, salt crystallization

1 Introduction

In the field of tangible heritage conservation, the use of compatible, yet durable, restoration materials is of utmost importance, in order to prevent further irreversible damage on monuments and art objects that have survived over the centuries [e.g. 1-2]. Despite the fact that traditional cementless mortars (e.g. lime-based mortars) are generally weaker in mechanical performance, when compared to most of the modern cement-based composites, their physical properties, such as their relatively high permeability and flexibility, can significantly benefit the durability of the masonry [3]. Nevertheless, since deterioration primarily affects the weakest materials in a structure, mortars are usually much more prone to weathering damage than other masonry materials; therefore relevant durability studies should be thoroughly carried out before any application of repair mortars whatsoever. With salt crystallization being widely considered as one of the most important weathering factors in the field of porous materials [4], the resistance of repair mortars to salt damage is vital. This paper presents ongoing research on the effects of selected nano-materials (SiO_2 and TiO_2) in the performance of lime-based composites. At the same time, it investigates the influence of two different aggregates and lime binders on the nano-modified end-products and it focuses on their durability against salt weathering.

1.1 The use of nanosilica and nanotitania in construction materials

The application of nanotechnology in the field of construction materials has resulted in significant improvements in recent years. Existing relevant literature mainly focuses on cementitious composites. The use of nanosilica, in particular, in concrete, cement mortars and pastes, has been widely investigated [e.g. 5-8]. Well-dispersed silica nanoparticles have been found to accelerate the hydration process and enhance pozzolanic activity. Moreover, nanosilica improves the materials microstructure by providing a more homogeneous, denser and compact structure. Hence, it may lead to materials with higher compressive strength and lower porosity. Despite the relatively broad research on the use of nanosilica in cement-based composites, this additive has only recently been tested in lime-based materials [9-10]. In these cases, the addition of nanosilica dramatically changed the mesopores distribution, causing a decrease of pores in the range of 20-100 nm and a rise of gel pores (<10 nm). The nano-sized particles also provided a large reactive total surface that led to

the formation of Calcium Silicate Hydrate (C-S-H), thus accelerating the hydration process and the “filling” effect [11]. At the same time, the reduction of the mean pore size and porosity improved the mechanical properties of the composites. Nanotitania, on the other hand, has recently been used as an additive in cementitious mixtures, mostly due to its photocatalytic properties. It is considered an efficient and environmentally friendly photoactive material due to its non-toxic nature and ability to oxidize organic pollutants, producing harmless end-products [12]. Therefore, it has been used in the production of self-cleaning materials, which reduce structural maintenance costs [13]. Although significant research regarding the effects of nanotitania in cement-based composites has been published already, only very limited relative scientific data exists in the field of lime binders [14-15]. Yet, the results are promising and show an increase in the compressive and flexural strengths of the materials, while they also prove the enhancement of their elastic modulus over time. Acceleration of carbonation and hydration has also been noticed due to the addition of nanotitania in lime-based mixtures. Experimental data regarding the durability of optimized composites, after the addition of nanosilica and nanotitania, against different weathering phenomena, and in particular salt attack, are rather limited, even in the case of cement-based materials. However the results published so far regarding artificial weathering laboratory tests indicate the high potential of such additives. Frost resistance of concrete mixtures has been considerably improved by the addition of nano-SiO₂, which behaved not only as a promoter of the pozzolanic reaction but also as a filler, thus improving the pore structure and densifying the microstructure of the material [16]. A study on High Performance Concrete (HPC) mixtures, modified with different amounts of nanosilica, showed an increase in their freeze-thaw resistance [17-18], while improvement of the dynamic elastic modulus of frost-weathered HPC samples has also been reported [18]. Similar tests on air lime mortars have recently shown that the addition of nanosilica gives rise to more resistant composites [19]. Nanosilica has also been used as a potential additive for enhancing the properties of concrete in terms of salt resistance. The formation of a denser structure limited the transport of sodium sulphate ions and their subsequent reaction with Ca(OH)₂ [20]. Other studies showed that, when cement paste with added nanosilica was kept in sulphate solution for 180 days, less reduction in its compressive strength was observed, compared to the reference mixture [21]. Regarding the salt resistance of lime-based composites, very limited published data exists; this is, however, encouraging and shows that the presence of large amounts of nanosilica improves the durability of air lime mortars by delaying the decay evolution of magnesium sulphate solution

[19]. To the best of the authors' knowledge, no relevant results have been published regarding the effect of nanotitania.

The present study aims at expanding current knowledge on the effects of nanosilica and nanotitania on the salt crystallization resistance of lime-based mortars, thus triggering further research on this subject. Due to the lack of a suitable standardized methodology to study the salt weathering phenomenon on mortars under laboratory conditions, this attempt adopted the concept of full immersion in sodium sulphate solution and subsequent drying. It should be noted that this test is considered to be excessively aggressive and inconsistent with what occurs in the natural built environment, let alone the fact that it has been performed on relatively weak materials such as lime mortars. An alternative to the full immersion test could be considered the "Continuous Partial Immersion Test" that was firstly introduced by Lewin in 1982 [22]. This procedure lets the solution to be absorbed by capillarity forces and allows the water to evaporate naturally, leaving the salt ions behind [23]. Many scientists used this method [22-24], since they consider it beneficial over other methodologies, due to the fact that the results for different specimens and salt combinations can easily be compared. However, no standardized procedure exists for this method either.

2 Materials and experimental procedure

2.1 Design of mortars

Two different types of binder were used for the production of the nano-modified mortars: aerial lime (A: CL80 by Hellenic Mining Public Co.) and natural hydraulic lime (H: NHL 3.5 by Lafarge). 3% of the lime binder was occasionally replaced by either nanosilica (nSi: Submicron Silica 995, 993 by Elkem) or nanotitania (nTi: Aeroxide[®] TiO₂ P25 by Evonik Industries). Crushed local calcareous sands from Mitsero (M), derived from an extensively recrystallized reef limestone, and Potamia-Latouros (L), originating from a clastic limestone consisting of grains cemented with a calcite matrix, were also used in the mixtures [25]. The binder to aggregates ratio (B:A) was kept constant at 1:3, since this has been found to be the prevalent ratio in ancient lime mortars both in Cyprus and in other areas of the world [26-27]. The quantity of water required for every mixture was estimated based on a constant workability of 165±5 mm; the water to binder ratios (W:B) for the 12 different mortar mixtures produced in the laboratory are given in Table 1, together with the rest of mix design details. All quantities given in this table were measured by mass.

Table 1: Mix design, expressed in mass, of laboratory produced mortars. M: Mitsero sand, L: Potamia-Latouros sand, A: Aerial lime, H: Hydraulic lime, nSi: nanosilica, nTi: nanotitania

Mixture	Aggregates		Binder				Workability (mm)	B:A	W:B
			Lime		Additive				
	M	L	A	H	nSi	nTi			
MA	3		1				167.81	1:3	0.99
LA		3	1				163.41	1:3	0.91
MAnSi	3		0.97		0.03		167.73	1:3	1.04
LAnSi		3	0.97		0.03		166.05	1:3	0.92
MAnTi	3		0.97			0.03	160.85	1:3	1.00
LAnTi		3	0.97			0.03	162.67	1:3	0.92
MH	3			1			163.80	1:3	0.94
LH		3		1			160.30	1:3	0.84
MHnSi	3			0.97	0.03		162.16	1:3	0.96
LHnSi		3		0.97	0.03		166.15	1:3	0.86
MHnTi	3			0.97		0.03	161.93	1:3	0.96
LHnTi		3		0.97		0.03	160.68	1:3	0.84

2.2 Testing methodology

2.2.1 Physical and mechanical properties

In order to characterize both the physical and the mechanical behaviour of the mortars, several conventional laboratory tests were carried out and various analytical techniques were used, at different time intervals after the day of casting. In this paper, we present results recorded 180 days after the production day of each mixture. Open porosity (p_o) and apparent density (p_a) were measured on prismatic specimens (40x40x160 mm) by vacuum saturation, using water as the wetting liquid. Water capillary absorption (s) was also measured on the same specimens. Additionally, porosimetric analyses (e.g. open porosity, apparent density, average pore size, pore size distribution) were carried out on bulk samples using Mercury Intrusion Porosimetry (MIP). Prismatic specimens (40x40x160 mm) were also tested under flexural load (three point bending); the

materials mean flexural strength (FS) was estimated using the results from three specimens. The mean uniaxial compressive strength (UCS) of each mixture was also measured based on the results of six cubic test specimens (40x40x40 mm).

2.2.2 Salt crystallization resistance

In order to evaluate the durability of each mortar mixture against salt crystallization, artificial weathering was performed under controlled laboratory conditions. For the purposes of this test, cubic specimens (40x40x40 mm) were subjected to a maximum of 15 wetting and drying cycles using a 10% w/w aqueous solution of Na₂SO₄. The test for each mixture began 180 days after casting. During the wetting cycle, the specimens were fully immersed in the salt solution at 20 °C for two hours. After that, they were put in an oven at 105 ± 5 °C for at least 16 hours. In order to estimate the durability of each specimen after each crystallization cycle, two parameters were considered: a) qualitative evaluation based on visual inspection and b) quantitative evaluation based on percentage loss in mass. For the purposes of the qualitative evaluation, the specimens were macroscopically investigated and their condition was “scored”, following a five-level scale which is described in Table 2.

Table 2: Scale for visual inspection of the materials resistance to salt weathering.

Score	Description
Perfect	<i>Specimen intact</i>
Good	<i>Very minor damage or minor cracks</i>
Moderate	<i>Rounding of corners and several cracks or detachment of small fragments</i>
Bad	<i>Specimen with several major cracks or broken</i>
Fail	<i>Specimen in pieces or disintegrated</i>

3 Results and discussion

The results of the physico-mechanical characterization of the 12 laboratory mixtures carried out 180 days after the production day are summarized in Table 3.

Table 3: Physico-mechanical properties of the laboratory mortars. Values in brackets represent standard deviations of the calculated mean values. p_o : open porosity, p_a : apparent density, s : water capillary absorption, FS: flexural strength, UCS: uniaxial compressive strength. See Table 1 for sample abbreviations.

Sample	p_o		p_a		Av. pore size	s	FS	UCS
	(%)		(kg/m^3)		(nm)	$(\text{mm/min}^{1/2})$	(MPa)	
	Under vacuum	MIP	Under vacuum	MIP	MIP			
MA	32.3	30.4	1766	1579	288.4	0.28	0.91 (0.05)	3.5 (0.1)
LA	30.9	27.0	1802	1669	279.1	0.88	0.95 (0.02)	3.5 (0.1)
MAnSi	30.3	29.1	1758	1687	199.0	1.68	1.21 (0.07)	5.3 (0.1)
LAnSi	30.8	25.5	1777	1740	197.5	1.34	1.37 (0.11)	6.1 (0.2)
MAnTi	32.2	28.6	1749	1775	327.0	0.64	0.75 (0.04)	3.4 (0.1)
LAnTi	30.5	27.2	1776	1706	264.4	1.08	1.00 (0.07)	3.5 (0.1)
MH	35.1	29.0	1687	1790	32.7	0.88	1.66 (0.06)	7.3 (0.1)
LH	30.7	29.0	1704	1870	34.5	0.10	1.88 (0.08)	7.7 (0.1)
MHnSi	35.7	30.7	1679	2024	33.7	0.07	2.31 (0.09)	8.6 (0.4)
LHnSi	34.4	31.4	1701	2020	34.2	0.17	2.50 (0.14)	9.9 (0.2)
MHnTi	35.7	32.8	1671	1792	36.6	0.57	1.70 (0.06)	6.5 (0.1)
LHnTi	33.6	31.6	1717	1892	34.1	0.38	1.96 (0.07)	8.0 (0.1)

Higher flexural and mechanical strengths are attributed to the use of Latouros sand and hydraulic lime. Significant strength increases were also noticed in all mixtures where nanosilica was added, irrespective of the binder and aggregate type. Less significant improvements were observed with the addition of nanotitania to mixtures with Latouros sand, while decreases in strength were recorded in some cases where nanotitania was added to mixtures cast using Mitsero sand. It is worth noting that Latouros sand is much finer (0-2 mm) than the recrystallized Mitsero sand (0-4 mm). The latter also has a much different mineralogical composition, as it only consists of calcite and dolomite. The systematically lower porosity values given by MIP may be attributed either to the samples' highly tortuous pore network, which does not allow mercury to fully intrude them [28], or to the fact that the size of some pores may be outside the range (360-0.003 mm) which can be detected by the MIP system [29-31]. Generally, lower porosity values were observed when Latouros sand was used. The addition of nanosilica or nanotitania to aerial lime mortars also led to a decrease in open porosity and average pore size; the opposite trend was noticed in the case of hydraulic mortars. Lower porosity was surprisingly observed in most of the aerial lime mixtures, compared to the hydraulic ones. The latter could be considered rather misleading and can possibly be explained by carbonation effects on the external surfaces of the samples. With regards to the capillary absorption results, the addition of nanotitania seems to have led to significantly reduced (over 160%) sorptivity values in the case of aerial mortars (compared to the addition of nanosilica); the opposite applies to hydraulic mixtures. It is also worth mentioning that, despite the changes in the physical property values observed before and after the addition of nano-binders, the mode of pore size distributions and the intensity of peaks recorded by MIP for the relevant mixtures do not show any significant changes (see Figure 1). The positive effect of the nano-binders is also apparent in the qualitative and quantitative evaluation of the samples subjected to salt crystallization tests (Figures 2 and 3). For example, even though the reference mixture LH has survived the test, the addition of nanotitania significantly improved the quality of the specimens, which in this case scored "Perfect" (intact material) even at the end of the 15th cycle. The better performance of Latouros mixtures is obvious when comparing the qualitative salt crystallization test results of all five surviving mixtures. The latter was also clear in the case of reference mixtures (MA & LA, MH & LH).

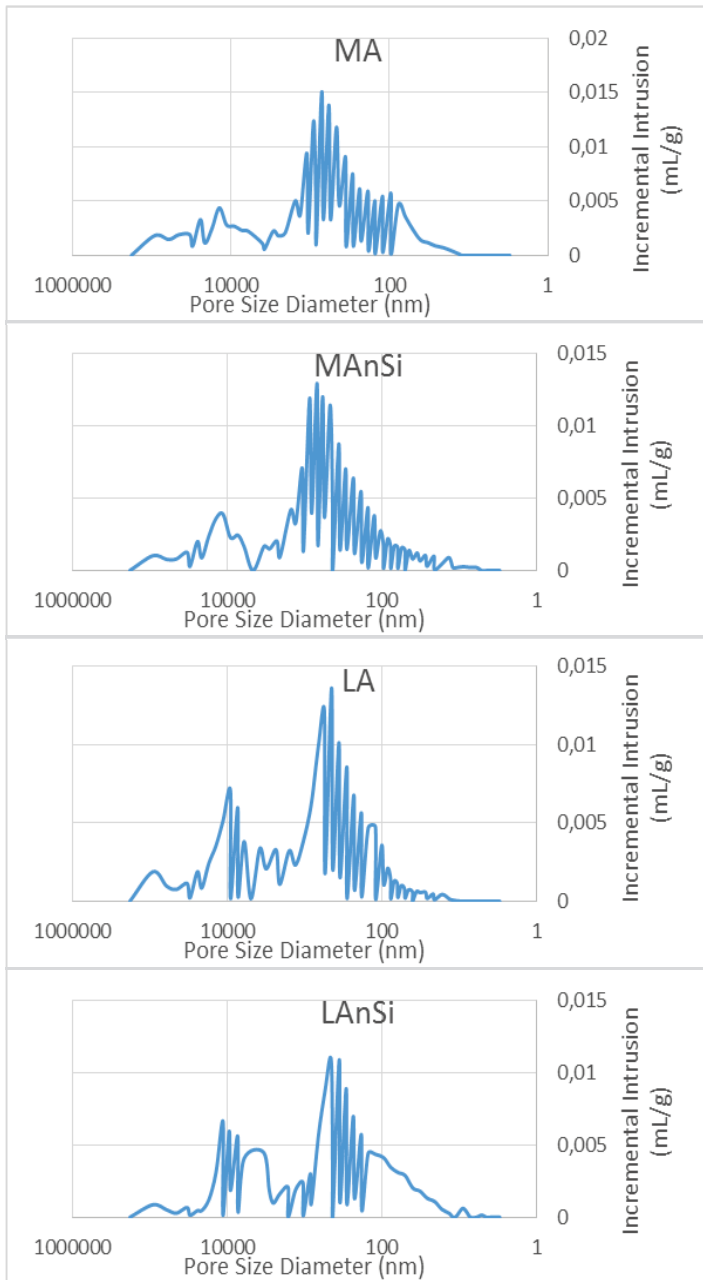


Figure 1: Indicative pore size distributions (see Table 1 for sample abbreviations).

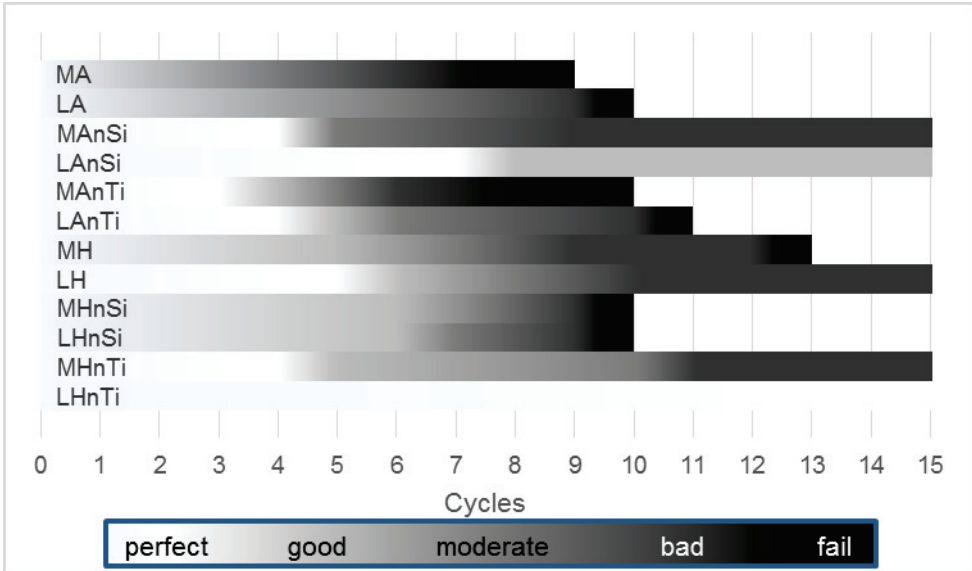


Figure 2: Qualitative evaluation of salt resistance by visual inspection of mortar mixtures. For explanation on the scale used see Table 2, while for sample abbreviations see Table 1.

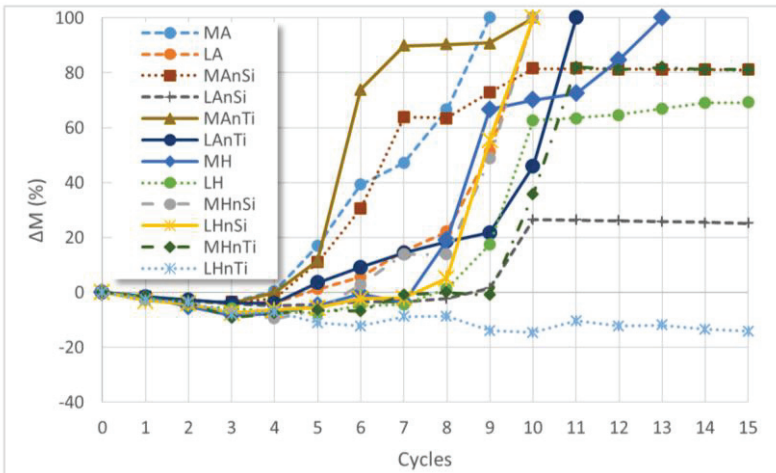


Figure 3: Weight loss (ΔM) of specimens after salt crystallization cycles (see Table 1 for sample abbreviations).

Quantitatively, the better durability results also corresponded to the mixtures with Latouros sand. This was found to be in agreement with the materials' relevant strengths and it can be attributed to the aggregate's finer particles, as well as to its mineralogical composition and in particular to the presence of significant amounts of hard minerals, such as silicates [25]. Only five mixtures survived the 15 cycles of artificial salt weathering test (MAnSi, LAnSi, LH, MHnTi and LHnTi). Irrespective of the aggregate type, nanosilica addition highly improved the performance of aerial lime mixtures, while nanotitania significantly enhanced the resistance of the two nano-modified hydraulic mixtures. The considerably positive effect of nanotitania on the durability of hydraulic lime mortars could be attributed to its known potential in enhancing the formation of hydraulic phases in the mixtures, which is in turn the result of its highly hydrophilic nature [15]. Complimentary thermal analyses of the same mixtures (not shown here) support this conclusion, while ongoing FTIR measurements aim to confirm the results achieved. Despite the fact that the addition of nanotitania in aerial lime mortars did not contribute to the successful accomplishment of the salt crystallization test, improvement of durability was nevertheless noticed, compared to the reference mixtures. Last but not least, lower amount of mass loss was generally noted in the case of hydraulic mortars (MHnSi & LHnTi), while the negative value of LHnTi could be attributed to insignificant loss of material and simultaneous accumulation of salt crystals in the pore structure of the specimens.

4 Conclusions

Generally higher strengths and better resistance to salt weathering were observed in the cases of mortars with Latouros sand. This can be attributed to the finer particle size distribution of this aggregate and to its mineralogical composition. Significant improvements of the materials' strengths were also noted when nanosilica was added in the mixtures. Less noticeable changes in strength, at the time interval of 180 days after the day of production, corresponded to the addition of nanotitania. Further testing at longer time intervals is needed to investigate this finding. The modifications of several physical property values due to the addition of nanomaterials did not lead to any noticeable change in the pore size distribution of the mixtures. The most durable aerial lime mortar samples in terms of salt resistance were found to be the mixtures with nanosilica additive; the use of nanotitania, on the other hand, proved to be efficient in the enhancement of the durability of hydraulic lime mortars. These findings are considered encouraging for meeting the goals of this ongoing

project, while further research is needed in the case of nanosilica addition to hydraulic lime binder. Despite the positive outcomes of this research, the selected methodology which was followed in order to test the durability of laboratory lime mortars against salt attack is considered highly aggressive; for this reason, most of the mixtures could not reach the end of the test. Visual inspection highly contributed to a better evaluation of the materials performance. Nevertheless, attention should be urgently drawn to the need for a standardized experimental approach, which would be more appropriate in the case of relatively weaker masonry materials, such as lime mortars, and could enable the comparison of results at an international level.

Acknowledgements

This research was partially carried out in the premises of Ledra Laboratory which was funded by the European Regional Development Fund and the Republic of Cyprus, through the Research Promotion Foundation (Project NEA ΥΠΟΔΟΜΗ/NEΚΥΠ/0308/17).

References

- [1] P. Maravelaki-Kalaitzaki, A. Bakolas, A. Moropoulou, Physico-chemical study of Cretan ancient mortars, *Cement and Concrete Research*, (33), (2003), 651-661.
- [2] B. Szemerey-Kiss, Á. Török, Time-dependent changes in the strength of repair mortar used in the loss compensation of stone. *Environmental Earth Sciences* (63), (2011), 1613-1621.
- [3] I. Brocklebank, *Building Limes in Conservation*, Donhead, UK 2012.
- [4] M. Steiger, Crystal growth in porous materials – II: Influence of crystal size on the crystallization pressure, *Journal of Crystal Growth*, (282), (2005), 470-481.
- [5] L.P. Singh, S.R. Karade, S.K. Bhattacharyya, M.M. Yousuf, S. Ahalawat, Beneficial role of nanosilica in cement based materials – A review, *Construction and Building Materials*, (47), (2013), 1069-1077.
- [6] M. Berra, F. Carassiti, T. Mangialardi, A.E. Paolini, M. Sebastiani, Effects of nanosilica addition on workability and compressive

- strength of Portland cement pastes, *Construction and Building Materials*, (35), (2012), 666-675.
- [7] S. Haruehansapong, T. Pulngern, S. Chucheeepsakul, Effect of the particle size of nanosilica on the compressive strength and the optimum replacement content of the cement mortar containing nano-SiO₂, *Construction and Building Materials*, (50), (2014), 471-477.
- [8] J.Y. Shih, T.P. Chang, T.C. Hsiao, Effect of nanosilica on characterization of Portland cement composite, *Materials Science and Engineering A*, (424), (2006), 266-274.
- [9] J.I. Alvarez, J.M. Fernández, I. Navarro-Blasco, A. Duran, R. Siera, Microstructural consequences of nanosilica addition on aerial lime binding materials: Influence of different drying conditions, *Materials Characterization*, (80), (2013), 36-49.
- [10] J.M. Fernández, A. Duran, I. Navarro-Blasco, J.Lanas, R.Siera, J.I. Alvarez, Influence of nanosilica and a polycarboxylate ether superplasticizer on the performance of lime mortars, *Cement and Concrete Research*, (43), (2013), 12-24.
- [11] A. Korpa, T. Kowland, R. Trettin, Hydration behavior, structure and morphology of hydration phases in advanced cement-based systems containing micro and nanoscale pozzolanic additives, *Cement and Concrete Research*, (38), (2008), 955-962.
- [12] M. Theodoridou, E. Charalambous, I. Ioannou, P. Maravelaki, Optimisation of repair lime-based composites using nano-binders, HMC2013 3rd Historic Mortars Conference, Glasgow 2013 (cd-rom).
- [13] M.V. Diamanti, M. Ormellese, M.P. Pedefferri, Characterization of photocatalytic and superhydrophilic properties of mortars containing titanium dioxide, *Cement and Concrete Research*, (38), (2008), 1349-1353.
- [14] I. Karatasios, M.S. Katsiotis, V. Likodimos, A.I. Kontos, G. Papavassiliou, P. Falaras, V. Kilikoglou, Photo-induced self-cleaning and carbonation of lime-TiO₂ mortars, *Applied Catalysis B*, (95), (2010), 78-86.
- [15] P. Maravelaki-Kalaitzaki, Z. Agioutantis, E. Lionakis, M. Stavroulaki, V. Perdikatsis, Physico-chemical and mechanical characterization of hydraulic mortars containing nano-titania for restoration applications, *Cement & Concrete Composites*, (36), (2013), 33-41.

- [16] K. Behfarnia, N. Salemi, The effects of nano-silica and nano-alumina on frost resistance of normal concrete, *Construction and Building Materials*, (48), (2013), 580-584.
- [17] Z. Peng, L. Chenhui, L. Qingfu, Application of gray relational analysis for chloride permeability and freeze-thaw resistance of high-performance concrete containing nanoparticles, *Journal of Materials in Civil Engineering*, (23), (2011), 1760-1763.
- [18] B. Wang, L. Wang, F.C. Lai, Freezing resistance of HPC with nano-SiO₂, *Journal of Wuhan University of Technology, Master. Sci. Ed.*, (23), (2008), 85-88.
- [19] A. Duran, I. Navarro-Blasco, J. M. Fernández, J. I. Alvarez, Long-term mechanical resistance and durability of air lime mortars with large additions of nanosilica, *Construction and Building Materials*, (58), (2014), 147-158.
- [20] J. Setina, A. Gabrene, I. Juhnevica, Effect of Pozzolanic Additives on Structure and Chemical Durability of Concrete, *Procedia Engineering*, (57), (2013), 1005-1012.
- [21] J.S. Dolado, I. Campillo, E. Erkizia, J.A. Ibáñez, A. Porro, A. Guerrero, S. Goñi, Effect of nanosilica additions on belite cement pastes held in sulfate solutions, *Journal of the American Ceramic Society*, (90), (2007), 3973-3976.
- [22] R. M. ESpinosa-Marzal, G. W. Scherer, Mechanisms of damage by salt, *Geological Society, Special Publications*, London 2010.
- [23] G. W. Scherer, Stress from crystallization of salt, *Cement and Concrete Research*, (34), (2004), 1613-1624.
- [24] T. Rivas, E. Alvarez, M. J. Mosquera, L. Alejano, J. Taboada, Crystallization modifiers applied in granite desalination: The role of the stone pore structure, *Construction and Building Materials*, (24), (2010), 766-776.
- [25] R. Fournari, I. Ioannou, D. Vatyliotis, A study of fine aggregate properties and their effect on the quality of cementitious composite materials, *IAEG XII Congress, Torino 2014*.
- [26] M. Theodoridou, I. Ioannou, M. Philokyprou, New evidence of early use of artificial pozzolanic material in mortars, *Journal of Archaeological Science*, (40), (2013), 3263-3269.

- [27] A. Moropoulou, A. Bakolas, S. Anagnostopoulou, Composite materials in ancient structures, *Cement & Concrete Composites*, (27), (2005), 295-300.
- [28] V. Cnudde, A. Wirzen, B. Masschaele, P.J.S. Jacobs, Porosity and micro-structure characterization of building stones and concretes, *Engineering Geology*, (103), (2009), 76-83.
- [29] M. Barsottelli, G.F. Cellai, F. Fratini, C. Manganelli Del fà, The hygrometric behavior of some artificial stone materials, *Materials and Structures* (34), (2001), 211-216.
- [30] M. Barsottelli, F. Fratini, G. Giorgetti, C.M. Manganelli Del Fà, Microfabric and alteration in the Carrara marble: a preliminary study, *Science and Technology for Cultural Heritage* (7, 2), (1998), 109-120.
- [31] M. Stefanidou, Methods for porosity measurement in lime-based mortars, *Construction and Building Materials* (24), (2010), 2571-2578.

Limestone resistance to sodium sulfate degradation after consolidation by hydroxyapatite and TEOS

E. Sassoni*, E. Franzoni, G. Graziani and F. Sagripanti

Department of Civil, Chemical, Environmental and Materials Engineering (DICAM), University of Bologna, Bologna, Italy

* enrico.sassoni2@unibo.it

Abstract

The use of aqueous phosphate solutions to produce hydroxyapatite (HAP) inside weathered carbonate stones has recently been proposed as a new consolidating technique. In this paper, the resistance of HAP-treated stone to soluble salt crystallization was investigated. Globigerina limestone, a porous stone typically used in historic architecture in Malta and often severely affected by salt crystallization, was used. After preliminary artificial weathering by heating at 400 °C for 1 hour, aimed at producing micro-cracks opening in the stone, cylindrical samples (5 cm height, 2 cm diameter) were treated by brushing application of a 3 M aqueous solution of diammonium hydrogen phosphate, followed by application of a limewater-impregnated poultice. For comparison's sake, a similar set of samples was treated with a commercial TEOS-based product, while a third set was left untreated. After proper curing, HAP- and TEOS-treated samples, together with untreated ones, were subjected to sodium sulfate crystallization cycles, by partial immersion in a 14 wt% sodium sulfate decahydrate solution for 7 hours and then drying at 50 °C for 15 hours. After each cycle, damage evolution was monitored by visual assessment and weight measurement. Five cycles were carried out in total. From the results of the study, the performance of the novel phosphate treatment can be regarded as promising, as HAP-treated samples exhibited less micro-cracking and lower mechanical damage than untreated and also TEOS-treated samples.

Keywords: ammonium phosphate, inorganic consolidants, pore size distribution, calcite, ethyl silicate

1 Introduction

Limestone consolidation is still a very challenging task, as a commercial product that satisfies all the requirements that consolidants must meet [1] does not currently exist. In fact, the available treatments exhibit significant limitations when applied to carbonate stones, with regard to their effectiveness (e.g., nano-limes and silicate consolidants), compatibility (e.g., silicate and polymeric consolidants) and/or durability (e.g., polymeric consolidants) [2, 3].

To overcome such limitations, the use of aqueous phosphate solutions to produce hydroxyapatite (HAP) inside weathered carbonate stones has recently been proposed [3]. The idea is that HAP can be formed directly inside the stone, as the reaction product between the phosphate solution and the calcitic substrate, so that cohesion between grains can be restored and mechanical properties can be improved [3]. The HAP-treatment has been found to provide a remarkable consolidating action, leaving the total porosity of treated stone substantially unaltered and preserving stone hydrophilic behavior [3-5]. According to results obtained so far, the effectiveness and compatibility requirements can hence be considered as fairly satisfied.

With regard to the durability requirement, preliminary tests have shown a good resistance of HAP-treated stones to wetting-drying cycles [3] and some mitigating effect towards thermal weathering [6]. However, no specific study aimed at evaluating resistance to salt crystallization, which is one of the main causes of limestone deterioration in the field, has been reported so far. The importance of evaluating the resistance to salt damage further derives from the fact that HAP formation has been found to cause a slight shift of pore size distribution towards smaller pores [3, 7], which may eventually increase the susceptibility of treated stone to salt crystallization.

Therefore, in this paper a preliminary evaluation of the durability of HAP-treated limestone to salt crystallization was carried out, by means of accelerated sodium sulphate crystallization cycles in laboratory conditions. Moreover, the HAP performance was compared with that of TEOS, which is currently the most frequently used consolidant for carbonate stones in the on-site practice (notwithstanding its reduced efficacy on this kind of substrate), basically because of the lack of more suitable alternatives.

2 Materials and methods

2.1 Stone

Globigerina limestone from Malta was used for the experimental tests. This lithotype is often severely affected by salt crystallization, especially sodium chloride and sodium sulphate coming from marine aerosol and rising damp

from the ground [8]. From a slab provided by Xelini Skip Hire and High-Up Service (Malta), cylindrical samples (5 cm height, 2 cm diameter) were core-drilled perpendicular to stone bedding planes.

Before consolidant application, the stone was artificially weathered by heating at 400 °C for 1 hour, according to a methodology previously developed by the authors [9]. Salt crystallization cycles could have been alternatively used for artificial weathering (they are actually the main cause of on-site deterioration of Globigerina limestone), but in the present study thermal weathering was preferred, because applying DAP on salt-contaminated samples would have made the effects of the treatment too hard to be assessed, at this stage of research on HAP.

An application procedure consistent with those usually followed in the field was chosen. For each consolidant six samples were treated by brushing 10 times on the whole external surface. Six samples were left untreated for comparison.

2.2 Hydroxyapatite-based treatment

The procedure recently proposed in [7] was followed. Firstly, a 3.0 M aqueous solution of diammonium hydrogen phosphate (DAP) was applied by brushing and then left to react for 48 hours, evaporation being impeded by sample wrapping in a plastic film. Then, after drying, samples were treated with a poultice, prepared by mixing dry cellulose pulp and limewater with a weight ratio of 1:6. After 24 hours of poultice application and wrapping in a plastic film, samples were finally left to dry in contact with the poultice until constant weight.

2.3 TEOS-based treatment

A commercial product, composed of 75 wt% ethyl silicate oligomers (also containing 1% dibutyltin dilaurate as catalyst) and 25 wt% White Spirit D40 (ESTEL 1000 by CTS s.r.l., Italy), was applied by brushing.

The samples were then left to cure in laboratory conditions ($T=20\pm 2$ °C, $RH=50\pm 5\%$) for 1 month. Even if this period is usually reported in commercial products technical data sheet as sufficient for TEOS hydrolysis-condensation reactions to be completed, TEOS-treated stone may exhibit hydrophobic behaviour for additional several months [2]. This may significantly alter the evaluation of TEOS-treated stone durability to salt crystallization, as stone temporary hydrophobicity hinders the salt solution ingress into the stone. For this reason, after 1 month curing in room conditions, TEOS hydrophobicity was eliminated according to a recently proposed novel methodology, which consists in boosting the curing reactions of ethyl silicate by water poulticing [10].

2.4 Salt crystallization cycles

A 14 wt% solution of sodium sulphate decahydrate and deionized water was used. According to the methodology reported in [11], each cycle consisted in: (i) sample impregnation by partial immersion in the salt solution for about 5 mm and soaking for 7 hours; (ii) drying at 50 °C for 15 hours; (iii) cooling to room temperature for 2 hours. In total, 5 cycles were carried out.

2.5 Characterization techniques

The mechanical effects of the consolidating treatments were evaluated in terms of dynamic elastic modulus (E_d , measured on cylindrical samples before and after consolidation by an ultrasonic instrument with 55 kHz transducers) and tensile strength (σ_t , measured by Brazilian splitting test on the same cylindrical samples as above). The microstructural alterations induced by the treatments were evaluated by mercury intrusion porosimetry (MIP), using a Porosimeter 2000 Carlo Erba with a Fisons Macropore Unit 120. Water sorptivity and water absorption after treatment (and after accelerated curing, in the case of TEOS) were determined on cylindrical samples subjected to capillary absorption for 24 hours, in the conditions described in EN 15801.

The effects of salt crystallization cycles were firstly evaluated by visually inspecting the samples and monitoring their weight after each cycle. Then, after the fifth cycle, for each condition two samples were taken by chisel (to avoid salt washing away by wet sawing) from the positions indicated in Figure 1. The two samples were: (i) a lower sample, coming from the bottom part of the cylinder directly immersed in the salt solution (labeled as "1") and (ii) an upper sample, coming from the top of the cylinder (labeled as "2"). During samples collection, particular care was given to avoiding the external surface, where efflorescences had grown.

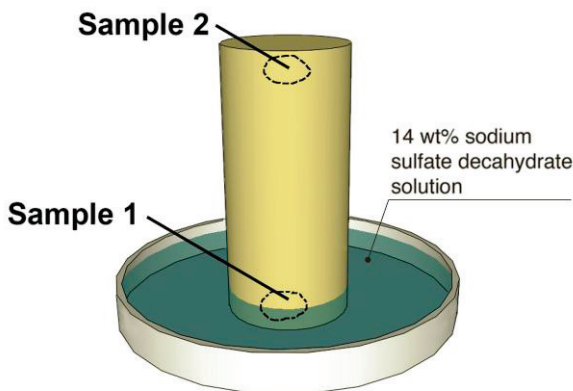


Figure 1: Scheme illustrating the sampling points in cylinders subjected to salt crystallization cycles.

Samples 1 and 2 were analyzed for determining their salt content and pore size distribution. The salt content was determined by ion chromatography (IC), using a Dionex ICS 1000, after sample grinding, salt extraction by deionized boiling water and filtering. The pore size distribution of the upper samples ("2") was evaluated by MIP immediately after the salt crystallization cycles and after removing the salts from the samples by poulticing (cellulose pulp and distilled water). Finally, the salt crystallization effect on sample integrity was evaluated by measuring E_d of cylindrical samples after salt removal by poulticing.

3 Results and discussion

Both treatments caused remarkable increases in dynamic elastic modulus and tensile strength, as reported in Table 1. Even if TEOS caused a higher improvement, the consolidating effectiveness of HAP is remarkable, being $\Delta E_d = +40\%$ and $\Delta \sigma_t = +40\%$. The very good performance of TEOS can be explained considering that Globigerina limestone naturally contains small amounts of quartz, that can allow some chemical bonding between the formed silica gel and the stone [12].

Neither of the two treatments was responsible for dramatic pore occlusion, even if TEOS caused a non-negligible 13% decrease in open porosity (Table 1). In terms of pore size distribution (Figure 2), HAP caused an increase in the amount of pores with radius 0.01-0.1 μm , whereas TEOS (and to a smaller extent HAP) led to a slight increase in the pores with radius $< 0.01 \mu\text{m}$. These increases in the relative percentage of the finest pores occurred mainly at the expense of the pores with radius 0.1-1 μm .

In terms of physical properties (Table 1), HAP caused only minor modifications in stone sorptivity and water absorption, consistent with previously obtained results [3, 7]. In the case of TEOS, a very little modification in water transport properties was found as well, which can substantially be ascribed to the good efficacy of the accelerated curing procedure, able to cause complete TEOS hydrolysis-condensation in a much shorter period of time than experienced on site [10].

Table 1: Mechanical, microstructural and physical properties of untreated and treated samples, before salt crystallization cycles (E_d = dynamic elastic modulus; σ_t = tensile strength; OP = open porosity; AC = absorption coefficient; WA_{24} = water absorption after 24 hours).

	E_d [GPa]	σ_t [MPa]	OP [%]	AC [mg/(cm ² √s)]	WA_{24} [%]
UNTR	11.6	2.5	37.1	20.5	14.6
HAP	16.3	3.5	34.7	19.3	13.9
TEOS	18.9	5.6	32.1	19.6	14.1

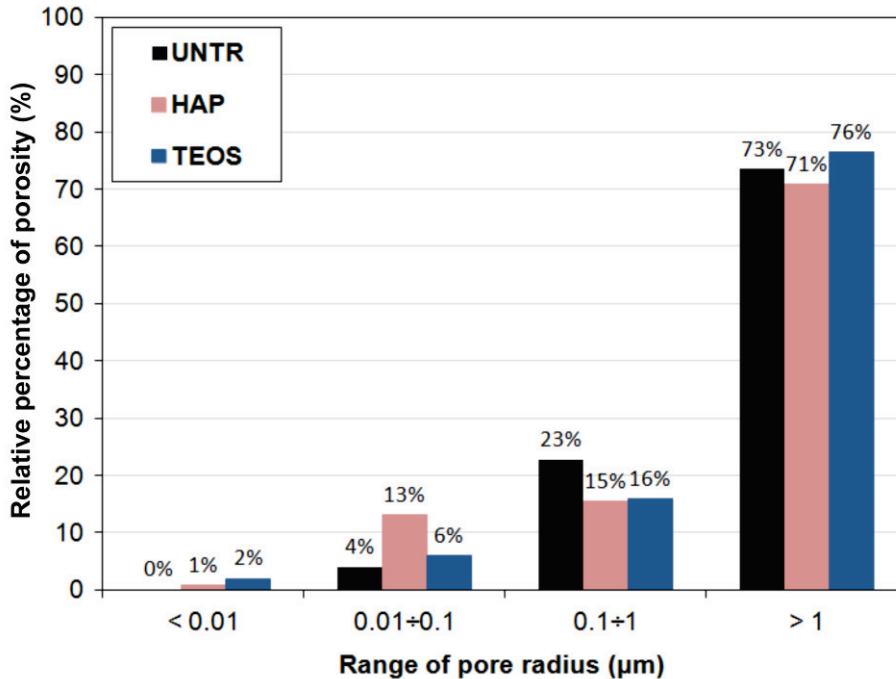


Figure 2: Distribution of pore size in untreated and treated samples.

The fact that both treatments left water transport properties basically unchanged and that open porosity was only slightly decreased after treatments allows to expect that also soluble salt-containing solutions will be able to exit from the treated stone, without causing sub-efflorescences formation and consequent stress inside the stone. However, the modifications in the pore structure induced by HAP and TEOS (Figure 2) may potentially be responsible for higher crystallization pressures inside the treated stone (the smaller the pore, the higher the crystallization pressure [13]). Therefore, the need of specifically evaluating resistance to salt crystallization after consolidation is confirmed.

When subjected to sodium sulphate crystallization cycles, untreated and treated samples underwent the weight changes reported in Figure 3. At the end of the fifth cycle, accelerated weathering was stopped as the samples exhibited marked visible decay and the appearance of untreated and treated samples, after salt washing away, was that illustrated in Figure 4. The untreated samples exhibited the most pronounced surface alteration, due to considerable flaking and pulverization, while HAP-treated samples apparently underwent the lowest deterioration.

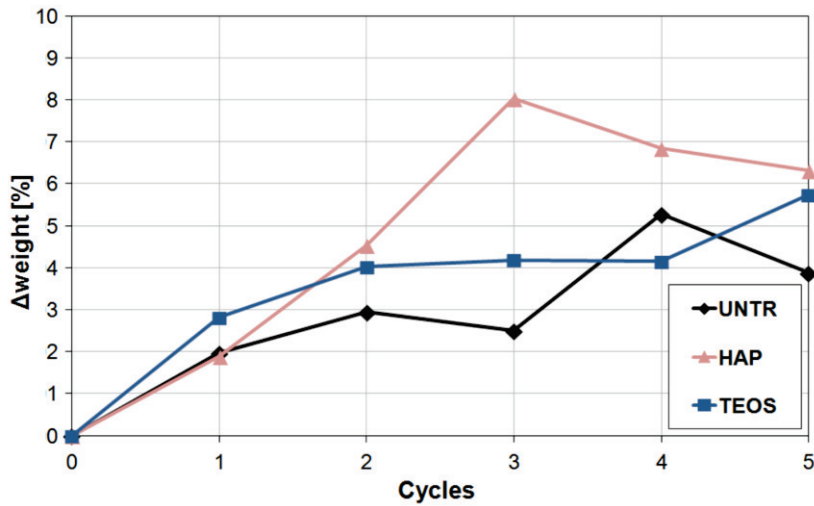


Figure 3: Percentage weight change of untreated and treated samples as a function of salt crystallization cycles.

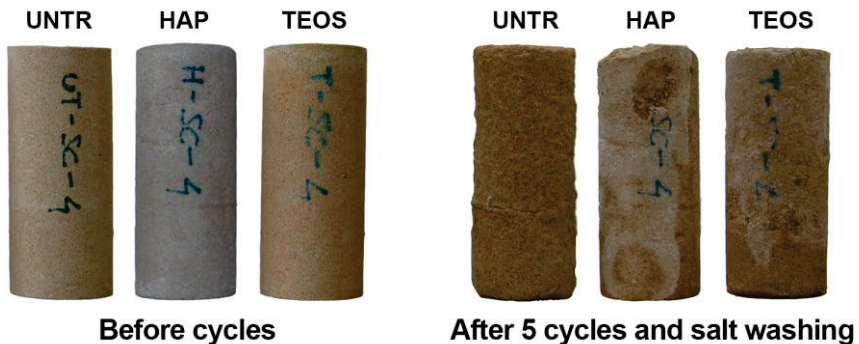


Figure 4: Appearance of untreated and treated samples, before and after 5 cycles and salt washing away.

The amounts of salts deposited in the untreated and treated samples are reported in Figure 5. As expected, the untreated samples exhibited a higher salt amount than treated samples, especially in the upper part (sample 2), where evaporation is more pronounced. TEOS-treated samples exhibited a similar trend in salt distribution, even if lower amounts were registered, whereas in the case of HAP no significant difference in salt content between the lower and upper parts was detected. The fact that untreated samples exhibited the highest salt content but, at the same time, the lowest weight increase (Figure 3) can be explained considering that these samples underwent the most severe flaking and material loss.

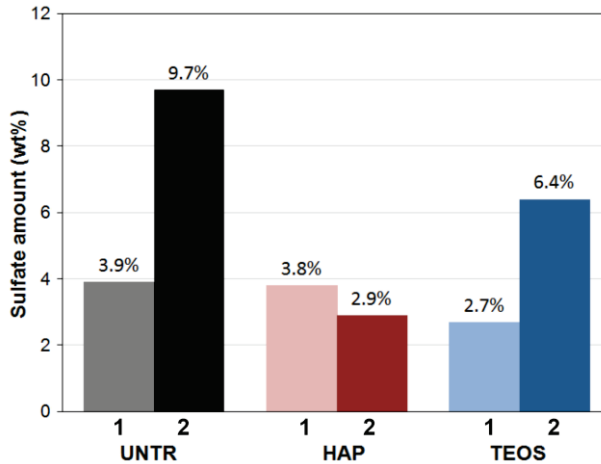


Figure 5: Sulfate content of untreated and treated samples after 5 cycles.

The effect of salts on sample microstructure was evaluated by MIP. In the case of salt-laden samples (dashed lines in Figure 6), some pore clogging was found for all the conditions. After salt removal by poulticing (dotted lines in Figure 6), remarkable differences in the pore size distribution were found. In particular, all the samples subjected to salt removal exhibited a higher open porosity than the corresponding salt-containing samples (according to IC results, salt content decreased from that reported in Figure 5 to about 0.2-0.3 wt.%). In the case of the untreated sample and, to a lower extent, of the TEOS-treated sample, after salt removal the open porosity was found to be even *higher* than the corresponding salt-free references. This can be attributed to the opening of new micro-cracks, as a consequence of stress exerted by growing salt crystals inside the pores. Notably, in the case of the HAP-treated sample, after salt removal, the resulting open porosity was however *lower* than that of the HAP-treated reference. This seems to suggest that no micro-cracking of the consolidated stone occurred (the difference with respect to the salt-free reference being owing to some residual salts retained in the pores).

To have a confirmation of this, dynamic elastic modulus measurement was repeated on two samples for each condition after salt removal. In agreement with indications obtained by MIP, remarkable decreases in E_d with respect to the condition before salt crystallization cycles were found for the untreated ($\Delta E_d = -15\%$) and TEOS-treated samples ($\Delta E_d = -20\%$). In the case of HAP, a much smaller decrease was found ($\Delta E_d = -3\%$), which seems to confirm that HAP-treated samples actually underwent less degradation than the other samples. Hence, since both TEOS- and HAP-treated samples exhibit similar E_d values after salt crystallization cycles (respectively, 15.7 and 15.5 GPa), any substantial advantage, in terms of mechanical properties, deriving from using TEOS rather than HAP seems to be lost after accelerated salt weathering.

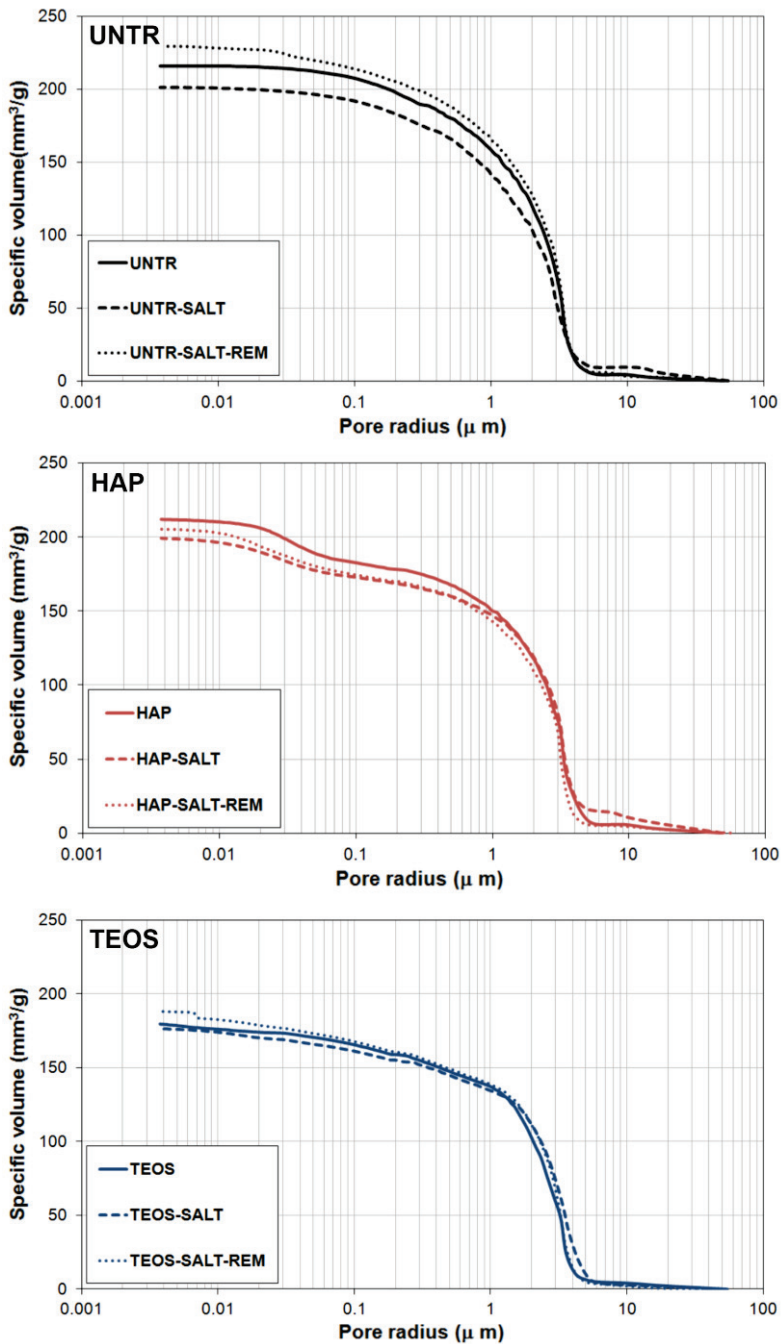


Figure 6: Pore size distribution of untreated and treated samples before, after 5 crystallization cycles ("-SALT" samples) and after salt removal ("-SALT-REM" samples).

4 Conclusions

In this paper, the durability of limestone samples consolidated by a novel phosphate-based consolidant was evaluated and compared to that of samples consolidated with a commercial TEOS-based product. Based on the results obtained in this study, by accelerated sodium sulphate crystallization cycles in laboratory conditions, a promising performance of the novel HAP-based consolidant was found. Indeed, HAP-treated samples exhibited less micro-cracking and lower mechanical damage than untreated and also TEOS-treated samples. In order to evaluate whether the HAP treatment may be responsible for sub-efflorescences formation at the interface between the unconsolidated substrate and the consolidated layer additional experimental tests are currently in progress. Future work will be also dedicated to evaluate the treatment performance when applied on already salt-contaminated substrates.

References

- [1] Italian Recommendation NORMAL 20/85, Conservazione dei materiali lapidei: Manutenzione ordinaria e straordinaria, Istituto Centrale per il Restauro (ICR), Rome, 1985
- [2] G.W. Scherer, G.S. Wheeler, Silicate consolidants for stone, *Key Engineering Materials*, 391 (2009) 1-25
- [3] E. Sassoni, S. Naidu, G.W. Scherer, The use of hydroxyapatite as a new inorganic consolidant for damaged carbonate stones, *Journal of Cultural Heritage*, 12 (2011) 346-355
- [4] E. Sassoni, E. Franzoni, B. Pigino, G.W. Scherer, S. Naidu, Consolidation of calcareous and siliceous sandstones by hydroxyapatite: comparison with a TEOS-based consolidant, *Journal of Cultural Heritage*, 14 (2013) 103-108
- [5] S. Naidu, C. Liu, G.W. Scherer, New techniques in limestone consolidation: Hydroxyapatite-based consolidant and the acceleration of hydrolysis of silicate-based consolidants, *Journal of Cultural Heritage* (2014) DOI: 10.1016/j.culher.2014.01.001
- [6] E. Sassoni, E. Franzoni, Evaluation of hydroxyapatite effects in marble consolidation and behaviour towards thermal weathering, *Proceedings of Built Heritage 2013 – Monitoring Conservation Management*, M. Boriani, R. Gabaglio, D. Gulotta (Eds), Milan (Italy) 18-20 November 2013, 1287-1295

- [7] E. Franzoni, E. Sassoni, G. Graziani, Brushing, poultice or immersion? Role of the application technique on the performance of a novel hydroxyapatite-based consolidating treatment for limestone, *Journal of Cultural Heritage* (2014), DOI: 10.1016/j.culher.2014.05.009
- [8] J. Cassar, Deterioration of the Globigerina limestone of the Maltese Islands, *Geological Society Special Publication* 205 (2002) 33-49
- [9] E. Franzoni, E. Sassoni, G.W. Scherer, S. Naidu, Artificial weathering of stone by heating, *Journal of Cultural Heritage*, 14 (2013) 85-93
- [10] E. Franzoni, G. Graziani, E. Sassoni, TEOS-based treatments for stone consolidation: acceleration of hydrolysis-condensation reactions by poulticing, *Journal of Sol-Gel Science and Technology* (submitted)
- [11] C. Miliani, M.L. Velo-Simpson, G.W. Scherer, Particle-modified consolidants: a study on the effect of particles on sol-gel properties and consolidation effectiveness, *Journal of Cultural Heritage*, 8 (2007) 1-6
- [12] P. Maravelaki-Kalaitzaki, N. Kallithrakas-Kontos, Z. Agioutantis, S. Maurigiannakis, D. Korakaki, A comparative study of porous limestones treated with silicon-based strengthening agents, *Progress in Organic Coatings*, 62 (2008) 49-60
- [13] G.W. Scherer, Stress from crystallization of salt, *Cement and Concrete Research*, 34 (2004) 1613-1624

Consolidation of fired-clay bricks by ethyl silicate: durability to salt crystallization

E. Franzoni*, E. Sassoni, G. Graziani and A. Fregni

Department of Civil, Chemical, Environmental and Materials Engineering (DICAM), University of Bologna, Bologna, Italy

* elisa.franzoni@unibo.it

Abstract

The resistance of ethyl silicate-consolidated bricks to sodium sulfate crystallization cycles was evaluated. A commercial ethyl silicate (ES) based product was applied by brushing with 5 or 10 strokes to assess the effect on distribution/accumulation of the consolidant inside the pores. After long-term curing, aimed at making ES-treated samples lose their temporary hydrophobicity, samples were characterized by assessing the penetration depth of consolidants, tensile strength and modifications in open porosity and pore size distribution. Resistance to salt crystallization was evaluated by carrying out sodium sulfate crystallization cycles. The capillary suction of the salt solution was let occur through the untreated surface of cubic samples treated in the upper face, in order to investigate brick response to salts coming from behind the consolidated layer (the situation usually occurring when rising damp is present). Treatment with either 5 or 10 strokes provided protection against salt damage, and no accumulation of salt behind the consolidated layer was observed.

Keywords: terracotta, ethyl silicate, rising damp, sodium sulfate, bricks

1 Introduction

The need of finding suitable materials for consolidation of fired-clay elements in ancient buildings, such as bricks and terracotta decorative parts, is an urgent task, as they are widely diffused in historical architecture and severely affected by weathering phenomena, causing disaggregation, flaking and detachments [1]. Despite this urgency, however, the study of this topic is not as intensive as might be expected [1].

Recently, the effects of brick consolidation by ethyl silicate (ES), which is the most widely used consolidant for natural stone [2, 3], has been investigated [1]. ES was chosen because it exhibits good effectiveness when OH⁻ groups are present on the pore surface of materials, allowing chemical bonding with silica gel that forms due to curing reactions [3]. As bricks contain relevant silicate fractions, some chemical adhesion between material and consolidant is expected and indeed encouraging preliminary results have been obtained [1].

However, several aspects still need to be fully investigated about the use of ethyl silicate for brick consolidation, such as the effects of different treating procedures and the treatment durability. Indeed, the application procedure is a key factor in determining the effects of a consolidation treatment, as it controls the consolidant penetration depth and product uptake and hence the final performances [4, 5].

With regard to durability, the behaviour of brick consolidated by ethyl silicate has not been fully elucidated yet. This topic seems to be particularly relevant, especially when referring to brick behaviour towards salt weathering, since conservation works are often carried out without removing completely (or even without removing at all) rising damp, and salt crystallisation may continue after the intervention [6]. If variations in the substrate properties induced by the consolidant are not carefully considered, the degradation processes could even be aggravated by the intervention. On this topic, different opinions can be found in the literature about the effects of ethyl silicate. According to some authors, ES should increase resistance to salt crystallization, by increasing samples tensile strength [2]. However, depending on the support, ethyl silicate treatment might increase the fraction of smaller pores, hence increasing material susceptibility to salt damage [7].

In this paper the resistance to salt crystallization of brick consolidated with ethyl silicate was investigated. Two different application procedures (involving a different number of brushing strokes) were followed and their effects were compared, in terms of efficacy and compatibility. The two application procedures involve brushing, as it is the easiest and hence the most used on site [4, 8]. Even though technical data sheets of commercial products usually recommend brushing until apparent refusal, a much lower number of applications is normally performed in the field. Therefore, two treatment procedures were tested: an application number closer to

apparent refusal (10 strokes) and one closer to the common on-site practice (5 strokes).

The behaviour of the treated samples towards salt weathering was taken into consideration, by evaluating the microstructure alteration and salt content of samples subjected to crystallization cycles of a 14 wt.% sodium sulphate solution. Particular attention was devoted to the behaviour of the treated layer with respect to the underlying one, in order to determine whether the consolidated part would allow the salts to exit the samples, or whether it would act as a clogging layer, possibly resulting in the detachment of the treated portion of the samples.

2 Materials and methods

2.1 Bricks

Commercial fired-clay bricks ($25 \times 12 \times 5.5 \text{ cm}^3$, RDB, Pontenure, Italy) were cut into $4 \times 4 \times 4 \text{ cm}^3$ cubes and cylinders with 2 cm diameter and 5 cm height. All the samples of the same shape were taken from the same brick, so that the obtained results could be unaffected by heterogeneities in the starting materials.

2.2 Ethyl silicate treatments

The ethyl silicate consolidant was applied by 5 brush strokes (samples "T5") and by 10 brush strokes (samples "T10").

A commercial product, composed of 75 wt.% ethyl silicate (including 1% dibutyltin dilaurate as catalyst) and 25 wt.% white spirit (ESTEL 1000 by CTS s.r.l., Italy) was used.

Cylinders were treated on the whole external surface, while cubes were treated on one face only. All treated samples were left curing for 1 month prior to mechanical and microstructural testing, as suggested by the consolidant technical data sheets. Samples to be subjected to salt crystallization cycles were cured for 1 year, to avoid possible surface hydrophobicity owing to incomplete ES hydrolysis-condensation, reportedly lasting as much as 6-7 months [3].

2.3 Characterization techniques

Treatment efficacy was determined in terms of weight gain after treatment, penetration depth and tensile strength, determined on both untreated and treated samples.

Weight gain was measured by weighing cylindrical samples before treatment and after 1 month curing. It was also evaluated whether the higher number of brush strokes of treatment "T10" had resulted in a higher product uptake. Penetration depth was measured after 72 hours curing, as

it might increase in the first hours after treatment, due to some redistribution of the consolidant [9]. Penetration depth was visually assessed by fracturing treated samples and wetting them to highlight the consolidated part (hydrophobic). Indeed, after ES treatment, samples remain temporary hydrophobic until consolidant ethoxy groups fully react [10]. Tensile strength was determined on brick cylinders by the tensile splitting test (loading rate 4 mm/min).

The compatibility of the treatment was evaluated in terms of alterations in sample microstructure, by mercury intrusion porosimetry (MIP), using a Porosimeter 2000 Carlo Erba with a Fisons Macropore Unit 120. MIP was performed on samples obtained by chisel from cylinders used for tensile strength measurement. As increases in the fractions of smaller pores are known to increase a material's susceptibility to salts decay, the percentages of pores in the following ranges were calculated: radius $r > 1 \mu\text{m}$, $1-0.1 \mu\text{m}$, $0.1-0.01 \mu\text{m}$, $<0.01 \mu\text{m}$. Particular attention was devoted to possible increases in the latter two ranges.

After evaluation of treatment efficacy and compatibility, samples were subjected to 5 salt crystallization cycles, performed as described below. Cubic samples treated on one face only were oven dried and then immersed for about 0.5 cm in a 14 wt.% solution of sodium sulphate in deionized water, and kept immersed for 7 hours. Samples were placed in the containers with the treated face up, so that the saline solution would penetrate from the untreated area of the samples and the ability of the consolidated layer to let salts exit from the samples could be evaluated. Immersion was followed by a drying phase, where samples were oven-dried for 15 hours at 50 °C, the temperature being chosen not to damage the consolidant. Finally, samples were left cooling for 2 hours prior to the next cycle.

The effect of salt crystallization cycles was determined by evaluating the weight variation at each cycle, the salt content of treated and untreated samples and the sample total open porosity at the end of the cycles.

Salt content of the samples was determined by ion chromatography (IC), using a Dionex ICS 1000. IC was performed on fragments obtained by chisel from a depth comprised between 0 and 8 mm from the treated face (labelled as "-top"), corresponding to the depth of the consolidated layer, and from a depth comprised between 20 and 40 mm (labelled as "-bottom"), corresponding to the part not reached by the consolidant. Samples were taken at the same depths also in untreated references, for comparison. The salt contents in the consolidated and non-consolidated layers were compared to determine whether the treated layer tends to act as a weir against salt transport. All the upper samples were obtained by excluding efflorescence formed on sample surface. Salt content is reported only in terms of sulphate percentage, as the amount of other salts was found to be negligible.

Sample microstructure was investigated by MIP, performed on samples obtained by chisel from the upper layer of cubes (0-8 mm from the treated surface), near the sample edge, where salt damage was expected to be maximal. To evaluate the opening of micro-cracks due to salt decay, salts were removed from the samples before MIP, by boiling chisel-fractured samples for 30 minutes in deionized water. The efficacy of this procedure in removing salts from brick samples was verified by ion chromatography in preliminary tests (not reported here for brevity's sake).

3 Results and discussion

Physical, mechanical and microstructural properties of treated and untreated samples are reported in Table 1. Both treatments resulted in a remarkable weight increase 1 month after the consolidant application, suggesting that ethyl silicate was retained in pores. T10, as expected, resulted in a higher weight increase compared to T5, consistent with the higher number of brush strokes applied. Consistent with the higher weight increase, treatment T10 reached a higher penetration depth compared to T5 (Table 1), suggesting that the additional amount of consolidant did not form a surface-clogging layer. In both cases, the penetration depth of the consolidant can be considered as satisfactory, also considering that the bricks used for the experiments were highly porous, but they were not subjected to artificial decay prior to the consolidant application.

Tensile strength was found to increase significantly after both treatments, but T10-treated samples exhibited a higher mechanical improvement than T5-treated samples, consistent with their higher consolidant absorption.

Open porosity and pore size distribution of untreated and treated samples are reported in Table 2. Both treatments resulted in some pore occlusion, more marked in the case of T10; however, these alterations are rather limited, hence both treatments can be considered as fairly compatible with bricks in terms of pore occlusion. Regarding pore size distribution, both T5 and T10 led to an increase in the amount of pores in the finest ranges (radius $r < 0.01 \mu\text{m}$ and $r < 0.1 \mu\text{m}$), hence some increase in sample susceptibility to salts might be expected, especially in the case of T10, where the increase is more significant. To ascertain whether this is actually the case, salt crystallization cycles were carried out.

Table 1: Weight gain, penetration depth and strength of treated samples (T5 and T10) compared to untreated references (UT)

	Weight gain after 1 month curing [g/cm ²]	Penetration depth [mm]	Tensile strength [MPa]
UT	-	-	3.3
T5	0.02	8	4.3
T10	0.07	11	4.8

Table 2: Total open porosity (OP) and share of the porosity in the indicated pore ranges, for untreated (UT) and treated samples (T5 and T10)

	OP [%]	Porosity shared in different pore ranges [%]			
		r < 0.01 μm	0.01 μm < r < 0.1 μm	0.1 μm < r < 1 μm	r > 1 μm
UT	38.0	0.1	2.9	11.2	85.8
T5	30.1	0.8	3.4	9.7	86.2
T10	26.7	2.1	7.1	14.5	76.3

Weight variations after each cycle are reported in Fig. 1. In all treated and untreated samples, weight increased after 5 cycles, hence the contribution of salt accumulation seems to be greater than salt-induced material loss. As weight increase is lower in treated samples, it seems that consolidation was effective in limiting salt accumulation inside the samples. This is probably due to the lower porosity of the treated layer, slowing down the rate of the capillary rising flux of the saline solution and hence reducing the final amount of salts deposited inside the samples.

Salt content in untreated and treated samples is reported in Table 3. Sulphate amount is higher in untreated references, compared to T5 and especially T10-treated samples. This seems to confirm that consolidants did reduce capillary rise rate and hence salt accumulation.

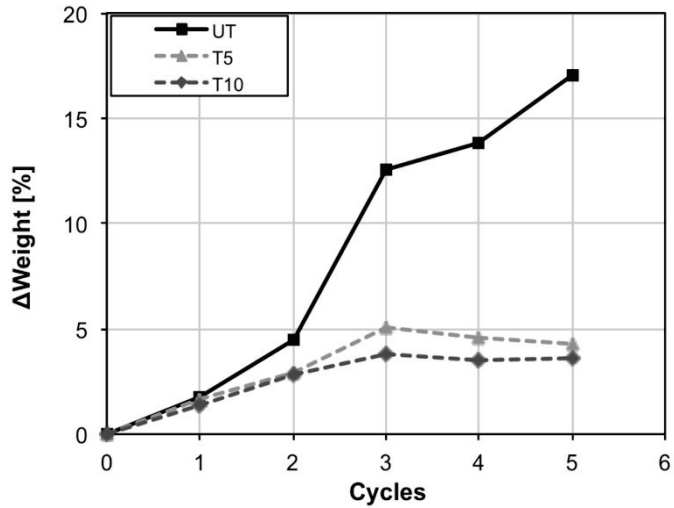


Figure 1: Weight variations in untreated and treated samples at each cycle.

Table 3: Sulphate content in untreated and treated samples after 5 cycles.

Samples	SO ₄ ⁼ amount [%]
UT-top	4.3
UT-bottom	3.7
T5-top	3.6
T5-bottom	2.6
T10-top	3.0
T10-bottom	2.4

In both untreated and treated samples, salts amount is higher in the top part of the samples, consistent with the higher evaporation rate in this region. In treated samples, salts are not concentrated only in the untreated volume, as would happen if the consolidated layer had acted as a clogging layer preventing their movement, but their distribution is similar to that in the untreated references (higher in the top, lower in the bottom part). Therefore, ethyl silicate did not cause any pore clogging layer and, consequently, no flaking or detachment of the treated area from the underlying part.

The influence of salt weathering on the samples' microstructure can be deduced from pore size distribution curves, reported in Fig. 2.

In untreated samples, porosity was found to be almost unaltered after weathering cycles, thus no salt-related damage (i.e. opening of micro-cracks) seems to have occurred after the cycles, despite accumulation of ~4 wt% salt (see results of IC). T5-treated samples, similarly, have suffered a very slight increase in porosity.

On the other hand, T10-treated samples, despite the lower salt content, experienced a remarkable increase in pore size distribution after the cycles. This might be due to the increase that T10 caused in the percentage of the finest pores, raising susceptibility to salt decay. As a matter of fact, the increase in the finest pores was greater in T10-treated samples than in T5-treated samples, which exhibited a much lower sensitivity to salt crystallization.

The increase in total open porosity of T10-treated samples after salt weathering suggests that some micro-cracks had opened as a result of the cycles. However, the total open porosity of T10-treated samples remained lower than that of untreated references, suggesting that some benefit was maintained after treatment and that salt decay had damaged the consolidant layer more than the sample itself.

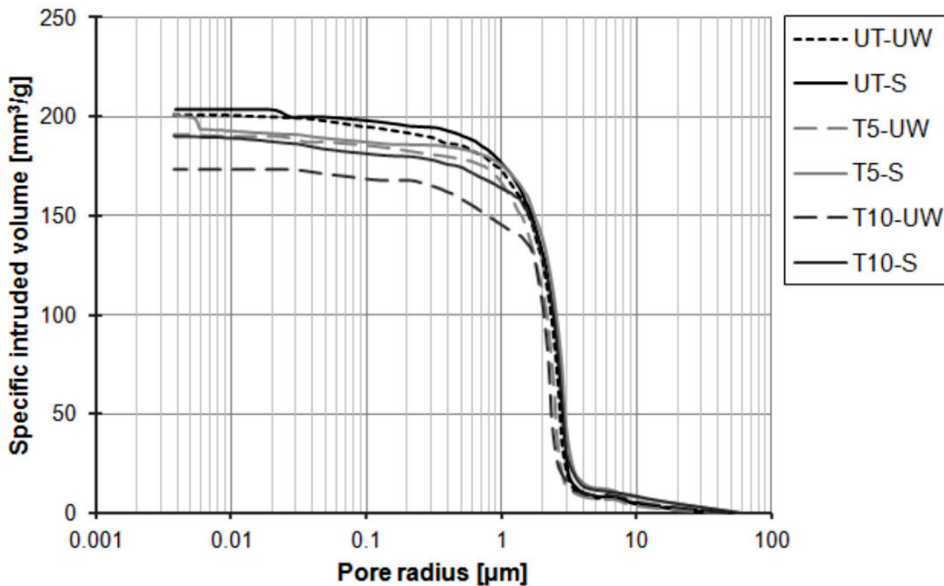


Figure 2: Pore size distribution of untreated (UT) and treated (T5 and T10) samples, both unweathered (-UW) and salt-weathered (-S), the latter after salt removal.

Further tests are currently in progress to promote a more intense decay by salt crystallization cycles and to investigate the change in mechanical properties induced by salt damage.

4 Conclusions

From the test results, the following conclusions can be derived:

- Ethyl silicate proved to be effective for the consolidation of bricks. Ten brush strokes gave better results than 5 strokes from the point of view of penetration depth and mechanical performance, hence they gave a better consolidation effectiveness. However, very good results were achieved also with the lower application number.
- Both treatments did not stop the salt transport towards the external surface and they were effective in reducing salt accumulation inside the sample by slowing down the capillary rise of the saline solution. After 5 cycles, the porosity of the consolidated bricks was still slightly lower than in the untreated samples, suggesting that some benefits from the treatments were still present. Further studies concerning mechanical properties of weathered samples are currently in progress.
- Despite T10 treatment being more effective than T5 treatment, its durability has proved to be a critical issue. The treatment was more effective in reducing salt accumulation; however, it increased brick susceptibility to salt weathering, so that no benefit is maintained after salt weathering, compared to T5 treatment. This is probably to be ascribed to the much higher increase in the fraction of smaller pores.

Acknowledgements

Dr. Ginevra Bacilieri, Dr. Claudia Castelli and Dr. Veronica Zulli are gratefully acknowledged for collaboration on brick characterization.

References

- [1] Franzoni E., Pigino B., Leemann A., Lura P., Use of TEOS for fired-clay bricks consolidation, *Materials and Structures*, DOI: 10.1617/s11527-013-0120-7
- [2] Maravelaki-Kalaitzaki P., Kallithrakas-Kontos N., Korakaki D., Agioutantis Z., Maurigiannakis S., Evaluation of silicon-based strengthening agents on porous limestones, *Progress in Organic Coatings* 57 (2006) 140-148
- [3] Scherer G.W., Wheeler G.S., Silicate consolidants for stone, *Key Engineering Materials* 391 (2009) 1-25
- [4] Ferreira Pinto A.P., Delgado Rodriguez J., Stone Consolidation: The role of treatment procedures, *Journal of Cultural Heritage* 9 (2008) 38-53

- [5] Ferreira Pinto A.P., Delgado Rodriguez J., Consolidation of carbonate stones: Influence of treating procedures on the strengthening action of consolidants, *Journal of Cultural Heritage* 13 (2012) 154-166
- [6] Franzoni E., Rising damp removal from historical masonries: a still open challenge. *Construction and Building Materials* 54 (2014) 123–36.
- [7] G.W. Scherer, Stress from crystallization of salt, *Cement and Concrete Research*, 34 (2004) 1613–1624
- [8] Franzoni E., Sassoni E., Graziani G., Brushing, poultice or immersion? Role of the application technique on the performance of a novel hydroxyapatite-based consolidating treatment for limestone, *Journal of Cultural Heritage* (2014), DOI:10.1016/j.culher.2014.05.009
- [9] Franzoni E., Graziani G., Sassoni E., Bacilieri G., Griffa M., Lura P., Solvent based TEOS consolidant for stone: influence of the application technique on penetration depth, efficacy and pore occlusion, *Materials and Structures* (submitted)
- [10] Wheeler G., *Alkoxysilanes and the consolidation of stone*, The Getty Conservation Institute, Los Angeles, 2005

Testing the durability of hemp-based mortars under Mediterranean climatic conditions in coastal and inland areas: does the presence of salt alter hemp bio receptivity?

A. Arizzi^{1*}, H. Viles¹, I. Martin-Sanchez² and G. Cultrone³

¹School of Geography and the Environment, University of Oxford, UK

²Department of Microbiology, University of Granada, Spain.

³Department of Mineralogy and Petrology, University of Granada, Spain.

* anna.arizzi@ouce.ox.ac.uk

Abstract

In this study, we assessed the durability of hemp-based mortars by means of accelerated weathering tests, simulating coastal and inland areas with a Mediterranean climate. Mortars were produced with dry hemp hurds (i.e. inner part of the stem) and three binders: dry hydrated lime, lime putty and natural hydraulic lime. Simulation of temperature and relative humidity variations, rainfall and salt attack were carried out in an environmental cabinet and programmed according to the Mediterranean climatic conditions. Only one cycle (lasting 12 days) was simulated, composed of four main steps (each step corresponding to one season). After the test, mortars did not show any apparent damage apart from the loss of some fibres from the edges of samples. Mineralogical (by means of X-ray diffraction), microscopical (by means of environmental scanning electron microscopy) and microbiological studies on samples allowed a more detailed assessment of the response of the three types of mortars to weathering conditions, especially when they were combined with the attack of salt. In particular, it was found that the presence of salt delayed mortar hardening under the simulated weathering conditions and that it induced the colonization of more microbial species. However, salt was mainly washed away by the rainfall simulated in the cabinet; therefore it did not cause any efflorescence on, or damage to, the samples. Among the three mortar types, the one with natural hydraulic lime showed the least deterioration (lowest mass variation and chromatic change) and was attacked by the lowest number of microbe species. This study

demonstrates that hemp-lime mortars perform well under Mediterranean climates and that their use in coastal areas is also suitable, provided that natural hydraulic lime is used and that protective measures against salt attack are adopted during the first weeks after mortar application.

Keywords: hemp hurd, lime, weathering, sodium chloride, microbes

1 Introduction

The addition of fibres (e.g. animal hairs, plant fibres) to mortars is an ancient and effective method of improving flexibility, adhesion and strength of these building materials. In addition, hemp hurds (i.e. inner woody part of the stem) provide thermal and insulating properties [1] and are efficient CO₂-sequesters [2], reasons why their use is being strongly encouraged in recent decades for the elaboration of lime-based mortars.

Despite these advantages, hemp hurds increase the water absorption of mortars [3], which may reduce their durability. Moreover, although lime acts as a disinfectant (because of its high pH), hemp mortars are still likely to be subjected to microorganism attack when exposed to humidity variations for long period, due to the organic nature of hemp that enhances mortar bioreceptivity. Since the growth of microorganisms is strongly influenced by conditions of temperature and relative humidity, it is fundamental to study hemp mortar behaviour under real environmental conditions in order to evaluate the advantages and disadvantages of the use of hemp-based building materials in specific areas.

In this work, hemp mortar durability was assessed by simulating one accelerated weathering cycle under the environmental conditions registered during the year 2012 in different cities/countries with a Mediterranean climate. Half of the mortar samples were also exposed to salt spray to simulate the effects of airborne salt on mortar durability in coastal area. Considering that soluble salts may affect microorganism growth, favouring halophytic (i.e. salt tolerant) species [4], we studied how bioreceptivity of hemp-based mortars is influenced by the presence of sodium chloride (e.g. growth of different number or type of microbe species). Hemp mortars were produced with three types of lime (aerial dry hydrated and putty and natural hydraulic), so as to investigate also the influence of the binder on the durability of this peculiar building material.

Although one weathering cycle, corresponding to one year, is not sufficient to fully predict the durability that mortars will exhibit in the building, where they will be exposed to the same conditions repeatedly and for a longer period of time, the present work still represents an important step in the comparative study that needs to be undertaken before the use of any repair materials. Comparing the weathering behavior of hemp mortars

made with different lime types, indeed, is helpful to decide which type of lime is most suitable under specific environmental conditions.

2 Materials and Methods

2.1 Materials

Mortars were prepared with commercial hemp hurds (Cannhabitat®, produced by AgroFibre, Euralis, Cazeres, France, and supplied by Cannabric, Guadix, Granada, Spain) and three types of lime: aerial dry hydrated lime in the form of powder (CL90S, [5], produced by ANCASA, Seville, Spain), aerial lime in the form of putty stored under water for 2 years (CL90-S PL, [5], produced by ComCal, Barcelona, Spain); and natural hydraulic lime (NHL3.5, [5], produced by Socli, Italcementi Group, Izaourt, France). The lime:hemp:water dosage by volume was 3:5:2.5 (in the case of the lime putty the same volume of lime and hemp but a lower amount of water were used). Mortars were named as C, N and P, according to the type of lime (CL90S, NHL 3.5 and CL90S PL, respectively). They were cured in the Cannabric factory base for three months under average conditions of $T = 17\text{ }^{\circ}\text{C}$ and $\text{RH} = 75\%$ before the study.

2.2 Weathering test

In order to simulate Mediterranean climatic conditions a synthetic year of data was obtained from temperature and relative humidity variations and rainfall registered during the year 2012 in different cities/countries with a Mediterranean climate (Fig. 1a). The data were used to provide an accelerated simulation in a Sanyo-FE 300H/MP/R20 environmental cabinet (Fig. 1b), with one year condensed into 12 days.

As shown in Fig. 1, the whole year was simulated (one cycle composed of four main steps), with conditions changing seasonally (a step every season). The values of temperature and relative humidity represented in each step were obtained from the main highest and lowest T and RH values registered during each season of 2012. Rainfall was simulated at the beginning of each season (as indicated by the arrows in Fig. 1) applying mist water by a hose placed inside the cabinet. The time of water application was calculated by converting the amount of rain received seasonally (from millimetres to minutes of application) by means of an experimental rain gauge. To reproduce the same environment in coastal areas, the presence of airborne salt was also simulated, by spraying half of the mortar samples with a half-saturated NaCl solution. The attack of salt was programmed at the beginning of every season as well as the rainfall, to be able to compare sample behaviour in presence and absence

of salt. In the cabinet, six samples per mortar type (2×2×4 cm) were placed with the largest surface (4×4 cm) facing the spray.

Samples were weighed (to an accuracy of ± 0.01 g) and photos taken at the end of each cycle (season) in order to record any visible change in mortars.

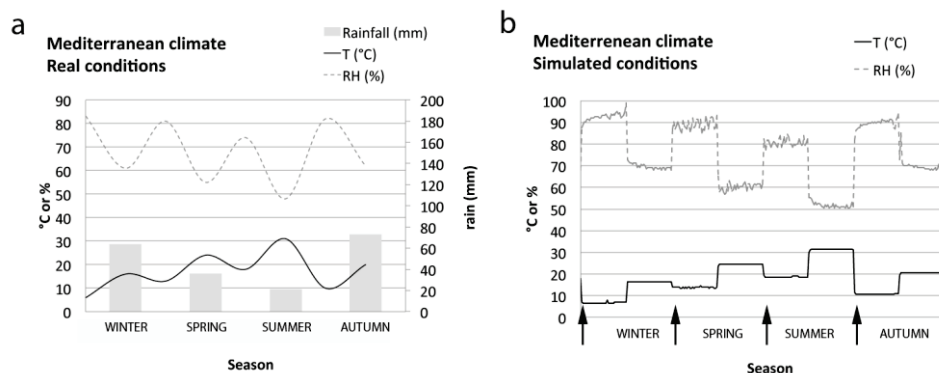


Figure 1: Mediterranean climate: real in 2012 (a) and simulated (b) conditions of temperature (T, in °C), relative humidity (RH, in %) and rainfall over one year cycle. In b, conditions were registered by means of an ibutton® Hygrolog. Arrows indicate the rainfall events.

2.2.1 Study before and after the weathering test

Mortar mineral phases were studied by means of X-ray diffraction (XRD) analysis, using a Panalytical X'Pert PRO MPD diffractometer, with automatic loader. Analysis conditions were: radiation $\text{CuK}\alpha$ ($\lambda=1.5405$ Å), 3 to 60 °2 θ explored area, 45 kV voltage, 40 mA current intensity and goniometer speed using a Si-detector X'Celerator of 0.01 °2 θ /s. The interpretation and identification of the mineral phases was performed using the X-Powder© software [6].

Microscopic observations of mortars were performed by means of a Philips Quanta 400 environmental scanning electron microscope (ESEM), which worked at a fixed temperature of 2 °C. Small pieces of mortars (~5 mm) were directly put in the chamber, which was initially purged 5 times at a range of pressures between 2.5 and 5.5 torr (RH ~ 50% and 100% at T = 2 °C). Once equilibrium was achieved, pressure was fixed at 3.5 torr (RH ~ 70% at T = 2 °C).

Mortar chromatic parameters (L^* , lightness; a^* and b^* , chromatism) were measured by means of a portable Konica-Minolta CM-700d spectrophotometer. The CIELab system was chosen [7] and the measurement conditions were as follows: measurement area of 8 mm, D65 standard illuminant and observer 10° with modes SCI/SCE and a

wavelength range from 400 nm to 700 nm with a wavelength interval of 10 nm. Ten measurements per mortar type were performed. The overall colour difference (ΔE) of the three mortar types before and after the weathering test was determined as follows.

$$\Delta E = \sqrt{(L_1^* - L_2^*)^2 + (a_1^* - a_2^*)^2 + (b_1^* - b_2^*)^2} \quad (1)$$

where L_1^* , a_1^* and b_1^* are respectively the lightness and the chromatic coordinates of the untreated samples and L_2^* , a_2^* and b_2^* are those of samples after the water absorption-drying or the capillary tests.

Finally, a microbiological study was performed on the mortars after the weathering test. Swab samples (sterilized by ethylene oxide and individually wrapped in peel-pack) deemed suitable for isolations in culture media (Class IIa) (Eurotubo, Deltalab, Rubí, Spain) and adhesive tape samples were collected to characterize the microbial community present in the mortars, both from areas showing colour changes. Samples were inoculated onto plates containing Trypticase soy agar (TSA, Scharlau Chemie S.A., Barcelona, Spain) and Sabouraud chloramphenicol agar (Scharlau) media (100 μ L of the suspension obtained per plate) and incubated at 28 °C for one week. During this period, colonies exhibiting different morphology and appearance were transferred to new culture plates of TSA medium for bacteria and potato dextrose agar (PDA) for fungi, to obtain pure strains. Phenotypic characterization of isolated microorganisms was performed by observation of macroscopic features such as colour, shape and texture of colonies appeared in the culture media. Hyphae, sporangia and spores of fungi have been visualized by staining with lactophenol blue. Bacteria were identified by Gram staining. Observation of the samples was performed with a Leitz Dialux 22 optical microscope with objectives of 60X/100X. Images were obtained with an Olympus Camedia C-5060 camera coupled to the microscope.

3 Results and discussion

3.1 Mortar mass variation and appearance before and after the weathering test

The variations of mortar weight due to the weathering conditions in the cabinet are shown in Fig. 2. Sample weight increased accordingly with the amount of rainwater sprayed in the cabinet and the temperature conditions of each season. As shown in Fig. 1a, indeed, the rainiest periods (winter and autumn) follow the warmest ones (spring and summer) and vice versa. In samples without salt (Fig. 2a), a slight weight increase was registered after the winter season ($\Delta M \sim 5\%$), but a much greater water absorption happened during autumn ($\Delta M \sim 20\%$), due to both the greater amount of rain water during this season and the higher temperature

values simulated in summer (Fig. 1a), which dried samples and increased their water absorption capacity. Samples with salt followed a similar trend during winter and autumn although a lower weight increase was registered ($\Delta M \sim 3\%$ and 10% after winter and autumn, respectively) compared to samples without salt. This finding could suggest that the presence of salt reduced the water absorption by the hemp hurds or, more likely, that the water was mainly absorbed by the sodium chloride, which was totally or in part washed away, due to the action of falling water. The second reason would explain why the weight increase in samples with salt is not higher than in samples without salt, as expected.

Regarding the behaviour of the three types of lime, the N samples (made with natural hydraulic lime) absorbed less water/salt solution during the weathering test, compared to samples made with aerial lime (C and P). This is in agreement with a previous study on the hygric behaviour of these mortars [8], where it was found that hemp mortars made with natural hydraulic lime have a lower water absorption capacity compared to those made with aerial lime.

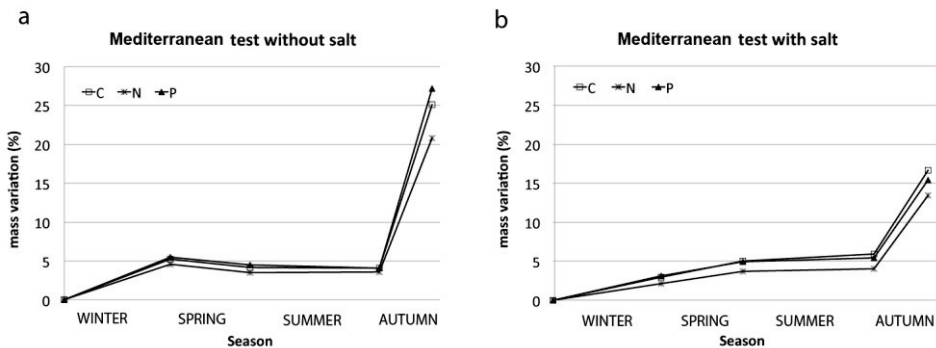


Figure 2: Mass variation (in %) of C, N and P samples (hemp mortars with CL90S, NHL 3.5 and CL90S PL limes, respectively) over one year cycle during the Mediterranean test without (a) and with (b) salt.

Images taken before and after the test show that mortar samples maintained the same appearance during the whole duration of the weathering test, both without and with the application of salt. In particular, Fig. 3 shows the appearance of samples with salt, before and after the weathering test. No efflorescences can be seen on the sample surface but only the loss of few hemp hurds, possibly caused by sample handling more than by the weathering conditions simulated in the cabinet.

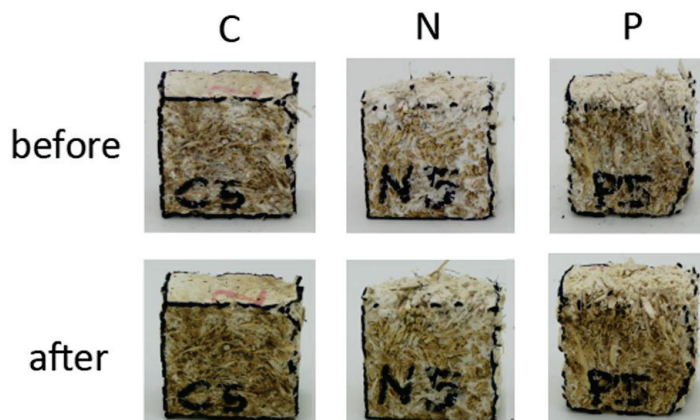


Figure 3: Appearance of C (left), N (middle) and P (right) samples (hemp mortars with CL90S, NHL 3.5 and CL90S PL limes, respectively) before and after the Mediterranean test with salt.

3.2 Mortar mineral phases and microscopic observations

Weathering clearly improved mortar hardening in comparison with control samples not exposed to the 12 days of weathering simulation, as it increased carbonation in samples produced with aerial lime (C, with dry hydrated lime and P, with lime putty) and hydration in samples with natural hydraulic lime (N). This can be observed from the decrease in the content of portlandite (Table 1) that turned into calcium carbonate (mainly calcite but also vaterite) in C and P samples, as well as in the decrease in the content of calcium silicate phases (CS) that turned into calcium silicate hydrates (CSH) in N samples.

Table 1: Semi-quantitative analysis of the mineral phases present in C (a), N (b) and P (c) samples (hemp mortars with CL90S, NHL 3.5 and CL90S PL limes, respectively), carried out by X-ray diffraction after the Mediterranean test without and with salt. Legend: Port: portlandite; Cal: calcite; Vat: vaterite; CS: calcium silicates; CSH: calcium silicate hydrates; Hal: halite; - absent; tr \leq 2%; * < 10%; ** = 10-20%; *** = 30-50%; **** = 60-80%

C sample						
	Port	Cal	Vat	CS	CSH	Hal
Before weathering	***	***	**	-	-	-
After weathering without salt	*	****	**	-	-	-
After weathering with salt	**	****	**	-	-	tr
N sample						
	Port	Cal	Vat	CS	CSH	Hal
Before weathering	*	***	**	***	**	-
After weathering without salt	*	***	**	**	**	-
After weathering with salt	*	***	**	**	**	tr
P sample						
	Port	Cal	Vat	CS	CSH	Hal
Before weathering	****	***	**	-	-	-
After weathering without salt	**	***	**	-	-	-
After weathering with salt	***	***	**	-	-	tr

The presence of salt, however, delayed this further carbonation, since a slightly higher amount of portlandite was found in all samples compared to those not subjected to salt application. This might have been caused by the closure of some pores in the matrix where sodium chloride precipitated. Halite (NaCl), however, was only detected in traces in the three mortar types and this suggests that it has been mostly washed away during rainfall simulated in the cabinet. This was verified by means of ESEM, as no halite crystals were recognized in the mortar matrix of the three samples with salt. Instead, some spores were observed in the C sample with salt (Fig. 4).

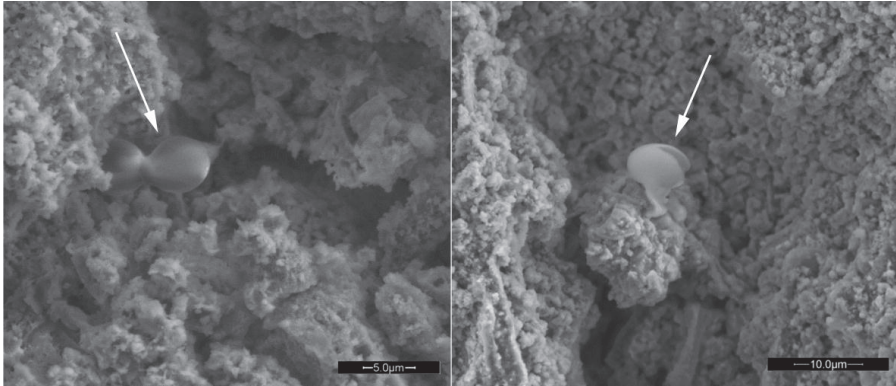


Figure 4: ESEM images of C sample (hemp mortars with CL90S) after the Mediterranean test with salt. Arrows indicate spores.

3.3 Chromatic changes and microbiological study

Sample color was measured before and after the weathering test to determine any chromatic change due to the environmental conditions or the presence of salt. Figure 5 shows that the biggest chromatic change occurred in samples made with aerial lime (especially C, with dry hydrated lime and P, with lime putty) and in those not subjected to salt application.

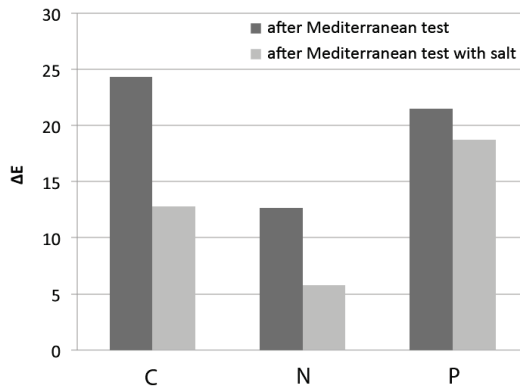


Figure 5: ΔE values of C, N and P samples (hemp mortars with CL90S, NHL 3.5 and CL90S PL limes, respectively) showing the colour difference before and after the Mediterranean test without and with salt, representing the chromatic changes of mortars.

Among the three mortar types, C and P samples were also the ones that presented a bigger mass variation (Fig. 2); therefore they absorbed more water during the test, which may have induced a more intense chromatic change with respect to N samples. The change in color (represented by the ΔE value) resulted in a general yellowing (increase of the b^* value) and darkening (decrease in L^* value, i.e. loss of lightness) of the sample surface. In samples with salt, this chromatic change might have been balanced by the whiteness conferred by the salt, giving a lower value of ΔE in the three mortar type. These chromatic variations, however, were not recognizable at first sight (Fig. 3), since neither visible efflorescences nor microbial attack (in the form of dark stains or mould) were observed in mortar samples. Notwithstanding, in all samples Gram-positive bacilli (of the *Bacillus* group, forming endospores) and in C and P samples Gram-positive cocci (of the *Micrococcus* group) were detected. These are very common bacteria, as they are resistant to most environmental conditions. Also different types of fungi and one type of yeast (*Rhodotorula*) were isolated, as indicated in Table 2.

Table 2: Species isolated in C, N and P samples (hemp mortars with CL90S, NHL 3.5 and CL90S PL limes, respectively) after the Mediterranean test without and with salt.

Species	C samples		N samples		P samples	
	Without salt	With salt	Without salt	With salt	Without salt	With salt
<i>Alternaria</i>					X	X
<i>Aspergillus</i>	X				X	
<i>Chaetomium</i>		X				
<i>Cladosporium</i>		X				
<i>Penicillium</i>	X		X	X	X	X
<i>Phoma</i>		X		X		
<i>Trichoderma</i>		X				
<i>Ulocladium</i>			X			X
<i>Rhodotorula</i>		X				

The bacteria isolated in mortars after weathering were already present in the hemp hurds. The presence of hemp, indeed, is the main cause of bio deterioration in these mortars, due to its organic nature and its ability of retaining large amounts of water. The other species, instead, formed during weathering in the cabinet. The number of species increases in mortars treated with salt, indeed it is higher in samples produced with dry hydrated lime (C samples) and it is the same in the other two mortar types (N and P). In summary: *Aspergillus* was present only in samples without salt; *Chaetomium*, *Cladosporium*, *Phoma*, *Trichoderma* and *Rhodotorula* were only present in samples with salt; *Alternaria*, *Ulocladium* and mainly

Penicillium were isolated in both samples (without and with salt). Isolated filamentous fungi belong to the phylum Ascomycota, whilst *Rhodotorula* is yeast belonging to the phylum Basidiomycota.

The species isolated in samples with salt are halotolerant/xerotolerant, which means that they can survive and grow in high concentration of salt, although the best growth occurs in the absence of salt [9]. Halotolerant microorganisms are indeed able to grow at low water activity (a_w is the partial vapor pressure in the growing medium (P) divided by the partial vapor pressure of pure water (P_0)). This parameter (a_w) refers to the amount of water metabolically available to microorganisms and it decreases with increasing amounts of solutes in the medium. The lowest values of water activity for filamentous fungi and yeast are $a_w > 0.80$ and $a_w > 0.85$ respectively. The tolerance to low a_w was demonstrated for fungi from Ascomycota and Basidiomycota fila. Yeast and yeast-like *Rhodotorula*, *Debaryomyces*, *Aureobasidium*, *Trichosporum*, as well as filamentous fungi *Cladosporium*, *Scopulariopsis*, *Alternaria* [9], *Phoma*, *Trichoderma* [10], *Chaetomium* [11] and different species of the genera *Aspergillus* and *Penicillium* [12] are described as halotolerant.

When a microorganism is on a substrate with a water activity lower than the needed one, growth stops but the microorganism remains capable of resistance for certain period of time. For spores, the phase of resistance in a salty environment (low a_w) can be considered virtually unlimited. Indeed, spores are very likely to remain in a quiescent state in samples, until environmental conditions are again favourable for their growth.

Water activity is influenced by other environmental parameters such as pH, temperature and relative humidity. In the specific case of the weathering test performed here, the washing of the sample surface undertaken by water during the rainfall period in the cabinet, at least reduced the possibility of salt efflorescences, thus ensuring a limited damage by microorganisms, since the deposit of salt is an ideal habitat for the development of more halophile microbes [4].

4 Conclusions

This study claimed to assess the durability of hemp-based mortars under Mediterranean climatic conditions. In particular, the influence of the presence of sodium chloride on the bio receptivity of these materials was studied here, to compare the behavior of these mortars in coastal vs inland areas.

In general, the behavior of the hemp mortars under variable temperature and relative humidity conditions and rainfall shows improved mortar hardening, with accelerated carbonation and hydration processes in aerial and hydraulic limes, respectively. The same happened in samples subjected to salt attack, although in this case carbonation and hydration were slower than in samples without salt. This indicates that the presence of salt in coastal areas delays hardening of hemp-based mortars, one reason why protective measures to reduce salt attack need to be taken during the first weeks after mortar application.

As expected, the presence of salt influenced mortar bio receptivity, indeed five new species (of fungi and yeast) were isolated only in samples subjected to salt attack, in addition to two types of bacteria already present in the non-weathered hemp mortars. The presence of nutrients (organic matter proceeding from hemp) and pre-existent microorganisms (bacteria) in the material substrate, as well as the variable environmental conditions and the attack of salt were determinant in the bio-colonization of the hemp mortars. Biological attack is an unavoidable deterioration factor in building materials and obviously the bio receptivity is increased when natural components, such as fibers and hurds, are used. However, the addition of hemp hurds to mortars is still a convenient solution in specific cases where the thermal and acoustic insulating properties of a building need to be improved. Investigating the weathering behavior of this peculiar building material allows better information about its response to different climatic conditions with the consequence that specific preventive measures can be taken to ensure longer durability. In this regard, disinfectant pre-treatments of the hemp hurds would be beneficial to reduce mortar bio receptivity.

Regarding the binder type, natural hydraulic lime was found to be the most suitable for use in combination with hemp hurds, since it slightly reduced the water absorption compared to the aerial lime and it also ensured reduced chromatic change and bio deterioration. Samples prepared with natural hydraulic lime, indeed, presented the least amount of fungi species (only three types in all samples), compared to samples with aerial lime (up to seven different species isolated).

It is worth highlighting that mortar samples did not show any apparent damage during or at the end of the durability test, apart from a slight darkening and yellowing of the sample surface, not even evident at first

sight. In particular, salt deposition in form of efflorescences was hindered by the continuous washing undertaken by water during rainfall. This means that, using the correct binder (natural hydraulic lime) and taking the necessary preventive measures as suggested above, hemp-based mortars would be totally suitable for use in inland and coastal areas with Mediterranean climate.

Acknowledgements

This study was financially supported by the European Commission under the Marie Curie program (FP7-PEOPLE-2012-IEF call, research project "NaturaLime") and by the Spanish research group RNM179 and MAT-2012-34473. We are grateful to Arch. Monika Brümmer (Cannabric factory, Guadix, Spain) for providing the hemp-based mortars.

References

- [1] Newman G. European decortication and fibre make. Biomaterials-back to the future. Plant fibre technology. (2008) From: http://www.compositesinnovation.ca/biofibre_workshop/, consulted on-line in January 2014.
- [2] Pervaiz M., Sain M.M. Carbon storage potential in natural fiber composites. Resources, Conservation and Recycling (39) (2003) 325-340.
- [3] Nozahic V, Amziane S, Torrent G, Saïdi K, De Baynast H. Design of green concrete made of plant-derived aggregates and a pumice-lime binder. Cem Concr Comp (34) (2012) 231-241.
- [4] Altieri A., Pinna D. Monumenti e manufatti in ambienti costieri. La biologia vegetale per i Beni Culturali. Vol. I Biodeterioramento e conservazione. Caneva G. Nugari M.P., Salvadori O. Collana Arte e Restauro, Nardini Ed., Firenze (2005) 196-199.
- [5] BS-EN 459-1. Building Lime. Part 1: Definitions, specifications and conformity criteria. BSI, Standards Publication, London (2010).
- [6] Martín Ramos, J.D. X Powder. A software package for powder X-ray diffraction analysis. Lgl. Dep. GR 1001/04 (2004).
- [7] UNE-EN 15886. Conservation of cultural property - Test methods - Colour measurement of surfaces. Spanish Association for Standardization and Certification, Madrid (2011).

- [8] Arizzi A, Brümmer M, Martín Sánchez I, Cultrone G, Viles H. The influence of the type of lime on the hygric behaviour of hemp-based mortars. Submitted to *Cem Concr Compos* (2014).
- [9] Kivistö, A. T., and Karp, M.. 1,3-propanediol production and tolerance of a halophilic fermentative bacterium, *Halanaerobium saccharolyticum* subsp. *saccharolyticum*. *J. Biotechnol.* (152) (2011) 114–124.
- [10] López-Archilla, A.I. , A.E. González, M.C. Terrón, and R. Amils. Diversity and ecological relationships of the fungal populations of an acidic river of Southwestern Spain: The Tinto river. *Can. J. Microbiol.* (50) (2004) 923–934.
- [11] Qasemian L , Billette C , Guiral D , Alazard E , Moinard M , Farnet AM . Halotolerant laccases from *Chaetomium* sp., *Xylogone sphaerospora*, and *Coprinopsis* sp. isolated from a Mediterranean coastal area. *Fungal Biol.* (116) (2012) 1090-1098.
- [12] Butinar L, Zalar P, Frisvad JC, Gunde-Cimerman N. *FEMS Microbiology Ecology* (51) (2005) 155–166.

Effect of ethyl silicate on salt crystallization resistance of Maastricht limestone

B. Lubelli^{1,2}, R.P.J. van Hees^{1,2}, T.G. Nijland¹ and J. Bolhuis¹

¹TNO, Delft, The Netherlands

²Delft University of Technology, Faculty of Architecture, Delft, The Netherlands

* barbara.lubelli@tno.nl

Abstract

Consolidant treatments aim to re-establish the cohesion in decayed materials showing decay patterns as sanding or powdering. Ethyl silicate (TEOS) is the most used type of consolidant for inorganic porous materials in the last 30 years. This product, which works through precipitation of silica gel in the pores of the material, is known to have a good chemical compatibility with siliceous substrates (sandstone and brick), but much less with lime based materials as limestone and mortar. In order to encounter this shortcoming, in the last years, research has been focused on the modification of ethyl silicate products to make them more compatible with lime-based substrates.

In this study the effect of an ethyl silicate product, commercialized for application on limestone, has been investigated. The research concerned more specifically the resistance of Maastricht limestone with respect to salt crystallization. The penetration depth and the strengthening effect of the treatment have been assessed, using respectively dithizone and the Drilling Resistance Measurement Method (DRMS). Further the influence of the treatment on water absorption and drying, measured by standard test procedures, has been assessed. An accelerated salt crystallization test has been carried out to assess the effect of the treatment on the salt resistance of the Maastricht limestone. All tests have been performed on fresh stone as well as on artificial analogues for decayed stone, obtained by re-aggregating the original stone following a method developed by the authors.

The results showed that the studied ethyl silicate product is able to reach a very good penetration depth in the Maastricht limestone and to confer a significant strengthening to the substrate, without significantly altering the overall drying behavior of the material. However, a not homogenous distribution of the product and of its strengthening effect in the impregnated zone has been measured. This has, for the salt crystallization test on specimens with the re-aggregated layer, caused salt accumulation behind the outer zone, enriched in ethyl silicate, which consequently resulted in the detachment of this 2-3 mm thick layer.

The differences in extent and type of damage observed during the crystallization test between fresh stone and re-aggregated stone specimens underline the necessity to test consolidant products on (artificially) decayed and not on fresh substrates in order to obtain reliable results.

Keywords: Maastricht limestone, ethyl silicate, salt crystallization test, analogues for decayed stone.

1 Introduction

Consolidant treatment can be defined as the impregnation with a product that, penetrating in depth in a material, improves the cohesion of the decayed part and possibly the adhesion of this to the sound material beneath. The expected result is a better resistance of the consolidated material to decay phenomena.

Amongst organic consolidants, products based on ethyl silicate (TEOS; tetra-ethylorthosilicate) are the most commonly used in the last decades. The chemical reaction leading to consolidation can be summarized as follows: in contact with water, present in the stone, the ethyl silicate breaks down into ethyl alcohol (which evaporates) and silicic acid. The latter forms a silica gel, that is deposited in the pores and the fissures of the materials, thus re-establishing cohesion. As silica is the main component of ethyl silicate, this consolidant is particularly suitable for materials containing silica, as sandstone and brick. However, because of the lack of effective alternatives, ethyl silicate is also often used for consolidation of lime-based mortar and limestone. In the last years different solutions for this problem have been looked for, including pre-treatment of the lime-based material in order to improve the adhesion of TEOS to the substrate [1], and modification of TEOS for improvement of its compatibility with lime-based substrates. [2, 3] In this research, a commercial ethyl silicate product, on purpose modified to increase its compatibility with lime-based substrates, has been tested.

Especially when assessing the feasibility of a consolidant product for application on substrates with a heritage value, the fulfilment of requirements related to its compatibility with the substrate should be considered [e.g. 4-7]. A treatment can be defined as compatible if it does not cause or enhance any damage (technical or esthetical) to the historic material. Damage processes such as salt crystallization should therefore not be enhanced by the consolidation. This might occur if the treatment significantly modifies the properties of a material: for example, a decrease in the evaporation rate due to the presence of the consolidant, may lead to salt accumulation behind the treated layer, with possible subsequent spalling of the last.

Moreover, as a consolidant aims at re-establishing the cohesion and increasing the strength of a decayed substrate, an effective consolidation is expected to improve the resistance of a material with respect to damage processes as e.g. salt crystallization. The effect of a consolidation on the salt crystallization resistance of a material can be assessed by an accelerated crystallization test comparing the behavior of treated and untreated specimens.

An important limitation, when testing the effect of a consolidant, is given by the difficulty of applying the product on a sufficient number of representative, weathered specimens. In laboratory tests, consolidants are usually applied on sound, fresh materials, which might invalidate the obtained results or complicate their interpretation. This choice is due to the difficulty of finding representative, reproducibly decayed substrates for testing. These might be either sampled from the field or produced in the laboratory. The first option is seldom applicable in the field of conservation: it is in fact generally not desirable nor allowed to sample a sufficient amount of materials from monumental buildings and/or objects. Moreover, differences in properties (as e.g. salt content, strength) among the specimens might be present.

In this research, reproducibly weathered specimens, obtained by a novel method developed by the authors, have been used [8].

2 Materials and methods

2.1 Stone type and properties

This research has been carried out on Maastricht limestone, a stone widely used for building purposes in the southern part of The Netherlands and in adjacent Belgium [9]. The Maastricht limestone is a very soft, yellow coloured and highly porous limestone composed by calcium carbonate bioclasts of about 300-500 μm diameter, poorly cemented by sparite. Its open porosity (51 vol%) is very high and constituted by coarse pores in the range of 40 μm [8]. Its CaCO_3 content is very high, up to 94-

98 wt.% [9]. Weathering often manifests in Maastricht limestone as loss of cohesion and powdering of the surface (figure 1).



Figure 1: Loss of cohesion and powdering of Maastricht limestone (castle ruine, Valkenburg, The Netherlands)

2.2 Specimens

Two types of specimens have been used in this research:

- Cylinders of fresh Maastricht limestone of 45 mm diameter and 50 mm height
- Cylinders of 45 mm diameter consisting of a core of 40 mm height fresh Maastricht limestone with a 10 mm re-aggregated layer on top (figure 2).

The cylinders of fresh stone were drilled out of slabs, with the natural layering of the stone perpendicular to the surface of the cores. This choice was made to reproduce the practice situation, where stone blocks are generally laid with the natural layering perpendicular to the surface.

The re-aggregated layer reproduces a decayed surface and it has been made following a procedure developed by the authors. This procedure, described in detail in [8], consists in grinding the limestone, sieving the

obtained particles in an appropriate grain size range and re-aggregating them by the use of an air lime binder in suitable proportions. The obtained “mortar” is then applied as a layer on the sound material and allowed to carbonate. The final result is a reproducible substrate, having a similar chemical composition as the original material but an increased open porosity and main pore size. These characteristics are representative for a decayed material [10]. The open porosity and pore size distribution of fresh and re-aggregated Maastricht limestone are compared in figure 3: the open porosity of the re-aggregated layer is 54%, with mostly pores in the range of 80 μm . As expected for a decayed material, the open porosity and the main pore size of the re-aggregated layer are larger than those of the fresh stone. Figure 4 shows a thin section of the re-aggregated layer on the fresh stone illustrating the higher and coarser porosity of the re-aggregated part with respect to the original stone. A zone slightly enriched in binder is visible at the interface between re-aggregated and fresh stone.

All specimens were coated on the cylindrical side with a two component epoxy resin in order to avoid absorption of the treatment (during the application) and water (during the water absorption and the salt crystallization tests) from this side.

Next to the small specimens described above, 15 x 15 x 10 cm specimens of fresh stone and of stone with re-aggregated layers were prepared to be used for assessing the penetration depth of TEOS.



Figure 2: Specimen of Maastricht limestone with re-aggregated layer on top

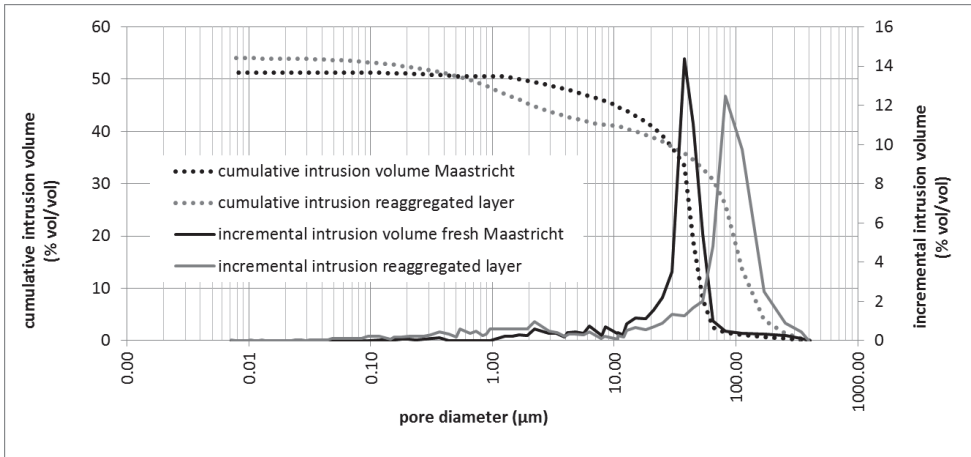


Figure 3: Open porosity and pore size distribution of the fresh Maastricht limestone and of the re-aggregated layer.

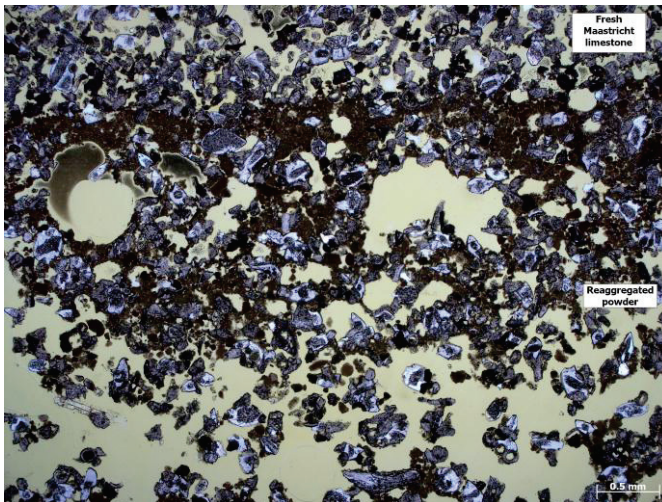


Figure 4: Plane polarized microphotograph of re-aggregated layer (below) on fresh Maastricht limestone (above) (original size: 5.4 x 3.5mm)

2.3 Application of the consolidant

The selected consolidant is a commercial product based on ethyl silicate. According to the information from the producer, this product has improved adhesion properties and it is especially suitable for application on

limestone substrates. According to the producer's technical sheet, the percentage of active components in the product is 95%, leading to about 30% gel formation after reaction.

Both specimens of fresh stone and specimens with re-aggregated layer were treated. The specimens were conditioned 20 °C 50% RH before treatment. The product was applied by brush on the surface, in two applications at a distance of one day. In order to define the amount of product to be used, some trial applications were carried out: in the trials, the treatment was applied until a penetration depth of 10 mm (assessed visually) was reached; this penetration depth corresponds to the thickness of the re-aggregated layer. The average amount of product absorbed was then calculated and the specimens were treated with this amount of product. The average consumption was slightly higher for specimens with re-aggregated layer than for those of fresh stone: 8.4 l/m² and 8 l/m², respectively. The high consumption is due to the very high absorption typical for this type of limestone.

After treatment, the specimens were cured at 20°C, 50% RH for at least three weeks before the start of the tests.

2.4 Penetration depth

Different methods exist to check the penetration depth of consolidant products. Some of these only assess the penetration of the product (as for example by the use of an indicator or microscopy observations), while other methods assess the extent and depth of its consolidating effect. In this research the depth of impregnation has been indicatively evaluated by spraying a solution of dithizone (diphenylthiocarbazone) in acetone on a cross section of some treated specimens few weeks after the treatment: a change in color from green to pink/orange indicates the presence of the product. The principle at the base of this colour change is the reaction of dithizone with metallic elements, often present in the catalyzing agents of ethyl silicate products [11]. Additionally, scanning electron microscopy, equipped with Energy Dispersive X-ray Spectroscopy (SEM-EDS) (FEI NovaNanoSEM650) has been used to investigate the distribution of the product in the porous system of the stone.

Moreover, the extent and depth of its consolidating effect have been measured by means of the Drilling Resistance Measurement Method (DRMS) by Sint Technology. This instrument can assess the consolidating effect by measuring the resistance the substrate opposes to the penetration of a drill; both the rotation speed and the penetration speed of the drill are constant and can be adjusted depending on the strength of the stone [12].

In this research, DRMS measurements have been carried out on fresh Maastricht limestone and on re-aggregated substrates, before and after treatment. Measurements were carried out up to 30 mm depth. A rotation speed of 40 rotations per minute and a penetration speed of 40 mm per

minute were used. 10 DRMS profiles were drilled for each specimen from which the average was calculated. For an optimal consolidation, the strength of the decayed and consolidated material should be equal to that of the sound stone.

2.5 Water absorption and drying test

The effect of the treatment on the absorption and drying behavior was determined, both on specimens with re-aggregated layer and on fresh stone specimens. The water absorption was determined and the water absorption coefficient (WAC) calculated, according to the CEN standard EN 1925-1999. In order to minimize the variance between the specimens, the absorption and drying were measured on the same specimens before and after treatment. Besides, the drying was assessed on the same specimens on which water absorption had been measured. Absorption and drying were measured in a climatic chamber at 20 °C, 50% RH. All experiments were carried out in threefold.

2.6 Salt crystallization test

The effect of the consolidant on the salt resistance of the stone to NaCl and Na₂SO₄ crystallization was assessed on specimens with a re-aggregated layer on top (treated and untreated) and on fresh stone specimen (treated). The crystallization experiment was carried out in threefold.

The accelerated salt crystallization test was carried out according to an adapted version of the procedure developed in the EC projects SCOST [13] and COMPASS [14].

The procedure used in this research includes the following steps:

1. The specimens are contaminated with NaCl and Na₂SO₄ solutions. The amount of solution is equal to the capillary water content, i.e. to the amount of solution necessary to wet the upper surface of the specimen when its bottom surface is in contact with the solution. In this way it is ensured that the salt solution reaches the upper (treated) surface of the specimen. The concentration of the salt solutions (10% and 5% for NaCl and Na₂SO₄, respectively) is calculated in such a way as to obtain a salt content in the specimens of 3 and 1.5% by weight, for NaCl and Na₂SO₄, respectively. The different salt concentrations were chosen because of their different damaging effect. Higher Na₂SO₄ concentrations might result in immediate damage in all the tested specimens, making a comparison impossible; a lower NaCl concentration might be insufficient to cause damage within the test period.

2. The specimens are dried. The drying includes two periods:
 - a. a first period, in which the specimens are dried at temperature and RH conditions cycling between 20°C, 65% RH (8 hours) and 40°C, 20% RH (16 hours), until 80% of the absorbed water is evaporated;
 - b. a second period, in which the RH crosses the RH of equilibrium of the salts, in order to stimulate hygroscopic moisture uptake and release and thus dissolution/crystallization cycles. Two cycles of 20°C, 96% RH and 60°C, 0% RH for a total period of one week are foreseen.
3. The appearance of efflorescence and the occurrence of damage are described and photographically recorded. The specimens are brushed and the material loss (salt + debris) measured. The debris is then separated from the salt, by dissolving the salt and filtrating the aqueous solution.
4. The specimens are re-wetted with an amount of demineralized water equal to the amount of salt solution used at the start
5. Steps 2-4 are repeated 4 additional times.

3 Results

3.1 Penetration depth

The test with dithizone, carried out on specimens of fresh and re-aggregated stone specimens, showed a very deep penetration of the consolidant, which reached more than 30 mm in both fresh and re-aggregated stone (figure 5).

The SEM-EDS observations confirmed the presence of the consolidant in the depth of the stone. The product is present in a large amount in the re-aggregated layer, where it can be easily distinguished because of the presence of shrinkage cracks, a typical feature of hardened ethyl silicate (figure 6).

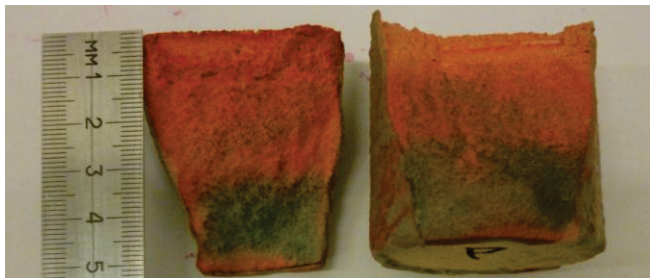


Figure 5: Penetration depth of ethyl silicate in a specimen with re-aggregated top layer (the pink-orange colour indicates the presence of the treatment)

The DRMS profiles of sound Maastricht stone before and after treatment are reported in figure 7. The results show that the 'hardness' of the stone has increased after treatment up to the whole measured depth (30 mm); this means that the impregnation depth is at least 30 mm, and confirms the results of the dithizone test and of the SEM observations. The very deep impregnation depth (deeper than the 10 mm desired) is due to the strong capillary suction / absorption of this stone as a result of the coarse pore structure of the Maastricht limestone. Further, due to the fact that the application was carried out on a horizontal surface, gravity might also have played a role to the transport of the consolidant to this depth. The profile of the consolidated stone shows a higher hardness at the surface, indicating that an accumulation of the strengthening product occurred in the outer 3-4 mm. This may have consequences for moisture and salt transport.

The DRMS measurements on the fresh stone, before and after treatment, allow to assess the strengthening effect of the treatment; however, it is difficult, only on the basis of these results, to evaluate whether consolidation is suitable or excessive. An objective evaluation can be better obtained by comparing the strength of the sound stone with that of the decayed layer after consolidation: for an optimal consolidation, the strength of the decayed and consolidated material should be equal to that of the sound stone. Besides, in any case the strength of the consolidated layer should not be higher than that of the sound stone.

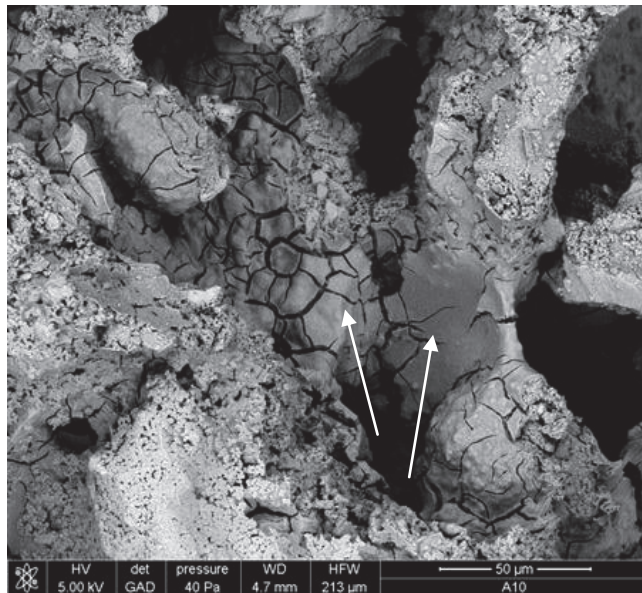


Figure 6: SEM microphotograph of the re-aggregated top layer of a specimen treated with ethyl silicate. The arrows indicate the product bridging stone particles.

In figure 8, the DRMS profiles of specimens with re-aggregated layer, before and after consolidation, are reported. After treatment, there is an overall increase of the strength up to 30 mm depth in the stone, but the strengthening effect is not as homogenous as desired. Peaks in the DRMS profile are visible at the surface (as observed in the untreated specimen) and at the interface between the re-aggregated layer and the fresh stone underneath (probably due to the abrupt change in pore size distribution and to the presence of a slightly denser layer at the interface). At both these locations, the strength of the consolidated re-aggregated layer is much higher than that of the sound (fresh) stone. This constitutes an undesired effect, which may have consequences for the durability of the consolidated material: because of the differences in strength, decay phenomena as scaling and/or spalling may occur.

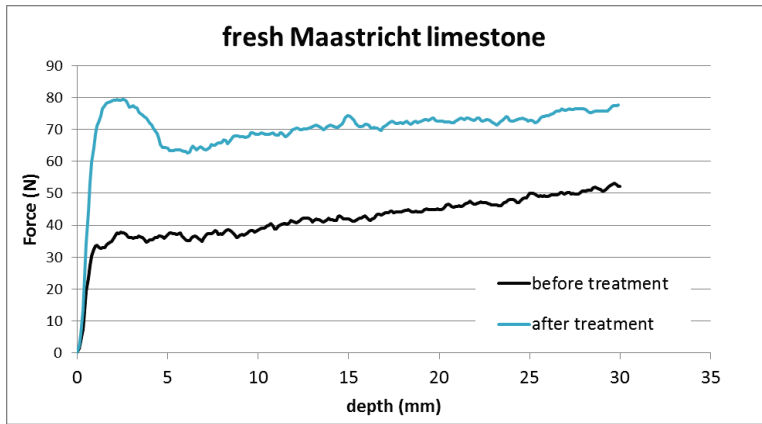


Figure 7: DRMS profile of sound Maastricht limestone before and after treatment (each profile is the average of 10 measurements).

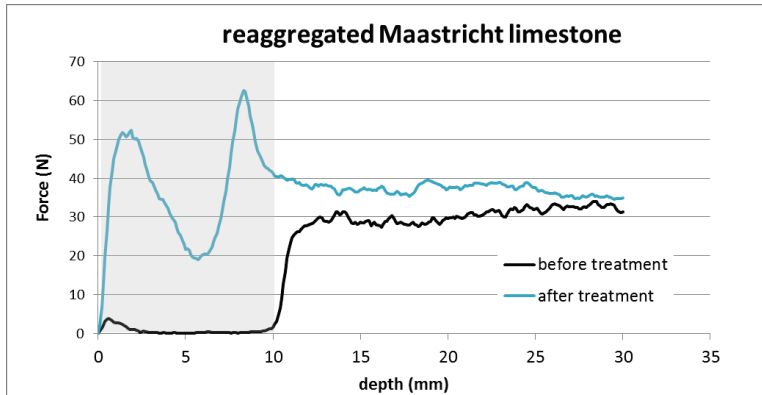


Figure 8: DRMS profile of re-aggregated Maastricht limestone before and after treatment; the grey area indicates the thickness of the re-aggregated layer (each profile is the average of 10 measurements).

3.2 Absorption and drying behavior

The water absorption of fresh Maastricht limestone specimens, before and after treatment, is reported in figure 9. The water absorption of the fresh stone decreases after treatment with ethyl silicate; a reduction of about 40% of the Water Absorption Coefficient (WAC) is measured.

Also for the re-aggregated specimens, a reduction of the water absorption rate is measured after treatment, though less pronounced than for the fresh stone specimens. In this case, it is difficult to quantify the effect of the ethyl silicate on the WAC, since the first part of the absorption curve of the treated specimen is not linear.

In the evaluation of the compatibility of a surface treatment, the effect of the product on the drying behaviour is of primary importance. A consolidant treatment should not considerably delay the drying [4].

The results of the drying measurements (figure 10) show that the ethyl silicate slightly delays the drying, both in sound and re-aggregated specimens: after 14 days the untreated specimens (both fresh and re-aggregated stone) have lost 99% of the absorbed water, whereas the same specimens, after consolidation, have lost 95% (fresh stone) and 92% (re-aggregated stone) of the absorbed water. This represents a slight delay in the drying which can be considered acceptable.

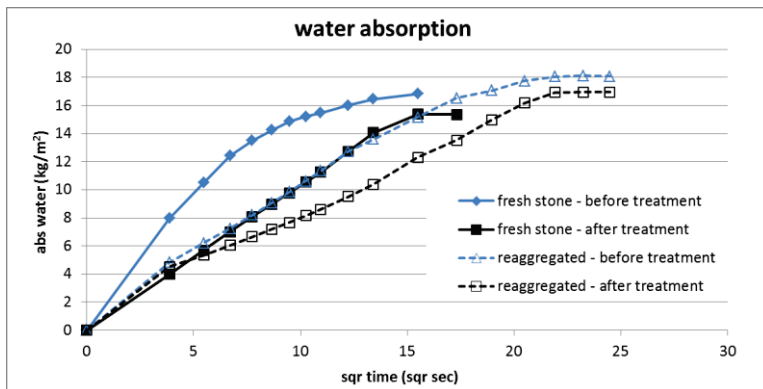


Figure 9: Water absorption of fresh and re-aggregated stone specimens, before and after treatment with ethyl silicate.

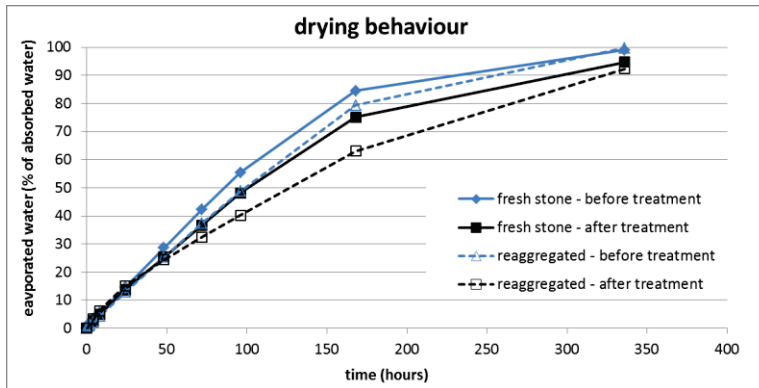


Figure 10: Drying behaviour of fresh and re-aggregated stone specimens, before and after treatment with ethyl silicate.

3.3 Salt crystallization test

The loss of material of re-aggregated specimens subjected to salt crystallization test during 4 complete cycles (about 12 weeks) is reported in figure 11.

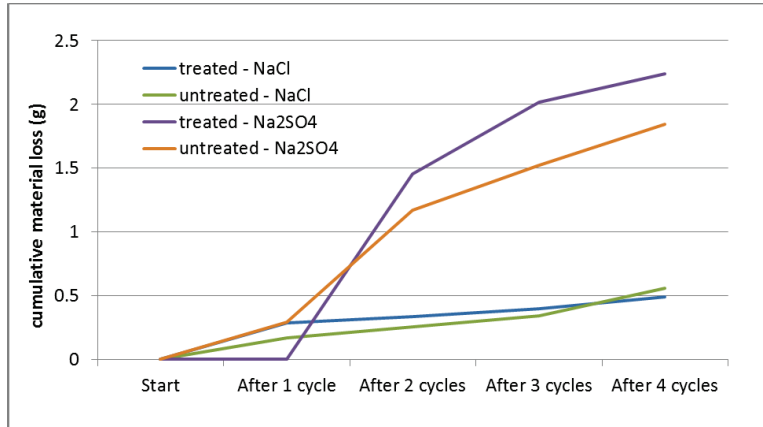


Figure 11: Cumulative material loss in specimens with re-aggregated layer during the salt crystallization test.

The specimens wetted with demineralized water (treated and untreated) did not suffer any damage. In the case of specimens contaminated with sodium chloride, very little damage was observed in untreated and treated specimens in the form of powdering of the surface. The specimens

showed a salt crust at the surface at the end of the drying period; the salts dissolve and migrate back into the specimen during the high RH periods.

The specimens contaminated with sodium sulfate showed a significant material loss. Damage appeared after the first (in untreated specimens) or second (in treated specimens) re-wetting. This is due to dissolution of thenardite followed by rapid re-precipitation of mirabilite at high supersaturation, with consequent generation of high crystallization pressures [15]. Most probably, the strengthening provided by the consolidant initially delayed the occurrence of the damage in treated specimens. However, after 4 re-wetting cycles, the loss of material in specimens treated with ethyl silicate was more relevant than in untreated specimens. Material loss occurred in the form of powdering of the re-aggregated layer in the case of the untreated specimen, whereas in the case of the treated specimen, a complete layer of about 2-3 mm thickness detached, due to the pressure developed by the crystallization of the salts accumulated under the outer layer. The thickness of the detached layer does not correspond to the full impregnation depth of the treatment (which is much deeper), but to the zone showing a very high strength in the DRSM profiles, due to an enrichment in ethyl silicate (figure 8). Most probably, the inhomogenous distribution of the treatment caused discontinuities in the moisture transport, which led to salt accumulation behind the zone rich in ethyl silicate and to development of locally high crystallization pressures and damage. In the untreated specimens, the more homogenous distribution of the salts beneath the surface, explains the observed limited damage in the form of powdering.

For comparison, the crystallization test was also carried out on fresh stone, treated with ethyl silicate and contaminated with sodium chloride and sodium sulfate. As for the re-aggregated specimens, no significant damage was observed in the case of sodium chloride. Specimens contaminated with sodium sulfate showed only 1/10 of the material loss observed in the specimens with re-aggregated layer, occurring in the form of powdering. No layering of the surface was observed, in spite of the clear enrichment in ethyl silicate in treated fresh stone noticed in the DRMS profiles (figure 7). It is not possible to foresee whether layering would occur in a later stage, after a larger number of cycles.

However, it is clear that significantly different results on the effects of a consolidant on the resistance of a material with respect to salt weathering can be obtained, depending on the state of conservation of the specimens (fresh or decayed) on which the consolidant is tested. This consideration underlines the importance of using (artificially) decayed specimens when testing the behaviour of consolidant products.

4 Discussion and conclusions

This research investigated the effect of an ethyl silicate product for consolidation of limestone on the resistance of Maastricht limestone to salt crystallization damage. With this aim the product was tested on fresh stone, as well as on specimens with a re-aggregated stone layer, constituting artificial analogues for decayed stone.

The results showed that this product applied on Maastricht limestone is able to reach a very deep penetration and to confer a significant strengthening to the substrate without significant altering the overall drying behavior of the material. However, a not homogenous distribution of the product and of its strengthening effect occurs in the impregnated zone. This has led, in the case of specimens with a re-aggregated layer, to salt accumulation behind the surface zone with accumulation of ethyl silicate, resulting in the detachment of this 2-3 mm thick layer.

The parallel execution of the salt crystallization test both on fresh stone and on re-aggregated specimens (reproducing the decayed substrate) has shown that the initial state of conservation of the substrate can significantly affect the results. Considered that in the conservation practice consolidant treatments are applied on decayed substrates, consolidants should be tested on (artificially) decayed substrates or on representative and reproducible replicas of these (as done in this research) in order to obtain reliable results with respect to their performance and compatibility.

Acknowledgements

This research has been developed in the framework of the EU project Nanomatch - Nano-systems for the conservation of immovable and moveable polymaterial Cultural Heritage in a changing environment (Grant agreement no: 283182).

References

- [1] Ferreira Pinto, A.P., & J. Delgado Rodrigues, 2008, 'Hydroxylating conversion treatment and alkoxy silane coupling agent as pretreatment for the consolidation of limestones with ethyl silicate', in: Delgado Rodrigues, J. & Mimoso J.M. (Eds.), Stone consolidation in cultural heritage: research and practice, LNEC, Lisbon, 131-140.
- [2] Wheeler, G. (et al.), 2000, 'Evaluation of alkoxy-silane coupling agents in the consolidation of limestone', in: Fassina, V. (Ed.),

- Proceedings of the 9th International Congress on Deterioration and Conservation of Stone, Venetië. Elsevier, Amsterdam, 541-545.
- [3] Steinhauser, U., & R. Wendler, 2004, 'Conservation of limestone by surfactants and modified ethylsilicate'. In: Kwiatkoski, D. & R. Lofvendhal (Ed.), Proceedings of the 10th International Congress on Deterioration and Conservation of Stone. ICOMOS Sweden, Stockholm, 439-446.
- [4] Sasse H.R., Snethlage R., 1996, Methods for evaluation of stone conservation treatments, In : Baer N.S. , Snethlage R. (Eds.), Saving our architectural heritage : the conservation of historic stone structures, Report of the Dahlem workshop, Berlin, March 3-8, 1996, Chichester ; New York ; Weinheim : J. Wiley, 1996, 223-243.
- [5] Siegesmund S., Snethlage R., Stone in architecture: properties, durability / Fourth edition, Springer, Berlin, 2011
- [6] Snethlage, R., 2005, Leitfaden Steinkonservierung. Planung von Untersuchungen und Maßnahmen zur Erhaltung von Denkmälern aus Naturstein. 2nd ed., Fraunhofer IRB Verlag, Stuttgart.
- [7] van Hees, R.P.J., Lubelli B, Nijland T.G., 2014, Compatibility and performance criteria for nano-lime consolidants, to be published in Proceedings of 9th International Symposium on the Conservation of Monuments in the Mediterranean Basin, Ankara (Turkey), 2-5 June 2014.
- [8] Lubelli B., van Hees R.P.J., Nijland T.G., Bolhuis J., A new method for making reproducible artificially weathered stone specimens, submitted to Journal of Cultural Heritage
- [9] Dubelaar C.W, Duser M, Dreesen R., Felder W.M., Nijland T.G., (2006) Maastricht limestone: a regionally significant building stone in Belgium and the Netherlands. Extremely weak, yet time-resistant, In: International Conference on Heritage, Weathering and Conservation, Madrid, 21-24 June 2006.
- [10] Franzoni E., Sassoni E., Scherer G.W., Naidu S., 2013, Artificial weathering of stone by heating, J Cult Heritage 14S, 85–93.
- [11] Leroux L., Verges-Belmin V., Costa D., Delgado Rodriguez J., Tiano P., Snethlage R., Massey S., De Witte E., 2000, Measuring the penetration depth of consolidating products: comparison of six products, in Fassina V (Ed.), Proceedings of the 9th International

Congress on Deterioration and Conservation of Stone., Venice, June 19-24, 2000, Vol. 2, 361-369.

- [12] Fratini F., Rescic S., Tiano P., 2006, A new portable system for determining the state of conservation of monumental stones, *Materials and Structures* 39 (286), 125-132.
- [13] De Witte E. (ed.), *Salt Compatibility of Surface Treatments (SCOST)*, Final report of the EU project ENV4-CT98-0710, 2002, 302 pp.
- [14] Wijffels T., Lubelli B., 2006, Development of a new accelerated salt crystallization test, *Heron* 51 (1), 63-75.
- [15] Shahidzadeh-Bonn, N., Desarnaud, J., Bertrand, F., Chateau, X., Bonn, D., 2010, Damage in porous media due to salt crystallization, *Physical review E*, (81), 066110, 1-6.

Sodium sulphate test on lime-based mortars: attaining degraded material to test conservation products and assessing salt resistance

C. Nunes*¹, Z. Slížková¹ and J. Delgado Rodrigues²

¹Institute of Theoretical and Applied Mechanics, Prague

²National Laboratory for Civil Engineering, Lisbon

* nunes@itam.cas.cz

Abstract

Four mortar mixtures were subjected to a sodium sulphate test, formulated to obtain degraded material for the further testing of conservation products and to estimate its salt resistance based on their hydric and hygric parameters. The ageing test involves cyclic conversion of thenardite-mirabilite. The cycle comprises of: the drying stage, salt absorption by capillarity, cooling and finally a total immersion in water. Water absorption by capillarity and microporosity determined by mercury porosimetry, were found to have a significant effect on the amount of salt absorbed consequently reflecting the induced damage. The experimental results support the theoretical view that micropores smaller than 0.1 μm in radius have a critical influence on the damage induced by sodium sulphate. Lime-metakaolin mortar proved to be extremely salt-susceptible in respect to lime mortar. The addition of linseed oil to both lime and lime-metakaolin mortar improved the salt resistance of both materials by granting hydrophobicity and restraining the absorption of salt. The ageing test used was successful in attaining lime mortar specimens to exhibit degradation patterns parallel to naturally exposed material, therefore can now be used for the testing of conservation products.

Keywords: sodium sulphate, lime, metakaolin, microporosity, hydrophobicity

1 Introduction

Salt damage is currently considered one of the main weathering processes of porous construction materials [1] and it is especially relevant in old buildings. Salt degradation progresses faster in old masonries because these are based on lime mortars, which are mechanically weaker than the porous materials in new buildings. One way to improve the strength and durability of air lime mortars is to partially replace air lime by other materials such as pozzolanas. Metakaolin is a promising pozzolanic material in this regard because it can grant higher mechanical strength than pure air lime mortar but not high enough to generate stress leading to failure of the original system [2].

Since liquid transport is one of the key factors influencing durability, materials that grant hydrophobic properties to mortars have become of great interest to the scientific community [3]. Research on the usage of traditional compounds to improve repairing mortars durability has also become of great interest [4, 5, 6] due to their harmless nature, compatibility with the traditional construction materials and cost-effectiveness.

Under the impossibility of sampling damaged materials from the historic buildings, *in situ* tests are the only means of evaluating the behaviour of the treatments in real field conditions. Nevertheless, the controlling of the variable parameters and the measuring conditions impose great difficulties in gathering reliable information [7]. This situation forces the investigations to simulate the testing of sound materials, which may not be quite representative of the onsite reality. The results obtained are limited in what concerns the evaluation of the treatment efficiency because there is an information lack about its action in the weathered material, which has different characteristics from the sound material. The contrast of properties is also expected to be lower in sound materials and therefore the harmful potential of the tested situations may result severely underestimated when compared to reality.

The values of the material properties, namely the hydric and hygric parameters (e.g. porosity, water capillary coefficient, pore size distribution, drying behaviour) are of utmost importance in the immediate action, namely in the cohesive properties and durability of the product. This aspect was the main goal for the formulation of the salt ageing test used in the present study.

Sodium sulphate was selected as the ageing salt due to its highly aggressive nature, to its worldwide occurrence in the architectural heritage and to its common use in building material durability studies [8, 9]. However, the definition of a testing protocol based on the action of sodium sulphate to produce a controlled artificial ageing has shown to be a more difficult task than it was initially expected because degradation is not a simple regular process. In fact, trying to induce slight modification of the

specimen through the action of sodium sulphate may destroy it completely within one or two cycles [10].

2 Experimental design

2.1 Materials

In the present study, four mortar types were designed and subjected to a sodium sulphate ageing test: lime mortar and lime with metakaolin to improve the mechanical strength; linseed oil was mixed in both reference mortars to grant hydrophobicity and investigate its salt resistance effectiveness.

Aerial dry hydrated lime in the form of powder (classified as CL90S) was used as the basic reference binder for all the specimens. Pure siliceous sand with controlled granulometry (0 to 4mm) was used as aggregate. The hereby-designated metakaolin corresponds to the burnt Czech clay shale Mefisto L05 described in [11]. The linseed oil used was extracted by the cold press method from flax seeds.

The binder/aggregate ratio used to prepare all mortar specimens is shown in Table 1. The amount of water was added in order to achieve 170 ± 5 mm consistency with the flow table test. Binder and aggregate were mixed in an automatic mortar mixer at low speed for 6 min. Water was then added and the mixture was blended for another 3 min. Linseed oil was added in 1.5 wt.% in respect to the binder weight, following the results obtained by [5] and was mixed with the mortar mixture before adding water.

The mortars were moulded in prismatic 40×40×160 mm casts using a jolting table to compact them. The specimens were demoulded after 1 day and the fresh young samples were cut in half to obtain 40×40×80 mm specimens. For the following 6 days the specimens were kept under high RH conditions (90 ± 10 %) and at 20 ± 5 °C. After this period, the mortar prisms were stored for 83 days in a room with controlled RH and T (60 ± 10 % and 20 ± 5 °C) lain on a 40×80 mm face over grid lined plastic shelves. Therefore, the prepared mortars were hardened for 90 days previously to carry out the tests. A more detailed description about the materials and sample preparation can be found in [12].

2.2 Test methods

The ageing test was elaborated based on a previous study with the aim of weathering stone specimens for further treatment [10] and in the present study it was applied on mortars and also used to test the durability of the hydrophobic mortars with linseed oil.

The samples were initially oven dried at 40 °C to constant weight and impregnated by capillarity with a 14 wt.% sodium sulphate solution at 40°C for 5 min. After the impregnation step, the samples were immediately placed in a climatic chamber at 5 °C temperature and 70 % RH, which is above the equilibrium humidity for the $\text{Na}_2\text{SO}_4 - \text{Na}_2\text{SO}_4 \cdot 10\text{H}_2\text{O}$ transition, during 60 min. The samples were then dried at 40 °C during 24 h and afterwards immersed in water at room temperature for 24h. This sequence of procedures corresponds to 73 h weathering cycle. Four samples were used for this test.

The selection of the time interval for the salt solution absorption was preceded by a pilot test with samples with the lateral surfaces unsealed in order to follow the salt solution front along the sample thickness. After 5 minutes the salt solution reached the following depth on each mortar type: Lime (L) – 32 mm; Lime + Oil (LO) – 11 mm; Lime - metakaolin (LM) – 20 mm; Lime-metakaolin + Oil (LMO) – 10 mm. These values already point out the hydrophobic effect in mortars with oil and the material thickness that becomes more exposed to the sodium sulphate action.

The goal of the immersion in water is to include a desalination stage to extract the salt in order to use the degraded material for further investigation of conservation treatments. In the previous study performed with stones [10] it was observed that the immersion in water stage was the one inducing the most severe degradation, regardless of the temperature of the immersion bath (20 °C and 40 °C). In this study the immersion in water was run at room temperature because it is technically more accessible and the degradation is faster as also concluded from the literature [13]: samples subjected to impregnation-drying tests showed no damage during drying at 105 °C and immersion at 50 °C after 7 ageing cycles. Degradation occurred only when immersion was done at 20 °C.

The environmental conditions, i.e., temperature and relative humidity, of the tests were selected based on the phase diagram of sodium sulphate presented in [14].

The amount of salt solution absorbed was registered after each cycle. The mass loss was also monitored after each cycle by measuring the mass remaining in the vessel used for the specimen immersion bath because the degradation expressed as loss of material occurred mostly during immersion in water.

Each mortar type was analysed with mercury intrusion porosimetry after the salt solution impregnation step of the cycle that preceded the most severe degradation or destruction of the material. Prior to this measurement the samples were dried at 40 °C. MIP was used in order to investigate the pore sizes involved in Na_2SO_4 crystallization. The measurements were performed in two specimens of each mortar type on 10 mm layers sampled from the surface of the 40 mm thick mortar specimens.

3 Results and discussion

Figure 1 presents the amount of salt solution absorbed per surface unit. L and LM mortars absorb the highest amount of salt solution as it was expected from the results of water absorption by capillarity. However, LM mortar absorbs a higher amount of salt solution than L mortar although the capillary coefficient is significantly lower. The same phenomena occurred with LMO mortar, which absorbs a similar amount of solution as L mortar on the first 3 cycles, although the capillary coefficient is remarkably lower.

The changes in the samples dimensions were measured with a caliper (resolution of 0.01 mm) after wetting and drying. No differences were detected on the samples dimensions but the method used to measure it is of low precision. The linear hydric coefficient of a lime and lime-metakaolin mortar has been determined [15]: the coefficient of a LM mortar between the dry state and the capillary water saturated state was almost two times higher than for the lime mortar. The mortar used in this study has lower metakaolin content (25 wt.% of binder weight) compared to that of [15] (50 wt. %) but given the important effect that the addition of metakaolin can have on the hydric expansion, this property can have an important influence on the absorption by capillarity and on the degradation process of lime-metakaolin mortars.

Therefore, the capillary absorption result can be misleading e.g. due to reaction between metakaolin and water, which tends to cause swelling and lower the capillary absorption. This is not expected with the salt solution, hence the higher absorption.

The amount of salt solution absorbed during ageing is increasing progressively for both reference and hydrophobic mortars, which means that the water-repellent effect decreases during ageing.

Table 1: Mortars composition, hydric and hygric properties. The values correspond to the average \pm standard deviation.

Mortar code	Composition (L - Lime; M - Metakaolin; S - Sand)	Open porosity ^a [%]	Capillary coefficient ^b [$\text{kg}\cdot\text{m}^{-2}\cdot\text{h}^{-0.5}$]	Drying index ^c
L	L:S(1:3)	32.0 \pm 0.2	28.5 \pm 0.42	0.70 \pm 0.01
LO	L:S (1:3) + Oil	34.4 \pm 0.6	3.95 \pm 1.66	0.63 \pm 0.03
LM	L:M:S (0.75:0.25:3)	34.4 \pm 0.1	13.4 \pm 0.30	0.53 \pm 0.03
LMO	L:M:S (0.75:0.25:3) + Oil	32.4 \pm 0.5	1.98 \pm 0.04	0.57 \pm 0.02

^a Open porosity test was performed with 4 samples according to [16].

^b Sorptivity corresponds to the slope of the curve representing the weight gain per unit surface area as a function of the square root of time and was calculated with 3 samples according to [17].

^c The evaporation curve was determined with 4 samples according to [18] at 40 \pm 5% relative humidity and the drying index was calculated according to [19] which is also described by [20] in English.

Figures 2 and 3 show, respectively, the mass loss and the aspect of the mortars during ageing. On the 8th cycle L mortar showed severe damage throughout the total sample thickness whereas degradation of LO mortar was limited to a layer of the surface. LM and LMO mortar were severely cracked after 2 and 5 cycles, respectively.

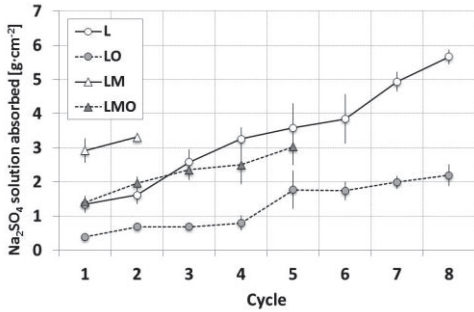


Figure 1: Salt solution absorbed by the samples during ageing.

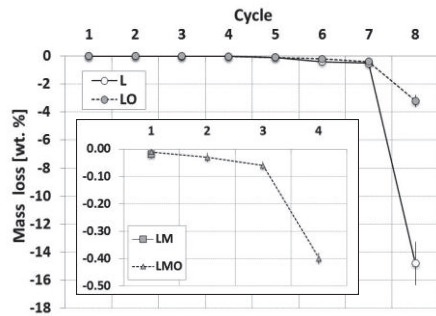


Figure 2: Mortars mass loss during ageing.

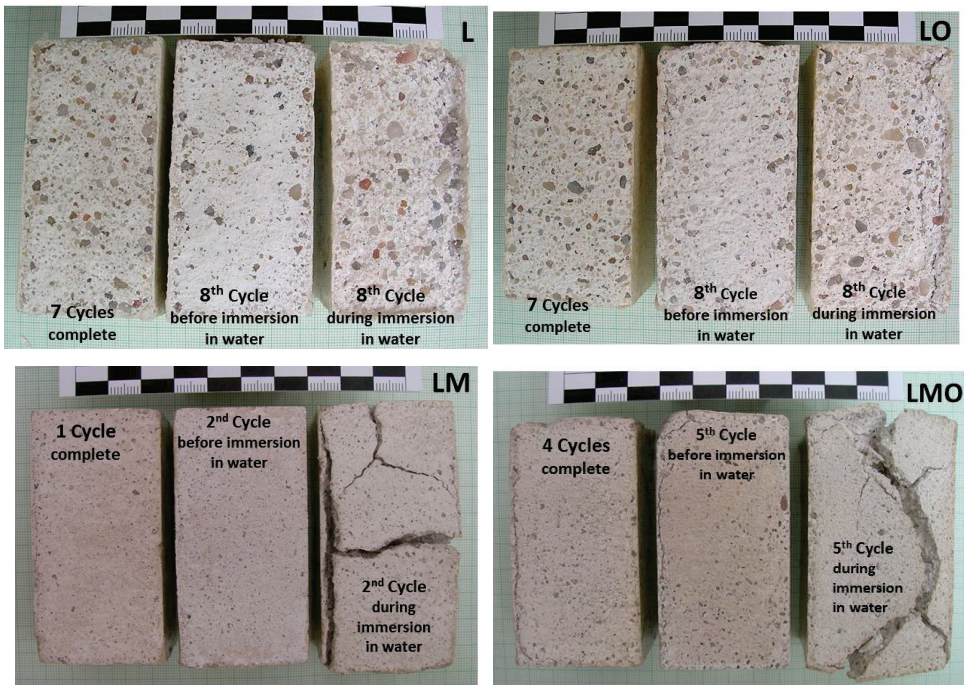


Figure 3: Aspect of mortar specimens during ageing (scale above the specimens shows 1mm intervals).

The mass variation during ageing is rather low during all cycles except for L and LO mortars on the 8th cycle after which full crumbling and severe surface damage, respectively, is noticed. During the previous ageing cycles the material loss of L and LO mortars is mostly assigned to powdering and sanding. After 6 to 7 cycles L mortar seems properly aged for the testing of conservation products as it exhibits moderate powdering and sanding.

On the 8th cycle the L mortar loses a layer of ca. 10-15 mm thickness on both top (in contact with the salt solution) and bottom part, although on the 1st salt absorption stage the solution front only reached 31 mm. The remaining material part is very fragile and it is the resin used to seal the lateral surfaces that sustains it (this is not clear in Figure 3). The reason for the integral damage is probably assigned to salt diffusion during the immersion stage. LO mortar loses only a top layer of 4-6 mm thickness, which reveals the protective effect of oil addition by restraining salt transport.

LM and LMO mortars are the most affected by the salt ageing test: destruction occurs on the 2nd and 5th cycle, respectively. The damage was not evidenced in terms of weight loss but the samples did suffer considerable deformation and cracking during immersion as shown in Figure 3. Higher tensile strengths usually result in more durable materials to salt weathering. Therefore, the crystallization pressure developed in mortars with metakaolin has to be much higher than in mortars with lime because the tensile strength of lime-metakaolin mortar is around 98% higher (1.65 MPa) than that of lime mortars [10].

Taking into account that the tensile strength is a macroscopic quantity and a high crystallization pressure in a single pore does not necessarily cause damage, two additional conditions must be met according to [21]. First, a sufficiently large fraction of the pore wall needs to be in contact with the growing crystal that generates stress. Second, the stress generated by the growing crystals must be large enough to propagate existing flaws in the material. That is, the crystals generating the stress must propagate through a volume of the material sufficiently large compared to the flaw sizes.

The higher hydric expansion coefficient of lime-metakaolin mortar in respect to lime [15] can possibly lead to a higher susceptibility of crack formation.

The thin section of not aged LM mortar analysed by optical microscopy and SEM did not show cracks, as was also the case for L mortar [12]. Therefore, in LM mortar, one cycle is sufficient to generate micro-flaws through the porous structure of the material leading to its destruction on the 2nd cycle.

It was observed that the cooling stage promoted hair-like cracks on the surface, probably due to the hydration distress caused by the supersaturation in respect to mirabilite as the sample temperature decreases. Under the conditions the cooling stage was performed (rapid cooling from a sodium sulphate solution at 40 °C) it is possible that the heptahydrate phase forms rather than the decahydrate as reported in older and recent literature [22]. However, another study [23] using nuclear magnetic resonance to measure Na_2SO_4 solubility in bulk and in pores of 5, 10 and 30nm has suggested that the heptahydrate phase cannot cause significant stress in a porous medium because no supersaturation or subsaturation is observed.

It is during the immersion stage that the degradation expressed as loss of material is evident. The loss of small amounts of surface material during the first ageing cycles immediately after immersion in water can partially be attributed to the cementing effect of sodium sulphate [24]. No particle detachment occurs during the cooling and drying stage as the accumulated salts are simultaneously filling the micro-cracks developed.

When the specimen is submerged in water the dissolution of the cementing salts produces an immediate loss of material surface, even before the precipitation of hydrated phases could commence, as also described in another experimental study [25]. Therefore, surface powdering and sanding occurs as soon as the specimens are submerged because of the immediate dissolution of the salts accumulated at the surface.

The severe cracking phenomena along the specimen thickness takes several hours to occur and can be assigned to the hydration distress, which takes longer time to develop. In the previous study [10], severe degradation of the stone samples also occurred when performing the immersion in water at 40 °C, but the process was less destructive and occurred at a later cycle. It has been recently shown that thenardite alone can inflict substantial damage to building stones in both cyclic total immersion and continuous partial immersion tests without involving mirabilite precipitation [25]. Therefore, the observed degradation can be partially attributed to the cementing effect of salt crystals.

According to [13] noticeable damage can commence once enough salt has accumulated in the porous network. This is due to the fact that salt crystals themselves should act as a confining barrier by occupying and narrowing down the pore spaces, thereby preventing unrestrained crystal growth as well as increasing the chances of confining newly precipitating crystals and thus of crystallization pressure [26]. In this study the water immersion stage contributes to salt extraction but at the same time induces hydration distress. Therefore, it can be inferred that the observed abrupt damage that occurs at a determined cycle for each mortar is not solely assigned to the accumulation of salt but rather develops once the generated flaws reach the threshold of the material resistance.

The MIP technique was used to investigate the pore sizes involved in Na_2SO_4 crystallization. Figure 4 presents the pore size distribution of the samples before and after ageing. The salt loaded samples studied were aged until the cycle that precedes its severe degradation in order to investigate the porometry of the aged specimens. Table 2 presents the porosity, microporosity and density obtained with MIP as well as the amount of salt solution absorbed by the specimens before performing the measurement. Microporosity is defined in this study as the percentage of the porosity expressed in pores less than $1\mu\text{m}$ radius. According to [27] pore sizes under $1\mu\text{m}$ facilitate crystallization damage as also concluded in the previous experiment with limestone [7].

Mortars with oil present higher porosity and less micropores because the triglycerides present in the oil hydrolyse to glycerol when mixed with the alkaline lime based materials [6] and this reaction has a similar effect to that of the saponification (formation of air bubbles), causing air entrainment and shifting the main pore diameter to higher sizes [12].

Mortar L exhibits a trimodal distribution with the main pore volume maxima located at ca. $0.46\mu\text{m}$ showing a small percentage of pores within the region $0.04 - 0.08\mu\text{m}$ and $12.5 - 71.8\mu\text{m}$. The latter pore range is probably assigned to shrinkage cracks and it is through these that water moves faster by capillary transport [28]. LO mortar also shows pores within this size range, however the pores in LO mortar are lined with hydrophobic non-polar hydrocarbon molecules, which prevent the water and salt solution absorption. The pore structure of LM and LMO mortars is mostly constituted of pores below $1\mu\text{m}$ in size. This is due to the presence of hydraulic phases such as CSH (calcium silicate hydrate) [29].

L and LO mortars showed a significant porosity decrease after the 7th cycle solution absorption: 22 and 11 % reduction, respectively. The porosity decrease was considerably higher for L mortar, which is in accordance with the higher amount of salt solution absorbed. A relevant percentage of the porosity decrease in L mortar is assigned to pore sizes below $1\mu\text{m}$ (28 %). LM and LMO mortars did not show significant changes in the porosity values but the microporosity after ageing was slightly higher (1 % increment).

The decrease in microporosity is due to salt crystallizing in and closing the pores. Regarding L and LO mortars, changes in larger pore sizes, between 10 and $100\mu\text{m}$ were also measured. They may be related not only to crystallization of salt partially filling the large pores but also to modifications in the porous structure (cracking). However, no clear shift towards bigger pore radii is registered in samples subjected to the salt crystallization test. Only LM mortar shows a significant increment of the main peak that can be related to modifications in the porous structure (micro-cracking) due to damage development. In this mortar the salt seems to precipitate preferentially in the pore size range between 0.04 and $0.3\mu\text{m}$.

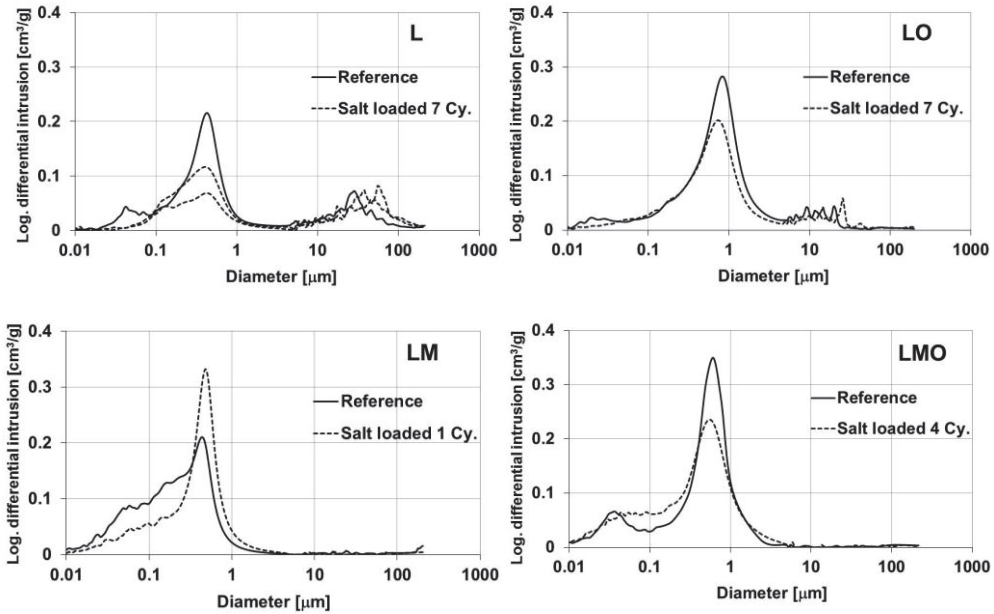


Figure 4: Pore size distribution of reference mortars and salt laden mortars. Only one curve from the two measurements performed in two different specimens is shown since both curves were very similar, except for L mortar aged specimens.

Table 2: Mortar properties determined with MIP of reference and salt laden samples and amount of salt solution absorbed before performing the analysis. Microporosity is defined in this study as the percentage of the porosity expressed in pores less than 1 μm radius.

Mortar code		Porosity [%]	Micro-porosity <1 μm) [%]	Density [g/cm ³]	Amount of salt solution absorbed [wt. %]
L	Reference	32.0 ±0.5	74 ±0.5	1.88 ±0.01	–
	Salt – 7 Cy.	24.9 ±5.1	58 ±2.1	2.15 ±0.10	6.3 ±0.9
LO	Ref.	37.0 ±0.2	69 ±0.2	1.69 ±0.05	–
	Salt – 7 Cy.	33.1 ±2.9	68 ±0.6	1.87 ±0.06	2.7 ±0.7
LM	Ref.	32.9 ±0.4	89 ±0.3	1.78 ±0.02	–
	Salt – 1 Cy.	31.3 ±1.4	90 ±0.2	1.84 ±0.05	4.1 ±1.1
LMO	Ref.	34.9 ±0.6	85 ±0.0	1.69 ±0.03	–
	Salt – 4 Cy.	34.4 ±1.7	86 ±0.3	1.71 ±0.03	3.1 ±0.8

The salt cementing effect is well expressed on the density values of the salt laden material that increases for all mortar types.

Sorption pores (pore size diameter less than $0.1\ \mu\text{m}$) are mostly related to the presence of hydraulic phases such as CSH [29] and according to [30] pore radius smaller than $0.1\ \mu\text{m}$ facilitate the crystallization damage. In the present study, the micropores of LM mortar, that are not present in the reference L, lie within the range of $0.04 - 0.3\ \mu\text{m}$. Therefore, this pore size range seems to be the culprit behind the observed salt crystallization damage. Other studies have pointed pore radius smaller than $0.5\ \mu\text{m}$ [24] and between 0.5 and $5\ \mu\text{m}$ [31] as the micropores that facilitate the crystallization damage.

It can be concluded that the observed damage in all mortar types is mostly related to the pore size distribution and water absorption by capillarity. The open porosity and drying behaviour of the materials tested do not seem to play such an important role since they are relatively similar. However, it is noteworthy that only the lime-metakaolin mortars (LM and LMO) developed a significant amount of salt efflorescences during drying, which is contradictory since these materials show lower drying index in respect to the lime mortars. However, the drying curve of lime mortars is characterized by a straight line meaning the drying rate remains constant during the total drying process whereas for lime-metakaolin, the drying rate does not drop in the beginning, later it does.

It can be inferred that the evaporation in lime mortars more rapidly retracts to the interior, not giving time for the development of salt efflorescences. In lime-metakaolin mortars the retraction of the moisture front progresses more slowly at the beginning, therefore salt efflorescences can develop. Thus, the drying behaviour of lime-metakaolin mortars should account for a higher salt resistance of these materials by promoting the development of salt efflorescences but it was proved to be negligible compared to the other physical properties.

4 Conclusion

It can be concluded that the mass variation during the applied ageing process is not a good indicator for monitoring the mortar degradation because the damage is not clearly evidenced in terms of the weight loss. This is possibly due to the fact that sodium sulphate induces a structural degradation, i.e., in the bulk of the sample, whereas the loss of material is only sensitive to the processes of surface degradation. Therefore, the collapse of the materials at a determined cycle is drastic because the propagation of cracks, with the consequent reduction of the materials resistance, has the character of a cumulative and exponential process and the specimen disintegrates once the threshold of the material resistance is reached. The MIP results in the cycle that precedes the material breakdown already show accumulation of damage, which is in accordance with the degradation mechanism observed. The evolution of the salt solution absorption proved to be a better method to follow the mortar ageing because it reveals the progressive degradation (formation of cracks) of the material expressed as a faster capillarity absorption rate.

The observed damage in all materials can be attributed to the double attack of thenardite (during drying) and mirabilite (during cooling and possibly during immersion) although in this study visible damage is only registered during cooling and water immersion stages.

After 6 to 7 cycles L mortar seems properly aged and useful for the testing of conservation products as it exhibits moderate powdering and sanding. LM mortar manifested itself as a very salt-susceptible mortar by being destroyed on the 2nd cycle.

In the present study it has been shown that the replacement of 25 wt. % of lime by metakaolin has a negative effect on the material resistance towards cycles of thenardite-mirabilite. Although the mechanical strength is improved by metakaolin addition, the microporosity is significantly higher than in the L reference. This is probably the cause for the salt-susceptible degradation of lime-metakaolin mortars because in a smaller sized pore the pressure developed by crystal growth is higher than in larger pores. This factor is so important that not even the addition of oil to lime-metakaolin, which significantly reduces the salt solution absorption, was able to attain the same level of salt resistance as the lime mortar. Further tests should be performed with a mix design with less metakaolin content (e.g. 16.8 wt. % [9]), which does not alter the pore size distribution in respect to the reference and probably decreases the hydric expansion.

The present ageing method proved to be promising to produce weathered mortar and to test its salt resistance. The fact that a complete desalination is difficult to achieve after ageing should be taken into account for the testing of conservation products.

Acknowledgements

The present study was supported by the Czech national project MK ČR NAKI DF11P01OVV008 entitled “High Valuable and Compatible Lime Mortars for Application in the Restoration, Repair and Preventive Maintenance of the Architectural Heritage” and by the Research Development Plan RVO 68378297 at the Centre of Excellence of Telč, built with the support from the EC, from the Czech Ministry of Education, Youth and Sports (CZ.1.05/1.1.00/02.0060). The authors are grateful to Dr. Krzysztof Niedoba for helping with MIP measurements.

References

- [1] Goudie, A., Viles H., Salt Weathering Hazard, John Wiley & Sons, Chichester, 1997.
- [2] Fortes-Revilla, C., Martínez-Ramírez, S., Teresa Blanco-Varela, M., Modelling of slaked lime-metakaolin mortar engineering characteristics in terms of process variables, *Cement and Concrete Composites* (28) (2006) 458-467.
- [3] Izaguirre, A., Lanas, J., Álvarez, J.I., Ageing of lime mortars with admixtures: durability and strength assessment, *Cement and Concrete Research* (40) (2010) 1081-1095.
- [4] Ventolá, L., Vendrell, M., Giraldez, P., Merino, L., Traditional organic additives improve lime mortars: new old materials for restoration and building natural stone fabrics, *Construction and Building Materials* (25) (2011) 3313–3318.
- [5] Čechová, E., Papayianni, I., Stefanidou, M. Properties of lime-based restoration mortars modified by the addition of linseed oil, *Proc. 2nd Historic Mortars Conf.*, Válek, J., Groot, C. and Hughes, J.J. (eds.), ITAM, Prague, 2010, 937-945.
- [6] Vikan, H., Justnes, H. Influence of vegetable oils on durability and pore structure of mortars, *Proc. 7th CANMET/ACI International Conference on Durability of Concrete*, Montreal, 2006, ACI SP-234-25, 417-430.
- [7] Delgado Rodrigues, J., Consolidation of decayed stones: a delicate problem with few practical solutions, *Proc. 3rd Int. Seminar on Historical Constructions: possibilities of numerical and experimental techniques*, Universidade do Minho, Guimarães, Lourenço, P.B., Roca, P. (Editors) (2001) 3-14.

- [8] RILEM PEM/25, Essais recommandées pour l'altération des pierres et évaluer l'efficacité des méthodes de traitement, *Mater Constr*, 17 (1980), 216–220.
- [9] ASTM C 88-90, Standard test method for soundness of aggregate by use of sodium sulfate or magnesium sulfate, *Annu Book ASTM Stand*, 4.2 (1997) 37–42.
- [10] Nunes, C., Methods for the artificial ageing of stone by salt crystallization for use in investigation of stone conservation treatments, MSc thesis, IST - LNEC, Lisbon, 2008.
- [11] Vejmelková, E., Keppert, M. Rovnaníková, P., Keršner Z., Cerny R. Application of burnt clay shale as pozzolan addition to lime mortar. *Cement & Concrete Composites* (34) (2012) 486–492.
- [12] Nunes C., Slížková, Z., Křivánková, D., Lime-based mortars with linseed oil: sodium chloride resistance assessment and characterization of the degraded material, *Periodico di Mineralogia*, (83) Special Issue Ancient and Modern Mortars (2013) 411-427.
- [13] Tsui, N., Flatt, R.J., Scherer, G.W., Crystallization damage by sodium sulphate, *Journal of Culture Heritage* (4) (2003) 109-115.
- [14] Steiger, M., Asmussen, S. Crystallization of sodium sulfate phases in porous materials: the phase diagram $\text{Na}_2\text{SO}_4\text{-H}_2\text{O}$ and the generation of stress, *Geochimica et Cosmochimica Acta* (72) (2008) 4291-4306.
- [15] Černý, R., Drchalová, J., Kunca, A., Tydlilát, V., Rovnaníková, P., Thermal and hygric properties of lime plasters with pozzolanic admixtures for historical buildings, *Proc. 2nd International Conference on Building Physics*, Vermeir, G.L.G., Hens, H., Carmeliet, J. (eds.), 2003, 27-33.
- [16] UNE-EN 1936, Natural stone test methods. Determination of real density and apparent density and of total porosity and open porosity (2007).
- [17] UNE-EN 1015-18, Methods of test for mortar for masonry. Part 18: Determination of water absorption coefficient due to capillary action of hardened mortar (2003).
- [18] RILEM II. 5, Evaporation curve, RILEM 25-PEM: Recommendations provisoires. Essais recommandés pour mesurer l'altération des

- pierres et évaluer l'efficacité des méthodes de traitement, *Matér. Constr.* 75 (13) (1980) 205–207.
- [19] NORMAL – 29/88, Misura dell'indice di asciugamento, CNR/ICR, Roma, 1991.
- [20] Couto, S., Gonçalves, T.D., Lopes, J.M.G., Drying of red ceramic brick. Effect of five silicone based water-repellent treatments, *Hydrophobe VI: Proc. 6th Int. Conf. on Water Repellent Treatment of Building Materials*, Aedification Publishers, 2011, 81-92.
- [21] Scherer, G. W., Crystallization in pores. *Cement and Concrete Research* (29) (1999) 1347–1358.
- [22] Saidov, T.A., Espinosa-Marzal, R.M., Pel, L., Scherer, G.W., Nucleation of sodium sulphate heptahydrate on mineral substrates studied by nuclear magnetic resonance, *Journal of Crystal Growth* (338) (2012) 166-169.
- [23] Rijniers, L.A., Pel, L., Huinink, H.P., Kopinga, K., Salt crystallization as damage mechanism in porous building materials – a nuclear magnetic resonance study, *Magnetic Resonance Imaging* (23) (2005) 273-276.
- [24] Rossi-Manaresi, R., Tucci, A., Pore structure and the disruptive or cementing effect of salt crystallization in various types of stone, *Studies in Conservation* (36) (1991) 53–58.
- [25] Yu, S., Oguchi, C.T., Is sheer thenardite attack impotent compared with cyclic conversion of thenardite-mirabilite mechanism in laboratory simulation tests? *Engineering Geology* (152) (2013) 148-154.
- [26] Scherer, G.W., Stress from crystallization of salt. *Cement and Concrete Research* (34) (2004) 1613–1624.
- [27] Benavente, D., García del Cura, M.A., Fort, R., Ordóñez, S., Durability estimation of porous building stones from pore structure and strength, *Engineering Geology* (74) (2004) 113–127.
- [28] Wendler, E. and Charola, A.E. Water and its interaction with porous inorganic building materials, *Hydrophobe V: Proc. 5th Int. Conf. on Water Repellent Treatment of Building Materials*, H. De Clercq, A.E. Charola (eds.), Aedification Publishers, 2008, 57-74.

- [29] M. Thomson, Porosity of mortars, in: Groot, C., Ashall, G., Hughes, J. (eds.), *Characterisation of Old Mortars with Respect to their Repair*, RILEM TC 167-COM, Springer, New York, 2004, 77-106.
- [30] Ordóñez, S., Fort, R., García del Cura, M.A., Pore size distribution and the durability of a porous limestone, *Quarterly Journal of Engineering Geology* (30) (1997) 221-230.
- [31] Zehnder, K., Arnold, A., Crystal growth in salt efflorescence, *Journal of Crystal Growth* (97) (1989) 513-521.

Electrodesalination of sandstones with irregular shapes and uneven distribution of salts

L. M. Ottosen*, G. Skibsted and T. Præsthholm

Department of Civil Engineering, Technical University of Denmark

* LO@byg.dtu.dk

Abstract

Electrochemical desalination of stone is based on application of an electric potential gradient. In case the electrodes are placed in a poultice, which buffer the acid from oxidation of water at the anode, the method has shown very effective. Most investigations have been carried out in laboratory scale on stones with an even salt distribution. This investigation was designed to answer different questions arising if the method is to be applied to sculptures and monuments with an uneven salt distribution and irregular shapes. Laboratory experiments were made with stones samples from a historic warehouse. The sampling was in connection to renovation. Before the renovation an on-site experiment was made as a part of the investigation.

The initial concentration in the stone segments for the different laboratory experiments varied reflecting the inhomogeneous distribution in the wall. Whether the electrodes were placed on the same side of the stone or on two opposite sides did not influence the removal rate of Cl^- and NO_3^- . A stone part, which was not placed directly between the electrodes, was desalinated, but with a slower rate than the other parts. Two stone parts were isolated from each other during the desalination, and the current mainly passed through the part with high salt concentration. The on-site experiment was successful. Chloride was removed to a very low level in all depth of the investigation (10 cm) and from cathode end to anode end, though the desalination had not finished as the concentration was still little too high in the anode end. All together 131 g Cl^- was removed during 5½ month. All results showed that the method had potential for desalination of monuments with irregular surfaces and salt distribution.

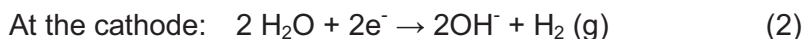
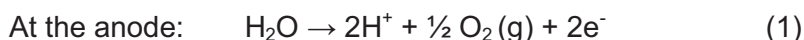
Keywords: electrodesalination, sandstone, electrode placement

1 Introduction

Electrochemical desalination is a method for desalination of salt infected monuments and buildings. An electric DC field is applied from electrodes, which are placed on the surface. In the applied electric field the main transport mechanism for the salt ions is electromigration. Positive ions in the pore solution will move towards the negative electrode and the negative ions will move towards the positive electrode. During the process the concentration of ions from the salts will thus decrease in the salt infected material as the ions concentrate around the electrodes.

Electrochemical desalination has shown large potential treatment of different matrices both through laboratory scale experiments: baked clay bricks [1-5], sandstones [6-8], granite [9] and glazed tiles [10-11] and pilot scale tests [12-13]. Also a numerical model over the process has been developed [14].

At the electrodes there are pH changes due to electrolysis reactions:



As seen from (1) and (2) pH decreases at the anode and increases at the cathode. It is necessary to neutralize acidification at the anode in order to prevent decay of the material to be desalinated. Hendrix et al. 2011 [7] underlined how important it is to avoid the acidification, as in experiments without pH neutralization the stones were severely damaged close to the anode. Also in order to obtain sufficient desalination pH neutralization can be crucial. Kamran et al. 2012 [4] showed that without neutralization at the electrodes, the desalination process in bricks stopped due to formation of a sharp transition zone between the acidic and alkaline region. This zone resulted in a large electrical potential gradient due to a local depletion of ions here. So for different reasons, the metallic electrodes should not be placed directly on the material to be desalinated.

Carbonate rich clay poultice can be placed between the electrodes and the stone for neutralization of pH changes. Calcareous clay for brick production or a mixture of kaolinite and calcite were tested both efficiently neutralized the acid from electrolysis at the anode [8]. The acid was neutralized by the CaCO_3 in the poultices. When using the CaCO_3 rich poultices, the transition zone between low and high pH is moved from the stone to the anode poultice [14]. The increased concentration of OH^- ions in the material must be counterbalanced by cations (electro-neutrality) and in [14] it is suggested from numerical-chemical simulations that these are mainly Ca^{2+} from dissolution of calcium-carbonate in the anode poultice. There may thus be precipitation of $\text{Ca}(\text{OH})_2$ in the material. Over time $\text{Ca}(\text{OH})_2$ reacts with CO_2 from air and form CaCO_3 , but neither $\text{Ca}(\text{OH})_2$

nor CaCO_3 are considered damaging, because aqueous solutions of calcium hydroxide (limewater) have been used for many centuries to protect and consolidate limestone. In addition to neutralizing the acid, the poultice also gives good electrical contact between metallic electrode and stone, and it serves as sink for removed ions. When the clay poultices are removed after the desalination, the ions of the salts are removed with it.

The present work is conducted with salt infected sandstones removed from a historic warehouse during renovation. The previously published laboratory work on electrodesalination has been conducted with samples contaminated with salts in the laboratory. The present investigation is focused on the influence from electrode placement on the desalination process in relation to both the stone shape and salt distribution.

2 Experimental section

2.1 Stones of the investigation

The experiments were conducted with Obernkirchner sandstones (Bremersandstones) from a historic warehouse, Eigtveds Pakhus, in the harbor area in Copenhagen, Denmark. The sandstones were from the outer surface of the building, and they were removed during a renovation action due to salt decay (scaling and delamination of the surface). Figure 1 shows how the sandstones were cut from the wall in long pieces. The laboratory experiments are made with such pieces after further



segmentation. A small on-site experiment was conducted at another section of the masonry before the renovation and removal of sandstone.

The stone segments were brought to the laboratory where they were placed in a closed bucket over (but not in contact with) water in order to keep the stones moist. Figure 2 shows one of the stone pieces after it was segmented (into a reference segment and segments for experiments 1 and 2). The stone segment for experiment 2 is a corner, so two sides from this segment has been exposed to free air.

Figure 1: Removal of experimental stone pieces from wall



Figure 2: Segmentation of a stone piece into a reference segment (Ref) and segment 1 and 2 for desalination experiments.

2.2 Electrochemical desalination experiments

Four electrochemical electrodesalination experiments were conducted in the laboratory. The stones were cut in different shapes, and the electrodes placed in different positions on the stones. Figure 3 is an overview of the different setups. The salt distribution was investigated in a reference stone. In addition an on-site experiment was made on the site (before the stones were replaced during the renovation).

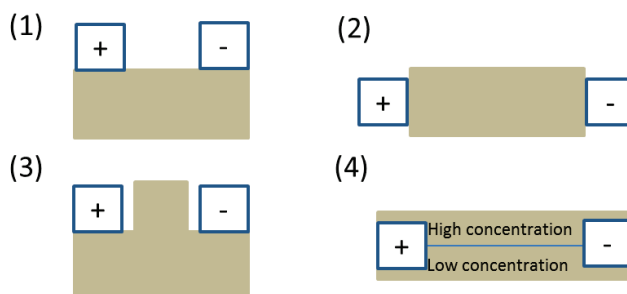


Figure 3: Summary of the four different laboratory setups for electrochemical desalination in this investigation

The laboratory experiments were designed to investigate: (a) the influence on the desalination from the placement of electrodes on opposite side or same side of the stone (comparison of lab experiments 1 and 2); (b) desalination of a part of the stone which is not placed directly in the electric field (lab experiment 3), (c) simultaneous desalination of volumes with low and high salt concentration (lab experiment 4), and (d) removal on-site compared to in the lab (on-site experiment)

Plastic frames with clay poultice (one for each electrode) were placed on the surface of the sandstone segments in positions shown in figure 1. The clay poultice was a mixture of kaolinite and CaCO_3 [15]. Inert electrode meshes were placed on the top of the poultice. Finally the electrodes were connected to a power supply (Hewlett Packard E3612A), which supplied a constant current. The whole setup with stone segment and electrode units were wrapped in plastic film to hinder evaporation.

During the experiments, the poultices were replaced regularly and the contents of Cl^- , NO_3^- and SO_4^{2-} were measured in the removed poultice to follow the progress in the desalination. At the end of the experiments the stone segments were sliced using hammer and chisel and the concentrations of the same anions were measured.

2.2.1 Reference segment

Concentration profiles of Cl^- , NO_3^- and SO_4^{2-} in depth for a reference segment (the middle segment figure 2) were measured. The reference segment was analysed directly and had not been subjected to placement of electrode units or an applied electric field. The reference segment was sliced into 6 slices starting from the original outer surface of the wall. The slices were approximately 1-1.5 cm thick.

2.2.2 Experiments 1 and 2. Poultice at same or opposite side of stone

The stone segments for experiment 1 and 2 were taken from the same long stone piece (figure 2) on both sides of the reference segment.

Experiment 1: electrodes were placed on the same side of the stone segment. The electrodes were placed on the original outer surface (figure 4(a)). At the end of the desalination experiment the stone segment was segmented into 5 slices as shown in figure 4(b).

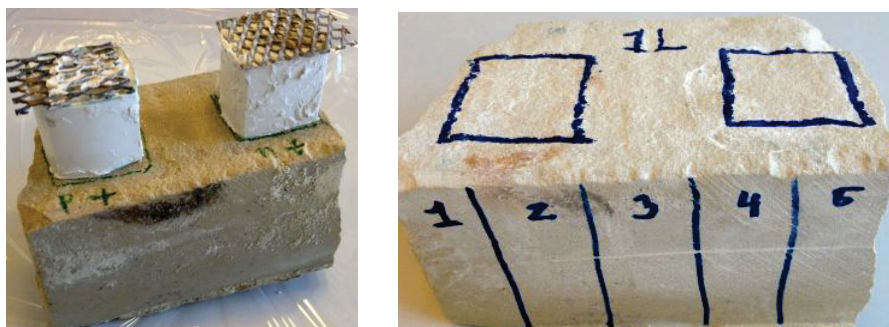


Figure 4: Experiment 1. (a) Placement of the electrode units and (b) Segmentation of the stone segment into slices at the end of the experiment

Experiment 2: The electrode units were placed in each end of the stone segment opposite to each other. The cathode unit was placed on an original outer surface (the stone segment had an original corner from the building). At the end of the experiment, the stone segment was sliced into 5 slices of approximately same sizes running from anode to cathode.

Experiments 1 and 2 were run simultaneously. During the first 24 hours 5 mA was applied, but as the voltage increased the current was decreased to 2 mA in the remaining 77 days of the experiments.

2.2.3 Experiment 3. Part of stone outside the electric field

The shape of the stone for experiment 3 is seen in figure 5. The electrodes were placed horizontally on parts 4.1 and 4.3. There was no physical contact between electrodes and part 4.4. The original outer surface was represented in all four parts to have the most similar salt concentration and distribution. Anion content was measured in the cutoffs over 4.1 and 4.3. At the end the segment was parted in four parts (figure 5).



Figure 5: Stone segment for experiment 3

2.2.4 Experiment 4. High and low initial concentration

The stone segment was cut in two pieces of equal size. One piece was submerged one week in distilled water and the other in 79.6 g/l NaCl. This was in order to have one piece with high concentration and one with low. An initial sample was taken from both parts. For the desalination experiment the two pieces were placed together again, but with plastic between, to hinder transport of ions between the two parts.



Figure 6: Stone segments for experiment 4

The two pieces were kept together by tape during the desalination experiment. The electrodes were placed on the same side as indicated by the markings for the electrode units at figure 6. The electrode units covered approximately the same area from the two stone pieces. At the end of the experiment five slices were made from each of the two stones. This experiment is focused on Cl removal, as the stone with the high concentration was submerged in NaCl.

2.2.5 On-site experiment

A set of electrodes were placed on the surface of the building (see figure 7a) before renovation. The electrode units were designed as the units described in [12-13]. The electrode units were placed in the height of 45 cm (to lower edge). The distance between the electrodes was 20 cm.

The electrode casings (50 cm long) were made from plastic and consisted of two parts; a box and a movable bottom (see figure 7b). The purpose of the movable bottom was to ensure mechanical pressure between poultice and masonry. This is crucial to passage of current. As the poultice dries slightly during desalination it loose volume and the bottom is moved closer to the masonry due to pressure from springs. It is further possible to tighten the springs by tightening the three buttons at the back of the casing. An inert metallic electrode mesh was placed on top of the bottom and the casing was filled with poultice. The experiment lasted 5½ month (July-Dec. 2010). Poultices were changed four times. A constant current of 50 mA was applied.

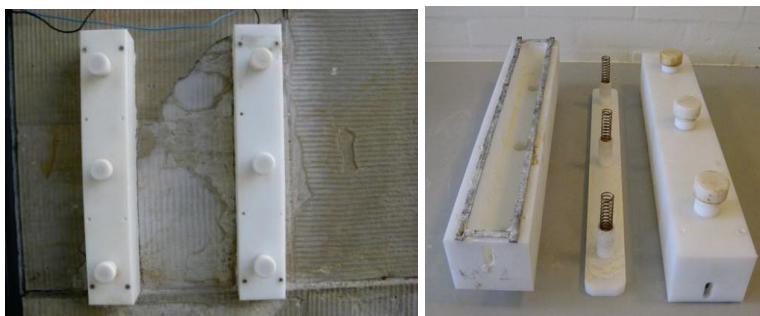


Figure 7: (a) the electrode units mounted on the wall, (b) The design of the electrode casings. To the left the hole in the box is shown, in which the movable bottom in the middle is placed with the springs down.

Samples from the masonry for determination of salt concentrations were taken during mounting of electrodes. The drilling powder from the holes made to fasten each electrode was collected (in the heights 45 and 95 cm). The holes were 6 mm in diameter and about 5 cm deep. By the end of the test drilling samples from masonry were taken to the depth 10 cm. The samples were divided in intervals: 0-1 cm; 1-2 cm; 2-5 cm and 5-10 cm. Samples were taken in the height of 70 cm (middle of electrode placement). The sampling positions were where the electrodes had been placed and one in between. Sampling from the poultice was done each time it was changed. Three sub-samples of the same size were taken from each unit (from top, middle and bottom) and these sub-samples were mixed before analysis to have a representative sample.

2.2.6 Overview of experimental conditions

An overview of the experiments is given in table 1.

Table 1: Conditions for the conducted experiments.

Experiment	Stone weight (g)	Current (mA)	Duration (d)
Ref. No current	0.59	0	-
1 Electrodes same side	1.05	2	77
2 Electrodes on opposite sides	0.83	2	77
3 Stone part outside electric field	0.99	2	42
4 High-low part concentrations	0.61/0.57	2	29
On-site	-	50	164

2.3 Analytical

Extractions were made with 10 g dry, powdered sandstone (powdered by hand in a mortar), drilling powder or poultice and 25 mL distilled water. The suspensions were agitated 24 hour. The suspension filtered and Cl^- , NO_3^- and SO_4^{2-} concentrations of were measured by ion chromatography.

3 Results and discussion

3.1 Concentration profiles in the reference segment

Concentration profiles of Cl^- , NO_3^- and SO_4^{2-} in the reference segment are in figure 8. To evaluate the concentrations the ONORM [16] is used. The norm is debated, but the only one of its kind. The Cl^- conc. is rather constant throughout the depth of the stone at a level of about 0.4 wt% exceeding the upper level from [16] (0.1 wt%). The SO_4^{2-} concentration is also about constant and at 0.04 wt%, which is less than the lower limit from [16] (0.1 wt%). The pattern for NO_3^- is very different from the two others, as the concentration decreases almost linearly from the outer surface (0.3 wt%) to 0.1 wt% in the depth of the sample (7-8 cm).

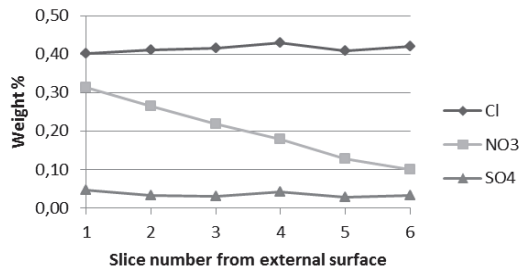


Figure 8: Concentration profiles of Cl^- , NO_3^- and SO_4^{2-} in the reference stone running from the original outer surface over the depth of 7-8 cm

3.2 Desalination with electrodes on the same side of the stone or on opposite sides

Experiments 1 and 2 are discussed together. The removal of the anions into the poultices as a function of the applied charge (Q) is shown in figure 9 ($Q = I \cdot t$, where I is current [A] and t is time [s]). Figure 10 shows the concentration profiles of the anions in the stone at the end of the experiments. Finally the average initial concentrations in the reference segment and calculated initial concentrations for experiments 1 and 2 are in table 2. The average concentrations in the reference segment are calculated on basis of dry weight and concentration in the six different slices. The average concentrations from experiments 1 and 2 are calculated on basis of final concentrations in the stone pieces and mass removed into the poultices (and dry weight of the corresponding matrices). The calculated average Cl^- concentration is underestimated as an unknown amount of Cl^- is lost from the anode process $2\text{Cl}^- \rightarrow \text{Cl}_2(\text{g}) + 2\text{e}^-$ (this reaction did take place as some of the removed poultices smelled of chlorine). It is seen from the table that even within one stone piece there

are significant concentration variations and thus this parameter is differing between all experiments of this investigation.

The most important transport mechanism involved in removal of ions from the salts into the poultice is electromigration. Diffusion may also be significant, due to the concentration gradient between the high concentration in the pore water of the sandstone and the extremely low concentration in the pore water of the poultice. This means that the anions removed into the anode poultice is a sum of the ions transported by electromigration and diffusion, whereas the concentration in the cathode poultice is due to diffusion alone. The difference is clearly seen from the differences in the level of mass of removed anions into the two poultices (figure 9 a and b).

A higher mass of the anions is transported into both anode and cathode poultice in experiment 1 than 2. The graphs for each of the anions in the anode poultice from the two experiments are almost parallel (figure 9a). The major difference between the levels of the two graphs is related to the different level in transport from diffusion. This can be seen from the removal into the cathode poultice (figure 9b), where the level is significantly higher in experiment 1 than 2. The reason is the placement of electrodes in relation to the original outer stone surface. Both electrodes were placed on the original outer surface in experiment 1, whereas the electrodes were placed on original internal parts in experiment 2. For NO_3^- this makes a major difference, as it was found that the NO_3^- concentration was highest at the surface (figure 8). The higher diffusion of NO_3^- than Cl^- (experiment 1) is though not at first sight explained by the difference in concentration gradient, as the concentration of Cl^- was found highest in the first slice from the original surface (figure 8), however as figure 8 shows average concentrations for the slices, it is not known if a fraction of NO_3^- in the first slice was actually soluble salt crystals at the surface and if so the surface concentration of NO_3^- could have been higher than Cl^- .

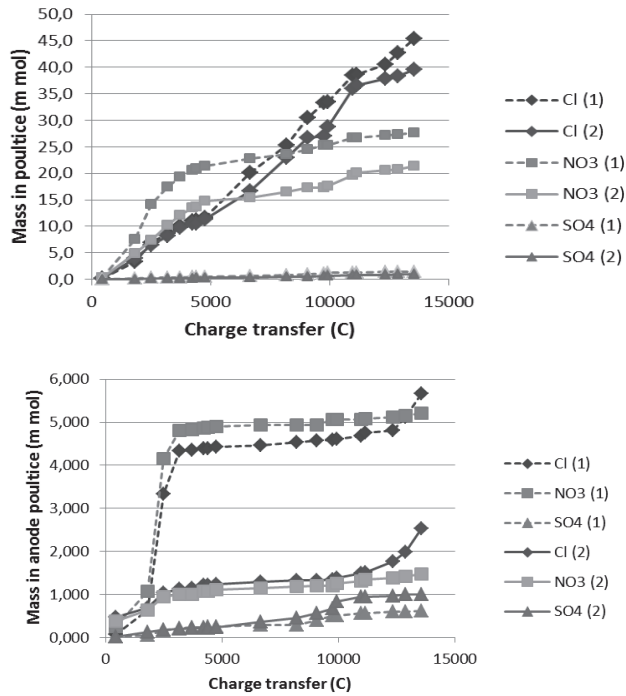


Figure 9: Accumulated mass of Cl^- , NO_3^- and SO_4^{2-} in the poultices as a function of the charge transfer in experiments 1 and 2 (top) anode poultice and (bottom) cathode poultice

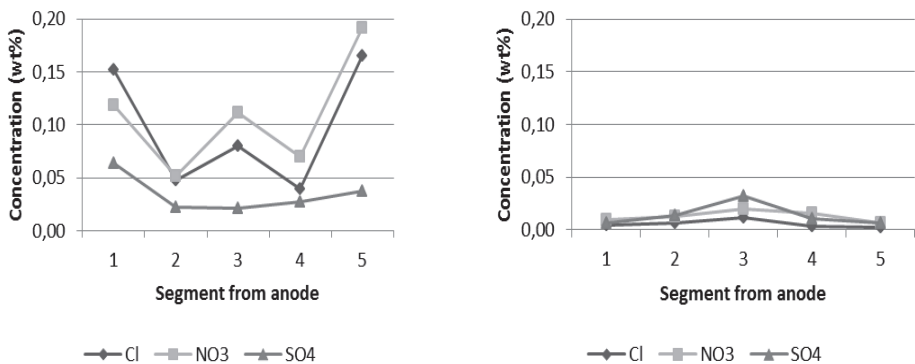


Figure 10: Concentrations of Cl^- , NO_3^- and SO_4^{2-} in the stone segments at the end of experiment 1 (left) and experiment 2 (right)

Table 2: Calculated average initial concentrations in the stone segments of the reference and desalination experiments 1 and 2. (*Chloride concentration is underestimated as an unknown amount is lost in the anode reaction)

Experiment	Cl ⁻ (mg/kg)	NO ₃ ⁻ (mg/kg)	SO ₄ ²⁻ (mg/kg)
Reference	4110	2190	350
Experiment 1	2540*	2900	470
Experiment 2	1910*	1890	370

Final Cl⁻, NO₃⁻ and SO₄²⁻ concentrations in the stone from experiment 2 are very low, and much lower than in experiment 1. So even if a higher mass was removed in experiment 1, the lowest concentrations were obtained in experiment 2. This is because both stone mass and initial concentrations were highest in experiment 1. Unfortunately this means that direct comparison of the electrode placements is not possible. The removal rates from electromigration are though very similar (figure 9a), which implies that there is no major difference. The Cl⁻ transport numbers for the two experiments are 0.32 and 0.28, respectively.

3.3 Experiment 3. Part of stone outside the electric field

Figure 11 shows the overall results from experiment 3. The Cl⁻, NO₃⁻ and SO₄²⁻ concentrations are shown for each of the stone parts and the initial concentrations (reflected by the concentrations in the parts, which were cut off before the desalination), are shown as well. The concentrations in each piece are considered relatively similar before desalination as the stone was cut so each part contained the original outer surface. The Cl⁻ and NO₃⁻ concentrations are also in the same level in the two initial samples, but the SO₄²⁻ concentration was double as high in one sample as in the other. Compared to the reference stone (figure 8) the concentration of Cl⁻ was only half in this stone, the NO₃⁻ concentration in the same level and the SO₄²⁻ was less in the left sample and in the same level in the right.

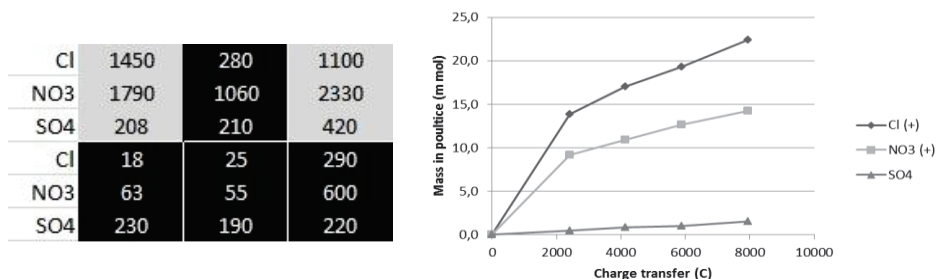


Figure 11: left: Concentrations (mg/kg) Cl⁻, NO₃⁻ and SO₄²⁻ in the different parts of the stone in experiment 3 (black). Light grey parts show initial concentrations found from cutoffs; right: Removal to anode poultice as function of charge transfer.

After desalination the Cl^- and NO_3^- concentrations are lowest in the parts placed directly between the electrodes (three lower parts). Concentrations in the first two parts here are very low and also concentrations in the part closest to the cathode are decreased significantly. The removal into the poultice shows good and stable removal (figure 11). The piece, which had not been directly in the electric field (the central upper piece), has decreased Cl^- and NO_3^- concentrations compared to the initial. Especially the Cl^- concentration was lowered. The result indicates that also salt infected volumes, which are not placed directly between the electrodes, can be desalinated, though with a slower rate. This is important if the method is applied to sculptures with different attributes. Electrodes need not to be placed on top of these often very fragile parts.

3.4 Experiment 4. High and low concentration

Figure 12 shows the Cl^- concentration in the two initial samples and the profiles in the samples after electrodesalination. The concentration was lowered in both samples, compared to the initial concentrations. In respect to the removed moles from the two sides it can be concluded, that the major part of the current passed through the part with high initial concentration. Initially pH was 7.5 and 8.0. At the end of the experiment pH was 7.6-8.5 in the sample with low concentration and 8.3-9.1 in the one with high concentration. This supports that the major part of the current passed through the stone with high concentration. The result shows that the electric field is strongest where the conductivity is highest i.e. parts of e.g. a wall with highest salt contamination.

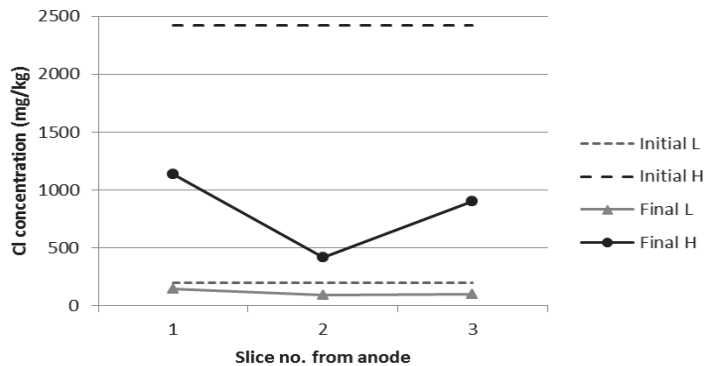


Figure 12: Initial and final concentrations in the two parts (L part with low initial Cl^- concentration and H part with high initial Cl^- concentration)

3.5 On-side experiment

The concentrations measured in the drilling powder when mounting the electrodes were 0.40 – 1.38 wt% Cl^- ; 0.03 – 0.33 wt% NO_3^- ; 0.01 – 0.03 wt% SO_4^{2-} . The Cl^- concentration was much higher than the highest level from the ÖNORM (0.1 wt%) [16], whereas the SO_4^{2-} concentration was much lower and only one of the initial samples did exceed the limit for NO_3^- . The initial Cl^- concentration was much higher than in the reference segment for the lab experiments (table 2).

Figure 13 shows the Cl^- concentration profiles in the wall from anode to cathode in four different depths. It is clearly seen that in every depth the concentration is much lower in the cathode side than in the anode side, which corresponds to the direction of electromigration. The profile shows, that the desalination was not finished as the concentration in the anode side still exceeded 0.1 wt%, but compared to the initial concentrations which was >0.4 wt% the concentration had decreased significantly here as well. The overall transport number for Cl^- in the experiment was 0.38 which is even better than in the lab experiments 1 and 2 (where it was about 0.3), and the removal could have progressed in case of prolonged duration, as the transport number in the last period was 0.25.

The on-site experiment gave very good results. The desalination has been efficient in the outer 10 cm of the wall (at least) and all together 131 g Cl^- was removed into the anode poultice at a relatively high transport number.

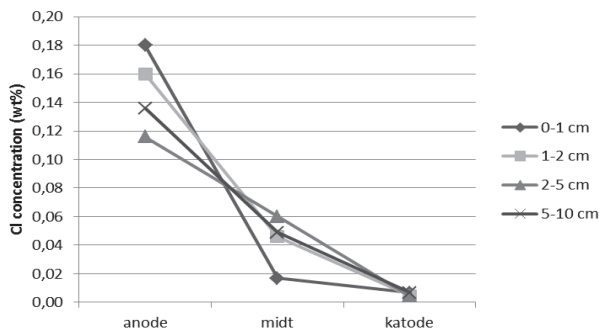


Figure 13: On-site experiment. Cl^- concentration profiles from anode to cathode in four different depths

4 Conclusions

This investigation was focused on some major questions in relation to full scale desalination of monuments and buildings. The experiments were made with sandstones from a historic warehouse. The Cl^- removal rate was very similar whether the electrodes were placed on the same side or opposite sides of the stone to be desalinated. Diffusion into the poultice is important in the first day of electrodesalination only. A part of a stone which is not placed directly between the electrodes was desalinated, but with a slower rate than the part between the electrodes. The electric field is strongest in the part of the stone with highest concentration of ions. The experiments in the present investigation were made with stone samples which were contaminated with salts from environmental exposure and thus the salt concentrations varied significantly between samples and in each sample. The experiments could be repeated with stones prepared so the salts were initially homogeneously distributed in order to verify these findings. An on-site experiment with electrodes at the same side of the wall gave a very good result, and even better than the laboratory experiment with electrodes at same side. The transport number was 0.38 and 0.32 in pilot and laboratory scale, respectively. The desalination had progressed and at least into the depth of 10 cm, from where the deepest samples were taken.

References

- [1] Ottosen, L.M.; Rørig-Dalgård, I. Electrokinetic removal of $\text{Ca}(\text{NO}_3)_2$ from bricks to avoid salt induced decay. *Electrochimica Acta* (52)(10) (2007) 3454-3463
- [2] Rørig-Dalgaard, I. Preservation of masonry with electrokinetics – with focus on desalination of murals. PhD Thesis. Department of Civil Engineering, Technical University of Denmark, 2009
- [3] Ottosen, L.M.; Rørig-Dalgaard, I. Desalination of a brick by application of an electric DC field. *Materials and Structures*, 42(7) (2009) 961-971
- [4] Kamran, K.; van Soestbergen, M.; Huinink, H.P; Pel, L. Inhibition of electrokinetic ion transport in porous materials due to potential drops induced by electrolysis. *Electrochimica Acta* (78) (2012) 229– 235
- [5] Rørig-Dalgaard, I.; Ottosen, L.M.; Hansen, K.K. Diffusion and electromigration in clay bricks influenced by differences in the pore system resulting from firing. *Construction and Building materials* (27)(1) (2012) 390-397
- [6] Petersen, G.; Ottosen, L.M.; Jensen, P.E. (2010) The possibility for using electrokinetics for desalination of sandstone with low porosity.

- Proceedings from 8th fib International PhD Symposium in Civil Engineering. Kgs. Lyngby, Denmark, 2010, 455-460
- [7] Herinckx, S.; Vanhellefont, Y.; Hendrickx, R.; Roels, S.; De Clercq, H. (2011) Salt removal from stone building materials using an electric field. In: I. Iannou & M. Theodoridou (eds.) Proceedings from the international conference on salt weathering on building and stone sculptures, Limassol, Cyprus 19-22 October 2011, pp 357-364
- [8] Ottosen, L.M.; Christensen, I.V. Electrokinetic desalination of sandstones for NaCl removal - Test of different clay poultices at the electrodes. *Electrochimica Acta*. (86) (2012) 192– 202
- [9] Feijoo, J.; Nóvoa, X.R.; Rivas, T.; Mosquera, M.J.; Taboada, J.; Montojo, C.; Carrera, F. Granite desalination using electromigration. Influence of type of granite and saline contaminant. *Journal of Cultural Heritage* (14) (2013) 365–376
- [10] Ottosen, L.M.; Ferreira, C.D.; Christensen, I.V. Electrokinetic desalination of glazed ceramic tiles. *Journal of Applied Electrochemistry* (40) (2010) 1161-1171
- [11] Ottosen, L.M.; Ferreira, C.; Christensen, I.V. (2011) Electrochemical desalination of historic Portuguese tiles, Azulejos, in laboratory scale, Proceedings of SWBSS2011 Salt Weathering on Buildings and Stone Sculptures (eds. I. Iannou & M. Theodoridou), Limassol, Cyprus, 19-22 October, 349-356
- [12] Ottosen, L.M.; Christensen, I.V.; Rørig-Dalgaard (2012) Electrochemical desalination of salt infected limestone masonry of a historic warehouse. *Structural Faults and Repair*, Edinburgh 2012. Proceedings – CD Rom. Ed MC Forde, 15 pages
- [13] Ottosen, L.M.; Rørig-Dalgaard; I., Villumsen, A. (2008) Electrochemical removal of salts from masonry - Experiences from pilot scale. *Salt Weathering on Buildings and Stone Sculptures*. Copenhagen, 22-24 October 2008, 341-350
- [14] Paz-Garcia, J.M.P.; Johannesson, B.; Ottosen, L.M.; Alshawabkeh, A.; Ribeiro, A.B.; Rodriguez-Maroto, M.(2012) Modeling of electrokinetic desalination of Brick, *Electrochim. Acta*. (86) (2012), 213-222.
- [15] Rørig-Dalgaard, I.; Ottosen, L.M. (2009) Method and device for removing an ionic impurity from building structures (Patent WO/2009/124890)
- [16] Austrian Önorm B 3355-1 "Trochkenlegung von Feuchtem Mauerwerk – Bauwerksdiagnostik und Planungsgrundlagen" 1999

Salt extraction of limestone by means of electrophoresis: some results on type of contact material and electrode position

H. De Clercq^{1*}, Y. Vanhellemont² and V. De Swaef³

¹Royal Institute for Cultural Heritage (KIK-IRPA), Brussels, Belgium

²Belgian Building Research Institute (BBRI), Brussels, Belgium

³KU Leuven@KAHO Sint-Lieven-Campus Gent-Technologiecluster Bouw, Leuven, Belgium

* hilde.declercq@kikirpa.be

Abstract

This paper describes some results of salt extraction by means of electrophoresis on limestone contaminated with two types of salts: NaCl and Na₂SO₄. Limestone plates in various dimensions have been tested. The electrophoresis is evaluated in terms of the measured current during the electrophoresis process and the remaining amount of salts in the samples, determined by conductivity measurements of the water extract. Three different contact materials have been tested: cotton, cellulose fibers and a mixture consisting of calcite powder and cellulose fibers. Results have shown that the last is the most efficient one. Two different electrode configurations have been tested on one type of the limestone plates. Results have shown that salts are removed from zones not necessarily positioned right between or physically in contact with the electrodes. There are indications that a better efficiency is obtained in case the electrodes are positioned on opposite sides, compared to an electrode-layout by which the electrodes are on the same side of the sample. It seems that the efficiency of the electrophoresis does not depend on the size of the electrodes, as long as the contact material is spread over the entire surface of the sample to be salt extracted.

Keywords: electrophoresis, limestone, contact material, sodium chloride, sodium sulphate

1 Introduction

Moisture and salt contamination is a major cause of degradation to historic building materials, in the form of aesthetic or mechanical damage. In Belgium, impermeable or salt resistant materials are quite often used in practice; interventions that have a tendency of hiding the salt problem instead of solving it and hence as such not contributing to a sustainable management of our built heritage. An alternative approach attempts to extract salts through poulticing or electrophoresis.

During electrophoresis, a wet sample contaminated with salts is subjected to a direct current enabling ions to migrate to the oppositely charged electrode where they are stored in the contact material. In case of sodium salts, sodium hydroxide is formed at the cathode or negatively charged electrode [1]. An alkaline environment as such is not damaging a limestone. At the positively charged anode, water is transformed into oxygen and hydrogen ions. Chlorides form chlorine gas or combine with hydrogen ions to form hydrochloric acid. Sulfates present in solution will similarly combine with the hydrogen ions and form sulfuric acid. An acidic environment can chemically attack the calcium carbonate of limestone and hence cause damage to it.

This paper describes some results of salt extraction by means of electrophoresis on limestone contaminated with two types of salts: NaCl and Na₂SO₄. Tested parameters are the type of contact material and the position of the electrode. Two types of limestone plates, more precisely 15x15x4 cm and 45x45x4 cm, are tested using a similar electrode having a size of 15x15 cm. Concerning the bigger plates, two different electrode configurations are tested: in the middle and at opposite sides of the plate on one hand and in the middle at the left and right and same side of the plate. The efficiency of the electrophoresis is expressed in terms of the measured current during the electrophoresis process and the remaining amount of salts. For the last, samples are crushed and poured into distilled water that is submitted to conductivity measurements. Three different contact materials are tested: cotton, cellulose fibers and a mixture consisting of calcite powder and cellulose fibers.

2 Materials

2.1 Substrates

Two types of limestone were tested in this investigation: Savonnières and Euville limestone, being respectively a semi-coarse oölitic and a coarse crinoidic French limestone. Savonnières limestone is characterized by a porosity accessible to water, determined by immersing dry samples in

demineralized water for 48 h, of 9.2 % while that of the Euville stone is 3.9 %. The limestones were cut into plates (15x15x4 cm or 45x45x4 cm).

Samples are dried at 105 °C till constant weight (difference between two weighings is less than 0.1 %).

2.2 Moisture and salt contamination

Limestone plates of 15x15x4 cm are contaminated with a saturated sodium chloride (NaCl) or sodium sulfate (Na_2SO_4) solution. The bigger plates are only contaminated with a saturated NaCl solution. The dry samples are poured into a saturated solution, containing or 369 g NaCl or 172 g Na_2SO_4 per liter water, during 48 hours. After that, the surfaces are made surface dry using a moistened cotton and the samples are weighed to determine their moisture and salt content. Prior to the electrophoresis, the samples contaminated with a saturated salt solution are covered with a plastic foil during 1 week to assure a homogeneous distribution of moisture and salt.

2.3 Contact materials – overview of samples

Three types of contact materials were included in this investigation: cotton, calcite powder and a mixture of cellulose and calcite powder. The choice of calcite powder is based on the research results obtained by L. Ottosen et al [2,3,4] in which a calcium carbonate rich clay was used as contact material. The calcite neutralizes the acids formed at the anode preventing a chemical damage of the lime substrate subjected to electrophoresis. Clay was not included in our research for its dense structure. It is supposed that calcite powder, characterized by a more open structure, will stimulate the evacuation of formed gaseous compounds, such as Cl_2 , O_2 and H_2 .

In case of calcite and calcite/cellulose, water is added to obtain a workable paste-like material and to assure a good contact with the limestone sample surface and the electrode. The paste-like contact material is added at a thickness of 1 cm. The cotton is also wetted prior to its attachment to the limestone plate samples. For plate samples of 45x45x4 cm, only a calcite/cellulose mixture is tested as contact material.

An overview of the samples is given in table 1.

2.4 Electrodes - electrophoresis

Results obtained during previous investigations have shown that stainless steel, copper as well as graphite net-electrodes got severely damaged during the electrophoresis process [5]. Hence, for present research plate graphite electrodes (15x15 cm) were selected for their good resistance in

an acidic and alkaline environment, low cost and easy availability. They are linked to the power supply by means of a titanium nut.

For the electrophoresis procedure, the ensemble, consisting of salt contaminated limestone plates, contact material and electrode, is protected by means of a plastic foil to minimize the evaporation of water. Little holes in the plastic foil enable the evaporation of formed gaseous compounds. In case of the 15x15x4 cm sized plate, the ensemble is kept together by means of a clip (figure 1). For the limestone plates of 45x45x4 cm, two different electrode configurations are tested: in the middle and at opposite sides of the plate on one hand and in the middle at the left and the right and same side of the plate (45x45 cm). The calcite/cellulose mixture is applied at a thickness of 1 cm on the complete surface (45x45 cm) of both opposite sides for the first configuration and on one side for the second configuration. The electrodes positioned in the middle of the opposite sides (first configuration) are kept in place using a wooden panel on both sides held together by means of screws (figure 2). A plastic plate between the wooden panel and the contact material serves as protection for the underlying contact material. For the second configuration, the electrodes are fixed similar to the small plate samples.

A voltage of 10 V was applied during 1 week. The current is measured continuously to follow up the electrophoresis process.



Figure 1: Setup for the limestone plates of 15x15x4 cm

Salt extraction of limestone by means of electrophoresis: some results on type of contact material and electrode position

Table 1: overview of the samples

Salt / contact material	cotton	calcite	calcite/cellulose
	Sample code		
Euville limestone (15x15x4 cm), electrodes (15x15cm) on opposite side			
NaCl	E1'	E2	E3
Na ₂ SO ₄	E4'	E5	E6
Savonnières limestone (15x15x4 cm), electrodes (15x15cm) on opposite side			
NaCl	S1'	S2	S3
Na ₂ SO ₄	S4'	S5	S6
Euville limestone (45x45x4 cm), electrodes (15x15cm) on opposite side			
NaCl	-	-	EX
Euville limestone (45x45x4 cm), electrodes (15x15cm) on same side			
NaCl	-	-	E
Savonnières limestone (45x45x4 cm), electrodes (15x15cm) on opposite side			
NaCl	-	-	SX
Savonnières limestone (45x45x4 cm), electrodes (15x15cm) on same side			
NaCl	-	-	S



Figure 2: The electrodes, applied in the middle of the opposite sides of limestone plates of 45x45x4 cm, are kept in place using a wooden panel on both sides and positioned by means of screws. A plastic plate applied between the wooden panel and the contact material serves as protection for the contact material underneath it.

2.5 Electrophoresis efficiency

After 1 week electrophoresis, the contact material is removed from the limestone samples which are dried at 105 °C till constant weight. After that, samples of 15x15x4 cm are entirely crushed and poured into 4 l of demineralized water to determine the remaining amount of salts through conductivity [5]. Limestone plates of 45x45x4 cm are divided in 9 equal parts of 15x15x4 cm that are further treated similarly. Conductivity results are interpreted based on a calibration procedure using aqueous solutions with known NaCl or Na₂SO₄ concentrations.

3 Results and discussion

3.1 Plates of 15x15x4 cm

Figures 3 and 4 present by means of illustration the evolution of the measured current during the electrophoresis of respectively Euville limestone contaminated with a saturated Na₂SO₄ solution and Savonnières limestone with a saturated NaCl solution, for the three types of contact materials. From both figures, it can be noticed that the highest current is obtained in case calcite/cellulose mixtures are used as contact

material, while generally the lowest in case of calcite. Similar results were obtained for Euville limestone saturated with NaCl and Savonnières limestone with a Na_2SO_4 solution (figure 5). By comparing the results presented in figures 4 and 5, it can generally be noticed that a higher current is measured in case of a contamination with NaCl compared to one with Na_2SO_4 . This can be explained by a higher mobility of chlorides compared to sulfates. Higher currents are measured for the Savonnières limestone compared to the Euville limestone (figures 5 and 3 respectively).

The efficiency of the salt removal by means of electrophoresis is presented in table 2.

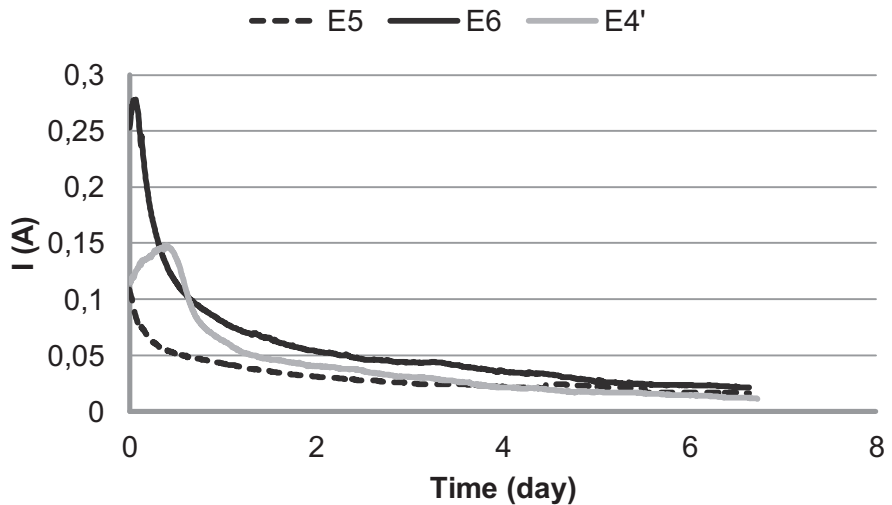


Figure 3: Evolution of the current during electrophoresis of Euville stone plates of 15x15x4 cm contaminated with a saturated Na_2SO_4 solution using cotton (E4'), calcite (E5) or a mixture of calcite and cellulose (E6) as contact material.

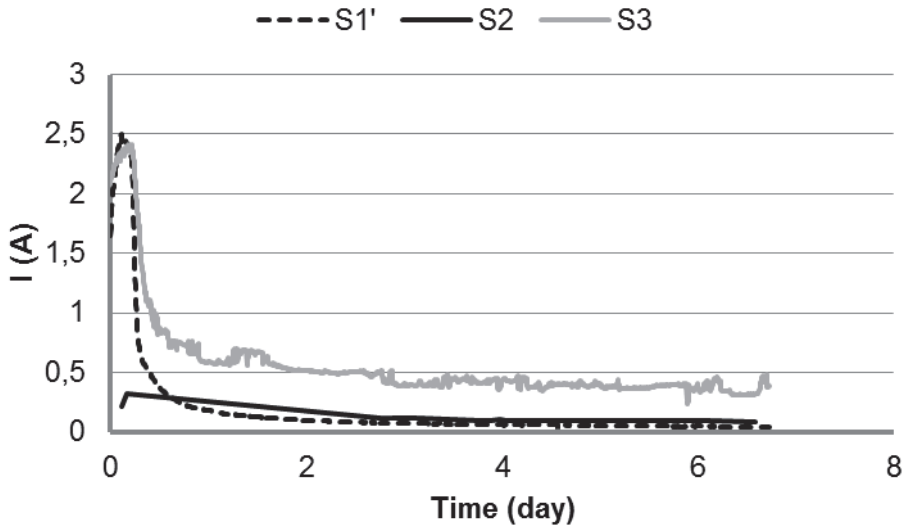


Figure 4: Evolution of the current during electrophoresis of Savonnières stone plates of 15x15x4 cm contaminated with a saturated NaCl solution using cotton (S1'), calcite (S2) or a mixture of calcite and cellulose (S3) as contact material.

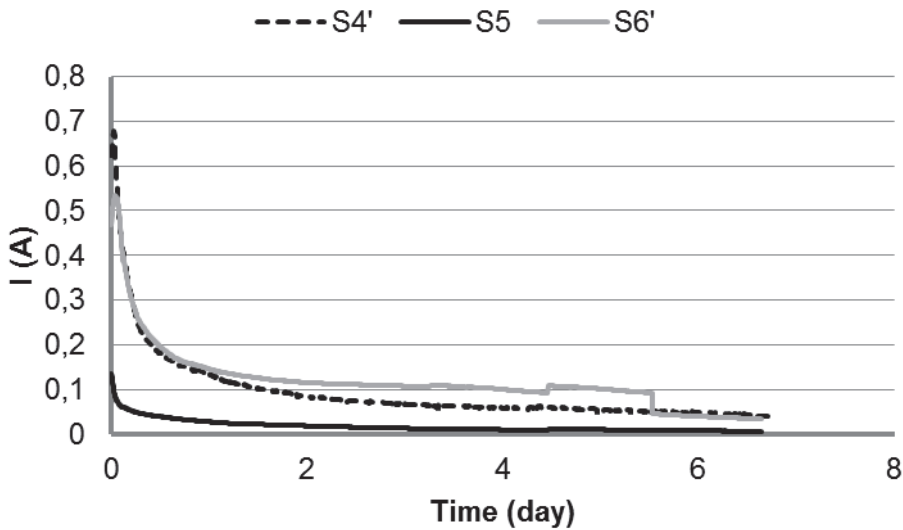


Figure 5: Evolution of the current during electrophoresis of Savonnières stone plates of 15x15x4 cm contaminated with a saturated Na₂SO₄ solution using cotton (S4'), calcite (S5) or a mixture of calcite and cellulose (S6) as contact material.

Table 2: efficiency (%) of salt removal by means of electrophoresis using three kinds of contact materials for Savonnières and Euville limestone plates of 15x15x4 cm contaminated with a saturated NaCl or Na₂SO₄ solution.

salt	cotton		calcite		calcite/cellulose	
	Sample code	Efficiency (%)	Sample code	Efficiency (%)	Sample code	Efficiency (%)
Euville limestone						
NaCl	E1'	52.3	E2	41.7	E3	49.4
Na ₂ SO ₄	E4'	31.2	E5	34.5	E6	52.9
Savonnières limestone						
NaCl	S1'	31.2	S2	35.7	S3	40.2
Na ₂ SO ₄	S4'	18.3	S5	12.7	S6	53.5

The three main conclusions are:

- The results in table 2 show that generally the highest efficiency is obtained for a calcite/cellulose mixture as contact material. This corresponds well with the higher current obtained with this poultice type (figures 3-5)
- Except for the last type of contact material, a higher removal is measured for Euville and Savonnières limestone contaminated with NaCl compared to Na₂SO₄, despite its higher solubility, and hence higher absolute initial content after contamination with a saturated solution. In addition, precipitation of Ca(SO₄) may have immobilized the sulphate. Formation of gypsum has indeed been observed in other research [6].
- Comparing the influence of the type of limestone, better results are noticed for the coarser Euville limestone. It should be remarked here that this crinoidic limestone contained, in absolute values, initially less salts as its porosity accessible to water is remarkably lower (3.9%) compared to the Savonnières limestone (9.2%). This finding again corresponds to the higher current in the Savonnières limestone.

3.2 Plates of 45x45x4 cm

In the test procedure using plates of 15x15x4 cm, the plate electrode covers completely both opposite sides (15x15 cm). It should be more practical to reduce the size of the plate compared to the surface subject of a salt extraction procedure. For on-site applications, it's rather illogic to cover a complete façade surface to be salt extracted with electrodes. It might be more advantageous to apply a series of electrodes at a fixed distance between each other. As a first approach to evaluate to what distance salts can be extracted by means of electrophoresis, preliminary tests are carried out on bigger limestone plates (45x45x4 cm) using the same plate electrodes as tested on the little plates and calcite/cellulose fibers as contact material. Two different electrode configurations are tested: in the middle and at opposite sides (45x45 cm) of the plate (1) and in the middle at the left and the right and same side of the plate (2). The second configuration mimics a situation where a wall is only accessible from one side, as is the case for cellars, or in the case of presence of constructions on the other side of the wall. One could think of a frame by which the electrodes are positioned as vertical forms on one side of a wall and at a certain distance, as was investigated by Ottosen et al [4]. A crucial parameter for such type of application is related to the distance between the electrodes, which should preferably be as high as possible to reduce eventual (mechanical) damage associated with the fixation of the electrodes to the wall.

Figure 6 illustrates the evolution of the measured current for Euville and Savonnières limestone contaminated with a saturated NaCl solution during the electrophoresis according to the two test configurations.

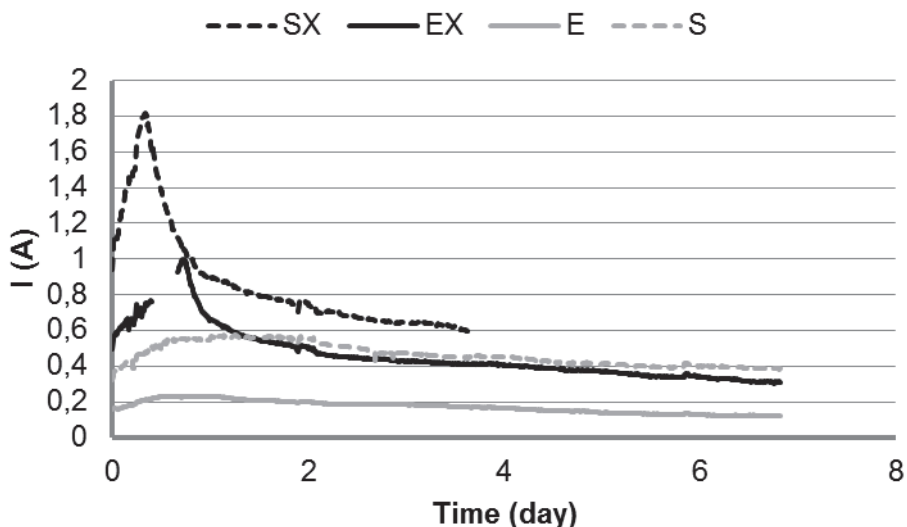


Figure 6: current measured during electrophoresis of Euville (E) and Savonnières (S) limestone plates of 45x45x4 cm contaminated with a saturated NaCl solution according to two configurations (EX and SX refer to the configuration by which the electrodes are positioned in the middle at both and opposite sides of the limestone plate; E and S refer to the configuration by which the electrodes are positioned in the middle at the left and the right and same side of the plate).

The electrophoresis by which the electrodes are applied in the middle of the opposite sides (SX and EX), results in a higher current compared to a procedure by which the electrodes are positioned on the same side (S and E), which is explained by a shorter distance in between, respectively 4 and 15 cm. If the resistance in the stone is considered homogeneous, a longer distance between the electrodes will result in a higher distance and a lower current (as the voltage is kept constant in these experiments). Similar as for the smaller plates, a higher current is measured for Savonnières plates than for Euville ones.

Results of extraction efficiency, based on conductivity measurements, are presented in tables 3 and 4. In order to calculate the efficiency of the electrophoresis, the assumption is made that initially the salts are distributed homogeneously over the volume of the sample.

Table 3: electrophoresis efficiency (%) of 9 equal parts (15x15x4 cm) of Euville (EX) and Savonnières (SX) limestone plates (45x45x4 cm) contaminated with a saturated NaCl solution and subjected to electrophoresis. The electrodes were applied in the middle of the opposite sides. The electrode position is marked in grey.

position	EX			SX		
	Left	Middle	Right	Left	Middle	Right
Top	60,8	65,7	58,8	52,0	57,2	47,9
Middle	63,4	66,1	62,0	56,1	53,1	54,8
Bottom	64,9	65,4	59,9	53,4	57,1	49,1
Global average	63			53		

Table 4: electrophoresis efficiency (%) of 9 equal parts (15x15x4 cm) of Euville (E) and Savonnières (S) limestone plates (45x45x4 cm) contaminated with a saturated NaCl solution and subjected to electrophoresis. The electrodes were applied in the middle at the left and the right and same side of the plate. Their position is marked in grey.

position	E			S		
	Left	Middle	Right	Left	Middle	Right
Top	35,1	42,8	39,8	27,2	39,1	24,5
Middle	42,2	57,4	49,9	27,8	45,9	29,4
Bottom	40,2	52,3	46,9	36,0	39,5	30,2
Global average	45			33		

The results presented in the tables 3 and 4 illustrate that a higher efficiency is obtained in case the electrodes are applied at opposite sides of the plate at a distance of 4 cm than at the same side at a distance of 15 cm between each other, corresponding to the higher current. With respect

to the first configuration (table 3), the difference in salt extraction efficiency between the different parts of the same limestone plate is rather small and unsystematic. An expected higher efficiency for the limestone part right between the electrodes is only obtained in case of the Euville limestone. For electrode configuration 2 (table 4), the highest efficiency is obtained for the limestone part right between both electrodes, hence the middle part of the plate. Nevertheless, it is still lower than the average efficiency obtained for electrode configuration 1 (table 3). These findings are very important, because they show that also volumes not directly covered by electrode units are desalinated. This gives some freedom when choosing placement of the electrodes.

4 Conclusions

It has been shown that electrophoresis might be a suitable method to extract salts from a salt-laden substrate. A suitable contact material such as a mixture of calcite/cellulose better protects the masonry against the acidic environment formed at the anode. The extraction rate may vary significantly, depending on the type of salt, the type of substrate, and the type of contact material between the electrodes. Extraction percentages between 20% and 60% were found. This can be obtained in ideal circumstances by which electrodes are positioned at opposite sides of a relatively thin salt laden substrate. Up-scaling to real masonry might prove to be problematic, since real walls are significantly more massive. As a consequence, larger electric tension and more time would be necessary to obtain similar extraction rates.

A possibility to obtain more easily an efficient salt extraction would be the application of electrodes on one side of the masonry. It has been shown that it is possible to perform an efficient extraction by placing electrodes on one side of the masonry. It is not necessary to cover the entire wall with electrodes. A continuous layer of contact material (a wet mixture of cellulose fiber and calcite) that may be 'sprayed' over the wall surface, combined with electrodes covering only part of the wall surface, might be enough for an electrophoresis. Although successfully tested out a wall section of 14 cm thickness [7], it is expected that such desalination will not always be effective in the entire depth of the wall. Most probably the depth of desalination will be similar to the average distance between the positive and negative electrodes, even though this still has to be confirmed through experiments.

References

- [1] Herinckx, S., Vanhellemont, Y., Hendrickx, R., Roels, S., De Clercq, H. Salt removal from stone building materials using an electric field. SWBSS Proceedings, Limassol, Cyprus, 2011, pp 357-364
- [2] Ottosen, L.M., Christensen, I.V., Electrokinetic desalination of sandstone for NaCl removal: Test of different clay poultices at the electrodes. Elsevier – Electrochimical Acta. NO. 86, 2012, 192-202.
- [3] Ottosen, L.M., Pedersen, A.J., Rørig-Delgaard, I. Salt-related problems in brick masonry and electrokinetic removal of salts. Journal of Building Appraisal. (3), (2007), 181-194.
- [4] Ottosen, L.M., Rørig-Dalgaard, I., Villumsen, A., Electrochemical removal of salts from masonry – Experiences from pilot scale, SWBSS Proceedings, Copenhagen, 2008, pp 341-350.
- [5] Nieuwe technieken ter remediëring van zoutbelast metselwerk, report IWT project WTCB-KIK-KUL (2010)
- [6] Skibsted, G., Ottosen, L.M., Jensen, P.E., Electrochemical desalination of limestone spiked with Na_2SO_4 – importance of buffering anode produced acid. Appendix to the PHD-thesis 'Matrix changes and side effects induced by electrokinetic treatment of porous and particulate materials', Gry Skibsted, BYG DTU – Department of civil engineering, Technical University of Denmark, 2013
- [7] Rørig-Dalgaard, I., Ottosen, L.M., Hansen K.K., Preservation of murals with electrokinetic – with focus on desalination of single bricks, PHD-thesis, Department of civil engineering, Technical University of Denmark, 2008

Poulticing sandstone: implications for subsequent weathering response

C.M. Gerrow^{1*}, C. Gerdwilker², P.A. Warke¹, S. McCabe¹ and J.M. McKinley¹

¹School of Geography, Archaeology and Palaeoecology, Queen's University Belfast, UK.

²Historic Scotland, Edinburgh, UK

* cgerrow01@qub.ac.uk

Abstract

This research investigates application of desalinating poultices to Locharbriggs Sandstone and Peakmoor Sandstone using different poultice mixes and application methods. The project has two aims, first, to determine the impact of poulticing on subsequent stone weathering response to simulated weathering cycles and, second, to evaluate the effectiveness of different poultice mixes and application methods on removing salt from substrate material. Analysis of surface to depth samples from blocks using Ion Chromatography and Atomic Absorption Spectroscopy identified spatial patterns of substrate salt retention. Visual recording of samples during weathering simulations identified differential weathering response of blocks with Peakmoor Sandstone exhibiting the most extensive surface deterioration. This deterioration was related to the incomplete removal of salts and mobilisation of 'deep' substrate salt deposits that were drawn up to near surface material. These data demonstrate the importance of appropriate poultice selection and adherence to 'best practice' during the application process. They also have implications for consideration of adverse effects of incomplete salt removal from heavily contaminated stone.

Keywords: poultice, sandstone, weathering, Locharbriggs, Peakmoor

1 Introduction

Since removal from a quarry and placement into a building or monument stone blocks will have acquired a complex stress history [1–4] that reflects exposure conditions, for example, a polluted urban environment or general weathering activity associated with the subaerial environment. Stone is traditionally seen as an immutable building material [5], which should withstand internal breakdown but with an understanding of decay processes comes the recognition that stone has a ‘finite life’ [6]. However with repetitive exposure to chemical, physical and biological weathering processes the structure of stone becomes altered and the stone can become ‘contaminated’ by agents of weathering such as salt. This can significantly curtail the durability and lifespan of a building or monument [7, 8].

Sandstones are common in historic and new-build structures because of their availability, aesthetic appeal and comparative ease of working. However, because of their relatively high porosities (c. 20%), moisture and any contaminants such as salts can gain access to the material. The significance of salt penetration and accumulation lies in its long and short term weathering effects that result due its changes in state i.e. in a dissolved or crystalline state that may be controlled by micro-environmental factors. Both salt crystallization and the volumetric expansion associated with phase changes exploit pre-existing weaknesses such as micro-fractures and pore spaces. For that reason salt phase changing takes advantage of inherited (whether diagenetic or caused by emplacement) weaknesses to develop microfracture networks. It is well documented [1, 6, 8–12] that the presence of salt is often associated with active surface deterioration and loss of material and hence architectural detail.

Stone cleaning can be contentious [13–17] and has generated great debate and a large body of literature detailing the problems and often common mistakes which have in some instances led to accelerated deterioration of stone and discoloration of facades. Aggressive chemical and physical cleaning of stonework in the 1980’s contributed to the creation of many dilapidated facades by the 1990’s in the United Kingdom, [13] but it is important to note that many buildings have been successfully cleaned, yet the successes were over-shadowed by those that were less successful. With many conservation grants, a certain proportion of funding is allocated to surface cleaning and there are several different approaches

that have commonly been used. Poulticing is one such process and it has successfully been used in many cases (e.g. Kelvingrove art gallery and museum, Glasgow). However many arguments have been put forward addressing the suitability and efficacy of poultices as to whether they should be used and how often poultices should be applied, particularly due to the cost and time needed for their repeated application within a conservation project.

Poulticing as a 'cleaning' method was originally designed to remove salt but additives are often now introduced to remove stains, referred to as 'active' or 'chemical' poultices. In this study, poulticing has been used as a mechanism to remove salt contaminations from historical stone substrates.

An abundance of research has been carried out into the efficacy of different poultices and carrying mediums [18–24]. However, once the process of poulticing has been completed, our knowledge of the short and long-term impact on subsequent weathering response appears to be limited as the post application weathering response has been an area of neglect in the research.

This paper reports data from a laboratory based experimental study aimed at identifying the implications of poulticing for subsequent salt weathering response in sandstone under controlled laboratory conditions.

2 Methodology

Information provided in this section gives insight into the stone types, materials used, the artificial weathering regime samples were subjected to and the subsequent analytical techniques used for analysis.

2.1 Materials

Two different sandstones were used in this study: Locharbriggs a red to brown coloured sandstone of fine to medium grained texture with inherent clay laminations and Peakmoor a buff coloured sandstone of fine to medium grained texture. For further characteristic information on these sandstones see Table 1.

Table 1: Stone types and their properties used in this study

Name	Geological Age	Mineralogy and Structure	Porosity (%)	Average Permeability (mD)	Standard Deviation (σ)
Locharbriggs	Permian	Quartz, Iron-Oxide, feldspars, Silica, Mica and Smectite clays	24.9%	743 (range 119 to 2028)	432
Peakmoor	Carboniferous	Quartz, feldspars, Mica and chlorite clays	16.5%	32 (range 9 to 88)	22

The pre-mixed poultice application used in this study is not a commercial pre-packed product but rather an admixture of sepiolite clay and Poraver® (Table 2). Two poultice mixes of various ratios were tested (Table 3), as the quantity of different granular sized mediums is directly related to the advective quality of a mix.

Table 2: Poultice mixture constituents

Constituent	Type	Characteristics
Binder	Sepiolite	A complex magnesium silicate clay with a high porosity content
Filler	Poraver®	An expanded lightweight glass granulate made from recycled glass

Poraver® granular size *P1- 0.1-0.3mm **P2- 0.25-0.5mm ***P3- 0.5-1.0mm

Table 3: Poultice ratio of mixture constituents

Poultice Mix	Volumetric Ratio of Constituents	Sub-set Ratios
Poultice 1	4:1 – Poraver®: Sepiolite	Poraver®: 2 x 'P1'*, 1 x 'P2'**, 1 x 'P3'*** 1 x Sepiolite
Poultice 2	5:1 – Poraver®: Sepiolite	Poraver®: 3 x 'P1', 1 x 'P2', 1 x 'P3' 1 x Sepiolite

Poultice mixes were applied on top of an interface material to prevent clay contamination on the surface of the substrate. The interface materials used in the study were: Arbocel® PWC 500 cellulose fibres (fibre length: 500 μ m) and Japanese tissue paper made from vegetable fibres, both commonly used in poultice application practices.

2.2 Procedures

Rock specimens were cut into blocks of 10 x 10 x 7.5cm and loaded with a one-off application of salt solution, in this case 1.709 moles per litre of sodium chloride was used. This salt and the concentration of solution was chosen due to its common association with salt weathering and the concentration is relative to what is found in the natural environment within the United Kingdom, a widely maritime environment. The one-off application of salt solution was carried out via capillary rise for 5 days and subsequently air dried for 6 days at a background Relative Humidity (RH) of c. 60% until block weights remained stable. Weight data were collected before and after salt loading. After drying all specimen blocks were coated on 5 sides with a clear varnish (Ronseal), and embedded in expanded polystyrene to ensure heating and cooling primarily occurred via the one exposed face (10 x 10 cm). The gap between block edges and the polystyrene were closed using a plastic sealant in an attempt to prevent multilateral mobilisation of the salt in its soluble state (see other experiments using this technique [25–27]). Moisture could then only be lost from one exposed surface.

Prior to the poultice applications the interface materials were applied as such:

- Japanese tissue (grade L2): the surface of the stone samples were sprayed lightly with distilled water before the tissue was set onto the surface. To ensure a sound adhesion to the surface the tissue was lightly sprayed with distilled water and stippled with a soft bristle brush to ensure connectivity.
- Cellulose fibres: used as an isolating layer between the clay and stone fabric. The Arbocel fibres were mixed with enough water to form a fluid paste, which allows the mass to be troweled onto the surface easily without breaching or puncturing the isolating layer.

Poultice materials were mixed with 1 part of distilled water to form a putty like paste, the poultice mixes were applied directly after the interface materials were applied and applied to pairs of specimen samples that were covered with PVC film for 72hrs to prevent initial evaporation of water. The poultice mixes were left *in situ* upon the sandstone samples for a total of 5 days, until the poultice appeared dry and to prevent re-impregnation of the salts into the sample blocks, then carefully removed and individually stored for subsequent analysis. Sample blocks with a cellulose interface were brushed lightly with a soft bristle brush to remove

any remaining cellulose fibres. Blocks were placed in an environmental chamber and exposed to the temperature cycles shown in Figure 1 for a total of 30 24hour cycles.

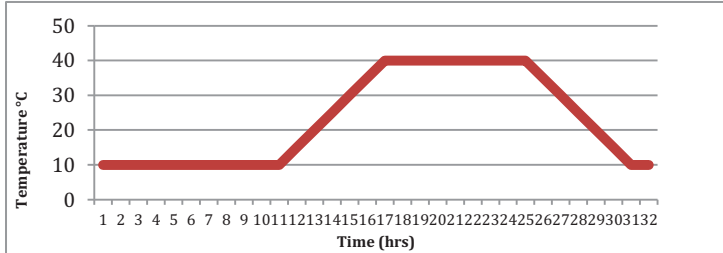


Figure 1: Temperature cycle

Samples were sprayed daily before the start of each cycle with 11ml of distilled water. At the end of the 30 cycles the exposed face of each sample block was lightly brushed to remove any loosened material which was retained and weighed.

2.3 Analysis

The following information provides specifications for sandstone and removed poultice samples post application and the analyses conducted.

2.3.1 Sandstone samples

Sandstone blocks, post poultice and post poultice with simulated weathering, were dry-cut in half from the exposed block surface to the base, to expose a cross-sectional face. Sub-sampling was conducted by extracting lateral powder samples through dry-drilling at 5mm intervals from surface to depth of each specimen. 1g of dried powdered sample was dissolved in 10ml of distilled H₂O for 24hrs on an orbital shaker and filtered through 0.22µm filter membranes. This water extraction was then used to conduct elemental analysis (Atomic Absorption Spectroscopy (AAS) and Ion Chromatography (IC)).

2.3.2 Removed poultice samples

The removed poultices were sub-sampled using a riffle splitter and placed in a temperature oven at 105°C for 24hrs. The sample weight was recorded at this point. 100ml of distilled water was added to the sub-sampled poultice, placed on a magnetic stirrer for 30mins and left in the solution for 24hrs. 40ml was decanted into centrifuge tubes and

centrifuged at 3000rpm for 5mins. Water extractions were manually filtered for 24hrs, which were then used for elemental analysis using AAS and IC.

3 Results

3.1 Salt profile results and weight loss for Locharbriggs and Peakmore samples

Figure 2 presents the salt profiles of Locharbriggs samples while in figure 3 those of Peakmore samples.

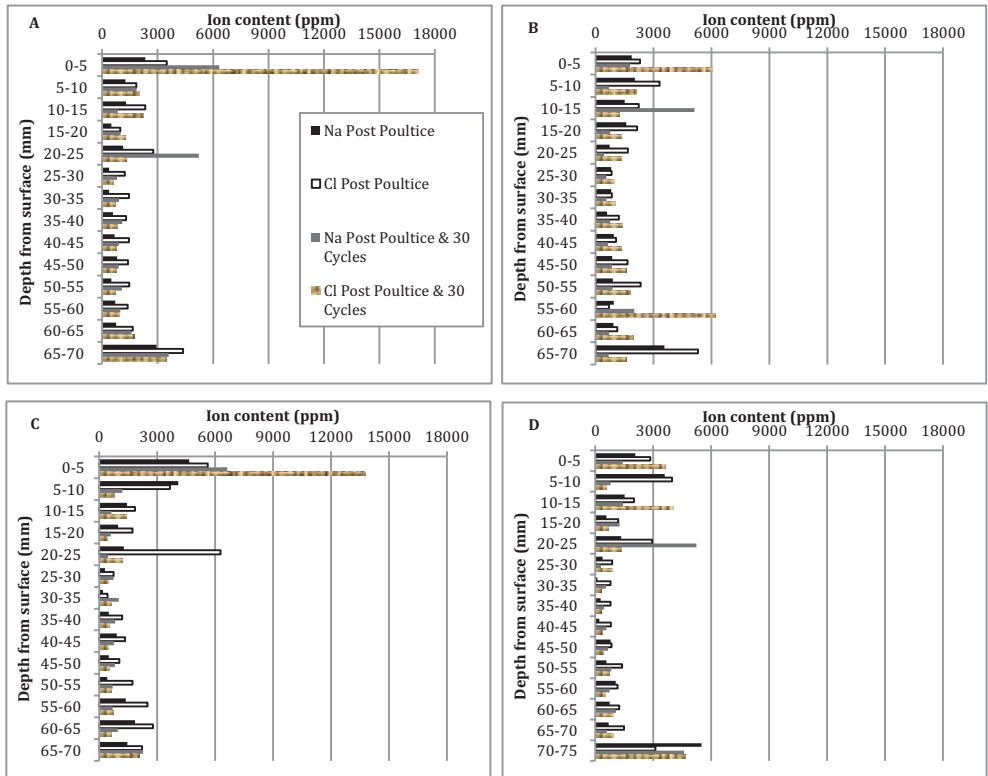


Figure 2: Combined post poultice and post poultice with simulated weathering salt profile results (ppm) on Locharbriggs samples (A with poultice 1 applied to cellulose interface, (B) with poultice 1 applied to Japanese tissue interface, (C) with poultice 2 applied to cellulose interface and (D) with poultice 2 applied to Japanese tissue interface.

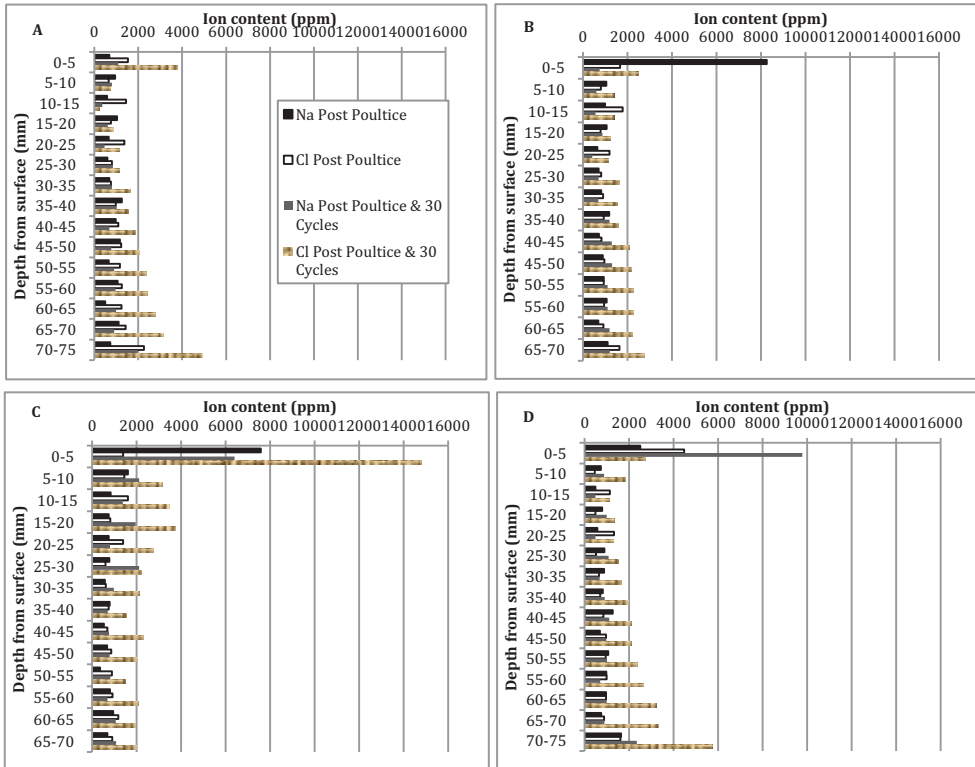


Figure 3: Combined post poultice and post poultice with simulated weathering salt profile results (ppm) on Peakmoor samples (A) with poultice 1 applied to cellulose interface, (B) with poultice 1 applied to Japanese tissue, (C) with poultice 2 applied to cellulose interface and (D) with poultice 2 applied to Japanese tissue interface.

The weight loss values of stone material are presented in Table 4.

Table 4: Weight loss data of Locharbriggs and Peakmoor samples post poultice with simulated weathering, and related to non poulticed salt free (blank) sample and one loaded with 10% NaCl.

Poultice Application	Locharbriggs initial weight before weathering (g)	Weight loss		Peakmoor initial weight before weathering (g)	Weight loss	
		(g)	(%)		(g)	(%)
Blank Sample	1323.54	N/A	0.00	1316.74	N/A	0.00
10% NaCl loaded sample	1379.58	2.09	0.15	1603.54	2.26	0.14
Poultice 1 - Cellulose interface	1365.66	1.51	0.11	1637.89	0.04	0.00
Poultice 1 - Japanese tissue interface	1399.73	1.57	0.11	1634.2	0.19	0.01
Poultice 2 - Cellulose interface	1347.67	2.37	0.18	1561.04	6.68	0.43
Poultice 2 - Japanese tissue interface	1395.02	2.42	0.17	1559.22	0.1	0.01

3.2 Salt extraction results from removed poultices

Pure poultice and natural stone sodium and chloride concentrations were tested prior to use. Table 5 reveals the minimal amount of both ions present in the materials before use while Table 6 presents Locharbriggs and Peakmoor sodium and chloride concentrations of removed water extractions from individual poultices.

Table 5: Pure poultice and natural stone sodium and chloride concentration

Materials	Na (ppm)	Cl (ppm)
Poultice 1 4:1 – Poraver®: Sepiolite	62	81
Poultice 2 5:1 – Poraver®: Sepiolite	54	46
Locharbriggs sandstone	1.5	2.5
Peakmoor sandstone	1.2	2.2

Table 6: Locharbriggs and Peakmoor sodium and chloride concentrations of removed water extractions from individual poultices.

Poultice - interface combination	Locharbriggs		Peakmoor	
	Na (ppm)	Cl (ppm)	Na (ppm)	Cl (ppm)
Poultice 1 - cellulose	11281	35052	4308	9097
Poultice 1 - cellulose	14113	46976	2813	6505
Poultice 1 - Japanese tissue	15214	46335	68323	16882
Poultice 1 - Japanese tissue	25818	48709	98385	92805
Poultice 2 - cellulose	63202	21699	6112	9663
Poultice 2 - cellulose	92822	27661	3328	5907
Poultice 2 - Japanese tissue	9843	35630	5046	8907
Poultice 2 - Japanese tissue	12868	38879	7653	7592

Duplicates of each block and poultice/interface combination were tested in this study to insure that the results (Table 6) were synonymous with each other. However, the results above indicate some differences between duplicate blocks with the same treatment combination applied. These differences in Na and Cl concentrations extracted from the near surface of the stone substrates may be due to the ionic diffusion of NaCl throughout the stone as well as the available pore connectivity. As it is already known that crystallised salts can block pore throats resulting in lesser connective pore pathways within the substrate [28].

Yet it is important to keep in mind structural controls within the stone, which will also play a part in where salt will reside, for instance Locharbriggs is heavily clay bedded which highlights the importance of micas and clays due to their “potential to ‘fix’ ions in the interlamellar spaces of the structure” [29]. McCabe goes on to explain that diagenetic processes in Locharbriggs disaggregated the mica-rich metamorphic rock liberating a pseudo-matrix that in addition to contributing to decreased porosity and increased tortuosity they also contribute to adsorption of hydrated ions. This may explain why more chlorides are detected in removed poultice 1 from Locharbriggs but the inverse can be seen in the

removed poultice 2, wherein more sodium was detected. As ions have been fixed within the clay material and hence not extracted to the same degree. Micas are also present in Peakmoor but, these are 'trapped' within the granitic rock fragments and do not exert the same influence.

Although iron was not tested for in this study, it is essential to understand that iron grains and iron coatings can also modify the diffusion of salt. As McCabe [29] has acknowledged iron 'grain coatings modify both the free charges on the pore surfaces and the contact angle (wettability) between salt solutions and the silicate grains in comparison to sandstones without grain coatings'. Locharbriggs' red- to brown colour is derived from such coatings and is noted to show well-developed iron oxide and hydroxide coatings, however Peakmoor is not abundant in iron minerals.

With these mineralogical difference kept in mind, it may explain the differences in results for the Peakmoor substrate treated with poultice 1 on Japanese tissue. One theory may be the concentration of mica within each sample block is different and therefore limiting the concentration of adsorbed ions, which could be removed via the poultice. Undoubtedly differing results between duplicate samples subject to the same treatment can be explained by the varying heterogeneity of each individual sample.

3.3 Initial results post-poultice removal

3.3.1 Locharbriggs

The salt profile results post-removal of the poultice application to the Locharbriggs specimens (Figure 2) suggest that the interface used between the stone substrate and the poultice mixture can have a significant influence over the efficacy of the applied poultice. This could be due to the interface altering the pore size of the poultice, which is designed to have a finer porosity than the substrate, so when applied an advective quality can be achieved. Poultices with pores of different sizes can be obtained by varying the component types and properties such as: clay type, grain size, and cellulose fibre length but also by varying the ratios between them [23], which could either be beneficial or disadvantageous to its overall efficacy.

Some specimens, such as those of Figure 2c, show a large concentration of sodium chloride at the near surface area in comparison to other specimens. One possible interpretation is that this poultice/interface combination did not produce a sufficient advective quality to effectively remove salts out of the top surface area following one application, but rather mobilised salts to create a greater concentration in that area.

However, the analysis conducted on the removed poultices (Table 6) contradicts this interpretation due to the high concentration of sodium chloride (taken out of the stone by the poulticing) present in this poultice/interface combination. This may be a reflection of porosity and the connectivity of the pores of the Locharbriggs sample drawing salts from a reservoir of salt at depth creating a 'feeding' effect to the surface zone. Duplicate blocks were treated with the same poultice/interface combination to ensure that this result was not an anomaly. These results reveal that this combination of poultice and interface is in fact very effective at removing chlorides when applied to a Locharbriggs substrate but it is likely that a second application of the poultice treatment would have been effective in removing salts from the near surface zone. As initial results indicate it has a strong advective quality, however leaving such a high concentration of sodium chloride in the near surface zone after only one application leaves the stone vulnerable to mechanical breakdown by salt weathering mechanisms as it creates a 'reservoir' of salts that are available for driving subsequent decay.

3.3.2 Peakmoor

The results post poultice removal for the Peakmoor specimens initially suggest that the poultice 1 mixture might not have been very successful in aiding salt reduction, as the overall salt profiles of Figures 3a and 3b have not been dramatically altered. However in comparison to the results of Figures 3c and 3d it is evident that salt has been mobilised to the near surface area.

Analysis of the removed poultices (Table 6) reveal that the most effective mix for reduction of salt was the combination of the poultice 1 mix used with a Japanese tissue interface. Suggesting that poultice mix 2 with either interface used has not generated sufficient advection to remove the salts from the top surface with one application. It is important to note that all poultices applied did remove salt, however as poultice applications are a time consuming and costly method of salt reduction it is important to choose the most effective poultice mix and interface combination in relation to the specific substrate being treated.

It must be remembered that in reality the salt concentration within a historic substrate of a building is usually unknown without the use of invasive testing i.e. sample coring of stone. Therefore removed poultices should be tested for their salt concentration to ensure the concentration of salt is reducing after each application to prevent high concentrations of salt being left at the surface, and hence the possibility of exacerbating surface loss.

3.4 Post weathering simulation results

After 30 diurnal simulated weathering cycles all salt profiles changed significantly.

3.4.1 Locharbriggs

Due to Locharbriggs characteristic of greater open porosity and connected permeability there appears to be a greater mobility of salt transportation, specifically to the exposed surface area within the top 25mm of the test blocks. It is this mobility and ability for salt to be transported which undoubtedly causes damage and encourages material breakdown and therefore material loss.

The overall substrate weight loss data recorded (Table 4) from this study demonstrates that 50% of the Locharbriggs samples treated with a one-off poultice application lost more material following the simulated diurnal cycling than the salt control block. Such material loss is at odds with the reason for applying poultice treatments, which is to limit breakdown by reducing salt load within the substrate. However, to understand these results all data must be considered holistically, for instance, if Figure 2a and Figure 2c results are viewed comparatively due to similarities in salt profiles. A combination of poultice 2/cellulose interface extracted the most salt within this category (Figure 2c) but also inflicted the most material loss of 0.18%, whereas in case of poultice 1/cellulose interface, the sample was left with the highest concentration of sodium chloride within the top 5mm (Figure 2a) but generated the least material loss, 0.11%. Salts need to be removed through the surface, therefore a tension arises between the need to remove salts and the danger of leaving increased salt concentrations in the near surface zone. The solution to this problem is not straightforward, even subsequent applications may simply continue to draw salts from depth and leave them in the near surface zone rather than completely removing the threat of salt decay giving potential for setting up a salt 'conveyor belt' from depth back to the surface.

It is evident from these results that the use of different interfaces upon a Locharbriggs substrate leads to very different salt profile outcomes post-weathering, such as Figure 2b in comparison to Figure 2c. Wherein the former poultice/interface combination extracted the second highest amount of salt but similarly resulted in the second highest material loss, even though the top surface of Figure 2b had significantly less salt concentrated in the top 5mm. Although, the overall salt profiles differ between same poultice/different interface combinations the substrate weight loss percentages have been fairly similar, e.g. 0.01% difference

between samples related to Figures 2a and 2b, whereas those related to Figures 2c and 2d showed exactly the same weight loss. This seemingly contradiction where high concentrations of salt in the near surface zone generated similar loss as those samples with lesser concentrations within the near surface zone suggests that the simulated weathering cycles may have been stopped prematurely before a major breakdown threshold was crossed. Thus only a small insight into Locharbriggs behavioural response to weathering has been witnessed and could be considered episodic rather than steady in terms of the rate of breakdown [10].

3.4.2 Peakmoor

The behaviour of Peakmoor samples provided contrasting results. The poultice/interface combination shown in Figure 3a extracted the most salt from the substrate (Table 6) and did not generate a large concentration of salt within the top 25mm. It also resulted in minimal material loss of 0.01% of the initial block weight, significantly less in comparison to the Peakmoor salt control block (Table 4). Although the sample considered in Figure 3a shows no material loss, in relation to its counterpart Figure 3b, the poultice/interface combination used extracted a considerably lower amount of salt, suggesting that this poultice/interface combination is not as effective on a Peakmoor substrate.

The greatest amount of material loss recorded during the simulation experiment was from a Peakmoor sandstone sample treated with poultice 2/cellulose interface. Analysis showed that significant amounts of NaCl had accumulated in the upper 5mm of stone (Figure 3c), which subsequently contributed to surface blistering and granular disintegration resulting in a loss of 0.43% of the initial block weight. Finally, Figure 3d shows a very different salt profile in comparison to its counterpart (Figure 3c) where to a lesser extent salt is concentrated within the top 5mm which led to much less material loss from the surface (0.01% of the total block mass). Such differing results between the same poultice mixes appear to reflect the type of interface used indicating that a cellulose interface potentially improved the advective effectiveness of the poultice in comparison to the Japanese tissue. However, these data must be viewed with caution as this experiment only tested the subsequent weathering response after one poultice application. The difference in results may also reflect the fact that the experimental cycles stopped before the block considered in Figure 3d shifted from a relatively stable condition to one of instability and breakdown.

4 Discussion

The results provided have brought to light areas of impact wherein these results could prove to be beneficial, which will be discussed below. In the context of practitioners approaching historic stone, the present study is significant. Data reported here highlight the importance of avoiding single poultice applications, as a one-off poultice treatment may allow damaging salts drawn towards the surface to remain in the near surface zone, where a second application could potentially remove these. However, if project funding is not sufficient for applying poultices multiple times it may be considered that it might be more beneficial not to poultice at all than to apply the treatment once.

4.1 Interface suitability

These data also illustrate the importance of selecting an appropriate poultice interface as this can have a significant impact on efficiency of salt removal. The use of a cellulose interface proved to be most efficient in aiding the mobility of salt, which may be due to several reasons:

- 1) A fibre length of 500 μ m or less can create a finer porosity at the surface zone creating a more effective advective quality.
- 2) To apply the cellulose interface it must be soaked to create an unbroken layer of approximately 1.5cm thick. The addition of water enables salt solubility and therefore increased salt mobility.
- 3) The layer of cellulose provides a greater area and pore space for salt to relocate to rather than the use of Japanese tissue interface.
- 4) A cellulose interface is usually favoured because of its 'sticky' quality, providing better adhesion to vertical facades.

However, despite these advantages cellulose also has several disadvantages:

- 1) Difficulties when the poultice is removed as cellulose fibres can remain on the stone surface, especially if the surface is rough and uneven. This can be removed by aggressive brushing but may jeopardise a friable surface.
- 2) Previous research [24] indicates that cellulose can be prone to mould development. In relation to the previous point, if cellulose fibres are left on the stone substrate and cannot be removed by agitation there is a risk that mould could develop or become a breeding ground for organic material.
- 3) Using cellulose to prevent clay contamination of the substrate surface means that it should be used as an individual layer

between poultice and substrate. However, cellulose as part of the poultice admixture will not prevent clay contamination and sometimes a powdered veil will be left on the stone surface that has been poulticed, causing discolouration and difficulty in removal.

- 4) The addition of water is necessary to make cellulose adhere to stone, however cellulose has a poor water retention, therefore the addition of too much water can make application to vertical surfaces difficult. There is also a risk that the wet cellulose can saturate the stone beneath, therefore mobilising salts deeper into the block, which may lead to a re-emergence of efflorescences [18, 30].
- 5) Furthermore, when a large amount of water is used to bind the cellulose, it may take a longer time to dry out in comparison to a clay poultice, resulting in the cessation of its advection and recontamination of salt from the wet cellulose back into the substrate if the poultice is not promptly removed.

This research shows the significance of attempting to understand the behavioural response of sandstone post-treatment, as this area has generally been neglected in the assessment of conservation treatments with focus being on the effectiveness of the stone treatment. It is when issues are ill addressed that problems concerned with treatment based conservation methods can result in detrimental damage rather than preservation. It is well known in the conservation world that treatments cannot be applied on a one-case fits all scenario basis but must be case-specific.

4.2 Ethics of conservation intervention

Intervention via conservation treatments to historic stone fabric is ruled by 'ideal' vs 'reality' ideology; in terms of the expected outcome of the treatment results, these expectations can differ greatly between the building owner and the skilled practitioner. This can be an area of contention between both parties when a building owner expects to see a remarkable change in the appearance of the masonry post treatment application. It is common for compromises to be made in overall expectations of conservation projects in order to seek the balance between 'best practice', funding available, building owners expectations and the desire and quality of expertise available.

The decision to intervene via conservation treatments is undoubtedly dictated by the on going debate and ethical approaches associated with

conservation. Building conservation is distinctly different from the physical processes of repair and adaptation. According to English Heritage [30] “it is an attitude of mind, a philosophical approach, that seeks first to understand what people value about a historic building or place beyond its practical utility, and then to use that understanding to ensure that any work undertaken does as little harm as possible to the characteristics that hold or express those values”.

Masonry behavioural response then, as well as now, is still not fully understood, but attempts into understanding the response is vital to prevent the mistakes of the past and to aid successful application of surface treatments for the future.

5 Conclusions

This study highlights the need for further research into the behavioural response of masonry post surface treatment applications. As an initial small-scale laboratory investigation it has revealed that applying one poultice application could potentially accelerate the degradation rate of the masonry surface instead of slowing the weathering process, but also highlighted the importance of interface selection. In order to adhere to best practice, it now appears to be significant to include trial panels for poulticing, not only to assess the efficacy but also to monitor the behavioural response of the substrate post-application. However, the monitoring period is up for debate as this is circumstantial to locality, exposure to moisture ingress, as well as threat of freeze and thaw in the natural environment. It is apparent from the results presented that if project funding is limited or does not cover the costs for repeated poultice applications it may be more beneficial for the future of the masonry to not apply poultices. This must be carefully considered by a skilled practitioner who can investigate the extent of salt contamination of the masonry before progressing with a desalinating surface treatment.

Furthermore, the mineralogical composition of the stone type being treated much be kept at the fore, as this may or may not exert limitations in the extractability of the poultice and the subsequent weathering response after removal. With this in mind it must be remembered that masonry stone such as sandstone is inevitably variable in its heterogeneity and mineralogical composition that may dictate to what extent salt extraction is possible.

These initial results into the behavioural response of sandstone post surface treatment applications have widened the scope for future

research. Rationale for proposed future research into sandstone behavioural response post surface treatment applications at Queen's University Belfast has been derived from the lack of geomorphological knowledge post treatment and what the subsequent weathering response impact has on the material. Data obtained will be beneficial to the debate of conservation intervention by inheriting the viewpoint that stone is a complex material and this must be remembered when addressing the issue.

Acknowledgements

The authors would like to thank the technical staff at Queen's University Belfast for their aid in sample preparation. This work was funded by Historic Scotland, who are thankfully acknowledged.

References

- [1] McCabe, S., Smith, B.J., Warke, P.A. Preliminary observations on the impact of complex stress histories on sandstone response to salt weathering: laboratory simulations of process combinations. *Environmental Geology*, (52) (2006), 251-258
- [2] McCabe, S., Smith, B.J., Warke, P.A. Sandstone response to salt weathering following simulated fire damage: a comparison of the effects of surface heating and fire. *Earth Surface Processes and Landforms* (32) (2007) 1874-1883
- [3] McCabe, S., Smith, B.J., Warke, P.A. A Legacy of Medieval Mistreatment in NE Ireland. Geological Society: Special Publications 333, London, 2010
- [4] Smith, B.J. Scale problems in the interpretation of urban stone decay In: *Processes of Urban Stone Decay* (Eds.) B.J. Smith & P.A. Warke. Donhead Publishing LTD, London, (1996), 3-18
- [5] McAlister, J.J. Analytical techniques for the examination of building stone. In: *Processes of Urban Stone Decay* (Eds.) B.J. Smith & P.A. Warke. Donhead Publishing LTD, London, (1996), 32-43
- [6] Smith, B.J., Gomez-Heras, M, McCabe, S. Understanding the decay of stone-built cultural heritage. *Progress in Physical Geography* 34, (4) (2008), 439-461

- [7] Camuffo, D. Acid rain and the deterioration of monuments: how old is the phenomenon? *Atmospheric Environment* (26B), (1992) 241-247
- [8] Turkington, A.V. Stone durability In: *Processes of Urban Stone Decay* (Eds.) B.J. Smith & P.A. Warke. Donhead Publishing LTD, London, (1996), 19-31
- [9] Price, C.A., Brimblecombe, P. Preventing salt damage in porous materials. In: *Preventive Conservation: Practice, Theory and Research*. International Institute for Conservation, London, (1994), 90-93
- [10] Smith, B.J., Magee, R.W., Whalley, W.B. Breakdown patterns of quartz sandstone in polluted urban environment: Belfast N. Ireland. In Robinson, D.A., Williams, R.B.G. (Eds.) *Rock weathering and landform evolution*. Wiley, Chichester, (1994), 131-150
- [11] Goudie, A. & Viles, H. *Salt Weathering Hazards*. John Wiley and Sons, Chichester, 1997
- [12] Warke, P.A., McKinley, J., Smith, B.J. Variable weathering response in sandstone: factors controlling decay sequences. *Earth Surface Processes and Landforms* (31) (2006), 715-735
- [13] Ashurst, N.A. *Cleaning Historic Buildings: Volume 1 substrates, soiling and investigations*. Donhead, London, 1994.
- [14] Maxwell, I. Stone cleaning, for better or worse? An overview. In Webster, R.G.M (Ed) *Stone Cleaning: and the nature, soiling and decay mechanisms of stone*. Donhead, London, 1992.
- [15] Andrew, C.A, Young, M.E., Tonge, K.H. *Stone Cleaning: A guide for practitioners*. Historic Scotland & The Robert Gordon University, Aberdeen, (1994), 1-3
- [16] Vicente, M.A., Vicente-Tavera, S. Clay poultices in salt extraction from ornamental stones: A statistical approach, *Clay and Clay Minerals*, (49:3) (2001), 227-235
- [17] Coath, J. Sandstone conservation and repair in *The Building Conservation Directory: Twentieth Anniversary Edition*. Cathedral Communication Limited, (2013), 106-109

- [18] Auras, M. Poultrices and mortars for salt contaminated masonry and stone objects In *Salt Weathering on Buildings and Stone Sculpture*, Proceedings of SWBSS, Ottosen, L.M., Rørig-Dalgaard, I., Larsen, P.K, Brajer, I., Bøllingtoft, P., Marciniak, M., Svane, M. (Eds.) National Museum Copenhagen, Denmark, Technical University of Denmark, Lyngby, (2008), 197-217
- [19] Bourgès, A., Vergès-Belmin, V. Comparison and Optimization of five desalination systems on the inner wall of Saint Philibert Church in Dijon, France. In *Salt Weathering on Buildings and Stone Sculpture*, Proceedings of SWBSS, Ottosen, L.M., Rørig-Dalgaard, I., Larsen, P.K, Brajer, I., Bøllingtoft, P., Marciniak, M., Svane, M. (Eds.) National Museum Copenhagen, Denmark, Technical University of Denmark, Lyngby, (2008), 29-40
- [20] Bourgès, A., Vergès-Belmin, V. Application of fresh mortar tests to poultrices used for the desalination of historical masonry. In *Materials and Structures* (44:7) (2011), 1233-1240
- [21] Doehne, E., Price, E. *Stone Conservation: Overview of Current Research*. The Getty Conservation Institute, Getty Publications, California, 2010
- [22] Lubelli, B., van Hees, R.P.J. Desalination of masonry structures: fine tuning of pore size distribution of poultrices to substrate properties. *Journal of Cultural Heritage* (11) (2010), 10-18
- [23] Lubelli, B., van Hees, R.P.J., De Clercq, H. Fine tuning of desalination poultrices: try-outs in practice. In *Salt Weathering on Buildings and Stone Sculptures*, Proceedings of SWBSS, I. Ioannou & M. Theodoridou (Eds.), Limassol, Cyprus, (2011), 381-388
- [24] Vergès-Belmin, V., Heritage, A., Bourgès, A. Powdered Cellulose Poultrices in Stone and Wall Painting Conservation Myths and Realities. *Studies in Conservation*, (56: 4), (2011), 281-297
- [25] McKinley, J.M., McCabe, S. A Geostatistical Investigation into Changing Permeability of Sandstone During Weathering Simulations. *Geographical Analysis* (42) (2010), 180-203
- [26] McCabe, S., McKinley, J.M., Gomez-Heras, M., Smith, B.J. Dynamic instability in surface permeability characteristics of building sandstones in response to salt accumulation over time. *Geomorphology* (130) (2011), 65-75

- [27] Smith, B.J., Srinivasan, S., Gomez-Heras, M., Basheer, P.A.M., Viles, H.A. Near-surface temperature cycling of stone and its implications for scales of surface deterioration. *Geomorphology* (130) (2011), 76-82
- [28] McCabe, S., Smith, B.J., McAlister, J.J., McAllister, D., Srinivasan, S., Basheer, P.A.M., Curran, J.M. Linking climate change, moisture dynamics and salt movement within natural building sandstones: implications for salt transport by diffusion. In *Salt Weathering on Buildings and Stone Sculpture, Proceedings of SWBSS, Limassol, Ionnou, I. & Theodoridou, M. (Eds.) University of Cyprus, (2011), 63-70*
- [29] McCabe, S., Smith, B.J., McAlister, J.J., Gomez-Heras, M., McAllister, D., Warke, P.A., Curran, J.M., Basheer, P.A.M. Changing climate, changing process: implications for salt transportation and weathering within building sandstones in the UK. *Environmental Earth Science* (69) (2013), 1225-1235
- [30] Sawdy, A., Heritage, A., Pel, L. A review of salt transportation in porous media, assessment methods and salt reduction treatments. In *Salt Weathering on Buildings and Stone Sculpture, Proceedings of SWBSS, Ottosen, L.M., Rørig-Dalgaard, I., Larsen, P.K, Brajer, I., Bøllingtoft, P., Marciniak, M., Svane, M. (Eds.) National Museum Copenhagen, Denmark, Technical University of Denmark, Lyngby, (2008), 1-28*
- [31] Martin, B., Wood, C., McCaig, I. (Eds.) *Practical Building Conservation: Conservation Basics*, English Heritage, Ashgate Publishing Limited, Surrey, 2011

Salt extractions of brickwork: a standard procedure?

H. De Clercq* and S. Godts

Royal Institute for Cultural Heritage (KIK-IRPA), Brussels, Belgium

* hilde.declercq@kikirpa.be

Abstract

Crystallization of salts is recognized as a major factor in the degradation of porous materials in built heritage. Salt damage occurs in the presence of salts and moisture, in liquid or vapour form. This implies that, in case one of both can be excluded, salt damage can be mitigated. A salt extraction aims to reduce a maximum amount of salts present. In practice salt extractions are often executed without scientific background or control of its effect or durability. This paper deals with the results of salt extractions using a poultice consisting of a mixture of kaolin, sand and cellulose fibers applied on salt contaminated brickwork of two cases, the abandoned coal mine site named C-mine in Winterslag and two chapels of the Cathedral of Our Lady in Antwerp. Results have shown that several factors influence the salt extraction effect: the amount and distribution of salts, the pre-wetting properties, the physical properties of the building materials as well as the environmental conditions of the salt extraction execution. From the experimentally determined salt contamination and distribution as well as the properties of the poultice and the building materials of the masonry, the salt extraction execution parameters and its effect were first approached theoretically through modelling. The predicted effect was compared to the one experimentally determined. Concerning the last, powder drill samples were lifted from brick and mortar, before and after each salt extraction from which the ion content was determined quantitatively. From the results it was concluded that the optimum conditions for the execution of a salt extraction cannot be considered as a standard copy-paste application suitable for all types of salt contaminated brickwork. A critical note is to be tackled with respect to the term "salt extraction" as the reality shows that an important part of the salts migrate deeper into the brickwork.

Keywords: brickwork, salt extraction, poultice

1 Introduction

The crystallization of salts is a major cause of damage on historic built heritage and stone sculptures. Compared to new buildings, historic ones suffer more severely from salt damage due to their higher salt contamination accumulated over time. Mitigating of salt damage contributes to a sustainable preservation of our precious historical and architectural heritage. The occurrence of salt damage implies the presence of salts and moisture, in liquid or vapor form. Moisture can be regarded as the main catalyst for salt damage; without moisture transport processes and dissolution-crystallization cycles of the salts there would be no salt damage of porous material [1].

While the removal of salts from movable stone objects by means of the water bath method is quite well known [2], salt extraction of masonry by means of salt extraction poultices is often applied 'ad hoc', in most cases without control of the effect deeper in the masonry [3, 4] or a long term monitoring.

In the framework of a European project "Desalination" (FP6, project number SSPI 22714) a so-called modular system for poultices was developed [5, 6], by which the pore structure of the poultice was tailored towards that of the support to be extracted. Promising results were obtained with salt extraction products based on a mixture of kaolin, sand (0.5 – 1 mm grain size) and cellulose fibers (200 μm) in a weight ratio of 2-1-1 and a water weight content of 0.8 related to the total solid material.

This paper goes deeper into the salt extraction technique using such a poultice and focuses on the influence of some of the experimental parameters on the salt extraction effect on brickwork of two test cases, the abandoned coal mine complex in Winterslag, named C-mine, and two chapels of the Cathedral of Our Lady in Antwerp.

2 Methodology

For both cases drilled samples are lifted on numerous locations from the mortar and the brick at different heights and at least two different depths (0-2 and 2-5 cm). From each lifted powder sample the ambient moisture content is determined by comparing the initial weight to the weight reached after drying at 60°C. The hygroscopic moisture content is determined by conditioning the dried sample at 95% RH until constant weight. The hygroscopic moisture content is calculated from the increase in weight.

Demineralized water is added to the samples. The solution is left to mix for 4 hours to dissolve all ions present followed by a filtration. From the extract, sodium (Na^+), potassium (K^+), calcium (Ca^{2+}) and magnesium (Mg^{2+}) cations and chlorine (Cl^-), nitrate (NO_3^-) and sulphate (SO_4^{2-}) anions

are quantitatively determined with Ion Chromatography (IC, Metrohm). The quantitative ion data, expressed as mole-fractions, are entered into the ECOS/RUNSALT thermodynamic model (Environmental Control Of Salts) that determines the crystallization behaviour of the salt mixture at changing climatic conditions [7, 8]. After evaluation of the salt content in the walls, a zone characterized by a high salt content is selected for the extraction test. Experimental conditions of salt extractions were designed by simulations using the porous media transport model DELPHIN 5.5 [9].

3 Results and discussion

The *Kempen*, the eastern part of Belgium, was during the 20th century known for its coal mine activities. One of the seven coal mines was located at Winterslag (Figure 1), active from 1917 till 1988. After a period of neglect, the entire mine site became the subject of stepwise rehabilitation projects. The C-mines, where the “C” stands for “creativity”, comprise a unique industrial heritage and a witness of historical industrial activities typical for the region.



Figure 1: Coal mine site in Winterslag (wikipedia)

A section of the old C-mine buildings was transformed into workshops and exhibition rooms for a local artist designing ceramics. Salt analyses on mortar and brick samples revealed a high salt content, principally composed of sodium chloride at contents up to 7.5 w% in the mortar while at least 1 w% in the brick, crystallizing around 75% RH (ECOS/RUNSALT output, not shown here) and causing damage to the finishing layers as shown in Figure 2.

Climate control of the rooms in the large complex was for financial reasons not considered, nor technically possible due to the activities of the artists' team working with mortars for the preparation of ceramics;

therefore, it was advised to carry out salt extractions to decrease the salt content in the walls. The paint layer was carefully removed followed by a pre-humidification (2 l/m^2) prior to the application of a poultice for the salt extraction. The poultice, with a composition as described earlier, was applied on 1 m^2 four times, such that a new application immediately followed the previous one, again after pre-humidification (2 l/m^2). The poultice was easily mixed and applied to the wall; it dried equally starting at the borders curling off the substrate. No shrinkage cracks were noticed. During all four application it took approximately ten days before it partly sagged down. Because it still adhered to the wall it was then removed mechanically. After each application, drill powder samples were lifted from the brick and the mortar at a depth of 0-2 and 2-5 cm from which the salt content was quantitatively determined [10]. The results of the total ion content before and after 4 salt extractions are shown in Figure 3.

Initially, the brick contains a lower salt content compared to the mortar. The results show that after one poultice application the salt content in the brick is reduced to an acceptable value and even more so after two applications. This is not the case for the mortar for which at least three applications seem necessary. An inconsistency was noticed within the depth of the mortar as the salt content increased after the fourth application at a depth between 2-5 cm. This could indicate that the dissolved ions are being pushed deeper into the wall rather than being extracted. In the following case study the sample depth was increased to understand this phenomenon.



Figure 2: interior wall with salt damage due to the presence of up to 7.5 w% sodium chloride in the mortar and at least 1 w% in the brick

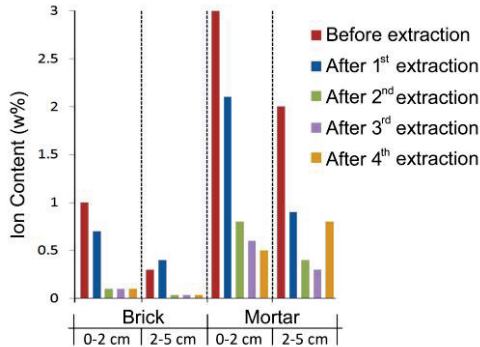


Figure 3: results of the total ion content before and after 4 salt extractions of brick and mortar samples, 0-2 and 2-5 cm.

The 19th century mural paintings of the St.-Vincentius- and St.-Jozeph Chapel of the Antwerp Our Lady Cathedral showed salt efflorescence and severe damage. Figure 4 illustrates an example of the typical damage. The restoration vision includes the preservation and restoration of the mural paintings and underlying plaster layer, if advised from a material-technical point of view. To scientifically approach this vision, the salt contamination of the plaster and underlying brick masonry was mapped out according to the damage patterns (discoloration, staining and/or loss of the paint layer and lack of adhesion and powdering of the plaster). Similar to the previous case study, samples were lifted from the plaster and underlying brickwork to a depth of 5 cm from which the salt content was determined.

As an example Figure 5 illustrates the results of the salt content in plaster, brick and mortar at several heights and depths. Excluding gypsum the salt contamination consisted of mainly sodium chloride and nitrates.



Figure 4: typical damage pattern of a 19th century mural painting in the St-Vincentius Chapel.

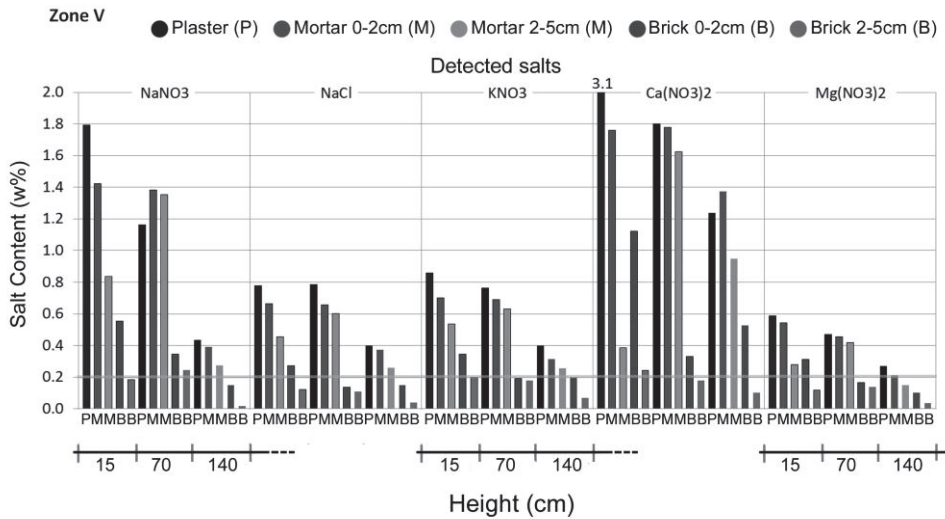


Figure 5: zone V, content of sodium chloride and nitrates of plaster and underlying brick and mortar at two depths and several heights.

As the salt content decreases with depth, the testing of the effect of a salt extraction by means of a poultice was considered. At selected test locations additional samples were lifted to a depth of 10 cm and the finishing layers were removed. For the salt extraction, the same type of poultice as used on the test zone at C-mine was applied.

Prior to the experimental poultice application, the execution parameters were approached theoretically through modelling (Delphin 5.5). To do so the material parameters of brick, mortar and poultice were determined, as described in [11]. From the salt extraction simulation results, it was predicted that:

1. Pre-wetting (2 l/m^2) has a positive effect on the salt extraction in terms of time and efficiency;
2. A salt extraction is more effective on brick (46% extracted) compared to mortar (1 to 8%);
3. A humid environment (95% instead of 50% RH) drastically slows down the extraction process (application times of 20 days instead of 6) mainly due to a reduced drying rate of the poultice.

Following the results of the simulated extraction process, a poultice was applied three times on two different zones of about 2 m height and 1 m length of a brick wall. The effect of the salt extraction was controlled by moisture and salt content measurements. Figures 6 and 7 illustrate the results expressed as total average salt content for respectively brick and mortar before and after the third application.

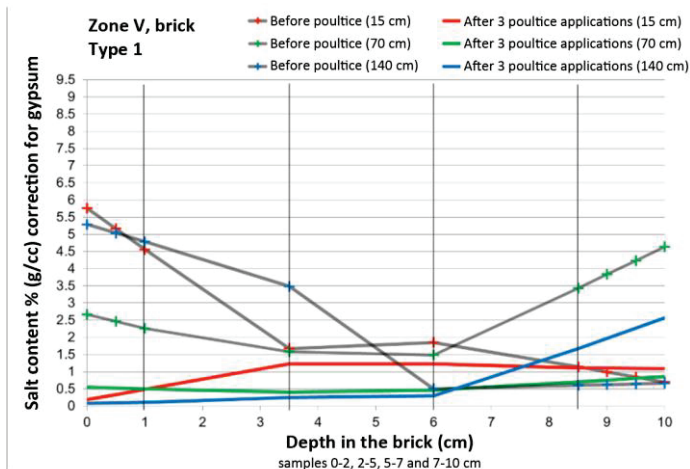


Figure 6: average salt content (% , g/cc) before and after the third salt extraction of brick samples lifted at different heights and to a depth of 10 cm.

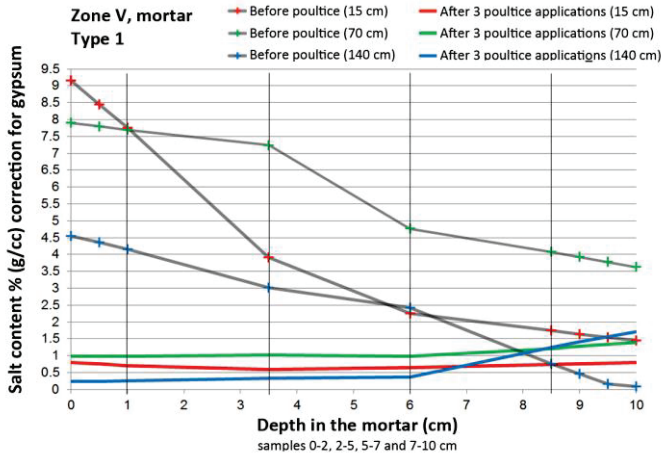


Figure 7: average salt content (% , g/cc) before and after the third salt extraction of mortar samples lifted at different heights and to a depth of 10 cm.

The experimental results were compared to the ones theoretically determined by modelling (Dephin 5.5) (Figure 8) from which a good agreement was concluded.

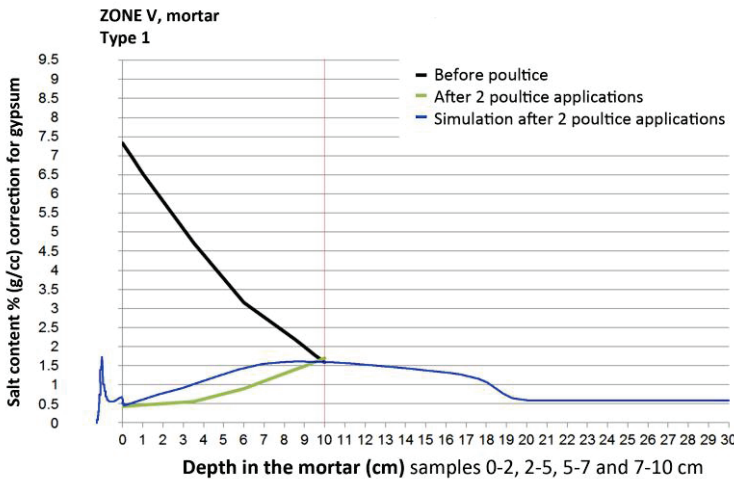


Figure 8: experimental average salt content (% , g/cc), before and after the second salt extraction of the mortar and related to the theoretical one.

Both experimental and simulated results show that the salt content was significantly reduced, especially in the first 5 cm. However, especially at a

height of 140 cm, an increase of the salt content was noticed starting at a depth of about 6 cm, indicative for a salt migration deeper into the masonry. In terms of durability of the restoration strategy, the extent of their migration back to the surface is a crucial point.

Hence, in order to address the influence of the application of a 1 cm thick lime plaster layer on the long-term salt distribution of brickwork, and hence the risk assessment of salt damage to the future plaster and paint layer, further simulations were carried out. For example, Figure 9 illustrates the simulated total salt content for mortar of brickwork, without a plaster layer, after 1 year, while in Figure 10 that for brickwork including a plaster layer over a longer time span (3 years).

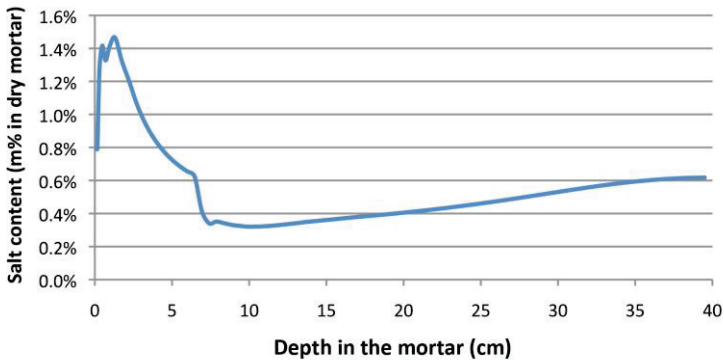


Figure 9: simulated total dissolved salt content (m%) in the mortar for a brick masonry after 1 year.

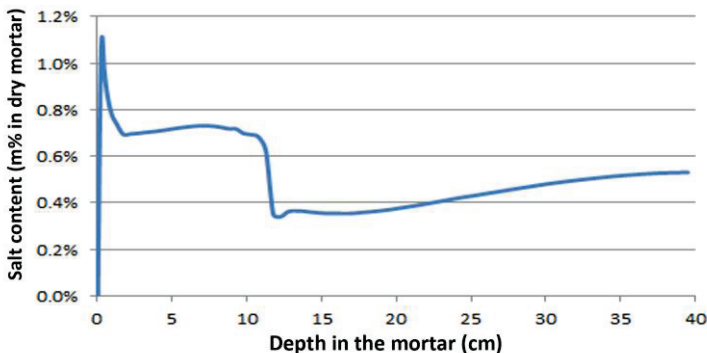


Figure 10: simulated total dissolved salt content (m%) in the mortar for a brick masonry containing a 1 cm thick plaster layer after 3 years.

The simulated results revealed that, without plaster, the water introduced during the pre-wetting of the three salt extractions, dries out very slowly; after one year the outer 5 cm of the mortar is quite dry, while the underlying part is still quite wet (not shown here). In this surface layer, the salt content increases to 1.1 w% on average. Applying a plaster of 1 cm thickness results in a further decrease of the drying, and hence of the amount of salts migrating back to the surface; in this case the outmost 5 cm contains on average 0.8 w% of salts after 3 years. Taken into account that initially, before salt extraction, the average salt content of this surface layer was maximum 4.9 w%, this corresponds to a long-term decrease of at least 80 %. Moreover, it is supposed that the paint layer as such will further reduce the drying process and hence the migration of salts to the surface.

4 Conclusions

From the experimental results of test salt extractions it can be concluded that after three applications of aforementioned poultice materials, the salt content in the first centimetres of the wall is reduced to an acceptable amount of 0.5 w% on average, while the content increases in the depth. These experimental results were also identified by means of computer simulations. As a major part of the salts is pushed inwards, the application of the term "salt extraction" by means of this technique is questioned.

The phenomenon of migration of salts deeper in walls seems to be inevitable. According to the simulations, salts migrate back to the near surface of a non-plastered wall till a content of 1.1 w% after 1 year, while on a plastered wall this may take several years. This amount corresponds to about 20 % of the initial total salt content. As such, the risk of salt damage to the future murals was considered rather low.

References

- [1] A. Sawdy, A. Heritage, L. Pel. A review of salt transport in porous media, assessment methods and salt reduction treatments. in: Salt Weathering on building and Stone Sculptures, SWBSS Proceedings from the International Conference, 22-24 October 2008, The National Museum, Copenhagen, 1-28
- [2] C. Franzen, F. Hoferick, S. Laue, H. Siedel, Water Bath desalination of sandstone objects, Proceedings 11th Int. Congress on Deterioration and Conservation of Stone, 15-20 sept 2008, Torun, Vol II, 881-888.

- [3] V. Vergès-Belmin, H. Siedel, Poultrice desalination of masonries and monumental sculptures: a review, *Restor. Build. Monum.* 11 (6) (2004), 1-18.
- [4] A. Heritage, A. Sawdy, F. Funke, V. Vergès-Belmin, A. Bourgès. How do conservators tackle desalination? An international survey of current poulticing methods, Postprints from the 8th European Conference on Research for Protection, Conservation and Enhancement of Cultural Heritage, 10-12 November 2008, Ljubeljana, Slovenia, 89-93
- [5] B. Lubelli, R.P.J. van Hees, H. De Clercq. Fine tuning of desalination poultices, try-outs in practice, *Proceedings of the 2nd Int Conference on Salt Weathering on Buildings and Stone Sculptures*, Limassol, 19-22 October 2011, 381-388.
- [6] B. Lubelli, R.P.J. van Hees. Desalination of masonry structures: Fine tuning of pore size distribution of poultices to substrate properties, *Journal of Cultural Heritage* (11) (2010), 10-18.
- [7] C.A. Price, Predicting environmental conditions to minimise salt damage at the Tower of London: a comparison of two approaches, *Environmental Geol.* (52) (2007), 369 – 374
- [8] D. Biondia, P. Storemyr, Modeling the behavior of salt mixtures in walls: a case study from Tenaille von Fersen, Suomenlinna, Finland, in: *The study of salt deterioration mechanisms. Decay of brick walls influenced by interior climate changes*, T. Von Konow, Editor, (2002), 95 -101
- [9] A. Nicolai, Modeling and numerical simulations of salt transport and phase transitions in unsaturated porous building materials, dissertation, University of Dresden, Germany (2007)
- [10] C. Vicentini, M. Jovanovic, H. De Clercq, Influence of Extreme Moisture and Salt Load on the Consolidation Properties of TEOS – Part II: Strengthening Effect and Salt Profiles, *Restoration of Buildings and Monuments*, (18), No 2 (2012), 71-80
- [11] H. De Clercq, S. Godts, R. Hendrickx, Zoutbestrijding. Zoutextracties op metselwerk: een standaardprocedure? *Handboek Onderhoud Renovatie Restauratie*, Kluwer, III (2013), 1-78

Desalination of the painted vault ribs of the Franciscan monastery church of Zeitz

W. Wedekind^{1*} and Y. Rieffel²

¹Geoscience Centre of the University of Göttingen, Göttingen, Germany

²Berlin Monument Authority, Berlin, Germany

* wwedekind@gmx.de

Abstract

The former Franciscan monastery church was mentioned for the first time in 1266 and is located on the periphery of the old town of Zeitz, Saxony-Anhalt, Germany. After several decades of neglect, the building was in the acute danger of collapse. In the 1990s parts of the roof collapsed and the groin vaults of the church were exposed to bad weather conditions.

Along with the structural problems, the structurally damaging salts, principally magnesium sulfate, were regarded as the main cause of damage to the historical substance of the building. In many areas, the painting on the ashlar blocks and mortar was already lost or in acute danger of loss due to salt degradation.

After making a map of the damages and prior testing, the ribs and the vault stones were extensively desalinated by cyclical sprinkling in order to ensure a contact-free treatment.

In this case, the sprinkling proved to be both an economical procedure for a sustained salt reduction.

Keywords: sulfates, desalination, sprinkling method, painted surfaces

1 Introduction

The city of Zeitz is located in the Burgenland (which roughly means “land of castles”) in the state of Saxony-Anhalt, where most of the German UNESCO World Heritage Sites are located. Zeitz, first mentioned under the name of Cici in the Synod of Ravenna in 967, as well as the region were of great historical significance. The town was at times the main fortress of the March of Zeitz and a bishop’s residence.

The city is situated along the river Weiße Elster, in the middle of the triangle of the federal states Saxony-Anhalt, Thuringia in the south, and Saxony in the east (Fig 1b). While the cathedral and fortress were built in the valley, the medieval town was erected on a hill above. The former Franciscan monastery church of St. Francisco, Antonius and Clara was mentioned for the first time in 1266. The church is located on the north-western periphery of the old town hill (Fig. 1, b and c).

1.1 The Franciscan monastery church

The Franciscan Gothic church is 61 meters long and is one of the biggest hall churches in Germany. The long extended vault consists of 11 vault bays and a semicircular choir built in the thirteenth century. The vault was built in the fifteenth century. The gussets were painted with floral decoration. The ribs were painted with simple stone imitation of red ashlars with white joints. The building was used by the Reformation movement of the sixteenth century, and the Reformation leader Martin Luther (1483-1546) gave a speech here.

After several decades of neglect, the building was in acute danger of collapse.

In the 1990s parts of the roof collapsed and the groin vaults of the church were exposed to bad weather conditions that caused water infiltration and much damage (Fig. 2a).

Along with the structural problems, the structurally damaging salts were regarded as the main cause of damage to the historical substance of the building. These were principally magnesium sulfate. Possibly, the building stones and mortar are the source of the salts.

1.2 Geological setting and rock material

The church was constructed out of dolomite bound sandstone that was used throughout this region and that often shows alveolar weathering as a result of salt weathering, as has been also found in buildings in the neighbouring state of Saxony [1].

Hirschwald mentions quarries near Kretschau and Kuhndorf that could be former medieval quarries (Figure 1b) [2]. Other bigger quartzite bound formations can be found in the north-eastern region of Bösau and near

Profen and Elsterstrebritz, where according to Pietzsch, sandstone formation with a quarry height of up to 5 meters can be found (Fig. 1b) [3]. Younger identified numerous quarries around the town like in Droysig-Hassel, Schkauditz, Haynsburg, Kleinporthen and Pölzig (Fig. 1b) [4].

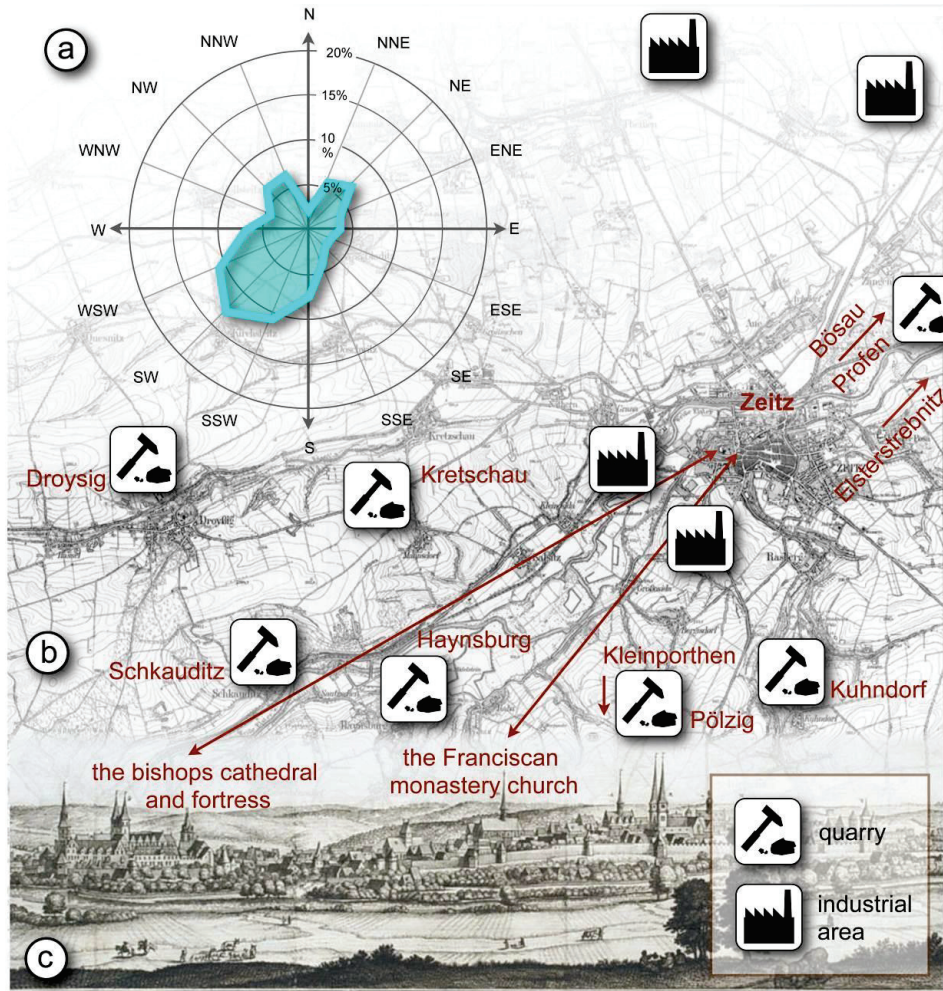


Figure 1: a) the main wind and rain directions in percent (www.windfinder.com). b) Zeitz and its environs around 1912 with location of quarries and industrial areas. c) Lithograph of the medieval city of Zeitz from the "Topographia Germaniae" by Matthäus Merian (1593-1650), showing the outstanding historical buildings and topography.

Sandstone can also be found on the monastery hill itself, but only thin layers.

The sandstone of Zeitz mostly has a yellow colour. Besides these varieties, which clearly dominate the stone architecture of the town, greyish to greenish types are also present. These colours are due to high concentrations of feldspar, mica and clayish substances.

The rock material has a low porosity that varies between 3 and 15 % with a dominance of micropores, and contains a homogeneous fine to middle grain size with a clearly visible layered structure. The Zeitz sandstone has a dolomite cementation that varies between 13 and 76 % volume. Due to the high amount of dolomite cement, the density reaches 2.72 g/cm^3 . As a consequence of the high density and low porosity with an averaged value of around 5 % the stone has a low water uptake rate (averaged $0.8 \text{ [kg/m}^2\sqrt{\text{t}}]$). The water uptake rate varies as much as 46% with the bedding direction. Compressive strength, 100 N/cm^2 , is quite high comparable to other sandstones.

1.2.1 Environmental impacts and geographical setting

During the industrial revolution Zeitz became one of the main centres for charcoal extraction and coal briquette production, starting in 1800 and continuing up to the 1990s. Today the last existing historical briquette factory in Europe, "Hermannschacht", is declared as monument and can be visited in the industrial area of Zeitz. Especially the processing of lignite produces a high content of sulfur within industrial pollution. From 1865 to 1905 charcoal production in Zeitz increased from more than one million square meters to more than six million a year [5]. The briquette production factories were located near the mining areas west of the town. The monastery complex is located at the western end of the city mountain (Figures 1b & 1c). The main wind and rain direction with 13.4 % is the southwest, followed by the west-southwest with 11.6 %, and the south-southwest with 10.9 % (Fig 1a). Consequently, sulfur pollutants were transported continuously in the direction of the historical city over a period of nearly two hundred years. The impact can be seen today on several historical buildings such as the Michaelis Church, which exhibits dramatic forms of alveolar weathering on the western and south-western side of the building (Fig. 2b).

2 Salt and weathering forms

In the case of historical buildings in Zeitz, the industrial pollution in combination with the binding material of the sandstone and lime mortar creates a dangerous salt with a high potential for damage: magnesium sulfate. The salt can result in extensive salt weathering in historical monuments as well if dolomite cemented stone or mortar and gypsum mortars are present [6-8]. The system of magnesium sulfate is already

well investigated and described (www.salzwiki.de). It consists in three stable crystalline phases in the terrestrial atmosphere with a different number of water molecules bound within the crystalline structure: epsomite ($\text{MgSO}_4 \cdot 7\text{H}_2\text{O}$), hexahydrate ($\text{MgSO}_4 \cdot 6\text{H}_2\text{O}$) and kieserite ($\text{MgSO}_4 \cdot 1\text{H}_2\text{O}$) [9]. At least 8 identified metastable crystalline phases with 1 to 12 water molecules can form by hydration or dehydration of the stable salts according to the relative humidity and temperature [10]. The damage potential of magnesium sulfate can be traced back to the stress generated by crystallization and hydration. The main stress is induced by salt crystallization of epsomite and hexahydrate precipitated from solution [11].

Salt weathering in Zeitz is characterized by alveolar weathering (Fig 2a). The ashlars of the vault ribs show different weathering forms, such as sanding, flaking and the out weathering of clayish components (Fig. 2b-d).

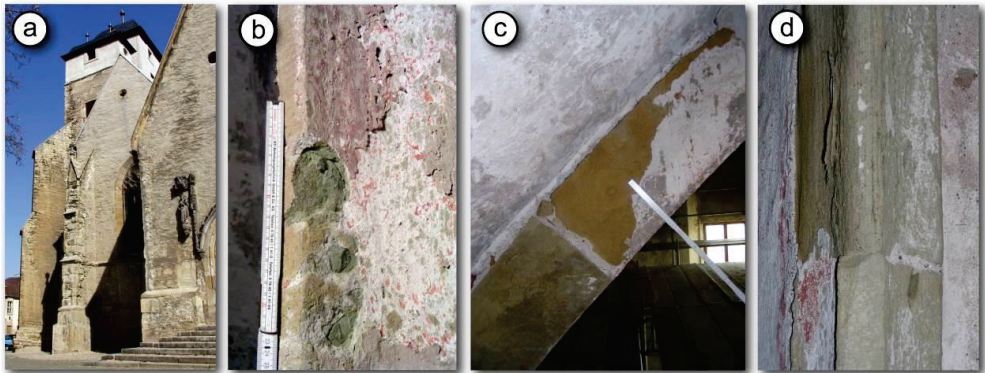


Figure 2: a) At the south-western side of the Michaelis Church, effected by the main wind and rain direction, alveolar back weathering can be found. b) Weathering of clayish material and flaking of painting. c) Back-weathering of single ashlars of the vault ribs. d) Lamination parallel to the bedding.

2.1 Method of desalination

In the 2000s preservation and restoration of the church vault were carried out and a desalination in the painted ribs, main arch, and abutments was performed.

In many areas, the painting on the ashlar and mortar was already lost or in acute danger of loss due to salt degradation (Fig. 2b, 3b).



Figure 3: a) The church before conservation. b) An exemplary mapping of damages of the ribs of vault no. 9. c) The church during conservation. In the front the first restored vaults are visible.

After making a map of the damages (Fig. 3b) and prior testing on loose material of the stone surface, the ribs and the vault stones were extensively desalinated. The desalination technique by cyclical sprinkling (rinsing method) was used, in order to ensure a contact-free treatment. A similar technique was used successfully for the desalination of brick architecture in Venice [12] and to desalinate the salt contaminated tafoni on a tomb facade in Petra, Jordan [13]. For smaller objects like tomb stones the sprinkling method also produces good results [14]. If there are fragile wall paintings, contact-free methods such as sprinkling, as employed at the Neues Museum in Berlin [15], or flushing for partial salt-reduction, as used for the Tiepolo frescos in the residential castle in Würzburg [16], are especially suitable.

2.2 Evaluation of the method

Each treatment in conservation or restoration, with the exception of preventive conservation, induces stress to the object. By cleaning, removing unsuitable materials, as well as in desalination a minimum of original substance will be lost.

As a conservator, one has to evaluate the risks and benefits of each method and choose the one that promises the best results and generates the least damage.

In case of the vault ribs, in general the use of the poultice-method would also be an option. The execution parameters of the poultice-method depend on the condition of the object, the climatic conditions, the type of salt and the depth of contamination. With respect to the stone material of the vault ribs and its pore structure, a lot of fine aggregate, such as kaolinite, would have to be used in the poultice to create a pore size distribution dominated by micropores. Once the humidity of the poultice has migrated into the pore system of the stone, these micropores are

necessary to create a capillary flow of humidity back into the poultice [17-19].

In case of fragile layers of paint, desalination by poultices can cause damage to the original substance. The problem occurs mostly when removing the poultice after drying. Often the poultice sticks to the original substance by forming a solid bond, especially if the poultice consists of a high amount of clayish material, as would be necessary in this case study. Therefore largely contact-free methods were considered as promising the best results. The chosen sprinkling method was first tested by desalination of one rib. A good efficacy was assessed and no serious damage to the painting could be observed.

In most cases, salt-contaminated areas already show back-weathering and surface loss, as was also the case on the vault ribs. The goal of the sprinkling method is to target the strongly stressed zones and to keep moisture movement at a minimum, reducing thereby that salts get concentrated on the stone surface by capillary transport, diffusion and subsequent drying. Their crystallization can cause damage in the near surface zone of the porous material, a risk that has to be kept in mind.

2.3 The treatment

In the following, the step-by-step procedure for the ensuing treatment is described.

For the desalination of the vault ribs their position as well as their form was helpful. The upper area of the contaminated zone was sprinkled with a spray head; subsequently the water flowed down the ribs. As sprinkling water normal tap water with a defined conductivity (because of the lime content) was used (Fig 4b). At the beginning of the procedure the water is predominantly absorbed by the porous stone surface through capillary forces. Water absorption is dependent upon the transport properties of the material. These are controlled by the pore space properties, such as porosity and pore radii distribution, and are a time-dependent process [20]. In the case of the treated sandstone vault ribs, salt contamination was analyzed from drill cuttings obtained in the first two centimetres of the stone in relevant amounts. The salt contaminated zone was sprinkled for washing and moisture penetration during a period of ten minutes, in accordance with the determined infiltration rates for the Zeitz sandstone variety. At the lower end of the treated area a drain gutter was constructed from clay, so that the eluate can be funnelled into a sample container. Excess water not absorbed by the stone was collected in five-liter amounts and checked for electrical conductivity (mS/cm) (Fig. 5a). The correlation between the electrical conductivity and the real content of soluble substances within the eluate was calculated by evaporation of different samples consisting of 1-liter eluate in a drying oven and weighing. After a treatment of about 10 minutes, the sprinkling was terminated and a drying period of at least two days followed. After every

sprinkling cycle, a break of ca. 48 hours was observed in order to initiate the drying procedure, which leads to the concentration of salts in the near-surface area of the stone. A complete drying out of the stone material did not take place and salt efflorescence could not be observed. Over a period of one month, a total of up to seven sprinkling cycles was completed.

At the end of the sprinkling cycles a compress was applied to the treated area and the stone could dry out completely within one week. The poultice was made out of sand, bentonite and cellulose in a proportion by volume of 2 : 1 : 1.

3 Results

The highest values of electrical conductivity were relate to the first measurement in the course of a respective sprinkling treatment by washing away the high salt concentration from the surface (Fig. 4b). Compared with the first dataset, the second values showed a decrease ranging between 30 and 50% after sprinkling. A continuous decrease in the electrical conductivity occurred in the following measurements. The last conductivity value was about one-fourth of the initial sprinkling cycle value.

The highest amount of about half a kilo of salt was extracted from a central pillar integrated in the western facade (Fig. 4c). This facade was heavily weathered due to its orientation and topographic position on the edge of the city hill (Fig. 1c). From the contaminated areas of the ribs and main arches of the vault of the bays 1-5, merely 350 g of dissolved substances were extracted whereas a total of ca. 2.5 kg from 209 stones of the ribs and main arches of the bay 6 to the choir.

In general, it might be possible that also other salts were removed by sprinkling that show a slightly different electric conductivity and therefore another mass content of solvent goods. Therefore the total amount from all measurements of almost 3.4 kg extracted salts should thus be regarded as an approximate value.

The results confirmed the intensity of weathering of the vault, which in the mentioned 6 vault bays displayed the most damage in the vault plaster and painting as well. In this area also the biggest damages could be observed in the roof of the church.

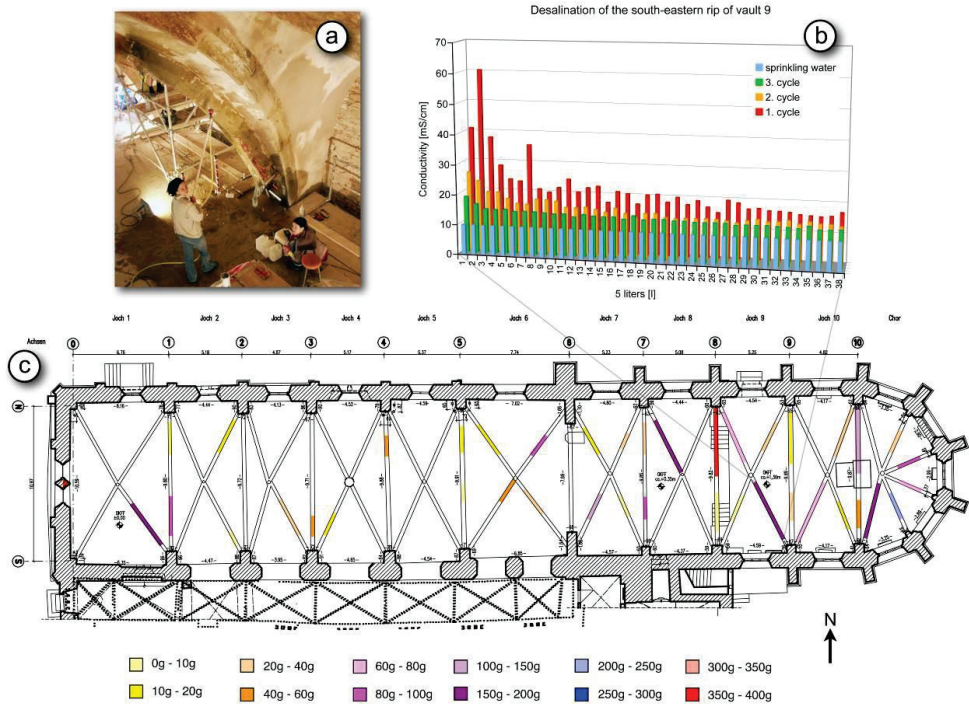


Figure 4: a) The sprinkling method and measurement of the electric conductivity in action. b) Exemplary diagram of a typical desalination treatment by sprinkling of the south-eastern rib of vault no. 9. c) The results of desalination of treated areas of the vault ribs.

3.1 Conservation-Restoration

After desalination, the ashlar of the ribs was conserved by using a fine mortar made from crushed sandstone and lime in order to use the natural pigmentation of the sand as a colour (Fig. 5b). Bigger gaps and missing parts were repaired by dry slaked lime mortar according to the historical technique (Fig. 5c). A reduced application of the mortar was considered in a way that the material only remains in the weathered areas to equalize the surface and to integrate the remainder of the decorative painting (Fig. 5d). Flaking parts of the paint were stabilized by backfilling with a lime suspension and reapplication.

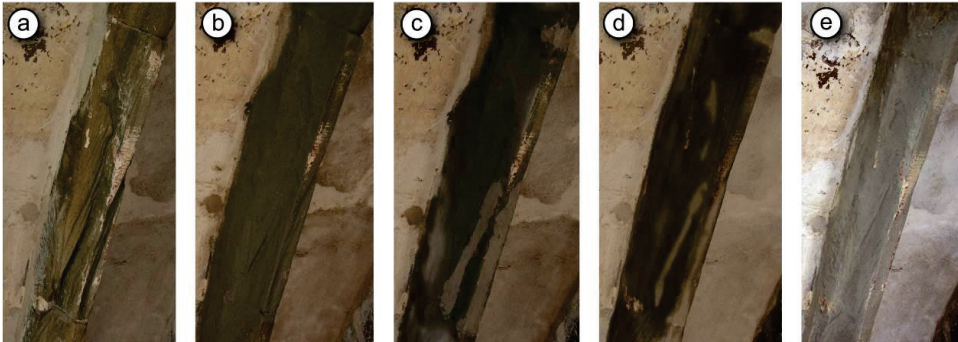


Figure 5: a) Ashlar of a rip after desalination. b) The fine mortar was applied with a brush. c) Bigger gaps were filled with dry slaked mortar. d) After the beginning of hardening, waste mortar was reduced with a wet sponge. E) The ashlar after restoration.

4 Conclusions

By using the described sprinkling technique for desalination, a control of the process was immediately possible by electric conductivity measurements. This allows a calculation of the contamination as well as the planning and application of the whole desalination process.

In this case, the sprinkling method proved to be both an economical procedure for a sustained salt reduction and an extremely gentle method for the partially loose remains of the decorative painting: only one poultice was applied and removed after the desalination by sprinkling and only one month was used to complete the hole procedure of treatment.

Today visitors can experience the church in its restored condition, which serves as a location for cultural events.

References

- [1] Siedel H., Alveolar weathering of Cretaceous building sandstones on monuments in Saxony, Germany, *Natural Stone Resources for Historical Monuments*, Prikryl R. and Torok A. eds., Geological Society special publication, no. 333, Geological Society, London 2010, 11-23.
- [2] Hirschwald J., *Die bautechnisch verwertbaren Gesteins-Vorkommnisse des Preussischen Staates und einiger Nachbargebiete: eine tabellarische Zusammenstellung der in Betrieb*

- befindlichen, zu gelegentlicher Benutzung erschlossenen und aufgelassenen Steinbrüche, nach Provinzen, Regierungsbezirken und Kreisen geordnet, mit Angabe der Verwendung der betreffenden Gesteine zu älteren Bauwerken und des an ihnen beobachteten Wetterbeständigkeitsgrades des Materials, Bornträger, Berlin 1910.
- [3] Pietzsch K., Abriss der Geologie von Sachsen, Volk und Wissen, Berlin 1951.
- [4] Ehling A., Unterer Bundsandstein 51, Zeitzer Sandstein 5.1.1., in Bausandsteine in Deutschland, Band 2. Ehling, A., Siedel, H. eds., Schweizerbart, Stuttgart 2011, 84 – 90.
- [5] Wohlfahrt H., Die Anbindung von Zeitz an das Eisenbahnnetz Mitteldeutschlands, in Industriestadt Zeitz – Verkehr Gewerbe und Fabriken, Otto K., Deye D., Rittig R. eds., Mitteldeutscher Verlag, Halle 2012, 35-47.
- [6] Siedel H., Dolomitmalkmörtel und Salzbildung an historischer Bausubstanz, in Mauersalze und Architekturoberfläche - Tagungsbeiträge, Leitner H., Laue S., Siedel H. eds., Hochschule für bildende Künste, Dresden 2003, 57-64.
- [7] Lopez-Arce P., Garcia-Guinea J., Benavente D., Tormo L., Doehne E., Deterioration of dolostone by magnesium sulfate salt: an example of incompatible building materials at Bonaval Monastery, Spain, *Constr Build Mater* (23) (2008), 846–855.
- [8] Wedekind W., Schwierige Ruinen - Zur Erhaltung der Ruinen an der Unstrut, in *Natur - Stein - Kultur - Wein - zwischen Saale und Unstrut*, Siegesmund S., Hoppert M., Epperlein K. eds., Mitteldeutscher Verlag, Leipzig 2014, 289-316.
- [9] Steiger M., Linnow K., Juling H., Gülker G., El Jarad A. Brüggerhoff S., Kirchner D., Hydration of $MgSO_4 \cdot H_2O$ and Generation of Stress in Porous Materials, *Crystal Growth and Design* 1 (8), (2008), 336-343.
- [10] Chipera SL., Vaniman DT. Experimental stability of magnesium sulfate hydrates that may be present on Mars, *Geochim Cosmochim Acta* (71), (2007), 241-250.
- [11] Balboni E., Espinosa-Marzal RM., Doehne E., Scherer GW., Can drying and re-wetting of magnesium sulfate salts lead damage of stone?, *Environ Earth Sci*, (63, Issue 7-8) (2011), 1463-1473.
- [12] Schubert, L., La realizzazione del progett., in *Un restauro per Venezia.*, Millership, J., Schubert, L. eds., Mazotti, Milano 2006, 69-85.
- [13] Wedekind W., Rüdrieh J., Salt-weathering, conservation techniques and strategies to protect the rock cut facades in Petra/Jordan, in

- Heritage, Weathering and Conservation, Fort R., Álvarez de Buergo M., Gomez-Heras M. and Vazquez-Calvo C. eds., Taylor & Francis, London 2006, 261-268.
- [14] Wedekind W., Baumeister A., Schellhase L., Die Salzreduzierung im Nordkuppelsaal, in *Das Neues Museum Berlin - Konservieren, Restaurieren, Weiterbauen im Welterbe*, Staatliche Museen zu Berlin - Stiftung Preußischer Kulturbesitz, Bundesamt für Bauwesen und Raumordnung and Landesdenkmalamt Berlin eds., Seemann, Leipzig 2009, 211 - 213.
- [15] Wedekind W., Taube E., Hüttich C., Entwicklung und Anwendung objektspezifischer Salzreduzierungsverfahren, in *Konservierung, Restaurierung und Ergänzung im Neuen Museum Berlin*, VDR (Verband der Restauratoren) ed., A Siegl, Munich 2013, 97-103.
- [16] Eiden M., Die Behandlung der Salzschäden, in *Die Restaurierung eines Meisterwerks: das Tiepolo-Fresko im Treppenhaus der Würzburger Residenz*. Staschull, M., Rösch, B. eds., Berlin: Deutscher Kunstverlag, Berlin 2009, 87 – 86.
- [17] Sawdy A., Lubelli B., Voronina V., Pel L., Optimizing the extraction of soluble salts from porous materials by poultices, *Studies in conservation* (55, 1) (2010), 26-40.
- [18] Lubelli, B., van Hees R.P.J, De Clercq H., Fine tuning of poultices: try-outs in practice, in *Salt weathering on buildings and stone sculptures: SWBSS 2011*, 19-22 October, Limassol, Cyprus. Ioannou, I. and Theodoridou, M. eds., University of Cyprus, Nicosia 2011, 381-388.
- [19] Setina J., Kirilova S., Clay based poultices for desalination of building materials, *Journal of sustainable architecture and civil engineering* (1) (2012), 52-57.
- [20] Wittmann FH., Feuchtigkeitstransport in porösen Werkstoffen des Bauwesens, in *Verfahren zum Entsalzen von Naturstein, Mauerwerk und Putz*, Goretzki L. ed., Aedificatio-Verlag, Freiburg 1996, 6-16.

In-situ 'vacuum' desalination - case study of a baroque tombstone

H. Siedel,^{1*} C. Franzen² and E. Pummer³

¹TU Dresden, Institute of Geotechnical Engineering, Dresden, Germany

²Institut für Diagnostik und Konservierung und Denkmälern in Sachsen und Sachsen-Anhalt, Dresden, Germany

³Atelier Erich Pummer GmbH, Rossatz / Wachau, Austria

*heiner.siedel@tu-dresden.de

Abstract

A combined 'vacuum' and poultice desalination procedure was applied to a tombstone made of Cotta sandstone. The desalination steps were controlled analytically by salt profiles in the stone, as well as by analyses of waste water and poultice material. A remarkable reduction of high total salt contents to a depth of 1-2 cm could be achieved, with the best effects in the lower part of the monument (at 50 cm height). In particular, high gypsum contents within the Cotta sandstone were significantly reduced, which could hardly be achieved only by poultice treatments. With respect to the better soluble nitrate compounds, the results are contradictory. Although nitrate could be extracted near the surface, large parts were moved into the stone by advection. The results suggest that the 'vacuum' procedure could be considered as an effective in-situ bath desalination with frequent water exchange rather than a "convective" desalination where the salt ions follow the water streaming through the object. The method has some potential for in-situ desalination of smaller stone objects and should be further developed.

Keywords: desalination techniques, sandstone, negative pressure/underpressure, poultices

1 Introduction

Desalination of salt contaminated objects is an important and common practice in stone restoration. For in-situ conservation measures the most frequently applied technique is desalination with poultices [1]. Recent investigations within an EU-FP 7 funded project [2] helped to better understand the factors controlling the desalination process, such as the pore size distribution within the poultice material related to that of the stone substrate [3]. However, one has to generally accept some limits about efficiency of that procedure, especially with respect to less soluble salts such as gypsum [4]. The alternatives on site to desalination with poultices are scarce.

In the case study presented, such an alternative in-situ approach for smaller objects like sculptures or tombstones started with water circulation and the application of 'vacuum' (negative pressure) of up to 600 mbar on a mainly gypsum-laden sandstone object. The equipment used was modified from the patented vacuum circulation strengthening technique for stone consolidation (VKV = Vakuum-Kreislauf-Verfahren; European Patent no. 1295859, EU ownership hold by Atelier Erich Pummer, Rossatz, Austria). The 'vacuum desalination' was followed by a traditional desalination with a cellulose poultice in the drying stage to additionally take advantage of the drying process and the connected advective transport, as recommended by [5]. To assess the effect of the applied method, a thorough analytical control of the salt content was carried out before, during and after desalination.

2 Materials and methods

2.1 The sandstone object

The sandstone object to be desalinated was a baroque tombstone from a cemetery in Dresden, Saxony (Innerer Neustädter Friedhof, Fig. 1). It consists of a Cotta type Elbe sandstone, a fine to medium grained, clay bearing Cretaceous quartz sandstone (arenite) from the Elbe Valley near Dresden. This sandstone has been a widely used material for buildings and sculptures in Saxony for centuries [6]. Its total porosity of about 20 % is distributed over a broad pore size range. The monumental object shows severe deterioration patterns especially in the lower part of its front side, where the original surface is nearly completely lost. This side has been exposed southwards whereas the back side stood close to a sandstone wall. Although there had been no direct contact between the wall and the tombstone, the small gap in between was filled with mud, rotten leaves, pieces of plaster fallen down from the wall etc. The material in the gap

was permanently wet. For desalination the object was removed from the wall and saved from tipping over by temporarily mounting it on a pedestal.



Figure 1: The baroque tombstone in its original position (left) and from the backside after removing it from the wall and mounting it on a pedestal for desalination (right).

2.2 Equipment and technical procedure

The main principle of the VKV procedure is a deep impregnation of a porous stone material with a liquid by applying an underpressure ('vacuum') to the stone objects. Generally the liquid is a stone consolidant, but due to high salt loads here an adaptation towards a technique for desalination as a first step of restoration was considered. Therefore, the liquid is water.

A schematic sketch of the technical set up and the equipment is given in Fig. 2, while in Fig. 3 different steps of the VKV procedure are illustrated.

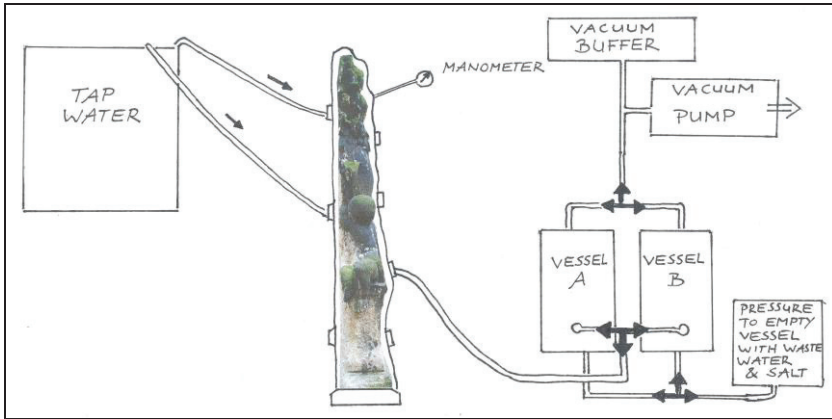


Figure 2: Schematic sketch of the technical set up for vacuum desalination (VKV procedure)

During desalination the object was completely wrapped in a plastic foil which was heat-sealed to isolate it from the surrounding air. The foil bag was fitted with several valves positioned at different heights to be connected with a vacuum pump or with a vessel with water. The sandstone surface of the object right under the foil 'skin' was protected by a highly permeable textile gauze layer to avoid a mechanical stress. By slowly increasing the underpressure via a hose mounted on a valve in the plastic bag, the generously cut plastic foil was moulded perfectly to the object's surface. Maintaining an underpressure of 150-600 mbar within the foil bag for some hours, the air in the stone pores was evacuated. Afterwards, several hoses were attached to the valves at the backside of the tombstone to suck tap water unidirectionally in the foil bag from a big vessel, hereby regularly changing the position of the connections between valves in different positions on the backside and the hoses. The underpressure is maintained during the whole procedure. By opening and closing the valves respectively, fresh tap water could be sucked in from the vessel or tap water with dissolved salt from the object could be sucked off to a smaller vessel. All in all, about 7650 litres of fresh tap water (tempered at 22 °C) were sucked during 7 working days (about 8 hours each day). Overnight the process was stopped, i.e. some water remained in the setup for about 16 hours and was replaced by fresh one again in the next morning. The foil bag was removed on working day eight, and a cellulose poultice was applied immediately after on the entire surface of



Figure 3: The object during the desalination procedure: Protecting the sandstone surface by permeable textile gauze (left), 'vacuum' desalination in progress (middle), and final application of cellulose poultice (right).

the wet object. The poultice remained there for another five weeks. During the drying process the object was sheltered from rain by a roof.

2.3 Analytical control

In a first step, samples (diameter 10 mm) were drilled at three different heights above the ground from the front side as well as from the back side to get information about the salt content and its distribution. Since the thickness of the tombstone is low (22 cm at 50 cm height, 21 cm at 122 cm, and 18 cm at 195 cm), a drilling depth of maximum 10 cm nearly covered a complete cross-section through the object at different heights. The drill powder was weighed on site immediately after sampling and again after drying in the laboratory at 60°C until constant mass was reached. Although there could be side effects due to heat production during drilling, the measured water content in the samples roughly describes the moisture distribution in the sandstone.

Sampling was performed similarly immediately after the 'vacuum desalination' procedure as well as five weeks later after the removal of the poultice. At that time parts of the poultice material (10 x 10 cm each) were also lifted near the drill powder sampling zones to analyze the amount of extracted salts collected in the poultice.

Soluble salts from the drill powder samples and the poultice material were extracted with deionized water. The total salt content of the samples was determined by evaporating the solution and weighing the remaining dry solid matter. Mg, Ca, K, SO₄, Cl, and NO₃ were quantitatively analysed in the aqueous solution by means of a HACH spectrophotometer using standardized reagents. Na was determined with an ion selective electrode. The results were related to the dry sample mass [wt%].

During the first four days of 'vacuum desalination' the salt content of the water sucked off the foil bag was regularly controlled by measuring the electric conductivity several times a day.

3 Results

3.1 Salt contents and salt distribution before desalination

Fig. 4 shows the initial total soluble salt content within the object before desalination. It can be seen that its distribution generally follows a steep profile from the surface to the depth, and the concentration is generally high near the stone surface up to 2 cm. Compared to the back side, concentrations near the surface are significantly higher at the exposed front side.

The moisture content (Fig. 5) is high and nearly equally distributed through the whole cross-section at 50 cm height. At 122 and 195 cm height, moisture content generally decreases with a trend to somewhat dryer surfaces on the front side.

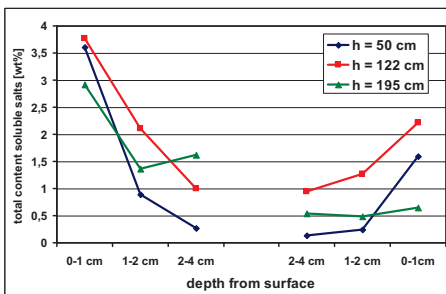


Figure 4: Profile of the total soluble salt content before desalination

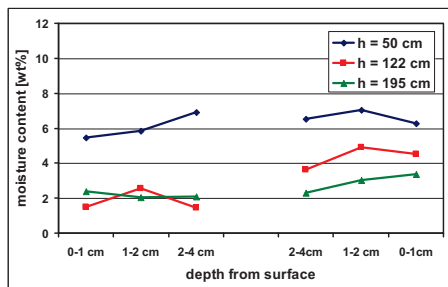


Figure 5: Profile of the moisture content before desalination

This might be due to the free southward exposure of the object at this side, compared to the back side which has been standing against a sandstone wall for decades, with a gap behind, filled with moist material up to a height of about 120 cm (see 2.1). The obtained moisture distribution can be interpreted as a hint towards rising damp from the ground, mainly affecting the lower parts of the object.

The analyses of the single ions show low contents of chloride (< 0.06 wt% in all samples), sodium (< 0.01 wt% in all samples) and potassium (< 0.04 wt% in most of the samples), which are neglected in the further discussion. The distribution of sulphate contents is displayed in Fig. 6. Distribution patterns of sulphate are very similar to those of calcium (Fig. 8) and of the total salt content, which means that gypsum is the predominant salt compound. In addition, remarkable contents of nitrate can be found especially at 122 cm height (Fig. 7). There, its distribution correlates well with magnesium (Fig. 9).

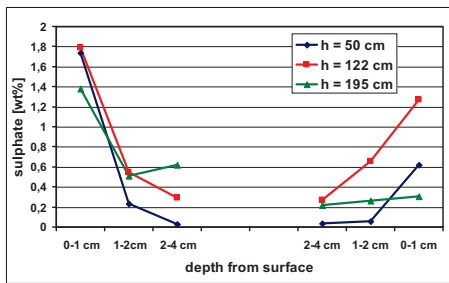


Figure 6: Distribution of sulphate before desalination

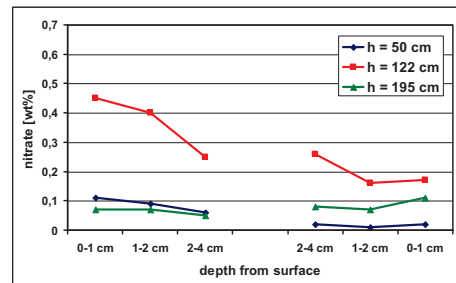


Figure 7: Distribution of nitrate before desalination

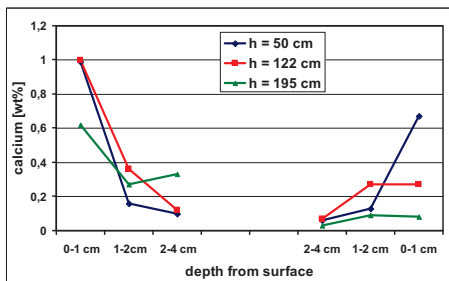


Figure 8: Distribution of calcium before desalination

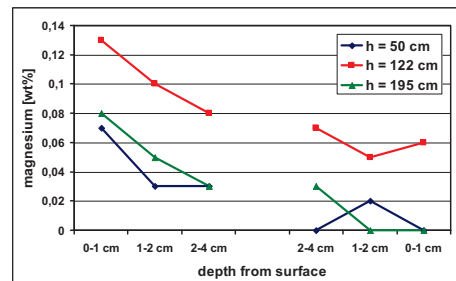


Figure 9: Distribution of magnesium before desalination

Assessing the salt contents it can be stated that the object is contaminated by a significant amount of gypsum (particularly near the surface, at all heights) and high levels of nitrate (throughout the profile, at 122 cm height). The latter might be attributed to rising damp from the ground, whereas the first is most likely a result of environmental pollution [7]. The salt contents found indicate that desalination is a crucial precondition for a further conservation treatment of the object.

3.2 Salt contents and salt distribution after 'vacuum' desalination

Changes in total soluble salt content after the 7 days 'vacuum' desalination are shown in Fig. 10. The total salt content was reduced in the first two centimetres from the surface; in particular the high contents in the first centimetre were significantly lowered. The best desalination effect can be found at 50 cm height, where the salt content is equally reduced to less than 0.35 wt%. This might be explained by the role of gravity with respect to water movement within the tombstone. As can be seen from Fig. 11, water content of the sandstone at 50 cm height increased to 8-10 wt% in the entire cross-section, which is near saturation of the pore space. Moisture content in the sandstone has increased throughout the object, as can be seen also at heights of 122 and 195 cm, respectively. However, the profile of water content is steeper at these places, indicating that the 'inner core' of the tombstone has not been saturated.

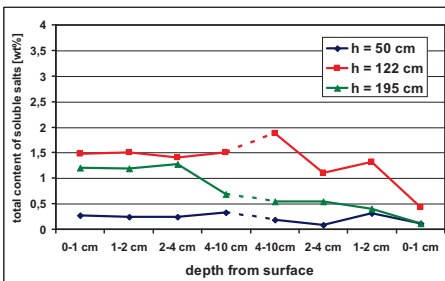


Figure 10: Profile of the total soluble salt content after 'vacuum' desalination

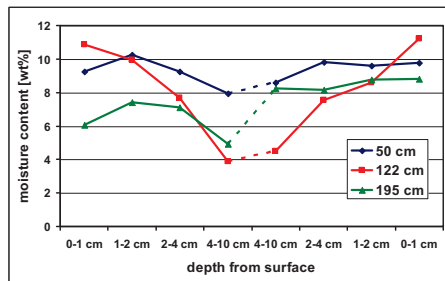


Figure 11: Profile of the moisture content after 'vacuum' desalination

Regarding sulphate and nitrate ions (Figs. 12 and 13), in both cases a significant reduction of contents can be observed near the surface (0-1 cm depth). In case of nitrate, also contents at 2 cm depth are lowered. However, there is an increase of nitrate contents towards the inner core, which might be attributed to the deep penetration of water and the advective transport of dissolved nitrate compounds from surface to the

depth. This can be seen at a height of 122 cm, where the nitrate content is highest.

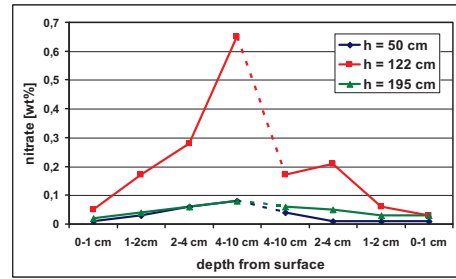
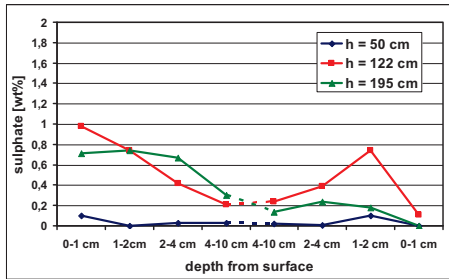


Figure 12: Distribution of sulphates after 'vacuum' desalination

Figure 13: Distribution of nitrates after 'vacuum' desalination

3.3 Salt contents and salt distribution after final poultice treatment

Salt and moisture distribution after 5 weeks final poulticing and drying are displayed in Figs. 14 and 15. Moisture content profiles are comparable to the starting point at 195 cm height or even somewhat lower both at 122 and 50 cm height. It can be concluded that the drying process has finished to a large extent, i.e. the moisture content of the sandstone object is nearly in equilibrium with the surrounding air. The total salt content at 50 cm height has decreased towards zero (< 0.1 wt%, apart from the near-surface sample at the back side with 0.31 wt%). The profile at 122 cm shows an increase of salt contents near the surface and a slight decrease deeper inside; the profile at 195 cm has not changed significantly.

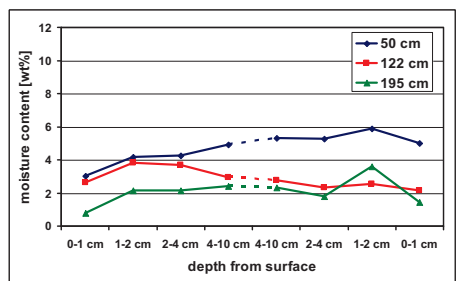
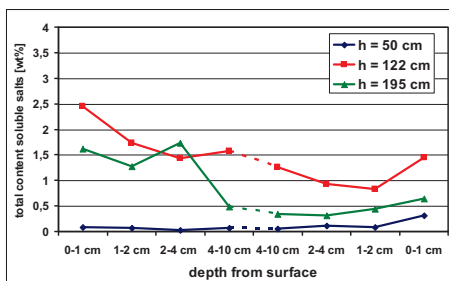


Figure 14: Total soluble salt content after poulticing and drying for 5 weeks

Figure 15: Moisture content profile after poulticing and drying for 5 weeks

Looking at the distribution of sulphate and nitrate, one can see they behave differently. Sulphate is reduced to zero at 50 cm height and shows

a slight, continuous decrease from the surface to the interior at 122 and 195 cm height after poulticing (Fig. 16). The concentrations near the surface (0-2 cm) are significantly reduced, compared to the starting point. Nitrate contents have increased again near the surface but are still high in the interior of the stone (Fig. 17). Likely the penetrating water front has moved highly soluble salts deep inside by advection, but the backward advective transport is interrupted when the sandstone becomes dryer and dryer, resulting in increased ion concentrations in the core and near the surface. Depending on future climatic influences, current distribution of the mobile nitrate might change again towards a more even one.

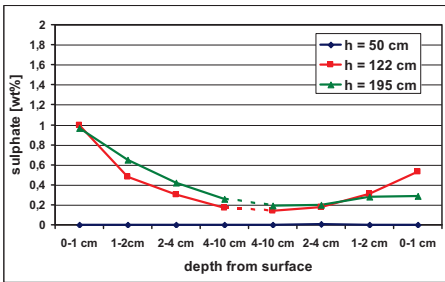


Figure 16: Distribution of sulphate after poulticing and drying for 5 weeks

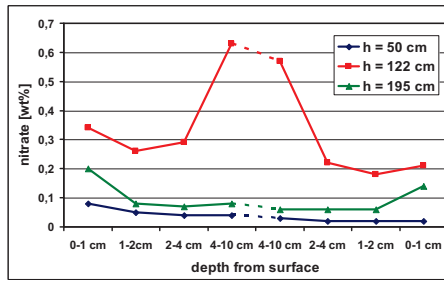


Figure 17: Distribution of nitrate after poulticing and drying for 5 weeks

4 Discussion: Efficiency of desalination and effective mechanisms

4.1 Efficiency of salt extraction

The efficiency of the desalination approach with the combined VKV and cellulose poultice method can be assessed by comparing starting concentrations with those analyzed after the procedure. The results are shown in Figs. 18 and 19. Fig. 18 displays the relative change of total salt concentration in %, with regard to the starting concentration. Since this comparison doesn't provide information about changes of the absolute amount of salt it is completed by another diagram showing the absolute difference between starting and final concentration in weight % (Fig. 19). All in all it can be stated that desalination was most successful in the lower part of the tombstone (at 50 cm height) where the salt concentration could be reduced by more than 80 % at the front side, reaching 4 cm depth. At the back side the effect is somewhat lower. However, the absolute starting concentrations were lower there, too. Bearing in mind that the starting

concentration in the steep profiles was already low at 2-4 cm depth (Fig. 4), a decrease in efficiency towards the inner core does not affect the excellent results. However, the efficiency is significantly lower at heights of 122 and 195 cm. At 122 cm, a reduction by less than 40 % can be found at up to 2 cm depth. At deeper depths the reduction is zero, or even an increase in salt content can be detected (2-4 cm from the front side). At 195 cm height, the salt content near the surface has been reduced by 40 % at the front side, whereas the low concentrations at the back side have not changed significantly.

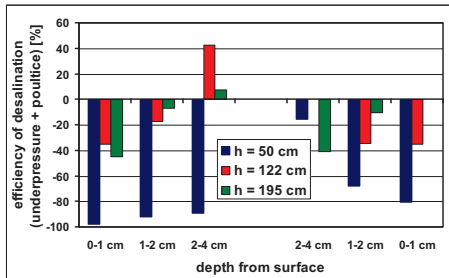


Figure 18: Efficiency of desalination as a function of depth from the surface ('vacuum' desalination + poulticing) in %. Negative values indicate a reduction, positive ones an increase of salt content.

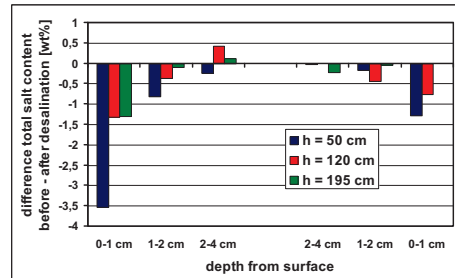


Figure 19: Difference between the total salt content before and after desalination as a function of depth from the surface ('vacuum' desalination + poulticing); absolute decrease (negative) / increase (positive) with respect to starting concentration [wt%]

Assessments with regard to the amount of calcium + sulphate (indirectly describing the gypsum content) and nitrate are given in Figs. 20 and 21. It can be demonstrated that the reduction of gypsum worked very well at heights of 50 and 122 cm, down to a depth of 2 cm from surface. Even at greater depths a reasonable reduction can be achieved. At 195 cm high, a contradictory effect can be found at 1-2 cm depth, where the gypsum content slightly increases. However, compared to repeated poultice treatments with cellulose as well as with cellulose-clay-mixtures, the efficiency of gypsum reduction in Cotta type sandstone with the technique applied here is much higher. The gypsum content of sandstone surfaces of the Dresden Zwinger could only be reduced by 25 % at maximum during 3 cycles of poulticing [4].

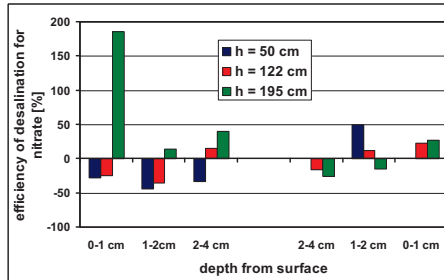
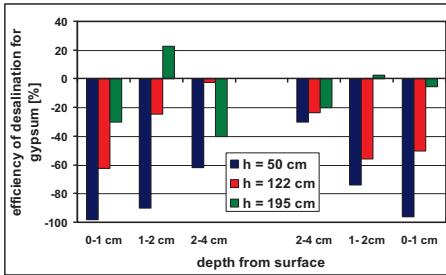


Figure 20: Efficiency of the desalination of gypsum as a function of depth from the surface ('vacuum' desalination + poulticing) in %. Negative values indicate a reduction, positive ones an increase of gypsum content.

Figure 21: Efficiency of nitrate desalination as a function of depth from the surface ('vacuum' desalination + poulticing) in %, with regard to the starting concentration. Negative values indicate a reduction, positive ones an increase of nitrate content.

4.2 Analytical control of waste water

Random samples of 'waste water', i.e. samples of the water sucked off from the foil bag with the object inside, were taken daily during the 'vacuum' desalination process (1.5 litres each). The results (Fig. 22) clearly display the difference between their salt contents during the first day and at the following days. From the second day onward, the total salt content extracted decreased to nearly a quarter of the starting concentration. The concentration of sulphate was continuously decreasing, whereas the (lower) nitrate concentration shows a somewhat higher variation.

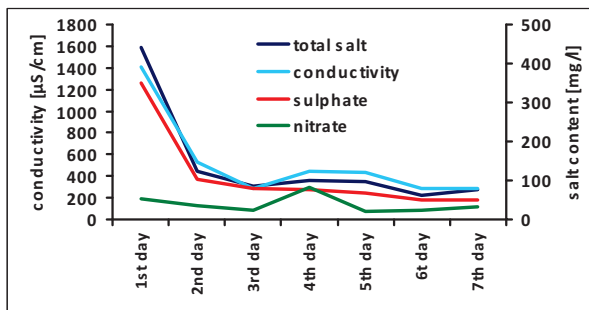


Figure 22: Salt contents and electric conductivity measured on waste water random samples, taken once a day during the entire 'vacuum' desalination procedure

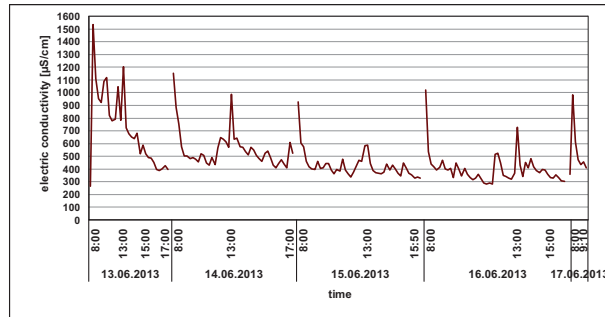


Figure 23: Results of continuous measurements of the electric conductivity of waste water from 'vacuum' desalination

During the first 4 days of 'vacuum' desalination, samples of waste water were regularly controlled by measurements of the electric conductivity. The results are displayed in Fig. 23. According to these results, the extraction of salts was most effective within the first 5 hours of 'vacuum' desalination, when the salts on the surface of the tombstone were dissolved and extracted with the waste water. Afterwards, the concentration was continuously decreasing until the end of the first working day. The repeated increase at the next morning, as well as at the following mornings, can be explained by the longer contact of fresh tap water with the object's surface, allowing transport by diffusion from the outermost parts of the sandstone to the surrounding water. A similar, but reduced effect could be observed daily at 13:00, when the first measurement after the lunch break was done. During the break, the extraction of waste water was temporarily stopped, and the water was longer in contact with the stone surface, which facilitated the diffusion process. The results found are similar to those obtained from conductivity measurements during water bath desalination [5], where the starting ion concentration in the bath was also high and increased again every time after adding fresh water. Consequently, the effective transport mechanism of ions outside the stone during 'vacuum' desalination is due to diffusion. Underpressure is thought to result in a deeper and faster penetration of water into the stone. The fast capillary transport by advection with penetrating water is the cause for the observed backward movement of more soluble salts, such as nitrates, deeper into the stone (cf. Fig. 13). Despite the underpressure applied, the given pore structure of Cotta sandstone with a high amount of smaller capillary pores (between 10 and 0.1 µm) does not allow a fast 'flow' of water through the pore space. Consequently, an outward advective transport of salts only takes place at the drying stage, i.e. during the poultice treatment.

4.3 Analytical control of poultices

Poultice samples taken from the areas near the sampling points for the profiles at 50, 122 and 195 cm height, respectively, were analyzed for their total salt content. The results are shown in Fig. 24. They are in good accordance with the salt profiles obtained from measurements after the final poultice treatment (Fig. 14). The lowest salt contents extracted by the poultice can be found at 195 cm, where the changes in the salt profiles before and after poultice treatment are accordingly low (cf. Figs. 10 and 14). At 50 cm height, where the salt concentration was already very low after the 'vacuum' desalination, the concentration was reduced to nearly zero (Fig. 14). The extraction effect (salt content in the poultice) is remarkable, compared to that at 195 cm, where the remaining salt content in the sandstone is higher. This might be due to the high moisture content throughout the cross-section at this height after the 'vacuum' desalination, which allows even the transport of small amounts of remaining salts from deep inside to the poultice while drying.

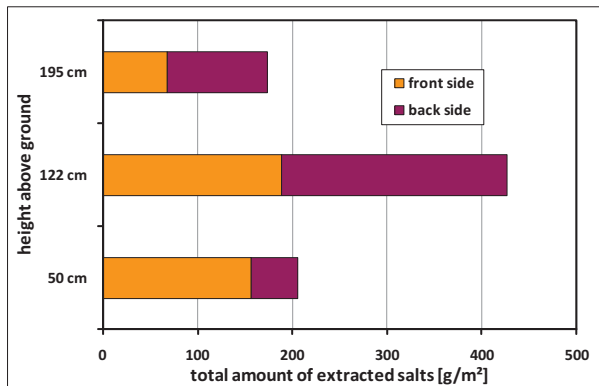


Figure 24: Total salt contents in samples from the cellulose poultice, taken 5 weeks after poultice application at different heights

At 122 cm, the poultice extraction was most efficient. This corresponds well with the high content of highly soluble nitrates in the sandstone at this height (Fig. 17). However, the transport processes had contradictory effects here: while high amounts of nitrates were transported to the stone surface and within the poultice by advection, some nitrates also remained deep inside the object.

5 Conclusions

The applied combination of 'vacuum' desalination and subsequent cellulose poulticing showed good results by reducing the very high gypsum content in Cotta sandstone. Gypsum had been the main salt compound in the treated sandstone object and can be hardly extracted from the Cotta sandstone by usual poultice treatments [4]. Although a reduction of sulphate (gypsum) contents to low / medium levels (referred to WTA Guideline 3-13-01/E [8]) was only achieved at the lower part of the sandstone object, the very high concentrations near the surface could be nearly halved, thus allowing a sustainable further conservation treatment. However, high concentrations of nitrate could not be significantly reduced due to the high mobility of these very soluble compounds. VKV desalination is a promising technical development in restoration. Permanent supervision of the running system ensures safe application. Thus the technical and man power needs are significant. However, it allows a thorough desalination treatment in-situ, which might reduce the risk of and the costs for dismantling and transport of smaller objects. As shown in the discussion about efficiency and the effective mechanisms, the efficiency might be improved by better controlling the dynamic of water change. The results suggest that the procedure could be looked at as effective in-situ bath desalination with frequent water exchange rather than a "convective" desalination where the salt ions follow the water streaming through the object. Moreover, the permanent water stream along the surface is a significant factor which is different to all other desalination methods. Combining the technique with poultice treatments might open new chances for an alternative in-situ desalination method, which could be appropriate especially for the treatment of stone sculptures of high artistic rank.

Acknowledgements

Funding of parts of the project by the German Federal Foundation for the Environment (DBU, Az 30408) is gratefully acknowledged. Thanks are due to Ernst Wandl and Jörn Wichert for technical assistance.

References

- [1] Vergès-Belmin, V., Siedel, H., Desalination of masonries and monumental sculptures by poulticing: a review. *Restoration of Buildings and Monuments* 11(6), (2005), 391-408.
- [2] Heritage, A., Desalination of Historic Buildings, Stone and Wall Paintings. Heritage, A., Zezza, F. (eds.) Archetype Publications, London (2013)
- [3] Pel, L., Sawdy, A. & Voronina, V., Physical principles and efficiency of salt extraction by poulticing. *Journal of Cultural Heritage* 11(1) (2010), 59-67.
- [4] Siedel, H., Experiences from desalting of tuffstone and sandstone monuments by compresses. In: *Le dessalement des matériaux poreux. Proc. 7^{es} Journées d'études de la SFIIC, Poitiers, 9-10 May 1996*, (1996), 191-198.
- [5] Franzen, C., Hoferick, F., Laue, S. & Siedel, H., Water bath desalination followed by poultice treatment. In: Heritage, A., Heritage, A., Zezza, F. (eds.) *Desalination of Historic Buildings, Stone and Wall Paintings*. Archetype Publications, London, (2013), 74-78.
- [6] Götze, J., Siedel, H., A complex investigation of building sandstones from Saxony (Germany). *Materials Characterization* 58 (11/12) (2007), 1082-1094.
- [7] Siedel, H., Klemm, W., Evaluation of the environmental influence on sulphate salt formation at monuments in Dresden (Germany) by sulphur isotope measurements. In: Fassina, V. (ed.) *Proc. 9th International Congress on Deterioration and Conservation of Stone, Venice 2000*, Elsevier Amsterdam (1) (2000), 401-409.
- [8] WTA Guideline 3-13-01/E, Non-destructive desalination of natural stones and other porous materials with poultices. WTA Publications, Munich (2005)

Salt conversion, backfilling, and back anchoring: the securing of the painted ceiling of the Red Hall in the Neues Museum, Berlin

W. Wedekind* and J. Rüdrieh†

Geoscience Centre of the University of Göttingen, Göttingen, Germany

* wwedekind@gmx.de

Abstract

In connection with the restoration of the Red Hall in the Neues Museum, located on the museums-island in Berlin (2006-2008), a procedure for salt conversion and backfilling of hollow painted plaster areas with the help of low-pressure injection technology was developed and successfully implemented. The precipitation reaction resulting from the salt conversion was assessed using electrical conductivity measurements and identification of the precipitate by x-ray diffractometric analyses (XRD). For an additional securing of the plaster areas, an extensive injection was carried out and a suspension system for the back anchoring in the hollow pot bricks was developed and implemented.

Keywords: Salt conversion, low-pressure injection technology, back anchoring

1 The Red Hall

In the course of the recent restoration of the Neues Museum, surely no other room experienced such an extensive transformation as the Red Hall. Located on the third floor of the historic museum building by Friedrich August Stüler (1843-1855), the Red Hall originally housed the reading room of the Prints and Drawings collection of the Berlin Museums.

The Red Hall owes its name to its red wallpaper. The ceiling and window frames were decorated with contrasting light-coloured mouldings and trompe l'oeil decoration (Fig. 1c). The areas above the windows on both sides are decorated with portrait medallions of well-known printmakers and illustrators of the seventeenth to nineteenth century. In the middle of the western side is the sumptuously stuccoed "Dürer Niche", where a bust of the German renaissance artist once stood. The building section is divided into two rooms. In the southern quarter there is the so-called servant's room with a passage to the roof.

The rectangular Red Hall's dimensions are 24 m x 9.7 m and a wall height of 4.60 m. The servant's room is 5.45 m x 9.70m. The ceiling in both rooms consists of a segmented arched vault with a crown height of 5.40 m.

1.1 The ceiling construction

A special aspect of the ceiling construction in the second and third floors of the still extensively preserved northeast wing is the aforementioned segmented arched vault on a foundation of a steel structure made of arch trusses and lengthwise running girders. The steel trusses consist of two symmetrical steel arches in the form of a T-profile and are bolted together at the crown [1]. Stüler had designed the part in highly detailed drawings as monolithic, a design that apparently was abandoned for a two-part segmented arch (Fig. 1a). They span the whole breadth of the room and were covered with profiled iron sheets and decorated with figural and hanging ornaments [2]. Only in the so-called servant's room between the Red Hall and the stairway are the arch trusses constructed without coverings. Stüler planned to document the mode of construction in compositional form in the rather unassuming side room. Optically, the deep-set girders rest on ornamented cast-iron consoles. On the load-bearing segmented arches, iron girders were placed in 1-meter intervals, which were held in position by pins arranged on the left and the right of the arches. The spaces between the iron girders were lined with hollow clay pots, also a specially developed material. High-fired gypsum plaster served as the mortar for the hollow pots. The spandrel areas were masoned up out of coarse-pored light construction bricks. Here chalk mortar was used for setting mortar. As floor mortar to the roof a ca. 3 cm strong, bituminous tamped screed was laid.

The 2.8 meters long and 1 meter wide fields of hollow pots were plastered with lime and gypsum mortar finished with an additional smooth and coloured with stencilled painting (Fig. 1b).

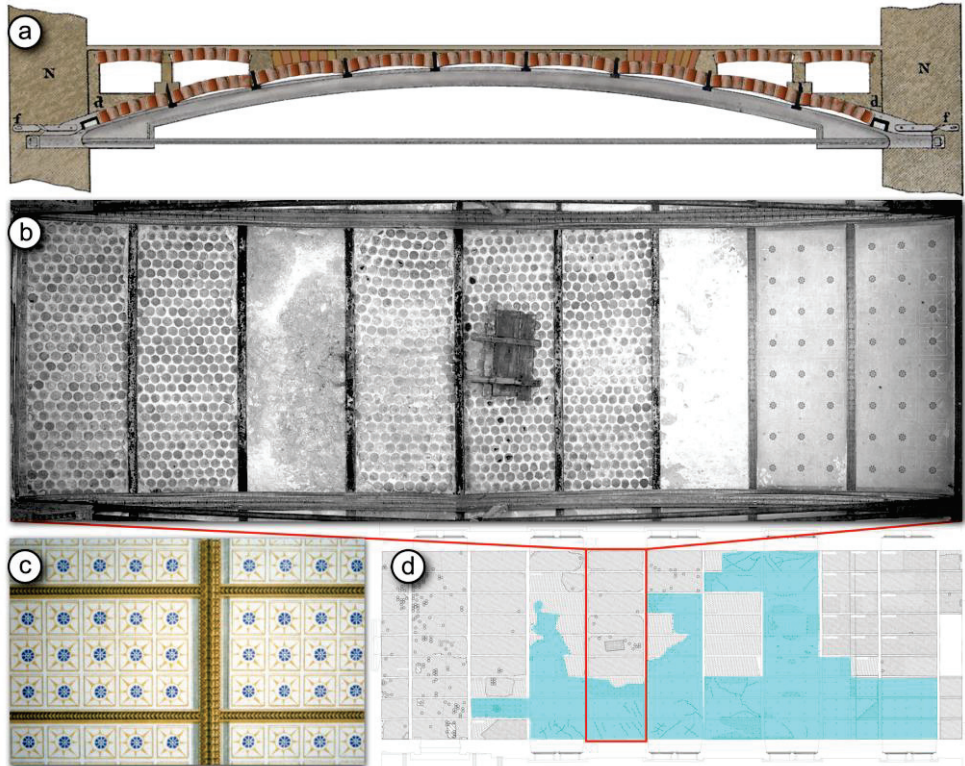


Figure 1: a) Colour Ink Drawing of the steel trusses and the construction of the ceiling with hollow pots after Stüler. b) A segment of the ceiling before restoration. c) Design for the decorative painting of the ceiling in the Red Hall by Friedrich August Stüler. d) Ceiling with extant sections and section designations (adapted from pro Denkmal). The conservation state of the ceiling before restoration remains only 40% of the original plaster and painting (blue).

Not least the construction of the vaulted ceiling out of a steel frame, hollow pots, and light construction bricks are characteristic of the broad spectrum of unusual and newly developed construction methods and materials that make the Neues Museum one of the outstanding works of industrial construction engineering of the nineteenth century [3].

But the clay pots that were used to reduce the weight in the ceiling construction were not a completely novel invention. Roman builders under

Emperor Hadrian in 119-125 AD had already built amphorae into the coffered dome of the Pantheon.

Stüler, who had first-hand knowledge of the Pantheon, used its rotunda as a model for the construction of the two cupola halls of the museum. This is evident not only aesthetically, but also with respect to the construction technique. Instead of amphorae or clay pots, the upper two coffered rings of the still preserved cupola of the North Cupola Room are masoned up with light construction bricks [4]. These have a high porosity of 57 % and a density of 1.1 g/cm³. By contrast, the traditional bricks from which the Neues Museum is built have porosity of 21 % and with 1.8 g/cm³ almost twice the density.

2 On the history of construction and damages

During the Second World War, the Neues Museum sustained serious damages, as did the other buildings on the Museum Island in the centre of Berlin. During the bombing on November 23, 1943, the central stairway with the wall frescos illustrating the history of mankind was completely destroyed by fire. During the Battle of Berlin in February 1945 bombs destroyed the northwest wing as well as the passage to the Altes Museum, damaged the southwest wing as well as the southeast projection, while the roofing of the whole building complex burned.

In the 1980s provisional roofs were constructed. The systematic work on the reconstruction first began in 1986.

Due to water infiltration and the connected chemical conversion of the processed white lead, the foundation tone of the ceiling painting today shows varying intensities of greying and has lost much of its original design as a light-coloured coffered ceiling creating the illusion of stucco (Fig. 1c).

Much more serious, however, was the impact of the development of damaging salts, which led to further total loss of the old plasterwork of the vault, of which at the beginning of restoration only about 40 percent was still present (Fig. 1d).

2.1 Damage diagnosis

As became evident in the course of the restoration work, large parts of the plasterwork below the paint layer on the ceiling was in acute danger of falling. Between the plaster and the plaster base massive salt efflorescence had developed, causing the plasterwork to separate from the substrate (Fig. 2). The salts were primarily magnesium sulphates, as was determined by testing by an external material testing laboratory, and grew up to 8 mm deep salt blooms of needle-like crystals [5]. The salt concentration in the surface areas of the material samples was in the

middle to high range, with 0.5-1 M%.



Figure 2: Massive salt efflorescence under the fallen ceiling area.

Most of the ceiling areas were in acute danger. Light vibrations or changes in the room climate led to the danger of a permanent separation of the often hollow plaster parts from the substrate material.

One plaster area fell in the course of the project evaluation. Sections of another plaster area were lost through falling more recently and during the restoration in 2007. Observations after the removal of the salt-contaminated plaster areas support the drastic hypothesis of an acute endangerment.

2.2 The source of the magnesium – investigations on the construction materials

The construction materials are a possible source of the high magnesium contamination in the Neues Museum and the secondary formations are a possible source of the sulphate. In high-fired gypsum, contamination with magnesium oxide (MgO) of ca. 2 M% could be detected [6]. An intentional addition of MgO can also lead to an accelerated setting behaviour of high-fired plaster [7], which can be a technical advantage. According to photometrical investigations (by monoparameter photometer) in our own laboratory ca. 0.4 M % - 0.55 M % magnesium could be detected in the

floor screed gypsum mortar of the North Cupola Room. On the other hand, the natural cement used in many parts of the museum turned out to be a possible source of contamination. In this material the soluble magnesium sulphate contamination was with 4 M-% higher by a power of ten. The natural cement was often used as a ground mortar layer under the screed mortar layer.

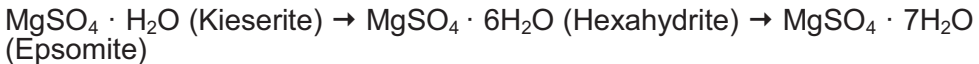
In the extremely heavy bitumen screed above the Red Hall between 0.4 M % and 0.5M % magnesium sulphate also could be detected. This corresponds to a potential soluble magnesium sulphate content of almost 40 g per square meter and calculated for the entire ceiling surface a theoretical potential of over 116 kg. But it is doubtful whether the mortar originally used as a barrier layer could be a direct source of damage, as it has an extremely low water uptake capacity. Theoretically, however, a partial dissolution of the magnesium sulphate could have occurred in the areas affected by crack formation and water infiltration. Therefore, primarily the plaster mortar with which the hollow clay pot bricks were set needs to be addressed as a confirmable source of the magnesium sulphate contamination.

The massive entry of water during the extinguishing of the fires in the wake of the wartime destruction and from rainfall during the ca. 30 years of neglect of the building are considered to be responsible for the mobilization and accumulation processes.

The accumulation of the damaging salt between the plaster base and the plaster can be traced back to the weak zone, a result of the manufacturing, between both materials as a consequence of the upside down position. The compact plaster layer was originally without a preliminary spraying directly applied to the partially smooth covers of the clay pots and then plastered, which hampered the adhesion of the two materials. In some areas where the adhesion between the two materials is evidently better, the salted moisture diffused all the way to the paint layer and there led to alveolar weathering.

3 The damaging salt magnesium sulphate

The damaging effect of magnesium sulphate is due to its different possible degrees of hydration. The salt is capable of taking up six to seven water molecules per molecule, depending on relative humidity and temperature.



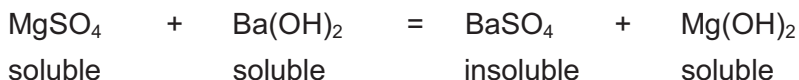
Along with these three salt forms, there are four further hydrate stages in which up to 12 water molecules are consumed per unit cell.

The incorporation of water molecules is connected to an increase in weight and a significant increase of the volume of the salt. In such

systems, damage is generally recognized not to come from volume change. Rather it originates after drying, when water causes an anhydrous phase to dissolve and produce a solution highly supersaturated with respect to a hydrated phase [8]. The conversion is dependent on the relative humidity and temperature and starting from a water-free form to the incorporation of seven water molecules in epsomite, attains an increase in volume of 223.2 percent [9]. The critical phase in the formation of the water-rich form epsomite is at a temperature ranging from 0 to 40 °C with a relative air humidity of 25 % to 95 %.

3.1 Salt passivation by salt conversion

Magnesium sulphates are easily soluble structurally damaging salts that can be converted into a largely insoluble compound by ion exchange with another salt solution. Barium hydroxide in an aqueous solution is used for this:



The magnesium hydroxide (Mg(OH)_2) combines with carbon dioxide in the air in a second step to form largely insoluble magnesium carbonate.

The reaction products of the salt conversion are lower in volume than the original magnesium sulphate. They are considered to be insoluble and stable. Moreover, according to some authors the final product (barium sulphate) also has a consolidating effect [10-11].

In restoration work, barium hydroxide has already been successfully used for decades for the conversion of sulphate salts on wall paintings [12-14].

For the Neues Museum in Berlin, Friese und Protz developed a concept for salt conversion by means of applying barium hydroxide to bricks and plaster surfaces, which had been already used in many areas of the building with success [15]. In this procedure, a high-percentage barium hydroxide solution was sprayed in several cycles on the contaminated masonry and plaster areas. Up to 100 g of magnesium sulphates were found per square metre. To be sure that the concentration was sufficient a little more than 300 g barium hydroxide was used within 8 litres of a saturated solution [16].

In the case of the extant plaster in the Red Hall, however, there was the difficulty that the damaging salt had accumulated in the hollow spaces between the plaster and the plaster base, which necessitated the development of a new conservation method.

4 Task, concept development and preliminary investigations

The dramatic damage dynamics became clear first in the course of the restoration work. Subsequently, a procedure and concept for solving the problem was developed by the former restoration firm Wandwerk Restaurierung GbR in close cooperation with the supervisors (pro Denkmal).

For the securing of the original plasterwork and painted surfaces the following tasks were foreseen: a salt treatment in the described interstices, a filling of the hollow space, the binding of the plaster to the plaster base, and development of an additional suspension and anchoring system.

In the course of concept development and comprehensive preliminary tests, a series of parameters was established and the qualities and possible changes in the plaster and the paint layer in connection with the treatment with barium hydroxide, as well as an appropriate backfilling mortar, were evaluated. Tests were carried out using Ledan D1, a back-fill mortar of Tecno Edile Toscana from Italy that has been used with success for many years in restoration work. The binders of the mortar are lime and cement.

Older publications had already shown that for Ledan products, the bonding values when used in securing of plasterwork on wooden beam systems were slight, with an average tensile strength of 0.018 N/mm^2 [17]. Therefore, an additional securing by means of a back-anchoring was foreseen. Corresponding measurements in situ by an external company (FEAD GmbH) confirmed this hypothesis: the bonding values between Ledan and the brick masonry, tested on a first test surface, were assessed as slight.

For the additional securing, an anchoring system made of stainless steel tubes for the suspension of the plaster areas was developed and tested. The tested samples consisted of the anchors casted in the clay pots with Ledan D1. The attachment and pull-out strength of anchoring systems were tested at the University of Applied Sciences in Kassel. [18], (Fig. 3).

The testing of the implemented system yielded a high variation in pull-out strength. The values varied between 0.56 and 1.52 kN. The number of samples was too small and the distribution of the values too large to achieve statistically significant results. The values thus can only be regarded as sample values. The surface load a securing bolt needs to hold in the case of a homogeneous distribution of mass is 12.5 kg. This corresponds to a weight of 0.123 kN. This value is by a factor of 5 among the lowest of the determined pull-out strength values and was assessed to be definitely sufficient. When pulling the anchors they were pulled out only a few millimetre and wedged again, the clay pots remain undamaged (Figure 3 a-d). The results let to the conclusion, that in case of a break the plaster area can be lowered but will not fall down.

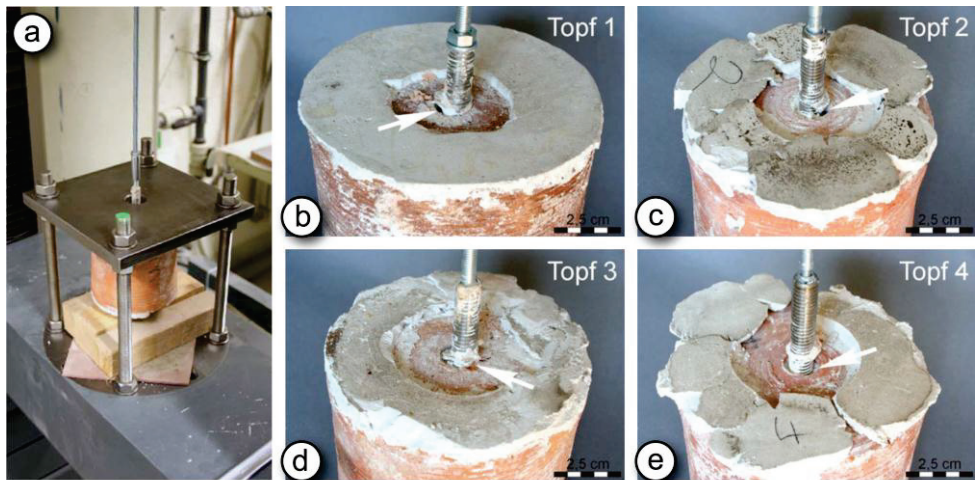


Figure 3: a) the testing equipment by using a universal testing machine. b - e) Crack pattern on tested clay pots. The white arrows mark the edges of the breaks.

4.1 Results of preliminary investigations and stocktaking

The investigation program encompassed the determination of the maximal water absorption, the density, as well as the diffusion properties of water and barium hydroxide solution for the assessment of possible alterations in the paint layer and spot formation. Compact pieces of plaster from the fallen ceiling field served as test samples.

The under layer of plaster was evidently a dense and compact, grey-ochre coloured gauged mortar plaster, in which calcareous spars were clearly discernable. This speaks in favour of a dry hydrated coarse material as the starting material, to which a binder portion of gypsum was added immediately before the processing.

The plaster density including the 1-2 mm thick final plaster layer is 1.66 g/cm^3 . The dry plaster of a ceiling area with an area of 2.8 m^2 can have a weight of up to ca. 140 kg. After water absorption by storage in water for 24 hours, the plaster increased in weight by 12 M-%. This corresponds to an open porosity of ca. 21 %. Therefore, the maximum water uptake of a single plaster area results in a weight increase of ca. 16.5 kg.

In the diffusion tests, the water and barium hydroxide solution were precisely dripped using a drop funnel positioned on the rough plaster area on the back of the sample. The solution diffused into the porous body and spread in a radial pattern. After drying, the paint layer was visually evaluated: after the various tests, only the most minimal, barely perceptible colourations of the paint layer surface could be observed.

For each plaster area to be treated cracks, hollow spaces and all subsequent measures were mapped. Detection of the hollows was done by simple knocking. The mapping of the hollowed areas yielded different results (Fig. 4): the extent of the hollow areas varied between 10 and 100% with an average of 63%.

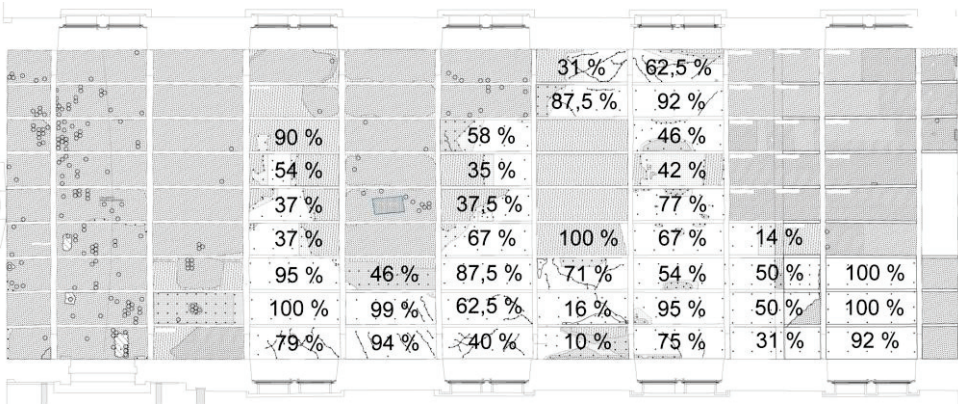


Figure 4: Hollows in percent (drawing adapted from pro Denkmal).

5 The securing concept

The protection of the wall paintings and plasterwork in danger of falling is a central concern in the restoration of architectural surfaces [19]. In the past, within numerous restoration projects flexible and reversible suspension systems for anchoring in wooden girders have been used [20-23]. In such procedures the support was achieved by using a Plexiglas or metal sheet that lay chromatically matched on the paint layer and was bolted to the mostly wooden supporting structure. For aesthetic reasons such a form of securing did not come into question for the ceiling of the Red Hall.

A further difficulty in back-filling large hollow spaces consists in the need to maintain a consistent flow of material and pressure in the low-pressure range [24]. In stone conservation, low pressure techniques for the continual application of consolidation material have already been used [25]. The low-pressure injection technology was developed for the renovation of cement and is usually used for injection into even the finest fractures [26].

The concept for the securing of the plasterwork areas consists of three points:

- 1) Salt conversion
- 2) Flat backfilling
- 3) Implantation of stabilizing bolts

A reconversion of oxidized white lead, as has been successfully implemented in other restoration projects [27], was not an option in the case of the ceiling painting in the Red Hall.

5.1 Securing and installation of the construction

During the conservation work the respective plaster areas were supported by at least six corner steadies (Fig. 5).



Figure 5: Installation of the hose and packer system (photo: Hüttich).

In a first step, the drilling down to the plaster base (13 mm) was carried out. This was done as needed on the basis of the detection of hollow spaces. Holes were placed in the centre of the rosette stencils. They were arranged in a grid over the painted area, so that at least 12 openings for injections were distributed over each area of 2.8 m². 4 injection openings and anchors thus secured each square meter of plaster surface. These had to be capable, if necessary, to continuously support a weight of 12.5 kg.

The painted layer areas of each bay run parallel to the segmented arch vault, each with a different slant. At the crown in the centre of the vault

(see Fig. 1a&b and Fig. 5) there is a slight slant in both directions toward the adjacent metal girders. Going toward the walls, the slant increases from 8 % to 13.5 %, 21 %, and up to 28 %. The danger of an accumulation of moisture and the development of damages is thus highest along the lowest parts of the plaster areas. To prevent a moisture build-up and the development of water spots, holes (6 mm) for drainage tubes were placed along the lowest parts. These were placed in the corner areas of the light-coloured square stencils. The drainage tubes were set in the holes, sealed with Teflon tape and a hose was installed on each that connected them to the suction apparatus.

To prevent an uncontrolled leakage of liquid through cracks in the plasterwork, all visible cracks were sealed using a solution of volatile hydrocarbons (cyclododecane) that was applied multiple times. In the course of the work, the flanks of the plaster areas on the vault girders turned out to be a further weak point. Here the metal along the flank of the connecting areas had been smoothed over with a thin and today predominantly loose and brittle lime mortar. The loose strips of mortar were removed and the metal surfaces cleaned of loose particles and dust. In the flank area a commercial bonding compound was used as a new mortar, since this also produces the needed adhesion on the metal material.

The holes for the injection of the hollow spaces and the surrounding paint layer were protected with cyclododecane and two-ply Japanese paper. Filling packer was put into the injection openings. For that, rubber plugs with an opening in the centre were fixed after inserting a light metal pipe in these openings. On the lower end of the opening a transparent filling hose was attached fitted with a closing valve for the flexible dosage of material.

The filling apparatus used was a low-pressure membrane pump (Model 2041 101-0 MC-Bauchemie). The pump is driven by compressed air and the injection pressure is continuously variable from 1 to 10 bar. A maximum of 6 filling hoses per injection cycle was connected to the pump. To produce the suction, a commercial industrial wet vacuum with a 1200-watt suction capacity was used. To maintain a sufficiently strong suction, only 6 drainage tubes were attached.

5.2 Salt conversion

Through the upper row of the hose system an amount of 5 litres highly concentrated barium hydroxide solution was directed into the hollow space between plaster and the plaster base. The electrical conductivity of the reaction liquid was measured beforehand. A possible liquid excess was sucked out through the lower row of hoses with help of a low vacuum of around 0,5 bar.

In the hollow space between the plaster and plaster base the magnesium sulphate dissolves and reacts directly with the dissolved barium hydroxide.

Insoluble barium sulphate is directly precipitated. The precipitate was partially in the form of white precipitate in the interstice and the excess was sucked out as a clear milky liquid (Fig 6b). Each plaster area was divided into two subareas and about half of each area was treated. The results obtained varied in most cases. Electron conductivity measurements revealed a reduction up to 36 %, with an average value of 9%, in relation to the initial solution (Fig 7), which indicates a successful precipitation reaction. In the individual subareas, however, much more significant results were obtained and the result of the salt reduction was evaluated. For example, the right half of a test field treated with 4 l barium hydroxide solution, of which almost 2 l could be removed by suction. In this case the electrical conductivity of both the applied liquid and the extracted liquid was measured. The applied liquid had an electrical conductivity of 26.6 mS/cm; this corresponds to a content of 9.6 g/l barium hydroxide. The sucked out solution, on the contrary, had an electrical conductivity of only 16.96 mS/cm and thus could be reduced by ca. 36 % and corresponds to a content of 7.8 g/l dissolved substances. The concrete examples as well as the results of the whole campaign speak for a successful precipitation reaction of magnesium sulphate into slightly soluble barium sulphate in the hollow area.

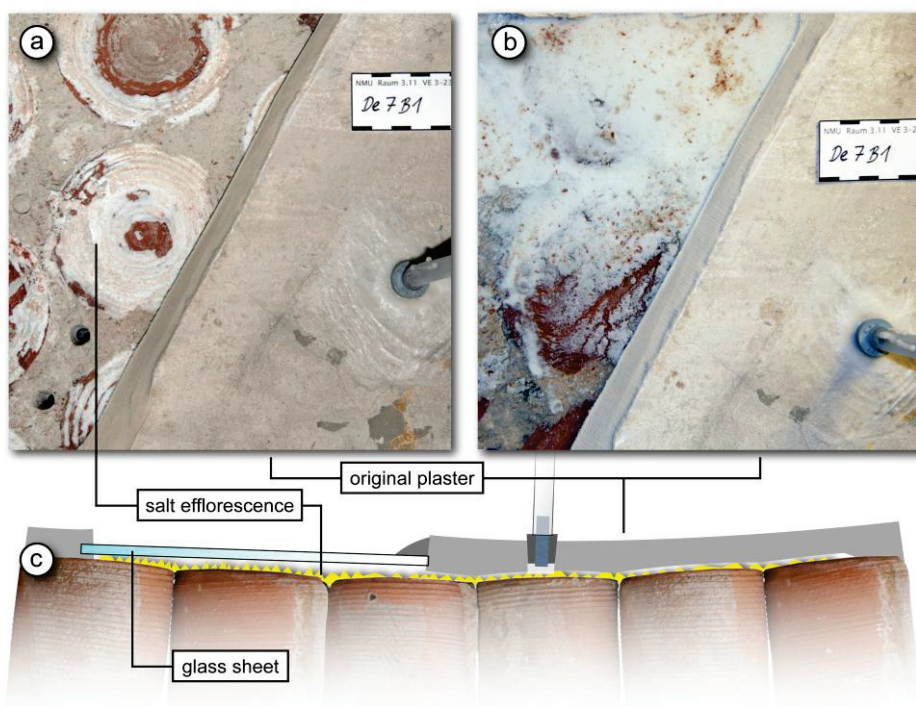


Figure 6: a) A test field area with massive salt efflorescence b) showing white deposit during the treatment. c) The preparation of the test field.

cautionary measures could not always be prevented. In one test area, changes of the paint layer manifested after the barium hydroxide treatment. After the filling of about 3 l, diffuse dampness could be discerned solely along some of the finely cracked areas. Also immediately after filling with the Ledan suspension, no changes in the paint layer were visible. After a dwell time of two days, however, brown stains and water markings emerged on the paint surface. The brown stains were most probably caused by the organic components of the glue painting. Water markings that developed and spots consisting of organic floating particles could be successfully almost completely repelled with a hydrogen peroxide solution (30 %) in the course of the evaluation of the measures. For this an application of the solution in up to 10 steps was necessary.

5.3 Backfilling

After the salt conversion and drying, the hollow space was filled using the same apparatus. For this step the plaster was secured partially lengthwise with cushioned slats and corner steadies (see Fig. 5).

Via the upper hose and packer row, backfilling mortar (Ledan D1) was filled into the hollow space with the help of a membrane piston pump under low pressure. Here a continuous filling pressure of 2 bar was used. The ratio of dry powder to water was 2:1. The pump was not able to transport a backfilling mortar with a high proportion of solid material with sufficient reliability. The backfilling was carried out half a surface at a time, the filling of the Ledan suspension in batches. A precise visual observation of the plaster area during the measure was crucial to mitigate uncontrolled leaking backfill suspension or to interrupt the process if water stains occurred. During the discharge of the mortar from the hoses in the lower plaster area, the flow was interrupted, and in order to reach all hollow areas the mortar was injected again for a few seconds. A further available control was the discharge tubes for the drainage, out of which often backfill mortar was discharged in a successful backfilling. For each area, depending on the state of the hollows, between 5 and 15 l of Ledan-suspension was injected. The mortar created a force-locked bond between the base and the plaster material. This could be confirmed both by knocking tests and in the course of the follow-up examination by the firm FEAD GmbH on a test area.

After backfilling and a dwell time of 3 days, the cyclododecane could be removed. The removal was carried out by blow-drying, whereby the hydrocarbon evaporated without leaving any residue.

5.4 Back anchoring

To achieve a recommended additional protection, after the removal of the hoses from the fill holes a new drilling was made in the same holes that went into the stable base material (7-10 cm). In the cases in which the drilling of one of the thin-walled tops of the pot bricks was punctured, a

pecially developed suspension system brought results. The restorer Carsten Hüttich and the mechanical engineer Martin Reußner were decisively involved in the development of the system. The stainless steel tubes served as stabilizing bolts, on which an external threading was cut. These were pushed over light metal tubes and both tubes inserted into the bore hole and into the hollow pot brick. Both tubes were fixed with rubber plugs in the middle of the hole. In order to increase the stability and load capacity of the component a defined amount of fill mortar (350 ml) was injected with a hand gun through the light metal tube into the pot brick. The mortar filled up the clay pot to a height of about 5 cm and ensured an interlocking of the stabilizing bolt with the hollow pot brick (Figs. 8 b). Per hollow pot filling this leads, as preliminary testing had established, to a weight increase of ca. 500 g. In the case in which the compact setting mortar was drilled, the borehole expanded upwards conically and as already described was injected with mortar.

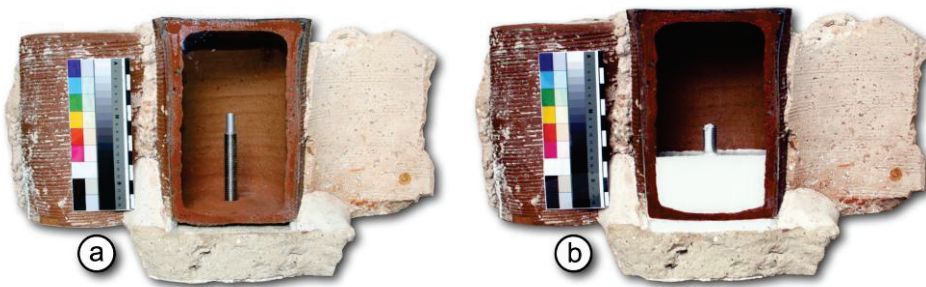


Figure 8: Model of the suspension system with stabilizing bolts in a clay pot before (a) and after (b) filling.

After a dwell time of three days the filling tubes could be pulled out of the stainless steel anchors and the bore hole below the level of the paint layer force-closed sealed with a gypsum-lime mortar. In a further step a final rendering stuff was applied and smoothed flush with the paint layer. After drying of this rendering layer the chromatic retouching was carried out on a new stencilling.

6 Summary and evaluation

37 plaster areas altogether were treated over a period of three months. The ca. 103 square meters large original plasterwork is today secured by about 400 securing bolts. 290 l highly concentrated barium hydroxide solution was applied, of which about 50 l could be recovered. The conservation and passivation of the damaging salt could be determined by

conductivity measurements and through analysis of the extracted residues. 340 l of backfilling suspension was injected all over as backfilling mortar.

The use of a low-pressure injection pump made possible a controllable and complete treatment of large hollow areas. By using the filling system in a grid process, several steps of the process could be carried out using the same apparatus. This made the work easier, reduced costs, and minimized an endangering of the painted surface.

The missing areas of the ceiling and wall surfaces were newly plastered and the ceiling vault areas reconstructed in a tonally contrasting stencil painting. After the restoration under the direction of the restorer Eberhard Taube and the reconstruction of mouldings and decorative painting and with the new red wallpaper the exhibition hall presents itself today again in a condition befitting its name [28-30].

Acknowledgements

We thank architect Stefan Schäfer for advice and instruction in the low-pressure injection technique; and we thank restorer Eberhard Taube, Carsten Hüttich, Bernhard Irmer, Annett Baumeister and the restoration planning by restorer Claudia Vollmann (pro Denkmal) for their constructive cooperation.

References

- [1] Lorenz, W., Kernform und Kunstform - Preußische Konstruktionskunst im Zeichen der Industrialisierung, in Das Neue Museum Berlin - Konservieren, Restaurieren, Weiterbauen im Welterbe, Stiftung Preußischer Kulturbesitz, Staatliche Museen zu Berlin (SMB), Bundesamt für Bauwesen und Raumordnung (BBR) & Landesdenkmalamt Berlin (LDA), eds., Leipzig 2009, pp. 38 - 43.
- [2] Haber, G.J., Riemann, M. "Metallische Bauplastik", in Das Neue Museum Berlin - Konservieren, Restaurieren, Weiterbauen im Welterbe, SMB, BBR & LDA, eds., Leipzig 2009, pp. 194 - 195.
- [3] Lorenz, W., The Berlin „Neues Museum“ - a microcosm of Prussian building technology against the background of beginning industrialization, in Structural Studies, Repairs and Maintenance of Historical Buildings VI., Brabbia, C.A., Jager, W., eds., Southampton 1999, 389-398.
- [4] Wedekind, W. Baumeister, A. Schellhase, L. 2009 Die Salzreduzierung im Norkuppelsaal, in: SMB, BBR & LDA (eds.). Das

Neues Museum Berlin - Konservieren, Restaurieren, Weiterbauen im Welterbe. Leipzig 2009, 211 - 213.

- [5] Höpcke, M., Ergebnisse der IC-Messungen, Pendelbögen zu den Entnahmebereichen 50/51, unpublished investigation report, Gesellschaft für Materialprüfung und Baustofforschung mbH (MBF), Berlin 08.08.2007.
- [6] Siebel, E. ed., Handbuch der Werkstoffprüfungen, Bd. 3: Die Prüfung nichtmetallischer Werkstoffe, Berlin 1941.
- [7] Lucas, G., Die stofflichen Besonderheiten von Hochbrandgipsmörtel, ZKG International (56) (2003) 54-65.
- [8] Steiger, M., Crystal growth in porous materials – I: The crystallization pressure of large crystals, Journal of Crystal Growth, (282), Issues 3-4, (2005), 455-469.
- [9] Goudie, A. S., Sodium sulphate weathering and the disintegration of Mohenjo-Daro, Pakistan, Earth Surface Processes (2) (1977) 75-86.
- [10] Toniolo, L., Colombo C., Realini, M., Peraio, A., Positano, M., Evaluation of barium hydroxide treatment efficacy on a dolomitic marble”, Annali di Chimica (91) (2001) 813-821.
- [11] Sayre. E.V., Direct deposition of barium sulphate from homogenous solution within porous stone, in Conservation of Stone. 1970 New York Conference on Conservation of Stone and Wooden Objects, Volume 1, second edition, The International Institute for Conservation of Historic and Artistic Works (IIC) ed., London 1971, 115 - 118.
- [12] Matteini, M. Moles, A., Twenty years of application of “barium” on mural paintings: Fundamentals and discussion of the methodology, ICROM Committee for Conservation: Preprints of the 7th triennial Meeting, Copenhagen, 10-14 September 1984, 15-19.
- [13] Matteini. M., In Review: An Assessment of Florentine Methods of Wall Painting Conservation Based on the Use of Mineral Treatments, in The Conservation of Wall Paintings: Proceedings of the symposium organized be the Courtauld institute of Art and the Getty Conservation Institute, London, 13-16 Juli 1987, Gather, S. ed., London 1991, 137-48
- [14] Leitner, H., The treatment of wall paintings affected by salts: an interdisciplinary task as seen from a conservator's perspective,

- Bauinstandsetzen und Baudenkmalpflege: eine internationale Zeitschrift (11) (2005) 365-380.
- [15] Friese, P., Protz, A., Salze im Mauerwerk – Möglichkeiten zur Entsalzung und Salzwandlung, in Entfeuchtung/Entsalzung, ed. H. Venzmer, FAS Schriftenreihe (10) (1999) 211 – 220.
- [16] Schwieger, O. Die Barium-Hydroxid-methode als Möglichkeit der Salzpassivierung, in Konservierung, Restaurierung und Ergänzung im Neuen Museum Berlin - Zwischen ursprünglichen Intentionen und neuen Entwicklungen, Verband der Restauratoren e.V., Siegl Verlag, Munich 2013, 92-96.
- [17] Ettl, H., Schuh, H., Putzsicherung mit Ledan TB 1, in Putzsicherung. Sicherung von Malerei auf gemauerten und hölzernen Putzträgern. Beiträge einer Fortbildungsveranstaltung der Restaurierungswerkstätten des Bayerischen Landesamtes für Denkmalpflege am 17. November 1992, ed. M. Petzet, Arbeitshefte des Bayerischen Landesamtes für Denkmalpflege, Vol. 79, Munich 1996, 37-42.
- [18] Rüdlich, J., Ausreißfestigkeiten von Ankersystemen aus Tontöpfen des Neuen Museums (Museumsinsel Berlin)“, unpublished investigation report, Angewandte Materialuntersuchungen (AM Göttingen), Göttingen, 09.23.2006.
- [19] Petzet, M. ed., Putzsicherung. Sicherung von Malerei auf gemauerten und hölzernen Putzträgern. Beiträge einer Fortbildungsveranstaltung der Restaurierungswerkstätten des Bayerischen Landesamtes für Denkmalpflege am 17. November 1992. Arbeitshefte des Bayerischen Landesamtes für Denkmalpflege, Band 79. Munich 1996.
- [20] Leitner, H., Paine, S., Is wall-painting restoration a representation of the original or a reflection of contemporary fashion?: An Austrian perspective, in Restoration: is it acceptable? Oddy, A. ed., London 1994, 51-65.
- [21] Hošek, J., Skupin, L., Aufhängung der Decke des Hauptsaaes im Schloss Troja, Wiener Berichte über Naturwissenschaft in der Kunst (6-8) (1991) 67 - 84.
- [22] Furdyna, J., Conservation Work in the Interior of the Kupe Synagogue in Kazimierz/Krakow, Biuletyn - Journal of Conservation Restoration (14) (2003) 48-61.

- [23] Wendler, E., Die Wiederbefestigung der Putzschale durch rückseitig fixierte Anker, *Denkmalpflege Informationen*, edition A (92) (2005) 22-25.
- [24] Adams, G.W., A practical technique for injection of consolidants behind wall and ceiling paintings, *APT bulletin* 37, (2-3) (2006) 33-36.
- [25] Schoonbrood, J.W.M., Low pressure application technique for stone preservatives, in Thiel, M.-J. (Hrsg.) *Conservation of stone and other materials: proceedings of the International RILEM/UNESCO Congress "Conservation of Stone and Other Materials: Research-Industry-Media"*, Paris, June 29-July 1, 1993, E. & F.N. Spon Ltd., London 1993, 512-518.
- [26] Schäfer, S., Zur Injektion mineralischer Füllgüter, unpublished Diploma Thesis, Civil Engineering Faculty, field of study Architecture at the Hochschule für angewandte Wissenschaft und Kunst (HAWK), Holzminden 2004.
- [27] Leitner, H., Rückwandlung von oxydiertem Bleiweiß an Deckenmalereien in der Burg Strechau, Steiermark", in *Wandmalerei, Sgraffito, Stuck*, Koller, M., Prandtstetten, R. eds., *Restauratorenblätter*, Vol. 9, IIC Austrian section, (1988) 116-119.
- [28] Taube, E. Roter Saal und Dienerzimmer, in *Das Neue Museum Berlin - Konservieren, Restaurieren, Weiterbauen im Welterbe*, SMB, BBR & LDA eds., Leipzig 2009, 173-176.
- [29] Taube, E., Hüttich. C., Wedekind, W. "Der Rote Saal im Neuen Museum", in *Konservierung, Restaurierung und Ergänzung im Neuen Museum Berlin - Zwischen ursprünglichen Intentionen und neuen Entwicklungen*, Verband der Restauratoren e.V., Siegl Verlag, Munich 2013, 184-189.
- [30] Walter, L.J. Eine Tapete mit Durchblick – Die Entwicklung einer transparenten Japanpapiertapete zur Wiedergewinnung der raumprägenden Farbigkeit des Roten Saales, in *Konservierung, Restaurierung und Ergänzung im Neuen Museum Berlin - Zwischen ursprünglichen Intentionen und neuen Entwicklungen*, Verband der Restauratoren e.V., Siegl Verlag, Munich 2013, 190-196.

Wall paintings salt induced decay in residential buildings in Hierapolis of Phrygia (Turkey)

E. Cantisani, B. Sacchi*, S. Bracci, C. Riminesi and S. Vettori

Institute for the Conservation and Valorization of Cultural Heritage,
National Council of Research, Sesto Fiorentino (FI), Italy

* b.sacchi@icvbc.cnr.it

Abstract

Hierapolis of Phrygia (Turkey) was an ancient city located on hot springs in south western Anatolian peninsula. The site was designated as a UNESCO World Heritage Site in 1988. It comprises an archaeological museum and most of the ruins are currently under excavation and studied by archaeologists and specialists from different countries, under the auspices of the Italian archaeological mission.

Inside the wide archaeological site, Insula 104 is a residential area dated back at proto-byzantine period. Many buildings were excavated starting from 1989, and the presence of several rooms with painted walls illustrating coloured marble columns and panels suggests the attribution to high-level residences. Currently, the wall paintings of some rooms of great historical and artistic importance, present tangible damages due to salt crystallization and therefore, new conservative interventions, besides some actions that already took place in the last years, are necessary.

Keywords: salt induced decay, wall paintings, efflorescence

Experimental procedures

In order to plan pertinent and focused actions, different analytical techniques were used to determine the nature and the origin of the soluble salts present on the wall paintings in two different areas of the Insula 104.

Samples were scratched out from the efflorescence on the surface of the wall paintings in *The House of the Doric Courtyard* (room A 1207, probably utilized for feasts and banquets till to VI century), and in the

House of the Painted Inscription (room A 1267, known as *Room of the Prayer of Manasseh*). Four samples were collected from room A 1207, *House of the Doric Courtyard*, and six samples from room A 1267, *Room of the Prayer of Manasseh* (see Figure 1).

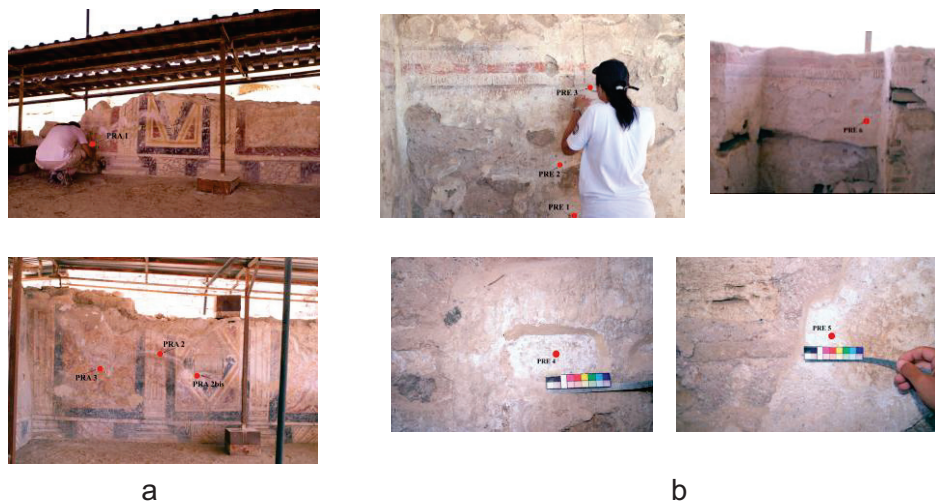


Figure 1: Location of collected samples in room A 1207 (a) and room A 1267 (b).

Collected samples were investigated by means of optical microscopy (OM), X-ray diffraction (XRD) and Ion Chromatography (IC).

Detailed images were acquired *in situ* using a digital microscope Scalar DG-2A instrument, equipped with an optical zoom ranging from 25x to 200x. All shots were recorded with a 25x magnification (corresponding to a 13x8 mm² area).

X-Ray Diffraction (XRD) was performed with a PANalytical X'Pert Diffractometer, using a Cu K α 1 radiation ($\lambda=1.545$ Å), an X-ray tube 40 KV, 30 mA, the investigated angular range was $3^\circ < 2\theta < 70^\circ$.

For chromatographic analyses, a given amount of water was added to a weighted amount of the sample. Then, the solution was stirred for 24 hours, decanted and filtered with hydrophilic PTFE filters (pore size 0.45 μm). Ion Chromatography (IC) was performed on the extract with a Dionex ICS-1000 Instrument, equipped with a suppressed conductivity detector, IonPac[®] columns and ion self-generating suppressors.

Results and discussion

The efflorescence on the mural paintings of the studied rooms of Insula 104 consists of sulfates (mainly thenardite, apthitalite and syngenite), nitrates and chlorides (halite and sylvite).

In room A 1207, sulfates are prevalent in the efflorescence of the lower part of the wall, whilst nitrates are prevailing at higher levels. In room A 1267 chlorides and nitrates are prevalent: from bottom to the top of the wall, the amount of chlorides increases, while that of nitrates decreases. In Table 1 the main results of XRD and IC analyses are presented.

Table 1: Main constituents of analyzed samples.

ID SAMPLE	XRD	IC
PRA1	<u>Sulfates</u> (thenardite (Na_2SO_4), apthitalite ($(\text{K},\text{Na})_3\text{Na}(\text{SO}_4)_2$), syngenite ($\text{K}_2\text{Ca}(\text{SO}_4)_2 \cdot \text{H}_2\text{O}$)); <u>carbonates</u> (calcite (tr))	Na^+ ; K^+ ; Ca^{2+} (tr); SO_4^{2-} ; NO_3^- (tr); Cl^- (tr)
PRA2	<u>Nitrates</u> : (sodium nitrate, potassium nitrate); <u>silicates</u> (quartz (tr))	Na^+ ; K^+ ; Ca^{2+} (tr); NO_3^- ; Cl^- (tr); SO_4^{2-} (tr)
PRA2bis	<u>Nitrates</u> : (sodium nitrate and potassium nitrate); <u>sulfates</u> (gypsum); <u>silicates</u> (quartz (tr) and micas)	K^+ ; Ca^{2+} (tr); Na^+ (tr); NO_3^- ; Cl^- (tr); SO_4^{2-} (tr)
PRA3	<u>Sulfates</u> (thenardite, picromerite ($\text{K}_2\text{Mg}(\text{SO}_4)_2 \cdot 6\text{H}_2\text{O}$), apthitalite, syngenite); <u>carbonates</u> (calcite (tr))	Na^+ ; K^+ ; Mg^{2+} ; Ca^{2+} ; SO_4^{2-} ; NO_3^- (tr); Cl^- (tr)
PRE1	<u>Chlorides</u> (halite); <u>nitrates</u> (potassium nitrate); <u>sulfates</u> (gypsum (tr))	Na^+ ; K^+ ; Ca^{2+} (tr); Mg^{2+} (tr); Cl^- ; NO_3^- ; SO_4^{2-} (tr)
PRE2	<u>Chlorides</u> (halite); <u>nitrates</u> (potassium nitrate and ammonium and potassium nitrate)	Na^+ ; K^+ ; Ca^{2+} (tr); Mg^{2+} (tr); Cl^- ; NO_3^- ; SO_4^{2-} (tr)
PRE3	<u>Chlorides</u> (halite, sylvite); <u>nitrates</u> (potassium nitrate); <u>sulfates</u> (gypsum)	Mg^{2+} ; Ca^{2+} ; Na^+ (tr); K^+ (tr); SO_4^{2-} ; Cl^- (tr); NO_3^- (tr)
PRE4	<u>Sulfates</u> (gypsum, magnesium sulfates with different hydration)	Ca^{2+} ; Mg^{2+} ; Na^+ (tr); K^+ (tr); SO_4^{2-} ; Cl^- (tr); NO_3^- (tr)
PRE5	<u>Chlorides</u> (halite); <u>sulfates</u> (gypsum)	Na^+ ; K^+ (tr); Mg^{2+} and Ca^{2+} ; Cl^- ; SO_4^{2-} (tr); NO_3^- (tr)
PRE6	<u>Sulfates</u> (hexahydrate - $\text{MgSO}_4 \cdot 6\text{H}_2\text{O}$, starkeyite - $\text{MgSO}_4 \cdot 4\text{H}_2\text{O}$, gypsum); <u>silicates</u> (quartz)	Mg^{2+} ; Ca^{2+} ; Na^+ (tr); K^+ (tr); SO_4^{2-} ; Cl^- (tr); NO_3^- (tr)

Note: (tr) = in trace elements

Conclusion

A correct definition of the provenance of salts present in the studied mural paintings of Insula 104 is essential in order to plan an appropriate removal of the decay reasons and a good conservative intervention.

The deposition of sulfates and nitrates can be ascribed to rising damp or to infiltration from filling soils that are in contact with the wall. The presence of significant amounts of chlorides is instead quite unusual in a place that is far from the sea-side (at least at present time), and could be due to the particular re-utilization of the room as a building materials warehouse.

Further investigations are foreseen in order to better understand causes and dynamics of soluble salts contamination in Insula 104.

Acknowledgments

The authors acknowledge the financial support of the Italian FIRB Project "Marmora Phrygiae". Thanks are given to Prof. F. D'Andria and Dr. G. Scardozzi for their assistance and useful comments.

References

- [1] D'Andria F., Hierapolis of Phrygiae, Ed. Yayınları 2003 (9758070703).
- [2] Zaccaria Ruggiu A.P., Un quartiere residenziale: l'insula 104, in, Hierapolis di Frigia V. Le attività delle campagne di scavo e restauro 2004-2006, edited by F. D'Andria, M.P. Caggia and T. Ismaelli, Istanbul, 2012.

Salt weathering processes of reconstituted stone used in the Orval Abbey (Belgium)

M. Gommeaux^{1*}, C. Thomachot-Schneider¹, G. Fronteau¹, S. Eyssautier¹, K. Mouhoubi², T. Fujimaki³ and C.T. Oguchi³

¹GEGENAA, Université de Reims Champagne-Ardenne, Reims, France

²GRESPI, Sciences Exactes et Naturelles, Campus du Moulin de la Housse, Reims CEDEX 2, France

³Geosphere Research Institute (GRIS), University of Saitama, Sakura-ku, Japan

* maxime.gommeaux@univ-reims.fr

Abstract

In its present state, the Orval Abbey, in southern Belgium (49.64°N, 5.35°E), comprises two parts. The mediaeval part, which is currently in the state of ruins, was built in Bajocian and Sinemurian limestones of local origin. The Sinemurian stone (SN) is a siliceous limestone with a low total porosity (7.6 ±0.2%) with no clearly dominant pore access radius. The Bajocian limestone (BJ) has a higher total porosity (31.1±0.7%) with pore access thresholds at 0.5 and 12 µm.

The modern part of the Abbey was built from 1926 to 1948, on the foundations of buildings dating from the late 18th century that have been destroyed in the meantime. A reconstituted stone (RS) was produced during the last major building phase (1933-1948), and used in complement to the natural stones mentioned above. Although the production process is not known, microscopic observations and chemical analyses are consistent with the very scarce historical archives and have shown that the RS was made from a mixture of crushed fragments of both natural stones and cement [1].

The RS is highly susceptible to salt weathering, whereas the natural stones not. The aim of this study is to assess these damage phenomena.

Earlier results have shown that some physical characteristics of the RS are in-between those of both natural stones, whereas others are very close to those of the BJ. Chemical analyses, however, have shown that

the RS, even in an un-weathered state, contains sulphur minerals that may constitute a source of salts within the stone itself.

Keywords: salt weathering, thermography, reconstituted stone

Mapping of salts in a weathered zone

Soluble-salt and moisture content of drilled samples

Stone powder samples have been collected by means of drilling (diameter 5 mm) on a damaged wall made of RS (Figure 1). Samples were lifted beneath (at 2, 10 and 19 cm height) and above (at 22 and 42 cm) a weathering fringe visible at a height of approximately 20 cm. The uppermost point was selected reasonably far from the fringe in order to serve as a reference for un-weathered material.

A quantity of 100 mg of stone powder was poured into 500 ml of distilled water for 24 h in order to ensure complete dissolution of soluble salts. The concentration in salts was determined by ion chromatography (DIONEX ICS 2000, for anions) and ICP-OES (Thermo ICAP 6000, for cations). The highest concentrations were observed for the samples just below and just above the weathering fringe.

Mapping of salts by means of portable X-ray fluorescence

Measurements of the elemental composition of the outer surface were carried out by means of a portable X-ray fluorescence (pXRF) device (Thermo Niton XL3t), at the same heights where drilled samples were lifted. The results (Figure 1) indicated a clear increase of the concentration in sulphur (S) when moving from the un-weathered zone to the weathered one. The values obtained at a height of 22 cm, slightly above the weathering fringe, were higher than those for the reference point, suggesting that salt damage will likely progress upwards.

Infrared thermography

Passive and active infrared thermography (IRT) images of the same test zone were acquired. A thermo signal (TS) image can be interpreted in terms of surface temperature, although the emissivity plays an important role. The obtained TS-images confirmed (Figure 1) that a thermal gradient exists over the zone before flash illumination, likely related to a moisture content gradient. Images acquired during flash illumination (either with or without subtraction of the initial TS) revealed a different thermal response in a zone that is not weathered macroscopically but enriched in salts, according to results of IC analyses of aqueous extracts of drilled samples and pXRF measurements.

Laboratory experiments

Time-release of ions through aqueous extraction

Un-weathered samples of the three types of stone (approximately 19 g of each) were poured into 50 ml of demineralized water. Samples of the aqueous solution were collected at different time intervals up to 48 h. The concentration in Cl^- and SO_4^{2-} was measured by IC.

For all types of stone, a continuous release of salts was observed

Continuous evaporation experiment

A continuous evaporation experiment was conducted by ensuring continuous supply of water through the bottom face of a RS core (3.5x7 cm) and evaporation of water through the upper face (for 54 days).

Surface colorimetric measurements revealed a progressive change of the colour of the stone, more precisely the development of a yellowish ring and whitening of the surface.

At the end of the experiment, the core was sawn longitudinally to allow for a pXRF study of the variations in the elemental composition. A clear gradient in the elemental concentration of S was observed. This showed that sulphur migrates within the RS together with the flow of water and accumulates near the evaporation surface.

Conclusions

On-site measurements with infrared thermography and a portable X-ray fluorescence device offer an easy and handsome way to characterize salt accumulation, even at stages when no damage is visible.

The laboratory results have shown that the weathering of the RS is due to mobilization of salts that are present within the stone itself, and that can be easily mobilized by water. To date, analyses revealed that sulphur-containing minerals are present in the reconstituted stone and are likely the source of the sulphate observed (thenardite, gypsum). However, the source of the cations, especially Na^+ , is not known yet.

Acknowledgements

This study was partly funded by the Hybriprotech grant as part of the INTERREG IV programme. The authors warmly thank Brother Xavier for permitting work in the Orval Abbey.

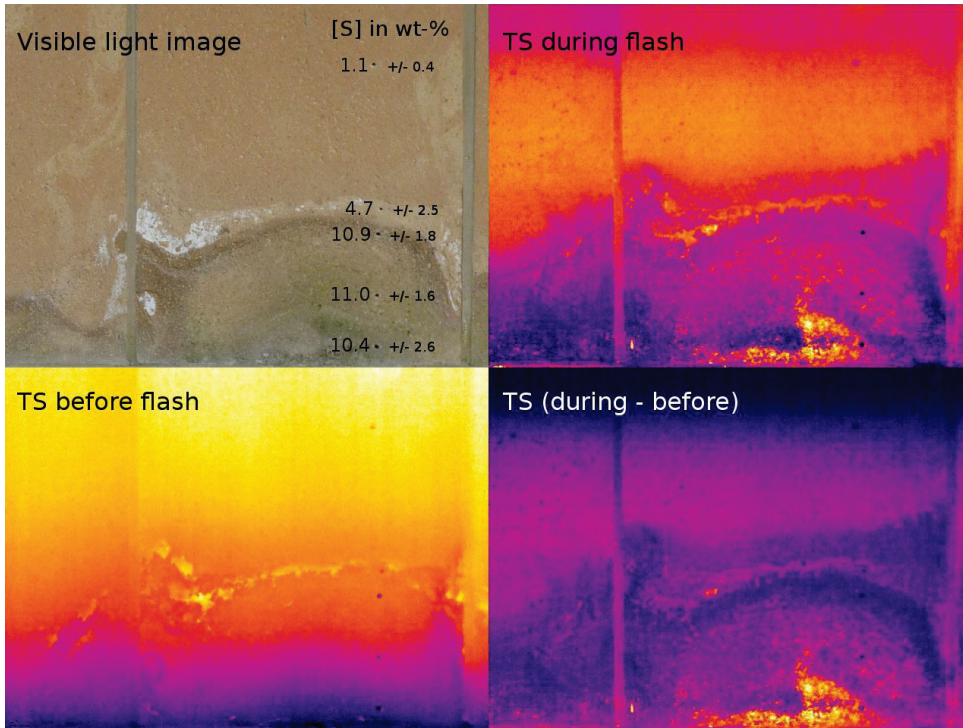


Figure 1: Weathered zone of a reconstituted-stone wall. Mapping of S obtained from pXRF (expressed in weight percent); thermal image obtained before flash illumination revealing a bottom-to-top increase of surface temperature; thermal image obtained during flash illumination revealing a thermo signal response extending further than what is visible to the naked eye; subtractive image enhancing the contrast between salt-rich and salt-poor zones.

Reference

- [1] Thomachot-Schneider C., Gommeaux M., Fronteau G., Oguchi C.T., Eyssautier S. & Kartheuser B.; A comparison of the properties and salt weathering susceptibility of natural and reconstituted stones of the Orval Abbey (Belgium); *Environmental Earth Sciences*, (63), issue 7-8, (2011), 1447-1461.

Limiting salt crystallization damage in lime mortar by using crystallization modifiers

S.J.C. Granneman*¹, N. Shahidzadeh², B. Lubelli^{1,3} and R.P.J. van Hees^{1,3}

¹Delft University of Technology, Delft, The Netherlands

²University of Amsterdam, Institute of Physics, Amsterdam, The Netherlands

³TNO Technical Sciences, Delft, The Netherlands

*s.j.c.granneman@tudelft.nl

Abstract

Salt crystallization is a recurrent cause of damage in porous building materials. Lime-based mortars, which were widely used in construction of ancient masonry, are especially prone to salt damage, due to their low mechanical strength. Existing solutions to tackle salt damage in mortars have been mainly focused on increasing the mechanical strength of the mortar by the replacement of lime with (Portland) cement, or on reducing the moisture transport capacity by the addition of silicone-based water repellent products. Both solutions often showed to have a limited resistance to salt decay and a low compatibility with historical buildings.

In the last years research has started to explore the possibility of influencing the crystallization mechanism by the use of crystallization modifiers. Modifiers are ions or molecules that prevent nucleation (inhibitors), promote nucleation of a certain crystal polymorph (promoters) and/or modify the habit of the crystals (habit modifiers). The modifiers can alter the level of supersaturation at the moment of crystallization, as well as the rate of crystallization, which may result in a lower crystallization pressure and/or enhanced drying and increased salt crystallization at the surface of the material. Consequently, they may reduce salt damage development.

In previous research, borax ($\text{Na}_2\text{B}_4\text{O}_7 \cdot 10\text{H}_2\text{O}$) has been identified as a potential modifier for sodium sulphate, being one of the most damaging salts [1]. Borax is expected to promote the crystallization of mirabilite, the

decahydrate polymorph of sodium sulfate, at a lower supersaturation level than without modifier. A reduced supersaturation level at the moment of crystallization leads to a lower crystallization pressure and consequently less damage. The effective concentration of borax in sodium sulfate solution has been defined to be in the range of 0.01 to 0.1 M [1]. The promotion of mirabilite instead of for example thenardite, the anhydrate polymorph, is possibly the result of the formation of a template layer of borax. The crystal lattice parameters of borax and mirabilite have a high similarity, resulting in epitaxial growth [2].

However, there are still many fundamental questions to be answered about the impact of such a modifier before the ideal outcome is achieved for our specific application in the area of cultural heritage.

In this poster we show some microscale experiments using direct imaging and optical microscopy [3] in order to study the dynamics of crystallization of sodium sulfate in the presence of borax. The nucleation and growth and the crystallization patterns of sodium sulfate are followed during droplet evaporation on a glass plate at controlled relative humidity and temperature for different concentrations of borax in the solution. Additionally the impact of the borax concentration on the surface tension and the wetting properties of sodium sulfate solution were measured using the drop weight technique and the KRUSS apparatus.

Future research will also include crystallization experiments in glass micro capillaries, in order to simulate crystallization in pores. The ultimate aim of this research is to develop a lime-based repair mortar, with built-in crystallization modifiers.

Keywords: crystallization modifiers, lime mortar

References

- [1] S.J.C. Granneman, E. Ruiz-Agudo, B. Lubelli, R.P.J van Hees, C. Rodriguez-Navarro. Study on effective modifiers for damaging salts in mortar. 1st International conference on Ageing of Materials and Structures (AMS'14), Delft, the Netherlands, 2014.
- [2] E. Ruiz-Agudo, C. Rodriguez-Navarro. Limestone in the built environment: present-day challenges for the preservation of the past, Chapter: Suppression of salt weathering of porous limestone by borax-induced promotion of sodium and magnesium sulphate crystallization, pages 93-102. Geological Society, London, Special Publications, 2010.
- [3] N. Shahidzadeh-Bonn, S.Rafai, D. Bonn, G. Wegdam. Salt crystallization during evaporation: impact of interfacial properties. *Langmuir*. 2008, 24, 8599-8605.

A salt-storing modular mortar system developed for the salt loaded brick masonry of the Kampischen Hof, Stralsund (Germany)

G. Hilbert¹, J. Weber² and P. Butz³

¹ gh-DenkMalPlan, Magdeburg, Germany

² University of Applied Arts Vienna, Wien, Austria

³ Rocem Plaster Baustoff GmbH, Regensburg, Germany

* office@gh-denkmalplan.de

Abstract

Along the coastline of the Baltic Sea, cities like Wismar or Stralsund are characterised by an architectural style named “brick gothic”. Two issues are typical for this architectural style and geographical location:

1. Bricks fired at a low temperature are often not resistant to internal crystallization pressures resulting from frost or salt activity.
2. An important part of the building materials is contaminated with a mixture of chlorides and nitrates. Exposed to environmental conditions of which the relative humidity ranges between 50 and 75%, the crystallization cycling of salts is a major parameter of destructive activity of the bricks.

The monastery of the Middle Ages called Kampischer Hof in the city of Stralsund is one of the “brick gothic” monuments that was the subject of detailed investigation in the 1990s, funded by the German government. From the results, it was concluded that the high salt load was the major decay vehicle.

The design of a suitable mortar and plaster for the durable restoration of this type of brickwork was crucial. The mortar concept has to address and fulfil different restoration tasks, such as grouting, salt-buffering, plastering and restoring of detached brick surface material – and each of them should be capable of being applied in an extreme salt loaded environment.

Salt-storing mortars as a typically hydrophilic mortar system have been known since the 1990s. Beside their hydrophilic character, in contrast to the hydrophobic WTA-restoration plasters, a volume porosity >60%, a

consciously shaped pore size distribution influencing the capillary suction and a salt crystallization pressure resistant binder are key features of these mortars. Up to now, only mortars characterized by variations in mechanical strength were produced and applied. A first approach in adapting this mortar for special grouting tasks in Baku / Azerbaijan was presented by the author at SWBSS 2011. In this project, the very first steps towards adaptation of the pore structure to increase the salt storing or salt buffering capacity of the mortar have been addressed in order to fulfil the above mentioned restoration tasks. Depending on the specific properties of the mortar (salt storing or salt buffering), the amount of capillary active pores is different. To increase the capillary suction of the mortar, Roman cement was tested, known as a capillary-active hydraulic binder, resulting in a significant increase in the salt storage rate. Subtle differences in the binder matrix of mortars modified or not with Roman cement are not readily apparent when observed in the microscope (SEM) – but for the practised eye the influence of Roman cement on the structure is visible. Besides the tuning of the structure it is possible to produce this kind of plaster in different coloured versions so that it may be used as a brick supplementary mortar.

The work represents the first step in assessing the prospects offered by Roman cement as the primary binder of salt-storing mortars. However, much practical investigation is required to reach an optimised solution for a major European restoration problem.

Keywords: salt-storing mortar, salt storage, pore structure modelling, Roman cement

Measurement of salt solution uptake by ceramic brick using γ -ray projection

D. Ogura^{1,*}, M. Abuku², S. Hokoi¹, C. Iba¹, S. Wakiya³, and T. Uno⁴

¹Graduate School of Engineering, Kyoto University, Kyoto, Japan

²Faculty of Architecture, Kinki University, Higashi-Osaka, Japan

³Nara National Research Institute for Cultural Properties, Nara, Japan

⁴Department of Architecture, Mukogawa Women's University, Nishinomiya, Japan

* ogurad@archi.kyoto-u.ac.jp

Abstract

Measurements of pure water/salt (NaCl) solution uptake by ceramic brick that use γ -ray attenuation have been conducted. A measurement set-up is described to determine the average pure water/salt solution content in the measured spot of a specimen. Two different types of specimens are prepared: a specimen of 3 x 5 x 10 cm with all surfaces made vapour tight, except the bottom and top sides which absorb pure water/salt solution or evacuate air and vapour; the other specimen that has the same dimensions and vapour barriers but being initially salt laden. Differences in pure water/salt solution uptake rate in the specimen are quantified. From the obtained data the liquid water permeability is determined, that is influenced by dissolved salts and salt crystals. The effect of salts on the sorption isotherm of the material is also implemented in the model.

Keywords: non-destructive measurement, liquid water uptake, sodium chloride, liquid water permeability, viscosity

Introduction

Prediction of water and salt transport and the resulting salt crystallisation that leads to salt damages of cultural heritage porous materials is feasible when the material properties such as the sorption isotherm and liquid water permeability, are well known. To date much advanced experimental and numerical research for such purpose has been made. In this work, pure water/aqueous NaCl solution uptake by ceramic brick is measured using γ -ray projection, in order to determine the influence of dissolved salts on the liquid water permeability.

Methodology

This study employs the model to analyse transport of a salt solution at a constant concentration in porous materials. The model is thus formulated in a simplified manner, based on an existing model and assuming a constant salt concentration, to assess the influence of salt on the sorption isotherm and liquid permeability of the material. The following three steps are taken:

- (1) The time evolution and spatial distribution of the content of pure water/salt solution in the material during uptake processes are experimentally determined using γ -ray attenuation.
- (2) The sorption isotherm and liquid water permeability of the material that contains pure water are determined by evaluating the experimental data for pure water uptake.
- (3) The experimental data are numerically treated, where the model implements the influences of salts on the sorption isotherm and permeability. Because the permeability is considered to depend on not only on the amount and type of salt but also on the porous material itself, the permeability of the material that absorbs a salt solution has to be determined to obtain a good agreement between measured and modelled data .

Experimental set-up and conditions

The volumetric pure water/salt solution content was measured in laboratory conditions of $\sim 23^{\circ}\text{C}$ and 50% RH using the set-up illustrated in Figure 1. The set-up consists of a stage, γ -ray source, collimators and detector as well as a sample holder placed on the stage. The (measured) circular spot has a diameter of approximately 10 mm. A single spot is measured every second during 40 seconds to determine the moisture content averaged over the last 7 seconds.

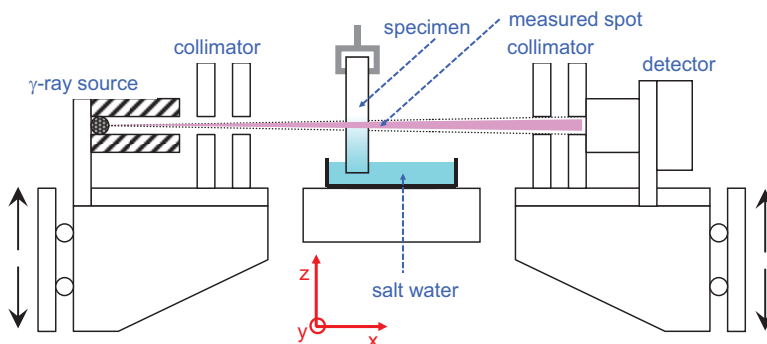


Figure 1: Schematic representation of the measurement set-up

Results and discussion

The time evolution of measured volumetric pure water/ salt solution contents at five different heights above the liquid surface in the container is shown in Figures 2 and 3. Each symbol in the figures depicts the content averaged over the measured spot. The time interval between two successive measurements corresponding to a difference in position of 1 cm is 80 seconds.

Significant differences in uptake rate between pure water and saturated salt solution are observed. Comparison of the two figures suggests that the uptake rate of pure water is almost three times that of a saturated salt solution.

At the end of the uptake, the pure water content is slightly higher than the salt solution content. This can be explained by a higher viscosity and higher surface tension of a saturated salt solution compared to pure water, resulting in a slower or limited absorption into pores of the material.

Acknowledgement

This work was supported by JSPS KAKENHI Grant Numbers 23560694 (Grant-in-Aid for Scientific Research (C)) and 26709043 (Grant-in-Aid for Young Scientists (A)). We also thank Mr. W. Kotera and Mr. K. Wada for their assistance in the experiments.

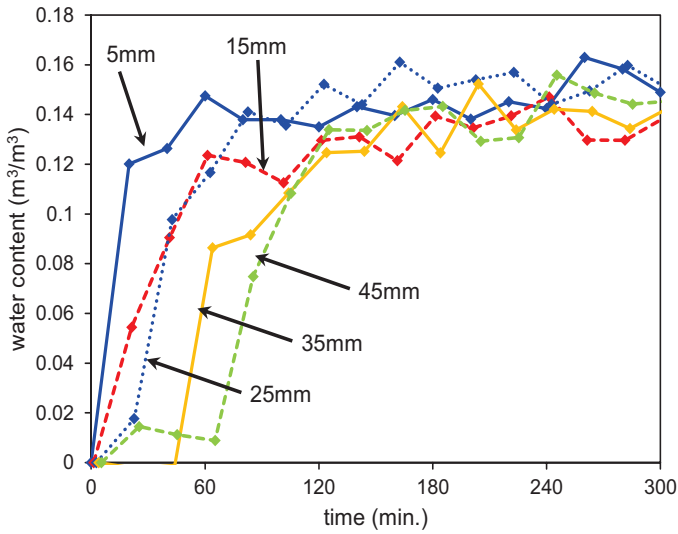


Figure 2: Evolution of water content during pure water uptake measurements

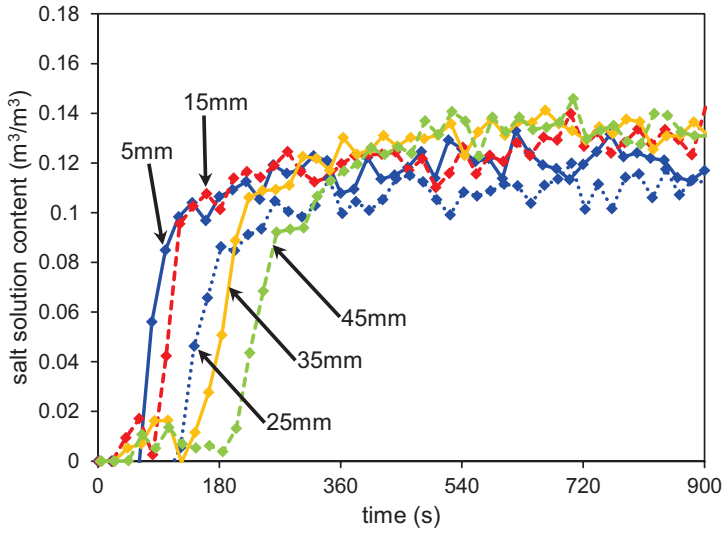


Figure 3: Evolution of salt solution content during saturated salt solution uptake measurements

The effect of salt crystallization on the drying kinetics of building materials

M. D. Seck^{1,2*}, **P. Faure**¹, **M. Van Landeghem**² and **P. Coussot**¹

¹Université Paris-Est, Laboratoire Navier, Champs-sur-Marne, France

²Saint-Gobain Recherche, Aubervilliers Cedex, France

* mamadou.diaga.seck@ifsttar.fr

Drying, and imbibition-drying cycles are two important phenomena known to play a major role during the production and the lifetime of building materials. Herein we study the evaporation of a saline solution in porous media. The critical physical phenomena in work are the migration and redistribution of ions within the porous medium. Indeed the crystallization of solids induced by the evaporation of the liquid phase has major impact on the drying kinetics. These phenomena are encountered during the production of building materials such as cement or plaster based building materials during their drying. Also we found them in the form of imbibition-drying cycles in buildings as in the case of capillary rising damp. The impact of the saline solution on the drying kinetics of porous media is not yet fully understood, nor has this impact been well quantified.

Results obtained by MRI (Magnetic Resonance Imaging), SEM (scanning electron microscopy), binocular microscopy, microtomography and weight measurement instruments, have shown that, compared to the ones filled with pure water, drying kinetics of porous media filled with ionic solution is quite well slower. For this purpose, a plaster sample was submitted to imbibition-drying cycles. Drying is assessed through the evolution of the mass loss and the setup of saturation profiles by means of MRI (fig.1). The results of these experiments show that the drying kinetics decrease after each cycle. With the help of imaging technics, the crystallization properties at the surface and within the pores are assessed. A crystallization close to the surface, forming a dense layer of which the thickness can be approached, seems to explain the slowing down of the

drying kinetics. This enables the establishment a model for ion transport in porous media capable to predict the slowing down of the drying process of saline solution saturated building materials.

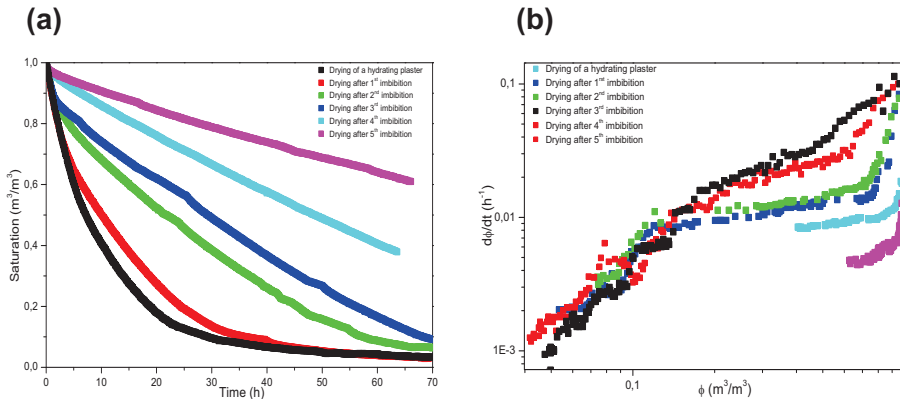


Figure 1: (a) Total water saturation as a function of time during the drying of a plaster sample. (b) Drying rate as a function of saturation during the drying of a plaster sample. From pasty state (black), after a first (red), a second (green), a third (blue), a fourth (turquoise) and a fifth (purple) saturation with a saturated gypsum solution.

Keywords: drying, building materials, ions, crystallization

Nanocomposite coatings for the protection of marble against salt weathering

P. Spathis^{1*}, I. Karapanagiotis², P. Manoudis², A. Zacharopoulou¹, V. Melfos³ and G. Vourlias⁴

¹School of Chemistry, Aristotle University of Thessaloniki, Greece

²Department of Management and Conservation of Ecclesiastical Cultural Heritage Objects, University Ecclesiastical Academy of Thessaloniki, Greece

³School of Geology, Aristotle University of Thessaloniki, Greece

⁴School of Physics, Aristotle University of Thessaloniki, Greece

*spathis@chem.auth.gr

Abstract

Moisture presence, salt precipitation and crystallization are main deterioration problems of the building materials of historic monuments. The presence of moisture in a material is due to rising and falling damp. The total moisture content and the contributions to salt damage of these forms of damp in a specific material will depend on the amount and nature of the salts in the soils beneath, on the humidity and temperature. For salt attack to occur the presence of a combination of conditions is needed, which are a permeable material, moisture, soluble salts and evaporation circumstances. The presence of salts changes the liquid transport properties of marbles, influencing also their structure and surface stability. Many commercial stone consolidation and some water repellent products contain tetraethoxysilane (TEOS). A drawback of these materials is their tendency to form gels susceptible to cracking. Nanomaterials resulting from the addition of TiO₂ nanoparticles to TEOS based commercial products, Rhodorsil RC-70 and RC-90, were synthesized. The protective

properties of the nanomaterials on a dolomite marble substrate against salts weathering were examined by water capillary absorption tests and accelerated aging tests. The consolidating and hydrophobic properties of the treatments were found to depend on the type of the nanomaterial and the type of salt. The type of the polymeric material and the presence of the nanoparticles affect in different ways the examined properties. Capillary rise is correlated with the rate of evaporation, the crystallization of salts and the growth of salt crystals within the pores of the marble. The aging behaviour of the treatment was found to depend on the type of the polymeric material and the presence of the nanoparticles.

Keywords: consolidant, nanomaterial, salt crystallization, dolomite marble, titanium oxide

Experimental

Five series of specimens of dolomite marble were prepared. Bare marble and marble treated with four types of consolidants, Rhodorsil RC-70, Rhodorsil RC-90, Rhodorsil RC-70 with 3% TiO₂ nanoparticles and Rhodorsil RC-90 with 3% TiO₂ nanoparticles. The capillary tests were carried out, for a period of seven days, in three different saturated solutions of sodium chloride, sodium sulphate and mixture of these salts. The behaviour of the treatments, the moisture presence and distribution, the form and the amount of the salts crystallized on the surface as well as the height of the capillary rise were investigated. The investigation was performed by gravimetric, optical microscopy, X-R Diffraction, X-R Fluorescence methods. The accelerated aging tests were carried out, for a period of three months, in 40°C temperature, 90% relative humidity, UV light conditions. Analysis by FTIR was performed and contact angle and colour alteration measurements were carried out.

Results and discussion

The gravimetric results of the capillary tests are shown in Table 1. The water absorption and salts crystallization is greater in the case of sodium chloride. All treatments show a decreased water absorption. The addition of TiO₂ further decreases the water absorption, and this more extensively

for Rhodorsil RC-90 compared to the RC-70 product, probably due to the presence of methyl-phenyl resin in the first one. Similar results were observed in the optical examination (Fig. 1) concerning the height of the capillary rise and salts crystallization on the surface of the specimen.

Table 1: Results of capillary tests, absorption, w % increase

	Marble	Rhodorsil RC-70	Rhodorsil RC-90	Rhodorsil RC-70 + TiO ₂	Rhodorsil RC-90 + TiO ₂
NaCl	2.97	2.10	0.61	1.53	0.41
Na ₂ SO ₄	0.86	0.58	0.28	0.42	0.17
Mixture	1.55	0.75	0.48	0.62	0.31

The results of the optical examination of the specimens after the capillary tests are shown in Figure 1. XRD analysis was carried out on the powder of the salts crystallized on the surfaces of the various series of the specimens, after their removal from the surface. The results showed that in the case of untreated marble the salts consist of sodium chloride and calcium and magnesium chlorides, sodium sulphate and calcium and magnesium sulphates or mixtures of these, according to the solution exposed. In all cases of treated marbles the calcium and magnesium salts exist, but their presence is significantly lower, indicating the protective properties of the products against the dissolution and transportation effects of salts. XRF analysis was carried out on the surfaces of the specimens after the removal of the salt layers. The results indicated the presence of sodium or sulphur ions that remained on the surface of the marble and also the existence of titanium in the case of a treatment to which TiO₂ was added.

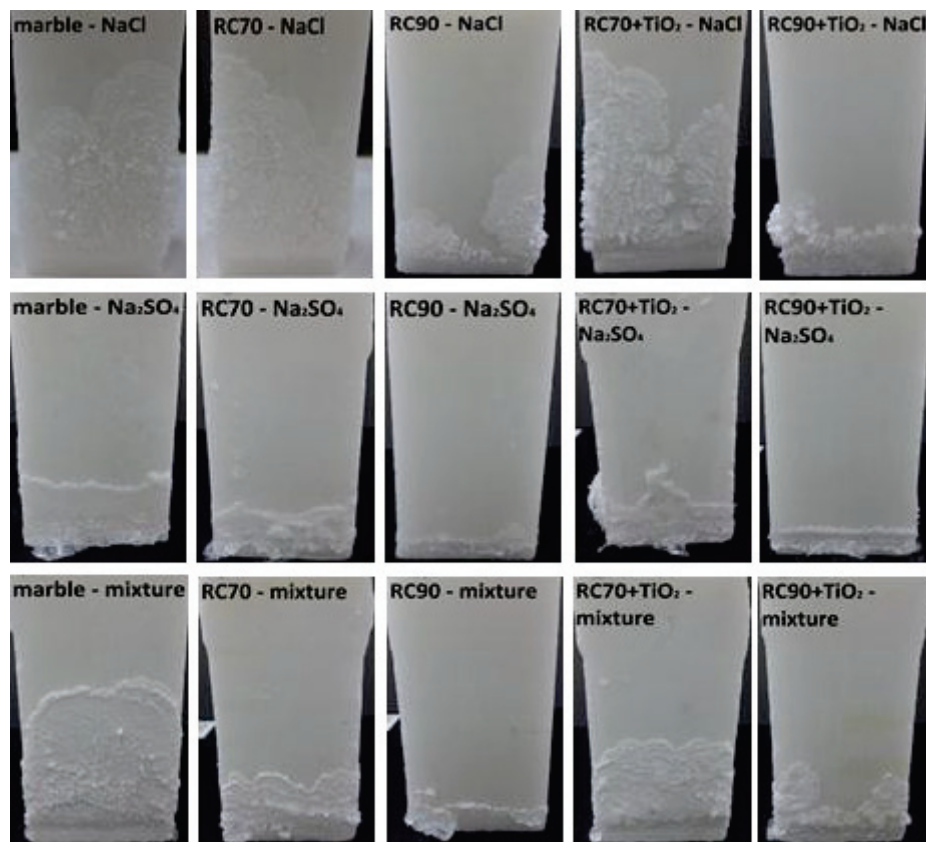


Figure 1: Capillary test, optical examination of bare and treated specimens after 7 days exposure in various salt solutions

Contact angle and colour alteration measurements, as well as FTIR analysis were carried out, before and after exposing in aging conditions. The results are shown in Table 2 and Figure 2.

Table 2: Contact angle and colour alteration results before (initial) and after (final) aging

	Marble	Rhodorsil RC-70	Rhodorsil RC-90	Rhodorsil RC-70 + TiO ₂	Rhodorsil RC-90 + TiO ₂
Contact angle initial, degree	71	92	95	93	101
Contact angle final, degree	82	98	104	103	108
Colour variation initial, ΔE^*	-	4.1	5.2	2.0	4.8
Colour variation final, ΔE^*	-	2.1	4.8	1.5	3.4

The results of the contact angle showed that the polymerised products all behaved water repellent, and this more intensively in case nanoparticles were added. After aging, the contact angle values increased slightly. This behaviour should be correlated to changes on surface microstructure and roughness during aging but further work is needed to confirm this supposition.

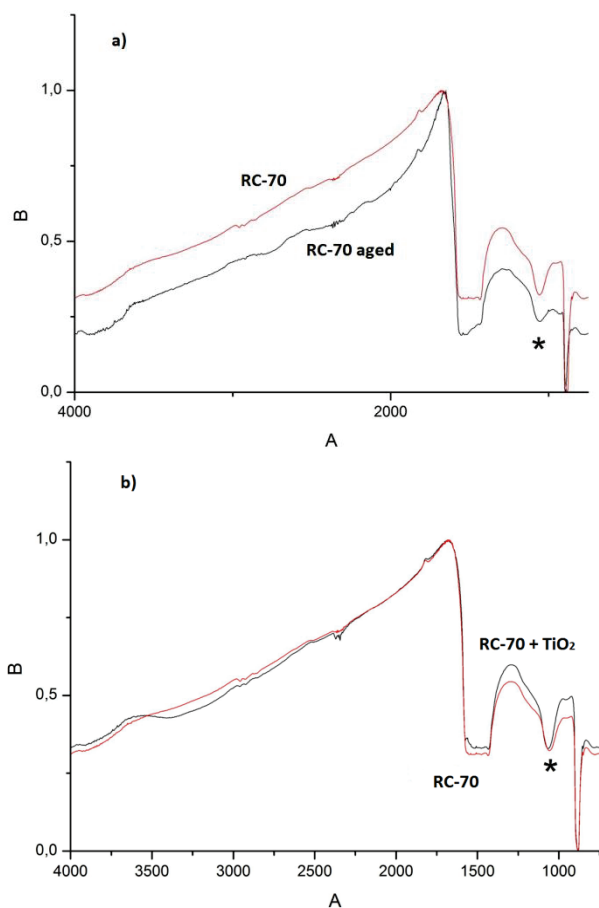


Figure 2: FTIR diagrams, a) before and after exposing in aging conditions, b) polymer and nanopolymer layer

In both FT-IR spectra of the samples treated with RC-70 (figure 2a), the (*) peak corresponds to the polymerised RC-70 product, which is wider and weaker for the sample after aging. From the results obtained for samples treated with RC-70 + TiO₂ (fig. 2b), it can be noticed that the addition of titanium oxide results in the formation of a better layer on the marble surface, as indicated from the closer and stronger form of the peak. Similar results were obtained for the samples treated with the RC-90 product.

Conclusions

The consolidating and hydrophobic properties of the tested products depend on the type of the nanomaterial and the type of the salt. The type of product and the presence of nanoparticles affect in different ways the examined properties as well as the aging behaviour.

All products used protect marble against salts weathering by decreasing the water absorption, salt crystallization and transportation effects. The addition of titanium oxide nanoparticles increases these protective properties.

The tested products had hydrophobic properties that further increase with the addition of the nanoparticles.

The application of a product having methyl and phenyl groupings and the addition of nanoparticles lead to the formation of a kind of modified resin with better surface and structure properties, enabling to increase its protective properties against salts weathering.

Thermal behaviour of building stones contaminated with Na₂SO₄

C. Thomachot-Schneider^{1*}, P. Vázquez¹, N. Lelarge¹, A. Conreux¹, C. Bouvy¹, M. Gommeaux¹, K. Mouhoubi² and J.L. Bodnar²

¹GEGENAA, Université de Reims Champagne-Ardenne, Reims, France

²CATHERM, Université de Reims Champagne-Ardenne, Reims, France

* celine.schneider@univ-reims.fr

Abstract

The Orval Abbey (Belgium) was rebuilt from 1928 to 1936 using the two original limestones of the previous Abbey and a reconstituted stone produced by mixing debris of the two natural stones with cement. These three materials have different resistance towards salt crystallisation; especially the reconstituted stone is highly salt-prone. The major salt found in the walls and at the surface of walls is thenardite (Na₂SO₄).

A previous study [1] showed that sulphates originate from the reconstituted stone itself. Active infrared thermography (IRT) recorded on parts of the Abbey show that the thermal response of salt-weathered part of walls is different from that of unweathered ones (Gommeaux et al., actual proceedings). This method is commonly used in heritage to detect thermal anomalies due to for example the presence of moisture or cracks or material change.

In this study, we applied the technique in the laboratory on samples of the three building materials used in the Orval Abbey. The aim was to understand the different behaviour of these materials and to see if there could be a relation between the extent of salt contamination and thermal response.

Keywords: infrared thermography, wetting-drying cycles, Na₂SO₄, limestone

Materials

The two natural stones are limestones from the surroundings of the Abbey: one from the Bajocian (BJ) and one from the Sinemurian (SN), while the reconstituted stone (RS) is composed of debris of SN and BJ mixed with cement [1]. The last was made on site during the last-century reconstruction; the recipe is unfortunately not known.

The natural and reconstituted materials are quite similar in visual aspect, except that the reconstituted stone often shows bubbles. Its russet colour is intermediate between those of the BJ and the SN.

The BJ limestone is a calcareous limestone rich in bioclasts and with very low silica content while the SN is a siliceous limestone. The reconstituted stone has a composition that is intermediate between the two natural stones and contains besides elements typical for cement, such as aluminium and iron.

Although porosity and water transfer properties of the RS are similar to the BJ limestone, its pore access distribution is centred at 0.1 μm which is the main pore access family of the SN (Figure 1). These three materials are similar but different enough to be distinguished through their porous network and transfer properties.

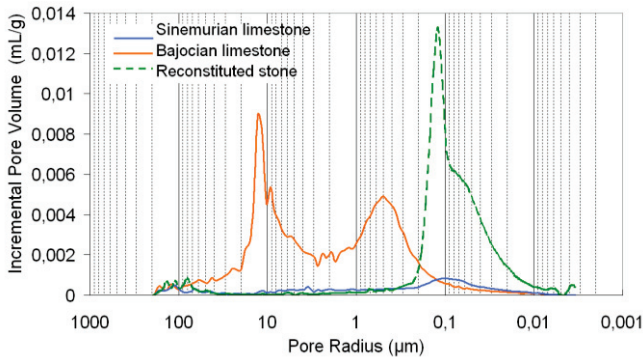


Figure 1: Pore size distribution of the three stones obtained by mercury porosimetry.

Salt ageing tests

45 disk-shaped samples (diameter: 30 mm; height: 5 mm) of each material were submitted to immersion-drying tests in Na_2SO_4 solutions of different concentrations: 7, 14 and 26 w%. 15 cycles of 24 h each were performed, consisting of 2 h immersion and 22 h of drying in boxes with silica gel.

The weight of the samples and the surface colour were recorded after each cycle. The samples were observed under a binocular magnifier.

After 1, 5, 10 and 15 cycles, 3 samples of each stone were selected for infrared thermography measurements.

Active infrared thermography

Active IRT was conducted by means of a FLIR infrared thermography camera SC655 operating in the long-wave infrared spectra range [7.5-14 μm] and providing images of 640 x 480 pixels. Two flash lights were placed at 45° of the sample, symmetrically along the axis of the camera (Figure 2), producing light of 4800 J during 5 ms. The flux of photons emitted by the flash excites the sample leading to an increase of its temperature. Part of the heat is absorbed while the other part is emitted back and recorded by the camera. The emitted infrared radiation depends on the physical parameters of the material: density, porosity and pore structure, specific heat, thermal emissivity, thermal conductivity and thermal diffusivity, as well as on the surface properties (rugosity, color) and mineralogical composition. To minimize the effect of the surface aspect of the samples on the thermal response, samples were covered with a black high-temperature resistant paint layer. The thermal effusivity b (indicating the stones' ability to exchange thermal energy with their surrounding) was computed from the thermal curves (in $\text{J} \cdot \text{K}^{-1} \cdot \text{m}^{-2} \cdot \text{s}^{-1/2}$).

Images were recorded each 10 milliseconds (100Hz), further treated and analysed with the ThermoCAM Researcher 2.10 software (FLIR).

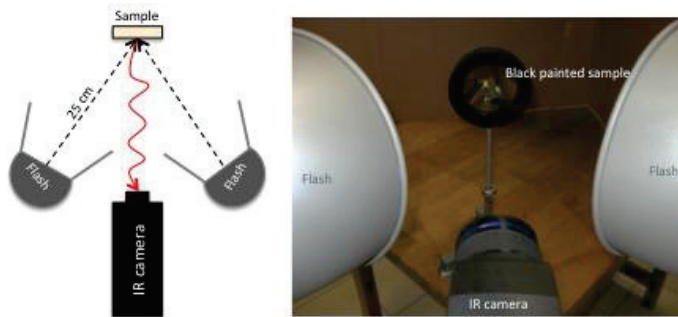


Figure 2: Scheme and picture of the setting of active IRT measurements.

Results

The salt crystallization at the surface of the samples of the three stones led to whitening that increased with the salt solution concentration. At the end of the 15th cycle, the color change ΔE was about 25 for the SN using a salt solution of 26w%, while about 20 for the BJ and the RS at the same concentration.

The weight change of the samples is a balance between salt uptake and loss of stone debris due to salt damage. While very little change in weight was noticed on SN for all three salt concentrations, related to a low salt uptake and damage, the BJ showed a weight increase up to 3% using the 14 and 26w% solutions. However, sanding of the BJ occurred all over the experiment. From cycle 12 on, important loss of material (and in some cases, complete collapse) occurred. The salt uptake of RS was higher than for the other stones (maximum weight increase between 2% for the 7w% salt solution to 7% for the 26w% solution). This was likely due to the high porosity of the RS consisting of a high content of micropores (0.1 μm) which favor salt crystallization. Sanding on the edges and surface of the samples occurred over the entire experiment; some samples disaggregated completely from cycle 13.

For each of the three stones, the changes in thermal properties were very similar for all three salt concentrations. The thermal effusivity of the BJ and the RS was similar over the course of the experiment (initial value close to $2300\text{J}\cdot\text{K}^{-1}\cdot\text{m}^{-2}\cdot\text{s}^{-1/2}$, constant until cycle 5, increase to $4000\text{J}\cdot\text{K}^{-1}\cdot\text{m}^{-2}\cdot\text{s}^{-1/2}$ after cycle 10 and little decline up to cycle 15). The evolution of the thermal effusivity of the SN showed a very different pattern. Yet after cycle 1, there was a large increase in thermal effusivity (from 3900 to $7000\text{J}\cdot\text{K}^{-1}\cdot\text{m}^{-2}\cdot\text{s}^{-1/2}$) that showed a further decreasing trend.

Conclusions

The results of IRT confirm that the properties of the RS are close to those of the BJ limestone. The initial purpose of making a RS suitable to replace the natural stones to complete the building of the Abbey was thus mostly fulfilled. However, the RS has properties closer to the BJ (which is used as freestone) than to the SN (used as rubblestone).

Furthermore, this study showed a clear link between salt uptake and a change in thermal properties of the stones. Although the relationship needs to be refined, this confirms that active IRT may be a valuable tool to distinguish similar-looking materials and for the diagnosis of salt accumulation in building materials.

Acknowledgements

This study was partly funded by the Hybriprotech grant as part of the INTERREG IV programme. The authors warmly thank Brother Xavier for permitting work in the Orval Abbey.

References

- [1] C. Thomachot-Schneider , M. Gommeaux, G. Fronteau, C.T. Oguchi, S. Eyssautier, B. Kartheuser; A comparison of the properties and salt weathering susceptibility of natural and reconstituted stones of the Orval Abbey (Belgium); *Environmental Earth Sciences*, (63), Issue 7-8 (2011) 1447-1461
- [2] J.L. Bodnar, J.C. Candoré, J.L. Nicolas, G. Szatanik, V. Detalle, J.M. Vallet, Stimulated infrared thermography applied to help restoring mural paintings, *NDT&E International* 49 (2013) 40-46



FHP:~)



.be

ISBN 978-2-930054-24-7

